PLANT SPECIALIZED METABOLISM FOR PLANT PROTECTION: GENOMICS AND BIOTECHNOLOGY

EDITED BY: Zhihua Liao, Lei Zhang and Felipe A. Vázquez-Flota

PUBLISHED IN: Frontiers in Plant Science

frontiers Research Topics

Frontiers eBook Copyright Statement

The copyright in the text of individual articles in this eBook is the property of their respective authors or their respective institutions or funders. The copyright in graphics and images within each article may be subject to copyright of other parties. In both cases this is subject to a license granted to Frontiers.

The compilation of articles constituting this eBook is the property of Frontiers.

Each article within this eBook, and the eBook itself, are published under the most recent version of the Creative Commons CC-BY licence. The version current at the date of publication of this eBook is CC-BY 4.0. If the CC-BY licence is updated, the licence granted by Frontiers is automatically updated to the new version.

When exercising any right under the CC-BY licence, Frontiers must be attributed as the original publisher of the article or eBook, as applicable.

Authors have the responsibility of ensuring that any graphics or other materials which are the property of others may be included in the CC-BY licence, but this should be checked before relying on the CC-BY licence to reproduce those materials. Any copyright notices relating to those materials must be complied with.

Copyright and source acknowledgement notices may not be removed and must be displayed in any copy, derivative work or partial copy which includes the elements in question.

All copyright, and all rights therein, are protected by national and international copyright laws. The above represents a summary only. For further information please read Frontiers' Conditions for Website Use and Copyright Statement, and the applicable CC-BY licence.

ISSN 1664-8714
ISBN 978-2-83250-896-1
DOI 10.3389/978-2-83250-896-1

About Frontiers

Frontiers is more than just an open-access publisher of scholarly articles: it is a pioneering approach to the world of academia, radically improving the way scholarly research is managed. The grand vision of Frontiers is a world where all people have an equal opportunity to seek, share and generate knowledge. Frontiers provides immediate and permanent online open access to all its publications, but this alone is not enough to realize our grand goals.

Frontiers Journal Series

The Frontiers Journal Series is a multi-tier and interdisciplinary set of open-access, online journals, promising a paradigm shift from the current review, selection and dissemination processes in academic publishing. All Frontiers journals are driven by researchers for researchers; therefore, they constitute a service to the scholarly community. At the same time, the Frontiers Journal Series operates on a revolutionary invention, the tiered publishing system, initially addressing specific communities of scholars, and gradually climbing up to broader public understanding, thus serving the interests of the lay society, too.

Dedication to Quality

Each Frontiers article is a landmark of the highest quality, thanks to genuinely collaborative interactions between authors and review editors, who include some of the world's best academicians. Research must be certified by peers before entering a stream of knowledge that may eventually reach the public - and shape society; therefore, Frontiers only applies the most rigorous and unbiased reviews.
Frontiers revolutionizes research publishing by freely delivering the most outstanding research, evaluated with no bias from both the academic and social point of view. By applying the most advanced information technologies, Frontiers is catapulting scholarly publishing into a new generation.

What are Frontiers Research Topics?

Frontiers Research Topics are very popular trademarks of the Frontiers Journals Series: they are collections of at least ten articles, all centered on a particular subject. With their unique mix of varied contributions from Original Research to Review Articles, Frontiers Research Topics unify the most influential researchers, the latest key findings and historical advances in a hot research area! Find out more on how to host your own Frontiers Research Topic or contribute to one as an author by contacting the Frontiers Editorial Office: frontiersin.org/about/contact

PLANT SPECIALIZED METABOLISM FOR PLANT PROTECTION: GENOMICS AND BIOTECHNOLOGY

Topic Editors:
Zhihua Liao, Southwest University, China
Lei Zhang, Second Military Medical University, China
Felipe A. Vázquez-Flota, Unidad de Bioquímica y Biología Molecular de Plantas, Centro de Investigación Científica de Yucatán, Mexico

Citation: Liao, Z., Zhang, L., Vázquez-Flota, F. A., eds. (2022). Plant Specialized Metabolism for Plant Protection: Genomics and Biotechnology. Lausanne: Frontiers Media SA. doi: 10.3389/978-2-83250-896-1

Table of Contents

frontiers | Frontiers in Plant Science

TYPE Editorial
PUBLISHED 15 November 2022
DOI 10.3389/fpls.2022.1080939

Check for updates

OPEN ACCESS

EDITED AND REVIEWED BY
Laigeng Li,
Center for Excellence in Molecular Plant Sciences (CAS), China

*CORRESPONDENCE
Felipe Vázquez-Flota
felipe@cicy.mx

SPECIALTY SECTION
This article was submitted to Plant Metabolism and Chemodiversity, a section of the journal Frontiers in Plant Science

RECEIVED 26 October 2022
ACCEPTED 01 November 2022
PUBLISHED 15 November 2022

CITATION
Liao Z, Zhang L and Vázquez-Flota F (2022) Editorial: Plant specialized metabolism for plant protection: Genomics and biotechnology. *Front. Plant Sci.* 13:1080939. doi: 10.3389/fpls.2022.1080939

COPYRIGHT
© 2022 Liao, Zhang and Vázquez-Flota. This is an open-access article distributed under the terms of the Creative Commons Attribution License (CC BY). The use, distribution or reproduction in other forums is permitted, provided the original author(s) and the copyright owner(s) are credited and that the original publication in this journal is cited, in accordance with accepted academic practice. No use, distribution or reproduction is permitted which does not comply with these terms.

Editorial: Plant specialized metabolism for plant protection: Genomics and biotechnology

Zhihua Liao[1,2], Lei Zhang[3] and Felipe Vázquez-Flota[4]*

[1]State Key Laboratory of Silkworm Genome Biology, Integrative Science Center of Germplasm Creation in Western China (CHONGQING) Science City & Southwest University, SWU-TAAHC Medicinal Plant Joint R&D Centre, School of Life Sciences, Southwest University, ChongqingChina, [2]Chongqing Academy of Science and Technology, Chongqing, China, [3]Department of Pharmaceutical Botany, School of Pharmacy, Naval Medical University, Shanghai, China, [4]Unidad de Bioquímica y Biología Molecular de Plantas, Centro de Investigación Científica de Yucatán, Mérida, Yucatán, México

KEYWORDS

biosynthesis, chemical diversity, plant-environment interactions, specialized metabolites, transcriptional factors

Editorial on the Research Topic
Plant specialized metabolism for plant protection: genomics and biotechnology

Introduction

The philosophical conception of the now called plant specialized metabolites (PSM) has radically changed over the last three decades. Up to the late 1980's, it was common to find extensive literature reviews analyzing conditions leading to the synthesis of these low molecular weight compounds and discussing their probable physiological roles. Despite of numerous reports of chemically mediated plant-insect interactions already available at the time, they were considered as metabolic waste or a simple means to keep major metabolic pathways in operation (Haslam, 1986; Williams et al., 1989). This apparently superfluous character was the reason to refer them as *secondary metabolites*, a term that persists in the plant science's vocabulary up to now. Regardless of semantic preferences, all these compounds share some important structural and biological features, such as displaying a wide chemical diversity and presenting a limited taxonomical distribution. Besides, they are accumulated in only tiny amounts and under specific conditions. Most importantly, they exert physiological activities on other organisms.

However, as the molecular mechanism controlling PSM formation in response to environmental cues were discovered, it became evident that these compounds were part of a plant sophisticated set of chemical tools to interact with their surroundings (Erb and Kliebenstein, 2020; Jamil et al., 2020). With this, new venues were opened for these specialized chemicals' which for a long time, had been profited from straightforward processes of extraction-purification and product elaboration (Salim and De Luca, 2013).

This collection on Plant Specialized Metabolism for Plant Protection: Genomics and Biotechnology, illustrates the quick progress experienced in this field as the high-

throughput technologies are turning into common tools for non-model species. Most articles nicely merge metabolomic and transcriptomic data, drawing an integral view of the operating metabolic networks and the possible master genes that coordinate them. Ultimately, two aspects of PSM were taken as main motives for this collection; the transcriptional factors (TF) acting as such master regulatory genes and the environmental conditions that activate the intricate biosynthetic pathway involved.

Transcriptional control of plant specialized metabolism

Combining anthocyanin profiling and transcriptomic analysis of differentially colored flowers of *Fressia hybrida*, Zhu et al. reported the finding of four novel TFs, from the WRKY and AP2 protein families, involved in governing petal's colour. A similar approach was followed by Yang et al. to address the basis of colour differences in white and pink *Lycoris sprengeri* flowers.

Moreover, Shen et al. described the coordinated interplay of bHLH and MYC2 proteins for switching on and off artemisinin biosynthesis in *Artemisa annua*. This work not just reveals a novel mechanism for the fine tuning of the biosynthesis of this metabolite, but also opens biotechnological opportunities, considering the medicinal applications of this plant. The associations between growth promotion, specifically trough cell wall formation, and the synthesis of specialized metabolites, are elegantly addressed by Yu et al, who traced down domestication traits in *Panax notoginseng*. A new MYB protein, able to bind to *cis* elements in promotors from genes for cell wall and ginsenoside biosynthesis, was found in this work which also discussed how human selection with medicinal purposes greatly influenced root chemical composition. Genes coding for proteins of the relatively small, and less studied Teosinte branched1/Cycloidea/Proliferating cell factor (TCP) family are proposed as possible modulators of camptothecin formation, by Wang et al., through genomic analysis of *Ophiorriza pumila*. Candidates involved, in both forming these alkaloids, and furnishing precursors to the biosynthetic pathway, were described and analyzed with regard to their cell distribution and ability to activate selected promotors in this medicinally important Asian plant.

Besides these *trans* functioning elements, the role of chromatin conformation was analyzed in *Cannabis sativa* by Yang et al.. Up to 14 putative histone deacetylase genes displayed matching transcriptional profiles to a set of selected cannabinoids biosynthetic genes. A particularly interesting result is that five of them, which belong to the C subfamily were affected along cannabinoid formation in plantlets treated with Trichostatin A, a broad inhibitor of their action. This work is one of the few reports dealing with specialized metabolism at this early regulatory mechanism.

Additionally to these studies, Zhan et al. presented a comprehensive review linking metabolic pathways with the environmental stimuli triggering them and the responsible genetic regulators. A careful choice of examples among alkaloids, glucosinolates, terpenoids, phenols and flavonoids was included by the authors. As for alkaloids, Song et al. covers the state of the art on the distribution of alkaloids from different families and transcriptomic data in *Dendrobium* medicinal species. Based on the combined information, biosynthetic routes are proposed, setting the stage for actual gene isolation and further studies in this interesting plant.

Specialized metabolism in environmental interactions

The adaptative role of specialized metabolites under adverse plant-environment interactions has been profusely documented. In this issue, Peng et al analyzed two cultivars of *Angelica sinensis* exposed to enhanced UV-B radiation. A contrasting metabolic performance was found, related to ferulic acid and flavonoid synthesis. ROS scavenger systems were also analyzed in this work, and important variations in the ascorbate-glutathione cycle were found. An interesting study of the superoxide dismutase (SOD) gene family in protecting tobacco plants exposed to heavy metal was presented by Huo et al.. Effects of other metals, such as copper, were also approached in *Salvia mithiorrhiza*. Combining the data from metabolomics and transcriptomics, Xiang et al. found an increase in salvianolic acid accumulation that could be associated with a significative increase of laccase transcripts and the occurrence of specific MYB and zinc finger proteins.

On the other hand, since photovoltaic agriculture is quickly spreading as a promising sustainable farming alternative, a better understanding of plant adaptative mechanisms to these conditions is required. The study of Xie et al. on the effects of photovoltaic conditions on performance of the medicinal plant *Tetrastigma hemsleyanum* revealed a decrease in photosynthetic efficiency which could be alleviated by the external addition of stress hormones, such as jasmonate and salicylic acid (SA). An interesting interplay between SA and NO modulating photovoltaic adaptation was described in this work, which also showed that these innovative agricultural practises could be adapted to SM producing plants.

Plant specialized metabolism. The road ahead

Conservative estimations fix the number of phytochemicals in the order of hundred of thousands. Although many of them result from the occurrence of chiral centers and different

modification patterns on a common core structure, such wide diversity involves the operation of elaborate biochemical networks and regulation at the genetic level. Comprehensive 'omics' approaches to plant specialized metabolism had unveiled some remarkable differences from primary metabolism, which explain the basis for this impressive phytochemical diversity. Each plant presents its unique chemical mixture, which results from the particular tuning of its genetic potential and developmental program with the surroundings. The increased access of high-throughput technologies has allowed us to expand our knowledge on the critical points for reaching this chemical setting. Moreover, these tools also present opportunities for engineering metabolic and synthetic biology strategies for more sustainable uses of these valuable natural resources.

Author contributions

FV-F wrote the first draft, ZL and LZ corrected and provided input to the first and subsequent drafts. All authors contributed to the article and approved the submitted version.

Funding

FV-F received funding from National Research Council for Science and Technology (CONACYT México; CB-2016-0285887). LZ was financially supported by the National Natural Science Foundation of China (31970316;32170274;82225047) and National Key R&D Program of China (2022YFC3500098). ZL received funding from the NSFC project (81973420) and the National Key Research and Development Project (2019YFE0108700).

Acknowledgments

The authors wish to thank to all the contributors and the FPS editorial team for their efficient work. We would like to express our deep gratitude to all reviewers for their valuable participation in assuring the scientific quality of this collection. FV-F wish to thank Dr. ML Miranda-Ham for critical reviewing the first draft.

Conflict of interest

The authors declare that the research was conducted in the absence of any commercial or financial relationships that could be construed as a potential conflict of interest.

Publisher's note

All claims expressed in this article are solely those of the authors and do not necessarily represent those of their affiliated organizations, or those of the publisher, the editors and the reviewers. Any product that may be evaluated in this article, or claim that may be made by its manufacturer, is not guaranteed or endorsed by the publisher.

References

Erb, M., and Kliebenstein, D. J. (2020). Plant secondary metabolites as defenses, regulators, and primary metabolites: the blurred functional trichotomy. *Plant Physiol.* 184 (1), 39–52. doi: 10.1104/pp.20.00433

Haslam, E. (1986). Secondary metabolism–fact and fiction. *Nat. Prod Rep.* 3, 217–249. doi: 10.1039/np9860300217

Jamil, I. N., Remali, J., Azizan, K. A., Nor Muhammad, N. A., Arita, M., Goh, H. H., et al. (2020). Systematic multi-omics integration (MOI) approach in plant systems biology. *Front. Plant Scie* 11, 944. doi: 10.3389/fpls.2020.00944

Salim, V., and De Luca, V. (2013). Towards complete elucidation of monoterpene indole alkaloid biosynthesis pathway: *Catharanthus roseus* as a pioneer system. *Adv. Bot. Res.* 68, 1–37. doi: 10.1016/B978-0-12-408061-4.00001-8

Williams, D. H., Stone, M. J., Hauck, P. R., and Rahman, S. K. (1989). Why are secondary metabolites (natural products) biosynthesized? *J. Nat. Prod* 52 (6), 1189–1208. doi: 10.1021/np50066a001

frontiers in Plant Science

ORIGINAL RESEARCH
published: 07 October 2021
doi: 10.3389/fpls.2021.746648

Genome-Wide Identification and Comparative Analysis of the Teosinte Branched 1/Cycloidea/Proliferating Cell Factors 1/2 Transcription Factors Related to Anti-cancer Drug Camptothecin Biosynthesis in *Ophiorrhiza pumila*

Can Wang[1,2], Xiaolong Hao[2], Yao Wang[2], Min Shi[2], Zhi-Gang Zhou[1] and Guoyin Kai[2]**

[1] Key Laboratory of Exploration and Utilization of Aquatic Genetic Resources Conferred by Ministry of Education, Shanghai Ocean University, Shanghai, China, [2] Laboratory for Core Technology of TCM Quality Improvement and Transformation, School of Pharmaceutical Sciences, The Third Affiliated Hospital, Zhejiang Chinese Medical University, Hangzhou, China

OPEN ACCESS

Edited by:
Zhihua Liao,
Southwest University, China

Reviewed by:
Zhongxiong Lai,
Fujian Agriculture and Forestry University, China
Ling Li,
Shanghai Jiao Tong University, China

***Correspondence:**
Zhi-Gang Zhou
zgzhou@shou.edu.cn
Guoyin Kai
kaiguoyin@163.com

Specialty section:
This article was submitted to Plant Metabolism and Chemodiversity, a section of the journal Frontiers in Plant Science

Received: 24 July 2021
Accepted: 09 September 2021
Published: 07 October 2021

Citation:
Wang C, Hao X, Wang Y, Shi M, Zhou Z-G and Kai G (2021) Genome-Wide Identification and Comparative Analysis of the Teosinte Branched 1/Cycloidea/Proliferating Cell Factors 1/2 Transcription Factors Related to Anti-cancer Drug Camptothecin Biosynthesis in Ophiorrhiza pumila. Front. Plant Sci. 12:746648. doi: 10.3389/fpls.2021.746648

Ophiorrhiza pumila (*O. pumila*; *Op*) is a medicinal herbaceous plant, which can accumulate camptothecin (CPT). CPT and its derivatives are widely used as chemotherapeutic drugs for treating malignant tumors. Its biosynthesis pathway has been attracted significant attention. Teosinte branched 1/cycloidea/proliferating cell factors 1/2 (TCP) transcription factors (TFs) regulate a variety of physiological processes, while TCP TFs are involved in the regulation of CPT biosynthesis remain unclear. In this study, a systematic analysis of the TCP TFs family in *O. pumila* was performed. A total of 16 *O. pumila* TCP (*OpTCP*) genes were identified and categorized into two subgroups based on their phylogenetic relationships with those in *Arabidopsis thaliana*. Tissue-specific expression patterns revealed that nine *OpTCP* genes showed the highest expression levels in leaves, while the other seven *OpTCPs* showed a higher expression level in the stems. Co-expression, phylogeny analysis, and dual-luciferase (Dual-LUC) assay revealed that *OpTCP15* potentially plays important role in CPT and its precursor biosynthesis. In addition, the subcellular localization experiment of candidate *OpTCP* genes showed that they are all localized in the nucleus. Our study lays a foundation for further functional characterization of the candidate *OpTCP* genes involved in CPT biosynthesis regulation and provides new strategies for increasing CPT production.

Keywords: *Ophiorrhiza pumila*, TCP transcription factors, genome-wide analysis, expression pattern, CPT biosynthesis

Abbreviations: CPT, camptothecin; TCP, teosinte branched 1/cycloidea/proliferating cell factors 1/2; TB1, teosinte branched 1; CYC, cycloidea; PCF1/2, proliferating cell factors 1/2; bHLH, basic helix-loop-helix; MEP, 2-Cmethyl-Derythritol 4-phosphate.

INTRODUCTION

Ophiorrhiza pumila (O. pumila), belonging to the family Rubiaceae, is an important herbaceous medicinal plant and can accumulate camptothecin (CPT). CPT is a quinoline-type monoterpenoid indole alkaloid and an anticancer compound with potent DNA topoisomerase I inhibitory activity (Johnson et al., 2018). Two semi-synthetic water-soluble CPT analogs known as topotecan and irinotecan have been approved for the treatment of ovarian, colorectal, lung and cervix cancer, and HIV (Liu et al., 2015; Martino et al., 2017). Additionally, a number of other CPT derivatives have shown promising results in preclinical and clinical trials (Xie et al., 2016). Despite CPT with pharmacological relevance, its biosynthesis pathway is complex and partially deciphered (Sadre et al., 2016; Yang et al., 2021). CPT is produced by the iridoid and shikimate pathways, which supply the important precursors, such as secologanin and tryptamine. Subsequently, secologanin and tryptamine are converged into strictosidine, which is finally synthesized into CPT by some unknown catalytic enzymes (**Supplementary Figure 1**). At present, genomes and transcriptome data of many monoterpenoid indole alkaloid-producing plants, such as *O. pumila*, *Catharanthus roseus*, *Camptotheca acuminata,* and *Nothapodytes nimmoniana*, provided the foundation for understanding the biosynthesis and regulatory components of plant-specialized metabolites, followed by molecular characterization and functional validation of candidate genes (Kellner et al., 2015; Rather et al., 2018; Kang et al., 2021; Rai et al., 2021). At present, a few genes-encoding key enzymes, such as *OpTDC*, *OpTDC2*, *OpSTR*, *OpCPR*, *OpG10H*, *OpSLS*, *OpLAMT,* in the CPT biosynthetic pathway and several transcription factors (TFs), such as OpMYB1, OpWRKY1/2/3, and OpERF1/2/3, have been cloned and analyzed in *O. pumila* (Kai et al., 2015; Rohani et al., 2016; Udomsom et al., 2016; Shi et al., 2020; Hao et al., 2021; Yang et al., 2021; You et al., 2021). For example, OpWRKY2 acted as a positive regulator of CPT biosynthesis by directly binding and activating the gene *OpTDC* (Hao et al., 2021). Suppression of OpERF2 resulted in reducing expression of genes in the early steps that supplied a precursor for CPT biosynthesis, such as *OpTDC*, *OpG10H*, *OpSLS*, and *OpSTR* (Udomsom et al., 2016). Nevertheless, limited information is available about the regulatory mechanism of CPT biosynthesis in *O. pumila*, especially teosinte branched 1/cycloidea/proliferating cell factors 1/2 (TCP) TF.

The TCP family is a group exclusively present in the higher plants (Liu et al., 2019). The name of TCP was derived from three members of this family identified: teosinte branched 1 (TB1) in *Zea mays* (Doebley et al., 1995), cycloidea (CYC) in *Antirrhinum majus* (Luo et al., 1996), and proliferating cell factors 1/2 (PCF1/2) in *Oryza sativa* (Kosugi and Ohashi, 1997; Cubas et al., 1999). These proteins contained a highly conserved 55–59 residue-long basic helix-loop-helix (bHLH) structure at the N-terminus, known as TCP domain (Aggarwal et al., 2010). It was associated with protein nuclear localization, DNA binding, and protein–protein interaction (Cubas et al., 1999). According to the differential features in TCP domains, TCP family members were divided into two subfamilies: class I (also called PCF or TCP-P) and class II (TCP-C) (Martín-Trillo and Cubas, 2010). The most striking difference between these two subfamilies was the deletion of four-amino-acids at the N-terminal, which was exclusive in class I. Class II TCP proteins were further subdivided into the cincinnata (CIN) and cycloidea (CYC)/TB1 subclasses based on the alterations in several amino acids (Howarth and Donoghue, 2006; Horn et al., 2015). Besides the TCP domain, some members within class II had the R domain (18–20 residue arginine-rich motifs) and glutamic acid-cysteine-glutamic acid (ECE) motif (glutamic acid-cysteine-glutamic acid stretch) (Lupas et al., 1991).

Teosinte branched 1/cycloidea/proliferating cell factors 1/2 proteins were involved in diverse physiological and biological processes, such as phytohormone biosynthesis, transport, and signal transduction, leaf development, branching, embryonic growth, floral organ morphogenesis, pollen development, germination, senescence, circadian clock, and cell cycle regulation (Danisman et al., 2012; Manassero et al., 2013). Class I TCP genes, *A. thaliana* TCP (*AtTCP*)*14* and *AtTCP15*, played a vital role in seed germination and promoted embryo growth via the gibberellin signaling pathway (Resentini et al., 2015). For CIN subclass *TCP* genes, repression of *AtTCP3*, *AtTCP4*, and *AtTCP24* could disturb leaf development (Palatnik et al., 2003; Nag et al., 2009; Sarvepalli and Nath, 2011). Overexpression of CYC-like homolog GhCYC2 caused disk flowers to obtain characteristics typical for ray flowers in *Gerbera hybrida* (Broholm et al., 2008). Furthermore, several emerging lines of evidence revealed the multi-faceted role of TCP protein in plant specialized metabolism. For example, AtTCP3 interacted with R2R3-MYB proteins to stimulate flavonoid production in *Arabidopsis thaliana*, while AtTCP15 repressed anthocyanin biosynthesis when the plants were under high light intensity (Li and Zachgo, 2013; Viola et al., 2016). In *Lycium ruthenicum*, *LrTCP4* performed as a positive regulator in kukoamine biosynthesis and other secondary metabolites (Chahel et al., 2019). In *Artemisia annua* (*A. annua*), *AaTCP14* and *AaTCP15* were essential for jasmonate (JA)-induced artemisinin biosynthesis (Ma et al., 2018, 2021).

To date, genome-wide identification of the TCP family members has been identified and characterized in many dicots and monocots plants, such as *A. thaliana* (Li, 2015), *Solanum lycopersicum* (Parapunova et al., 2014), *Malus domestica* (Xu et al., 2014), *Citrullus lanatus* (Shi et al., 2016), *Nicotiana tabacum* (Chen et al., 2016), *Fragaria vesca* (Wei et al., 2016), *Glycine max* (Feng et al., 2018), *Gossypium barbadense* (Zheng et al., 2018), *Vitis vinifera* (Leng et al., 2019), *Solanum tuberosum* (Bao et al., 2019), *Phyllostachys edulis* (Liu et al., 2018), *Z. mays* (Ding et al., 2019), *Panicum virgatum* (Zheng et al., 2019), *Hordeum vulgare* subsp. vulgare (Gao et al., 2021), and so on. However, there is no research about the identification and functional characterization of TCP proteins in CPT-producing plants. Here, we first present a detailed and comprehensive analysis of the *TCP* gene family through the whole *O. pumila* genome, such as identification of all TCP family members, phylogenetic relationships, conserved motifs, gene structure, *cis*-elements in gene promoter regions, the expression levels of *O. pumila* TCP (*OpTCP*) genes in diverse tissues, co-expression analysis of key enzymes involved in CPT

biosynthesis, and subcellular localization, which could provide valuable information for understanding its classification and functions in *O. pumila*.

MATERIALS AND METHODS

Identification and Characteristics of *Teosinte Branched 1/Cycloidea/Proliferating Cell Factors 1/2* Gene Family in *Ophiorrhiza pumila*

All annotated protein sequences from *O. pumila* genome database[1] were obtained to comprehensively identify genomic TCP TFs (Rai et al., 2021). Moreover, to avoid missing any *OpTCP* genes, the Hidden Markov Model (HMM) of the TCP domain (Pfam, PF03634) was applied as a query to blast all TCP-containing sequences against our protein database by HMMER3.2 software.[2] Then, all candidate *OpTCPs* were manually further validate using the online programs of CDD,[3] Simple Modular Architecture Research Tool (SMART),[4] and Pfam[5] confirmed the existence of core domains. Finally, the *TCP* gene members were identified in *O. pumila*, after removing incorrect and redundant predicted proteins. The molecular weights (MWs), amino acid lengths, and isoelectric points (pI) of each OpTCP protein were computed by the ExPASy website[6] (Gasteiger et al., 2005). The subcellular localization of putative OpTCPs protein was predicted by PSORT[7] and pLoc-mPlant.[8] In addition, the sequences of the 24 *Arabidopsis* TCP proteins were downloaded from the *Arabidopsis* Information Resource (TAIR).[9] The sequences of the 23 *O. sativa* and 18 *Coffea canephora* TCP proteins were retrieved from PlantTFDB database.[10]

Chromosomal Localization and Gene Duplication

The physical locations of *OpTCP* genes on chromosomes were obtained from *O. pumila* genome database and visualized by TBtools software.[11] Multiple collinear scanning toolkits (MCScanX) and the Basic Local Alignment Search Tool (BLASTP) methods were used to analyze gene duplication events. Tandem repeats were identified based on the criteria defined in the previous report (Cheng et al., 2016), in which two or more genes should be located within a 100 kbp window and displayed at least 70% sequence similarity. The synonymous relationship between *OpTCP* genes and Arabidopsis, rice, and coffee *TCP* genes was visualized by TBtools software.

[1]http://pumila.kazusa.or.jp/

[2]http://hmmer.org/

[3]https://www.ncbi.nlm.nih.gov/Structure/cdd/wrpsb.cgi

[4]http://smart.embl-heidelberg.de/#

[5]http://pfam.xfam.org/

[6]http://web.expasy.org/protparam/

[7]https://psort.hgc.jp/

[8]http://www.jci-bioinfo.cn/pLoc-mPlant/

[9]http://www.Arabidopsis.org/

[10]http://planttfdb.gao-lab.org/

[11]https://github.com/CJ-Chen/TBtools

Multiple Sequence Alignment and Phylogenetic Analysis

Multi-sequence alignments of all conserved TCP core domains were determined using DNAMAN 6.0 software. The aligned sequences were visualized with WEBLOGO program[12] for the conserved amino acid residues analysis. To investigate phylogenetic relationships of OpTCPs and assist their classification, the full-length amino acid sequences of 24 AtTCP, 23 *O. sativa* TCP (OsTCP), 18 *C. canephora* TCP (CcTCP), 16 OpTCP, and some functional TCPs were aligned with CLUSTAL software. The protein sequences of those genes involved in the regulation of special secondary metabolism can be found under the following accession numbers: AtTCP3 (At1g53230), AtTCP15 (At1g69690), AaTCP14 (AYF60463.1), AaTCP15 (QKD77227.1), and MdTCP46 (MDP0000319941). The phylogenetic tree was constructed using Neighbor-joining (NJ) method implemented with MEGA 7.0, and its reliability was tested using bootstrapping with 1,000 replicates (Kumar et al., 2016). The display of the phylogenetic tree was performed by Interactive Tree of Life (iTOL).[13]

Gene Structure and Motif Composition Analysis

The exon-intron structures of *OpTCP* genes were determined by aligning their genomic sequences with corresponding coding sequences (CDS), while diagrams were visualized with online the program Gene Structure Display Server (GSDS v2.0)[14] (Hu et al., 2015). Additionally, the conserved motifs of OpTCP proteins were investigated using Multiple Expectation-Maximization for Motif Elicitation online program (MEME v5.1.1)[15] with the following parameters: the number of motifs searched was set as 10; optimum motif width of 6–100 amino acids; and sites of per motif set to $\geq$2 and $\leq$600 (Bailey et al., 2009). Subsequently, the TBtools software was used to display and re-edited the gene structure and conserved motif.

Promoter *cis*-Acting Elements Analysis

To analyze the promoter regions of the *OpTCPs* and key enzyme genes involved in CPT biosynthesis, genomic DNA sequences in the promoter region (−3,000 to −1 bp) were extracted by the TBtools. Identification of candidate CPT biosynthetic pathway genes in *O. pumila* by sequence identifies with characterized genes from the prestrictosidine biosynthetic pathway in *O. pumila* or *C. roseus* (**Supplementary Table 1**). These CDS sequences were mapped into the *O. pumila* genome to find the corresponding promoter regions. Subsequently, the promoter sequences of each *OpTCP* gene were scanned by Plantpan 3.0[16] database to predicate and identify *cis*-acting regulatory elements (Chow et al., 2019). Meanwhile, the identification of TBS elements on the promoter of 15

[12]http://weblogo.berkeley.edu

[13]http://itol.embl.de/

[14]http://gsds.cbi.pku.edu.cn/

[15]http://meme-suite.org/tools/meme

[16]http://plantpan.itps.ncku.edu.tw/

key enzyme genes in the CPT biosynthetic pathway was scanned with conserved TCP-binding sites by blast methods, such as GGNCCCAC, GGNCC, GCCCR, or G(T/C)GGNCCC (Aggarwal et al., 2010).

Plant Materials, RNA Extraction, and Quantitative Real-Time PCR Analysis

Sterile *O. pumila* seedlings were cultured on solid B5 medium (pH 5.5) under controlled glasshouse conditions at 25°C and 14 h light/10 h dark photoperiod. The roots, stems, and leaves of 2-month-old *O. pumila* seedlings were collected to detect the tissue expression pattern of the *OpTCP* and CPT biosynthetic pathway genes. All of the samples were immediately frozen in liquid nitrogen and then stored at −80°C until used for RNA extraction.

Total RNA was extracted via the RNApure Plant Kit (Tiangen, China). Then cDNA synthesis was performed with PrimeScript^{TM} II First Strand cDNA Synthesis Kit (Tiangen, China). qRT−PCR was performed by StepOnePlus platform (Bio-Rad, Hercules, CA, United States) with a SYBR Green PCR Master Mix Kit (SYBR® Premix Ex Taq^{TM}, Japan). Transcript abundance was calculated relative to *OpUBQ* (Ubiquitin) by $2^{-\Delta\Delta Ct}$ method. Primers were listed in **Supplementary Table 2**. Co-expression analysis of candidate genes was performed by Pearson's correlation test, and coefficients >0.8 indicated co-expression. Co-expression of candidate genes has been re-visualized as a network figure by Cytoscape_v3.7.2.

Dual-Luciferase Assay

To investigate the ability of OpTCP15 to regulate the expression of CPT biosynthesis pathway genes, the full-length coding sequence of *OpTCP15* was amplified and inserted into the pHB-yellow fluorescent protein (YFP) vector (effectors). The promoter regions of *Op7DLH* and *Op8HGO* were ligated into the pGreenII0800-LUC vector (reporters). The Renilla luciferase gene driven by the CaMV 35 S promoter was used as an internal control. Empty pHB-YFP was used as the negative control for the effector. Infiltration and detection were performed as described previously (Hao et al., 2021). The ratio of firefly luciferase to Renilla luciferase represents the relative activity of the promoter. All experiments were repeated three times for each combination. All primers used for these constructs are listed in **Supplementary Table 2**.

Subcellular Localization Assay

To investigate the subcellular localization of candidate OpTCP proteins, the full-length coding sequences were inserted into the pHB-YFP vector. The pHB-YFP (empty vector) was used as the negative control. The plasmids pHB-OpTCPs-YFP and pHB-YFP were transformed into the *Agrobacterium tumefaciens* strain GV3101, respectively. Then strains GV3101 harboring OpTCPs-YFP and pHB-YFP were transiently infected the epidermal cells of 5-week-old *N. benthamiana* leaves. YFP fluorescences were analyzed 2 days after infiltration with an LSM880 confocal laser microscope (Carl Zeiss, Germany). Nuclei were stained with 4' 6-diamidino-2-phenylindole (DAPI, Sigma), and three biological replicates were performed to verify the results (Hao et al., 2021).

RESULTS

Identification of Teosinte Branched 1/Cycloidea/Proliferating Cell Factors 1/2 Family Members in the *Ophiorrhiza pumila* Genome

To identify *TCP* genes in *O. pumila*, an HMM search was conducted using the HMM profiles of TCP domain (PF03634) as queries against the *O. pumila* genome dataset (see text footnote 1). A total of 16 non-redundant *TCP* genes were obtained and named as OpTCP1 to OpTCP16 according to their order in the *O. pumila* genomic sequence (**Table 1**). Each candidate gene was further analyzed to confirm the integrity of the TCP domain of TCP proteins with the online program of CDD, SMART, and Pfam. Meanwhile, MWs, amino acid lengths, pI, and subcellular location of OpTCP proteins were analyzed (**Table 1**). The MWs of OpTCP proteins ranged from 18.91 (OpTCP1) to 54.25 (OpTCP13) kDa, with an average of 37.51 kDa. The protein lengths were distributed from 174 (OpTCP1) to 504 (OpTCP13) amino acids, and pI varied from 5.60 (OpTCP11) to 10.01 (OpTCP6). They were all predicted to be located in the nucleus.

Chromosome Localization and Duplication of the *OpTCP* Gene Family

Sixteen *OpTCP* genes were disproportionately distributed on 8 of 11 *O. pumila* chromosomes (**Figure 1A** and **Supplementary Figure 2**). There was no distribution on Chr 2, 3, and 8. Four *OpTCP* genes on Chr 7; three *OpTCP* genes on Chr 9; two on Chr 4, Chr 5, and Chr 11; only one on Chr 1, Chr 6, and Chr 10. The possible relationships with the *OpTCP* genes and potential gene duplication type, collinear analyses were investigated in *O. pumila* genome. As illustrated in **Figure 1A**, seven genes involved in three segmental duplication events, such as Opu_chr05 (OpTCP4, 5)/Opu_chr09 (OpTCP12), Opu_chr04 (OpTCP3)/Opu_chr07 (OpTCP8), and Opu_chr07 (OpTCP7)/Opu_chr11 (OpTCP16). In contrast, no tandem duplication events were observed, suggesting that segmental duplications were the main causes for the amplification of the *OpTCP* gene family.

Microsynteny and Evolutionary Patterns of the *OpTCP* Genes in *O. pumila*

To further explore the functions and evolutionary relationships of *TCP* genes, large-scale comparative synteny maps between *O. pumila* and *Arabidopsis*, and *O. sativa* or *V. vinifera* were analyzed at genome-wide levels (**Figures 1B–D**). As a result, a total of 15 pairs of syntenic *TCP* genes were identified between *O. pumila* and *Arabidopsis* (**Figure 1B** and **Supplementary Table 3**), while 7 and 5 pairs of *TCP* genes were identified between *O. pumila*, *O. sativa*, and *V. vinifera* (**Figures 1C,D** and **Supplementary Table 3**), respectively. Among the synteny events, *O. pumila* between *Arabidopsis* and 5 *OpTCP* genes were found to be associated with two synteny events, such as OpTCP2-AtTCP12/AtTCP18, OpTCP3-AtTCP5/AtTCP17, and OpTCP5-AtTCP3/AtTCP4 (**Supplementary Table 3**). Interestingly, four of

TABLE 1 | Detailed information for 16 *OpTCP* genes in the *O. pumila* genome.

ID	Gene name	Type	Chr	Start	Stop	Strand	No. of Exon	CDS (bp)	Protein (aa)	MWs (Da)	pI	Loc
Opuchr01_g0001120-1.1	*OpTCP1*	PCF	chr01	578509	577985	–	1	525	174	18907.37	9.15	Nucleus
Opuchr04_g0008760-1.1	*OpTCP2*	CYC/TB1	chr04	4881540	4880265	–	2	1,179	392	44582.07	8.36	Nucleus
Opuchr04_g0064620-1.1	*OpTCP3*	CIN	chr04	32348228	32347020	–	1	1,209	402	44514.21	7.39	Nucleus
Opuchr05_g0002240-1.1	*OpTCP4*	CIN	chr05	1225789	1226784	+	1	996	331	36943.08	6.37	Nucleus
Opuchr05_g0060100-1.1	*OpTCP5*	CIN	chr05	27883069	27884421	+	1	1,353	450	48977.51	6.59	Nucleus
Opuchr06_g0114980-1.1	*OpTCP6*	PCF	chr06	56622961	56623614	+	1	654	217	23276.48	10.01	Nucleus
Opuchr07_g0000090-1.1	*OpTCP7*	PCF	chr07	67153	67995	+	1	843	280	29639.13	8.69	Nucleus
Opuchr07_g0005290-1.1	*OpTCP8*	CIN	chr07	2963107	2964165	+	1	1,059	352	38817.75	6.79	Nucleus
Opuchr07_g0006620-1.1	*OpTCP9*	CYC/TB1	chr07	3648191	3647069	–	2	1,203	400	44972.86	9.22	Nucleus
Opuchr07_g0038750-1.1	*OpTCP10*	PCF	chr07	19064610	19063813	–	1	798	265	27475.75	9.51	Nucleus
Opuchr09_g0004960-1.1	*OpTCP11*	PCF	chr09	3099165	3100307	+	1	1,143	380	39829.61	5.6	Nucleus
Opuchr09_g0016060-1.1	*OpTCP12*	CIN	chr09	10055733	10054717	–	1	1,017	338	37364.12	6.26	Nucleus
Opuchr09_g0061970-1.1	*OpTCP13*	CIN	chr09	28382461	28380947	–	1	1,515	504	54252.12	7.8	Nucleus
Opuchr10_g0056950-1.1	*OpTCP14*	PCF	chr10	28389738	28390955	+	1	1,218	405	42082.31	7.02	Nucleus
Opuchr11_g0082210-1.1	*OpTCP15*	PCF	chr11	36501516	36502670	+	1	1,155	384	41199.34	7.86	Nucleus
Opuchr11_g0088190-1.1	*OpTCP16*	PCF	chr11	39951958	39952734	+	1	777	258	27359.43	8.57	Nucleus

AA, amino acid residues; Chr, chromosome; MW, molecular weight; pI, theoretical isoelectric point; Loc, subcellular location; OpTCP, O. pumila TCP.

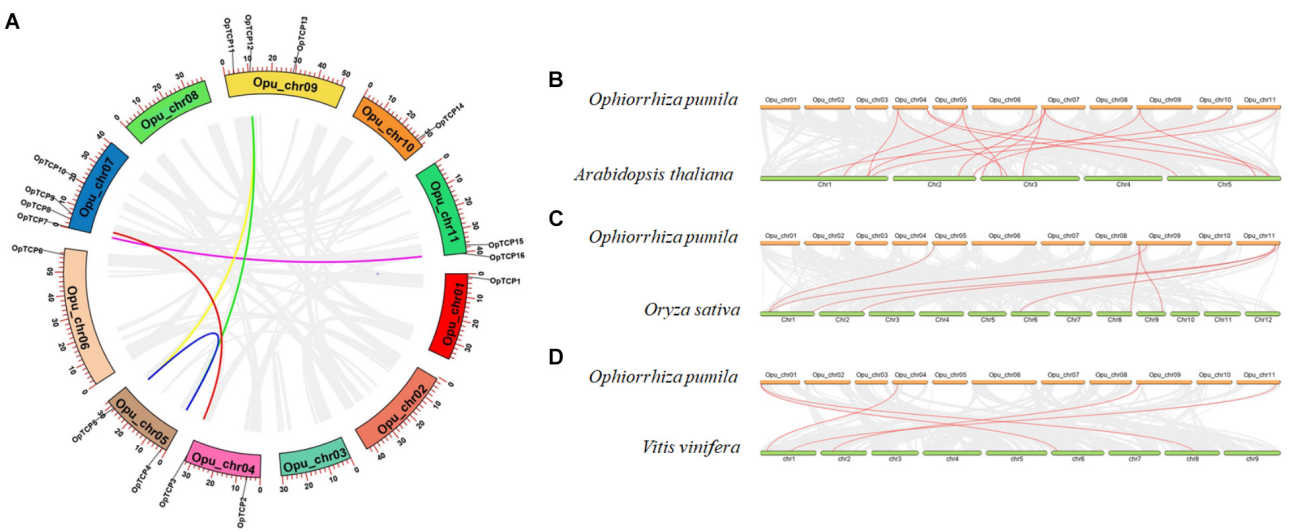

FIGURE 1 | The chromosomal location and synteny analysis of *OpTCP* genes. **(A)** Circos diagram illustrates the chromosomal locations of *OpTCP* genes and their synteny. The colored lines display similarity of different genes. **(B–D)** Synteny analysis of *TCP* genes between *O. pumila* and *Arabidopsis*, and rice, and *V. vinifera*, respectively. TCP, teosinte branched 1/cycloidea/proliferating cell factors 1/2; OpTCP, *O. pumila* TCP.

these five genes were in CIN and CYC/TB1subclade, indicating higher conservation of CIN and CYC/TB1 than PIF subclade in the *TCP* gene family. In addition, the *OpTCP15* gene had a homologous relationship in all three plants, indicating that this gene may have an important role in evolution.

Phylogenetic Analysis and Classification of *OpTCP* Genes

To explore the phylogenetic and evolutionary relationship of the *TCP* genes in *O. pumila* and group them with the established subfamilies, an unrooted NJ phylogenetic tree was constructed (**Figure 2A**). Sixteen *OpTCP* genes were clustered into classes I and II, each of which contained eight members. Additionally, class II could be further divided into the CIN and CYC/TB1 subgroups, which contained 6 (OpTCP3, OpTCP4, OpTCP5, OpTCP8, OpTCP12, and OpTCP13) and two TCP members (OpTCP2 and OpTCP9), respectively.

Multiple sequences alignments showed that two subgroups were distinguished by a four-amino-acids deletion at the N-terminal of class I (**Figure 2B**). Additional, three class II proteins, OpTCP2 and OpTCP9 from class II CYC/TB1, and OpTCP13 from CIN also shared an R domain at the C-terminus of the TCP domain (**Figure 2C**).

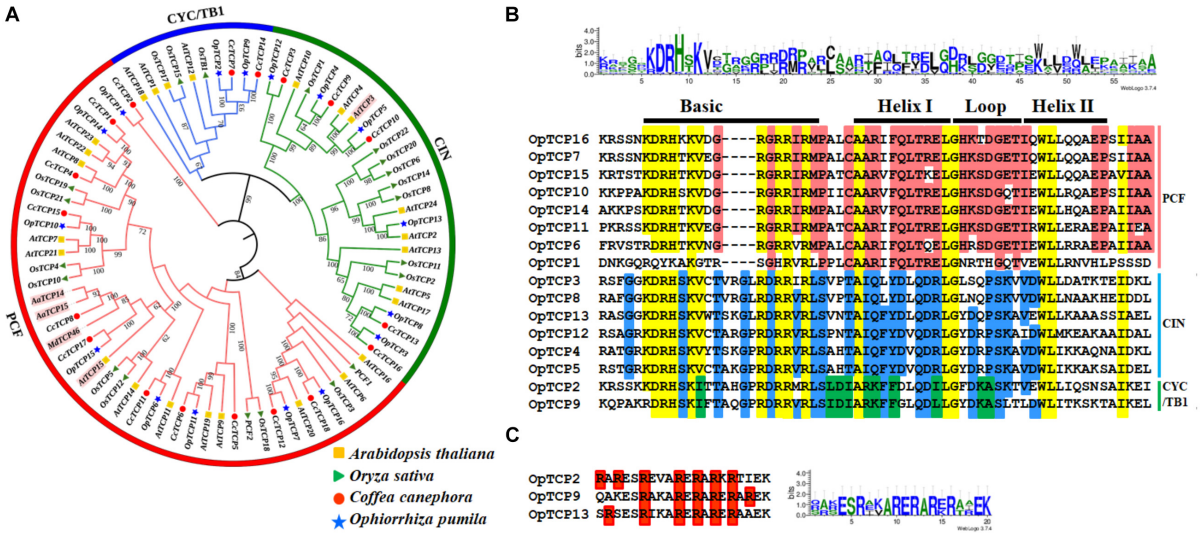

FIGURE 2 | Identification of TCP transcription factor genes in *O. pumila*. **(A)** Phylogenetic analysis of TCP proteins using the un-rooted Neighbor-Joining (NJ) method with 1,000 bootstrap replicates. Five *TCP* genes involved in special secondary metabolism are marked with pink shades. **(B)** The conserved TCP domains analysis using WebLogo and multiple sequence alignments by ClustalW. Each letter represents one amino acid, and the left column corresponds to the name of the gene. The yellow region indicates the highly conserved residues of the OpTCP family members, and the red region indicates residues conserved only in the class I subfamily. The blue region indicates residues conserved in the Class II subfamily. Green indicates the residues conserved in the CYC/TB1 class of proteins. The top black bar represents the conserved domain in TCP proteins. **(C)** The R domain in Class II members of the *OpTCP* gene family. TCP, teosinte branched 1/cycloidea/proliferating cell factors 1/2; OpTCP, *O. pumila* TCP.

Gene Structure and Motif Analysis of *OpTCP* Genes

To further understand the pivotal role that exon-intron structural features play in the evolution of *O. pumila* gene families, the structure of *OpTCP* genes was obtained through exon-intron organization analysis. The phylogenetic tree (**Figure 3A**) revealed the most OpTCP proteins in the same group with similar genetic structures, such as the length and number of the exon. As shown in **Figure 3B**, class I and class II CIN-type *TCP* genes had only one exon and no intron, while class II CYC/TB1-type *TCP* genes contained two exons. These results suggested that different OpTCP members tended to share different structure organizations.

The conserved motifs of TCP family proteins in *O. pumila* were analyzed by MEME online software, and 10 motifs were identified (**Supplementary Table 4**). These 10 motifs were distributed across different subgroups in the phylogenetic tree (**Figure 3C**). For OpTCP proteins, motif 1 was broadly distributed in all OpTCP proteins, which was corresponded to TCP domain. The OpTCPs in subfamily CIN had motif 2 and all members of the CYC/TB1 subfamily and OpTCP13 from CIN contained the motif 3 (R domain). Generally, proteins with similar motif compositions were clustered in the same class indicating that members of the same class may have similar functions.

Analysis of *cis*-Acting Elements

To further investigate the gene function and regulation mechanism of *OpTCP* genes, the *cis*-acting elements in promoter sequences were analyzed by Plantpan 3.0 software. As a result, a variety of *cis*-acting elements involved in plant growth and development, hormone responses, and stress responses were identified. As shown in **Figure 4**, CAT-box and CCGTCC-box involved in meristem expression were identified in the promoter region of 11 and 2 *OpTCP* genes, respectively. GCN4_motif was related to endosperm expression in plant growth and development. The zein metabolism regulation element (O2-site) and circadian control element (circadian) were found in 10 and 4 *OpTCP* genes, respectively. Additionally, leaf development correlated *cis*-acting regulatory elements (HD-Zip 1) and root-specific (motif I) regulatory elements were also found in the promoter region of the *OpTCP* genes (**Supplementary Table 5**).

In hormone responses, ABA-responsive *cis*-acting regulatory elements (ABREs) were found in the promoter region of 15 *OpTCP* genes, except for the *OpTCP5* gene. Two MeJA-responsive elements (CGTCA-motif and TGACG-motif) were found in the promoter region of 12 *OpTCP* genes. In addition, auxin-responsive element (AuxRR-core), ethylene-responsive element (ERE), three gibberellin-responsive elements (GARE-motif, P-box, and TATC-box), and salicylic acid-responsive element (TCA-element) were found in the promoter region of 4, 11, 10, and 11 *OpTCP* genes, respectively (**Supplementary Table 5**).

In stress responses, ARE elements essential for the anaerobic induction were found in the promoter region of 16 *OpTCP* genes. Moreover, low temperature-responsive element (LTR), drought-inducibility element (MBS), TC-rich repeats, and wound-responsive element (WUN-motif) were also found in the

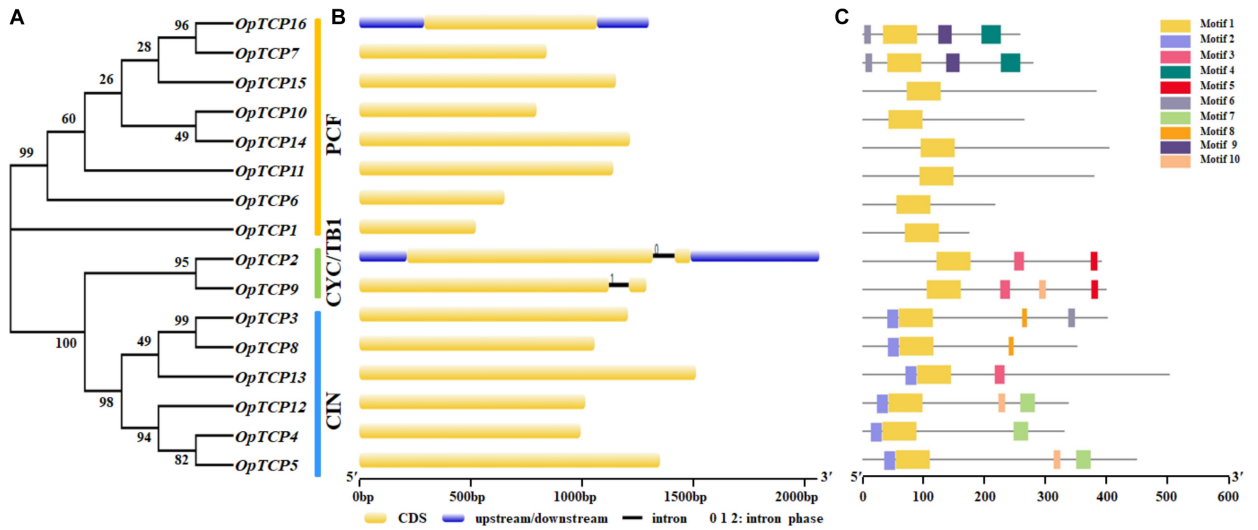

FIGURE 3 | Phylogenetic analysis, gene structure, and conserved motifs of TCP family in *O. pumila*. **(A)** The conserved TCP domain sequences of OpTCP proteins were constructed a Neighbor-Joining phylogenetic tree and the bootstrap test was performed with 1,000 iterations. **(B)** Exon-intron structure of the *OpTCP* genes. Blue indicates untranslated 5′- and 3′-regions, yellow indicates exons; black indicates introns; 0, 1, 2 indicates intron phase. **(C)** Distribution of conserved motifs of OpTCP proteins. Different motifs are shown by different colors numbered 1–10. TCP, teosinte branched 1/cycloidea/proliferating cell factors 1/2; OpTCP, *O. pumila* TCP.

	Plant growth and development							Phytohormone responsive								Abiotic and biotic stress				
								ABA	Auxin	Eth	GA			MeJA		SA					
	CAT-box	CCGTCC-box	GCN4_motif	HD-Zip 1	O2-site	circadian	motif I	ABRE	AuxRR-core	ERE	GARE-motif	P-box	TATC-box	CGTCA-motif	TGACG-motif	TCA-element	ARE	LTR	MBS	TC-rich repeats	WUN-motif
OpTCP1	1	1		1	3			3		2		2		2	2		3		4	2	
OpTCP2	1		1		1	1		3				1		2	2	2	3	2	1		1
OpTCP3					2			1	1							1	1		4		1
OpTCP4	1				1	1		1		1		1				1	3		5	1	2
OpTCP5	3				1						1	2	1			1	9			2	1
OpTCP6	1		2		1			2	1	1		1		2	2	1	2		1		
OpTCP7	2		1		3	1		1					1	2	2	4	4	1	2	2	4
OpTCP8			1					2		1				2	2	1	3	3	1	2	2
OpTCP9		1						3	1	1				1	1	1	1	1	1		1
OpTCP10	1			1			1	6		3		2		2	2	1	4				2
OpTCP11	1			1	1	1		3		2		1		4	4		6	1	1		
OpTCP12								2			1	2		1	1		4		2		
OpTCP13	1							3		3							4	1	1		2
OpTCP14			1					3	1	2				1	1	1	7		1	2	1
OpTCP15	1		1		1			5		3				3	3	1	2		1		1
OpTCP16	2				1			3		2		1	1	4	4		1	1		1	1

FIGURE 4 | Promoter *cis*-regulatory elements analysis of the *OpTCP* genes. Based on the functional annotation, the *cis*-acting elements were classified into three major classes: plant growth and development, phytohormone responsive, or abiotic and biotic stresses-related *cis*-acting elements (detailed results shown in **Supplementary Table 5**).

promoter region of 7, 13, 7, and 12 *OpTCP* genes, respectively (**Supplementary Table 5**).

Expression Patterns of *OpTCP* Genes in Various Tissues

To validate the gene expression profiles, roots, stems, and leaves of *O. pumila* were collected for RNA extraction and quantitative Real-Time PCR (qRT-PCR) analysis. We performed hierarchical clustering with the expression data and accomplished a heatmap to visualize the expression profiles of the *OpTCPs* in different tissues (**Figure 5**). From the heatmap, most of the *OpTCP* genes preferentially expressed in leaves or stems. For example, 9 *OpTCP* genes (OpTCP3, 4, 5, 6, 8, 11, 12, 13, and 14) had the highest expression levels in leaves, while the other *OpTCPs* (OpTCP1, 2, 7, 9, 10, 15, and 16) showed a higher expression level in stems.

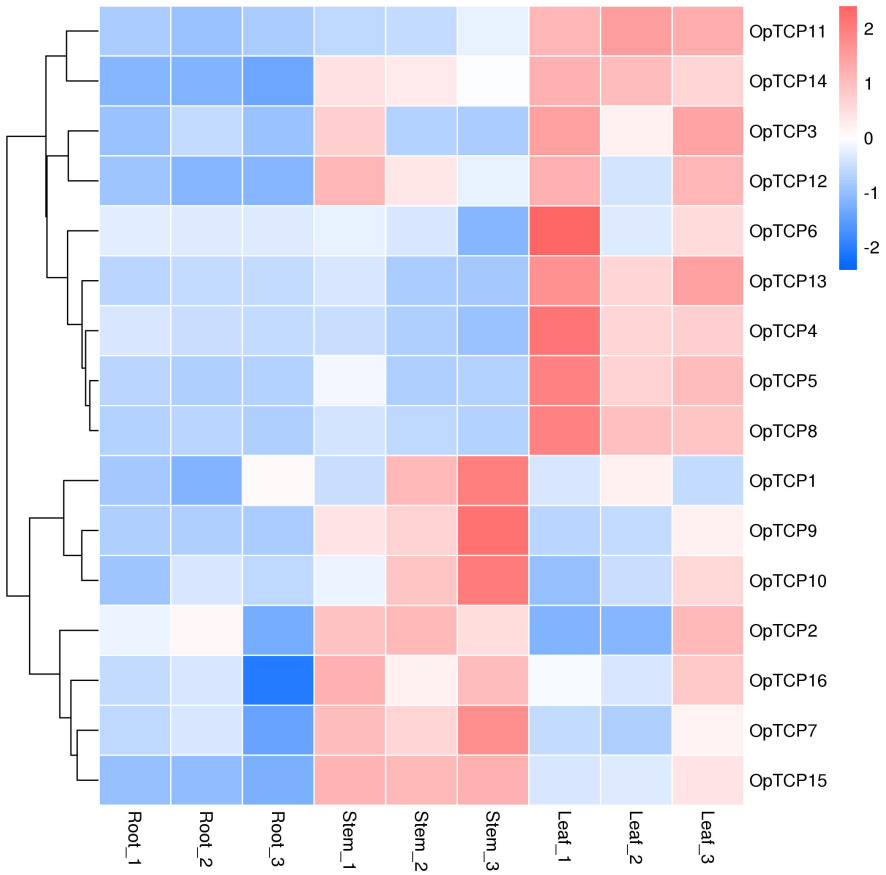

FIGURE 5 | Expression patterns of *OpTCP* genes in different tissues. TCP, teosinte branched 1/cycloidea/proliferating cell factors 1/2; OpTCP, *O. pumila* TCP.

In addition, OpTCP7, 10, 14, 15, and 16 consistently had high expression level in all tissues, while OpTCP1, 2, 3, 6, and 12 with low expression level.

Co-expression Analyses of Candidate Camptothecin Biosynthesis OpTCPs

Analysis was conducted to determine the co-expression of all *OpTCPs* with target genes in CPT biosynthesis pathways. The expression levels of key enzyme genes, such as *OpG10H*, *Op10HGO*, *Op8HGO*, *OpSLS1*, *Op7-DLGT*, *OpTDC*, *OpLAMT*, *OpIS*, *OpIO,* and *OpSTR*, were extremely higher in roots while *Op7-DLH* and *OpCPR* showed higher expression levels in stems (**Supplementary Figure 3**). The gene co-expression analysis revealed that six *OpTCP* (*OpTCP3*, *4*, *5*, *6*, *8*, and *13*) genes were in strong positive correlations with 2-C-methyl-Derythritol 4-phosphate (MEP) pathway genes (Pearson correlation coefficient $r > 0.8$ and $p < 0.05$, **Figure 6** and **Supplementary Table 6**), while *OpTCP12*, *OpTCP14,* and *OpTCP15* genes were in negative correlations with MEP pathway genes. In addition, *OpTCP14* and *OpTCP15* were in strong negative correlations with *OpG10H*, *Op7-DLGT, OpLAMT*, and *Op8HGO* ($r < -0.8$), respectively. Moreover, the Pearson coefficients of four OpTCPs (*OpTCP7*, *9*, *10*, *and 15*) and *Op7-DLH* were >0.8 (**Supplementary Table 6**). Overall, this result suggested that 12 of 16 *OpTCPs* might be associated with CPT and its precursor biosynthesis.

To identify the OpTCP TFs, which potentially involved in the regulation of CPT biosynthesis, we analyzed the phylogenetic relationships between the candidate OpTCPs and functional TCP TFs that regulated specialized metabolite biosynthesis (i.e., AaTCP14, AaTCP15, AtTCP3, AtTCP15, and MdTCP46). These TFs were grouped into two clades in the neighbor-joining tree (**Figure 2A**). The OpTCP6, OpTCP7, OpTCP10, OpTCP11, OpTCP14, and OpTCP15 proteins clustered with AaTCP14, AaTCP15, AtTCP15, and MdTCP46 in clade I, whereas AtTCP3 and other OpTCPs belonged to clade II. Interestingly, OpTCP5 and OpTCP15 clustered with AtTCP3 and AtTCP15, respectively, and may be most likely participated in regulating CPT and its precursor biosynthesis.

Finally, to identify the *cis*-elements of TCP TFs, the promoter sequences of the genes encoding enzymes in CPT biosynthesis pathway were analyzed. These results showed that the sequences of GGNCC and GCCCR were identified in the promoter regions of most studied genes (**Supplementary Figure 4** and **Supplementary Table 7**). For example, there were 18, 14, and 9 TBS-binding sites on the promoter sequences of *OpSLS*, *Op8HGO*, and *Op7DLH* genes in CPT biosynthetic pathway, respectively. The finding indicated that the expression of these

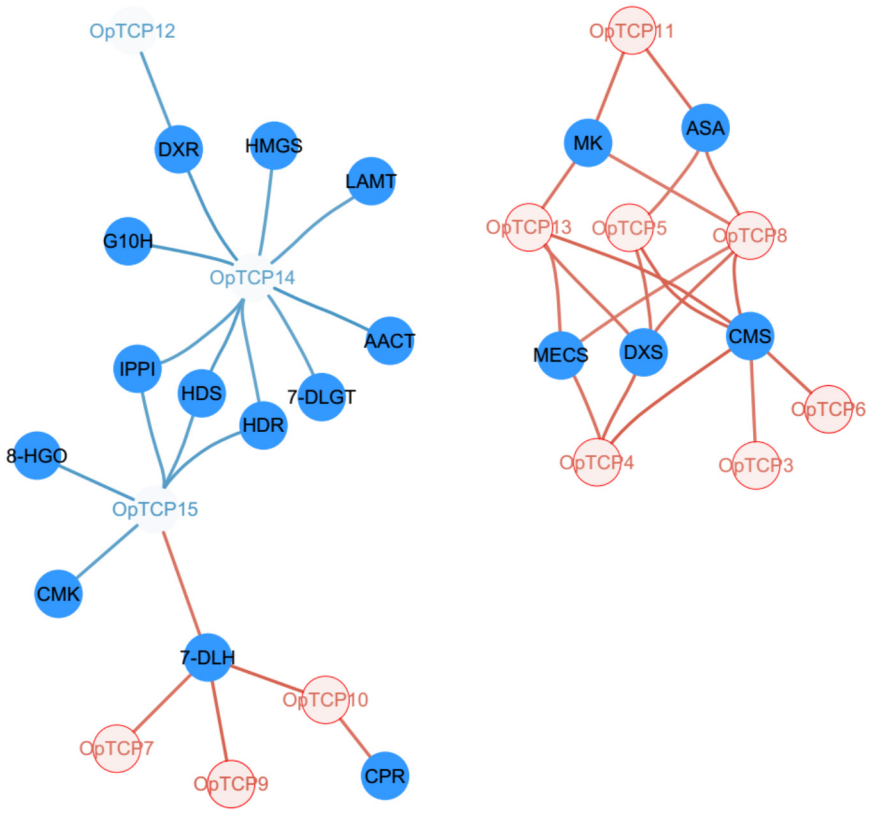

FIGURE 6 | Regulatory network of TCP transcription factors and key CPT-biosynthetic genes. The colored fonts represent TCP TFs and the solid blue circles represent CPT-biosynthetic genes. The edges are drawn when the absolute value of the linear correlation coefficient is >0.8. The blue and red line represents the negative correlation and positive correlation, respectively. TCP, teosinte branched 1/cycloidea/proliferating cell factors 1/2; CPT, camptothecin.

genes might be regulated by TCP TFs. Overall, *OpTCP5* and *OpTCP15* were likely to have a functional role in CPT and its precursor biosynthesis.

Dual Luciferase Assay

Subsequently, the dual luciferase (Dual-LUC) assay was performed to verify whether OpTCP15 protein affected the transcription of *Op7DLH* and *Op8HGO* or not. The results showed that *OpTCP15* significantly activated the *Op7DLH* promoter compared to the YFP control, while the *Op8HGO* was slightly upregulated (**Figure 7**). Together, *OpTCP15* was likely to have a functional role in CPT and its precursor biosynthesis.

Subcellular Localization Analysis of Selected OpTCPs

To determine the subcellular localization of five *OpTCP* genes, which were strongly related to the key enzyme genes of the iridoid pathway, pHB-OpTCP7/9/10/14/15-YFP and pHB-YFP were transiently expressed in *N. benthamiana* leaves. As shown in **Figure 8**, the *N. benthamiana* leaves transformed with pHB-YFP vector displayed fluorescence in nucleus and cytoplasm. In contrast, all fluorescence in cells transformed with pHB-OpTCP7/9/10/14/15-YFP was detected in the nucleus exclusively, suggesting that all five selected *OpTCP* genes encoded nuclear proteins. It was consistent with their putative role as TFs.

DISCUSSION

Evolution and Classification of Teosinte Branched 1/Cycloidea/Proliferating Cell Factors 1/2 Transcription Factor Family

Teosinte branched 1/cycloidea/proliferating cell factors 1/2 genes are a class of terrestrial plant-specific TF, which have been investigated in diverse plants (Liu et al., 2019). However, no systematical study of TCP TFs has been examined in *O. pumila*. In this study, 16 non-redundant *TCP* genes were identified and analyzed from the *O. pumila* genome. Furthermore, a multi-level analysis was performed, such as chromosome location, duplication events, phylogenetic analysis, gene structure, conserved motif, *cis*-acting elements, expression profiles in different tissues, co-expression analysis of key enzymes in CPT biosynthesis, and subcellular localization of candidate TCPs. Compared with those identified *TCP* gene family in the higher plant, the number of *OpTCP* genes was significantly small (**Supplementary Table 8**). It was consistent with the smaller size of *O. pumila* genome (439.90 Mb) and did not

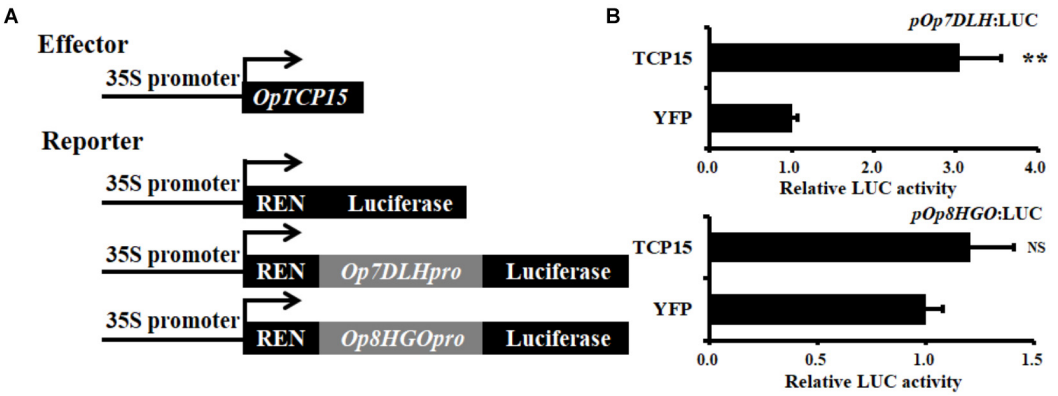

FIGURE 7 | (A) Schematic diagrams of the effector and reporter plasmids used in Dual-LUC assay. **(B)** Dual-LUC assay in *N. benthamiana* leaf cells using the constructs shown in panel **(A)**. The relative LUC activity was normalized to that of the reference Renilla (REN) luciferase. Error bars indicate the SD ($n = 3$). Student's *t*-test: $^{**}p < 0.01$; NS, no significance; Dual-LUC, dual-luciferase assay.

show signs of any recent whole-genome duplication (WGD) in *O. pumila* (Rai et al., 2021). It was found that some *TCP* genes in *O. pumila* had two counterparts in *Arabidopsis* and *O. sativa* (**Figures 1B,C**), indicating that the deletion of the TCP family in *O. pumila*. Furthermore, compared with the number of *TCP* genes in different subgroups (**Supplementary Table 8**), our results showed that the PCF subfamily had the largest number of genes, accounting for about 50%, while the CYC/TB1 subfamily had the least number of genes, accounting for about 15%. It was in agreement with the CIN clade being larger than the CYC clade in land plants (Liu et al., 2019).

Phylogenetic analysis and sequence alignment showed that OpTCPs in the same group or subgroup shared similar motifs composition and gene structures (**Figure 3**), which was consistent with the previously described in *Arabidopsis* (Li, 2015), maize (Ding et al., 2019), potato (Bao et al., 2019), and barley (Gao et al., 2021). For example, motif 2 in N-terminal TCP domain was only present in all CIN subclade, while the conserved R domain (motif 3) was not detected in the PCF subclass (**Figure 3C**). Additionally, almost all of the *OpTCP* genes within the same subgroup exhibited similar distribution patterns of exon/intron in terms of exon length and intron number. Taken together, the consistency of the motif compositions and the exon/intron structures of *OpTCP* genes further supported the close evolutionary relationships.

OpTCP Proteins Play Important Roles in Plant Development and Camptothecin Biosynthesis

Increasing evidence indicated that the main function of class I TCP proteins was to promote cell proliferation in leaves (Li et al., 2005; Resentini et al., 2015), while class II proteins played an important role in preventing tissues overgrowth and cell proliferation (Ori et al., 2007). For instance, AtTCP19 and AtTCP20 were class I TCP proteins that are involved in cell division and affect leaf development (Hervé et al., 2009; Danisman et al., 2013). Furthermore, repression of five CIN-like genes (*AtTCP2*, *3*, *4*, *10,* and *24*) in *Arabidopsis* disturbed leaf development (Schommer et al., 2008; Nag et al., 2009). *TB1* mutant increased the number of lateral branches in Maize (Doebley et al., 1995). According to previous studies, syntenic genes between different species may play similar functions (Angiuoli and Salzberg, 2011). In this study, the two class I clade genes *OpTCP7* and *OpTCP11* had orthologous genes *AtTCP20* and *AtTCP19* in *Arabidopsis* (**Figure 1B** and **Supplementary Table 3**), respectively, and might be involved in cell division. OpTCP13 was closely homology with AtTCP2 and highly expressed in *O. pumila* leaf (**Figure 2A**). These findings implied that OpTCP13 may be involved in regulating leaf and flower development. *OpTCP2*, the orthologous gene OsTB1 in *O. sativa*, was highly expressed in *O. pumila* stem, which implied that OpTCP2 played a role in regulating the lateral branching. In addition, qRT-PCR results showed that the expression level of *OpTCPs* in different tissues varied, implying that different *OpTCP* genes may take part in different organ development.

Interestingly, several TCP proteins were found to regulate special metabolism in plants. In *A. annua*, *AaTCP15* promoted artemisinin production by directly binding to and activating the promoters of *ALDH1* and *DBR2*, in which two genes involved in artemisinin biosynthesis (Ma et al., 2021). In this study, co-expression analysis of all *OpTCPs* with target genes in the CPT biosynthesis pathways revealed that nine of the 16 *TCP* genes were in strong correlations with some key enzyme genes in the MEP pathway. Such as the expression patterns of the two genes (*OpDXS* and *OpCMS*) in different tissues are consistent with the *OpTCP5* gene, and the correlation coefficient was >0.8. Additionally, two *TCP* genes (*OpTCP14* and *OpTCP15*) were in strong negative correlations with *OpG10H*, *Op7-DLGT*, *OpLAMT*, and *Op8HGO* ($r < -0.8$), respectively. Four OpTCPs (*OpTCP7*, *9*, *10*, and *15*) and *Op7-DLH* were >0.8 (**Supplementary Table 6**). Overall, most *OpTCPs* might be involved in CPT the biosynthesis pathway. Additionally, the phylogenetic tree was constructed using the protein sequences of *TCP* family genes from *A. thaliana*, *O. sativa*, *C. canephora,* and *O. pumila*, together with known metabolism-regulating TCPs

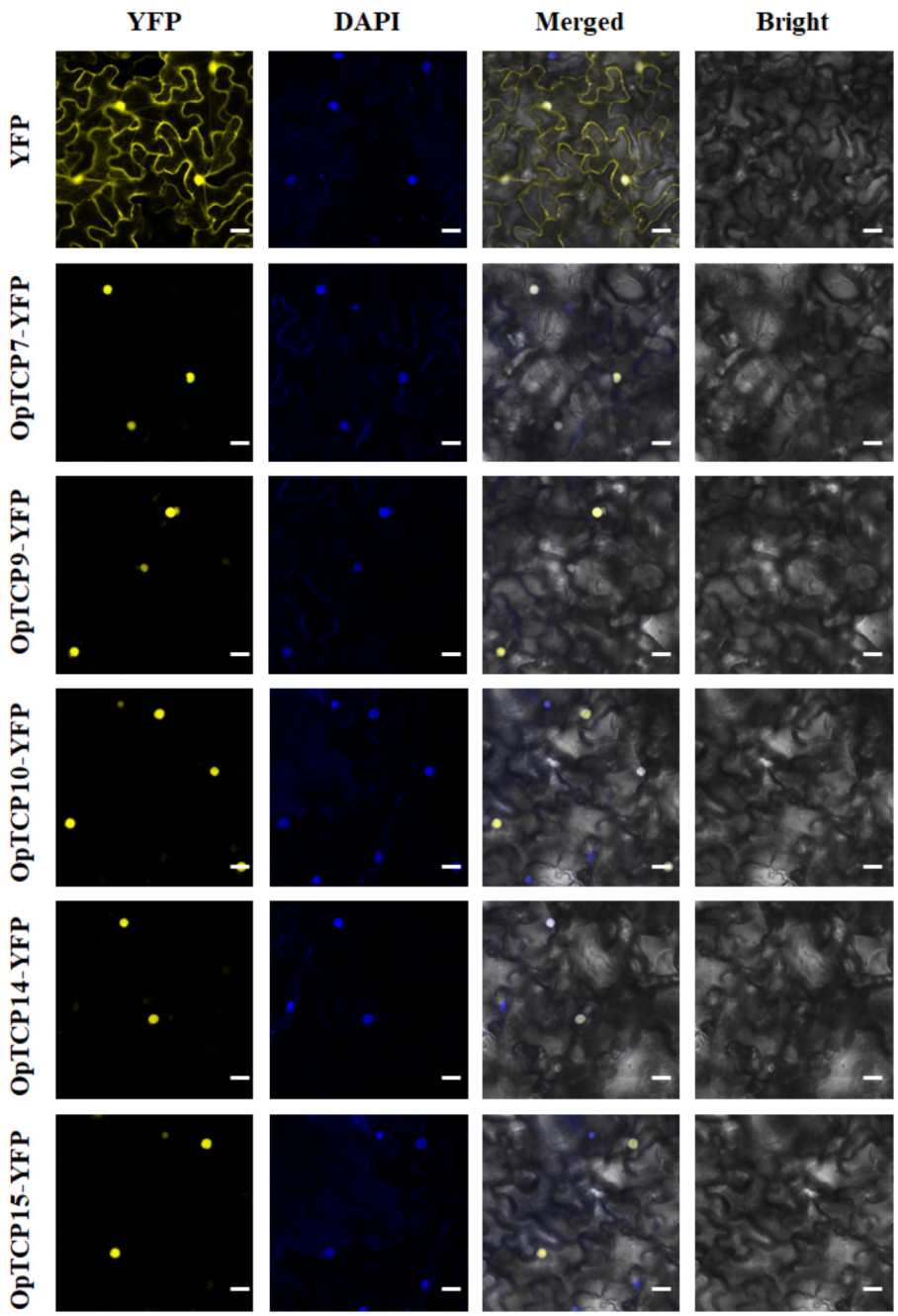

FIGURE 8 | The subcellular localization of the selected five OpTCPs. Scale bars: 20 μm. OpTCP, *O. pumila* TCP.

(AtTCP3, AtTCP15, AaTCP14, AaTCP15, and MdTCP46), to portray their evolutionary relationship. We found that OpTCP15 proteins clustered close with AtTCP15, AaTCP14, AaTCP15, and MdTCP46, while OpTCP5 exhibited a close relationship with AtTCP3 and AtTCP4. Meanwhile, collinearity analyses of *TCP* genes between *O. pumila* and *Arabidopsis* also revealed that *OpTCP5* and *OpTCP15* have a collinear relationship with *AtTCP3*, *AtTCP15*, respectively. In summary, *OpTCP5* and *OpTCP15* were likely to be involved in the biosynthesis process of CPT in *O. pumila*. The functions of two genes are worth exploring in the future.

To identify the *cis*-elements of TCP TFs, the promoter sequences of 15 enzyme-coding genes in CPT biosynthesis were analyzed including three functionally characterized genes (*OpSLS*, *OpTDC,* and *OpSTR*). These results showed that the sequences of GGNCC and GCCCR were identified in the promoter regions of most studied genes (**Supplementary Figure 4** and **Supplementary Table 7**). For example, there were

18, 10, and 7 TBS-binding sites on the promoter sequences of *OpSLS*, *OpSTR*, and *OpTDC* genes, respectively. The finding indicated that TCP TFs may influence the expression of these genes by binding to the TBS binding sites. Furthermore, the results of Dual-LUC assay showed that *OpTCP15* significantly activated the transcription of *Op7DLH* (**Figure 7**). Investigation on how *OpTCP15* is involved in regulating the biosynthesis of CPT needs to be further conducted. Yeast One-Hybrid (Y1H) and electronic mobility shift assays (EMSAs) were performed to examine OpWRKY2 binding W-box in *O. pumila* (Hao et al., 2021). However, additional methods and techniques are needed to analyze the possible regulatory mechanisms of OpTCP TFs.

CONCLUSION

This is the first genome-wide study, such as a systematic analysis of the *OpTCP* gene family in *O. pumila*. A total of 16 TCP family genes were identified and categorized into two classes based on phylogenetics. Expression patterns of all the 16 *OpTCP* and central enzyme genes in CPT biosynthetic pathway were investigated. Combining the results of co-expression, phylogeny analysis, and Dual-LUC assay revealed that *OpTCP15* potentially participated in the regulation of CPT and its precursor biosynthesis. Additionally, a subcellular localization experiment of five *OpTCP* genes showed that they were all localized in the nucleus. These results provided a foundation for further functional characterization of the candidate *OpTCP* genes with the potential to increase CPT production.

DATA AVAILABILITY STATEMENT

The original contributions presented in the study are included in the article/**Supplementary Material**, further inquiries can be directed to the corresponding author/s.

AUTHOR CONTRIBUTIONS

CW analyzed the data. CW and YW wrote the original draft of this manuscript. XH, MS, GK, and Z-GZ revised the manuscript. All authors have read and approved the final version.

FUNDING

This work was supported by the National Natural Science Foundation of China (Nos. 31571735, 82073963, 81522049, and 82003889), the Major Science and Technology Projects of Breeding New Varieties of Agriculture in Zhejiang Province (No. 2021C02074), the Zhejiang Provincial Ten Thousands Program for Leading Talents of Science and Technology Innovation (No. 2018R52050), the Zhejiang Provincial Program for the Cultivation of High-level Innovative Health Talents, Zhejiang Provincial Natural Science Foundation of China (LQ21H280004), the Research Project of Zhejiang Chinese Medical University (2021JKZDZC06), and the Opening Project of Zhejiang Provincial Preponderant and Characteristic Subject of Key University (Traditional Chinese Pharmacology), Zhejiang Chinese Medical University (ZYAOX2018009).

ACKNOWLEDGMENTS

We appreciate the experimental support from the Public Platform of Medical Research Center, Academy of Chinese Medical Science, Zhejiang Chinese Medical University.

SUPPLEMENTARY MATERIAL

The Supplementary Material for this article can be found online at: https://www.frontiersin.org/articles/10.3389/fpls.2021.746648/full#supplementary-material

REFERENCES

Aggarwal, P., Gupta, M. D., Joseph, A. P., Chatterjee, N., Srinivasan, N., and Nath, U. (2010). Identification of specific DNA binding residues in the TCP family of transcription factors in *Arabidopsis*. *Plant Cell* 22, 1174–1189. doi: 10.1105/tpc.109.066647

Angiuoli, S. V., and Salzberg, S. L. (2011). Mugsy: fast multiple alignment of closely related whole genomes. *Bioinformatics* 27, 334–342. doi: 10.1093/bioinformatics/btq665

Bailey, T. L., Mikael, B., Buske, F. A., Martin, F., Grant, C. E., Luca, C., et al. (2009). Meme suite: tools for motif discovery and searching. *Nucleic Acids Res.* 37, W202–W208. doi: 10.1093/nar/gkp335

Bao, S., Zhang, Z., Lian, Q., Sun, Q., and Zhang, R. (2019). Evolution and expression of genes encoding TCP transcription factors in *Solanum tuberosum* reveal the involvement of *StTCP23* in plant defence. *BMC Genet.* 20:91. doi: 10.1186/s12863-019-0793-1

Broholm, S. K., Tähtiharju, S., Laitinen, R. A., Albert, V. A., Teeri, T. H., and Elomaa, P. (2008). A TCP domain transcription factor controls flower type specification along the radial axis of the Gerbera (Asteraceae) inflorescence. *Proc. Natl. Acad. Sci. U.S.A.* 105, 9117–9122. doi: 10.1073/pnas.0801359105

Chahel, A. A., Zeng, S., Yousaf, Z., Liao, Y., Yang, Z., Wei, X., et al. (2019). Plant-specific transcription factor *LrTCP4* enhances secondary metabolite biosynthesis in *Lycium ruthenicum* hairy roots. *Plant Cell Tissue Organ Culture* 136, 323–337. doi: 10.1007/s11240-018-1518-2

Chen, L., Chen, Y. Q., Ding, A. M., Chen, H., Xia, F., Wang, W. F., et al. (2016). Genome-wide analysis of TCP family in tobacco. *Genet. Mol. Res.* 15:gmr.15027728. doi: 10.4238/gmr.15027728

Cheng, Y., Yao, Z. P., Ruan, M. Y., Ye, Q. J., Wang, R. Q., Zhou, G. Z., et al. (2016). In silico identification and characterization of the WRKY gene superfamily in pepper (*Capsicum annuum* L.). *Genet. Mol. Res.* 15, 1–12. doi: 10.4238/gmr.15038675

Chow, C. N., Lee, T. Y., Hung, Y. C., Li, G. Z., Tseng, K. C., Liu, Y. H., et al. (2019). PlantPAN3. 0: a new and updated resource for reconstructing transcriptional regulatory networks from ChIP-seq experiments in plants. *Nucleic Acids Res.* 47, D1155–D1163. doi: 10.1093/nar/gky1081

Cubas, P., Lauter, N., Doebley, J., and Coen, E. (1999). The TCP domain: a motif found in proteins regulating plant growth and development. *Plant J.* 18, 215–222. doi: 10.1046/j.1365-313X.1999.00444.x

Danisman, S., Van der Wal, F., Dhondt, S., Waites, R., de Folter, S., Bimbo, A., et al. (2012). *Arabidopsis* class I and class II TCP transcription factors regulate jasmonic acid metabolism and leaf development antagonistically. *Plant Physiol.* 159, 1511–1523. doi: 10.1104/pp.112.200303

Danisman, S., van Dijk, A. D. J., Bimbo, A., van der Wal, F., Hennig, L., de Folter, S., et al. (2013). Analysis of functional redundancies within the *Arabidopsis*

TCP transcription factor family. *J. Exp. Bot.* 64, 5673–5685. doi: 10.1093/jxb/ert337

Ding, S., Cai, Z., Du, H., and Wang, H. (2019). Genome-wide analysis of *TCP* family genes in *Zea mays* L. identified a role for *ZmTCP42* in drought tolerance. *Int. J. Mol. Sci.* 20:2762. doi: 10.3390/ijms20112762

Doebley, J., Stec, A., and Gustus, C. (1995). Teosinte branched1 and the origin of maize: evidence for epistasis and the evolution of dominance. *Genetics* 141, 333–346.

Feng, Z. J., Xu, S. C., Liu, N., Zhang, G. W., Hu, Q. Z., and Gong, Y. M. (2018). Soybean TCP transcription factors: evolution, classification, protein interaction and stress and hormone responsiveness. *Plant Physiol. Biochem.* 127, 129–142. doi: 10.1016/j.plaphy.2018.03.020

Gao, G., Kan, J., Jiang, C., Ahmar, S., Zhang, J., and Yang, P. (2021). Genome-wide diversity analysis of TCP transcription factors revealed cases of selection from wild to cultivated barley. *Funct. Integrative Genomics.* 21, 31–42. doi: 10.1007/s10142-020-00759-4

Gasteiger, E., Hoogland, C., Gattiker, A., Wilkins, M. R., Appel, R. D., and Bairoch, A. (2005). *Protein Identification and Analysis Tools on the ExPASy Server. The Proteomics Protocols Handbook*. Berlin: Springer, 571–607.

Hao, X., Xie, C., Ruan, Q., Zhang, X., Wu, C., Han, B., et al. (2021). The transcription factor *OpWRKY2* positively regulates the biosynthesis of the anticancer drug camptothecin in *Ophiorrhiza pumila*. *Horticulture Res.* 8, 1–14. doi: 10.1038/s41438-020-00437-3

Hervé, C., Dabos, P., Bardet, C., Jauneau, A., Auriac, M. C., Ramboer, A., et al. (2009). In vivo interference with *AtTCP20* function induces severe plant growth alterations and deregulates the expression of many genes important for development. *Plant Physiol.* 149, 1462–1477. doi: 10.1104/pp.108.126136

Horn, S., Pabon-Mora, N., Theuß, V. S., Busch, A., and Zachgo, S. (2015). Analysis of the CYC/TB1 class of *TCP* transcription factors in basal angiosperms and magnoliids. *Plant J.* 81, 559–571. doi: 10.1111/tpj.12750

Howarth, D. G., and Donoghue, M. J. (2006). Phylogenetic analysis of the "ECE"(CYC/TB1) clade reveals duplications predating the core eudicots. *Proc. Natl. Acad. Sci. U.S.A.* 103, 9101–9106. doi: 10.1073/pnas.0602827103

Hu, B., Jin, J., Guo, A. Y., Zhang, H., Luo, J., and Gao, G. (2015). GSDS 2.0: an upgraded gene feature visualization server. *Bioinformatics* 31, 1296–1297. doi: 10.1093/bioinformatics/btu817

Johnson, A. J., Rajan, R., and Baby, S. (2018). Secondary metabolites from Ophiorrhiza. *Nat. Products J.* 8, 248–267. doi: 10.2174/2210315508666180515104735

Kai, G., Wu, C., Gen, L., Zhang, L., Cui, L., and Ni, X. (2015). Biosynthesis and biotechnological production of anti-cancer drug Camptothecin. *Phytochem. Rev.* 14, 525–539. doi: 10.1007/s11101-015-9405-5

Kang, M., Fu, R., Zhang, P., Lou, S., Yang, X., Chen, Y., et al. (2021). A chromosome-level *Camptotheca acuminata* genome assembly provides insights into the evolutionary origin of camptothecin biosynthesis. *Nat. Commun.* 12, 1–12. doi: 10.1038/s41467-021-23872-9

Kellner, F., Kim, J., Clavijo, B. J., Hamilton, J. P., Childs, K. L., Vaillancourt, B., et al. (2015). Genome-guided investigation of plant natural product biosynthesis. *Plant J.* 82, 680–692. doi: 10.1111/tpj.12827

Kosugi, S., and Ohashi, Y. (1997). PCF1 and PCF2 specifically bind to *cis* elements in the rice proliferating cell nuclear antigen gene. *Plant Cell* 9, 1607–1619. doi: 10.1105/tpc.9.9.1607

Kumar, S., Stecher, G., and Tamura, K. (2016). MEGA7: molecular evolutionary genetics analysis version 7.0 for bigger datasets. *Mol. Biol. Evol.* 33, 1870–1874. doi: 10.1093/molbev/msw054

Leng, X., Wei, H., Xu, X., Ghuge, S. A., Jia, D., Liu, G., et al. (2019). Genome-wide identification and transcript analysis of *TCP* transcription factors in grapevine. *BMC Genomics* 20:786. doi: 10.1186/s12864-019-6159-2

Li, C., Potuschak, T., Colón-Carmona, A., Gutiérrez, R. A., and Doerner, P. (2005). *Arabidopsis TCP20* links regulation of growth and cell division control pathways. *Proc. Natl. Acad. Sci. U.S.A.* 102, 12978–12983. doi: 10.1073/pnas.0504039102

Li, S. (2015). The *Arabidopsis thaliana* TCP transcription factors: a broadening horizon beyond development. *Plant Signal. Behav.* 10:e1044192. doi: 10.1080/15592324.2015.1044192

Li, S., and Zachgo, S. (2013). TCP3 interacts with R2R3-MYB proteins, promotes flavonoid biosynthesis and negatively regulates the auxin response in *Arabidopsis thaliana*. *Plant J.* 76, 901–913. doi: 10.1111/tpj.12348

Liu, H. L., Wu, M., Li, F., Gao, Y. M., Chen, F., and Xiang, Y. (2018). TCP transcription factors in moso bamboo (*Phyllostachys edulis*): genome-wide identification and expression analysis. *Front. Plant Sci.* 9:1263. doi: 10.3389/fpls.2018.01263

Liu, M. M., Wang, M. M., Yang, J., Wen, J., Guo, P. C., Wu, Y. W., et al. (2019). Evolutionary and comparative expression analyses of TCP transcription factor gene family in land plants. *Int. J. Mol. Sci.* 20:3591. doi: 10.3390/ijms20143591

Liu, Y. Q., Li, W. Q., Morris-Natschke, S. L., Qian, K., Yang, L., Zhu, G. X., et al. (2015). Perspectives on biologically active camptothecin derivatives. *Med. Res. Rev.* 35, 753–789. doi: 10.1002/med.21342

Luo, D., Carpenter, R., Vincent, C., Copsey, L., and Coen, E. (1996). Origin of floral asymmetry in Antirrhinum. *Nature* 383, 794–799. doi: 10.1038/383794a0

Lupas, A., Van Dyke, M., and Stock, J. (1991). Predicting coiled coils from protein sequences. *Science* 252, 1162–1164. doi: 10.1126/science.252.5009.1162

Ma, Y. N., Xu, D. B., Li, L., Zhang, F., Fu, X. Q., Shen, Q., et al. (2018). Jasmonate promotes artemisinin biosynthesis by activating the TCP14-ORA complex in *Artemisia annua*. *Sci. Adv.* 4:eaas9357. doi: 10.1126/sciadv.aas9357

Ma, Y. N., Xu, D. B., Yan, X., Wu, Z. K., Kayani, S. I., Shen, Q., et al. (2021). Jasmonate-and abscisic acid-activated AaGSW1-AaTCP15/AaORA transcriptional cascade promotes artemisinin biosynthesis in *Artemisia annua*. *Plant Biotechnol. J.* 19, 1412–1428. doi: 10.1111/pbi.13561

Manassero, N. G. U., Viola, I. L., Welchen, E., and Gonzalez, D. H. (2013). *TCP* transcription factors: architectures of plant form. *Biomol. Concepts* 4, 111–127. doi: 10.1515/bmc-2012-0051

Martino, E., Della Volpe, S., Terribile, E., Benetti, E., Sakaj, M., Centamore, A., et al. (2017). The long story of camptothecin: From traditional medicine to drugs. *Bioorganic Med. Chem. Lett.* 27, 701–707. doi: 10.1016/j.bmcl.2016.12.085

Martín-Trillo, M., and Cubas, P. (2010). *TCP* genes: a family snapshot ten years later. *Trends Plant Sci.* 15, 31–39. doi: 10.1016/j.tplants.2009.11.003

Nag, A., King, S., and Jack, T. (2009). miR319a targeting of TCP4 is critical for petal growth and development in *Arabidopsis*. *Proc. Natl. Acad. Sci. U.S.A.* 106, 22534–22539. doi: 10.1073/pnas.0908718106

Ori, N., Cohen, A. R., Etzioni, A., Brand, A., Yanai, O., Shleizer, S., et al. (2007). Regulation of LANCEOLATE by miR319 is required for compound-leaf development in tomato. *Nat. Genet.* 39, 787–791. doi: 10.1038/ng2036

Palatnik, J. F., Allen, E., Wu, X., Schommer, C., Schwab, R., Carrington, J. C., et al. (2003). Control of leaf morphogenesis by microRNAs. *Nature* 425, 257–263. doi: 10.1038/nature01958

Parapunova, V., Busscher, M., Busscher-Lange, J., Lammers, M., Karlova, R., Bovy, A. G., et al. (2014). Identification, cloning and characterization of the tomato TCP transcription factor family. *BMC Plant Biol.* 14:157. doi: 10.1186/1471-2229-14-157

Rai, A., Hirakawa, H., Nakabayashi, R., Kikuchi, S., Hayashi, K., Rai, M., et al. (2021). Chromosome-level genome assembly of *Ophiorrhiza pumila* reveals the evolution of camptothecin biosynthesis. *Nat. Commun.* 12, 1–19. doi: 10.1038/s41467-020-20508-2

Rather, G. A., Sharma, A., Pandith, S. A., Kaul, V., Nandi, U., Misra, P., et al. (2018). *De novo* transcriptome analyses reveals putative pathway genes involved in biosynthesis and regulation of camptothecin in *Nothapodytes nimmoniana* (Graham) Mabb. *Plant Mol. Biol.* 96, 197–215. doi: 10.1007/s11103-017-0690-9

Resentini, F., Felipo-Benavent, A., Colombo, L., Blazquez Rodriguez, M. A., Alabadí Diego, D., and Masiero, S. (2015). TCP14 and TCP15 mediate the promotion of seed germination by gibberellins in *Arabidopsis thaliana*. *Mol. Plant* 8, 482–485. doi: 10.1016/j.molp.2014.11.018

Rohani, E. R., Chiba, M., Kawaharada, M., Asano, T., Oshima, Y., Mitsuda, N., et al. (2016). An MYB transcription factor regulating specialized metabolisms in *Ophiorrhiza pumila*. *Plant Biotechnol.* 33, 1–9. doi: 10.5511/plantbiotechnology.15.1117a

Sadre, R., Magallanes-Lundback, M., Pradhan, S., Salim, V., Mesberg, A., Jones, A. D., et al. (2016). Metabolite diversity in alkaloid biosynthesis: a multilane (diastereomer) highway for camptothecin synthesis in *Camptotheca acuminata*. *Plant Cell* 28, 1926–1944. doi: 10.1105/tpc.16.00193

Sarvepalli, K., and Nath, U. (2011). Hyper-activation of the TCP4 transcription factor in *Arabidopsis thaliana* accelerates multiple aspects of plant maturation. *Plant J.* 67, 595–607. doi: 10.1111/j.1365-313X.2011.04616.x

Schommer, C., Palatnik, J. F., Aggarwal, P., Chételat, A., Cubas, P., Farmer, E. E., et al. (2008). Control of jasmonate biosynthesis and senescence by miR319 targets. *PLoS Biol.* 6:e230. doi: 10.1371/journal.pbio.0060230

Shi, M., Gong, H., Cui, L., Wang, Q., Wang, C., Wang, Y., et al. (2020). Targeted metabolic engineering of committed steps improves anti-cancer drug camptothecin production in *Ophiorrhiza pumila* hairy roots. *Industrial Crops Products* 148:112277. doi: 10.1016/j.indcrop.2020.112277

Shi, P., Guy, K. M., Wu, W., Fang, B., Yang, J., Zhang, M., et al. (2016). Genome-wide identification and expression analysis of the ClTCP transcription factors in *Citrullus lanatus*. *BMC Plant Biol.* 16:85. doi: 10.1186/s12870-016-0765-9

Udomsom, N., Rai, A., Suzuki, H., Okuyama, J., Imai, R., Mori, T., et al. (2016). Function of AP2/ERF transcription factors involved in the regulation of specialized metabolism in *Ophiorrhiza pumila* revealed by transcriptomics and metabolomics. *Front. Plant Sci.* 7:1861. doi: 10.3389/fpls.2016.01861

Viola, I. L., Camoirano, A., and Gonzalez, D. H. (2016). Redox-dependent modulation of anthocyanin biosynthesis by the TCP transcription factor TCP15 during exposure to high light intensity conditions in *Arabidopsis*. *Plant Physiol.* 170, 74–85. doi: 10.1104/pp.15.01016

Wei, W., Hu, Y., Cui, M. Y., Han, Y. T., Gao, K., and Feng, J. Y. (2016). Identification and transcript analysis of the TCP transcription factors in the diploid woodland *strawberry Fragaria* vesca. *Front. Plant Sci.* 7:1937. doi: 10.3389/fpls.2016.01937

Xie, X., Lin, W., Liu, H., Deng, J., Chen, Y., Liu, H., et al. (2016). Ultrasound-responsive nanobubbles contained with peptide–camptothecin conjugates for targeted drug delivery. *Drug Delivery* 23, 2756–2764. doi: 10.3109/10717544.2015.1077289

Xu, R., Sun, P., Jia, F., Lu, L., Li, Y., Zhang, S., et al. (2014). Genomewide analysis of TCP transcription factor gene family in *Malus domestica*. *J. Genet.* 93, 733–746. doi: 10.1007/s12041-014-0446-0

Yang, M., Wang, Q., Liu, Y., Hao, X., Wang, C., Liang, Y., et al. (2021). Divergent camptothecin biosynthetic pathway in *Ophiorrhiza pumila*. *BMC Biol.* 19:122. doi: 10.1186/s12915-021-01051-y

You, D., Feng, Y., Wang, C., Sun, C., Wang, Y., Zhao, D., et al. (2021). Cloning, characterization, and enzymatic identification of a new tryptophan decarboxylase from *Ophiorrhiza pumila*. *Biotechnol. Appl. Biochem.* 68, 381–389. doi: 10.1002/bab.1935

Zheng, A., Sun, F., Cheng, T., Wang, Y., Xie, K., Zhang, C., et al. (2019). Genome-wide identification of members of the *TCP* gene family in switchgrass (*Panicum virgatum* L.) and analysis of their expression. *Gene* 702, 89–98. doi: 10.1016/j.gene.2019.03.059

Zheng, K., Ni, Z., Qu, Y., Cai, Y., Yang, Z., Sun, G., et al. (2018). Genome-wide identification and expression analyses of *TCP* transcription factor genes in *Gossypium barbadense*. *Sci. Rep.* 8:14526. doi: 10.1038/s41598-018-32626-5

Conflict of Interest: The authors declare that the research was conducted in the absence of any commercial or financial relationships that could be construed as a potential conflict of interest.

The handling editor declared a past collaboration with the author GK.

Publisher's Note: All claims expressed in this article are solely those of the authors and do not necessarily represent those of their affiliated organizations, or those of the publisher, the editors and the reviewers. Any product that may be evaluated in this article, or claim that may be made by its manufacturer, is not guaranteed or endorsed by the publisher.

Copyright © 2021 Wang, Hao, Wang, Shi and Zhou and Kai. This is an open-access article distributed under the terms of the Creative Commons Attribution License (CC BY). The use, distribution or reproduction in other forums is permitted, provided the original author(s) and the copyright owner(s) are credited and that the original publication in this journal is cited, in accordance with accepted academic practice. No use, distribution or reproduction is permitted which does not comply with these terms.

frontiers in Plant Science

ORIGINAL RESEARCH
published: 20 October 2021
doi: 10.3389/fpls.2021.755494

Identification of the Histone Deacetylases Gene Family in Hemp Reveals Genes Regulating Cannabinoids Synthesis

*Liu Yang[1,2†], Xiangxiao Meng[2†], Shilin Chen[2], Jun Li[2], Wei Sun[2], Weiqiang Chen[2], Sifan Wang[2], Huihua Wan[2], Guangtao Qian[3], Xiaozhe Yi[1], Juncan Li[1], Yaqin Zheng[1], Ming Luo[4], Shanshan Chen[2], Xia Liu[1]*and Yaolei Mi[2]**

[1]School of Chemistry, Chemical Engineering and Life Sciences, Wuhan University of Technology, Wuhan, China, [2]Key Laboratory of Beijing for Identification and Safety Evaluation of Chinese Medicine, Institute of Chinese Materia Medica, China Academy of Chinese Medical Sciences, Beijing, China, [3]Key Laboratory of Saline-alkali Vegetation Ecology Restoration, Ministry of Education, College of Life Sciences, Northeast Forestry University, Harbin, China, [4]Guangdong Provincial Key Laboratory of Applied Botany, South China Botanical Garden, Center of Economic Botany, Core Botanical Gardens, Chinese Academy of Sciences, Guangzhou, China

Histone deacetylases (HDACs) play crucial roles nearly in all aspects of plant biology, including stress responses, development and growth, and regulation of secondary metabolite biosynthesis. The molecular functions of HDACs have been explored in depth in *Arabidopsis thaliana*, while little research has been reported in the medicinal plant *Cannabis sativa* L. Here, we excavated 14 *CsHDAC* genes of *C. sativa* L that were divided into three relatively conserved subfamilies, including RPD3/HDA1 (10 genes), SIR2 (2 genes), and HD2 (2 genes). Genes associated with the biosynthesis of bioactive constituents were identified by combining the distribution of cannabinoids with the expression pattern of HDAC genes in various organs. Using qRT-PCR and transcription group analysis, we verified the expression of candidate genes in different tissues. We found that the histone inhibitor Trichostatin A (TSA) affected the expression of key genes in the cannabinoid metabolism pathway and the accumulation of synthetic precursors, which indirectly indicates that histone inhibitor may regulate the synthesis of active substances in *C. sativa* L.

Keywords: histone deacetylase, *Cannabis sativa*, gene family, bioinformatics, genome-wide

OPEN ACCESS

Edited by:
Lei Zhang,
Second Military Medical University, China

Reviewed by:
Dongming Ma,
Guangzhou University of Chinese Medicine, China
Lida Zhang,
Shanghai Jiao Tong University, China
Qinlong Zhu,
South China Agricultural University, China

****Correspondence:***
Xia Liu
lrx1125@126.com
Yaolei Mi
xiaomi20063@sina.com

[†]These authors have contributed equally to this work

Specialty section:
This article was submitted to Plant Metabolism and Chemodiversity, a section of the journal Frontiers in Plant Science

Received: *09 August 2021*
Accepted: *21 September 2021*
Published: *20 October 2021*

Citation:
Yang L, Meng X, Chen S, Li J, Sun W, Chen W, Wang S, Wan H, Qian G, Yi X, Li J, Zheng Y, Luo M, Chen S, Liu X and Mi Y (2021) Identification of the Histone Deacetylases Gene Family in Hemp Reveals Genes Regulating Cannabinoids Synthesis. Front. Plant Sci. 12:755494. doi: 10.3389/fpls.2021.755494

INTRODUCTION

Chromatin consists of nucleosomes, each of which is composed of an octamer of four key histones—H2A, H2B, H3, and H4, each of which is a dimer—around which is wrapped a strand of DNA (Yang and Nielsen, 2000; Lusser et al., 2001). Histone acetylases (HAT) are enzymes, which catalyzes the acetylation of histones, and histone deacetylase (HDAC) catalyzes the deacetylation of histones (Yang and Seto, 2007; Wang et al., 2009). When histones are acetylated, they release DNA due to the decrease in the affinity between histones and DNA, and subsequently promote the binding of transcription factors to DNA (Kurdistani and Grunstein, 2003). However,

these effects are counteracted by histone deacetylases (Liu et al., 2012). HAT and HDAC coexist in various tissues and organs of animals and plants and interact to regulate the availability of DNA (Graessle et al., 2001; Haigis and Guarente, 2006). The classification and function of HDACs in humans and yeast have been studied in depth (Brownell et al., 1996; Song and Galbraith, 2006). In yeast, the HDAC gene family is divided into two subfamilies according to the characteristics of the conserved domain sequences RPD3/HDA1 (reduced potassium dependency 3) and SIR2 (silent information regulator 2; Frye, 2000; Guarente, 2000). Histone deacetylation can directly affect the level of transcription by altering the structure of chromatin (Brownell et al., 1996; Pandey et al., 2002). Both subfamilies have also been studied in plants (Zhang et al., 2020). For example, *AtHDA1*, *AtSNLs,* and *AtHDA19* regulate flowering time by forming complexes (Lee et al., 2016); *AtHDA19* and *AtHSL1* together suppress the expression of seed maturation genes (Zhou et al., 2013). In rice, *OsIDS1* physically interacts with the transcriptional corepressors *OsTPR1* and *OsHDA1* (Cheng et al., 2018). Additionally, another subfamily of HDAC, HD2 (Histone Deacetylase 2), was shown to be plant-specific (Gu et al., 2011; Nicolas-Francès et al., 2018). In Poplar lignin, the *PtHDT1* mutant of *Populus tomentosa*, an HD2 subfamily member, has thinner stem nodes, more wood fiber cells, thicker wood fiber cell walls, and higher lignin than the wild type (Kornet and Scheres, 2009). *PtHDT1* interacts with *PtMYB* to regulate the development of xylem and cambium (Zhang, 2018). In banana, *MaERF1* recruits *MaHDA1* to represses the expression of *MaACO1*, thereby negatively regulating ethylene biosynthesis (Han et al., 2016; Zheng et al., 2020). Therefore, HDAC families exert vital effects on the synthesis of secondary metabolites.

Cannabis sativa (Cannabinaceae) is an annual herb, mostly dioecious (Zuardi, 2006). This plant has been used in many areas including food, fiber, cosmetics, and medicine (Schachtsiek et al., 2018). Cannabinoids, the main components found in *C. sativa*. L, include CBD and THC (Marks et al., 2009; Vindenes, 2017). *C. sativa* is divided into hemp and marijuana, according to the content of tetrahydrocannabinol (THC; Morimoto et al., 1997; Vindenes, 2017). CBD has anti-vomiting, analgesic, anti-inflammatory, anti-spasmodic, anti-cancer, and other activities (De Meijer and Hammond, 2005). For instance, epidiolex (purified CBD) is an oral drug approved for treating epilepsy. However, THC is a neuroactive compound and is addictive (Pacher et al., 2006; Burstein, 2015). In China, the cultivation of hemp with a THC content higher than 0.3% is prohibited. Therefore, our lab is committed to cultivating high-quality varieties of *C. sativa* with high CBD and low THC content. This aim will be achieved by studying the molecular mechanism related to the production of CBD to increase natural yield and response to external environmental stress. The biosynthetic pathway of cannabinoids has been elucidated (Lydon et al., 1987; Booth et al., 2020; **Figure 1**). However, the molecular mechanism of regulation of cannabinoid synthesis has yet to be clearly resolved. Posttranscriptional modification plays a pivotal role in the biosynthetic pathway of active substances in medicinal plants (Appendino et al., 2008; VanBakel et al., 2011; Luo et al., 2019). We aimed to systemically summarize the members of the HDAC family at the genome-scale level and explore histone deacetylation the effects of posttranscriptional modification on cannabinoid synthesis. In this study, we identified 14 HDACs in *C. sativa* genome and studied their structural characteristics, subcellular localization, alternative splicing events, and differential expression in different tissues and organs. We treated *C. sativa* L seedlings with histone inhibitors and measured the expression of key genes and the accumulation of precursor substances (olivetolic acid-OA and geranyl diphosphate-GPP). Based on these studies, we explored the role of deacetylation in the cannabinoid synthesis pathway.

MATERIALS AND METHODS

Plant Materials and Growth Condition

In this study, we used the hemp variety Diku (DK), a female plant crossing Purple Kush with Dinamed Autoflowering CBD. This variety has a short growth cycle and is a variety with high CBD and low THC content. It is an excellent reference variety for cannabis breeding. The plants were cultivated in the experimental field of the Institute of Chinese Materia Medica of the Chinese Academy of Chinese Medical Sciences, China. Flowers, bracts, leaves, stems, seeds, and roots of hemp were collected to analyze the expression patterns of HDAC genes. Hemp seeds were cultured in MS medium for 3 weeks. After the seedlings grew, they were transferred to an MS medium containing 0-μm (DMSO matrix), 0.25-μm, or 1.25-μm Trichostatin A (TSA) and cultured for 1 week to analyze the effect of TSA on the HDAC gene of hemp. All sample materials collected in this study were frozen in liquid nitrogen immediately and then reserved at −80°C for further analysis.

Data Sources

The genomic data (GCA_900626175.1) of hemp variety female CRBRX, with a high-CBDA cultivar (15% CBDA and 0.3% THCA) used in this study, were downloaded from the NCBI[1] database. *Arabidopsis thaliana* and soybean HDAC genetic data were obtained from the PlantTFDB database.[2] We measured the transcriptome of five different tissues and organs of Diku. The transcriptome data of its flowers, bracts, stems, leaves, and seeds were available at NCBI (NCBI accession number: flowers: SAMN16122886 ~ SAMN16122888; bracts: SAMN16122880 ~ SAMN16122882; stems: SAMN16122883 ~ SAMN16122885; leaves: SAMN16122889 ~ SAMN1612281; and seeds: SAMN20474456 ~ SAMN20474458).

Basic Information and Characteristics of CsHDACs

We downloaded the full gene set and annotation files of *C. sativa* (GCA_900626175.1), *Glycine max* (GCF_000004515),

[1]https://www.ncbi.nlm.nih.gov
[2]http://planttfdb.cbi.pku.edu.cn/

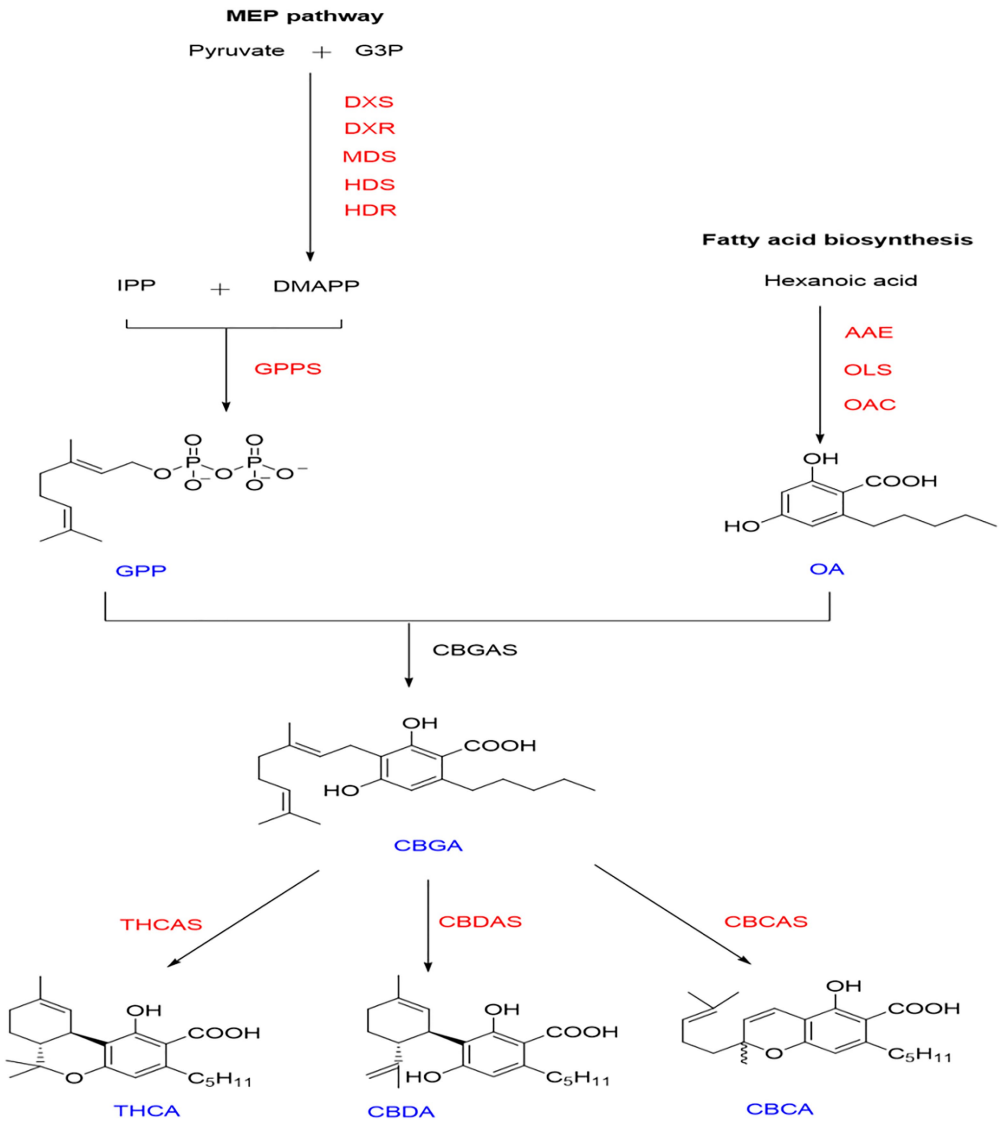

FIGURE 1 | Synthetic pathway of cannabinoids. Intermediates and final products are shown in blue. Enzyme names are shown in red. Fatty acid pathway—AAE, Acyl activating enzyme; OAC, Olivetolic acid cyclase; and OLS, Olivetol synthase. Methylerythritol phosphate (MEP) pathway—DXS, 1-deoxy-d-xylulose 5 phosphate DXP synthase; DXR, DXP reductase; MDS, 2-C-methyl-pyrophosphate synthase; HDS, (E)-4-Hydroxy-3-methyl-but-2-enylpyrophosphate (HMB-PP) synthase; HDR, HMB-PP reductase; and GPPS: Geranyl diphosphate synthase. Intermediates and final products—GPP, Geranyl diphosphate; OA, Olivetolic acid; CBGA, Cannabigerolic acid; THCA, Δ9-Tetrahydrocannabinolic acid A; CBDA, Cannabidiolic acid; and CBCA, Cannabichromenic acid.

and *A. thaliana* (GCA_000005425.2) from the NCBI Web site. We extracted the CDS sequence and protein sequence of hemp using the TBtools software (Chen et al., 2020). Using the protein sequence of AtHDAC and GmHDAC as query in BLASTp (score value of ≥100, e-value ≤ e^{-10}), we ran the extracted hemp data against the AtHDAC sequence to identify potential HDACs in hemp. Then, we initially established identity-reliable domains by manually searching the NCBI reserved domain database.[3] Finally, 14 HDAC family members were obtained. The basic characteristics, such as the protein molecular weight, isoelectric point, and amino acid number, were analyzed on the ExPASy Web site.[4]

Phylogenetic, Conserved Motif Analyses, Gene Structure, Chromosomal Locations, and Syntenic Analyses of CsHDACs

CsHDAC, GmHDAC, and AtHDAC domain amino acid sequences were aligned using MEGA 7.0 software. The neighbor-joining (NJ) adjacency method was used to build a phylogenetic tree against the *A. thaliana* and *G. max*. The bootstrap test

[3]https://www.ncbi.nlm.nih.gov/structure/cdd/wrpsb.cgi

[4]http://web.expasy.org/protparam/

was repeated 1,000 times, and the BLASTp cutoff was set as value of $E < 1 \times 10^{-10}$. The structure of the CsHDACs and their localization on the chromosomes were visualized using TBtools (Chen et al., 2020). The conserved motifs of CsHDAC proteins were carried out using MEME.[5] The parameters are set as follows: The maximum number of themes is 20, and the best theme width is 10–200. Conserved structural domains were analyzed using NCBI-CDD.[6] Subcellular localization was predicted using the wolf PSORT Web site.[7] Sequences 2000 bp upstream of the start codon of each CsHDAC gene were extracted, and the distribution of the *cis*-elements in the promoter regions was analyzed using PlantCARE software.[8] We downloaded the chromosomal locations of 14 HDAC genes in the *C. sativa* genome from the NCBI.[9] The HDAC gene locations were then represented using TBtools (Chen et al., 2020). Multiple collinear scanning toolkits (MCScanX) were used to detect gene duplication events (Wang et al., 2012).

Gene Expression in Different Tissues and Alternative Splicing Analysis

Differential expression analysis of CsHDACs and all isoforms of CsHDACs were performed, and heat maps were created using TBtools software. In short, SpliceMap was used to detect the junctions of Illumina short reads obtained from samples, and IDP was then used to predict and detect isoforms by integrating both Illumina short reads and SMRT long reads. The results of IDP show the sites where isoforms are located on the genome. Integrative Genomics Viewer was used to visualize the isoform structure that may exist for each HDAC gene family member.[10] Specific steps were referred to in our previous research (Gao et al., 2019; Xu et al., 2020). We took the original annotated genes as reference isoforms (ref isoforms). The other isoforms were divided into intron retained (IR), an exon skipping (ES), and alternative 3′ splice site (AA). Isoforms that did not belong to the aforementioned three types were defined as "others."

RNA Isolation and qRT-PCR

According to the manufacturer's instructions, we isolated total RNA from samples (Tiangen Biotech, Beijing, China). Using a Fast Quant RT Kit, the first cDNA strand was synthesized (Tiangen Biotech). The specific primers for qRT-PCR were designed using NCBI-Primer blast (**Table 1**). CFX96™ real-time system (Bio-Rad, Hercules, CA, United States) was used for qRT-PCR. Program: 95°C for 2 min, followed by 40 cycles of 95°C for 15 s, 56°C for 35 s, and 72°C for 15 s. A melting curve was generated and analyzed. The reference gene in this study was *EF1-α* (Nicot et al., 2005). Each sample was in triplicate experiments.

[5]http://meme-suite.org/tools/meme
[6]https://www.ncbi.nlm.nih.gov
[7]http://www.genscript.com/wolf PSORT. HTML
[8]http://www.plantcare.co.uk/
[9]https://www.ncbi.nlm.nih.gov
[10]http://software.broadinstitute.org/software/igv/IGV

Sample Preparation and UPLC-ESI-MS/MS Conditions

After adding liquid nitrogen in a mortar, leaves of hemp seedlings were crushed into a uniform powder. An ultrasonic ice water bath was used to dissolve approximately 0.1-g sample powder in 10.0-ml 95% aqueous methanol for 30 min. Approximately 12,000 rpm was applied for 10 min at 4°C to centrifuge the solution; then, the supernatant was filtered by a 0.22-μm hydrophilic organic nylon microporous membrane.

The Agilent UPLC 1290II–G6400 triple quadrupole mass spectrometer (QQQ; Agilent Technologies, Santa Clara, CA, United States) was used to determine the relative quality of synthetic precursors. We used the peak area to express the relative mass under each condition.

A bidirectional solvent delivery system, an autosampler, and a column compartment were used in the UPLC. A column (2.1 * 100 mm, 1.8 μm) of C18 was used for chromatographic separations at a temperature of 40°C. Mobile phase A contained water containing 0.1% formic acid; phase B is 100% methanol. Elution was proceeded linearly at a flow rate of 0.3 ml/min. In gradients, these settings were used as: 5% B → 70%B (0–2 min); 70% B → 100% B (2–10 min); 100% B (10–13 min); 100% B → 5% B(13–14 min); and 5% B (14–15 min). Autosampler was set to 4°C and 3-μl sample volume was injected. The experiment was performed in triplicate. The MRM diagrams of OA, GPP, and their standard products are shown in **Supplementary Figure S1**.

Statistical Analysis

All the data were analyzed by the Prism 8 Statistics programs, and the means were compared by the least significant difference test at the 0.05 and 0.01 level of significance.

RESULTS

Basic Information and Characteristics of CsHDACs

In our study, 14 HDAC genes were obtained, and RPD3/HDA1 subfamily contained 10 members, named *CsHDA1–CsHDA10*; two members of HD2 subfamily named *CsHDT1–CsHDT2*; and two members of SIR2 subfamily named *CsSRT1–CsSRT2*. Their sequences ranged in length from 432 to 1953 bp. The molecular weight of their translated protein ranged from 21702.17 to 56624.95 Da, and they had between 203 and 504 amino acids. The other characteristics, such as theoretical IP and subcellular localization, were shown in **Table 2**.

Evolutionary Analysis of the CsHDAC Family

To demonstrate the evolutionary relationships of CsHDAC in plants, we constructed a phylogenetic tree using amino acid sequences from model plant Arabidopsis, model food crop soybean, and hemp. The CsHDAC family was categorized into three subfamilies based on the difference in sequence features

TABLE 1 | qRT-PCR primers for genes.

Protein name	Forward primer	Reverse primer
CsHDA1	TCCCTGGTACCGGAGACATAG	CACTGAAGAACCACAGCCCC
CsHDA2	AGGTTGGAGGAACTATTGTGGC	CACAAAATCCCCCTCCTCTCC
CsHDA3	TGGAAAACCAGCTCTCACTTCT	CCCTCCACAAAACATCTTACCC
CsHDA4	GGGCTTGCCATAGTTGATTCC	GCATAACGAGCAGCTATTGCC
CsHDA5	GCGTCAAAAATGGGTTTGCCC	CAATGAGCACCTTCCTAGCCC
CsHDA6	TGGAGATGGTGTTGAGGAAGC	GGCCGAAAAAGACCACGAAAA
CsHDA7	CCGGTGATGTCAAGGATTCAGG	GAAGCAGCCTAAGCGATCTCC
CsHDA8	CTGCTTCCTTAACAATGCTGGTC	AGGATGAGATGAACCCCATGAAC
CsHDA9	TGCCCAAGGGAAAGTTGTGTT	GCAAGTGTAGGCCAGAATGGA
CsHDA10	GTTGGGTAGAGGCGAAGACC	ACGGCTACACAATACCTCCT
CsHDT1	TGAAAACTTGCAGTCTGGAGAAG	TGAATCGTTTTCTTCATCACCAC
CsHDT2	TCCGATGAGGAAGAAGAAGTCC	GCTTGGCTCCACAACCTTAACT
CsSRT1	ATGTTTGGGGACGAGCCTG	ATCATGGCACCCGAAACTACC
CsSRT2	GGAGTTTATTCGCTCAAGCCG	AGAGCGATATGAGCAGCACC

and the number of HDAC domains, SIR2, HD2, and RPD3/HDA1, with 2, 2, and 10 members, respectively (Zhang et al., 2020). Clades I–IV represented the RPD3/HDA1 subfamily, which is a type of Zn^{+}-dependent histone deacetylase. Clade V represented the HD2 subfamily, which are plant-specific HDACs. Clade VI represented the SIR2 subfamily, a type of nicotinamide adenine dinucleotide (NAD^{+})-dependent HDACs. The 10 members of RPD3/HDA1 subfamilies were further divided into four subgroups based on the similarities of the HDAC domain amino acid sequences, with Subgroup I including CsHDA1 and CsHDA7, Subgroup II including CsHDA6 and CsHDA10, Subgroup III including CsHDA2, and Subgroup IV including CsHDA3-5 and CsHDA8-9 (**Figure 2**).

Conserved Motifs and Gene Structure of CsHDACs

The conserved motifs of proteins may be related to their transcriptional activity, protein interactions, and nuclear localization (Ikeda and Ohme-Takagi, 2009; Causier et al., 2012). Thus, we studied the conserved motifs of all CsHDAC proteins combined with the evolutionary relationship of hemp (**Figure 3A**), and 20 conserved motifs were predicted (**Figure 3B**). The RPD3/HDA1 subfamily included numerous conserved motifs, while the SIR2 and HD2 subfamilies contained relatively fewer conserved motifs. According to the analysis of the conserved motifs, motifs 1 and 3 partly represented the distribution of the HDAC-conserved domain and were shared by all 10 members of the RPD3/HDA1 subfamily. Motifs 10, 13, and 14 were highly conserved and were included only in the Class II subgroup. The conserved motifs 16 and 17 were identified as a characteristic NPL domain, a structure that is unique to the HD2 subfamily. Motif 18 corresponded to the SIR2 conserved domain, which only existed in the SIR2 subfamily (**Figure 3E**). Multiple sequence comparison of important conserved motifs is shown in **Supplementary Figure S2**. Other conserved motifs were also found in CsHDACs, while the action mechanism of these motifs has not been analyzed. Overall, the conserved motif composition and gene structure within each family of CsHDAC members had a high similarity, and the results of the phylogenetic analysis advocated the validity of the population classification.

We investigated the exons and introns from their number and distribution to study the structural composition of the *CsHDAC* genes (**Figure 3C**). Two members of the SIR2 subfamily had eight exons, and two members of the HD2 subfamily contained 10 exons. The coding sequences of the entire RPD3/HDA1 subfamily were interrupted by introns, with the number of exons in the range of 1–17. The *CsHDAC* genes had three main domains, which were specifically distributed into three subfamilies (**Figure 3B**). The SIR2, RPD3/HDA1, and HD2 subfamilies consisted of the SIR2, HDAC, and NPL domains, respectively. Members of the HD2 subfamily of *C. sativa* had conserved MEFWG pentapeptide at the N-terminus and possibly had a zinc finger at the C-terminus. Generally, the number of exons within each subgroup was similar. The domain of each subfamily was conserved, although the structures of members within a particular subfamily were different. In addition, we analyzed the co-expression analysis of CsHDACs and key genes in the cannabinoid synthesis pathway (**Figure 3D; Supplementary Table S1**). We found that *CsHDA1*, *CsHDA5*, *CsHDA7*, and *CsSRT1* have obvious correlations with key genes.

Chromosomal Localization of *CsHDACs*

Chromosome mapping of the *CsHDAC* genes was performed using the latest *C. sativa* genome database. A total of 14 *CsHDAC* genes were unevenly distributed on six chromosomes (**Figure 4A**). Among them, chromosomes 1, 2, 3, 4, 6, and 8 harbored 5, 1, 4, 1, 3, and 1 genes, respectively. While chromosomes 5, 7, 9, and 10 did not contain any *HDAC* gene. We further studied the homologous genes of CsHDAC within and between species. No homologous genes are found on the chromosomes of *C. sativa*. The results of collinearity analysis between *C. sativa* and *A. thaliana* showed three orthologous genes (**Figure 4B**).

CIS-Acting Element Analysis of *CsHDACs*

Cis-acting element analysis was performed on the CsHDAC gene family members, and the results were visualized

TABLE 2 | Description of the HDACs in *C. sativa*.

Gene ID	Protein id	Protein name	Protein Length (aa)	Molecular Weight (Da)	Theoretical IP	Subcellular localization
LOC115702813	XP_030486110.1	CsHDA1	494	55699.25	5.00	Cyto. Nuc.
LOC115707169	XP_030490898.1	CsHDA2	388	43016.59	8.07	Nuc
LOC115710981	XP_030495193.1	CsHDA3	203	21702.71	6.02	Nuc
LOC115707945	XP_030491922.1	CsHDA4	422	45486.66	5.95	Nuc
LOC115711299	XP_030495493.1	CsHDA5	494	53597.21	5.48	Nuc
LOC115710180	XP_030494383.1	CsHDA6	422	52277.81	5.47	Cyto. Nuc
LOC115719134	XP_030503922.1	CsHDA7	432	49345.45	5.15	Nuc
LOC115718595	XP_030503266.1	CsHDA8	387	41888.25	5.47	Cyto. Nuc
LOC115709622	XP_030493624.1	CsHDA9	504	56624.95	5.81	Nuc
LOC115703044	XP_030486387.1	CsHDA10	464	52277.81	5.47	Cyto. Nuc
LOC115711643	XP_030495876.1	CsHDT1	296	31610.11	4.59	Nuc
LOC115719367	XP_030504240.1	CsHDT2	311	33030.00	4.63	Nuc
LOC115695686	XP_030478610.1	CsSRT1	484	53608.19	9.04	Chlo. Nuc
LOC115714802	XP_030499415.1	CsSRT2	397	43486.62	8.37	Chlo. Nuc

(**Figure 5**). The HDAC gene family contained 13 *cis*-type elements, and each member of the family contained multiple response elements. Among them, *HDAC9* contained many light-responsive elements, suggesting that *HDAC9* may be highly sensitive to light stimuli. *HDA10* contained the largest number of cis-elements, with six *cis*-elements, whereas *HDA8* had the least number of *cis*-elements, with only two *cis*-elements.

Alternative Splicing Analysis and Gene Expression Patterns

Alternative splicing, which causes polymorphisms in the function and structure of proteins, is extensive in eukaryotic organisms (Chaudhary et al., 2019). Therefore, we performed hypomorphic detection and prediction on the basis of data obtained *via* second-generation sequencing and third-generation sequencing and identified 21 splicing events in eight HDAC genes (**Figure 6A**). Compared with the eight selected reference isoforms, splicing events included seven intron retentions (IR), three alternative 3′ splice site (A3SS; AA), one exon skipping (ES), and two other isoforms ("others"). One gene may generate different alternative splicing events. For instance, NC_044372.1: 65918457–65940183.9 (*CsHDA5*) contained two cutting types: IR and "others." The expression of different transcripts of the same gene differed. In other words, some transcripts dominated the expression of the gene in all tissues. For instance, rna-XM_030622750.1 (*CsSRT1*) had higher expression in all tissues than the other transcripts. Additionally, different transcripts may be enriched in various tissues. For instance, the rna-XM_030643555.1 (*CsSRT2*) had the highest expression in roots, while another splice variant, rna-XM_030643556.1 (*CsSRT2*), had the highest expression in leaves.

To explore the expression patterns of the *CsHDAC* gene family in different organs, we drew heat maps based on the FPKM calculated from RNA-seq data of seeds, flowers, stems, leaves, and bracts of DK (**Figure 6B**). *CsHDA1*, *5*, *7,* and *13* were commonly expressed in all tissues. *CsHDA1* and *CsHDT2* were highly expressed in all tissues, especially in seeds. The expression of *CsHDA6* was also relatively higher in seeds. *CsHDA10* was highly expressed in the stem, while *CsHDA4* was enriched in leaves. Genes in flowers and bracts had a similar expression pattern, and the majority was expressed at lower levels than in other tissues. Expression patterns of CsHDAC genes in different tissues can be used as the foundation for identifying functional genes in *C. sativa*. According to previously published research, *MaDHAC1*, *AtHDA6*, and *AtHD2* were associated with plant secondary metabolism (Han et al., 2016). Therefore, we selected candidate homologous *CsHDAC* members by constructing NJ trees and performing motif analysis between these genes and *CsHDACs* (**Supplementary Figure S3**) and verified them *via* qRT-PCR analysis. *CsHDA1* and *CsHDA5* were evenly enriched in all tissues. *CsHDA7*, *CsHDA8,* and *CsSRT1* were less strongly expressed in the bracts (**Figure 6C**).

Gene Expression Pattern and Metabolite Determination After TSA Treatment

TSA can broadly inhibit the HDAC subfamily (Li et al., 2014; Su et al., 2015). To study whether HDAC is related to the synthesis of cannabinoids, we compared the changes in gene expression in hemp seedlings before and after TSA treatment. HDAC gene expression decreased significantly with increasing concentration of TSA. TSA could effectively inhibit the expression of all the *CsHDAC* genes in the exception of *CsHDA10* (**Figure 7A**). In this study, two kinds of synthetic precursors were unambiguously identified as OA and GPP, respectively, by comparing the retention times, adductions, and productions with those of authentic standards. We also tested the expression of representative genes in the cannabinoid metabolic pathway and the changes in the synthetic precursors OA and GPP. The expression of genes in the fatty acid synthesis pathway, *OAC*, *OLS*, and *AAE*, was generally downregulated (**Figure 7C**). However, the expression of *PP1* (HMB-PP reductase1), *PP2* (HMB-PP reductase2), and geranyl diphosphate synthase (*GPPS*) in the MEP pathway increased (**Figure 7B**). Correspondingly, the content of synthetic precursor OA was reduced, while GPP accumulated (**Figure 7D**). The above results indicated that TSA

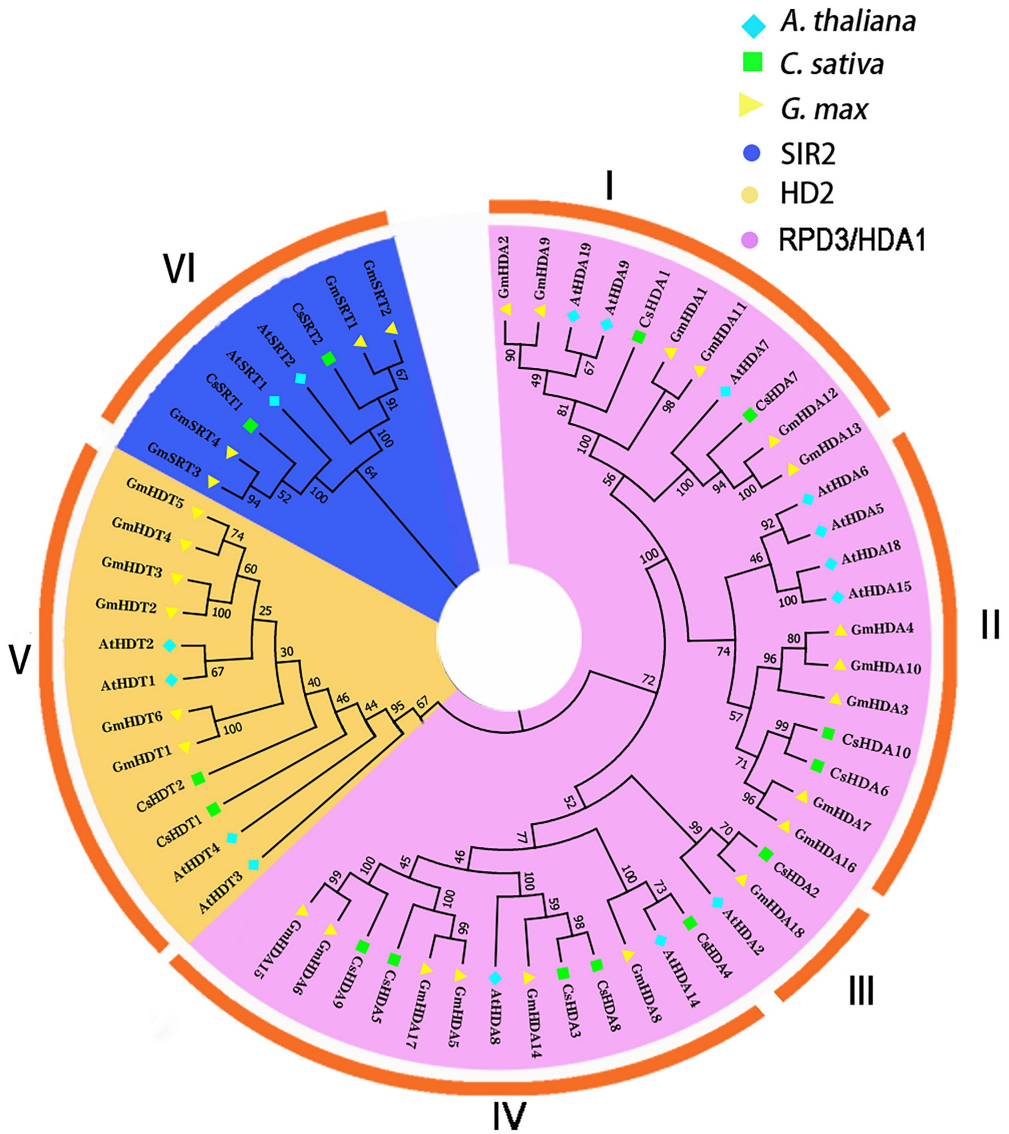

FIGURE 2 | An unrooted phylogenetic tree was constructed with the HDAC domain amino acid sequences of *Arabidopsis thaliana, Cannabis sativa*, and *Glycine max*. A neighbor-joining tree was constructed using MEGA7 with 1,000 bootstrap replicates. The tree was divided into six groups that contained the RPD3/HDA1, SIR2, and HD2 subfamilies (I–IV: RPD3/HDA1; V: HD2; and VI: SIR2). The blue rhombus represents *A. thaliana*; the green square indicates *C. sativa*; and the yellow triangle represents *G. max*. The purple background shows the SIR2 subfamily; the yellow background refers to the HD2 subfamily; and the blue background represents the RPD3/HDA1 subfamily.

inhibited the expression of *CsHDAC* genes and altered the contents of representative genes and synthetic precursors in the cannabinoid synthesis pathway.

DISCUSSION

Histone deacetylases are widely present in yeast, animals, and plants. The HDAC gene family has been isolated and characterized in several plants, involving 18 genes in *Arabidopsis* (Hollender and Liu, 2008), 18 genes in rice (Fu et al., 2007), 28 genes in soybean (Yang et al., 2018), 11 genes in litchi (Peng et al., 2017), and 15 genes in tomato (Zhao et al., 2015). In this study, we identified 14 *CsHDAC* members and surveyed their gene structures, expression profiles, phylogenetic relationships, and conserved motifs. CsHDACs can be classified into three subfamilies, RPD3/HDA1, HD2, and SIR2. The RPD3/HDA1 was the most highly represented CsHDAC subfamily in Arabidopsis (77%) and soybean (64%), suggesting that the RPD3/HDA1 subfamily may have undergone significant expansion during the process of evolution. The HD2 subfamily will be more likely to have a high affinity with the DNA-binding domain or mediate protein-protein interactions if it contains a C-terminal zinc finger (Wu et al., 2000; Dangl et al., 2001). For example, the interaction between

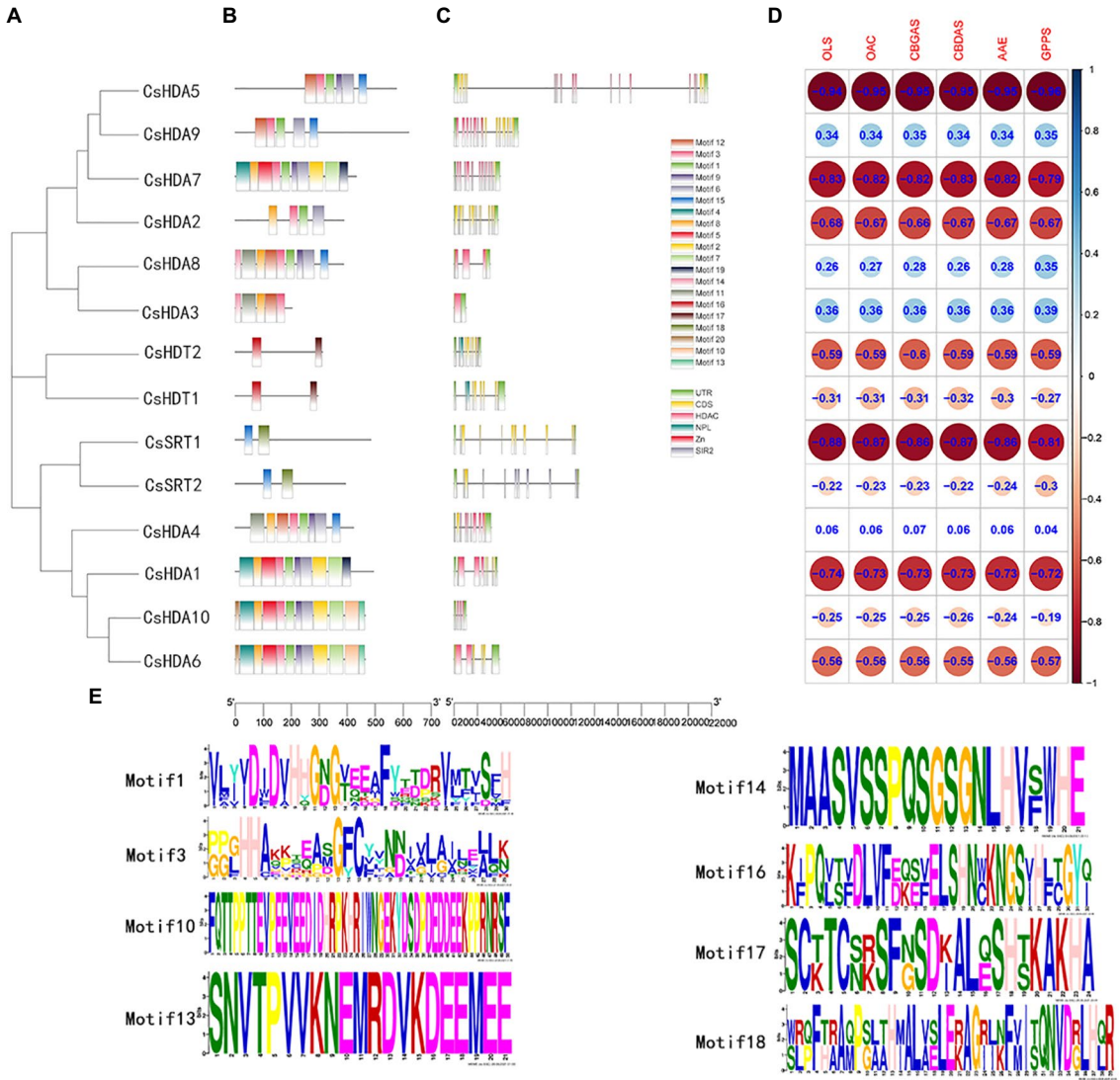

FIGURE 3 | The gene structures and the distribution of conserved motifs of CsHDACs. **(A)** Construction of phylogenetic tree based on the full-length sequence of CsHDAC protein. **(B)** The distribution of the motifs of each CsHDAC protein. **(C)** The gene structure and distribution of the conserved domains of CsHDACs. Green boxes, unrelated area; yellow boxes, exons; black lines, introns; pink boxes, HDAC domains; blue boxes; blue boxes, NPL domains; red box, zinc finger domain; and gray boxes, SIR2 domains. **(D)** Co-expression analysis of CsHDACs and key genes in the cannabinoid synthesis pathway. **(E)** The sequence information for representative motifs.

AtHDT2 and *AtDNMT2* (DNA methyl transfer) affected the expression of cold stress genes (Song, 2010), and *PtHDT1* interacted with *PtMYB to* regulate lignin biosynthesis (Zhang, 2018). In our study, *CsHDT2* had a C2H2 zinc finger in the C-terminus, suggesting that it may participate in protein-protein interactions. Motif 18 was unique to SIR2. We compared the SIR2 subfamily of Arabidopsis, soybean, and hemp, and found that they all contained motif 18, indicating that motif 18 was an important structural feature, that can be used to identify the SIR2 subfamily, and motif 18 could be the SIR2 subfamily structural basis with similar functions (König et al., 2014).

The expression of genes in tissues can help us infer the function of genes. In our study, we predicted and verified the expression of members of the CsHDAC family in different tissues. It was found that the expression of *CsHDA7* in flowers and bracts was relatively low when compared its expression in other organs, which was consistent with the contention that HDACs usually bind inhibitory regulators to exert a negative regulatory effect. *CsHDA1* was evenly distributed in all tissues, and in previous studies, its homologous gene *AtHDA6* significantly contributed to a variety of aspects of plant development and growth, such as abiotic stress responses, jasmine and ethylene signal transmission, and leaf and flower development (Probst et al., 2004; Yu et al., 2011). Both genes were predicted to be localized in the nucleus, suggesting that they were involved in transcriptional regulation. Therefore, *CsHDA1* may be a vital regulator throughout the life course of hemp.

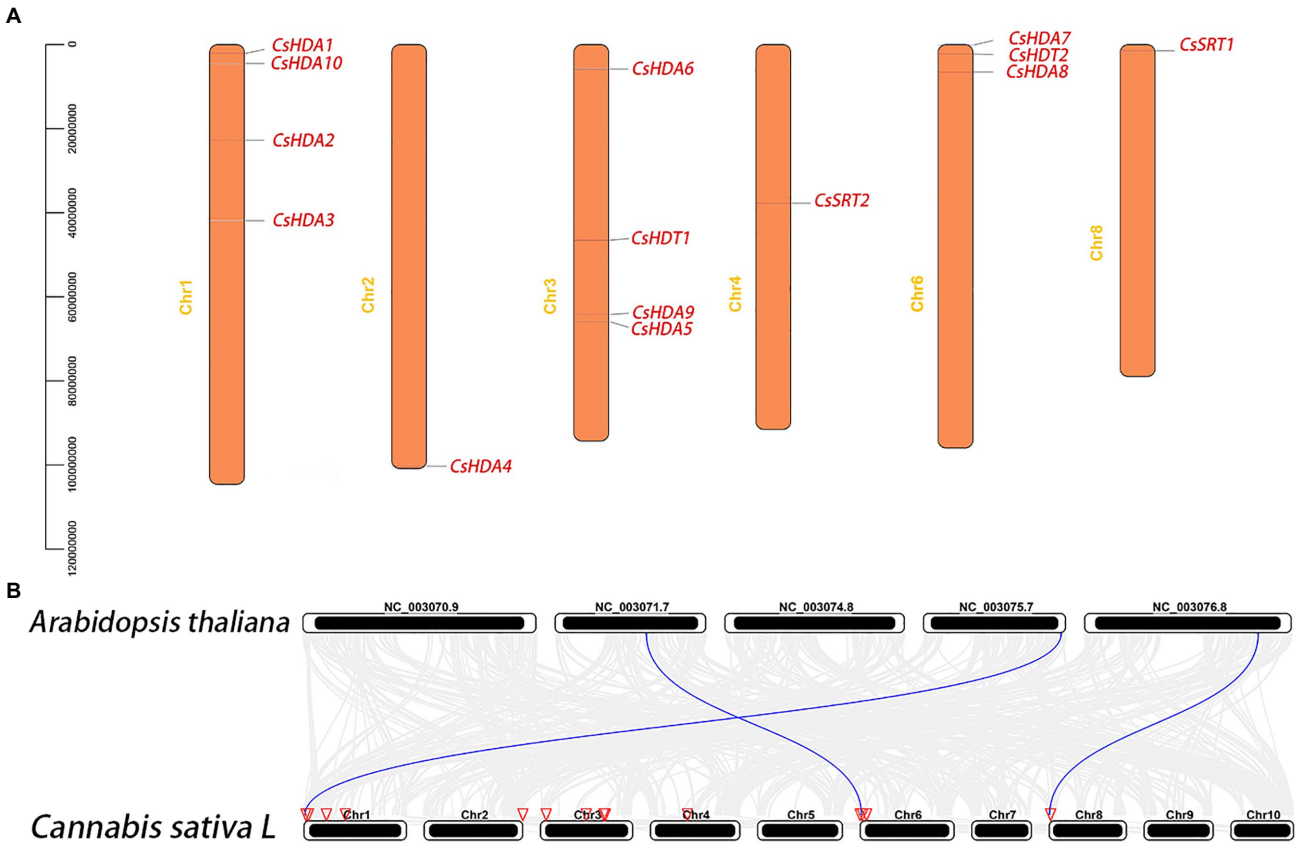

FIGURE 4 | (A) Chromosomal locations of the *CsHDAC* genes. The y axis shows the length of the chromosome (unit: bp). **(B)** Synteny analysis of HDAC genes between *Cannabis sativa* and *A. thaliana*. The red triangle side indicates the position of the HDAC gene on the chromosome. The blue lines represent the syntenic HDAC gene pairs.

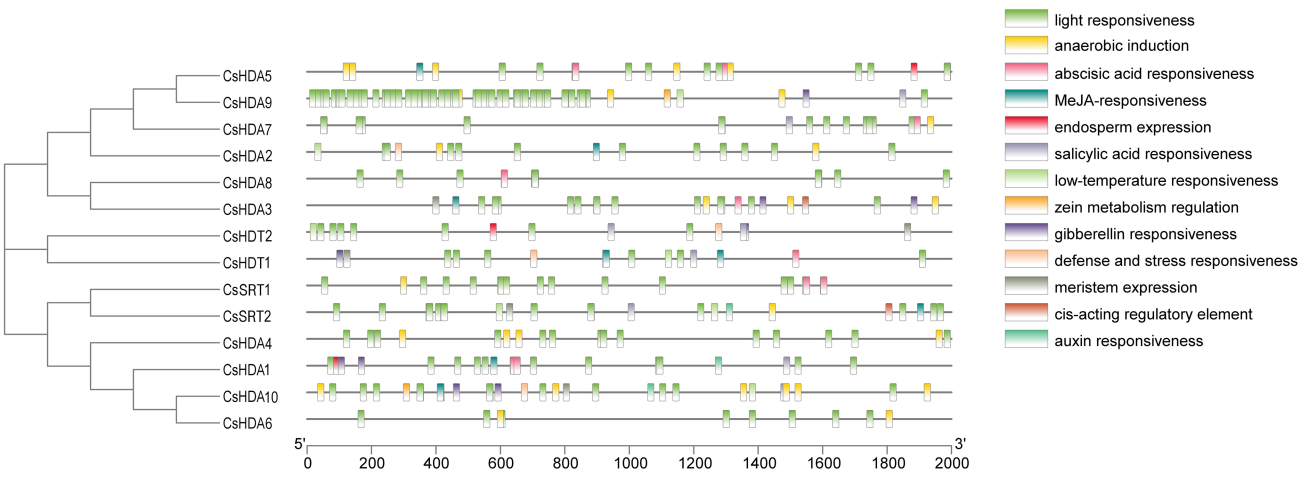

FIGURE 5 | *CIS*-acting elements of the *CsHDAC* genes.

Histone deacetylase is involved in the development of plants, the response to environmental changes, and the synthesis of secondary metabolites (Waterborg, 2011). HDAC usually forms a complex with transcription repressors to regulate target gene expression. In previous research, *AtHDA15* interacted with a negative regulator, *AtHY5*, to repress photomorphogenesis (Jing et al., 2020). *OsHDA1* physically interacted with *OsIDS1* and the transcriptional corepressor

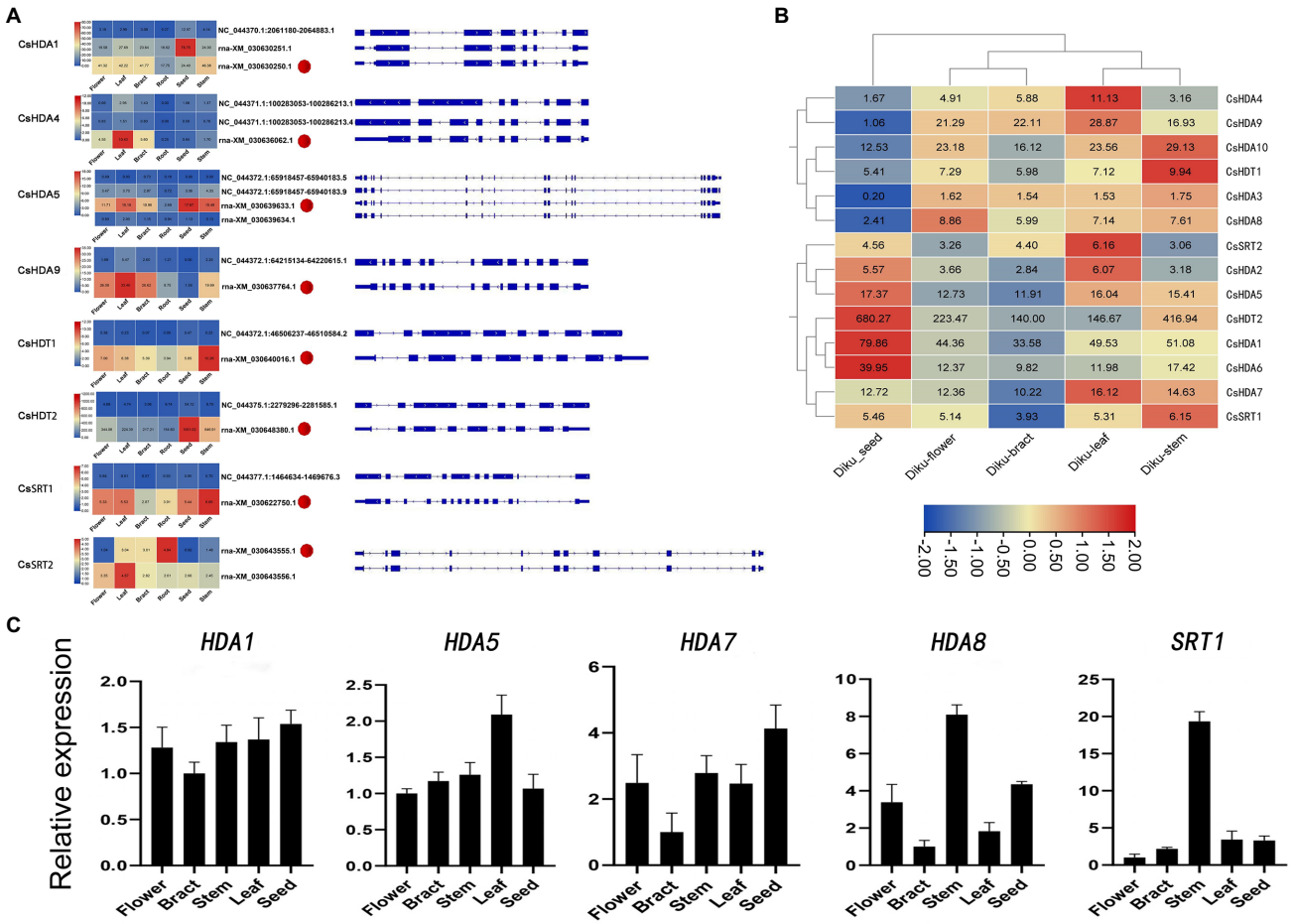

FIGURE 6 | (A) Alternative splicing isoforms and the expression pattern of eight *CsHDAC* genes. Red dots refer to the selected reference isoforms. **(B)** The gene expression profile of *CsHDACs* in the seed, flower, bract, leaf, and stem. The row scale on the values has been performed, and the FPKM value of each gene was presented in the figure. **(C)** Expression patterns of the selected *CsHDACs* genes in the flower, bract, stem, leaf, and seed. The characters on the x axis indicate different organs and tissues. The y axis shows the relative level of gene expression. The *EF1-α* gene was used as an internal reference.

OsTPR1 (topless-related 1) contributing to the repression of *OsLEA1* and *OsSOS1* expression (Cheng et al., 2018). *MaHDAC1* and the transcription repressor *MaERF11* inhibited the expression of genes related to maturation (Han et al., 2016). Combined with previous studies on the regulation of secondary metabolites by HDACs, tissue-specific expression, and co-expression analysis, we initially screened five candidate genes that may be related to cannabinoid regulation. Furthermore, we compared the domain amino acid sequences of CsHDACs and MaHDA1, constructed the NJ tree, and performed BLAST sequence alignment. The results showed that *CsHDA7* and *MaHDA1* had 86.98% amino acid similarity (**Supplementary Figure S5**), suggesting that *CsHDA7* and *MaHDA1* have a similar effect.

TSA has been shown to inhibit the activity of histone deacetylase. Similarly, the expression of CsHDACs was significantly depressed by TSA during this study. The synthesis of cannabinoids originated from the MEP pathway and fatty acid pathway. Both pathways differed after TSA treatment regardless of gene expression or metabolite accumulation, indicating that TSA can affect the biosynthesis of cannabinoids in several ways. However, it is still unclear whether TSA plays a role *via* inhibiting the expression of related genes or by mediating the structure of chromatin by repressing the activity of histone deacetylase in the cannabinoid synthesis pathway (**Supplementary Figure S4**).

CONCLUSION

We identified 14 CsHDAC family members and analyzed their structural characteristics, evolutionary relationships, and spatial expression patterns. By combining RNA-seq with qRT-PCR analysis, we predicted that five HDACs were associated with cannabinoid synthesis. Furthermore, the reduction of HDAC through TSA treatment directly contributed to the expression of related genes in cannabinoid synthesis and the changes in synthetic precursors of cannabinoids. However, both genes and the synthetic

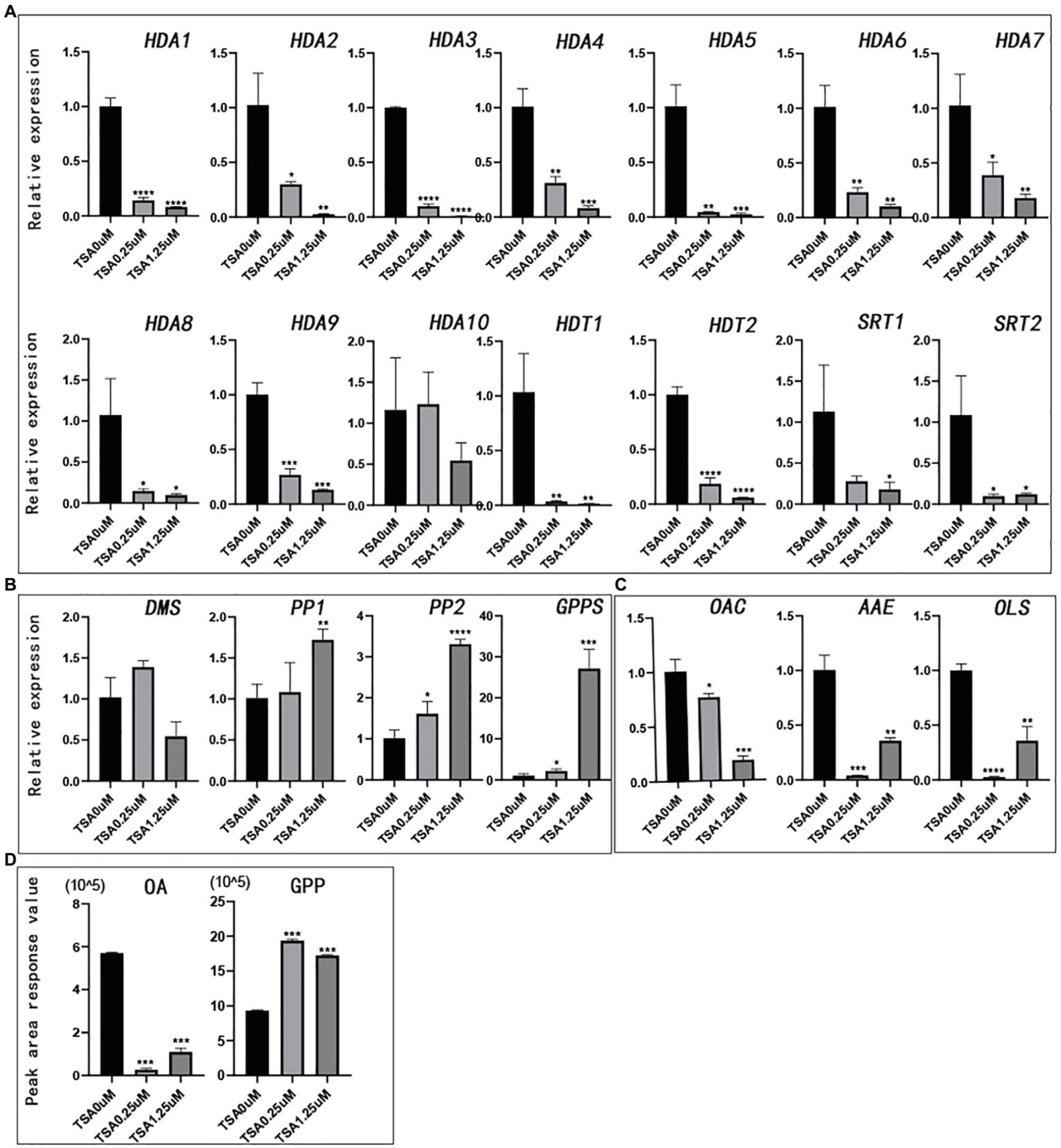

FIGURE 7 | The relative expression of genes and the peak area of synthetic precursors OA and GPP after TSA treatment. The control was performed with 0 μm TSA (DMSO matrix) treatment. n = 3. **(A)** The relative expression of partial histone deacetylase genes; **(B)** The relative expression of key genes in the MEP pathway; **(C)** The relative expression of key genes in the fatty acid pathway; and **(D)** Peak area of synthetic precursors OA and GPP. *value of $p < .05$, **value of $p < 0.01$, ***value of $p < 0.001$, and ****value of $p < 0.0001$.

precursors involved in the fatty acid and MEP pathways behaved opposite with the TSA treatment, implying the complexity of HDACs in cannabinoid synthesis. Therefore, the function of candidate genes in cannabinoid synthesis should be thoroughly studied in the future.

DATA AVAILABILITY STATEMENT

The datasets presented in this study can be found in online repositories. The names of the repository/repositories and accession number(s) can be found in the article/**Supplementary Material**.

AUTHOR CONTRIBUTIONS

ML, WS, and YM contributed to conception of the study. LY wrote the manuscript. LY, XM, XY, SC, and JCL conducted the bioinformatics analysis. LY, YZ, and SW contributed to data visualization. LY and YM performed the qRT-PCR experiment. JL, LY, and GQ performed the metabolic experiment. WC completed the data extraction. ML and WS revised the manuscript. SC, WS, and XL contributed to supervision. All authors have read and agreed to the published version of the manuscript.

FUNDING

This research received funding from the Scientific and Technological Innovation Project of China Academy of Chinese Medical Sciences (CI2021A04806 and CI2021A04008).

SUPPLEMENTARY MATERIAL

The Supplementary Material for this article can be found online at: https://www.frontiersin.org/articles/10.3389/fpls.2021.755494/full#supplementary-material

REFERENCES

Appendino, G., Gibbons, S., Giana, A., Pagani, A., Grassi, G., Stavri, M., et al. (2008). Antibacterial cannabinoids from *Cannabis sativa*: A structure-activity study. *J. Nat. Prod.* 71, 1427–1430. doi: 10.1021/np8002673

Booth, J. K., Yuen, M., Jancsik, S., Madilao, L. L., Page, J. E., and Bohlmann, J. (2020). Terpene synthases and terpene variation in *Cannabis sativa*. *Plant Physiol.* 184, 130–147. doi: 10.1104/pp.20.00593

Brownell, J. E., Zhou, J., Ranalli, T., Kobayashi, R., Edmondson, D. G., Roth, S. Y., et al. (1996). Tetrahymena histone acetyltransferase A: A homolog to yeast Gcn5p linking histone acetylation to gene activation. *Cell* 84, 843–851. doi: 10.1016/S0092-8674(00)81063-6

Burstein, S. (2015). Cannabidiol (CBD) and its analogs: A review of their effects on inflammation. *Bioorg. Med. Chem.* 23, 1377–1385. doi: 10.1016/j.bmc.2015.01.059

Causier, B., Ashworth, M., Guo, W., and Davies, B. (2012). The TOPLESS interactome: A framework for gene repression in Arabidopsis. *Plant Physiol.* 158, 423–438. doi: 10.1104/pp.111.186999

Chaudhary, S., Jabre, I., Reddy, A., Staiger, D., and Syed, N. (2019). Perspective on alternative splicing and proteome complexity in plants. *Trends Plant Sci.* 24, 496–506. doi: 10.1016/j.tplants.2019.02.006

Chen, C., Chen, H., Zhang, Y., Thomas, H. R., Frank, M. H., He, Y., et al. (2020). TBtools: an integrative toolkit developed for interactive analyses of big biological data. *Mol. Plant* 13, 1194–1202. doi: 10.1016/j.molp.2020.06.009

Cheng, X., Zhang, S., Tao, W., Zhang, X., Liu, J., Sun, J., et al. (2018). Indeterminate spikelet1 recruits histone deacetylase and a transcriptional repression complex to regulate rice salt tolerance1. *Plant Physiol.* 178, 824–837. doi: 10.1104/pp.18.00324

Dangl, M., Brosch, G., Haas, H., Loidl, P., and Lusser, A. (2001). Comparative analysis of HD_2 type histone. Deacetylases in higher plants. *Planta* 275, 280–285. doi: 10.1007/s004250000506

De Meijer, E. P. M., and Hammond, K. M. (2005). The inheritance of chemical phenotype in *Cannabis sativa* L. *Genitics.* 145, 189–198. doi: 10.1007/s10681-005-1164-8

Frye, R. A. (2000). Phylogenetic classification of prokaryotic and eukaryotic Sir2-like proteins. *Biochem. Biophys. Res. Commun.* 273, 793–798. doi: 10.1006/bbrc.2000.3000

Fu, W., Wu, K., and Duan, J. (2007). Sequence and expression analysis of histone deacetylases in rice. *Biochem. Biophys. Res. Commun.* 356, 843–850. doi: 10.1016/j.bbrc.2007.03.010

Gao, H., Li, F., and Xu, Z. (2019). Genome-wide analysis of methyl jasmonate-regulated isoform expression in the medicinal plant Andrographis paniculata. Ind. *Crops. Prod.* 135, 39–48. doi: 10.1016/j.indcrop.2019.04.023

Graessle, S., Loidl, P., and Brosch, G. (2001). Histone acetylation: plants and fungi as model systems for the investigation of histone deacetylases. *Cell. Mol. Life Sci.* 58, 704–720. doi: 10.1007/PL00000894

Gu, X., Jiang, D., Yang, W., Jacob, Y., Michaels, S. D., and He, Y. (2011). Arabidopsis homologs of retinoblastoma-associated protein 46/48 associate with a histone deacetylase to act redundantly in chromatin silencing. *PLoS Genet.* 7:e1002366. doi: 10.1371/journal.pgen.1002366

Guarente, L. (2000). Sir2 links chromatin silencing, metabolism, and aging. *Genes Dev.* 14, 1021–1026.

Haigis, M. C., and Guarente, L. P. (2006). Mammalian sirtuins - emerging roles in physiology, aging, and calorie restriction. *Genes Dev.* 20, 2913–2921. doi: 10.1101/gad.1467506

Han, Y. C., Kuang, J. F., Chen, J. Y., Liu, X. C., Xiao, Y. Y., Fu, C. C., et al. (2016). Banana transcription factor MaERF11 recruits histone deacetylase MaHDA1 and represses the expression of MaACO1 and expansins during fruit ripening. *Plant Physiol.* 171, 1070–1084. doi: 10.1104/pp.16.00301

Hollender, C., and Liu, Z. (2008). Histone deacetylase genes in Arabidopsis development. *J. Integr. Plant Biol.* 50, 875–885. doi: 10.1111/j.1744-7909.2008.00704.x

Ikeda, M., and Ohme-Takagi, M. (2009). A novel group of transcriptional repressors in Arabidopsis. *Plant Cell Physiol.* 50, 970–975. doi: 10.1093/pcp/pcp048

Jing, Y., Guo, Q., and Lin, R. (2020). The SNL-HDA19 histone deacetylase complex antagonizes HY5 activity to repress photomorphogenesis in Arabidopsis. *New Phytol.* 229, 3221–3236. doi: 10.1111/nph.17114

König, A. C., Hartl, M., and Pham, P. A. (2014). The Arabidopsis class II sirtuin is a lysine deacetylase and interacts with mitochondrial energy metabolism. *Plant Physiol.* 164, 1401–1414. doi: 10.1104/pp.113.232496

Kornet, N., and Scheres, B. (2009). Members of the GCN5 histone acetyltransferase complex regulate PLETHORA-mediated root stem cell niche maintenance and transit amplifying cell proliferation in Arabidopsis. *Plant Cell* 21, 1070–1079. doi: 10.1105/tpc.108.065300

Kurdistani, S. K., and Grunstein, M. (2003). Histone acetylation and deacetylation in yeast. *Nay. Rev. Mol. Cell Biol.* 4, 276–284. doi: 10.1038/nrm1075

Lee, K., Park, O. S., Jung, S. J., and Seo, P. J. (2016). Histone deacetylation-mediated cellular dedifferentiation in Arabidopsis. *J. Plant Physiol.* 191, 95–100. doi: 10.1016/j.jplph.2015.12.006

Li, H., Soriano, M., Cordeverer, J., Muiño, J. M., Riksen, T., Fukuoka, H., et al. (2014). Thehistone decetylase inhibitor trichostatin A promotes Totipotency in the malle gaming. *Plan Cell.* 26, 195–2009. doi: 10.1105/tpc.113.116491

Liu, X., Luo, M., and Wu, K. (2012). Epigenetic interplay of histone modifications and DNA methylation mediated by HDA6. *Plant Signal. Behav.* 7, 633–635. doi: 10.4161/psb.19994

Luo, X., Reiter, M. A., d'Espaux, L., Wong, J., Denby, C. M., Lechner, A., et al. (2019). Complete biosynthesis of cannabinoids and their unnatural analogues in yeast. *Nature* 567, 123–126. doi: 10.1038/s41586-019-0978-9

Lusser, A., Kölle, D., Loidl, P., and Lusser, A. (2001). Trends in plant science histone acetylation lessons from the plant kingdom. *Trends Plant Sci.* 6, 59–65. doi: 10.1016/S1360-1385(00)01839-2

Lydon, J., Teramura, A. H., and Coffman, C. B. (1987). UV-B radiation effects on photosynthesis, growth and cannabinoid production of two *Cannabis sativa* CHEMOTYPES. *Photochem. Photobiol.* 46, 201–206. doi: 10.1111/j.1751-1097.1987.tb04757.x

Marks, M. D., Tian, L., Wenger, J. P., Omburo, S. N., Soto-Fuentes, W., He, J., et al. (2009). Identification of candidate genes affecting Δ9-tetrahydrocannabinol biosynthesis in *Cannabis sativa*. *J. Exp. Bot.* 60, 3715–3726. doi: 10.1093/jxb/erp210

Morimoto, S., Komatsu, K., Taura, F., and Shoyama, Y. (1997). Enzymological evidence for cannabichromenic acid biosynthesis. *J. Nat. Prod.* 60, 854–867. doi: 10.1021/np970210y

Nicolas-Francès, V., Grandperret, V., Liegard, B., Jeandroz, S., Vasselon, D., Aimé, S., et al. (2018). Evolutionary diversification of type-2 HDAC structure, function and regulation in Nicotiana tabacum. *Plant Sci.* 269, 66–74. doi: 10.1016/j.plantsci.2018.01.007

Nicot, N., Hausman, J. F., Hoffmann, L., and Evers, D. (2005). Housekeeping gene selection for real-time RT-PCR normalization in potato during biotic and abiotic stress. *J. Exp. Bot.* 56, 2907–2914. doi: 10.1093/jxb/eri285

Pacher, P., Bátkai, S., and Kunos, G. (2006). The endocannabinoid system as an emerging target of pharmacotherapy. *Pharmacol. Rev.* 58, 389–462. doi: 10.1124/pr.58.3.2

Pandey, R., Mu, A., Ller, È., Napoli, C. A., Selinger, D. A., Pikaard, C. S., et al. (2002). Analysis of histone acetyltransferase and histone deacetylase families of *Arabidopsis thaliana* suggests functional diversification of chromatin modification among multicellular eukaryotes. *Nucleic Acids Res.* 30, 5036–5055. doi: 10.1093/nar/gkf660

Peng, M., Ying, P., Liu, X., Li, C., Xia, R., Li, J., et al. (2017). Genome-wide identification of histone modifiers and their expression patterns during fruit abscission in litchi. *Front. Plant Sci.* 8:639. doi: 10.3389/fpls.2017.00639

Probst, A. V., Fagard, M., Proux, F., Mourrain, P., Boutet, S., Earley, K., et al. (2004). Arabidopsis histone deacetylase HDA6 is required for maintenance of transcriptional gene silencing anddetermines nuclear organization of rDNA repeats. *Plant Cell* 16, 1021–1034. doi: 10.1105/tpc.018754

Schachtsiek, J., Warzecha, H., Kayser, O., and Stehle, F. (2018). Current perspectives on biotechnological cannabinoid production in plants. *Planta Med.* 84, 214–220. doi: 10.1055/s-0043-125087

Song, Y. (2010). Interaction and function study of Arabidopsis DNA methyltransferase DNMT2 and histone deacetylase family HD2. *Biochem. Biophys. Res. Commun.* 396, 187–192. doi: 10.7666/d.Y1704966

Song, C. P., and Galbraith, D. W. (2006). AtSAP18, an orthologue of human SAP18, is involved in the regulation of salt stress and mediates transcriptional repression in Arabidopsis. *Plant Mol. Biol.* 60, 241–257. doi: 10.1007/s11103-005-3880-9

Su, L. C., Ding, B., Liu, S., Limei, L., Yuting, Z., and Ling, L. (2015). Isolation and characterization of an osmotic stress and ABA induced histone deacetylasm. Arachis Hygogaea. *Font. PlantSci.* 6, 512–522. doi: 10.3389/fpls.2015.00512

VanBakel, H., Stout, J. M., Cote, A. G., Tallon, C. M., Sharpe, A. G., Hughes, T. R., et al. (2011). The draft genome and transcriptome of *Cannabis sativa*. *Genome Biol.* 12:R102. doi: 10.1186/gb-2011-12-10-r102

Vindenes, V. (2017). Increasing plant concentrations of THC and implications on health related disorders. *Handbook of Cannabis and Related Pathologies*. 3, 24–32.

Wang, Y. P., Tang, H. B., DeBarry, J. D., Tan, X., Li, J., Wang, X., et al. (2012). MCScanX: a toolkit for detection and evolutionary analysis of gene synteny and collinearity. *Nucleic Acids Res.* 40:e49. doi: 10.1093/nar/gkr1293

Wang, Z. B., Zang, C., Cui, K., Schones, D. E., Barski, A., Peng, W., et al. (2009). Genome-wide mapping of HATs and HDACs reveals distinct functions in active and inactive genes. *Cell* 138, 1019–1031. doi: 10.1016/j.cell.2009.06.049

Waterborg, J. H. (2011). "Plant histone acetylation: In the beginning …" in *Biochimica et Biophysica Acta Gene Regulatory Mechanisms*. ed. G. Grafi, *vol.* 1809 (Elsevier), 353–359.

Wu, K., Tian, L., Mallik, K., Brown, D., and Miki, B. (2000). Functional analysis of HD2 histone deacetylase homologues in *Arabidopsis thaliana*. *Plant J.* 22, 19–27. doi: 10.1046/j.1365-313x.2000.00711.x

Xu, Z. C., Ranran, G., Pu, X. D., Xu, R., Wang, J., Zheng, S., et al. (2020). Comparative genome analysis of Scutellaria baicalensis and Scutellaria barbata reveals the evolution of active flavonoid biosynthesis. *Geno. Proteo. Bioinfo.* 18, 230–240. doi: 10.1016/j.gpb.2020.06.002

Yang, Z., and Nielsen, R. (2000). Estimating synonymous and nonsynonymous substitution rates under realistic evolutionary models. *Mol. Biol. Evol.* 17, 32–43. doi: 10.1093/oxfordjournals.molbev.a026236

Yang, X. J., and Seto, E. (2007). HATs and HDACs: From structure, function and regulation to novel strategies for therapy and prevention. *Oncogene* 26, 5310–5318. doi: 10.1038/sj.onc.1210599

Yang, C., Shen, W., Chen, H., Chu, L., and Xu, Y. (2018). Characterization and subcellular localization of histone deacetylases and their roles in response to abiotic stresses in soybean. *BMC Plant Biol.* 18, 1–13. doi: 10.1186/s12870-018-1454-7

Yu, C. W., Liu, X., Luo, M., Chen, C., Lin, X., Tian, G., et al. (2011). Histonedeacetylase6 interacts with flowering locus D and regulatesflowering in Arabidopsis. *Plant Physiol.* 156, 173–184. doi: 10.1104/pp.111.174417

Zhang, Y. (2018). HDT1 histone deacetylase and MYB211 ellipse regulate the growth and development of plant cambium and xylem. doi: 10.26949/d.cnki.gblyu.2018.000130

Zhang, Z., Wang, B., Wang, S., Lin, T., and Yang, L. (2020). Genome-wide target mapping shows histone deacetylase complex1 regulates cell proliferation in cucumber fruit. *Plant Physiol.* 182, 167–184. doi: 10.1104/pp.19.00532

Zhao, L., Lu, J., Zhang, J., Wu, P. Y., Yang, S., and Wu, K. (2015). Identification and characterization of histone deacetylases in tomato (Solanum lycopersicum). *Front. plant science* 5:760. doi: 10.3389/fpls.2014.00760

Zheng, Y., Ge, J., Bao, C., Chang, W., and Liu, J. (2020). Histone deacetylase HDA9 and WRKY53 transcription factor are mutual antagonists in regulation of plant stress response. *Mol. Plant* 13, 598–611. doi: 10.1016/j.molp.2019.12.011

Zhou, Y., Tan, B., Luo, M., Li, Y., Liu, C., and Chen, C. (2013). Histone deacetylase19 interacts with HSL1 and participates in the repression of seed maturation genes in Arabidopsis seedlings. *Plant Cell* 25, 134–148. doi: 10.1105/tpc.112.096313

Zuardi, A. W. (2006). History of cannabis as a medicine: A review. *Revista Brasileira dePsiquiatria* 28, 153–157. doi: 10.1590/S1516-44462006000200015

Conflict of Interest: The authors declare that the research was conducted in the absence of any commercial or financial relationships that could be construed as a potential conflict of interest.

Publisher's Note: All claims expressed in this article are solely those of the authors and do not necessarily represent those of their affiliated organizations, or those of the publisher, the editors and the reviewers. Any product that may be evaluated in this article, or claim that may be made by its manufacturer, is not guaranteed or endorsed by the publisher.

Copyright © 2021 Yang, Meng, Chen, Li, Sun, Chen, Wang, Wan, Qian, Yi, Li, Zheng, Luo, Liu and Mi. This is an open-access article distributed under the terms of the Creative Commons Attribution License (CC BY). The use, distribution or reproduction in other forums is permitted, provided the original author(s) and the copyright owner(s) are credited and that the original publication in this journal is cited, in accordance with accepted academic practice. No use, distribution or reproduction is permitted which does not comply with these terms.

frontiers in Plant Science

ORIGINAL RESEARCH
published: 21 October 2021
doi: 10.3389/fpls.2021.746117

Integrative Omics Analyses Reveal the Effects of Copper Ions on Salvianolic Acid Biosynthesis

Yaping Xiang[1†], *Xiaoxiao Wang*[1†], *Wei Song*[1†], *Jinfa Du*[2] *and Xiaojian Yin*[1*]

[1] State Key Laboratory of Natural Medicines, Department of Pharmacognosy, Institute of Pharmaceutical Science, China Pharmaceutical University, Nanjing, China, [2] School of Traditional Chinese Pharmacy, China Pharmaceutical University, Nanjing, China

Salvianolic acids, a group of secondary metabolites produced by *Salvia miltiorrhiza*, are widely used for treating cerebrovascular diseases. Copper is recognized as a necessary microelement and plays an essential role in plant growth. At present, the effect of copper on the biosynthesis of SalAs is unknown. Here, an integrated metabolomic and transcriptomic approach, coupled with biochemical analyses, was employed to dissect the mechanisms by which copper ions induced the biosynthesis of SalAs. In this study, we identified that a low concentration (5 μM) of copper ions could promote growth of *S. miltiorrhiza* and the biosynthesis of SalAs. Results of the metabolomics analysis showed that 160 metabolites (90 increased and 70 decreased) were significantly changed in *S. miltiorrhiza* treated with low concentration of copper ions. The differential metabolites were mainly involved in amino acid metabolism, the pentose phosphate pathway, and carbon fixation in photosynthetic organisms. The contents of chlorophyll *a*, chlorophyll *b*, and total chlorophyll were significantly increased in leaves of low concentration of copper-treated *S. miltiorrhiza* plants. Importantly, core SalA biosynthetic genes (*laccases* and *rosmarinic acid synthase*), SalA biosynthesis-related transcription factors (*MYBs* and *zinc finger CCCH domain-containing protein 33*), and chloroplast proteins-encoding genes (*blue copper protein* and *chlorophyll-binding protein*) were upregulated in the treated samples as indicated by a comprehensive transcriptomic analysis. Bioinformatics and enzyme activity analyses showed that laccase 20 contained copper-binding motifs, and its activity in low concentration of copper ions-treated *S. miltiorrhiza* was much higher than that in the control. Our results demonstrate that enhancement of copper ions of the accumulation of SalAs might be through regulating laccase 20, MYBs, and zinc finger transcription factors, and photosynthetic genes.

Keywords: copper ion treatment, metabolomics, transcriptomic, *Salvia miltiorrhiza*, salvianolic acids

OPEN ACCESS

Edited by:
Lei Zhang,
Second Military Medical University, China

Reviewed by:
Shujuan Zhao,
Shanghai University of Traditional Chinese Medicine, China
Zhichao Xu,
Northeast Forestry University, China

***Correspondence:**
Xiaojian Yin
ajian.517@163.com

[†]These authors have contributed equally to this work and share first authorship

Specialty section:
This article was submitted to Plant Metabolism and Chemodiversity, a section of the journal Frontiers in Plant Science

Received: *23 July 2021*
Accepted: *21 September 2021*
Published: *21 October 2021*

Citation:
Xiang Y, Wang X, Song W, Du J and Yin X (2021) Integrative Omics Analyses Reveal the Effects of Copper Ions on Salvianolic Acid Biosynthesis. Front. Plant Sci. 12:746117. doi: 10.3389/fpls.2021.746117

INTRODUCTION

Copper, a necessary microelement in plants, plays an essential role in various physiological activities during plant growth and development, such as cell wall metabolism, hormone signaling, photosynthesis, and redox reactions (Choudhary et al., 2012; De Caroli et al., 2020; Ding et al., 2020; Saleem et al., 2020). Copper is a redox-active transition metal, and two valence states (Cu^{2+} and Cu^{+}) exist under physiological conditions. Copper can work as a metal cofactor in metalloproteins

involved in electron transport and oxidative stress response (Quist et al., 2017). In chloroplasts, copper is a constituent of plastocyanin (Pc), the most abundant copper protein in plant chloroplasts, which acts as an electron carrier in primary photosynthetic reactions (Droppa et al., 1984). Copper also works as a constituent of Cu/Zn-superoxide dismutase (Cu/Zn-SOD), localized in the stroma that protects against reactive oxygen species (Yruela, 2009). Due to these characters, copper ion plays an important role in regulating plant physiology.

Although copper is indispensable in plant development, most studies have reported that excessive copper causes toxicity to plants *via* the production of reactive oxygen species (ROS) that can oxidize biological macromolecules, such as lipids and nucleic acids, and cause enzyme inactivation (Andre et al., 2010). It has been reported that excessive copper causes rice cell death by increasing the ROS level in rice radicles (Zhang et al., 2017). However, a low dose of copper can enhance enzyme activity to increase the production of plant secondary metabolites (Ibrahim et al., 2017). Treatment of Arabidopsis seedlings with different concentrations of copper showed that the right amount of copper increased the meristem size of the seedlings (Song et al., 2017). Although pieces of research on copper have reported its role in several biological functions involving cytochrome c oxidase, plastocyanin, and ethylene receptors (Burkhead et al., 2009; Song et al., 2017), the majority of previous studies have not focused on whether copper ions are involved in plant secondary metabolism. Therefore, studies are needed to improve our understanding of the role of copper in plant secondary metabolism.

Salvia miltiorrhiza, a traditional Chinese herb, is widely used in the treatment of cardiovascular diseases. Water-soluble phenolic acids, such as salvianolic acid A, salvianolic acid B (Sal B), and rosmarinic acid (RA), are the essential active compounds in the roots of *S. miltiorrhiza* (Huang et al., 2019). There are two biosynthetic routes for phenolic acid in plants: the tyrosine-derived and phenylpropanoid pathways. In the tyrosine-derived pathway, tyrosine is converted to 4-hydroxyphenyllactate under the action of various enzymes, including tyrosine aminotransferase and 4-hydroxyphenylpyruvate reductase. In the phenylpropanoid pathway, phenylalanine is converted to 4-coumaroyl-CoA under the action of various enzymes, including phenylalanine ammonia-lyase, cinnamic acid 4-hydroxylase, and 4-coumarate: CoA ligase. Rosmarinic acid synthase catalyzes the transformation of 4-coumaroyl-CoA and 4-hydroxyphenyllactate to rosmarinic acid (Ma et al., 2013; Shi et al., 2019). The molecular mechanism by which rosmarinic acid converts to salvianolic acid B is still not completely understood. Recently, laccase has been found to catalyze the conversion of rosmarinic acid to salvianolic acid E, which is then transformed into salvianolic acid B and other compounds (Li et al., 2019a; Wang et al., 2019). Furthermore, many transcription factors also regulate the biosynthesis of phenolic acids (Xing et al., 2018; Sun et al., 2019; Deng et al., 2020a; Yin et al., 2020).

As ceruloplasmin oxidases, laccases are widely distributed in all kinds of organisms, including bacteria, fungi, insects, and plants. Laccases belong to the multicopper oxidases family, and four copper ions existed in laccase (Hoegger et al., 2006). Laccases contain three types of catalytic sites (T1, T2, and T3), and T1 site is capable of oxidating substrates, while T2/3 sites are responsible for the consumption of oxygen and the generation of water (Solomon et al., 1996; Riva, 2006). T1 site containing one blue copper ion is mainly responsible for taking the electrons from the substrate after the laccase protein binds to the substrate. The remained three copper ions existed in T2 and T3 sites; they, together, form into the T2/T3 trinuclear center (copper cluster) (Patel et al., 2019). After the T1-copper ion obtains electrons, the electrons will be transferred to the T2/T3 trinuclear center *via* the amino acid bridge, and oxygen molecules obtained from the environment are reduced to produce water (Jones et al., 2015). In a word, the process of laccase catalyzes the oxidation by taking electrons from the substrate and transferring them to the corresponding domains and reacts with oxygen in the environment to form water. Meanwhile, the substrate loses electrons and becomes free radicals. To date, a large number of laccases have been identified and reported to exert their function in plant lignin biosynthesis, cell wall biosynthesis, and flavonoid biosynthesis (Turlapati et al., 2011). In *Arabidopsis*, 17 laccases have been annotated, which are clustered into six distinct clades (McCaig et al., 2005; Turlapati et al., 2011). In *S. miltiorrhiza*, laccases were also systemically investigated and demonstrated to play a great role in plant growth, development, and secondary metabolites biosynthesis (Zhou et al., 2018; Li et al., 2019a).

When a plant encounters adverse stress, the plant's own stress resistance mechanism will be activated and related genes will control the process of protein synthesis to protect themselves against adversity. Here, metabolomics and transcriptomics approaches were applied to reveal how copper affects the biosynthesis of phenolic acids in *S. miltiorrhiza*. The genes that respond to copper and the genes in the biosynthetic pathway of salvanoic acids (SalAs) were analyzed. Our findings are of great significance in understanding the underlying mechanism of the induction of the biosynthesis of SalAs under copper treatment and provide potential approach to improve SalA content in *S. miltiorrhiza*.

METHODS

Plant Materials and Treatment

Salvia miltiorrhiza was cultivated at 25°C with a 16-h-light/8-h-dark cycle in MS basal medium containing 3% sugar and 8% agar. $CuSO_4{\cdot}5H_2O$ (Sinopharm Chemical Reagent Company., Ltd, China) was dissolved in distilled water to make concentrations of 5, 25, and 100 mM. All the prepared $CuSO_4{\cdot}5H_2O$ were sterilized through 0.22-μm filters and then added to MS basal medium to a final concentration of 5, 25, or 100 μM. *S. miltiorrhiza* was treated with different concentrations of $CuSO_4{\cdot}5H_2O$ for 5 days, and then plant matter was collected for the following experiments.

Phenotype and Fresh Weight

After 5 days of treatment with different concentrations of $CuSO4{\cdot}5H_2O$, a photo *of S. miltiorrhiza* planted in a culture flask was taken. To measure fresh weight, the whole plant of *S. miltiorrhiza* was taken out from the culture flask, washing away culture medicum, and measured with electronic balance. To

accurately reflect fresh weight changes, at least four plants were used each time, and average weight was calculated.

High-Performance Liquid Chromatography (HPLC)

To extract phenolic acids, fresh roots of copper-treated or non-treated *S. miltiorrhiza* were collected from a culture flask, dried at 55°C until the weight remained constant, and then grounded into powder. Each sample of 0.1 g was added to 1-ml methanol: water (70: 30, v v-1), followed by 1-h ultrasound and centrifugation at 12,000 rpm for 20 min. The supernatant was then removed and filtered through a 0.22-μm filter. HPLC was performed on an Agilent 1290 with a DAD detector (Agilent Technologies, USA), equipped with an Agilent ODS-SP 5-μm 4.6 mm × 250 mm column. The mobile phase was H_2O (0.1% formic acid, A) and acetonitrile (B). The HPLC program was set to the following line gradient: 10–25% of B for 0–10 min, 25–27% of B for 10–15 min, 27–55% of B for 15–20 min, 55–95% of B for 20–21 min, held 5 min, 95–10% of B for 26–27 min, and 10% of B for 27–30 min. The flow rate was 1 ml/min, the column temperature was set to 35°C, sample injection volume was 10 μl, and the wavelength was 280 nm. Sal B and RA standards (Shanghai Yuanye Bio-Technology Co., Ltd, China) were configured as a mixed standard solution with a concentration of 0.25 mg/ml. The standard curve method was used to calculate the content of Sal B and RA. The experiment was performed with four repetitions, and data were expressed as mean ± SD.

Ultra-Performance Liquid Chromatography-Quadrupole-Time of Flight-Mass Spectrometry (UPLC-QTOF MS)

For metabolomics analysis, the same samples were analyzed by LC-MS using an Agilent 6545A Q/TOF mass spectrometer equipped with an electrospray ion (ESI) source. In the negative ion mode, the following conditions were used: a drying N2 gas flow rate, 8 L/min; temperature, 320°C; nebulizer, 35 psig; capillary, 3,000 V; skimmer, 65 V; OCT RFV, 750 V. Mass spectra were recorded in a full-scan mode from 100 to 1,200 m/z range. Agilent 1290 Infinity Ultra-performance liquid chromatography (UPLC, Agilent technologies, USA), equipped with an Agilent ODS-SP 5 μm 4.6 mm × 250 mm column, was used to affect the separations. The mobile phase consisted of acetonitrile and 0.03% acetic acid (mobile phase A) and H2O with 0.03% acetic acid (mobile phase B), which were eluted as follows: 10–13% of B at 0–8 min, 13–23% of B at 8–13 min, 23% of B at 25 min, 23–27% of B at 25–45 min, 27–36% of B at 45–54 min, 36–70% of B at 54–65 min, 70–73% of B at 65–75 min, 73–93% of B at 75–85 min, 93–100% of B at 85–87 min, and then held for 5 min. The flow rate was 0.5 ml/min; the column temperature was set at 35°C, sample injection volume was 5 μl, and post-run time was 12 min.

For data analysis, raw LC-MS data were converted to mzData format using DA reprocessor software (Agilent), and the XCMS package in R was used to perform peak finding, filtering, and alignment. Metabioananlyst 4.0 (https://www.metaboanalyst.ca) was used to obtain normalized data. Metabolites with $P < 0.05$ and fold change (copper treatment/blank) >1.5 or <0.5 were regarded as differential metabolites. Metlin database, Human Metabolome database, and our in-house laboratory database were used to identify metabolites. The experiment was performed with four repetitions, and data were expressed as mean ± SD.

Global Transcriptomic Analysis

Total RNA was isolated from fresh root of copper-treated or non-treated *S. miltiorrhiza* using RNeasy Plus Kit with the genomic DNA removal step. The concentration and the quality of extracted RNA were evaluated. cDNA library construction and sequencing were performed by the Biomarker Technologies Corporation (Beijing, China). The raw sequence data were filtered to obtain clean data, which were then compared with the *S. miltiorrhiza* reference genome using HISAT2 software (https://ccb.jhu.edu/software/hisat2/manual.shtml). Fragments Per Kilobase of transcript per Million fragments mapped (FPKM) was used to calculate gene expression. Differential gene expression analysis used edgeR (Robinson et al., 2010), and genes with $p < 0.05$ and fold change >1.5 or <0.5 are regarded as differentially expressed genes (DEGs). The DEGs were classified into functional categories by blasting against the clusters of orthologous groups against the eukaryotic complete genomes (KOG) database (http://www.ncbi.nlm.gov/KOG) and the gene ontology (GO) database (http://geneontology.org/). The experiment was performed with three repetitions, and data were expressed as mean ± SD.

Total RNA Extraction and Reverse Transcription-Quantitative PCR (RT-qPCR)

Total RNA extraction was achieved using a plant total RNA extraction kit (Tiangene Biotech Co., Ltd., China). Briefly, a 0.5-g fresh *S. miltiorrhiza* root was grounded into powder with liquid nitrogen, and extraction was carried out according to the instructions. RNA reverse transcription (Hieff™ First Strand cDNA Synthesis Super Mix, Yeasen, China) and gene quantification (Hieff™ qPCR SYBR Green Master Mix kit, Yeasen, China) were performed following the protocols of the manufacturer. The qPCR conditions were as follows: 95°C for 5 min, followed by 40 cycles of 95°C for 10 s, 60°C for 30 s, and 70°C for 90 s. mRNA expression levels were calculated using the $^{2-\Delta\Delta}$Ct method and presented as a ratio to β-actin. Primer sequences are shown in **Supplementary Table 4**.

Quantification of Laccase Enzyme Activity

A Laccase Activity Detection kit (Solarbio Life Sciences, Beijing, China) was used to detect laccase activity. To detect laccase activity, a 0.1-g fresh *S. miltiorrhiza* root was added to a 1-ml extraction buffer, the mixture was homogenized on ice, and then centrifuged at 12,000 rpm for 20 min at 4°C. The supernatant was then moved to a new centrifuge tube, and the absorbance was measured at 562 nm to determine protein concentration of supernatant using a BCA kit (Good Laboratory Practice Bioscience, Montclair, CA, USA). Subsequently, 150 μL of supernatant was mixed with 850 μL of a working buffer and heated in an oven at 45°C for 3 min. As negative control, 150 μL of an extraction buffer was mixed with 850 μL of the

working buffer and heated in an oven at 45°C for 3 min. Then, the produced ABTS radical was determined through measuring mixture absorbance at 420 nm. Enzyme activity was calculated through measuring ABTS radical content change according to the instructions of the manufacturer.

Phylogenetic Construction of Laccase

The whole genome sequence and protein data from *S. miltiorrhiza* (BioProject: PRJNA287594) were downloaded from the Genome Warehouse in the BIG Data Center (http://gigadb.org/dataset/100164). The whole genome data and protein data of *Arabidopsis thaliana* were downloaded from the *Arabidopsis thaliana* information resource website (TAIR, https://www.arabidopsis.org/). In order to select all the laccases in the genomes of *Salvia miltiorrhiza* and *Arabidopsis thaliana*, we downloaded the unique HMM model (the hidden Markov model) of laccase from the Pfam database. HMMER 3.0 software with hmmsearch was used to search for laccase-conserved domain models, including PF00394, PF07731, and PF07732, in the protein database of *S. miltiorrhiza* and *Arabidopsis thaliana*. A phylogenetic tree was constructed using the maximum likelihood (ML) method with bootstraps in MEGA X software.

Correlation Analysis

FPKM values of genes in copper ion-treated and non-treated groups were used to calculate correlation coefficient. Gene co-expression analysis between the candidate transcription factors and the key genes was performed by the mean of the Pearson correlation test using IBM SPSS Statistics 20. Data are shown as the mean ± SD ($n = 3$) ($^{*}p < 0.05$ and $^{**}p < 0.01$). The correlation coefficient >0.8 was considered to be co-expressed, and the coexpression network was visualized using Cytoscape.

Copper-Response Element Predication in Laccases and Transcription Factors

The promoter sequences of analyzed genes (from 2,000 bp, relative to a translation start site) were extracted using gff file of *S. miltiorrhiza* genome. Core motif of copper-response element (GTAC) (Quinn et al., 2000; Kropat et al., 2005) and metal response-element (TGCxCxC) (Murphy et al., 1999) were predicted in extracted 2,000 bp promoter sequences of laccases and transcription factors using the Plantcare database (Lescot et al., 2002) and visualized by TB tools (Chen et al., 2020). In addition, transcription factors-binding motifs were also predicated in extracted 2,000 bp promoter sequences of laccases.

RESULTS

A Low Concentration of Copper Ions Promoted Plant Growth

To explore the effect of copper on the growth of *S. miltiorrhiza* plants, we exposed the plants to predetermined copper concentrations (0, 5, 25, and 100 μM) and determined the phenotypic changes thereafter. After 5 days of cultivation, the *S. miltiorrhiza* plants wilted under treatments with a greater copper concentration. Compared with the 0 and 5 μM treatments, *S. miltiorrhiza* plants grew slowly and the leaves withered and yellowed in the 25- and 100-μM treatments (**Figure 1A**). It is noteworthy that low concentration of copper (5 μM) significantly promoted plant growth compared with the blank (0 μM) group (**Figure 1A**). Thus, 5 μM of copper was optimum for the growth of the *S. miltiorrhiza* plants.

A Low Concentration of Copper Ions Promoted the Accumulation of Sal B and RA

As the major SalAs, Sal B, and RA are important active secondary metabolites in *S. miltiorrhiza*. To ascertain the most suitable concentration of copper that promotes SalAs biosyntheses, we used HPLC to determine the contents of Sal B and RA in the copper-stressed groups and the blank group. The low concentration of copper treatment increased Sal B by an average of 4.27-fold compared with the control, but the medium and high concentrations of copper treatments decreased Sal B by 2.16- and 2.06-fold, respectively, compared with the control (**Figure 1B** and **Supplementary Figure 1**). Compared with the blank group, low concentration of copper increased RA content 1.55-fold while medium and high concentrations of copper decreased its amount 4.22- and 2.37-fold, respectively (**Figure 1B** and **Supplementary Figure 1**). Based on these findings, it is evident that low concentration of copper promotes the biosyntheses of Sal B and RA.

A Low Concentration of Copper Increases the Content of SalAs

To further confirm the holistic effect of low copper on the accumulation of SalAs in *S. miltiorrhiza*, the plant samples exposed to low concentration of copper and the blank group were analyzed using UPLC-QTOF-MS. In the negative iron model, the total ion chromatogram was different between the control and the low copper treatment (**Supplementary Figure 2**). A total of 2,041 ions were detected (**Figure 2A**). Using the selection criteria of change ratio >1.5 (significant increase; $P < 0.05$) or <0.5 (significant decrease; $P < 0.05$), 90 increased and 70 decreased compounds were detected. The principal component analysis (PCA) analysis showed that the copper stress treatment and control clearly clustered into two categories (**Figure 2B**). Among the different metabolites, 13 SalAs, including Sal B, RA, lithospermic acid, salvianolic acid D, salvianolic acid A, and danshensu, were significantly increased in the low concentration of copper treatment compared with the control (**Figure 3A**), indicating that low copper stress can positively regulate the synthesis of SalAs. The pathway enrichment analysis of differential metabolites showed that copper ions had significant effects on amino acid synthesis and metabolism, the pentose phosphate pathway, and carbon fixation in photosynthesis in *S. miltiorrhiza* (**Figure 3B**).

Transcriptomics Analysis to Identify Genes That Responded to Copper Treatment in *S. miltiorrhiza*

To explore how the low concentration of copper treatment regulated the biosynthesis of SalAs in *S. miltiorrhiza*, a

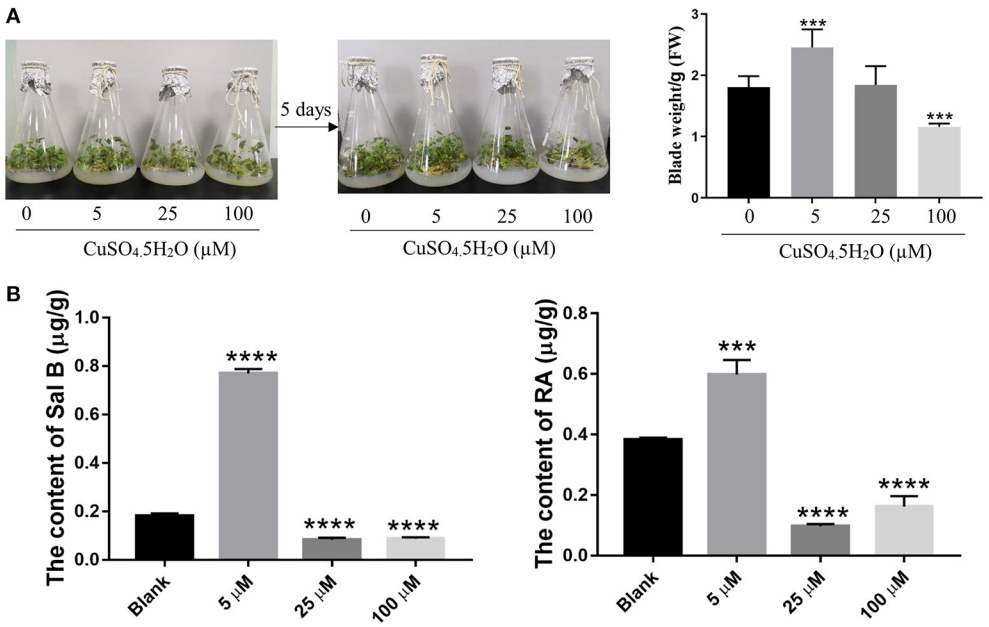

FIGURE 1 | Effect of copper ion treatment on the growth of *Salvia miltiorrhiza* and biosynthesis of salvinolic acids (SalAs). Two-month-old *S. miltiorrhiza* was treated with different concentrations of $CuSO_4.5H_2O$ (0, 5, 25, and 100 μM) for 5 days. **(A)** Phenotype change and weight change of *S. miltiorrhiza* were recorded before and after the treatment. **(B)** The content of salvianolic acid B and rosemarinic acid in untreated and treated *S. miltiorrhiza* using high-performance liquid chromatography (HPLC) with standards. Data represent the mean ± SD of three independent biological replicates. Significant differences between the treatment and control samples were determined using a Student's *T*-test (***$P < 0.001$ and ****$P < 0.0001$).

transcriptome analysis was performed between the control and low copper treatments. Using the selection criteria of the change ratio $P < 0.05$ and fold change >1.5 and <0.5, a total of 418 differential genes were obtained, of which 207 were upregulated and 211 were downregulated in the low copper-treated group compared with the blank group (**Supplementary Table 2**). Gene Ontology (GO) analysis showed that these significantly changed genes were mainly involved in copper ion binding, oxidoreductase, and ROS metabolism (**Figure 4A**). Pathway enrichment analysis showed that the differentially expressed genes are related to tyrosine and phenylalanine metabolism, chlorophyll biosynthesis, plant pathogene interaction, photosynthesis, and plant hormone signal transduction (**Figure 4B**).

A further gene expression pattern indicated that SalAs biosynthesis-related genes (*laccase 20*, *laccase 13*, *laccase 7*, and *rosmarinate synthase*), photosynthesis-related genes (*blue copper protein*, *basic blue protein*, and *chlorophyll A-B-binding protein*), and *zinc transporter 5* were upregulated in the copper-treated group compared with the blank group (**Figure 5A** and **Table 1**). In contrast, copper transport-related genes, such as *copper transporter 6*, *copper transporter 5*, *copper transport protein CCH*, and *copper-transporting ATPase RAN1*, were downregulated in the copper-treated group (**Figure 5A** and **Table 1**). In addition, transcription factors, such as *ethylene-responsive transcription factor 5*, *ERF012*, *ethylene-responsive transcription factor RAP2-7*, *ethylene-responsive transcription factor TINY*, *transcription factor MYB14*, *MYB33*, *MYB73*, *basic helix-loop-helix transcription factor*, and *transcription factor bHLH69*, were responsive to low copper treatment (**Figure 5A** and **Table 1**).

Effect of Copper Ions on the Chlorophyll Content in the Leaves of *S. miltiorrhiza*

To determine whether the gene expression changes corresponded to physiological changes, chlorophyll content and copper content in *S. miltiorrhiza* were measured. Chlorophyll, which plays an extremely important role in photosynthesis, is the main component of chloroplasts in leaves. After the copper ion treatment, we detected the difference in chlorophyll content between the 5-μM copper treatment and the control (**Figure 5B**). The chlorophyll a, chlorophyll b, and total chlorophyll of *S. miltiorrhiza* in the 5-μM copper treatment were 1.08, 0.31, and 1.39 mg/g, respectively. The chlorophyll a, chlorophyll b, and total chlorophyll of *S. miltiorrhiza* in the control were 0.49, 0.03, and 0.52 mg/g, respectively. Compared with the control, the 5-μM copper treatment increased chlorophyll a, chlorophyll b, and total chlorophyll by 2.19, 9.98, and 2.66 times, respectively. Copper content in the treatment group was also significantly increased compared with the control (**Figure 5C**). The greater chlorophyll content increased the photosynthetic ability of the copper treatment group, the growth state of the plant was healthier, the ability of the plant to resist adverse environments was increased, and the treatment was conducive to the accumulation of active products in *S. miltiorrhiza*.

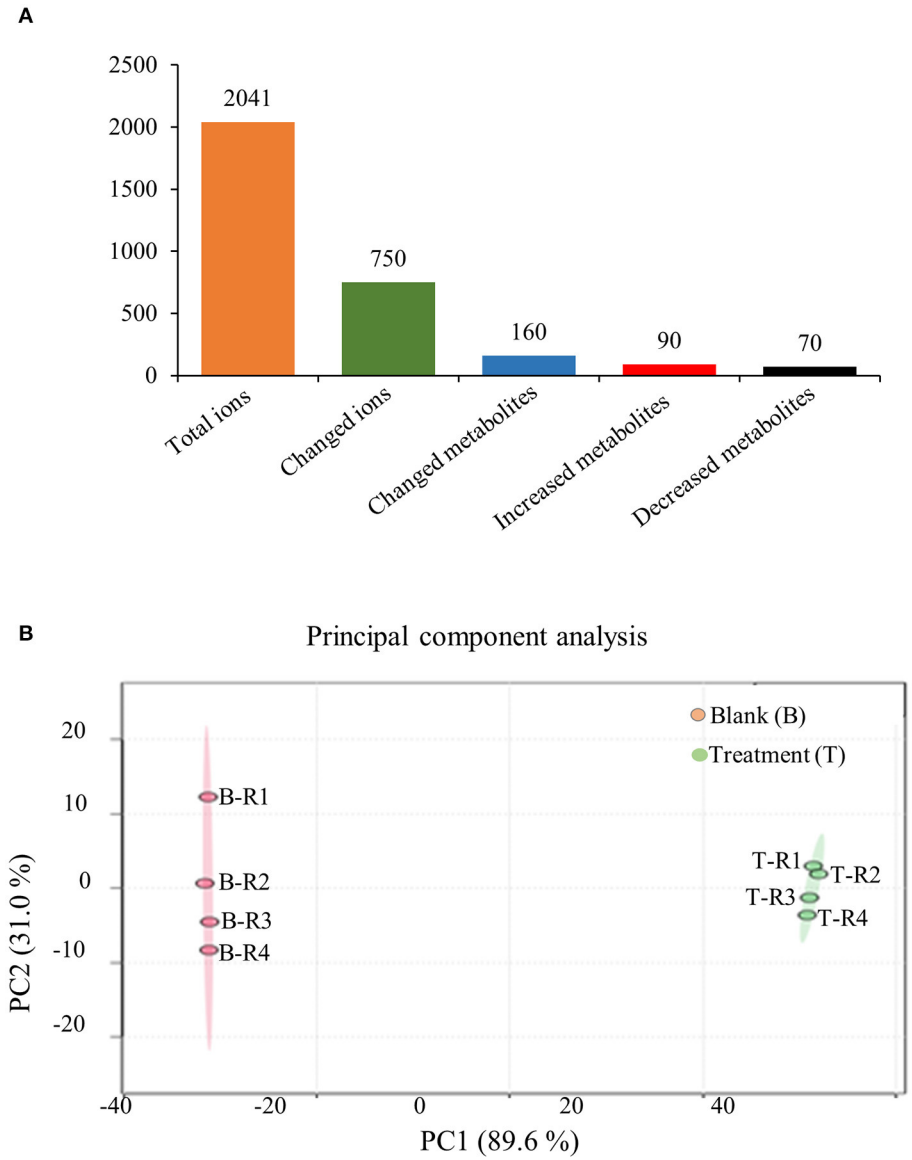

FIGURE 2 | Metabolomic analysis of low concentration of copper ion (LCCI) on the biosynthesis of salvinolic acids (SalAs) in *Salvia miltiorrhiza*. Two-month-old *S. miltiorrhiza* was treated with $CuSO_4.5H_2O$ (5 μM) for 5 days. Metabolites were extracted from roots and subjected to metabolomics analysis by untargeted ultra-performance liquid chromatography-quadrupole-time of flight mass spectrometry (UPLC-Q/TOF-MS). The total ions were counted within 90 min. **(A)** The statistical number of identified ions, metabolites, and significantly changed metabolites is listed. **(B)** Principal component analysis (PCA) and a volcano plot based on identified ions in control and treated samples. To characterize their ion profiles, the identified ions were estimated using a principal component analysis. The significantly changed ions are depicted with a volcano plot. Red dots indicate significantly changed ions.

Bioinformatics and Enzyme Activity Analysis of Copper Ion-Induced Laccase

Based on the transcriptomics result, we verified the mRNA expression of laccase 20, laccase 13, and laccase 7 using RT-qPCR. The results obtained showed 2.3 and 1.4-fold increases in laccase 20 and laccase 13 expressions, respectively, in the low-copper group relative to the control group. Consequently, laccase enzyme activity increased 3.19-fold in the low-copper group compared with the control group (**Figure 6A**). These findings suggest the pivotal role of laccase in the synthesis of salvianolic acids in the presence of low copper. To explore the evolutionary relationships among laccases, the sequences of laccases were extracted from *S. miltiorrhiza* and *A. thaliana*, and a phylogenetic tree was constructed using the ML method with bootstraps in MEGA X software (**Figure 6B**). Laccases in *S. miltiorrhiza* and *Arabidopsis thaliana* were grouped into seven clusters (I, II, III, IV, V, VI, and VII) based on similarity of amino acid sequence. The copper-induced laccases

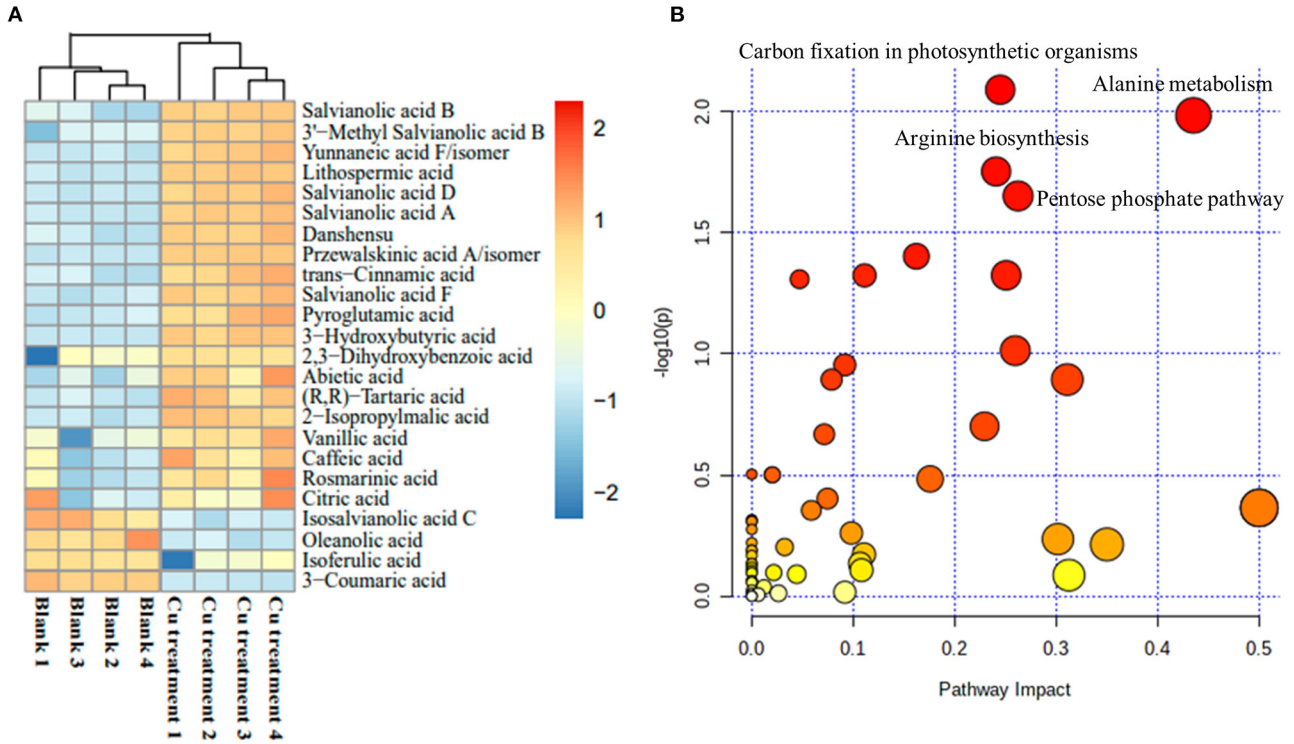

FIGURE 3 | Change of identified salvinolic acids (SalAs). Two-month-old *S. miltiorrhiza* was treated with $CuSO_4.5H_2O$ (5 μM) for 5 days. **(A)** The changes of identified SalAs in control and treated samples were analyzed using a Cluster analysis. **(B)** Pathway enrichment analysis of significantly changed metabolites was performed using the KEGG database.

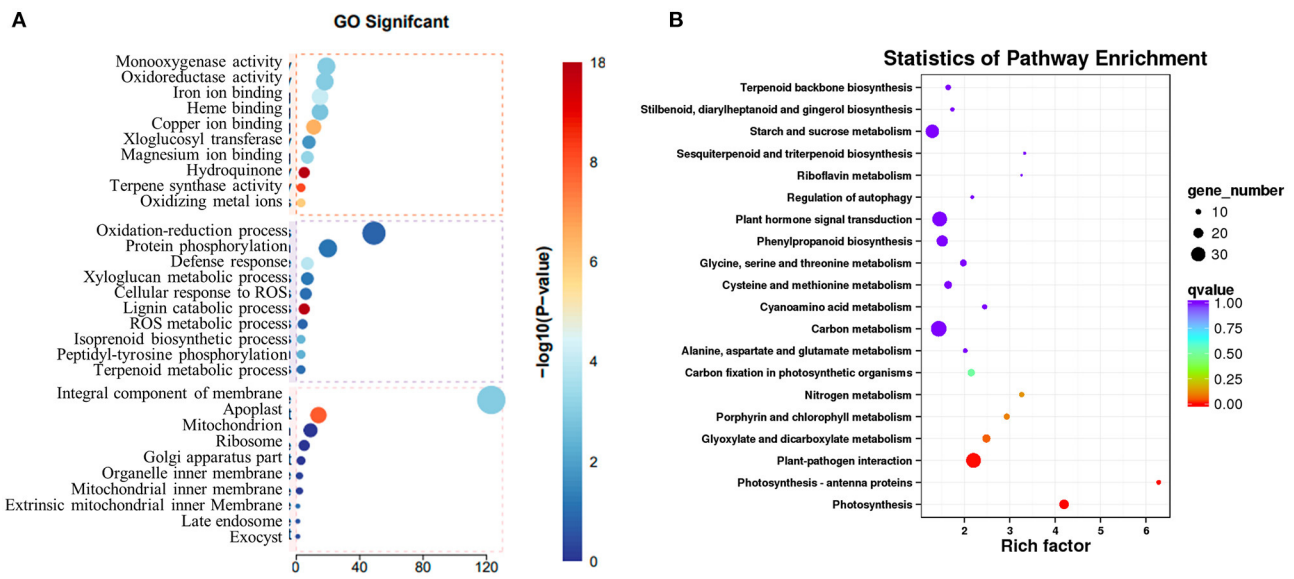

FIGURE 4 | Transcriptomic analysis of *Salvia miltiorrhiza* with low concentration copper treatment. **(A)** Two-month-old *S. miltiorrhiza* was treated with $CuSO4.5H_2O$ (5 μM) for 5 days, following which mRNA was extracted from roots and subjected to transcriptomic analysis. **(A)** Differentially expressed genes were identified by comparing gene expression in copper treated *vs*. untreated samples. Function of identified significantly changed genes was analyzed using the gene ontology (GO) database. **(B)** Pathway mapping of significantly changed genes was performed using the Kyoto Encyclopedia of Genes and Genomes database (http://www.genome.jp/kegg/).

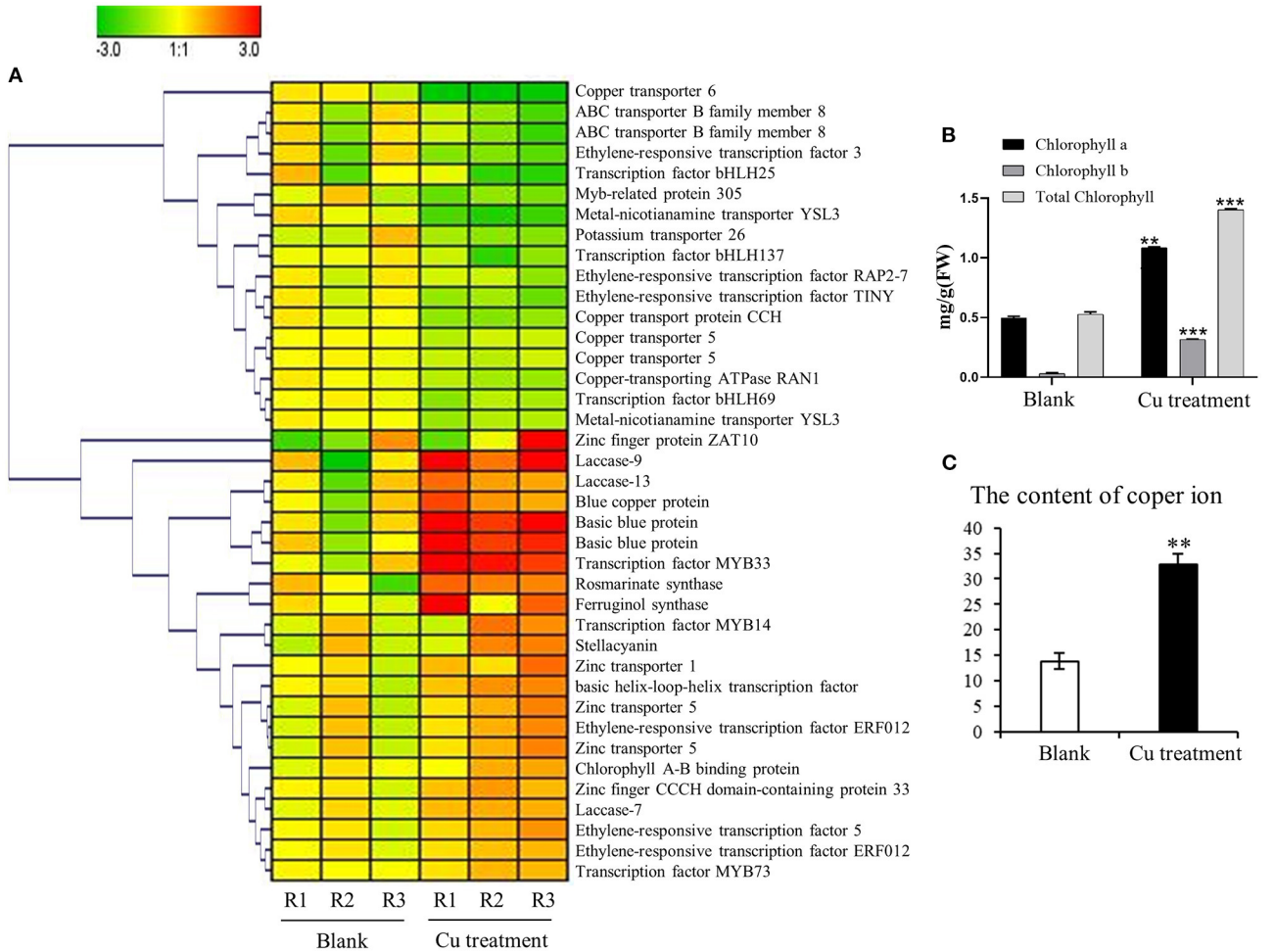

FIGURE 5 | Impact of the copper treatment on biosynthesis of salvinolic acids (SalAs), chlorophyll metabolism, and ion transport. **(A)** The change tendency of differentially expressed genes involved in the biosynthesis of SalAs, chlorophyll metabolism, and ion transport was analyzed based on their expression levels in untreated and treated samples. **(B)** The content of chlorophyll *a*, chlorophyll *b*, and total chlorophyll in untreated and treated samples was determined. **(C)** The content of copper ions in untreated and treated samples was measured. Data represent the mean ± SD of three independent biological replicates. Significant differences between treatment and control samples were determined using a Student's *T*-test (**$P < 0.01$, ***$P < 0.001$).

(marked with a red pentagram) were positioned in Cluster II and Cluster V (**Figure 6B**). Functional domain analysis found that the three key laccases had the same three motifs and conserved domains, which implies that they have functional similarity (**Figure 6C**).

To identify the upstream transcription factor involved in the regulation of copper-induced biosynthetic enzymes of SalAs, a coexpression analysis of biosynthetic genes related to SalAs (laccases and rosmarinate synthase) and 12 key transcription factors was carried out. As shown in **Figure 7**, transcription factors were positively correlated with key candidate genes in the biosynthetic pathways of SalAs. Among them, zinc finger protein ZAT10, Myb family transcription factor PHL5, ethylene-responsive transcription factor 5, and bZIP transcription factor 18 were significantly coexpressed with laccase 20 (gene 3); Zinc finger CCCH domain-containing protein 33/29, zinc finger A20 and AN1 domain-containing stress-associated protein 5, transcription factor MYB73, and ethylene-responsive transcription factor ERF012 were significantly coexpressed with laccase 7 (gene 1); Transcription factor MYB33 was significantly coexpressed with laccase 13 (gene 3) (**Supplementary Table 3**). To further explore the underlying mechanism by which copper induces expression of laccases and transcription factors, a copper-response element and metal-response elements were searched against 2,000 bp promoter sequences of laccases and transcription factors. As shown in **Supplementary Figure 3**, a core motif of a copper-response element (GTAC) (Quinn et al., 2000; Kropat et al., 2005) and a metal-response element (TGCxCxC) (Murphy et al., 1999) were identified in extracted 2,000 bp promoter sequences of laccases (laccase 20 and laccase 13) and transcription factors (zinc finger protein ZAT10, Zinc finger CCCH domain-containing protein 33,

TABLE 1 | Key genes involved in salvianolic acid biosynthesis that showed a significantly change in abundance in leaves and roots of Salvia miltiorrhiza in response to treatment with a low concentration of copper ions.

Gene ID	Description	Ratio	*P*-value
scaffold9670.3	Laccase 20	13.1784	0.0000
scaffold1005.5	Zinc finger protein ZAT10	12.5554	0.0017
scaffold4128.1	Basic blue protein	8.8272	0.0000
scaffold1723.6	Transcription factor MYB33	9.0328	0.0000
scaffold3548.4	Basic blue protein	6.5314	0.0000
newGene_16720	Ferruginol synthase	4.1724	0.0062
newGene_4005	Rosmarinate synthase	2.9856	0.0026
scaffold7426.5	Blue copper protein	2.9906	0.0006
scaffold9243.42	Laccase 13	2.5341	0.0144
scaffold6895.1	basic helix-loop-helix transcription factor	2.2409	0.0055
scaffold8762.12	Zinc transporter 1	2.1111	0.0096
scaffold696.10	Transcription factor MYB14	2.1066	0.0452
scaffold4780.1	Stellacyanin	2.0829	0.0466
scaffold720.3	Zinc transporter 5	1.9774	0.0255
C221085.11	Zinc transporter 5	1.9465	0.0297
scaffold7135.8	Ethylene-responsive transcription factor ERF012	1.9232	0.0284
scaffold9614.5	Zinc finger CCCH domain-containing protein 33	1.8885	0.0135
scaffold215.22	Laccase 7	1.8639	0.0068
scaffold10670.14	Ethylene-responsive transcription factor 5	1.8451	0.0114
scaffold726.5	Chlorophyll A-B binding protein	1.6674	0.0418
C219717.5	Transcription factor MYB73	1.6080	0.0458
scaffold12295.1	Ethylene-responsive transcription factor ERF012	1.5692	0.0432
scaffold4374.6	Copper transporter 5	0.6246	0.0357
scaffold1463.7	Copper transporter 5	0.6236	0.0404
scaffold5168.12	Ethylene-responsive transcription factor RAP2-7	0.5813	0.0393
scaffold239.4	Copper-transporting ATPase RAN1	0.4883	0.0021
C220963.1	Metal-nicotianamine transporter YSL3	0.4967	0.0018
newGene_9124	Transcription factor bHLH69	0.4776	0.0426
scaffold9212.4	Potassium transporter 26	0.4124	0.0269
scaffold4677.5	Putative ABC transporter B family member 8	0.4269	0.0170
scaffold4677.4	Putative ABC transporter B family member 8	0.4154	0.0254
scaffold3984.1	Transcription factor bHLH137	0.4101	0.0339
scaffold3771.63	Ethylene-responsive transcription factor TINY	0.3941	0.0243
scaffold3068.14	Copper transport protein CCH	0.3959	0.0000
C222313.14	Transcription factor bHLH25	0.4072	0.0314
scaffold8569.11	Myb-related protein 305	0.3426	0.0028
scaffold1219.23	Ethylene-responsive transcription factor 3	0.3299	0.0016
scaffold1040.9	Metal-nicotianamine transporter YSL3	0.1990	0.0000
scaffold4004.3	Copper transporter 6	0.0802	0.0000

transcription factor MYB73, and transcription factor MYB33). In addition, MYB transcription factor-binding motifs were also identified in promoter sequences of laccase 20 and laccase 13 (**Supplementary Figure 3**).

DISCUSSION

SalAs are important water-soluble compounds in *S. miltiorrhiza*, which contribute to the treatment of cerebrovascular and cardiovascular diseases (Chen et al., 2016; Zhou et al., 2016). Recently, increasing research has been conducted to increase the content of SalA in *S. miltiorrhiza* (Xiao et al., 2009; Zhang et al., 2010). In this study, we reported that a low concentration of copper (5 μM) could promote the biosynthesis of SalA in *S. miltiorrhiza*. Then, we conducted comprehensive, integrated metabolomic and transcriptomic analyses to provide insights into the mechanisms underlying low copper-induced SalA biosynthesis. Genes-encoding SalAs biosynthetic enzymes (laccases and rosmarinate synthase) and transcription factors were identified as potential key factors involved in low copper-induced SalA biosynthesis.

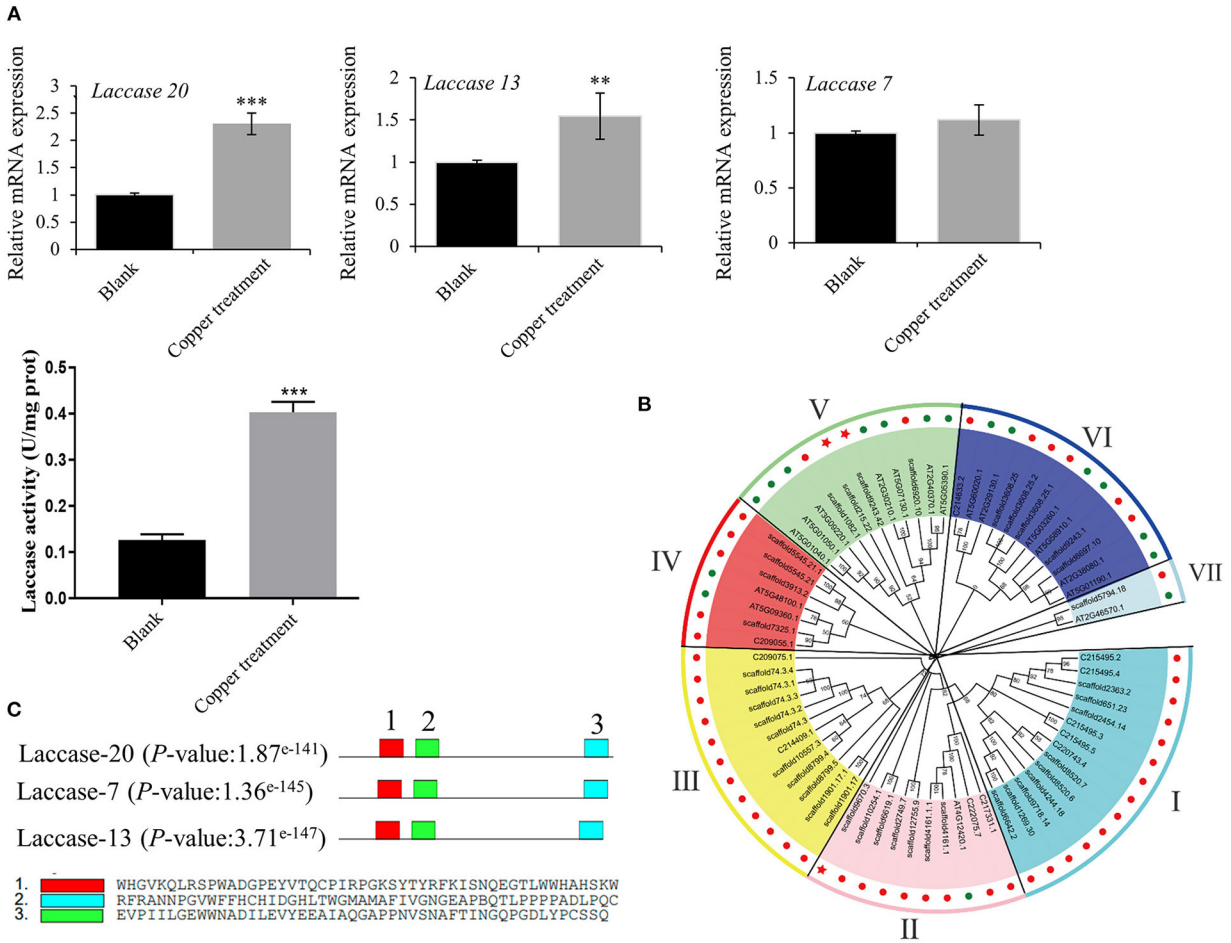

FIGURE 6 | Bioinformatics and enzyme activity analyses of copper ion-induced laccase. **(A)** mRNA expression levels of laccase 20, laccase 13, and laccase 7 in untreated and treated samples were checked by reverse transcription-quantitative PCR (RT-qPCR). Crude proteins were extracted from root of *Salvia miltiorrhiza*, and laccase activity was measured in untreated and treated samples using an ELISA kit. **(B)** A phylogenetic tree of laccases in *Salvia miltiorrhiza* (red dots) and *Arabidopsis thaliana* (green dots) was constructed using the maximum likelihood (ML) method with bootstraps in MEGA X software. Our target laccases (laccase 20, laccase 13, and laccase 7) were marked with a red pentagram. **(C)** A motif analysis of three key laccases was performed using MEME Suite. $^{**}P$-value < 0.01, $^{***}P$-value < 0.001.

A Low Copper Concentration Promotes SalA Biosynthesis in *S. miltiorrhiza* Through Regulating Plant Growth and Photosynthesis

Our results revealed that the growth status and fresh weight of *S. miltiorrhiza* were significantly improved in the low copper concentration treatment compared with the control. The metabolites involved in carbon fixation in photosynthesis were significantly increased by the low-copper concentration treatment. Importantly, chlorophyll a, chlorophyll b, and total chlorophyll, which play an important role in photosynthesis (Baker, 2008), showed an increase in accumulation in low copper-treated plants. Photosynthesis contributes greatly to the biosynthesis of secondary metabolites in plants (Landi et al., 2020). A previous study has shown that copper played a role in photosynthesis through strengthening the photosynthetic capacity of plants (Douglas and Jaqueline, 2019). In our study, blue copper protein and basic blue protein, which are involved in promoting photosynthesis through acting as electron acceptors (Skyes, 1991), were upregulated in low copper-treated plants. Sal B and RA, the two most representative secondary metabolites of phenolic acids in *S. miltiorrhiza* (Zhao et al., 2015; Shi et al., 2016, 2019; Zhou et al., 2017; Huang et al., 2019), were significantly increased in *S. miltiorrhiza* treated with a low concentration of copper. These results suggest that low concentrations of copper induce the accumulation of SalAs might be through regulating photosynthesis related genes such as blue copper proteins in *S. miltiorrhiza*.

Low Concentration of Copper Induces the Accumulation of SalAs by Activating Key Enzymes Involved in SalA Biosynthesis

Both tyrosine- and phenylalanine-derived pathways are the starting point for the biosynthesis of SalAs s (Hao et al., 2020). The data obtained in the transcriptomic analysis showed

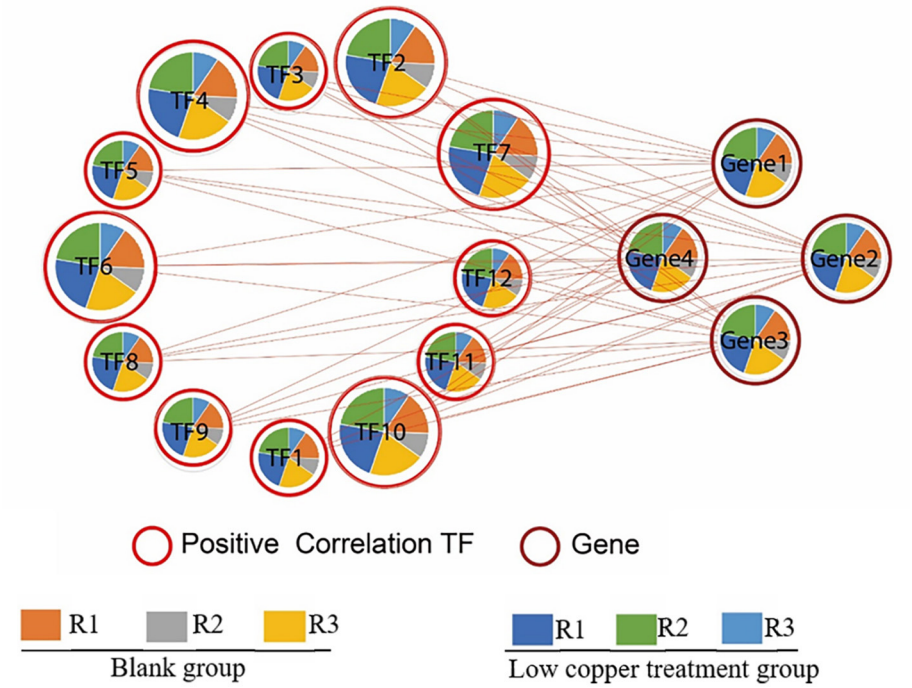

FIGURE 7 | Correlation analysis between significantly changed transcription factors and enzymes related to SalA biosynthesis. The correlation between significantly changed SalA biosynthetic enzymes and the relative expression of candidate transcription factors was analyzed using R software. A Spearman correlation analysis was performed to calculate the correlation coefficient.

that rosmarinate synthase and laccase were upregulated in plants treated with a low copper concentration compared with the control. Rosmarinate synthase is the key enzyme in the pathway of SalAs biosynthesis in *S. miltiorrhiza* (Zhou et al., 2018). A previous study has reported that phenolic acids, such as rosmarinic acid and lithospermic acid B, were decreased in rosmarinate synthase-knockdown hairy root lines of *S. miltiorrhiza* (Zhou et al., 2018). However, overexpression of rosmarinate synthase resulted in a higher content of phenolic acids (up to over 3-fold) in transgenic lines compared with the control (Fu et al., 2020). Recently, scientists have demonstrated that laccase plays a critical role in the biosynthesis of Sal B. The laccase gene family in *S. bowleyana* has undergone expansion, and it might catalyze the oxidative reaction from RA to Sal B (Zheng et al., 2021). At present, 29 laccase candidates have been found in *S. miltiorrhiza*, and they contained three signature Cu-oxidase domains (Li et al., 2019b). It is known that laccases are copper-containing enzymes, and their catalytic activity requires the presence of copper ions (Arregui et al., 2019). Here, a core motif of a copper-response element (GTAC) and a metal response-element (TGCxCxC) were identified in the promoter region of laccase 20 and laccase 13. Overexpression and silencing assays demonstrated *SmLAC7* and *SmLAC20* played an important role in the biosynthesis of Sal B (Li et al., 2019b). In our study, laccase 20, laccase 13, laccase 7, and rosmarinate synthase were significantly upregulated in *S. miltiorrhiza* in the low-copper treatment compared with the control, suggesting that treatment with a low concentration of copper may promote the accumulation of SalAs *via* the regulation of laccase 20/13 and rosmarinate synthase.

In addition to the upregulation of laccase 20/13 and rosmarinate synthase, transcription factors, such as ethylene-responsive transcription factor (*ERF*), transcription factor MYBs, and basic helix-loop-helix transcription factor (*bHLH*), were also responsive to the low-copper treatment. The content of SalAs was increased in *SmERF115*-overexpressing hairy roots and was decreased in silencing lines (Sun et al., 2019). Previous studies have reported that *SmMYB1* was a positive activator that improved the accumulation of phenolic acids in *S. miltiorrhiza* (Deng et al., 2020b; Zhou et al., 2021). However, *SmMYB36* was reported to inhibit the accumulation of phenolic acids (Ding et al., 2017). For the *bHLH* transcription factor, the overexpression of *SmbHLH37* substantially decreased yields of Sal B (Du et al., 2018). Here, zinc finger protein ZAT10, Myb family transcription factor PHL5, ethylene-responsive transcription factor 5, and bZIP transcription factor 18 were significantly upregulated and coexpressed with laccase 20 under low concentration of copper treatment in *S. miltiorrhiza*. In our study, a core motif of a copper-response element (GTAC) and a metal-response element (TGCxCxC) were identified in the promoter region of transcription factors (zinc finger protein ZAT10, Zinc finger CCCH domain-containing protein 33, transcription factor MYB73, and transcription factor MYB33). In addition, MYB transcription factor-binding motifs were

identified in promoter sequences of laccase 20 and laccase 13. In *Arabidopsis*, copper has been shown to induce expression changes of transcription factors, including bHLH, MYB, and ERF (Jakubowicz et al., 2010; Perea-García et al., 2010; Cai et al., 2021). Combined, these results suggest that transcription factors, such as ERF, MYB, and bHLH, play a role in copper-induced SalA biosynthesis in *S. miltiorrhiza*.

We systematically studied the effects of copper on SalA biosynthesis in *S. miltiorrhiza*. We identified a suitable copper ion concentration to promote the biosynthesis of SalA and provide a potential regulatory mechanism by identifying a series of copper-responsive genes. Our work provides an effective approach to induce SalAs and demonstrates a promising future for the metabolic regulation of *S. miltiorrhiza*.

DATA AVAILABILITY STATEMENT

The datasets presented in this study can be found in online repositories. The names of the repository/repositories and accession number(s) can be found here: https://www.ncbi.nlm.nih.gov/, PRJNA645746.

AUTHOR CONTRIBUTIONS

XY conceived and designed the research and revised the manuscript. YX, WS, XW, and JD analyzed the data and drafted the manuscript. WS and XW performed the experiments. All authors reviewed and approved the final manuscript.

FUNDING

This work was supported by the National Natural Science Foundation of China (Grant No. 81803654).

SUPPLEMENTARY MATERIAL

The Supplementary Material for this article can be found online at: https://www.frontiersin.org/articles/10.3389/fpls.2021.746117/full#supplementary-material

REFERENCES

Andre, C. M., Larondelle, Y., and Evers, D. (2010). Dietary antioxidants and oxidative stress from a human and plant perspective: a review. *Curr. Nutr. Food Sci.* 6, 2–12. doi: 10.2174/157340110790909563

Arregui, L., Ayala, M., Gómez-Gil, X., Gutiérrez-Soto, G., Hernández-Luna, C. E., Herrera de Los Santos, M., et al. (2019). Laccases: structure, function, and potential application in water bioremediation. *Microb. Cell Fact.* 18:200. doi: 10.1186/s12934-019-1248-0

Baker, N. R. (2008). Chlorophyll fluorescence: a probe of photosynthesis *in vivo*. *Annu. Rev. Plant Biol.* 59, 89–113. doi: 10.1146/annurev.arplant.59.032607.092759

Burkhead, J. L., Reynolds, K. A., Abdel-Ghany, S. E., Cohu, C. M., and Pilon, M. (2009). Copper homeostasis. *N. Phytol.* 182, 799–816. doi: 10.1111/j.1469-8137.2009.02846.x

Cai, Y., Li, Y., and Liang, G. (2021). FIT and bHLH Ib transcription factors modulate iron and copper crosstalk in *Arabidopsis*. *Plant Cell Environ.* 44, 1679–1691. doi: 10.1111/pce.14000

Chen, C. J., Chen, H., Zhang, Y., Thomas, H. R., Frank, M. H., He, Y. H., et al. (2020). TBtools: an integrative toolkit developed for interactive analyses of big biological data. *Mol. Plant* 13, 1194–1202. doi: 10.1016/j.molp.2020.06.009

Chen, X., Cheng, J., Chen, L., Zhang, G., Huang, H., Zhang, Y., Xu, L., et al. (2016). Auxin-independent NAC pathway acts in response to explant-specific wounding and promotes root tip emergence during de novo root organogenesis in Arabidopsis. *Plant Physiol.* 170, 2136–45. doi: 10.1104/pp.15.01733

Choudhary, S. P., Oral, H. V., Bhardwaj, R., Yu, J. Q., and Tran, L. S. (2012). Interaction of brassinosteroids and polyamines enhances copper stress tolerance in *Raphanus sativus*. *J. Exp. Bot.* 63, 5659–5675. doi: 10.1093/jxb/ers219

De Caroli, M., Furini, A., DalCorso, G., Rojas, M., and DiSansebastiano, G. P. (2020). Endomembrane reorganization induced by heavy metals. *Plants* 9:482. doi: 10.3390/plants9040482

Deng, C., Shi, M., Fu, R., Zhang, Y., Wang, Q., Zhou, Y., et al. (2020a). ABA-responsive transcription factor bZIP1 is involved in modulating biosynthesis of phenolic acids and tanshinones in Salvia miltiorrhiza. *J. Exp. Bot.* 71, 5948–5962. doi: 10.1093/jxb/eraa295

Deng, C., Wang, Y., Huang, F., Lu, S., Zhao, L., Ma, X., et al. (2020b). SmMYB2 promotes salvianolic acid biosynthesis in the medicinal herb *Salvia miltiorrhiza*. *J. Integr. Plant Biol.* 62, 1688–1702. doi: 10.1111/jipb.12943

Ding, K., Pei, T., Bai, Z., Jia, Y., Ma, P., and Liang, Z. (2017). SmMYB36, a novel R2R3-MYB transcription factor, enhances tanshinone accumulation and decreases phenolic acid content in *Salvia miltiorrhiza* hairy roots. *Sci. Rep.* 7:5104. doi: 10.1038/s41598-017-04909-w

Ding, Y., Ding, L., Xia, Y., Wang, F., and Zhu, C. (2020). Emerging roles of micrornas in plant heavy metal tolerance and homeostasis. *J. Agric. Food Chem.* 68, 1958–1965. doi: 10.1021/acs.jafc.9b07468

Douglas, H. B., and Jaqueline, C. S. (2019). The effects of copper on photosynthesis and biomolecules yield in *Chlorolobion braunii*. *J. Phycol.* 55, 1335–1347. doi: 10.1111/jpy.12914

Droppa, M., Terry, N., and Horvath, G. (1984). Effects of Cu deficiency on photosynthetic electron transport. *Proc. Natl. Acad. Sci. U.S.A.* 81, 2369–2373. doi: 10.1073/pnas.81.8.2369

Du, T., Niu, J., Su, J., Li, S., Guo, X., Li, L., et al. (2018). SmbHLH37 functions antagonistically with SmMYC2 in regulating jasmonate-mediated biosynthesis of phenolic acids in *Salvia miltiorrhiza*. *Front. Plant Sci.* 9:1720. doi: 10.3389/fpls.2018.01720

Fu, R., Shi, M., Deng, C., Zhang, Y., Zhang, X., Wang, Y., et al. (2020). Improved phenolic acid content and bioactivities of *Salvia miltiorrhiza* hairy roots by genetic manipulation of RAS and CYP98A14. *Food Chem.* 331:127365. doi: 10.1016/j.foodchem.2020.127365

Hao, X., Pu, Z., Cao, G., You, D., Zhou, Y., Deng, C., et al. (2020). Tanshinone and salvianolic acid biosynthesis are regulated by SmMYB98 in *Salvia miltiorrhiza* hairy roots. *J Adv Res.* 23, 1–12. doi: 10.1016/j.jare.2020.01.012

Hoegger, P. J., Kilaru, S., James, T. Y., Thacker, J. R., and Kues, U. (2006). Phylogenetic comparison and classification of laccase and related multicopper oxidase protein sequences. *FEBS J.* 273, 2308–2326. doi: 10.1111/j.1742-4658.2006.05247.x

Huang, Q., Sun, M., Yuan, T., Wang, Y., Shi, M., Lu, S., et al. (2019). The AP2/ERF transcription factor SmERF1L1 regulates the biosynthesis of tanshinones and phenolic acids in *Salvia miltiorrhiza*. *Food Chem.* 274, 368–375. doi: 10.1016/j.foodchem.2018.08.119

Ibrahim, M. H., Kong, Y., and Zain, N. A. (2017). Effect of cadmium and copper exposure on growth, secondary metabolites and antioxidant activity in the medicinal plant Sambung Nyawa (*Gynura procumbens* (Lour.) Merr). *Molecules* 22:1623. doi: 10.3390/molecules22101623

Jakubowicz, M., Gałgańska, H., Nowak, W., and Sadowski, J. (2010). Exogenously induced expression of ethylene biosynthesis, ethylene perception, phospholipase D, and Rboh-oxidase genes in broccoli seedlings. *J. Exp. Bot.* 61, 3475–3491. doi: 10.1093/jxb/erq177

Jones S. M., Solomon E. I. (2015). Electron transfer and reaction mechanism of laccases. *Cell Mol Life Sci.* 72, 869–883.

Kropat, J., Tottey, S., Birkenbihl, R. P., Depège, N., Huijser, P., and Merchant, S. (2005). A regulator of nutritional copper signaling in

Chlamydomonas is an SBP domain protein that recognizes the GTAC core of copper response element. *Proc. Natl. Acad. Sci. U.S.A.* 102, 18730–18735. doi: 10.1073/pnas.0507693102

Landi, M., Zivcak, M., Sytar, O., Brestic, M., and Allakhverdiev, S. I. (2020). Plasticity of photosynthetic processes and the accumulation of secondary metabolites in plants in response to monochromatic light environments: a review. *Biochim. Biophys. Acta Bioenerg.* 1861:148131. doi: 10.1016/j.bbabio.2019.148131

Lescot, M., Déhais, P., Thijs, G., Marchal, K., Moreau, Y., Van de Peer, Y., et al. (2002). PlantCARE, a database of plant cis-acting regulatory elements and a portal to tools for in silico analysis of promoter sequences. *Nucleic Acids Res.* 30, 325–327. doi: 10.1093/nar/30.1.325

Li, C., Li, D., Zhou, H., Li, J., and Lu, S. (2019a). Analysis of the laccase gene family and miR397-/miR408-mediated posttranscriptional regulation in *Salvia miltiorrhiza*. *Peer J.* 7:e7605. doi: 10.7717/peerj.7605

Li, Q., Feng, J., Chen, L., Xu, Z., Zhu, Y., Wang, Y., et al. (2019b). Genome-wide identification and characterization of *Salvia miltiorrhiza* laccases reveal potential targets for salvianolic acid B biosynthesis. *Front. Plant Sci.* 10:435. doi: 10.3389/fpls.2019.00435

Ma, P., Liu, J., Zhang, C., and Liang, Z. (2013). Regulation of water-soluble phenolic acid biosynthesis in *Salvia miltiorrhiza* Bunge. *Appl. Biochem. Biotechnol.* 170, 1253–1262. doi: 10.1007/s12010-013-0265-4

McCaig, B. C., Meagher, R. B., and Dean, J. F. (2005). Gene structure and molecular analysis of the laccase-like multicopper oxidase (LMCO) gene family in *Arabidopsis thaliana*. *Planta* 221, 619–636. doi: 10.1007/s00425-004-1472-6

Murphy, B. J., Andrews, G. K., Bittel, D., Discher, D. J., McCue, J., Green, C. J., et al. (1999). Activation of metallothionein gene expression by hypoxia involves metal response elements and metal transcription factor-1. *Cancer Res.* 59, 1315–1322

Patel, N., Shahane, S., Shivam, M. R., and Mishra, U. (2019). Mode of action, properties, production, and application of laccase: a review. *Recent Pat. Biotechnol.* 13, 19–32. doi: 10.2174/1872208312666180821161015

Perea-García, A., Andrés-Colás, N., and Peñarrubia, L. (2010). Copper homeostasis influences the circadian clock in Arabidopsis. *Plant Signal. Behav.* 5, 1237–1240. doi: 10.4161/psb.5.10.12920

Quinn, J. M., Barraco, P., Eriksson, M., and Merchant, S. (2000). Coordinate copper- and oxygen-responsive Cyc6 and Cpx1 expression in Chlamydomonas is mediated by the same element. *J. Biol. Chem.* 275, 6080–6089. doi: 10.1074/jbc.275.9.6080

Quist, D. A., Diaz, D. E., Liu, J. J., and Karlin, K. D. (2017). Activation of dioxygen by copper metalloproteins and insights from model complexes. *J. Biol. Inorg. Chem.* 22, 253–288. doi: 10.1007/s00775-016-1415-2

Riva, S. (2006). Laccases: blue enzymes for green chemistry. *Trends Biotechnol.* 24, 219–226. doi: 10.1016/j.tibtech.2006.03.006

Robinson, M. D., McCarthy, D. J., and Smyth, G. K. (2010). edgeR: a Bioconductor package for differential expression analysis of digital gene expression data. *Bioinformatics* 26, 139–140. doi: 10.1093/bioinformatics/btp616

Saleem, M. H., Ali, S., Rehman, M., Hasanuzzaman, M., Rizwan, M., Irshad, S., et al. (2020). Jute: a potential candidate for phytoremediation of metals-a review. *Plants* 9:258. doi: 10.3390/plants9020258

Shi, M., Huang, F., Deng, C., Wang, Y., and Kai, G. (2019). Bioactivities, biosynthesis and biotechnological production of phenolic acids in *Salvia miltiorrhiza*. *Crit. Rev. Food Sci. Nutr.* 59, 953–964. doi: 10.1080/10408398.2018.1474170

Shi, M., Luo, X., Ju, G., Li, L., Huang, S., and Zhang, T. (2016). Enhanced diterpene tanshinone accumulation and bioactivity of transgenic *Salvia miltiorrhiza* hairy roots by pathway engineering. *J. Agric. Food Chem.* 64, 2523–2530. doi: 10.1021/acs.jafc.5b04697

Skyes, A. G. (1991). Active site properties of blue copper proteins. *Adv. Inorg. Chem.* 36:377. doi: 10.1016/S0898-8838(08)60044-6

Solomon, E. I., Sundaram, U. M., and Machonkin, T. E. (1996). Multicopper oxidases and oxygenases. *Chem. Rev.* 96, 2563–2605. doi: 10.1021/cr950046o

Song, Y. J., Zhou, L. C., Yang, S. H., Wang, C. L., Zhang, T. J., and Wang, J. H. (2017). Dose-dependent sensitivity of *Arabidopsis thaliana* seedling root to copper is regulated by auxin homeostasis. *Environ. Exp. Bot.* 139, 23–30. doi: 10.1016/j.envexpbot.2017.04.003

Sun, M., Shi, M., Wang, Y., Huang, Q., Yuan, T., Wang, Q., et al. (2019). The biosynthesis of phenolic acids is positively regulated by the JA-responsive transcription factor ERF115 in *Salvia miltiorrhiza*. *J. Exp. Bot.* 70, 243–245. doi: 10.1093/jxb/ery349

Turlapati, P. V., Kim, K. W., Davin, L. B., and Lewis, N. G. (2011). The laccase multigene family in *Arabidopsis thaliana*: towards addressing the mystery of their gene function(s). *Planta* 233, 439–470. doi: 10.1007/s00425-010-1298-3

Wang, J., Xu, J., Gong, X., Yang, M., Zhang, C., and Li, M. (2019). Biosynthesis, chemistry, and pharmacology of polyphenols from Chinese salvia species: a review. *Molecules* 24:155. doi: 10.3390/molecules24010155

Xiao, Y., Gao, S. H., Di, P., Chen, J., Chen, W., and Zhang, L. (2009). Methyl jasmonate dramatically enhances the accumulation of phenolic acids in *Salvia miltiorrhiza* hairy root cultures. *Physiol. Plantarum* 137, 1–9. doi: 10.1111/j.1399-3054.2009.01257.x

Xing, B., Liang, L., Liu, L., Hou, Z., Yang, D., Yan, K., et al. (2018). Overexpression of SmbHLH148 induced biosynthesis of tanshinones as well as phenolic acids in *Salvia miltiorrhiza* hairy roots. *Plant Cell Rep.* 37, 1681–1692. doi: 10.1007/s00299-018-2339-9

Yin, X., Fan, H., Chen, Y., Li, L. Z., Song, W., Fan, Y., et al. (2020). Integrative omic and transgenic analyses reveal the positive effect of ultraviolet-B irradiation on salvianolic acid biosynthesis through upregulation of SmNAC1. *Plant J.* 104, 781–799. doi: 10.1111/tpj.14952

Yruela, I. (2009). Copper in plants: acquisition, transport and interactions. *Funct. Plant Biol.* 36, 409–430. doi: 10.1071/FP08288

Zhang, H., Lv, S., Xu, H., Hou, D., Li, Y., and Wang, F. (2017). H_2O_2 is involved in the metallothionein-mediated rice tolerance to copper and cadmium toxicity. *Int. J. Mol. Sci.* 18:2083. doi: 10.3390/ijms18102083

Zhang, Y. A., Yan, Y. P., and Wang, Z. Z. (2010). The Arabidopsis PAP1 transcription factor plays an important role in the enrichment of phenolic acids in *Salvia miltiorrhiza*. *J. Agric. Food Chem.* 58, 12168–12175. doi: 10.1021/jf103203e

Zhao, S., Zhang, J., Tan, R., Yang, L., and Zheng, X. (2015). Enhancing diterpenoid concentration in *Salvia miltiorrhiza* hairy roots through pathway engineering with maize C1 transcription factor. *J. Exp. Bot.* 66, 7211–7226. doi: 10.1093/jxb/erv418

Zheng, X., Chen, D., Chen, B., Liang, L., Huang, Z., Fan, W., et al. (2021). Insights into salvianolic acid B biosynthesis from chromosome-scale assembly of the *Salvia bowleyana* genome. *J. Integr. Plant Biol.* 63, 1309–1323. doi: 10.1111/jipb.13085

Zhou, W., Huang, Q., Wu, X., Zhou, Z., Ding, M., and Shi, M. (2017). Comprehensive transcriptome profiling of *Salvia miltiorrhiza* for discovery of genes associated with the biosynthesis of tanshinones and phenolic acids. *Sci. Rep.*7:10554. doi: 10.1038/s41598-017-10215-2

Zhou, W., Shi, M., Deng, C., Lu, S., Huang, F., Wang, Y., et al. (2021). The methyl jasmonate-responsive transcription factor SmMYB1 promotes phenolic acid biosynthesis in *Salvia miltiorrhiza*. *Hortic Res.* 8:10. doi: 10.1038/s41438-020-00443-5

Zhou, Y., Sun, W., Chen, J., Tan, H., Xiao, Y., Li, Q., et al. (2016). SmMYC2a and SmMYC2b played similar but irreplaceable roles in regulating the biosynthesis of tanshinones and phenolic acids in *Salvia miltiorrhiza*. *Sci. Rep.* 6:22852. doi: 10.1038/srep22852

Zhou, Z., Tan, H., Li, Q., Chen, J., Gao, S., Wang, Y., et al. (2018). CRISPR/Cas9-mediated efficient targeted mutagenesis of RAS in *Salvia miltiorrhiza*. *Phytochemistry* 148, 63–70. doi: 10.1016/j.phytochem.2018.01.015

Conflict of Interest: The authors declare that the research was conducted in the absence of any commercial or financial relationships that could be construed as a potential conflict of interest.

Publisher's Note: All claims expressed in this article are solely those of the authors and do not necessarily represent those of their affiliated organizations, or those of the publisher, the editors and the reviewers. Any product that may be evaluated in this article, or claim that may be made by its manufacturer, is not guaranteed or endorsed by the publisher.

Copyright © 2021 Xiang, Wang, Song, Du and Yin. This is an open-access article distributed under the terms of the Creative Commons Attribution License (CC BY). The use, distribution or reproduction in other forums is permitted, provided the original author(s) and the copyright owner(s) are credited and that the original publication in this journal is cited, in accordance with accepted academic practice. No use, distribution or reproduction is permitted which does not comply with these terms.

frontiers in Plant Science

ORIGINAL RESEARCH
published: 15 November 2021
doi: 10.3389/fpls.2021.756300

Composition of Flavonoids in the Petals of *Freesia* and Prediction of Four Novel Transcription Factors Involving in *Freesia* Flavonoid Pathway

*Jiayi Zhu[1], Xueying Guo[1], Xin Li[2] and Dongqin Tang[1]**

[1] School of Design, Shanghai Jiao Tong University, Shanghai, China, [2] Instrumental Analysis Center, Shanghai Jiao Tong University, Shanghai, China

Freesia hybrida is rich in flower colors with beautiful flower shapes and pleasant aroma. Flavonoids are vital to the color formation of its flowers. In this study, five *Freesia* cultivars with different flower colors were used to study on the level of accumulation of their flavonoids and expression of flavonoid-related genes and further explore new novel transcription factor (TF). Ultra-high-performance liquid chromatography and VION ion mobility quadrupole time-of-flight mass spectrometer (UPLC-Q-TOF-MS) were used to determine the flavonoids. Combined with transcriptome sequencing technology, the molecular mechanism of the flavonoid metabolism difference in *Freesia* was revealed. A total of 10 anthoxanthin components and 12 anthocyanin components were detected using UPLC-Q-TOF-MS. All six common anthocyanin aglycones in high plants, including cyanidin, delphinidin, petunidin, peonidin, malvidin, and pelargonidin, were detected in *Freesia* at first time in this study. In orange, yellow, and white cultivars, anthoxanthins gradually decreased with the opening of the petals, while in red and purple cultivars, anthoxanthins first increased and then decreased. No anthocyanin was detected in yellow and white cultivars, while anthocyanins increased with the opening of the petals and reached their maximum at the flowering stage (S3) in other three cultivars. The correlation analysis revealed that the color of *Freesia* petals was closely related to the composition and content of anthoxanthins and anthocyanins. Petals of five cultivars at S3 were then selected for transcriptome sequencing by using the Illumina Hiseq 4000 platform, and a total of 100,539 unigenes were obtained. There were totally 5,162 differentially expressed genes (DEGs) when the four colored cultivars were compared with the white cultivar at S3. Comparing all DEGs with gene ontology (GO), KEGG, and Pfam databases, it was found that the genes involved in the flavonoid biosynthesis pathway were significantly different. In addition, AP2, WRKY, and bHLH TF families ranked the top three among all differently expressed TFs in all DEGs. Quantitative real-time PCR (qRT-PCR) technology was used to analyze the expression patterns of the structural genes of flavonoid biosynthesis pathway in *Freesia*. The results showed that metabolic process was affected significantly by structural genes in this pathway, such as *CHS1*, *CHI2*, *DFR1*, *ANS1*, *3GT1*, and *FLS1*. Cluster analysis was performed by using all annotated WRKY and AP2 TFs and the above structural genes based on their relatively

OPEN ACCESS

Edited by:
Felipe Vazquez-Flota, Unidad de Bioquímica y Biología Molecular de Plantas, Centro de Investigación Científica de Yucatán, Mexico

Reviewed by:
Pengfang Zhu, Shenyang Agricultural University, China
Rongfang Guo, Fujian Agriculture and Forestry University, China

***Correspondence:**
Dongqin Tang
dqtang@sjtu.edu.cn

Specialty section:
This article was submitted to Plant Metabolism and Chemodiversity, a section of the journal Frontiers in Plant Science

Received: *10 August 2021*
Accepted: *18 October 2021*
Published: *15 November 2021*

Citation:
Zhu J, Guo X, Li X and Tang D (2021) Composition of Flavonoids in the Petals of Freesia and Prediction of Four Novel Transcription Factors Involving in Freesia Flavonoid Pathway. Front. Plant Sci. 12:756300. doi: 10.3389/fpls.2021.756300

expression. Four novel candidate TFs of WRKY and AP2 family were screened. Their spatiotemporal expression patterns revealed that these four novel TFs may participate in the regulation of the flavonoid biosynthesis, thus controlling its color formation in *Freesia* petals.

Keywords: *Freesia hybrida*, flavonoid, transcription factor, WRKY, AP2

INTRODUCTION

Plant pigments mainly include flavonoids, carotenoids, and betalain substances. Among them, flavonoids, an important kind of plant secondary metabolites, are most widely distributed in plants (Mierziak et al., 2014; Nabavi et al., 2020), and they can be divided into flavonols, flavones, anthocyanins, proanthocyanidins, and catechins, etc., based on the degree of oxidation and conformational differences of their three-carbon bonds (Singh et al., 2014). Commonly, flavonoids and flavonols are collectively called anthoxanthins (Kesavan et al., 2018).

Flavonoids have been proved to affect the coloration of many plants, which can make plants appear milky white, yellow, orange-red, blue-violet, and other colors and have a decisive effect on the color of a variety of plant fruits, leaves, and petals. For instance, a significant correlation was observed between the hue, brightness, and vividness of the petals of *Narcissus* cultivars and its flavonoids (Li et al., 2015); 29 anthocyanins were identified in iris, among which delphinidin contributes to the formation of the flower color of purple wild iris (*Iris dichotoma*), while the flower color of orange *I. domestica* is mainly determined by pelargonidin (Xu et al., 2018). In *Rhododendron* species, anthocyanins, such as delphinidin and cyanidin, and flavonols, such as quercetin and kaempferol, were detected in the petals. It was also found that anthocyanins promote the formation of red flowers of *Rhododendron* (Du et al., 2018).

Structural genes in the flavonoid biosynthesis pathway, including *CHS*, *CHI*, *F3H*, *F3′5′H*, *FNS*, *FLS*, *DFR*, *ANS*, and *UF3GT*, encode key enzymes to control the synthesis of corresponding flavonoids, thereby affecting the color development of petals. For instance, the *CHS* gene of *Hosta plantaginea* was introduced into tobacco (*Nicotiana tabacum*), which deepened the flower color of transgenic plants and significantly increased the flavonoid content (Zhang et al., 2020). In *Rosa hybrida*, the expression of *F3′5′H* gene led to the accumulation of delphinidin, which made the petals appear in a novel bluish flower color (Katsumoto et al., 2007). The *FLS* gene of *Rosa rugosa* was introduced into petunia, which made some petunia plants show a lighter flower color, and a new flavonol myricetin was detected at the same time (Tsuda et al., 2004). The *FLS* gene was antisensely expressed in *Eustoma grandiflorum*, which turned its flower color into magenta. The transgenic plants also contain new anthocyanin components and accumulate more dihydroflavonols (Nielsen et al., 2002). *DFR* and *ANS* are essential for the synthesis of anthocyanins. In tulip petals, it was suggested that the accumulation of the red pigment was positively related to the expression levels of *TfDFR1* and *TfANS1* (Yuan et al., 2013). Chen M. et al. (2018) found that the functional defect or mutation of the *ANS* gene may be the cause of the white flower cultivar of *Solanum melongena*. In *Freesia*, some members in an individual structural gene family, including *FhFLS1* and *FhFLS2* (Shan et al., 2020), *FhCHS1* (Sun et al., 2015), *FhDFR*s (Li et al., 2017), and *Fh3GT*s (Sun et al., 2016; Meng et al., 2019), were also isolated, which were confirmed to be related with the flavonoid biosynthesis so far.

Till present, various regulatory genes that directly control transcription of the structural genes involving in the flavonoid biosynthesis pathway had been identified from some plants. Among them, three transcription factors (TFs) families, namely, R2R3-MYB, basic helix-loop-helix (bHLH), and WD40 repeats (WD40), have been extensively studied. They can regulate the structural genes involving in the flavonoid pathway alone or in the form of MBW complex (Xu et al., 2015; Chen et al., 2019; Yuan et al., 2020). In *Freesia*, several reports focused on these three TFs, and their regulating mechanism in this pathway is also relatively clear (Li et al., 2016, 2019, 2020; Shan et al., 2020). With the discovery of more powerful TF families, scientists are also paying attention to whether there are other novel TFs other than the above three families, involving in the regulation of the flavonoid biosynthesis in a certain plant.

Freesia, a perennial herb belonging to the genus *Freesia* in the Iridaceae family, is native to southern Africa (Manning and Goldblatt, 2010). *Freesia hybrida* is a collective name for many horticultural cultivars in this genus and currently planted worldwide as a cut flower with rich colors and pleasant fragrance. The main colors of the petals in *F. hybrida* include white, yellow, red, and purple. It was already confirmed that flavonoids had a decisive effect on the color of *Freesia* flower (Zhong et al., 2009). Our previous study determined various flavonoid components in *Freesia* petals and found that the petal color of *F. hybrida* was related with the flavonoid components; meanwhile, the degree of petal coloration was proportional to the total amount of flavonoids in *Freesia* petals (Xu et al., 2016; Yu et al., 2020; Zhu et al., 2021). These results provide a good foundation to further study the mechanism of formation of flower color in *Freesia* on the basis of the metabolic and molecular levels.

MATERIALS AND METHODS

Plant Materials and Growth Conditions

Five cultivars of *F. hybrida* with different colors were used as materials, namely, 'Castor' (purple), 'SN Chenghuang' (orange), 'Gold River' (yellow), 'Red Passion' (red), and 'White River' (white) (**Figure 1**), shortened as CA, CH, GR, RP, and WR in the following text, figures, and tables, respectively.

The healthy corms of the above cultivars were planted in the standard farm shed at the Modern Agricultural Engineering Training Center of Shanghai Jiao Tong University in late October 2019, and the petal samples were collected at four developmental stages (S0–S3) of each cultivar during March to April, 2020. The description of each stage is presented in **Supplementary Table 1**.

Identification and Measurement of the Flavonol and Anthocyanin

Ultra-high-performance liquid chromatography and VION ion mobility quadrupole time-of-flight mass spectrometer (UPLC-Q-TOF-MS) (Waters Corporation, United States) with Optima LC/MS-grade methanol and trifluoroacetic acid (Thermo Fisher Scientific, United States) were used to identify flavonol and anthocyanin and measure their contents in petals of *Freesia*.

Several standards were used for the qualitative and quantitative identification of anthocyanins and anthoxanthins in *Freesia* petals. All standards are shown in **Supplementary Table 2**.

Ultra-high-performance liquid chromatography and VION ion mobility quadrupole time-of-flight mass spectrometer analysis conditions are as follows: The column is Ethylidene bridge hybrid particles (BEH) C18 1.7 μm (2.1 mm × 100 mm); mobile phase A, 0.1% formic acid H_2O; B, 0.1% formic acid acetonitrile. The elution gradient is 0 min, 5% B; 3 min, 20% B; 10 min, 100% B; 12 min, 100% B; 15 min, 95% B; 20 min, 95% B. The flow rate is 0.4 mL/min. The injection volume is 1 μl and the column temperature is 45°C. Mass spectrometry conditions are as follows: Acquisition mode is MSE (low-energy/high-energy switching scan); anthoxanthin detection ion mode is electrospray negative ion scan mode (m/z 50–1,000), anthocyanin is electrospray positive ion scan mode (m/z 50–1,000), the scanning speed is 0.2 s. The capillary voltage is 2 kV. The cone voltage is 40 V. The temperature of the atomizing gas is 450°C. The flow of atomizing gas is 900 L/h. The taper hole blowback gas is 50 L/h. The ion source temperature is 115°C.

The flavonoids in petals of *Freesia* were quantified by using the external standard method. The sum of the content of each anthoxanthin component was calculated and recorded as the total anthoxanthin content, that is, the total flavone and flavonol content [total flavonoid content (TFC)]; the sum of the content of each anthocyanin component was calculated and recorded as the total anthocynadin content (TAC).

RNA Extraction and Transcriptome Sequencing

The petals at S3 of each cultivar were then chosen as materials for transcription sequencing. Three biological duplicate samples were taken from each cultivar.

RNA of each sample was extracted using TRIzol Reagent (Kangwei Century Ltd., Beijing, China). The RNA quality test uses Nanodrop GX. Biomarker Technologies (Beijing, China) was responsible for transcriptome sequencing. The Illumina Hiseq 4000 platform was used for sequencing, and a large number of high-quality reads (raw data) were produced. Then, the clean data were obtained by filtering these raw data, discarding low-quality reads and the connector sequence.

De novo Transcriptome Assembling, Functional Annotation, and Classification of Unigenes

Trinity software[1] was used to assemble the obtained clean data. First, the reads were broken into shorter fragments (K-mer), then these small fragments were extended into longer fragments

[1]http://trinityrnaseq.sourceforge.net/

FIGURE 1 | Flower color phenotypes of five *Freesia hybrida* cultivars at different developmental stages.

(Contig), and the overlap between these fragments was used to obtain a fragment set (component). Finally, using the method of De Bruijn diagram and the sequencing read information, the transcripts were identified in each fragment set to obtain the unigene library of *Freesia* petals. The sequencing data have been uploaded to the NCBI database (BioProject: PRJNA656641).

The alignment of Freesia unigene sequences with gene ontology (GO)[2], KEGG[3], COG[4], Pfam[5], and other eight databases was conducted by using BLAST. The prediction of unigene amino acid sequence was performed by using HMMER[6], and the KEGG Orthology analysis is conducted by using KOBAS2.0[7].

Differential Expression Analysis of Unigenes

Bowtie was used to compare the read length obtained by sequencing with the unigene library and to estimate the expression level combined with RNA-Seq by Expectation-Maximization. Fragments per kilobase per million (FPKM) was used to indicate the expression abundance of the corresponding unigene.

DESeq2 is used for the differential expression analysis of genes between sample groups. The screening criteria are fold change (FC) ≥ 2 and false discovery rate (FDR) < 0.01. Subsequently, the differentially expressed gene (DEG) sets were obtained, named in the form of "A vs. B."

Screening of Key Genes in Flavonoid Biosynthesis Pathway

The transcriptome database was searched for key structural genes of the flavonoid biosynthesis pathway based on the functional annotation, and the selected genes were further confirmed by comparing with the known genes in the NCBI database through BLAST+. Genes with high matching degree and high expression abundance (FPKM) were selected for following validation by quantitative real-time PCR (qRT-PCR) detection.

The WRKY, AP2 family TFs were preliminarily screened from the transcriptome according to the functional annotation and then were used to cluster with the above selected structural genes. These TFs closer to the structural genes were selected as candidates. According to the relative gene expression multiples between samples, the software Multi Experience Viewer 4.9.0[8] was used for the gene cluster analysis and heat map drawing. Furthermore, the transcriptome data (BioProject: PRJNA656641) of *Freesia* corms measured by our group were compared, and TFs with high expression in petals and low expression in corms were chosen to perform the phylogenetic analysis and study their temporal and spatial expression characteristics *via* qRT-PCR. The gene phylogenetic tree was constructed by using the MEGA-X software, and the phylogenetic tree was constructed by neighbor-joining method with a step value of 1,000. The red cultivar RP with high flower pigments was used to conduct qRT-PCR, and the roots, stems, leaves, and petals at four developmental stages were sampled, respectively.

The Transcript Level Analysis of Flavonoid-Related Gene by Quantitative Real-Time PCR

The sequences of the selected genes were used to design primers by using the Primer 5.0 software[9]. Actin was used as the internal reference gene (Ding et al., 2020). All primer sequences are listed in **Supplementary Table 3**. The primers were synthesized by Tsingke Biotechnology Co., Ltd. (Shanghai, China).

The first-strand cDNA was obtained by using Prime Script™ RT reagent kit (TaKaRa, Dalian, China) and then used as the template for qRT-PCR. A total 20-μl PCR reaction system was prepared, including 10 μl of SYBR, 7.2 μl of ddH_2O, 0.4 μl of each forward primer and reverse primer, and 2.0 μl of cDNA. The reaction program was set to 94°C for 10 min, followed by 40 cycles with 94°C for 20 s, 55°C for 20 s, and 72°C for 20 s.

The relative expression amount of the selected genes was calculated according to the $2^{-\Delta\Delta Ct}$ method (Livak and Schmittgen, 2001). The sample with the lowest expression level was taken as the calibrator for each gene, and it was set to 1.

Statistical Analysis

Three biological replicates were included for the measurement of the anthoxanthin and anthocyanin and qRT-PCR for each gene. In figures, the values were present as the mean ± standard error (SE) of three replicates. Significance was determined by Duncan test ($p < 0.05$) by SPSS Statistics version 19.0.

RESULTS

Analysis of Flavonoid Accumulations in *Freesia* Flowers

Eight flavonol components and two dihydroflavonoid components were detected in the petals of *Freesia* by UPLC-Q-TOF-MS (**Table 1**). Among them, component 1, component 2, component 3, and component 4 were identified through the standard chemicals, which were kaempferol, quercetin, quercetin-3-*O*-rutinoside, and quercetin 3-galactoside, respectively. The other six components were inferred based on the mass spectrum data.

The anthocyanin components of *Freesia* petals were identified, and 12 anthocyanin components were obtained (**Table 2**). According to the standards, six components, namely, component 1, component 2, component 3, component 4, component 5, and component 6, were identified exactly, which are cyanidin 3-*O*-glucoside, delphinidin-3-*O*-glucoside, petunidin 3-*O*-glucoside, peonidin 3-*O*-glucoside, malvidin 3-*O*-glucoside,

[2]http://www.geneontology.org
[3]http://www.genome.jp/kegg
[4]https://www.ncbi.nlm.nih.gov/research/cog/
[5]http://pfam.sanger.ac.uk/
[6]http://www.hmmer.org/
[7]http://kobas.cbi.pku.edu.cn/help.do
[8]https://sourceforge.net/projects/mev-tm4/
[9]http://www.premierbiosoft.com/products/products.html

TABLE 1 | Identification of anthoxanthins component from *Freesia hybrida* petals.

Component	Retention time (min)	Quasi-molecular ions (m/z)	Fragment ions (m/z)	Tentative identification
1	10.62	285	151	Kaempferol*
2	9.13	301	107	Quercetin*
3	5.76	609	301	Quercetin 3-*O* rutinoside*
4	5.93	463	301	Quercetin 3-galactoside*
5	6.13	623	315	Isorhammetin-R
6	6.09	463	301	Quercetin-G
7	5.48	609	301	Quercetin-N
8	6.85	447	285	Kaempferol-G
9	5.71	433	271	Naringenin-G
10	6.93	447	271	Naringenin-Gr

**Stands for compounds identified by standards; G, glucoside; Gr, glucuronide; R, rutinoside; and N, neohesperidoside.*

TABLE 2 | Identification of anthocyanins component from *Freesia hybrida* petals.

Component	Retention time (min)	Quasi-molecular ions (m/z)	Fragment ions (m/z)	Tentative identification
1	5.46	449	287	Cyanidin 3-*O*-glucoside*
2	4.98	465	303	Delphinidin 3-*O*-glucoside*
3	5.80	479	317	Petunidin 3-*O*-glucoside*
4	6.31	463	301	Peonidin 3-*O*-glucoside*
5	6.56	493	331	Malvidin 3-*O*-glucoside*
6	5.94	433	271	Pelargonidin 3-*O*-glucoside*
7	4.32	773	287	Cyanidin-GGG
8	4.25	627	303	Delphinidin-GG
9	4.71	611	303	Delphinidin-R
10	4.95	641	317	Petunidin-GG
11	5.48	625	301	Peonidin-GG
12	5.65	655	331	Malvidin-GG

**Stands for compounds identified by standards; G, glucoside; GG, diglucoside; GGG, triglucoside; and R, rutinoside.*

and pelargonidin 3-*O*-glucoside, respectively. The other six components were inferred based on the mass spectrum data.

The relative quantification of TFC and TAC in petals at different developmental stages was carried out and the results were shown in **Figure 2**.

For anthoxanthin, the TFC of GR, WR, and CH (**Figures 2A–C**) reached the highest value in S0 and decreased with the opening of the petals significantly ($p < 0.05$). The TFC of RP and CA (**Figures 2D,E**) showed an increase and then a decline, reaching the highest value at S2 and S1, respectively. At S0, except for WR (**Figure 2B**), TFC of all other four cultivars showed a higher level of accumulation. From S1 to S3, the TFC of RP and CA (**Figures 2D,E**) was significantly higher than other cultivars at each stage ($p < 0.05$), especially RP.

For anthocyanins, TAC in the petals of CH, RP, and CA (**Figures 2C–E**) showed a significant upward trend ($p < 0.05$) with the opening of the petals, reaching the highest value at S3. Among them, the TAC of RP (**Figure 2D**) was significantly higher than the other cultivars ($p < 0.05$), reaching 1,334.09 μg/g FW at S3, followed by CA (**Figure 2E**), reaching 406.26 μg/g FW. The lowest TAC was observed in CH, corresponding to 57.38 μg/g FW (**Figure 2C**). Since anthocyanins were not detected in GR and WR (**Figures 2A,B**), they are not shown in the figure.

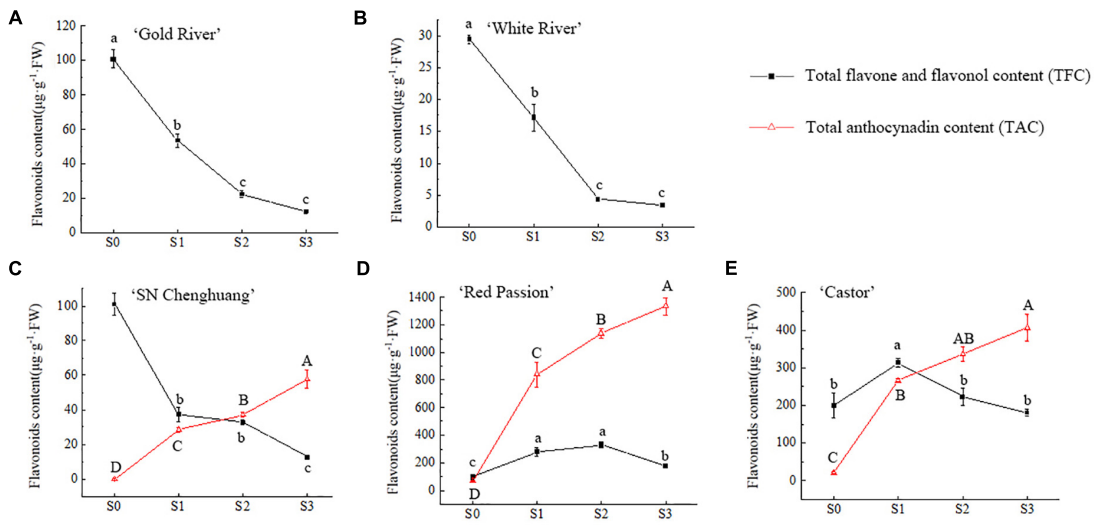

FIGURE 2 | Changes of total flavonoid content (TFC) and total anthocynadin content (TAC) in four flower developing stages of 'Gold River' **(A)**, 'White River' **(B)**, 'SN Chenghuang' **(C)**, 'Red Passion' **(D)**, and 'Castor' **(E)** petals. Uppercase and lowercase letters stand for significance of TAC and TFC in different stages, respectively. The significance of difference is at 0.05 level measured by using the Duncan test.

De novo Transcriptome Assembly and Functional Annotation of Unigenes

Since a significant difference was present in the accumulation of flavonoid among five *Freesia* cultivars at S3, petals at this stage of each cultivar were chosen as materials for transcription sequencing. Sequencing the petals of the five *Freesia* cultivars at S3, a total of 188.29 Gb clean data were obtained, and the clean data of each sample reached 4.59 Gb. After assembly, a total of 1,00,539 unigenes were obtained with a mean length of 1,126 nt. The N50 of unigene was 1,523 nt, and 24,917 unigenes were longer than 1,000 nt, showing a high assembly integrity. Other detailed data are shown in **Supplementary Table 4**.

Comparing the obtained unigenes with COG, GO, KEGG, and other eight databases, a total of 30,857 unigenes were annotated. The specific statistical results are shown in **Supplementary Table 5**.

Differential Expression Analysis of Unigenes

The transcriptome library of petal samples of four colored cultivars at S3 was compared with that of white cultivar (WR) at S3. A total of 5,162 DEGs were obtained from the four DEG sets (**Supplementary Table 6**).

The largest number of DEGs of 2,584 was present in CH3 vs. WR3, followed by 2,546 in RP3 vs. WR3. The least number of DEGs was observed in GR3 vs. WR3, with only 14 genes. Comparing WR3 with the other individual cultivars, it was found that there were more downregulated genes than the upregulated genes. A total of 1,545 genes were downregulated in WR3 compared with CH3. Comparing WR3 with CA3 and RP3, 1,191 and 1,307 genes were downregulated, respectively, while only eight genes were downregulated in GR3.

Comparing the 5,162 DEGs with the GO database, a total of 2,067 DEGs were annotated (**Supplementary Figure 1**). Among them, a large number of DEGs were enriched in the metabolic process, cell, and catalytic activity.

Comparing all above DEGs with the KEGG database, a total of 714 genes were annotated. Among them, the flavonoid biosynthesis pathway had the highest enrichment factor of 3.52 (**Supplementary Figure 2**), and 22 differential genes in this pathway were annotated. The comparison of these 22 DEGs based on FPKM values indicates that their expression differs among different flower-colored cultivars of *Freesia*, and a higher expression level was present in the dark-colored cultivars than in the light-colored cultivars. Thus, the expression of genes in the flavonoids biosynthesis pathway may be closely related to the color difference of *Freesia*.

Comparing the 5,162 DEGs with the Pfam database, the top 20 TF families with the largest number were counted (**Supplementary Figure 3**). Among them, *AP2*, *WRKY*, and *bHLH* were ranked as the top three TF families in *Freesia*. The largest number (15 in total) was present in the *AP2* family, followed by the *WRKY* family, 13 in total, and 10 in the *bHLH* family. It suggests that the expression of *AP2*, *bHLH*, and *WRKY* TFs is significantly different among these different cultivars at S3 and may be involved in the regulation of formation of flower color in *Freesia*.

Validation of Differential Expression of Structural Genes Involving in Flavonoid Biosynthesis by Quantitative Real-Time PCR

Based on the above results of the flavonoid components, the structural genes in this pathway were preliminarily searched in the transcriptome database by keywords of the components. Then, BLAST+ was used to compare the related genes in the flower transcriptome database with the known genes in the NCBI database, and 13 structural genes involving in the flavonoid synthesis pathway were screened with the higher matching degree. The gene number and nomenclature are shown in **Supplementary Table 7**. Notably, 7 out of above 13 genes were further verified by using qRT-PCR, and their expression patterns were analyzed (**Figure 3**).

In the light-colored *Freesia* cultivars (GR and WR), the expression levels of all selected seven structural genes were much lower than those in the dark-colored cultivars, RP, CA, and RP, at S3. The highest expression level of *CHS1*, *CHI2*, and *F3H1* was observed in RP3, CA3, and RP3, respectively, while the expression of these genes was much lower in GR3 and WR3. The expression of *DFR1* and *ANS1* was also high in the dark-colored cultivars, peaking in RP3 and CA3, respectively, which was much higher than that in the light-colored cultivars GR and WR, consistent with no anthocyanins detected in the two cultivars. The expression pattern of *3GT1* was similar to that of *CHI2*. The highest and the lowest expressions were observed in RP3 and WR3, respectively. Although similar expression pattern of *FLS1* with *DFR1* was present, the expression level of this gene was quite different. A significantly higher level of *FLS1* was detected in RP3 than in other three cultivars.

Explore Novel Candidate Transcription Factors Involving in Flavonoid Biosynthesis

Recently, it was confirmed that WRKY and AP2 TFs were involved in the regulation of the flavonoid biosynthesis in some plants other than *Freesia*. As mentioned above, the expression of WRKY and AP2 family TFs was significantly different in the petals of *Freesia* cultivars with different flower colors. Therefore, to explore more novel TFs that may affect the flavonoid synthesis pathway in the petal of *Freesia*, the WRKY and AP2 TFs and the above structural genes in this pathway were used for cluster analysis based on their FPKM values, and the candidate TFs were screened according to their consistent expression patterns.

A total of 32 WRKY family TFs with five key structural genes involving in the flavonoid biosynthesis pathway in the petals of *Freesia*, namely, *CHS1* (c80871.graph_c0), *CHI2* (c86861.graph_c0), *F3H1* (c91613.graph_c0), *DFR1* (c105946.graph_c0), and *ANS1* (c97452.graph_c0), were combined to perform cluster analysis, and the results are shown in **Figure 4**.

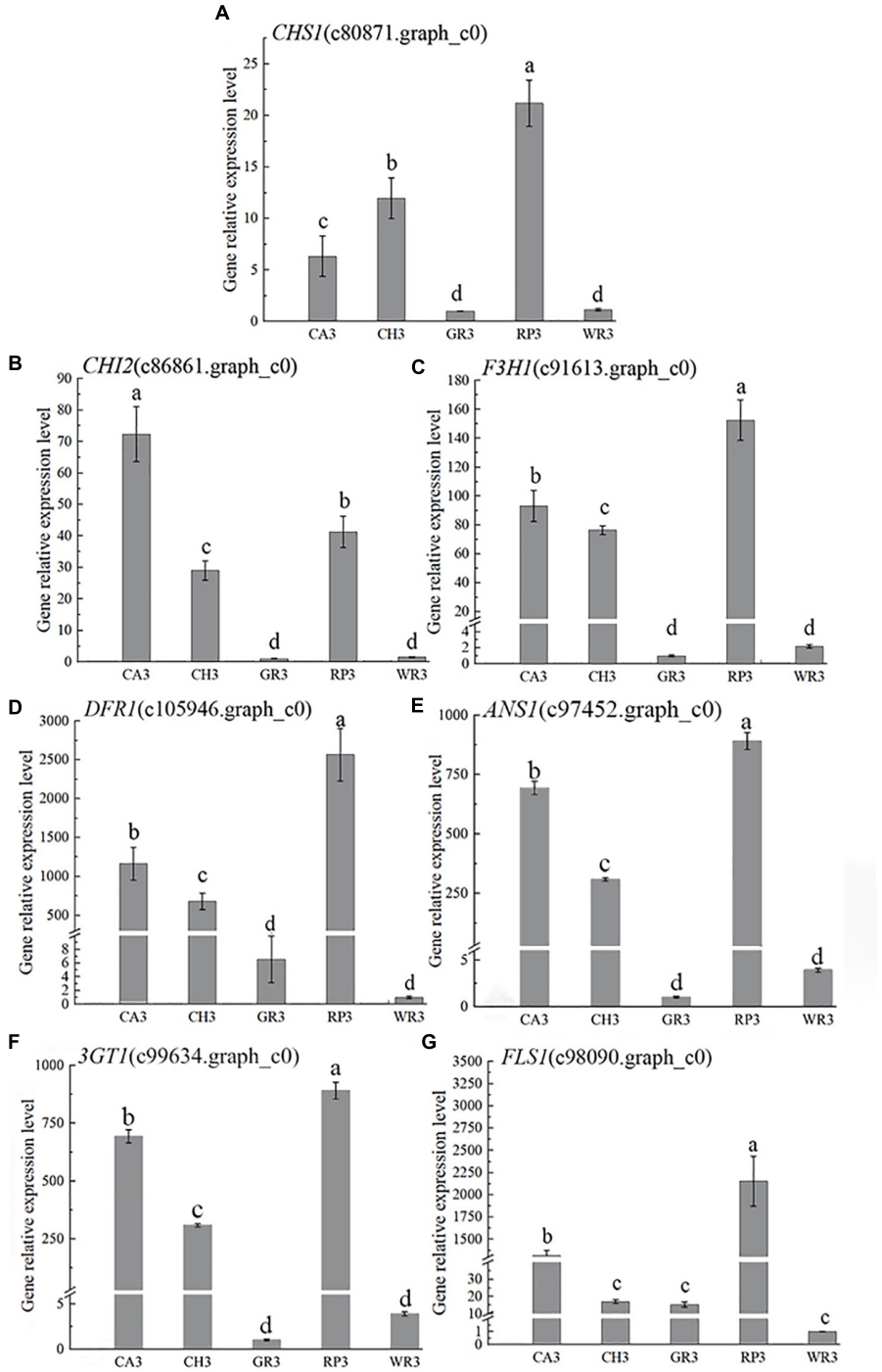

FIGURE 3 | The expression characteristics of seven structural genes of *Freesia hybrida*. **(A)** *CHS1*, **(B)** *CHI2*, **(C)** *F3H1*, **(D)** *DFR1*, **(E)** *ANS1*, **(F)** *3GT1*, and **(G)** *FLS1*. GR3 was chosen as calibrator sample of *CHS1*, *CHI2*, *F3H1*, and *3GT1*; WR3 was chosen as calibrator sample of *DFR1*, *ANS1*, and *FLS1*. Lowercase letters stand for the significance of difference at 0.05 level.

Among all the WRKY TFs clustered to closer branches with the structural genes, the unigenes c74453.graph_c0 and c103059.graph_c0 were screened due to their closest distance. These two genes were then compared with the *Freesia* corm transcriptome database, and it was found that their expression level in the *Freesia* corms was low. Therefore, the genes c103059.graph_c0 and c74453.graph_c0 were then selected as the candidate unigenes.

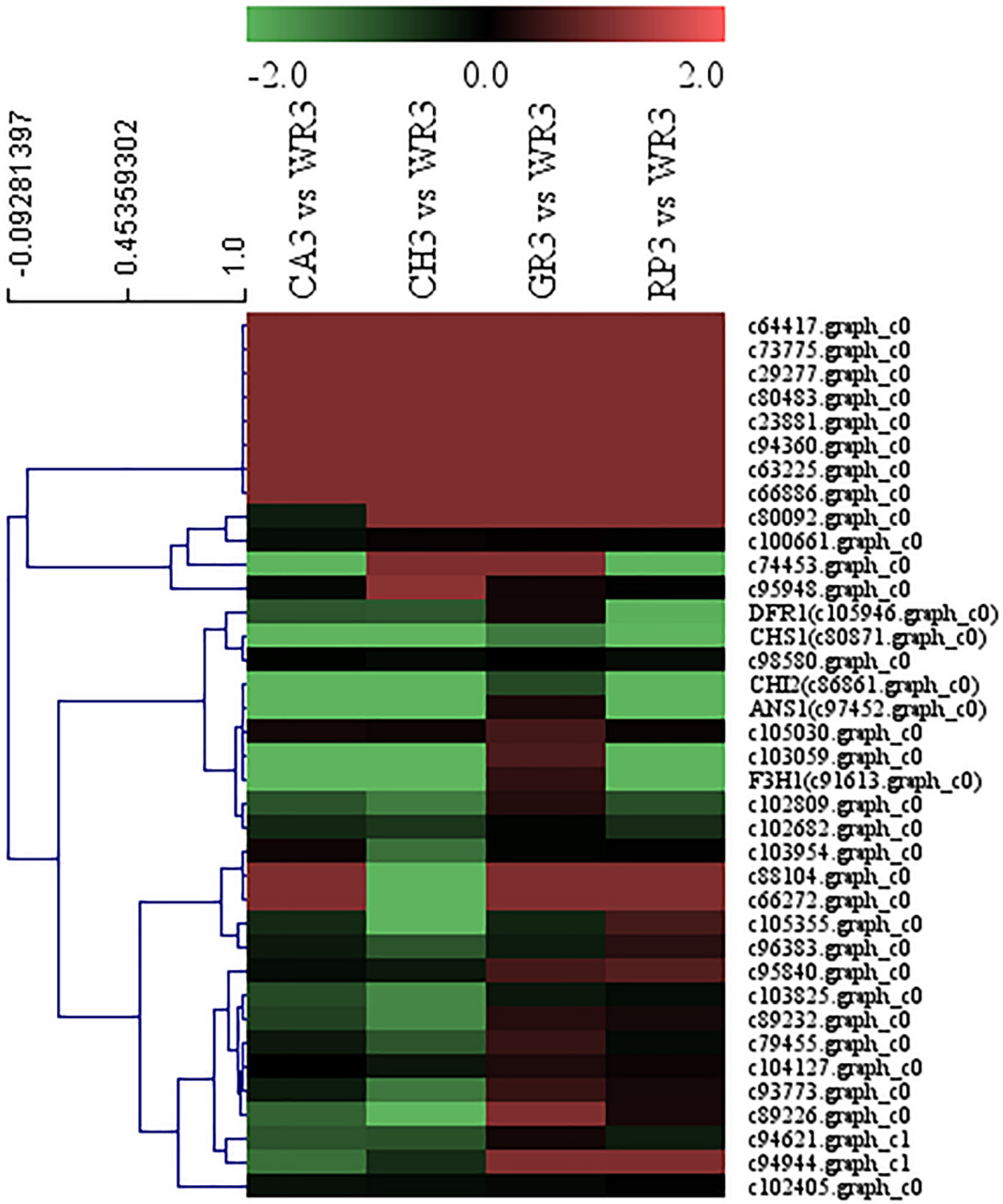

FIGURE 4 | Cluster thermogram of *WRKY* with key structural genes in flavonoid biosynthesis process of *Freesia hybrida*.

As discussed earlier, the highest expression abundance and the highest flavonoid content were observed in the red cultivar RP. Therefore, this cultivar was chosen to verify the temporal and spatial expression characters of selected candidate TFs by using qRT-PCR (**Figure 5**). The expression of the gene c103059.graph_c0 showed a gradual increase with the development of RP petals, reaching the maximum at S3 (**Figure 5A**), which was consistent with the accumulation of flavonoids. However, the expression levels of this gene in leaves and stems were much lower than that in petals. With the development of petals, another candidate gene, c74453.graph_c0, showed a slightly different trend, which peaked at S2 and then declined slightly at S3; meanwhile, its expression in roots, leaves, and stems was extremely low (**Figure 5B**).

After preliminary screening, 44 AP2 family TFs were combined with the above five structural genes to perform cluster analysis, and the results are shown in **Figure 6**. Similar to the above *WRKY* screening, two *AP2* family genes, c97095.graph_c0 and c101694.graph_c0, were chosen and compared with the *Freesia* corm transcriptome database, and the expression levels

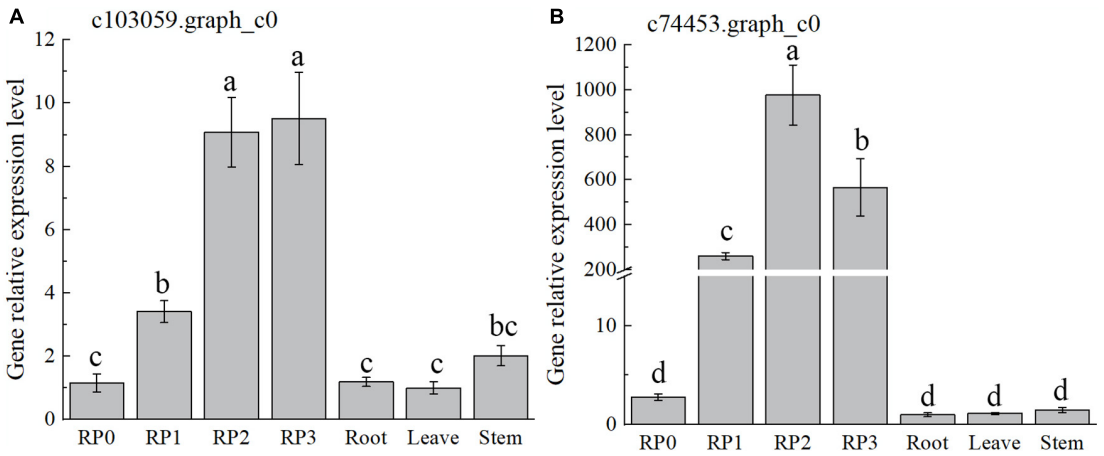

FIGURE 5 | Expression characteristics of two selected *WRKY* TFs in *Freesia hybrida* 'Red Passion' (RP). RP0, RP in the green bud stage; RP1, RP in the budding stage; RP2, RP in the early flowering stage; and RP3, RP in the flowering stage. The leaf was chosen as a calibrator sample of c103059.graph_c0 **(A)**. Root was chosen as a calibrator sample of c74453.graph_c0 **(B)**. Lowercase letters stand for the significance of difference at 0.05 level.

of the selected two TFs in the *Freesia* corms were also much lower than those in the petals, indicating that these two AP2 TFs had higher specificity in petals. Therefore, these two AP2 TFs were then selected as candidate unigenes to further study their pattern of gene expression of different flowering stages and different tissues by using qRT-PCR in the red cultivar RP.

The expression of both genes, c97095.graph_c0 and c101694.graph_c0, showed a gradual increase with the development of petals and reached the maximum at S3 (**Figure 7**), which was consistent with the accumulation of flavonoids in the petals of the cultivar. Meanwhile, the expression of these two genes, especially c97095.graph_c0, was significantly higher at S2 and S3 than that at S0 and S1 of petals and other tissues (**Figure 7**). The spatiotemporal expression pattern showed that these four TFs were expressed in large quantities in petals, revealing that they may play an important role in the regulation of flower color.

DISCUSSION

Flavonoid Accumulations Affect Color in *Freesia* Flowers

Four flavonoids and flavonol aglycones, namely, quercetin, kaempferol, isorhamnetin, and naringenin, and a total of 10 anthoxanthin components were detected in *Freesia* petals by UPLC-Q-TOF-MS in this present study. These components have been reported in some ornamental flowers. For example, quercetin, kaempferol, and isorhamnetin were reported in *Primula officinalis* (Karl et al., 1981), and the apigenins, luteolins, and hollandrins were detected in *Iris* × *hollandica* and *Iris rossii* but not reported in *Freesia* (Mizuno et al., 2012, 2013). Kaempferol and quercetin flavonoids were detected in water lilies (*Nymphaea* spp.) and lilies (*Lilium*) and confirmed to affect the appearance of flower color (Guo et al., 2015; Wu et al., 2016). A variety of flavonoids, such as naringenin, quercetin, kaempferol, and luteolin, were also identified in *Zantedeschia hybrida*, which were closely related to the color appearance of yellow, pink, and red calla lily cultivars (Lei et al., 2017).

Anthocyanins were detected in the petals of orange, red, and purple cultivars of *Freesia* but not in white and yellow cultivars. The six most common anthocyanins in plants, namely, cyanidin, delphinidin, petunidin, peonidin, malvidin, and pelargonidin, were all observed in the petals of *Freesia* in this present study. Among them, pelargonidin-3-*O*-glucoside, delphinidin-rutinoside, and cyanidin-triglucoside were first identified in *Freesia*. So far, it is the first proof that *Freesia* contains all the six anthocyanin aglycones.

In orange, yellow, and white cultivars of *Freesia*, the anthoxanthin peaked at S0, followed by a rapid decline, which was similar to the case with *Peony*, *Magnolia biondii*, and *Lonicera* (Yang et al., 2015; Wang et al., 2019; Liu et al., 2020), while in the red and purple *Freesia* cultivars, the anthoxanthin increased first up to S2 and then decreased at S3. Starting from S1, the anthoxanthins in the orange, yellow and white cultivars declined rapidly, while it increased in the red and purple cultivars. It suggested that the anthoxanthins in the petals of orange, yellow, and white cultivars of *Freesia* were synthesized faster than the red and purple cultivars, and the synthesis of the main anthoxanthins was basically completed at S0, while the red and purple cultivars required more anthoxanthins, so they continued to be synthesized at S1 and S2.

During the flower opening in orange, red, and purple cultivars of *Freesia*, anthocyanins showed an upward trend, reaching a maximum at S3, which was significantly higher than that at S0 and S1. This trend was similar to that of *Matthiola incana*, *Primulina swinglei*, and other plants (Hu et al., 2018; Nuraini et al., 2020). In CH, RP, and CA, the anthocyanin content kept a continuous increase from S0 to S3. Up to S3, the accumulation slowed down to some extent. The anthocyanin content in the petals of the red and purple cultivars of *Freesia* was always significantly higher than that of the orange cultivar, and the

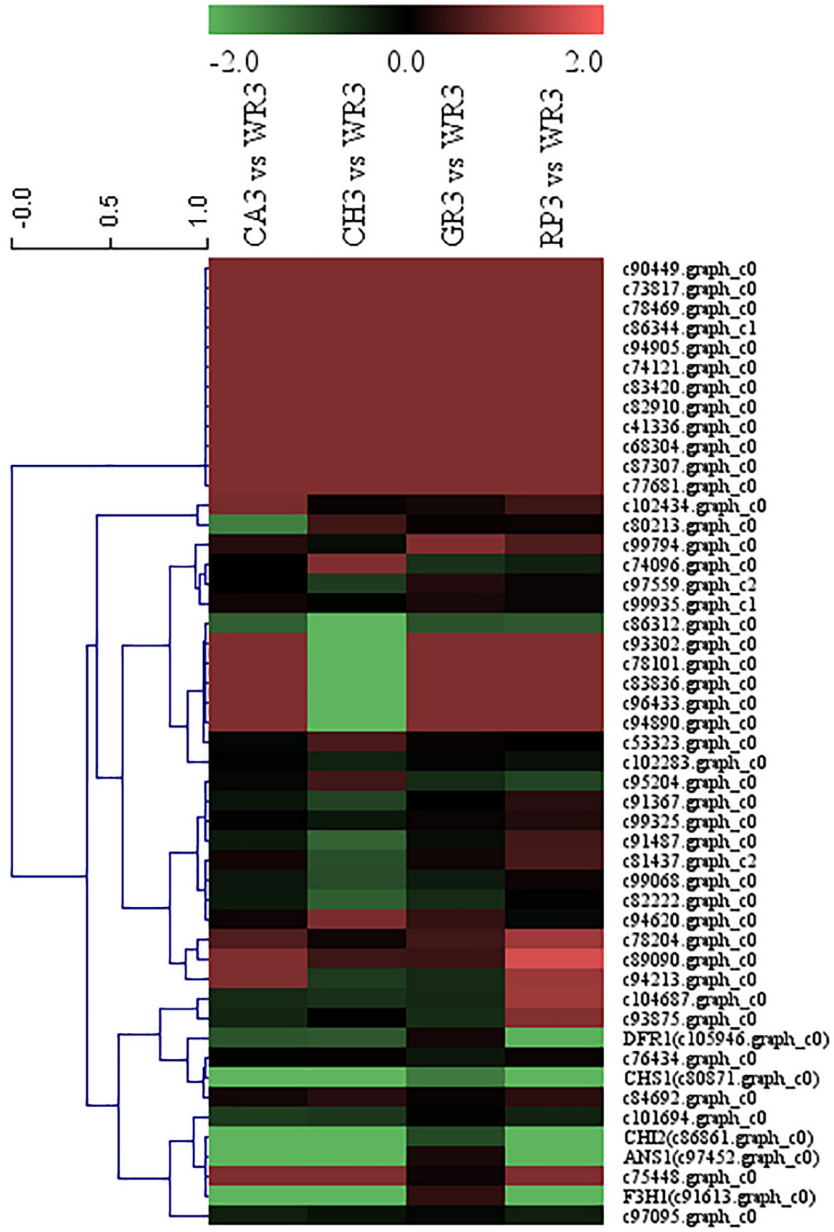

FIGURE 6 | Cluster thermogram of *AP2* with key structural genes in flavonoid biosynthesis process of *Freesia hybrida*.

anthocyanin content between the cultivars was significantly different. These results indicated that the accumulation of anthocyanins in different cultivars was different.

The correlation analysis (**Supplementary Table 8**) was further conducted based on the flavonoid contents and CIE L^* a^* b^* values of *Freesia* petals (data not shown). The results showed that the more accumulation of flavonoid, the less brightness, and the more redness were possessed in the petals of *Freesia*, revealing that the flavonoid accumulation affected directly the petal color of *Freesia*. It is already clear that the synthesis and accumulation of flavonoids are closely related to the structural genes and TFs in its synthesis pathway. Therefore, to clarify the mechanism of formation of flower color in *Freesia*, it is necessary to further study the expression differences of related genes and explore more novel TFs.

Expression of Genes Involved in Flavonoids Biosynthesis Is Correlated With the Flower Color of *Freesia*

Based on the above component analysis, it was the first time to detect all three branches of anthocyanin biosynthesis existed in *Freesia*. We further analyzed the gene expression in these pathways.

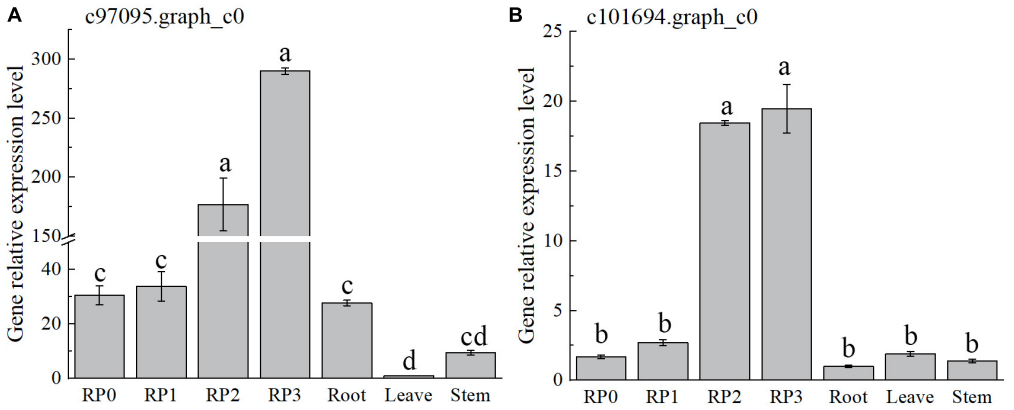

FIGURE 7 | Expression characteristics of two selected *AP2* in *Freesia hybrida* 'Red Passion' (RP). RP0, RP in the green bud stage; RP1, RP in budding stage; RP2, RP in early flowering stage; and RP3, RP in flowering stage. The leaf was chosen as a calibrator sample of c97095.graph_c0 **(A)**. Root was chosen as a calibrator sample of c101694.graph_c0 **(B)**. Lowercase letters stand for the significance of difference at 0.05 level.

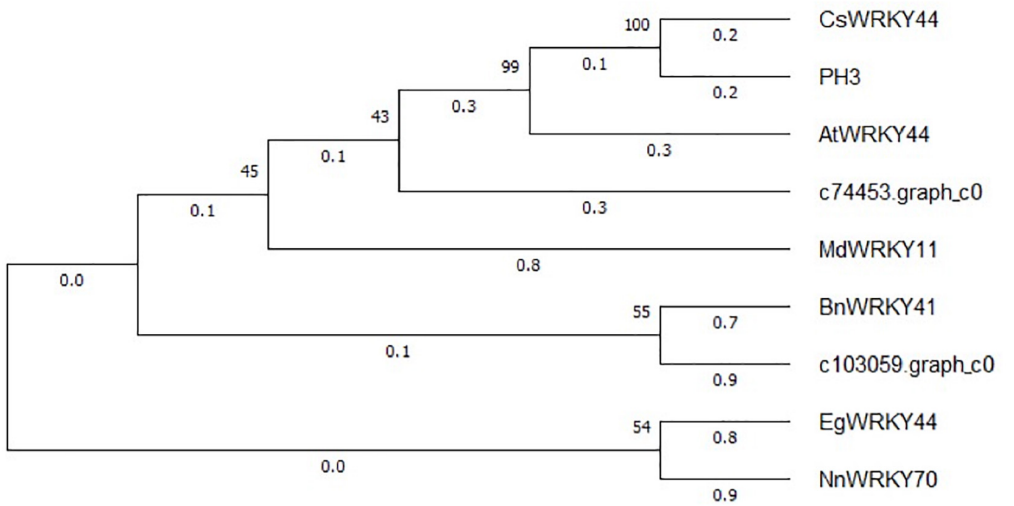

FIGURE 8 | Phylogenetic tree of two selected *WRKY* unigenes and *WRKY* TFs from other plant species. The sequences included *Camellia sinensis CsWRKY44* (MG298960.1), *Petunia hybrida PH3* (AMR43368.1), *Arabidopsis thaliana AtWRKY44* (NM_129282.4), *Malus domestica MdWRKY11*(HM122714.1), *Brassica napus BnWRKY41*(XM_013831080.2), *Elaeis guineensis EgWRKY44*(XM_029264803.1), and *Nelumbo nucifera NnWRKY70*(XM_010253742.2).

The structural genes in the flavonoid biosynthesis pathway played an important role in the synthesis of anthoxanthins and anthocyanins. It was already known that genes *CHS*, *CHI*, and *F3H* were the most upstream structural genes in this pathway, affecting the expression of downstream genes and the accumulation of flavonoids. For instance, in pomegranate, it was found that the expression of genes *CHS* and *CHI* was synergistic, and their synergistic expression was beneficial to the synthesis of downstream flavonoids (Zhao and Yuan, 2019). In Yunnan peony (*Paeonia delavayi*), the expression pattern of *PlCHS3*, *PlCHI1*, *PlF3H1*, and other genes in the purple-red cultivar was consistent with the pattern of flavonoid accumulation, which played an important role in the formation of its flower color (Shi et al., 2015). Similarly, in the tulip (*Tulipa fosteriana*), the expression levels of *TfCHS1*, *TfCHI2*, and *TfF3H1* continued to increase as the petal development, leading to the accumulation of anthocyanins and flavonols in the petals, and the color of the flower became darker (Yuan et al., 2014). Studies also showed that the blocked expression of *CHS* in the petals of *Parrya nudicaulis* affected the synthesis of flavonoids and made the petals appear white color (Dick et al., 2011). Our findings showed that in the light-colored *Freesia* cultivars GR and WR, the expression levels of *CHS1*, *CHI2*, and *F3H1* were lower, which may cause lower TFC and lighter color in their petals. Its synergistic upregulated expression can directly affect the accumulation of anthocyanins in the petal development of the dark-colored cultivars of *Freesia*.

DFR and *ANS* are the two key genes for anthocyanin synthesis branches. In *Freesia* petals, the expression of *DFR1* and *ANS1* was generally at a high level in the dark-colored cultivars. In contrast,

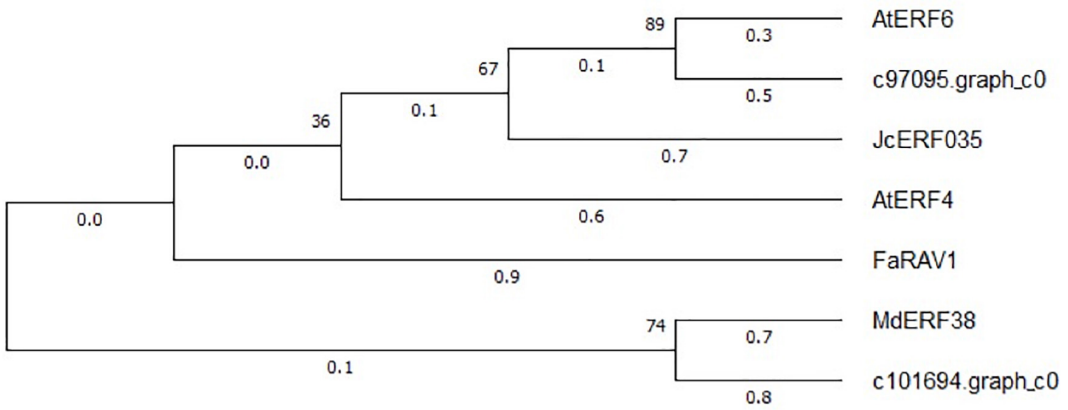

FIGURE 9 | Phylogenetic tree of two selected *AP2* unigenes and *AP2* TFs from other plant species. The sequences included *Arabidopsis thaliana AtEFR6* (AB013301.1), *Jatropha curcas JcERF035* (XM_012237693.3), *Arabidopsis thaliana AtERF4* (NM_112384.2), *Fragaria* × *ananassa FaRAV1* (XM_011466945.1), and *Malus domestica MdEFR38* (MG099847.1).

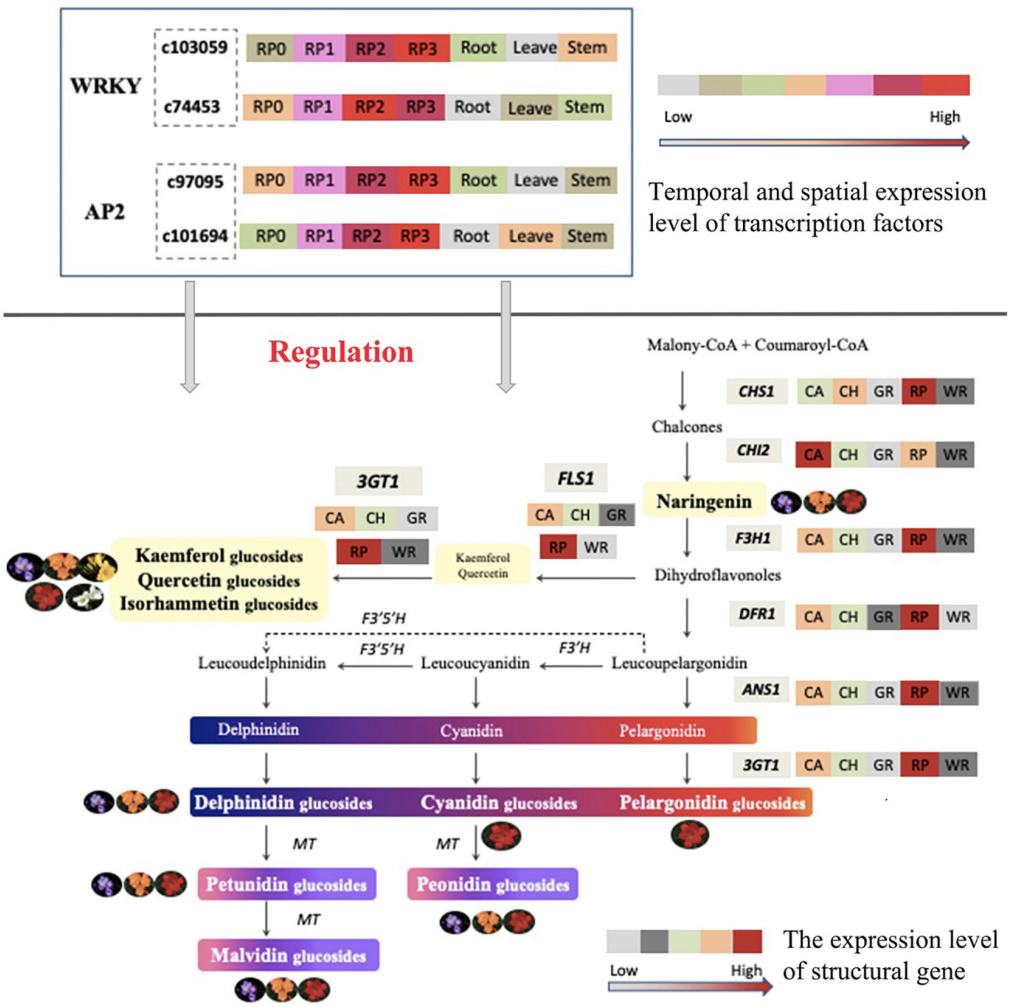

FIGURE 10 | Proposed model of the metabolism and gene regulation of flavonoid in the petals of *Freesia*.

anthocyanins were not detected in yellow and white cultivars (GR and WR). Accordingly, the expression of *DFR1* and *ANS1* in the two cultivars was present a very low level, in contrast to the dark-colored cultivars. The low expression led to the hindrance of anthocyanin synthesis, thereby affecting the appearance of flower color in the yellow and white cultivars. Similar results were reported in *Centaurea cyanus* and roses (*Rosa multiflora*) (Deng et al., 2019; Huang et al., 2019). *FLS*, catalyzing the synthesis of flavonols, competes with the anthocyanin synthesis branch gene *DFR* for the common substrate. The expression of gene *FLS1* in CA and RP was significantly higher than that in other cultivars, which was consistent with the accumulation pattern of anthoxanthin content in the petals of *Freesia*, indicating that the expression of *FLS1* affected anthoxanthin in petals of various cultivars. UF3GT was at the end of the flavonoid biosynthesis pathway, catalyzing the combination of flavonoid aglycone and glycosyl to form a more stable glycoside structure. It was verified that *Fh3GT2* in the *Freesia* red cultivar 'Red River' was preferentially involved in glycosylation of kaempferol, while *Fh3GT1* was involved in the glycosylation process of quercetin and anthocyanin (Meng et al., 2019). The expression of *3GT1* selected in this study was significantly higher in the dark-colored cultivars than that in the light-colored cultivars, consistent with the distribution of flavonoids, indicating that this gene had an effect on the glycosylation of flavonoids in the petals of *Freesia*.

Novel Candidate Transcription Factors Identified From the Transcriptome Database Might Regulate Flavonoids Biosynthesis in *Freesia* Flowers

As already known, some TF families can regulate the structural genes of the flavonoid synthesis pathway. Among them, three TF families, MYB, bHLH, and WD40, were extensively studied, including *Freesia*, and their regulating mechanism was relatively clear. It is natural to consider whether there exist other TFs except the above three TF families, which are involved in regulating the flavonoid synthesis in a certain plant. Recently, it is a hotspot to explore related novel TFs and enrich the mechanism of formation of flower color. So far, there have also been some studies focusing on other TF families related to flavonoid synthesis in some plant species. Among them, some TFs in WRKY, AP2, bZIP, NAC, and other families have been found to be closely related to the anthocyanin synthesis (Rameneni et al., 2020), especially the AP2 and WRKY TF families, which have become research hotspots in recent years. Therefore, some candidate WRKY and AP2 families were selected to explore the possible roles related to the flavonoid biosynthesis in petals of *Freesia*.

The expression patterns of the two WRKY TFs selected in this study were consistent with the accumulation pattern of flavonoids in the petals of *Freesia*, thus revealing that they may involve in functions related to flavonoid synthesis. By constructing the phylogenetic tree (**Figure 8**), we found that these two candidate *WRKY* genes were clustered with *AtWRKY44*, *PH3*, *CsWRKY44*, *MdWRKY11*, and *BnWRKY41*, suggesting that they may have similar functions to these genes. Earlier studies showed that *MdWRKY11* in apples had a positive regulatory effect on the expression of genes such as *F3H*, *DFR*, *ANS*, and *UFGT*, which can affect the synthesis of flavonoids (Wang et al., 2018). *AtWRKY44* in *Arabidopsis* affected the synthesis of proanthocyanidins (Johnson et al., 2002; Gonzalez et al., 2016), and the *PH3* of petunia can bind to *WD40* family TFs, thereby affecting the regulation of anthocyanin synthesis pathways (Faraco et al., 2014; Verweij et al., 2016). In tea plants, the gene *CsWRKY44* plays a key role in regulating the synthesis of catechins (Zhang et al., 2018). Duan et al. (2018) found that *BnWRKY41* in *Brassica napus* affected its anthocyanin accumulation when overexpressed in *Arabidopsis thaliana*. Similar to WRKY TFs, the expression of two selected AP2 TFs was also consistent with the flavonoid accumulation in the *Freesia* petals, and they were clustered with two known *AP2* TFs based on the phylogenetic analysis (**Figure 9**). In *Jatropha curcas*, the *AP2* family gene *JcERF035* was confirmed to affect the synthesis and accumulation of anthocyanins in its tracheal tissue (Chen Y. et al., 2018). In apples, *MdERF3* was also found to interact with *MdMYB1* to positively regulate anthocyanin synthesis (An et al., 2020). Hence, the candidate *AP2* TFs in *Freesia* may have similar functions to these genes.

In addition, the temporal and spatial expression of these four candidate TFs showed an increasing trend along with the development of flower, and a much higher level was present in petals than other tissues in the red cultivar RP. The above results indicate that the selected WRKY and AP2 family TFs may be involved in the regulation of flavonoid synthesis in the petals of *Freesia*.

CONCLUSION

Taken together, the composition and content of anthoxanthin and anthocyanin varied among *Freesia* cultivars with different flower colors and were relative to their flower color. All six common anthocyanin aglycones in plants were detected, and all three anthocyanin biosynthesis branches were proved as existing in *Freesia* at first time in this study. The expression of key structural genes was consistent with the component and accumulation of flavonoids in petals of different *Freesia* cultivars. Combined the transcriptomic and expression analysis, two WAKY TFs and two AP2 TFS were screened, and their spatiotemporal expression characters suggested that these novel candidate TFs may participate in the regulation of flavonoid synthesis in the petals of *Freesia*. A model of flavonoid metabolism and its gene regulation in *Freesia* petals is proposed in **Figure 10**. The findings of this study laid a solid foundation for the study of molecular mechanism and gene function of the formation of flower color in *Freesia* in future.

DATA AVAILABILITY STATEMENT

The original contributions presented in the study are publicly available. This data can be found here: National Center for

Biotechnology Information (NCBI) BioProject database under accession number PRJNA656641.

AUTHOR CONTRIBUTIONS

JZ performed the experiments, analyzed the data, and drafted the manuscript. DT and XG revised the manuscript and helped in completing the final manuscript. XL assisted in the UPLC-Q-TOF-MS analysis. DT designed the experiments, provided guidance on the whole study, and contributed with valuable discussions. All authors contributed to the article and approved the submitted version.

FUNDING

This work was funded by Shanghai Municipal Agricultural Commission, China, under Grant Hu Nong Ke Tui Zhi (2020) no. 1-1.

SUPPLEMENTARY MATERIAL

The Supplementary Material for this article can be found online at: https://www.frontiersin.org/articles/10.3389/fpls.2021.756300/full#supplementary-material

REFERENCES

An, J.-P., Zhang, X.-W., Bi, S.-Q., You, C.-X., Wang, X.-F., and Hao, Y.-J. (2020). The ERF transcription factor MdERF38 promotes drought stress-induced anthocyanin biosynthesis in apple. *Plant J.* 101, 573–589. doi: 10.1111/tpj.14555

Chen, K., Du, L., Liu, H., and Liu, Y. (2019). A novel R2R3-MYB from grape hyacinth, MaMybA, which is different from MaAN2, confers intense and magenta anthocyanin pigmentation in tobacco. *BMC Plant Biol.* 19:390. doi: 10.1186/s12870-019-1999-0

Chen, M., Xu, M., Xiao, Y., Cui, D., Qin, Y., Wu, J., et al. (2018). Fine mapping identifies SmFAS encoding an anthocyanidin synthase as a putative candidate gene for flower purple color in *Solanum melongena* L. *Int. J. Mol. Sci.* 19:789. doi: 10.3390/ijms19030789

Chen, Y., Wu, P., Zhao, Q., Tang, Y., Chen, Y., Li, M., et al. (2018). Overexpression of a phosphate starvation response AP2/ERF gene from physic nut in *Arabidopsis* alters root morphological traits and phosphate starvation-induced anthocyanin accumulation. *Front. Plant Sci.* 9:1186. doi: 10.3389/fpls.2018.01186

Deng, C., Li, S., Feng, C., Hong, Y., Huang, H., Wang, J., et al. (2019). Metabolite and gene expression analysis reveal the molecular mechanism for petal colour variation in six *Centaurea cyanus* cultivars. *Plant Physiol. Biochem.* 142, 22–33. doi: 10.1016/j.plaphy.2019.06.018

Dick, C. A., Buenrostro, J., Butler, T., Carlson, M. L., Kliebenstein, D. J., and Whittall, J. B. (2011). Arctic mustard flower color polymorphism controlled by petal-specific downregulation at the threshold of the anthocyanin biosynthetic pathway. *PLoS One* 6:e18230. doi: 10.1371/journal.pone.0018230

Ding, S., Li, X., and Tang, D. (2020). Screening on reference genes for real-time fluorescent quantitative PCR of Freesia hybrida. *J. Nanjing For. Univ. Nat. Sci. Edn.* 44, 19–25.

Du, H., Lai, L., Wang, F., Sun, W., Zhang, L., Li, X., et al. (2018). Characterisation of flower colouration in 30 *Rhododendron* species via anthocyanin and flavonol identification and quantitative traits. *Plant Biol.* 20, 121–129. doi: 10.1111/plb.12649

Duan, S., Wang, J., Gao, C., Jin, C., Li, D., Peng, D., et al. (2018). Functional characterization of a heterologously expressed *Brassica napus* WRKY41-1 transcription factor in regulating anthocyanin biosynthesis in *Arabidopsis thaliana*. *Plant Sci.* 268, 47–53. doi: 10.1016/j.plantsci.2017.12.010

Faraco, M., Spelt, C., Bliek, M., Verweij, W., Hoshino, A., Espen, L., et al. (2014). Hyperacidification of vacuoles by the combined action of two different P-ATPases in the tonoplast determines flower color. *Cell Rep.* 6, 32–43. doi: 10.1016/j.celrep.2013.12.009

Gonzalez, A., Brown, M., Hatlestad, G., Akhavan, N., Smith, T., Hembd, A., et al. (2016). TTG2 controls the developmental regulation of seed coat tannins in Arabidopsis by regulating vacuolar transport steps in the proanthocyanidin pathway. *Dev. Biol.* 419, 54–63. doi: 10.1016/j.ydbio.2016.03.031

Guo, H., Zhang, Y., Niu, L., and Luo, J. (2015). Petal pigments of eight wild *Lilium* species native to China. *J. Northwest A F Univ. Nat. Sci. Edn.* 43, 98–104.

Hu, B., Ding, D., Fu, X., Feng, C., and Kang, M. (2018). The changes of anthocyanin content during the development of *Primulina swinglei* flower. *Acta Hortic. Sin.* 45, 117–125.

Huang, P., Lin, F., Li, B., and Zheng, Y. (2019). Hybrid-transcriptome sequencing and associated metabolite analysis reveal putative genes involved in flower color difference in rose mutants. *Plants Basel* 8:267. doi: 10.3390/plants8080267

Johnson, C. S., Kolevski, B., and Smyth, D. R. (2002). TRANSPARENT TESTA GLABRA2, a trichome and seed coat development gene of *Arabidopsis*, encodes a WRKY transcription factor. *Plant Cell* 14, 1359–1375. doi: 10.1105/tpc.001404

Karl, C., Muller, G., and Pedersen, P. A. (1981). Flavonoids in the flowers of *Primula officinalis*. *Planta Med.* 41, 96–99. doi: 10.1055/s-2007-971683

Katsumoto, Y., Fukuchi-Mizutani, M., Fukui, Y., Brugliera, F., Holton, T. A., Karan, M., et al. (2007). Engineering of the rose flavonoid biosynthetic pathway successfully generated blue-hued flowers accumulating delphinidin. *Plant Cell Physiol.* 48, 1589–1600. doi: 10.1093/pcp/pcm131

Kesavan, P., Banerjee, A., Banerjee, A., Murugesan, R., Marotta, F., and Pathak, S. (2018). "An overview of dietary polyphenols and their therapeutic effects," in *Polyphenols: Mechanisms of Action in Human Health and Disease*, eds R. Watson, V. Preedy and S. Zibadi (Amsterdam: Elsevier), 221–235.

Lei, T., Song, Y., Jin, X., Su, T., and Pu, Y. (2017). Effects of pigment constituents and their distribution on spathe coloration of *Zantedeschia hybrida*. *Hortscience* 52, 1840–1848. doi: 10.21273/hortsci12229-17

Li, X., Lu, M., Tang, D., and Shi, Y. (2015). Composition of carotenoids and flavonoids in Narcissus cultivars and their relationship with flower color. *PLoS One* 10:e0142074. doi: 10.1371/journal.pone.0142074

Li, Y., Liu, X., Cai, X., Shan, X., Gao, R., Yang, S., et al. (2017). Dihydroflavonol 4-reductase genes from *Freesia hybrida* play important and partially overlapping roles in the biosynthesis of flavonoids. *Front. Plant Sci.* 8:428. doi: 10.3389/fpls.2017.00428

Li, Y., Shan, X., Gao, R., Han, T., Zhang, J., Wang, Y., et al. (2020). MYB repressors and MBW activation complex collaborate to fine-tune flower coloration in Freesia hybrida. *Commun. Biol.* 3:396. doi: 10.1038/s42003-020-01134-6

Li, Y., Shan, X., Gao, R., Yang, S., Wang, S., Gao, X., et al. (2016). Two IIIf Clade-bHLHs from *Freesia hybrida* play divergent roles in flavonoid biosynthesis and trichome formation when ectopically expressed in *Arabidopsis*. *Sci. Rep.* 6:30514. doi: 10.1038/srep30514

Li, Y., Shan, X., Zhou, L., Gao, R., Yang, S., Wang, S., et al. (2019). The R2R3-MYB factor FhMYB5 from *Freesia hybrida* contributes to the regulation of anthocyanin and proanthocyanidin biosynthesis. *Front. Plant Sci.* 9:1935. doi: 10.3389/fpls.2018.01935

Liu, A., Yu, Q., Wang, F., Bai, G., Wang, Q., Li, S., et al. (2020). Changes of floral color and pigment content during flowering in several species of *Lonicera* L. *J. Southwest Univ. Nat. Sci. Edn.* 42, 22–29.

Livak, K. J., and Schmittgen, T. D. (2001). Analysis of relative gene expression data using real-time quantitative PCR and the 2(T)(-delta delta C) method. *Methods* 25, 402–408. doi: 10.1006/meth.2001.1262

Manning, J. C., and Goldblatt, P. (2010). *Botany and Horticulture of the Genus Freesia (Iridaceae)*. Cape Town: South African National Biodiversity Institute.

Meng, X., Li, Y., Zhou, T., Sun, W., Shan, X., Gao, X., et al. (2019). Functional differentiation of duplicated flavonoid 3-O-glycosyltransferases in the flavonol and anthocyanin biosynthesis of *Freesia hybrida*. *Front. in Plant Sci.* 10:1330. doi: 10.3389/fpls.2019.01330

Mierziak, J., Kostyn, K., and Kulma, A. (2014). Flavonoids as important molecules of plant interactions with the environment. *Molecules* 19, 16240–16265. doi: 10.3390/molecules191016240

Mizuno, T., Okuyama, Y., and Iwashina, T. (2012). Phenolic compounds from Iris rossii, and their chemotaxonomic and systematic significance. *Biochem. Syst. Ecol.* 44, 157–160. doi: 10.1016/j.bse.2012.04.022

Mizuno, T., Yabuya, T., Kitajima, J., and Iwashina, T. (2013). Identification of novel C-glycosylflavones and their contribution to flower colour of the dutch iris cultivars. *Plant Physiol. Biochem.* 72, 116–124. doi: 10.1016/j.plaphy.2013.06.028

Nabavi, S. M., Samec, D., Tomczyk, M., Milella, L., Russo, D., Habtemariam, S., et al. (2020). Flavonoid biosynthetic pathways in plants: versatile targets for metabolic engineering. *Biotechnol. Adv.* 38:107316. doi: 10.1016/j.biotechadv.2018.11.005

Nielsen, K., Deroles, S. C., Markham, K. R., Bradley, M. J., Podivinsky, E., and Manson, D. (2002). Antisense flavonol synthase alters copigmentation and flower color in lisianthus. *Mol. Breed.* 9, 217–229. doi: 10.1023/a:1020320809654

Nuraini, L., Ando, Y., Kawai, K., Tatsuzawa, F., Tanaka, K., Ochiai, M., et al. (2020). Anthocyanin regulatory and structural genes associated with violet flower color of *Matthiola incana*. *Planta* 251:61. doi: 10.1007/s00425-020-03351-z

Rameneni, J. J., Choi, S. R., Chhapekar, S. S., Kim, M.-S., Singh, S., Yi, S. Y., et al. (2020). Red Chinese cabbage transcriptome analysis reveals structural genes and multiple transcription factors regulating reddish purple color. *Int. J. Mol. Sci.* 21:2901. doi: 10.3390/ijms21082901

Shan, X., Li, Y., Yang, S., Yang, Z., Qiu, M., Gao, R., et al. (2020). The spatio-temporal biosynthesis of floral flavonols is controlled by differential phylogenetic MYB regulators in *Freesia hybrida*. *New Phytol.* 228, 1864–1879. doi: 10.1111/nph.16818

Shi, Q., Zhou, L., Wang, Y., Li, K., Zheng, B., and Miao, K. (2015). Transcriptomic analysis of *Paeonia delavayi* wild population flowers to identify differentially expressed genes involved in purple-red and yellow petal pigmentation. *PLoS One* 10:e0135038. doi: 10.1371/journal.pone.0135038

Singh, K. S., Majik, M. S., and Tilvi, S. (2014). "Vibrational spectroscopy for structural characterization of bioactive compounds," in *Analysis of Marine Samples in Search of Bioactive Compounds*, eds T. Rocha-Santos and A. C. Duarte (Amsterdam: Elsevier), 115–148.

Sun, W., Liang, L., Meng, X., Li, Y., Gao, F., Liu, X., et al. (2016). Biochemical and molecular characterization of a flavonoid 3-O-glycosyltransferase responsible for anthocyanins and flavonols biosynthesis in *Freesia hybrida*. *Front. Plant Sci.* 7:410. doi: 10.3389/fpls.2016.00410

Sun, W., Meng, X., Liang, L., Jiang, W., Huang, Y., He, J., et al. (2015). Molecular and biochemical analysis of chalcone synthase from Freesia hybrid in flavonoid biosynthetic pathway. *PLoS One* 10:e0119054. doi: 10.1371/journal.pone.0119054

Tsuda, S., Fukui, Y., Nakamura, N., Katsumoto, Y., Yonekura-Sakakibara, K., Fukuchi-Mizutani, M., et al. (2004). Flower color modification of *Petunia hybrida* commercial varieties by metabolic engineering. *Plant Biotechnol.* 21, 377–386.

Verweij, W., Spelt, C. E., Bliek, M., de Vries, M., Wit, N., Faraco, M., et al. (2016). Functionally similar WRKY proteins regulate vacuolar acidification in *Petunia* and hair development in *Arabidopsis*. *Plant Cell* 28, 786–803. doi: 10.1105/tpc.15.00608

Wang, N., Liu, W., Zhang, T., Jiang, S., Xu, H., Wang, Y., et al. (2018). Transcriptomic analysis of red-fleshed apples reveals the novel role of MdWRKY11 in flavonoid and anthocyanin biosynthesis. *J. Agric. Food Chem.* 66, 7076–7086. doi: 10.1021/acs.jafc.8b01273

Wang, N., Zhang, C., Bian, S., Chang, P., Xuan, L., Fan, L., et al. (2019). Flavonoid components of different color Magnolia flowers and their relationship to cultivar selections. *Hortscience* 54, 404–408. doi: 10.21273/hortsci13462-18

Wu, Q., Wu, J., Li, S.-S., Zhang, H.-J., Feng, C.-Y., Yin, D.-D., et al. (2016). Transcriptome sequencing and metabolite analysis for revealing the blue flower formation in waterlily. *BMC Genomics* 17:897. doi: 10.1186/s12864-016-3226-9

Xu, W., Dubos, C., and Lepiniec, L. (2015). Transcriptional control of flavonoid biosynthesis by MYB-bHLH-WDR complexes. *Trends Plant Sci.* 20, 176–185. doi: 10.1016/j.tplants.2014.12.001

Xu, W., Luo, G., Yu, F., Jia, Q., Zheng, Y., Bi, X., et al. (2018). Characterization of anthocyanins in the hybrid progenies derived from Iris dichotoma and I. domestica by HPLC-DAD-ESI/MS analysis. *Phytochemistry* 150, 60–74. doi: 10.1016/j.phytochem.2018.03.003

Xu, Y.-Q., Yuan, Y., Tao, X.-H., Yang, J., Shi, Y.-M., and Tang, D.-Q. (2016). Main anthocyanin profiles in petals of *Freesia hybrida*. *Bull. Bot. Res.* 36, 184–189. doi: 10.7525/j.issn.1673-5102.2016.02.005

Yang, Q., Yuan, T., and Sun, X. (2015). Preliminary studies on the changes of flower color during the flowering period in two tree peony cultivars. *Acta Hortic. Sin.* 42, 930–938.

Yu, J., Tang, D., and Li, X. (2020). Anthocyanin compositions in petals of *Freesia hybrida*. *Guihaia* 40, 687–695.

Yuan, Y., Ma, X., Shi, Y., and Tang, D. (2013). Isolation and expression analysis of six putative structural genes involved in anthocyanin biosynthesis in Tulipa fosteriana. *Sci. Hortic.* 153, 93–102.

Yuan, Y., Ma, X., Tang, D., and Shi, Y. (2014). Comparison of anthocyanin components, expression of anthocyanin biosynthetic structural genes, and TfF3'H1 sequences between *Tulipa fosteriana* 'Albert heijn' and its reddish sport. *Sci. Hortic.* 175, 16–26.

Yuan, Y., Shi, Y., and Tang, D. (2020). Isolation and characterization of R2R3-MYB and basic helix-loop-helix (bHLH) transcription factors involved in anthocyanin biosynthesis in tulip tepals. *Acta Physiol. Plant.* 42:32. doi: 10.1007/s11738-020-3026-3

Zhang, J., Sui, C., Wang, Y., Liu, S., Liu, H., Zhang, Z., et al. (2020). Transcriptome-wide analysis reveals key DEGs in fower color regulation of *Hosta plantaginea* (Lam.) aschers. *Genes* 11:31. doi: 10.3390/genes11010031

Zhang, Y., Wei, K., Li, H., Wang, L., Ruan, L., Pang, D., et al. (2018). Identification of key genes involved in catechin metabolism in tea seedlings based on transcriptomic and HPLC analysis. *Plant Physiol. Biochem.* 133, 107–115. doi: 10.1016/j.plaphy.2018.10.029

Zhao, X., and Yuan, Z. (2019). Expression profiles of fruit color related genes CHS and CHI in *Punica granatum* L. *Genom. Appl. Biol.* 38, 2175–2182.

Zhong, H., Chen, Y., Huang, M., Lin, B., Ye, X., and Wu, J. (2009). The component and stability of anthocyanidins in petals of *Freesia refracta* cultivars. *J. Trop.Subtrop. Bot.* 17, 571–577.

Zhu, J., Tang, D., and Li, X. (2021). Analysis of composition and content of anthoxanthins in petals of *Freesia hybrida*. *Chin. J. Trop. Crops* 42, 1136–1144.

Conflict of Interest: The authors declare that the research was conducted in the absence of any commercial or financial relationships that could be construed as a potential conflict of interest.

Publisher's Note: All claims expressed in this article are solely those of the authors and do not necessarily represent those of their affiliated organizations, or those of the publisher, the editors and the reviewers. Any product that may be evaluated in this article, or claim that may be made by its manufacturer, is not guaranteed or endorsed by the publisher.

Copyright © 2021 Zhu, Guo, Li and Tang. This is an open-access article distributed under the terms of the Creative Commons Attribution License (CC BY). The use, distribution or reproduction in other forums is permitted, provided the original author(s) and the copyright owner(s) are credited and that the original publication in this journal is cited, in accordance with accepted academic practice. No use, distribution or reproduction is permitted which does not comply with these terms.

frontiers in Plant Science

ORIGINAL RESEARCH
published: 03 December 2021
doi: 10.3389/fpls.2021.747131

Comprehensive Transcriptome and Metabolic Profiling of Petal Color Development in *Lycoris sprengeri*

Feng Yang[1,2†], Chao-han Li[1†], Debatosh Das[2†], Yu-hong Zheng[3], Tao Song[2], Lan-xiang Wang[4], Mo-Xian Chen[4], Qing-zhu Li[1] and Jianhua Zhang[5]**

[1] Forestry and Pomology Research Institute, Protected Horticultural Research Institute, Shanghai Academy of Agricultural Sciences, Shanghai, China, [2] Shenzhen Research Institute, The Chinese University of Hong Kong, Shenzhen, China, [3] Ornamental Plant Research Center, Institute of Botany, Jiangsu Province and Chinese Academy of Sciences (Nanjing Botanical Garden Memorial Sun Yat-Sen), Nanjing, China, [4] Shenzhen Institute of Synthetic Biology, Shenzhen Institutes of Advanced Technology, Chinese Academy of Sciences, Shenzhen, China, [5] Department of Biology, Hong Kong Baptist University, and State Key Laboratory of Agrobiotechnology, The Chinese University of Hong Kong, Hong Kong SAR, China

OPEN ACCESS

Edited by:
Lei Zhang,
Second Military Medical University, China

Reviewed by:
Hong-Hwa Chen,
National Cheng Kung University, Taiwan
Chen Junfeng,
Shanghai University of Traditional Chinese Medicine, China

***Correspondence:**
Qing-zhu Li
1984yu1986@163.com
Jianhua Zhang
jzhang@hkbu.edu.hk

† These authors have contributed equally to this work

Specialty section:
This article was submitted to Plant Metabolism and Chemodiversity, a section of the journal Frontiers in Plant Science

Received: *25 July 2021*
Accepted: *18 October 2021*
Published: *03 December 2021*

Citation:
Yang F, Li C-h, Das D, Zheng Y-h, Song T, Wang L-x, Chen M-X, Li Q-z and Zhang J (2021) Comprehensive Transcriptome and Metabolic Profiling of Petal Color Development in Lycoris sprengeri. Front. Plant Sci. 12:747131. doi: 10.3389/fpls.2021.747131

Lycoris sprengeri (*L. sprengeri*) is an important ornamental bulbous plant, and its numerous varieties in different color forms are widely planted. Multiple color types of petals in *L. sprengeri* provide us with possibilities to delineate the complicated metabolic networks underlying the biochemical traits behind color formation in this plant species, especially petal color. In this study, we sequenced and annotated a reference transcriptome of pink and white petals of *L. sprengeri* and analyzed the metabolic role of anthocyanin biosynthesis in regulating color pigment metabolism. Briefly, white and pink petal samples were sequenced with an Illumina platform, to obtain the reads that could be assembled into 100,778 unique sequences. Sequences expressed differentially between white vs. pink petals were further annotated with the terms of Gene Ontology (GO), Clusters of Orthologous Groups (COG), Kyoto Encyclopedia of Genes and Genomes (KEGG), and eggNOG. Gene expression analyses revealed the repression of anthocyanin and steroid biosynthesis enzymes and R2R3 MYB transcription factor (TF) genes in white petals compared to pink petals. Furthermore, the targeted metabolic profiling of anthocyanins revealed that color-related delphinidin (Del) and cyanidin (Cy) pigments are lower in white petals, which correlate well with the reduced gene expression levels of anthocyanin biosynthesis genes. Taken together, it is hypothesized that anthocyanin biosynthesis, steroid biosynthesis, and R2R3 MYB TFs may play vital regulatory roles in petal color development in *L. sprengeri*. This work provides a valuable genomic resource for flower breeding and metabolic engineering in horticulture and markers for studying the flower trait evolution of *L. sprengeri*.

Keywords: *Lycoris sprengeri*, flavonoids, transcriptome, anthocyanin, petal color, metabolome

INTRODUCTION

Genus *Lycoris* belongs to the Amaryllidaceae family, which consists of approximately 20 species of flowering plants and is native to the moist warm temperate woodlands of eastern and southern Asia, nearly 15 of which (10 endemics) are spread throughout China (Ren et al., 2021). Most of the *Lycoris* species are commonly cultivated as bulbous plants in countries such as China, Korea,

Japan, and Vietnam (Ping-Sheng et al., 1994; Shi et al., 2006). In comparison to other well-known bulbous flowers, such as *Narcissus* spp. and *Lilium* spp., *Lycoris* has its specific traits and benefits. For example, it flowers at a time of the year during which others are not active. These flowers are characterized by their pastel, plentiful colors, and multiple flower shapes (Ping-Sheng et al., 1994). Thus, globally *Lycoris* species, such as *L. radiata*, *L. aurea*, and *L. sprengeri*, have been very popular as ornamental plants in the past few decades (Zhou et al., 2007). With an increasing demand for *Lycoris* as a commercial horticultural product, the breeding of different varieties with new petal forms and/or colors has become a valued necessity for *Lycoris*. Moreover, the bulbs of *Lycoris* have been used in traditional Chinese medicine (TCM) as some Amaryllidaceae alkaloids isolated from the bulbs of *Lycoris* have been reported to exhibit immunostimulatory, antitumor, antiviral, and antimalarial activities (Jin, 2009; Son et al., 2010; Wang et al., 2013).

The flower petal color of *L. sprengeri* varies widely from pure white color (with only the faintest pale purple stripe on the abaxial base of the petals) to an intense pink color (with blue color on the tips) (Cai et al., 2020). Flower pigmentation is mainly caused by the accumulation of pigments such as flavonoids, carotenoids, and betacyanin within epidermal cells (Zhao et al., 2012). Flavonoids consist of chalcones, anthoxanthins, and anthocyanin. Anthocyanin biosynthesis *via* flavonoid metabolism has been studied on flower development because of its high antioxidant content and UV protection properties in plants (Ithal and Reddy, 2004; Irani and Grotewold, 2005; Paśko et al., 2009; Ordidge et al., 2012; Feng et al., 2013). Anthocyanin pigment is the main pigment in flowering plants, and anthocyanin accumulation is tightly linked to floral development, including petal color changes (Weiss, 2000). Anthocyanin biosynthesis is catalyzed by two groups of genes, namely, structural genes and functional regulatory genes. The first group of structural genes includes flavanone 3-hydroxylase (*F3H*), chalcone synthase (*CHS*), anthocyanidin synthase (*ANS*), dihydroflavonol-4-reductase (*DFR*), flavonoid 3′-hydroxylase (F3′H), flavonoid 3′,5′-hydroxylase (F3′5′H), etc., which represent the enzymes responsible for the biochemical reactions of anthocyanin synthesis (Tanaka et al., 2008; Huang et al., 2012; Tan et al., 2013; **Figure 1**). DFR could catalyze a stereospecific reduction of the three dihydroflavonols to leucoanthocyanidins while flavonol synthase (FLS) catalyzes the conversion of dihydrokaempferol and dihydroquercetin to a variety of copigment flavanols and glycosidic derivatives that determine the petal color (white and/or pink) (Luo et al., 2015). The second group includes regulatory genes such as transcription factors (TFs), which regulate the expression of the abovementioned structural genes. It has been reported that the most important TFs for anthocyanin biosynthesis belong to the basic helix-loop-helix (*bHLH*), *MYB*, and *WD40* gene families (Zhou et al., 2012; Li et al., 2013). The coordinated expression of structural genes and TFs may lead to differential anthocyanin biosynthesis and accumulation during petal color development.

In recent years, transcriptome mapping has become a particularly effective method for genome annotation and discovery and the annotation of novel functional genes, especially in non-model plants, which lack a reference genome (Wang et al., 2009; Song et al., 2020). Sequencing technologies have dramatically accelerated genome-wide transcriptome studies and have been widely used to explore a novel gene structure and gene expression, even in plants without a reference genome (Chen et al., 2011; Liu et al., 2011; Shen et al., 2011). In previous studies related to *Lycoris*, the transcriptome sequencing analysis was performed to investigate the molecular basis of the synthesis of Amaryllidaceae alkaloids in *L. aurea* and *L. longituba* species (Wang et al., 2013; Park et al., 2019; Li et al., 2020). However, very few systematic studies have been performed to explore the molecular mechanism in the regulation of pigment accumulation in the different color forms of *Lycoris* petals. In this study, a comparative transcriptome and metabolome analysis of the gene expression and metabolite accumulation between white and pink petals of *L. sprengeri* was first carried out using Illumina sequencing and targeted metabolic profiling with the liquid chromatographic tandem mass spectrometry (LC-MS/MS) method, respectively. Thereby, we mainly focus on the identification of structural genes in anthocyanin biosynthesis, for example, enzymes, regulatory gene TFs, and on the differentially accumulating metabolites that may coregulate the observed color variation in *L. sprengeri* petals. The assembled and newly annotated transcriptome resource for *Lycoris* petals will provide an additional overview of genes involved in pigment pathways, including flavonoid biosynthesis. In summary, this work would enable us to understand the molecular changes behind the flower color variation in *L. sprengeri*.

MATERIALS AND METHODS

RNA Isolation, Library Preparation, and Illumina Sequencing

Lycoris sprengeri plants for this study were collected by Prof. Zheng Yu-hong (Institute of Botany, Chinese Academy of Sciences, Jiangsu Province, China). Voucher specimens of *L. sprengeri* (0653967) were deposited at the herbarium of the Institute of Botany, Chinese Academy of Sciences. A total amount of 1 μg isolated RNA per sample was used as input material for sequencing. RNA sequencing (RNA-seq) libraries were constructed using the NEB Next®Ultra™ RNA Library Prep kit for Illumina® (NEB, Ipswich, MA, United States) following the manufacturer's recommendations as described. Briefly, poly-T oligo magnetic extraction of messenger RNA (mRNA) from the isolated total RNA was carried out, followed by its fragmentation using divalent cations and heating in NEB Next Frist Strand synthesis reaction buffer and first strand synthesis with random hexamer and M-MuLV Reverse Transcriptase. Following this, a second strand cDNA synthesis was performed on the first strand with DNA Polymerase I and RNase H. In the process, the leftover overhangs in the second cDNA were filled *via* exonuclease/polymerase activities. After adenylation of 3' ends of DNA, NEBNext Adaptor carrying hairpin loop structure was ligated for hybridization. A 240-bp-long cDNA fragments were selected preferably by purifying the library fragments

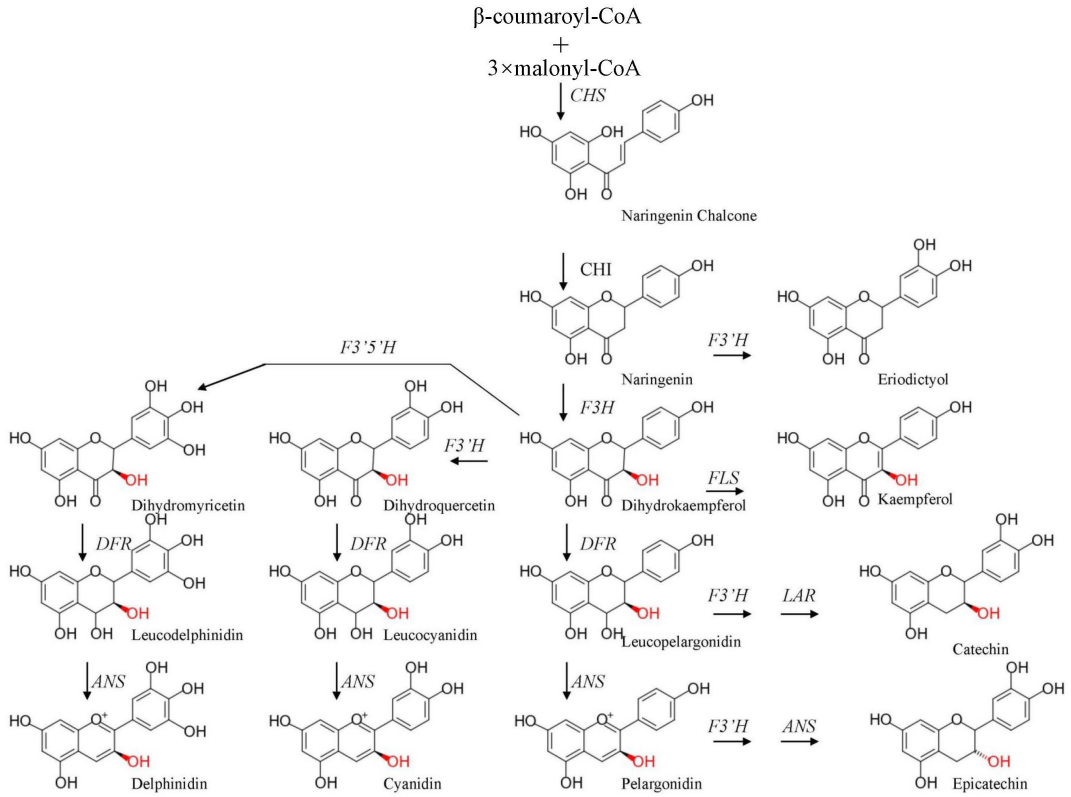

FIGURE 1 | Simplified model of the flavonoid pathway, comprising the general phenylpropanoid pathway, the anthocyanin branch, and other subgroups of flavonoid end products. CHS, chalcone synthase; F3H, flavanone 3-hydroxylase; DFR, dihydroflavonol-4-reductase; ANS, anthocyanidin synthase; F3′H, flavonoid 3′-hydroxylase; FLS, flavonol synthase; F3′5′H, flavonoid 3′,5′-hydroxylase; LAR, leucoanthocyanidin 4-reductase.

with the AMPure XP system (Beckman Coulter, Beverly, MA, United States). Following this, 3 μl USER Enzyme (NEB, Ipswich, MA, United States) was incubated with the abovementioned adaptor-ligated and size-selected cDNA, first for 15 min at 37°C followed by 5 min at 95°C. Following this, PCR was carried out using Phusion High-Fidelity DNA polymerase and Universal PCR primers and Index (X) Primer. At last, again AMPure XP system (Beckman Coulter, Beverly, MA, United States) was used to purify the extract of the synthesized PCR products. In the final step, the quality check of the constructed library was assessed using an Agilent Bioanalyzer 2100 system (Agilent, Santa Clara, CA, United States) (Lou et al., 2014). Samples were subsequently sequenced on an Illumina HiSeq platform.

Transcriptome Assembly, Annotation, and Differentially Expressed Genes (DEGs) Analyses

The raw reads obtained earlier were filtered to remove adaptors and reads where unknown nucleotides exceeded 5%. The filtered clean reads were *de novo* assembled with Trinity[1] using the following parameters: "K-mer = 25 and group pairs distance = 300" (Grabherr et al., 2011). Briefly, the assembly process was as follows: short reads from sequencing were assembled into longer contigs based on sequence overlaps. Following this, the different contigs from another transcript and the distance between them were further recognized by mapping the clean reads back to the corresponding longer contigs based on their paired-end information. In this way, the sequence of different transcripts was obtained. Finally, these potential transcript sequences were clustered (TGI Clustering) to obtain unitranscripts (Pertea et al., 2003). To identify a uni-transcript identity, they were aligned to multiple protein databases in BLASTx (E-value $\leq 10^{-5}$), including NCBI non-redundant (Nr[2]), Swiss-Prot[3], Trembl, Kyoto Encyclopedia of Genes and Genomes (KEGG[4]), Clusters of Orthologous Groups (COG[5]), euKaryotic Orthologous Groups (KOG[6]), eggNOG (v4.5[7]), Pfam (Protein family[8]), and Gene Ontology (GO[9]) databases. SOAP

[1]http://trinityrnaseq.sourceforge.net/

[2]ftp://ftp.ncbi.nih.gov/blast/

[3]http://www.uniprot.org/

[4]http://www.genome.jp/kegg/

[5]http://www.ncbi.nlm.nih.gov/COG/

[6]http://www.ncbi.nlm.nih.gov/COG/; https://ftp.ncbi.nih.gov/pub/COG/

[7]http://eggnogdb.embl.de/

[8]http://pfam.xfam.org/

[9]http://www.geneontology.org/

aligner[10] was used to realign all usable reads to each uni-transcript to evaluate the depth of data coverage.

This normalization was post-implemented to obtain reads per kilobytes per million reads (FPKM; Mortazavi et al., 2008). Afterward, uni-transcript abundance differences between white and pink petals were calculated based on the ratio of the FPKM values (Benjamini and Yekutieli, 2001). Here, prior to the differential gene expression analysis, read counts were adjusted, and the differential expression analysis of white vs. pink petals was performed using the EBSeq R package (Leng et al., 2015). The cutoff of $|\log_2(\text{fold change})| \geq 1$ and false discovery rate (FDR) ≤ 0.01 was set as the threshold cutoff for identifying DEGs.

Kyoto Encyclopedia of Genes and Genomes and Gene Ontology Enrichment Analyses

Kyoto Encyclopedia of Genes and Genomes (Kanehisa et al., 2007) was used for the characterization of enriched metabolic pathways (based on gene expression) in white vs. pink petals. KOBAS statistical test pipeline (Xie et al., 2011) was used to identify significantly overrepresented metabolic pathways for DEGs between white and pink petals. Unique sequences were represented with EC numbers for which BLASTX (against KEGG) scores were associated with *E*-value $\leq 10^{-5}$ and based on this, these unique sequences were mapped to match the specific biochemical pathways (according to the corresponding KEGG EC distribution).

To gain insights into the functional enrichments in DEGs or gene clusters, we conducted the GO enrichment test to find the overrepresented GO terms in gene lists using BiNGO (Maere et al., 2005). The *p*-values were adjusted using Benjamini and Hochberg's (1995) FDR correction method for multiple testing. GO terms with FDR ≤ 0.01 and consisting of at least five genes were considered as significantly enriched.

Quantitative PCR Analysis of Differentially Expressed Genes and Transcription Factors Identified in RNA-Seq Approach

All the petal color implicated unitranscripts differentially expressed in white vs. pink petals were subjected to real-time quantitative PCR (qPCR) with gene-specific primers (**Supplementary Table 10**). cDNA synthesis and qPCR were performed as described previously (Qi et al., 2013) on a MyiQ Single-Color Real-Time Detection System (Bio-Rad, Watford, United Kingdom). *LsUbiquitin* was used as a housekeeping gene.

Extraction and Quantification of Metabolites

Anthocyanin metabolites were determined according to the following method: 0.5 g white and pink with blue points of petal tips (pink), which are at the full-bloom stage were weighed and ground into powder in liquid nitrogen. About 7.5 ml of the extract was added and ultrasonically treated for 0.5 h in a 4°C water bath and centrifuged at 10,000 *g* under 4°C for 5 min. Subsequently, the supernatant was transferred to a new tube. A 5 ml of concentrated HCl was added and incubated at 90°C for 40 min, and the volume was finally fixed to 20 ml. After filtration with a 0.22-μm membrane, LC-MS/MS detection was performed. Metabolite contents were determined using Agilent 1290 high performance liquid chromatography (Aglient1290) in tandem with AB QTRAP6500 mass spectrometer (SciEx-6500QTRAP), and poroshell column 120 SB-C18 RP (2.1 × 150, 2.7 μm) was used in this approach.

To measure the contents of about 105 kinds of flavonoid-related metabolites and phenolic compounds, a broad-target metabolic analysis was employed to analyze an overview of metabolic changes between white and pink petals using LC-MS/MS. Briefly, 0.2 g of the petal was freeze-dried, and a 600 μl mixture of methanol and water (2/1, V/V) and 400 μl chloroform were added to each sample. The mixtures were ultrasonicated in an ice-water bath for 20 min, then the samples were centrifuged at 13,000 rpm for 10 min at 4°C. A 500-μl supernatants were removed to a new tube, and a 400 μl mixture of methanol and water (2/1, V/V) was added to the residue. The mixtures were ultrasonicated at an ice-water bath for 20 min, then the samples were centrifuged at 13,000 rpm for 10 min at 4°C. A 300-μl supernatants were combined into a new tube (total 800 μl). A 200-μl supernatants were vacuum-dried and redissolved in 200 μl of water-methanol (V/V = 18:7) for the LC-MS/MS analysis. A 2-chloro-L-phenylalanine (12 ng/ml) was used as an internal standard. All of the standard chemicals were purchased from Sigma-Aldrich. High performance liquid chromatography (HPLC) grade solvents were ordered from Thermo Fisher Scientific (Waltham, MA, United States). Metabolite analysis was performed with an AB ExionLC (AB Sciex, Framingham, MA, United States) equipped with a Waters UPLC HSS T3 column (100 mm × 2.1 mm, 1.7 μm). LC elution was monitored using a Qtrap 6500+ mass spectrometer (AB Sciex, Framingham, MA, United States) operating in a positive or negative detection mode. The binary gradient elution system consisted of (A) acetonitrile and (B) water (containing 0.1% formic acid, v/v). Separation was achieved using a gradient: 0 min, 0 B; 2 min, 0 B; 36 min, 55% B; 39 min, 95% B; 42 min, 95% B; 42.1 min, 0 B; and 45 min, 0 B. The flow rate was 0.30 ml/min. The main metabolites that may affect flavonoid compositions were quantified by using the following mother and daughter ion pair: delphinidin (Del) 303→229, epicatechin (Ep) 289→109, cyanidin (Cy) 287→231, catechin (Ca) 290→109, myricetin (My) 317→151, eriodictyol (Er) 287→151, and kaempferol (Km) 285→229. Experiments were conducted with three independent biological replicates.

Measurements of Brassinolide in White and Pink Petals in *Lycoris sprengeri*

All the petal samples were ground with precooled mortar in liquid nitrogen, and about 1.0 g of powder for each sample was transferred into fresh tubes. Precooled 95% methanol was added to the samples, and the samples were incubated at 4°C for 2 h. After that, the centrifugation was performed at 10,000 *g* under

[10]http://soap.genomics.org.cn/soapaligner.html

4°C for 5 min, the supernatant was taken and precipitation was performed repeatedly, and supernatants were combined. The sample was directly loaded onto the preloaded column (18 ml liquid was taken) and eluted with 3 ml methanol. Methanol was blow-dried with nitrogen, dissolved with 300 μl methanol, filtered through a 0.22-μm membrane, and examined by HPLC and tandem mass spectrometry (HPLC-MS/MS).

For the quantification of brassinolide (BL), 250 pg BL (Sigma-Aldrich, St. Louis, MO, United States) was used together as the standard with the extracts. All samples were injected onto a poroshell 120 (2.1 × 150, 2.7 μm) reverse phase column. The inlet method was set as follows: mobile phase A, methanol and B, 0.1% ammonium hydroxide in ddH_2O. Gradient: 0–2 min, 80% A; 2–3.5 min, 80–85% A; 3.5–6 min, 95% A; 6–6.1 min, 95–80% A; and 6.1–10 min, 80% A. BL was detected in an ESI source performed in a positive mode of MRM detection. The ESI parameters were set as follows: air curtain gas: 15 psi; spray voltage: +4,500 V, −4,000; atomizing gas pressure: 65 psi; auxiliary gas pressure: 70 psi; atomization temperature: 350°C.

Measurements of pH Values in White and Pink Petals in *Lycoris sprengeri*

The measurement of pH value between white and pink petals was performed as follows: about 1 g of fresh petals were mixed with 0.1 g of quartz sand and then fully ground in liquid nitrogen. Centrifugation was performed at 1,200 r·min^{-1} at 4°C for 1 min, and the supernatant was quickly transferred to a new 1.5-ml centrifuge tube. Immediately, a flat pH meter (pH5F, Shanghai Sanxin Instrument Company, Shanghai, China) was used to measure the pH value of the supernatant at room temperature. The three different sample replicates that were used from white and pink petals were taken, and each sample was repeated at least four times.

RESULTS

Phenotypic Characteristic Analysis of Pink and White Petals in *Lycoris sprengeri*

Though various studies have been performed to study the flower bud differentiation in *Lycoris* plants, limited investigations on the mechanisms of the color difference of Lycoris flowers were employed. In this study, the two contrasting colors of *L. sprengeri* petals, namely, white and pink petals, at full-bloom stages were obtained (**Figure 2A**) and the color difference prompts us to hypothesize that anthocyanin biosynthesis or other pigments biosynthesis was different from each other in *L. sprengeri*. The targeted LC-MS/MS results of the pigments-related metabolites suggested that major flavonoid biosynthesis metabolites, which may be involved in flower color development, have different accumulation levels (**Figure 2B**). For example, the accumulation levels of Del, Ep, and Cy are significantly lower in white petals than that in pink petals whereas the accumulation levels of Ca, Er, and Km were significantly higher in white petals than those in pink petals. As expected, pink *L. sprengeri* petals contained high levels of two anthocyanin compounds responsible for color pigmentation: Del and Cy. In contrast, significantly reduced levels of color anthocyanins and a few derivatives were detected in the white petals of *L. sprengeri* (**Figure 2B**). In addition, the accumulation levels of My in both pink and white petals were similar. To obtain the general overview of pigment metabolite levels, the composition of common copigment flavonoids, such as quercitrin, cyanin chloride, Del 3-glucoside, caffeic acid, 4-hydroxycinnamic acid, and other 105 metabolites in total for pink and white petals has been provided (**Supplementary Table 6**).

Sequencing and Transcriptome Assembly

To investigate the molecular basis regarding color development in *L. sprengeri* petals, genome-wide transcriptome analysis is employed to analyze the transcriptomic gene expressions. At first, the two cDNA libraries from white and pink petals were prepared in Illumina sequencing from three biological replicates per sample, which generated 25,822,803 sequences with 7,743,689,931 bp from white petals and 24,664,320 sequences with 7,378,331,053 nucleotides (basepair) from pink petals. After the removal of low-quality raw reads, which included too short, empty, too many Ns, we obtained an average of 25,822,803 (white) and 24,664,320 (pink) high-quality sequences, respectively (**Supplementary Table 1**). Transcriptome data obtained hereby have been uploaded to the Sequence Read Archive[11] and can be accessed with the accession number PRJNA714286. These reads were assembled into 34,336 total genes, 100,778 total isogenes, and 203,657,668 total reads with an average length of 1,037.74 bp. In total, 34,336 unique sequences were annotated using different databases (**Supplementary Table 2**). Unique sequences that were not among the GenBank sequences were considered to be the novel transcripts of *L. sprengeri*. The number of isogenes with over 1.0 kb length was 21,621, and the number of isogenes with less than 300 bp length was 28,908 (**Supplementary Table 3**). An overview of the sequence length distribution is shown, which displays good data assembly performance due to an optimal N50 (**Figure 3A** and **Supplementary Table 3**). A principal component analysis (PCA) suggested close clustering of replicates within the samples and hence obtaining excellent sample data reproducibility (**Supplementary Figure 1**). We suggest that a large quantity of unique sequences from *L. sprengeri* petals should cover a vast majority of genes in this species. This should provide, for the first time, a powerful gene expression resource for this medicinal and ornamental plant.

Functional Annotation

To analyze and annotate the identified unigenes, unigenes were searched against different databases. A 34,336 spliced *L. sprengeri* transcripts were assigned with GO terms based on sequence similarity with already known proteins and corresponding GO slim terms from TAIR. Among the 34,336 spliced transcripts, 17,213 annotated sequences could be annotated with GO terms while 17,123 lacked it (**Figure 3B**). GO annotations of unique

[11] https://submit.ncbi.nlm.nih.gov/subs/sra/SUB9202653/overview

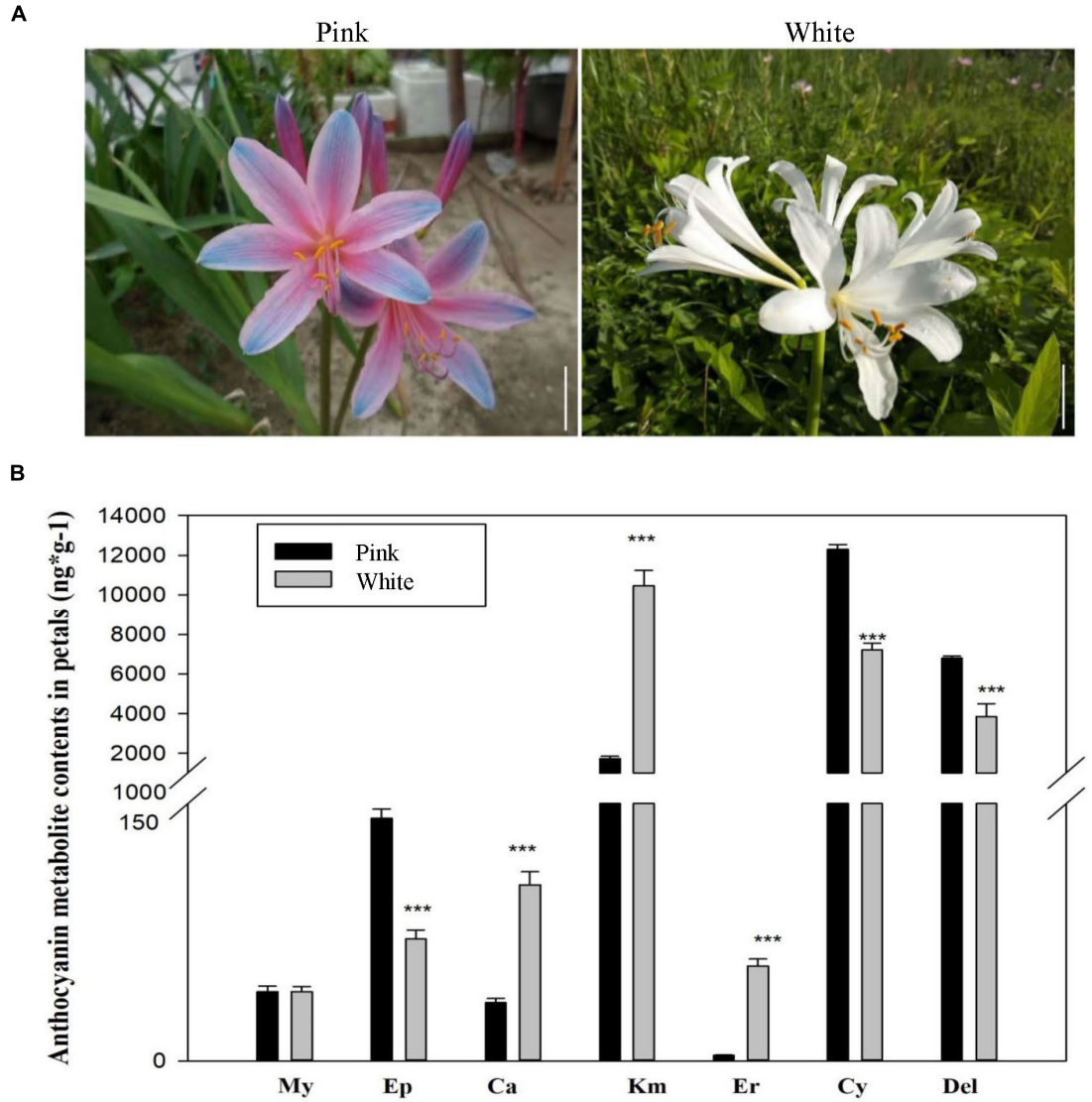

FIGURE 2 | Phenotypic characteristics analysis of pink and white petals in *Lycoris sprengeri*. **(A)** Morphological comparison of white and pink petals of *L. sprengeri* under wild conditions. **(B)** Liquid chromatographic tandem mass spectrometry (LC-MS/MS) analysis of core metabolites in flavonoid biosynthesis process.

sequences could be categorized into molecular function (37,971 unique sequences), biological process (19,342 unique sequences), and cellular component (33,505 unique sequences) (**Figure 3B**). GO term annotation provided a broad overview of the functional groups of genes cataloged in our *L. sprengeri* petal transcriptome.

To further examine the integrity of our transcriptome library and the effectiveness of the annotation process, we identified the unigene numbers based on the COG and eggNOG classification. Altogether, there were 9,395 unigenes identified by the COG (**Figure 3C**) and 19,760 unigenes by the eggNOG classification (**Figure 3D**). Among the 24 COG categories, the cluster of "Translation, ribosomal structure, and biogenesis" accounted for the largest proportion of unigenes (1,069, 11.51%) followed by "General function prediction only" (1,047, 11.27%), "Post-translational modification, protein turnover, chaperones" (942, 10.14%), and "Carbon hydrate transport and metabolism" (913, 9.83%).

Kyoto Encyclopedia of Genes and Genomes-Based Pathway Assignment of Unique Sequences

Overall, 12,416 unique sequences could be annotated with KEGG terms, and out of these 1,192 were assigned to the biosynthesis of the secondary metabolite pathway. Expectedly, metabolic pathways were well represented among *L. sprengeri* unique sequences (**Figure 4** and **Supplementary Table 4**). Most of the downregulated genes in white vs. pink petals were mapped to the pathways of circadian rhythm-plant, starch and sucrose metabolism, carotenoid biosynthesis, galactose metabolism, and

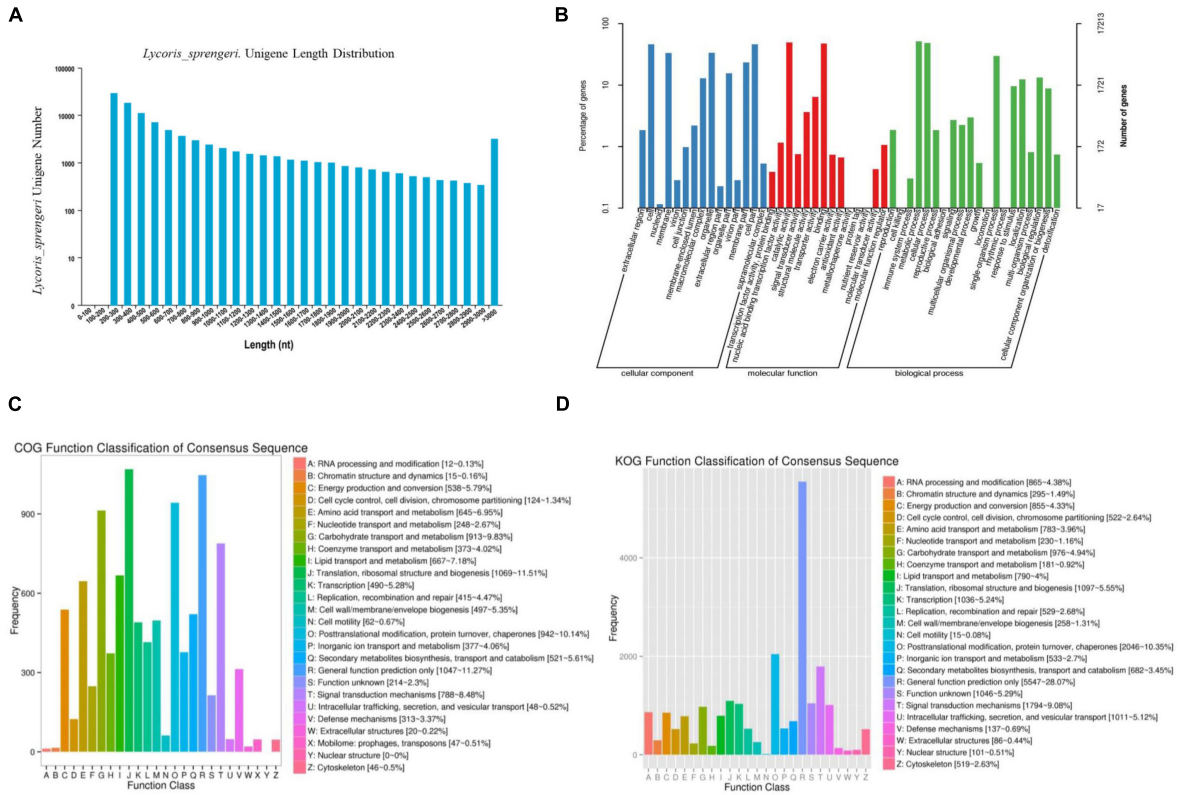

FIGURE 3 | An overview of the RNA sequencing (RNA-seq) data analysis in white and pink petals. **(A)** Unigene length distribution of sequencing reads and contigs in *L. sprengeri* RNA-seq. **(B)** Histogram representing Gene 02Ontology (GO) classification. GO categories, shown on the *x*-axis, were grouped into three main ontologies: biological process, cellular component, and molecular function. The right *y*-axis indicates the number of genes in each category, while the left *y*-axis indicates the percentage of total genes in that category. The "all gene" indicates that unigenes were those assembled from reads from pink and white petals. **(C)** Histogram representing clusters of orthologous groups (COG) classification. A total of 33,456 unigenes were assigned to 24 categories in the COG classification. **(D)** Histogram representing the eggNOG classification. The *y*-axis "frequency" indicates the number of genes in a specific functional cluster. The right side of the legend shows a description of the 24 functional categories.

flavonoid biosynthesis (**Figure 4A**) while most of the upregulated genes were mapped to plant hormone signal transduction, beta-alanine metabolism, phenylpropanoid biosynthesis, starch and sucrose metabolism, plant-pathogen interaction, and flavonoid biosynthesis (**Figure 4B**). Transcripts encoding flavonoid biosynthesis enzymes detected in our Illumina sequencing data set are tabulated under **Supplementary Table 5**.

Anthocyanin Biosynthesis Genes and Pigments Are Repressed in White vs. Pink Petals

It is hypothesized that flower pigmentation is mainly related to the genes involved in flavone, anthocyanin, and flavonoid biosynthesis pathways. After searching against the combined functional annotation, a total of 41 key structural genes (encoding pigment biosynthesis enzymes) were identified and 8 of them showed significant downregulation in white vs. pink petals. We compared the pigment metabolic process and its main branches (with core metabolites and enzymes) to figure out why some steps in the anthocyanin biosynthesis pathway are blocked in the white petals (**Figure 5A**). This included *CHS*, *F3H*, *FLS*, *ANS*, and *DFR*. The expression of leucoanthocyanidin reductase (*LAR*) was significantly upregulated in white vs. pink petals. However, among the unigenes matched to chalcone isomerase (*CHI*), c93521.graph_c0 was downregulated and c98816.graph_c0 was upregulated. Similarly, among the unigenes for caffeoyl-flavonoid 3′-monooxygenase (CYP75B1), c120123.graph_c0 was downregulated and c130176.graph_c2 was upregulated (**Figure 5A**). Interestingly, increased Ca in white vs. pink petals can be attributed to a higher LAR enzyme level. Based on the analysis of DEGs involved in anthocyanin biosynthesis, we may figure out that the DEGs of anthocyanin biosynthesis may give further evidence to interpret mechanisms, which may cause the different accumulations of anthocyanin-related metabolites and finally led to the different color forms in *L. sprengeri*, all the other core metabolites were also detected in the pink petal extracts (**Figure 2B**).

Annotation of Transcription Factor Gene Families

Plant TF database was searched for annotating the detected *L. sprengeri* transcripts as putative transcriptional regulators

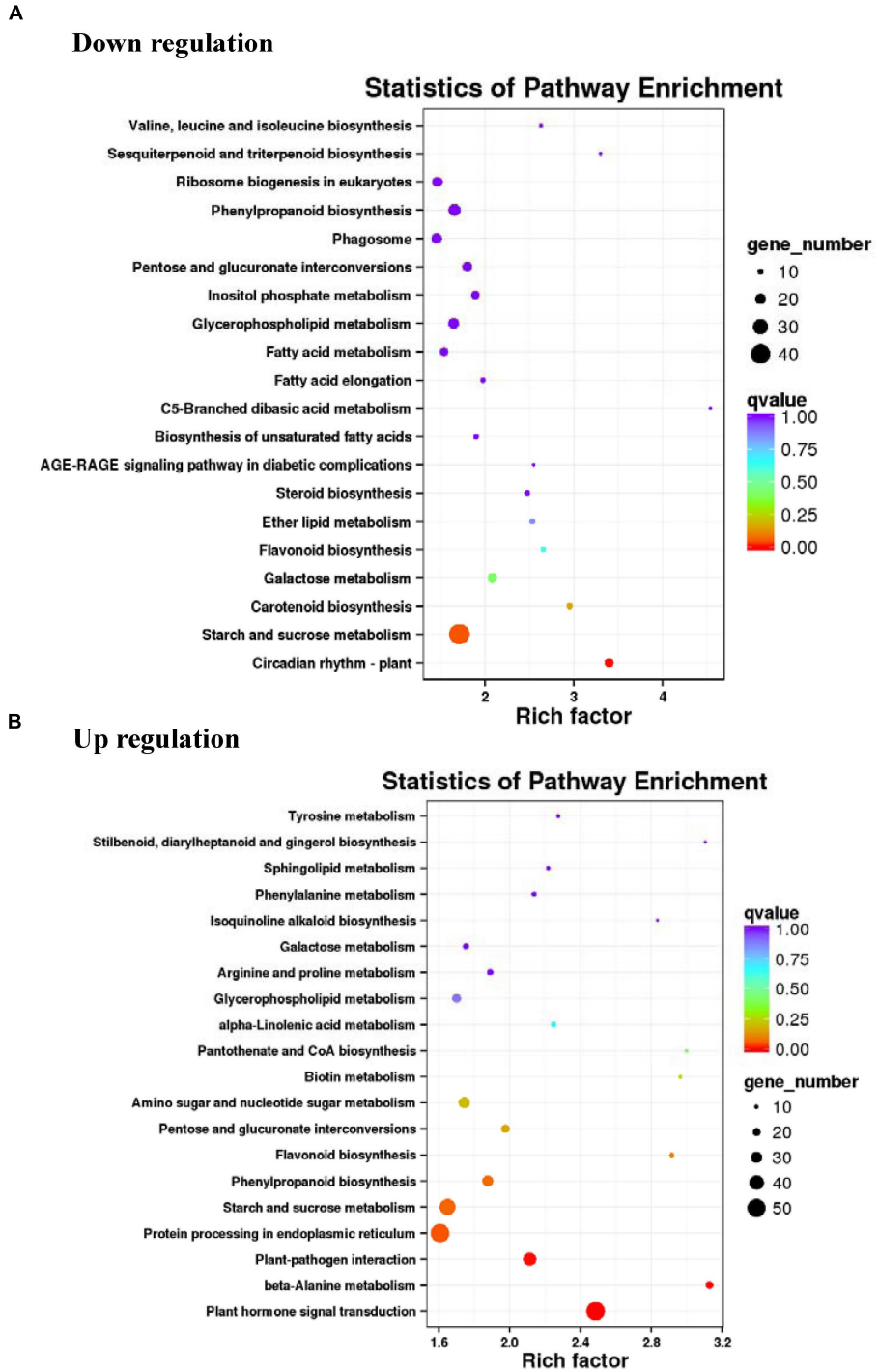

FIGURE 4 | Kyoto Encyclopedia of Genes and Genomes (KEGG) pathway analysis of differentially expressed genes (DEGs) in RNA-seq. Top 20 pathways were characterized among the upregulated **(A)** and downregulated **(B)** DEGs.

(Pérez-Rodríguez et al., 2010). In our study, a total of 164 transcripts were predicted as TFs, which mainly belonged to 6 families, including 50 bHLH, 33 ethylene responsive factor family (ERF), 25 MYB, 28 WRKY, 7 bZIP, and 6 NAC family TFs (**Figure 5B**). Of these, we identified three R2R3 TFs (c128273.graph_c0, c126227.graph_c2, and c105793.graph_c0), which were greatly repressed in white vs. pink petals. On the other hand, the expression of eight MYB family TFs (c120875.graph_c0, c124022.graph_c2, c118923.graph_c0, c116915.graph_c0, c123390.graph_c0,

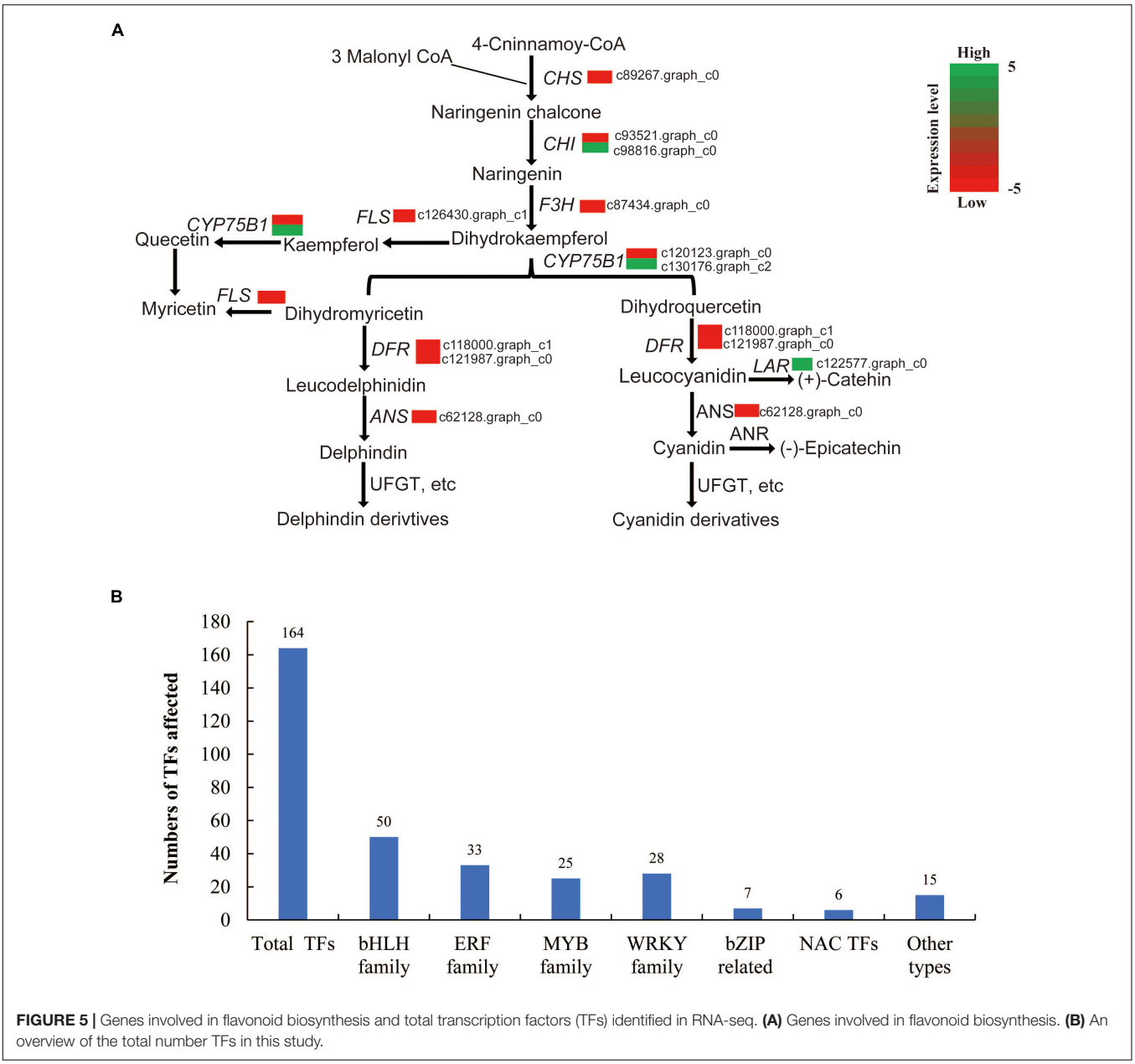

FIGURE 5 | Genes involved in flavonoid biosynthesis and total transcription factors (TFs) identified in RNA-seq. **(A)** Genes involved in flavonoid biosynthesis. **(B)** An overview of the total number TFs in this study.

c119914.graph_c0, c107135.graph_c0, and c102137.graph_c0) showed 4-fold or greater changes in white vs. pink petals while others are MYB-related proteins with unknown annotations, suggesting a potential involvement of these eight MYB TFs in the gene regulation of the expression of biosynthesis genes for pigment enzymes controlling contrasting factors, such as anthocyanin biosynthesis, petal color development, photosynthesis, and multiple biological processes in plants that may compensate for the petal color variations as well.

To analyze the relationships between those three R2R3 MYB TFs and the other eight MYB TFs, a phylogenetic analysis of the three R2R3 MYB TFs and the other eight MYB TFs identified was employed in our study. The results suggest that the three R2R3 are phylogenetically related while others belong to other types (**Supplementary Figure 3**). A qPCR analysis of these transcriptional factors demonstrated that all the 3 R2R3 are downregulated and the expression of the other 11 TFs is upregulated, and the obtained fold changes were consistent with those in the RNA-seq assay (**Supplementary Figure 4**).

Genes Involved in Steroid Biosynthesis and Brassinolide Levels Are Repressed While pH Is Higher in White Petals

In this study, a total of 10 genes, including *ERG1* (squalene monooxygenase), *CAS1* (cycloartenol synthase), *CYP51* (sterol 14-alfa-demethylase), *EBP* (cholestenol delta-isomerase), *SMO2* (alpha-monomethylsterol monooxygenase), *ERG3* (delta-7-sterol

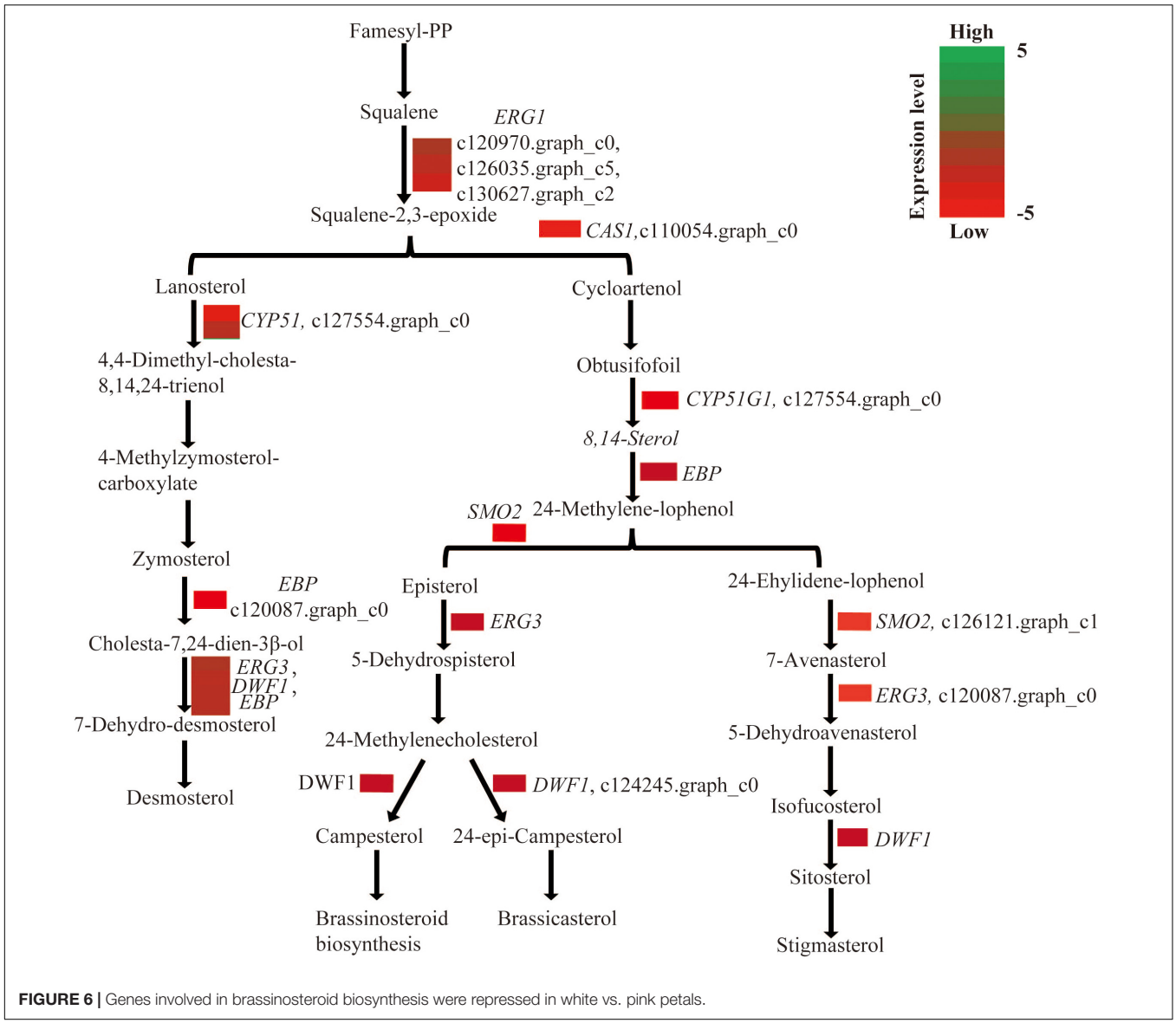

FIGURE 6 | Genes involved in brassinosteroid biosynthesis were repressed in white vs. pink petals.

5-desaturase), and *DWF1* (sterol reductase), which are all involved in steroid biosynthesis, were repressed in white vs. pink petals (**Figure 6**). To investigate the brassinosteroid contents in white and pink petals, HPLC-MS/MS was employed to compare the BL content between them. The BL content in white petals was about nine times lower than that in pink petals of *L. sprengeri* (**Supplementary Figure 2**). The pH inside white petals is significantly higher than that inside pink petals (**Supplementary Table 13**).

Gene Expression of Flavonoid Biosynthesis Genes

As the flower color in plants is mainly determined by the anthocyanin pathway, the expression levels of a few genes identified in our RNA-seq were quantified with a qPCR assay. Eight genes, *LsCHS*, *LsCHI*, *LsF3H*, *LsCYP75B1*, *LsFLS*, *LsDFR*, *LsANS*, and *LsLAR*, from the flavonoid biosynthetic pathway, were selected for qPCR validation. Most of the genes were greatly suppressed in white petals, and only the expression level of *LsLAR* was upregulated in white vs. pink petals (**Supplementary Figure 5** and **Supplementary Table 10**). The expression levels of *LsDFR*, *LsCHS*, *LsANS*, and *LsFLS* are supposed to be directly related to flower color development (Shan et al., 2020).

DISCUSSION

Lycoris sprengeri is an important herb, and the *Lycoris* genus has about 20 species, of which ten are commonly grown in China and Southern Asia (Shi et al., 2019). Previous transcriptomic studies relevant to the Amaryllidaceae family investigated *L. aurea* (Wang et al., 2013), *L. longituba* (Wang et al., 2013; Li et al., 2020), *Allium cepa* (Kim et al., 2015), *Narcissus pseudonarcissus*

(Singh and Desgagné-Penix, 2017), and *L. sprengeri* (Chang et al., 2011). Hereby, we profiled the transcriptome and metabolite profiles of white and pink petals of *L. sprengeri*. The transcriptome analysis was used to identify the differentially regulated genes that could explain the color differences and hence control flower coloration (**Supplementary Tables 3**, **4**). In comparison with the transcriptomic analysis in other *Lycoris* species, this study has better gene coverage and sequence assembly performance in total sequences and total unigenes (Wang et al., 2013; Park et al., 2019; **Supplementary Tables 11**, **12**).

Most unigenes were associated with molecular function terms, such as "binding" and "catalytic activity," cellular component terms such as "cell" and "cell parts" while the biological process terms mainly are "cellular process" and "metabolic processes" (**Figure 3B**). These results are consistent with a previous transcriptome study on *L. aurea* (Wang et al., 2013). Most unigenes in the study were reported to be involved in "translation, ribosomal structure, and biogenesis," "post-translational modification," "protein turnover, chaperones," and "general functional prediction only," "binding and catalytic activity," "cell," "cell parts," and "organelle and cellular and metabolic processes" (Wang et al., 2013). However, we obtained more unigenes in our transcriptomic study and present a more detailed GO annotation. Chang et al. (2011) also reported similar results for the GO annotation for the transcriptome of *L. sprengeri*. COG/eggNOG annotation analyses revealed that the pathways that were annotated to the identified unique transcripts belonged to lipid metabolism, transcriptions, signal transduction, translational, protein turn over and chaperone, and ribosomal biogenesis (**Figures 3C,D**). This suggested that the major category in COG annotation was "General function" and "lipid metabolism" while in eggNOG the largest metabolic pathway was "post-translational modification, protein turnover and chaperones." These categories may be quite important for the color development in *L. sprengeri* petals. The KEGG analysis revealed the enrichment of color development-related flavonoid biosynthesis pathway in both upregulated and downregulated genes (**Figure 4** and **Supplementary Table 9**). Furthermore, 20 color-related DEGs were identified between white and pink petals and associated with pigments: anthocyanins, flavonoids, and flavonols, which were considered to contribute to the flower color and their levels could determine the final flower color variation from pink to white (Tanaka et al., 1998; Aida et al., 2000). In the following section, we are going to discuss the candidate genes, which may be responsible for the petal coloration.

Candidate Genes Responsible for Loss of Pink Color in White Petals of *Lycoris sprengeri*

Anthocyanins are a type of flavonoids implied in the formation of different non-white petal colors (Tanaka et al., 1998; Zhao and Tao, 2015). Common enzymatic reactions in the anthocyanin pathway are catalyzed by *CHS*, *F3H*, and *CHI* while other genes are responsible for specific metabolite synthesis in the anthocyanin pathway (Xue et al., 2021). It is well known that Del and Cy are reported to be the direct reason for a color difference in petals (Lou et al., 2014). Our transcriptome analysis demonstrated that anthocyanin biosynthetic activities were repressed in white petals due to the repressed transcript levels of *CHS*, *FLS*, *F3H*, *ANS*, and *DFR* (**Figure 5A**). Gene expression repression of flavonoid biosynthesis enzyme genes was validated in white petals through qPCR to validate the accuracy and reproducibility (**Supplementary Figure 5**). These genes are reported to be involved in various biosynthesis stages of the anthocyanin biosynthesis process. For example, *ANS* is an α-ketoglutarate-dependent dioxygenase acting downstream of the anthocyanin biosynthesis pathway, which mediates the catalysis of anthocyanin formation from α-ketoglutaric acid and Fe^{2+} (Tan et al., 2013). *CHS* (encodes a chalcone synthase) and *F3'H* (encodes a flavanone 3-hydroxylase) are also important genes involved in the regulation of flower color and catalyzed the early enzymatic reactions in the flavonoid biosynthesis pathway (Lou et al., 2014). *DFR* (encodes dihydroflavonol reductase) is an enzyme, which reduces dihydroflavonols to colorless leucoanthocyanidins. This in turn is converted into colored anthocyanidins by *ANS*. These genes and their corresponding catalytic reactions might be occurred by key genes and speed-limiting steps leading to the loss of anthocyanins in white petals. Although the *DFR* gene effectively restricts the Cy metabolism branch, Ca was found in white petals, suggesting that white petals were without the lack of anthocyanin metabolism downstream genes. Meanwhile, the content of Km in white petals was higher than that in pink petals, indicating that the anthocyanin biosynthetic pathways (ABP) in white petals is restrained and some amounts of Km are accumulated (**Figure 2B**). The ANS gene also plays a key role in the ABP pathway, which could catalyze the synthesis of colorless anthocyanins into colored anthocyanins (Xue et al., 2019). The reduced expression of ANS gene might be a factor in its inability to accumulate anthocyanins in white petals (**Figure 5A**).

Metabolic Compounds Associated With Flower Coloration in *Lycoris sprengeri*

The metabolic regulation related to the formation of flower color is a complex metabolic pathway, which is regulated by the key genes of several branch metabolic pathways and regulatory factors. It was difficult to obtain an absolute coloration between the genes and the corresponding metabolites. The anthocyanin composition and content and copigment flavonol content in petals were analyzed to understand the biochemical basis of different flower colors and to predict the genetic differences. In this study, the metabolic profiling of anthocyanin-related metabolites was performed, which showed that Ep, Cy, and Del were significantly lower while Ca, Km, and Er were significantly more in white petals than in pink petals (**Figure 2B**). Lower Ep levels in white petals suggested that the color pigment Cy may either be present at a significantly lower level or maybe stable for a short time in white petals compared to pink petals. In the latter case, it is probable that the unstable Cy is converted to colorless Ep, which would prevent the production of a color pigment from Cy *via* later glycosylation and other reactions.

Interestingly, reduced products downstream of dihydromyricetin (DFR substrate) in the Del synthesis pathway (a substrate for the DFR enzyme) were detected in white vs. pink petals (**Figure 5A**), suggesting that *DFR* was the most likely target for Del suppression in the white petals of *L. sprengeri* (**Figure 2B**). *FLS* (encodes flavonol synthase) acts as a coregulator for controlling the amounts of dihydroflavonols for synthesizing the intermediates in the production of both the colored anthocyanins together with *DFR*. It was suggested in a recent study that the contents of Cy can be correlated to the expression levels of *FLS* and *DFR* (Lou et al., 2014). Thus, the repressed levels of *FLS* together with *DFR* may produce lower anthocyanin (Davies et al., 2003). A similar mechanism may act in white petals due to the repression of these enzyme genes.

Mechanism of Flower Coloration in *Lycoris sprengeri*

Even though the contents of some anthocyanins are relatively high in white flowers (**Figure 2B**), the type of flower color could be affected by other conditions including pH values such as the color form of anthocyanins is red in acidic pH, colorless or white in neutral or nearly neutral pH, and blue in alkaline pH. The pH values of pink petals are significantly lower than those in white petals (**Supplementary Table 13**). Four anthocyanin tautomers in different pH values: alkali blue quinone A, red–yellow molten cation AH+, colorless false base B, and colorless chalcone C could cause different colorful flower forms, and the pH can influence the three balance conversions between them (Zhao and Tao, 2015). The colorless false base B and colorless C may be the major form in white petals, and red-yellow molten cation AH+ represents the major anthocyanin in pink petals (Zhao and Tao, 2015).

The expression of structural genes in anthocyanin biosynthesis and brassinosteroid biosynthesis-related genes may be controlled by transcriptional regulators (Wang et al., 2021). Previously, 51 TFs were recognized as flower specific and belonged to MADS, MYB-related, NAC, and others (He et al., 2010). However, there is still no standardized reference genome for *Lycoris* and therefore TF annotation information is limited. We cataloged TFs in our petal transcriptome based on publicly available data sets (**Figure 5B**). Three major groups of TFs, belonging to bHLH, R2R3 MYB, and WD40 families, were predominantly reported to regulate genes in the anthocyanin biosynthesis pathway across the majority of plant species (Stracke et al., 2001; Allan et al., 2008). MYB proteins have been implicated in secondary metabolism, development, signal transduction, and disease resistance in plants (Jin and Martin, 1999). MYB TF contains 339 TFs reported in Arabidopsis (Feller et al., 2011), and is associated with the anthocyanin biosynthesis pathway. In this study, three R2R3 MYB TFs were greatly repressed in white vs. pink petals. R2R3 MYB are among the MYB TF types considered to be closely related to anthocyanin metabolism and regulation (Zhao and Tao, 2015). These three phylogenetically related R2R3 MYB TFs were grouped distinctly from the other eight MYB TFs (**Supplementary Figure 3**). Their relative expression levels were further confirmed to be consistent with their expression pattern in RNA-seq (**Supplementary Figure 4**). The evolutionary transition to white petals *via* multiple losses of floral anthocyanin production is associated with the mutation of an R2R3 MYB transcriptional activator (Gates et al., 2018). It is thus highly likely that the repression of R2R3 MYB TFs in our study may lead to white color petals in comparison with pink petals.

In addition, the genes involved in steroid and BR biosynthesis pathways were all downregulated in white petals (**Figure 6**). BR treatment enhances the coloration and increases the anthocyanin content in grape berries from veraison onset to full veraison (Zheng et al., 2020). Therefore, the reduced transcript levels of genes involved in the steroid biosynthesis may lead to lower BR contents in white petals of *L. sprengeri,* which may, in turn, affect the anthocyanidin biosynthesis and result in the fainter color variations of *Lycoris* petals. The most potent BR, BL, is produced by the campesterol (Wei and Li, 2020) in the BR biosynthesis pathway that could further affect the phytohormone, flowering time, plant growth, and seed yield in plants. Consistently, the BL content in white petals was about nine times lower than pink petals (**Supplementary Figure 2**). We, therefore, confirm that the suppressed levels of genes involved in steroid biosynthesis could lead to lower levels of BL contents and subsequently lead to reduced levels of anthocyanin biosynthesis in white petals. It was also reported that BR could increase the anthocyanin biosynthetic activity by an upregulation of the late anthocyanin biosynthetic genes, such as *DFR*, *leucoanthocyanidin dioxygenase* (*LDOX*), and *UDP-glucose: flavonoid-3-O-glucosyl transferase* (*UF3GT*) in Arabidopsis while the anthocyanin accumulation was reduced in a BR-gene deficient mutant that may be caused by the repressed expressions of late anthocyanin biosynthetic genes (Yuan et al., 2015). In our study, the anthocyanin accumulation levels are decreased in white petals, and as a result, the expression of BR biosynthesis pathway-related genes is greatly suppressed as well as the structural genes and downstream genes suggest that the accumulation of anthocyanins may be one of the reasons for regulating the biosynthetic activities in the BR biosynthesis pathway. However, a variation in the different color forms of petals is regulated by multiple factors, and the BR pathway may be one of the factors affecting anthocyanin accumulation and finally lead to different color types. However, we may need more experimental data to support the relationship between the BR biosynthesis and flower color development in plants.

The mechanism of different petal colorations in *L. sprengeri* was speculated. Overall, pink petals contained more types and higher levels of intermediate compounds in the flavonoid biosynthesis pathway compared to white petals, with a few exceptions. We assume that because of ABP's restrained effects in white petals, the upstream flux must flow into other branches of the flavonoid metabolic route. The underlying mechanism is probably more complex is what is described here. The mechanism would be clarified by identifying a characteristic structure of genes and by examining how the occurrence of TFs, transporters, or miRNA affected the flowers in our future work. Exploring the molecular mechanism of petal coloration might help apply genetic engineering to produce other novel colors of *Lycoris* spp.

CONCLUSION

Taken together, we can hypothesize that the regulation of petal color may be determined by the expression levels of steroid and anthocyanin biosynthesis genes regulated by MYB TFs. Further studies are needed to determine whether the three repressed R2R3 MYB TF genes (in white petals) could be related to the regulation of repressed BR and anthocyanin genes in white petals. Specifically, quantifying the level of these genes and pigments in the mutants (white petals) of these TFs and its further functional characterization in *L. sprengeri* or of orthologous genes in model species can be undertaken using the CRISPR genome editing technique. Altogether, our transcriptome and metabolite quantification approach provides evidence for the genes putatively responsible for the lack of color phenotype in the white petals. This could provide valuable information for breeders to produce the different colors of *L. sprengeri* petals in horticultural research.

DATA AVAILABILITY STATEMENT

RNA-Seq data obtained hereby have been uploaded to the Sequence Read Archive (https://www.ncbi.nlm.nih.gov/sra/SUB9202653/overview) and can be accessed with accession number PRJNA714286.

AUTHOR CONTRIBUTIONS

Q-ZL and JZ designed the experiments. FY, Q-ZL, and JZ got the funding. FY, DD, and C-HL performed the experiments. Q-ZL, DD, C-HL, Y-HZ, M-XC, TS, L-XW, and JZ analyzed the data. FY, Q-ZL, C-HL, DD, and JZ wrote the manuscript with contributions from all other authors.

FUNDING

This work was supported by the Basic and Applied Basic Research Foundation of Guangdong Province (2020A1515110586), the Shanghai Rising-Star Program, China (No. 20 QB1404100), the National Natural Science Foundation of China (31801889, 31761130073, and 31872169), the National Key Research and Development Program of China (2017YFE0118100 and 2018YFD02003025), the Shenzhen Virtual University Park Support Scheme to Shenzhen Research Institute of the Chinese University of Hong Kong, and the Hong Kong Research Grant Council (CUHK14122415, 14160516, and 14177617).

ACKNOWLEDGMENTS

We thank Beijing Biomarker Technologies (Beijing, China) for assistance in RNA-seq analysis. We thank Zheng Yuhong for assistance in plant material identification.

SUPPLEMENTARY MATERIAL

The Supplementary Material for this article can be found online at: https://www.frontiersin.org/articles/10.3389/fpls.2021.747131/full#supplementary-material

Supplementary Figure 1 | Principal component analysis (PCA) comparison between three pink and three white petals.

Supplementary Figure 2 | Comparison of brassinolide (BL) contents in white and pink petals in *Lycoris sprengeri.*

Supplementary Figure 3 | Phylogenetic tree analysis of MYB transcription factors (TFs) in *L. sprengeri*.

Supplementary Figure 4 | Quantitative PCR (qPCR) analysis of MYB TFs in white and pink petals in *L. sprengeri*.

Supplementary Figure 5 | qPCR analysis of genes involved in flavonoid biosynthesis identified in RNA sequencing (RNA-seq). *LsUbiquitin* (c105178.graph_c0) was used as an internal control. The expression levels of genes in WT plants were set to one.

Supplementary Table 1 | Quality control of RNA sequencing (RNA-seq).

Supplementary Table 2 | Overview of transcriptome data assembly.

Supplementary Table 3 | Data assembly results.

Supplementary Table 4 | Kyoto Encyclopedia of Genes and Genomes (KEGG) pathway analysis.

Supplementary Table 5 | Total differentially expressed genes (DEGs) identified in this study.

Supplementary Table 6 | Metabolic profiles of flavonoid biosynthesis-related metabolites in this study.

Supplementary Table 7 | Summary of numbers of single nucleotide polymorphism (SNP) in samples analyzed in pink and white petals.

Supplementary Table 8 | Total SNPs in this study.

Supplementary Table 9 | Simple sequence repeat (SSR) analysis in this study.

Supplementary Table 10 | Primers used for quantitative PCR (qPCR) analysis in this study.

Supplementary Table 11 | Comparison of the transcriptome analysis in recent studies.

Supplementary Table 12 | All annotated unigene numbers from different databases.

Supplementary Table 13 | pH measurements in white and pink petals.

REFERENCES

Aida, R., Yoshida, K., Kondo, T., Kishimoto, S., and Shibata, M. (2000). Copigmentation gives bluer flowers on transgenic torenia plants with the antisense dihydroflavonol-4-reductase gene. *Plant Sci.* 160, 49–56. doi: 10.1016/S0168-9452(00)00364-2

Allan, A. C., Hellens, R. P., and Laing, W. A. (2008). MYB transcription factors that colour our fruit. *Trends Plant Sci.* 13, 99–102. doi: 10.1016/j.tplants.2007.11.012

Benjamini, Y., and Hochberg, Y. (1995). Controlling the false discovery rate: a practical and powerful approach to multiple testing. *J. R. Stat. Soc.* 57, 289–300. doi: 10.1111/j.2517-6161.1995.tb02031.x

Benjamini, Y., and Yekutieli, D. (2001). The control of the false discovery rate in multiple testing under dependency. *Ann. Stat.* 29, 1165–1188. doi: 10.1214/aos/1013699998

Cai, J., Fan, J., Wei, X., Zhang, D., Ren, J., and Zhang, L. (2020). Differences in floral development between *Lycoris radiata* and *Lycoris sprengeri*. *Scienceasia* 46, 271–279. doi: 10.2306/scienceasia1513-1874.2020.032

Chang, L., Chen, J., Xiao, Y., and Xia, Y. (2011). De novo characterization of *Lycoris sprengeri* transcriptome using Illumina GA II. *Afr. J. Biotechnol.* 10, 12147–12155.

Chen, S., Luo, H., Li, Y., Sun, Y., Wu, Q., Niu, Y., et al. (2011). 454 EST analysis detects genes putatively involved in ginsenoside biosynthesis in *Panax ginseng*. *Plant Cell Rep.* 30:1593. doi: 10.1007/s00299-011-1070-6

Davies, K. M., Schwinn, K. E., Deroles, S. C., Manson, D. G., Lewis, D. H., Bloor, S. J., et al. (2003). Enhancing anthocyanin production by altering competition for substrate between flavonol synthase and dihydroflavonol 4-reductase. *Euphytica* 131, 259–268. doi: 10.1023/A:1024018729349

Feller, A., Machemer, K., Braun, E. L., and Grotewold, E. (2011). Evolutionary and comparative analysis of MYB and bHLH plant transcription factors. *Plant J.* 66, 94–116. doi: 10.1111/j.1365-313X.2010.04459.x

Feng, F., Li, M., Ma, F., and Cheng, L. (2013). Phenylpropanoid metabolites and expression of key genes involved in anthocyanin biosynthesis in the shaded peel of apple fruit in response to sun exposure. *Plant Physiol. Biochem.* 69, 54–61. doi: 10.1016/j.plaphy.2013.04.020

Gates, D. J., Olson, B. J. S. C., Clemente, T. E., and Smith, S. D. (2018). A novel R3 MYB transcriptional repressor associated with the loss of floral pigmentation in Iochroma. *New Phytol.* 217, 1346–1356. doi: 10.1111/nph.14830

Grabherr, M. G., Haas, B. J., Yassour, M., Levin, J. Z., Thompson, D. A., Amit, I., et al. (2011). Full-length transcriptome assembly from RNA-Seq data without a reference genome. *Nat. Biotechnol.* 29:644. doi: 10.1038/nbt.1883

He, K., Guo, A. Y., Gao, G., Zhu, Q. H., Liu, X. C., Zhang, H., et al. (2010). Computational identification of plant transcription factors and the construction of the PlantTFDB database. *Methods Mol. Biol.* 674, 351–368. doi: 10.1007/978-1-60761-854-6_21

Huang, W., Sun, W., and Wang, Y. (2012). Isolation and molecular characterisation of flavonoid 3′-hydroxylase and flavonoid 3′, 5′-hydroxylase genes from a traditional Chinese medicinal plant, *Epimedium sagittatum*. *Gene* 497, 125–130. doi: 10.1016/j.gene.2011.11.029

Irani, N. G., and Grotewold, E. (2005). Light-induced morphological alteration in anthocyanin-accumulating vacuoles of maize cells. *BMC Plant Biol.* 5:7. doi: 10.1186/1471-2229-5-7

Ithal, N., and Reddy, A. R. (2004). Rice flavonoid pathway genes, OsDfr and OsAns, are induced by dehydration, high salt and ABA, and contain stress responsive promoter elements that interact with the transcription activator, OsC1-MYB. *Plant Sci.* 166, 1505–1513. doi: 10.1016/j.plantsci.2004.02.002

Jin, H., and Martin, C. (1999). Multifunctionality and diversity within the plant MYB-gene family. *Plant Mol. Biol.* 41, 577–585. doi: 10.1023/A:1006319732410

Jin, Z. (2009). Amaryllidaceae and *Sceletium alkaloids*. *Nat. Prod. Rep.* 26, 363–381. doi: 10.1039/b718044f

Kanehisa, M., Araki, M., Goto, S., Hattori, M., Hirakawa, M., Itoh, M., et al. (2007). KEGG for linking genomes to life and the environment. *Nucleic Acids Res.* 36 (suppl_1), D480–D484. doi: 10.1093/nar/gkm882

Kim, S., Kim, M.-S., Kim, Y.-M., Yeom, S.-I., Cheong, K., Kim, K.-T., et al. (2015). Integrative structural annotation of de novo RNA-Seq provides an accurate reference gene set of the enormous genome of the onion (*Allium cepa* L.). *DNA Res.* 22, 19–27. doi: 10.1093/dnares/dsu035

Leng, N., Dawson, J., and Kendziorski, C. (2015). *EBSeq: An R Package For Dierential Expression Analysis Using RNA-Seq Data. R Package Version 1*. Available online at: https://www.biostat.wisc.edu/~kendzior/EBSEQ/EBSeq_Vignette.pdf

Li, Q., Xu, J., Yang, L., Zhou, X., Cai, Y., and Zhang, Y. (2020). Transcriptome analysis of different tissues reveals key genes associated with galanthamine biosynthesis in *Lycoris longituba*. *Front. Plant Sci.* 11:1444. doi: 10.3389/fpls.2020.519752

Li, Y., Zhang, T., Shen, Z.-W., Xu, Y., and Li, J.-Y. (2013). Overexpression of maize anthocyanin regulatory gene Lc affects rice fertility. *Biotechnol. Lett.* 35, 115–119. doi: 10.1007/s10529-012-1046-9

Liu, B., Jiang, G., Zhang, Y., Li, J., Li, X., Yue, J., et al. (2011). Analysis of transcriptome differences between resistant and susceptible strains of the citrus red mite *Panonychus citri* (Acari: Tetranychidae). *PLoS One* 6:e28516. doi: 10.1371/journal.pone.0028516

Lou, Q., Liu, Y., Qi, Y., Jiao, S., Tian, F., Jiang, L., et al. (2014). Transcriptome sequencing and metabolite analysis reveals the role of delphinidin metabolism in flower colour in grape hyacinth. *J. Exp. Bot.* 65, 3157–3164. doi: 10.1093/jxb/eru168

Luo, P., Ning, G., Wang, Z., Shen, Y., Jin, H., Li, P., et al. (2015). Disequilibrium of flavonol synthase and dihydroflavonol-4-reductase expression associated tightly to white vs. red color flower formation in plants. *Front. Plant Sci.* 6:1257. doi: 10.3389/fpls.2015.01257

Maere, S., Heymans, K., and Kuiper, M. (2005). BiNGO: a cytoscape plugin to assess overrepresentation of gene ontology categories in biological networks. *Bioinformatics* 21, 3448–3449. doi: 10.1093/bioinformatics/bti551

Mortazavi, A., Williams, B. A., McCue, K., Schaeffer, L., and Wold, B. (2008). Mapping and quantifying mammalian transcriptomes by RNASeq. *Nat. Methods* 5, 621–628.

Ordidge, M., García-Macías, P., Battey, N. H., Gordon, M. H., John, P., Lovegrove, J. A., et al. (2012). Development of colour and firmness in strawberry crops is UV light sensitive, but colour is not a good predictor of several quality parameters. *J. Sci. Food Agric.* 92, 1597–1604. doi: 10.1002/jsfa.4744

Park, C. H., Yeo, H. J., Park, Y. E., Baek, S.-A., Kim, J. K., and Park, S. U. (2019). Transcriptome analysis and metabolic profiling of *Lycoris Radiata*. *Biology* 8:63. doi: 10.3390/biology8030063

Paśko, P., Bartoń, H., Zagrodzki, P., Gorinstein, S., Fołta, M., and Zachwieja, Z. (2009). Anthocyanins, total polyphenols and antioxidant activity in amaranth and quinoa seeds and sprouts during their growth. *Food Chem.* 115, 994–998. doi: 10.1016/j.foodchem.2009.01.037

Pérez-Rodríguez, P., Riano-Pachon, D. M., Corrêa, L. G. G., Rensing, S. A., Kersten, B., and Mueller-Roeber, B. (2010). PlnTFDB: updated content and new features of the plant transcription factor database. *Nucleic Acids Res.* 38 (suppl_1), D822–D827. doi: 10.1093/nar/gkp805

Pertea, G., Huang, X., Liang, F., Antonescu, V., Sultana, R., Karamycheva, S., et al. (2003). TIGR Gene Indices clustering tools (TGICL): a software system for fast clustering of large EST datasets. *Bioinformatics* 19, 651–652. doi: 10.1093/bioinformatics/btg034

Ping-Sheng, H., Kurita, S., Zhi-Zhou, Y., and Jin-Zhen, L. (1994). Synopsis of the genus lycoris (*Amaryllidaceae*). *SIDA Contrib. Bot.* 16, 301–331.

Qi, Y., Lou, Q., Li, H., Yue, J., Liu, Y., and Wang, Y. (2013). Anatomical and biochemical studies of bicolored flower development in *Muscari latifolium*. *Protoplasma* 250, 1273–1281. doi: 10.1007/s00709-013-0509-8

Ren, Z., Lin, Y., Lv, X., Zhang, J., Zhang, D., Gao, C., et al. (2021). Clonal bulblet regeneration and endophytic communities profiling of *Lycoris sprengeri*, an economically valuable bulbous plant of pharmaceutical and ornamental value. *Sci. Hortic.* 279:109856. doi: 10.1016/j.scienta.2020.109856

Shan, X., Li, Y., Yang, S., Yang, Z., Qiu, M., Gao, R., et al. (2020). The spatio-temporal biosynthesis of floral flavonols is controlled by differential phylogenetic MYB regulators in *Freesia hybrida*. *New Phytol.* 228, 1864–1879. doi: 10.1111/nph.16818

Shen, G.-M., Dou, W., Niu, J.-Z., Jiang, H.-B., Yang, W.-J., Jia, F.-X., et al. (2011). Transcriptome analysis of the oriental fruit fly (*Bactrocera dorsalis*). *PLoS One* 6:e29127. doi: 10.1371/journal.pone.0029127

Shi, S., Qiu, Y., Li, E., Wu, L., and Fu, C. (2006). Phylogenetic relationships and possible hybrid origin of *Lycoris* species (Amaryllidaceae) revealed by ITS sequences. *Biochem. Genet.* 44, 198–208. doi: 10.1007/s10528-006-9023-4

Shi, T., Yue, Y., Shi, M., Chen, M., Yang, X., and Wang, L. (2019). Exploration of floral volatile organic compounds in six typical Lycoris taxa by GC-MS. *Plants* 8:422. doi: 10.3390/plants8100422

Singh, A., and Desgagné-Penix, I. (2017). Transcriptome and metabolome profiling of Narcissus pseudonarcissus 'King Alfred'reveal components of *Amaryllidaceae alkaloi*d metabolism. *Sci. Rep.* 7, 1–14. doi: 10.1038/s41598-017-17724-0

Son, M., Kim, A., Lee, J., Park, C.-H., Heo, J.-C., Lee, H.-J., et al. (2010). Ethanol extract of *Lycoris radiata* induces cell death in B16F10 melanoma via p38-mediated AP-1 activation. *Oncol. Rep.* 24, 473–478. doi: 10.3892/or_00000881

Song, T., Das, D., Yang, F., Chen, M., Tian, Y., Cheng, C., et al. (2020). Genome-wide transcriptome analysis of roots in two rice varieties in response to alternate wetting and drying irrigation. *Crop J.* 8, 586–601. doi: 10.1016/j.cj.2020.01.007

Stracke, R., Werber, M., and Weisshaar, B. (2001). The R2R3-MYB gene family in *Arabidopsis thaliana*. *Curr. Opin. Plant Biol.* 4, 447–456. doi: 10.1016/S1369-5266(00)00199-0

Tan, J., Wang, M., Tu, L., Nie, Y., Lin, Y., and Zhang, X. (2013). The flavonoid pathway regulates the petal colors of cotton flower. *PLoS One* 8:e72364. doi: 10.1371/journal.pone.0072364

Tanaka, Y., Sasaki, N., and Ohmiya, A. (2008). Biosynthesis of plant pigments: anthocyanins, betalains and carotenoids. *Plant J.* 54, 733–749. doi: 10.1111/j.1365-313X.2008.03447.x

Tanaka, Y., Tsuda, S., and Kusumi, T. (1998). Metabolic engineering to modify flower color. *Plant Cell Physiol.* 39, 1119–1126. doi: 10.1093/oxfordjournals.pcp.a029312

Wang, R., Xu, S., Jiang, Y., Jiang, J., Li, X., Liang, L., et al. (2013). De novo sequence assembly and characterization of *Lycoris aurea* transcriptome using GS FLX titanium platform of 454 pyrosequencing. *PLoS One* 8:e60449. doi: 10.1371/journal.pone.0060449

Wang, Y., Mao, Z., Jiang, H., Zhang, Z., Wang, N., and Chen, X. (2021). Brassinolide inhibits flavonoid biosynthesis and red-flesh coloration via the MdBEH2. 2–MdMYB60 complex in apple. *J. Exp. Bot.* 72, 6382–6399. doi: 10.1093/jxb/erab284

Wang, Z., Gerstein, M., and Snyder, M. (2009). RNA-Seq: a revolutionary tool for transcriptomics. *Nat. Rev. Genet.* 10, 57–63. doi: 10.1038/nrg2484

Wei, Z., and Li, J. (2020). Regulation of brassinosteroid homeostasis in higher plants. *Front. Plant Sci.* 11:583622. doi: 10.3389/fpls.2020.583622

Weiss, D. (2000). Regulation of flower pigmentation and growth: multiple signaling pathways control anthocyanin synthesis in expanding petals. *Physiol. Plant.* 110, 152–157. doi: 10.1034/j.1399-3054.2000.110202.x

Xie, C., Mao, X., Huang, J., Ding, Y., Wu, J., Dong, S., et al. (2011). KOBAS 2.0: a web server for annotation and identification of enriched pathways and diseases. *Nucleic Acids Res.* 39 (suppl_2), W316–W322. doi: 10.1093/nar/gkr483

Xue, L., Wang, J., Zhao, J., Zheng, Y., Wang, H.-F., Wu, X., et al. (2019). Study on cyanidin metabolism in petals of pink-flowered strawberry based on transcriptome sequencing and metabolite analysis. *BMC Plant Biol.* 19:423. doi: 10.1186/s12870-019-2048-8

Xue, Q., Zhang, X., Yang, H., Li, H., Lv, Y., Zhang, K., et al. (2021). Transcriptome and metabolome analysis unveil anthocyanin metabolism in pink and red testa of peanut (*Arachis hypogaea* L.). *Int. J. Genomics* 2021:5883901. doi: 10.1155/2021/5883901

Yuan, L., Peng, Z., Zhi, T., Zho, Z., Liu, Y., Zhu, Q., et al. (2015). Brassinosteroid enhances cytokinin-induced anthocyanin biosynthesis in Arabidopsis seedlings. *Biol. Plant.* 59, 99–105. doi: 10.1007/s10535-014-0472-z

Zhao, D., and Tao, J. (2015). Recent advances on the development and regulation of flower color in ornamental plants. *Front. Plant Sci.* 6:261. doi: 10.3389/fpls.2015.00261

Zhao, D., Tao, J., Han, C., and Ge, J. (2012). Flower color diversity revealed by differential expression of flavonoid biosynthetic genes and flavonoid accumulation in herbaceous peony (*Paeonia lactiflora* Pall.). *Mol. Biol. Rep.* 39, 11263–11275. doi: 10.1007/s11033-012-2036-7

Zheng, T., Dong, T., Haider, M. S., Jin, H., Jia, H., and Fang, J. (2020). Brassinosteroid regulates 3-hydroxy-3-methylglutaryl CoA reductase to promote grape fruit development. *J. Agric. Food Chem.* 68, 11987–11996. doi: 10.1021/acs.jafc.0c04466

Zhou, L.-L., Shi, M.-Z., and Xie, D.-Y. (2012). Regulation of anthocyanin biosynthesis by nitrogen in TTG1–GL3/TT8–PAP1-programmed red cells of *Arabidopsis thaliana*. *Planta* 236, 825–837. doi: 10.1007/s00425-012-1674-2

Zhou, S., Yu, B., Luo, Q., Hu, J., and Bi, D. (2007). Karyotypes of six populations of *Lycoris radiata* and discovery of the tetraploid. *Acta Phytotaxonomica Sin.* 45, 513–522. doi: 10.1360/aps050108

Conflict of Interest: The authors declare that the research was conducted in the absence of any commercial or financial relationships that could be construed as a potential conflict of interest.

Publisher's Note: All claims expressed in this article are solely those of the authors and do not necessarily represent those of their affiliated organizations, or those of the publisher, the editors and the reviewers. Any product that may be evaluated in this article, or claim that may be made by its manufacturer, is not guaranteed or endorsed by the publisher.

Copyright © 2021 Yang, Li, Das, Zheng, Song, Wang, Chen, Li and Zhang. This is an open-access article distributed under the terms of the Creative Commons Attribution License (CC BY). The use, distribution or reproduction in other forums is permitted, provided the original author(s) and the copyright owner(s) are credited and that the original publication in this journal is cited, in accordance with accepted academic practice. No use, distribution or reproduction is permitted which does not comply with these terms.

frontiers in Plant Science

ORIGINAL RESEARCH
published: 17 December 2021
doi: 10.3389/fpls.2021.805407

Physiological and Biochemical Responses, and Comparative Transcriptome Profiling of Two *Angelica sinensis* Cultivars Under Enhanced Ultraviolet-B Radiation

Tong Peng[1], Yinquan Wang[1,2], Tao Yang[3], Fusheng Wang[4], Jun Luo[1] and Yali Zhang[1]*

[1] College of Pharmacy, Gansu University of Chinese Medicine, Lanzhou, China, [2] Northwest Chinese and Tibetan Medicine Collaborative Innovation Center, Lanzhou, China, [3] Key Laboratory of Microbial Resources Exploitation and Application, Institute of Biology, Gansu Academy of Sciences, Lanzhou, China, [4] Dingxi Academy of Agricultural Sciences, Dingxi, China

In this study, we explored the adaptive mechanism of two varieties of *Angelica sinensis* exposed to enhanced Ultraviolet-B (UV-B) radiation. The radiation had different effects on the biomass, photosynthetic performance, oxidative damage, antioxidant defense system, and levels of bioactive compounds of Mingui 1 (C1) and Mingui 2 (C2). C2 outperformed C1 under enhanced UV-B radiation, compared to natural light. Using the Illumina RNA-seq, we obtained 6,326 and 2,583 DEGs in C1 and C2, respectively. Under enhanced UV-B radiation, the mRNA levels of genes involved in photosynthesis, antennae protein synthesis, carbon fixation, chlorophyll synthesis, and carotenoid synthesis were decreased in C1 but stable in C2, involving few DEGs. TFs were widely involved in the response of C1 to enhanced UV-B radiation; almost all *bHLH* and *MYB* coding genes were downregulated whereas almost all genes encoded *WRKY22*, *WRKY50*, *WRKY72*, *NCF*, and *HSF* were upregulated. These results indicate that enhanced UV-B radiation was not conducive to the synthesis of flavonoids, while disease resistance was enhanced. Regarding the ROS scavenging system, upregulated DEGs were mainly found in the AsA-GSH cycle and PrxR/Trx pathways. Remarkably, DEGs that those encoding biosynthetic key enzymes, including ferulic acid (*CHS*, *CHI*, *DFR*, and *ANS*) and flavonoid (*CHS*, *CHI*, *DFR*, and *ANS*), most upregulation in C2, leading to increased accumulation of ferulic acid and flavonoids and adversely affecting C1. Genes encoding key enzymes involved in the synthesis of lactone components (*ACX*, *PXG*) were mostly up-regulated in C1, increasing the content of lactone components. Our results reveal the DEGs present between C1 and C2 under enhanced UV-B radiation and are consistent with the observed differences in physiological and biochemical indexes. C1 was more sensitive to enhanced UV-B radiation, and C2 was more tolerant to it under moderate enhanced UV-B radiation stress. In addition, the large amount of *A. sinensis* transcriptome data generated here will serve as a source for finding effective ways to mitigate UV-B enhancement, and also contribute to the well-established lack of genetic information for non-model plant species.

Keywords: *Angelica sinensis*, UV-B radiation, transcriptome, physiological response, antioxidant defense system, bioactive compound

OPEN ACCESS

Edited by:
Zhihua Liao,
Southwest University, China

Reviewed by:
Lv Zongyou,
Shanghai University of Traditional Chinese Medicine, China
Guoyin Kai,
Zhejiang Chinese Medical University, China
Xiaozhong Lan,
Tibet Agricultural and Animal Husbandry College, China

***Correspondence:**
Yinquan Wang
kjkfpp@163.com

Specialty section:
This article was submitted to Plant Metabolism and Chemodiversity, a section of the journal Frontiers in Plant Science

Received: *30 October 2021*
Accepted: *30 November 2021*
Published: *17 December 2021*

Citation:
Peng T, Wang Y, Yang T, Wang F, Luo J and Zhang Y (2021) Physiological and Biochemical Responses, and Comparative Transcriptome Profiling of Two Angelica sinensis Cultivars Under Enhanced Ultraviolet-B Radiation. Front. Plant Sci. 12:805407. doi: 10.3389/fpls.2021.805407

INTRODUCTION

Radix Angelica Sinensis (RAS) is the dried root of *Angelica sinensis* (Oliv.) Diels, which has been used as both a medicine and for nourishment in the form of spice and tonic for more than 1,000 years in China, South Korea, and Japan. Today, it is still one of the most commonly used herbs by practitioners of Traditional Chinese Medicine (TCM) in China as well as Europe (Wei et al., 2016). More than 70 active compounds have been identified in RAS, including polysaccharides, ferulic acid, coniferyl ferulate, Z-ligustilide, E-3-butylidenephthalide, and other phthalides (Hook, 2014). These active compounds have numerous pharmacological actions, including anti-inflammatory, antitumor, immunostimulatory, hormone regulation, antihepatotoxic, neuroprotective, and anti-aging effects, among others (Chao and Lin, 2011).

RAS is mainly cultivated in the alpine wetland of southeast Gansu Province of China, in the northeastern margin of the Tibet Plateau. *A. sinensis* prefers a cold summer climate, sufficient rainfall, low light, and loose, organic-rich loam soil. In the past 10 years, due to global climate warming, and severe early bolting and root diseases, the planting area of *A. sinensis* has gradually changed from low-altitude mountain valleys to high-altitude slopes; thus, it is now being exposed to enhanced UV-B stress (An et al., 2020).

Mingui 1 (C1) is a popularized *A. sinensis* cultivar with dark purple petioles, dark green leaves in the growing period, and light purple flowers in the flowering and fruiting period. It has been cultivated throughout the planting area of *A. sinensis* but has suffered from problems such as biological contamination caused by agricultural residues and pathogenic microorganisms, and cultivar degradation, and so forth. Mingui 2 (C2) was bred from the mixed population of cultivated *A. sinensis* with combining methods of group breeding and systematic breeding by Dingxi Academy of Agricultural Sciences, Gansu Province, China. C2 shows a typical characteristic in its stem and leaf is light green leaves and petioles during the growing period; green stalks with white flowers, and light yellow and white seeds in the flowering and fruiting period. Nei's genetic of between Mingui 1 and Mingui 2 was 0.0690, and both were clustered by UPGMA into the same class at the genetic distance of 0.10, which indicated there were great genetic differences among different *A. sinensis* cultivars (Yan et al., 2014; **Figure 1**).

Ultraviolet-B (UV-B, 280∼315 nm) is a natural component of sunlight, and a small amount of it can have a great impact on organisms (Robson et al., 2019). Generally, there is a positive correlation between the UV erythemal dose and altitude (Xiao et al., 2019). The impact of UV-B on plant growth and development is largely dependent on radiation dose and plant species (Jenkins, 2009). Both UV-B-specific and non-specific pathways may be activated, leading to damage of photosystem II (PS II) and photosystem I (PS I), the loss of thylakoid membrane integrity, a decrease in chlorophyll level, and carbon fixation (Nawkar et al., 2013). The accumulation of reactive oxygen species (ROS) may damage cells, proteins, lipids, and DNA, and further damage the photosynthetic apparatus (Jansen et al., 1998). It can also have adverse effects on stress-related hormone synthesis (Mosadegh et al., 2019). A low dose of UV-B radiation can induce a photogenic morphological response and UV-B adaptive response in plants (Yin and Ulm, 2017), leading to an increase in chlorophyll levels (Vandenbussche et al., 2018) as well as antioxidants such as superoxide dismutase (SOD); peroxidase (POD), catalase (CAT), and nicotinamide adenine dinucleotide phosphate (NADP) dehydrogenase, and non-enzymatic defense systems such as glutathione, polyphenols, tocopherol, and ascorbic acid (Yu and Liu, 2013). At the same time, UV-B-absorbing metabolites, including flavonoids and other phenolic substances, will accumulate (Inostroza-Blancheteau et al., 2016). Some transcriptome studies have shown that UV-B regulates different functional genes in Asian ginseng (Panax ginseng) (Gong et al., 2020), Lycium ruthenicum (Chen et al., 2015), and other medicinal plants. This includes genes related to the photosynthesis pathway and photosynthetic pigment synthases, such as *Lhca*, the *Lhcb* gene family, and the Psb complex (Kataria et al., 2014). Transcription factors (TFs) are also involved in the plant response to UV-B stress. Among them, WRKY, MYB, NCF, and *bHLH* are the most well-known and are considered important regulators of UV-B response genes in plants. Hormone-related genes, such as those encoding biosynthesis and signal transduction pathways of indoleacetic acid (IAA), gibberellin (GA), cytokinin (CTK), jasmonic acid (JA), and salicylic acid (SA), are involved in the adaptive response of plants to UV-B stress (Vanhaelewyn et al., 2016). These include many structural and regulatory genes in the phenylalanine/flavonoid pathway, such as phenylalanine ammonia-lyase (*PAL*), chalcone synthase (*CHS*), dihydroflavonol 4-reductase (*DFR*), and flavanone-3-hydroxylase (*F3H*) (Neugart et al., 2014; Henry-Kirk et al., 2018). Other genes encoding lactone component synthase are less well studied.

As discussed above, the understanding of UV-B effects has shifted from general stress factors to specific regulators to promote metabolic and developmental changes in higher plants (Parihar et al., 2015). Previous studies on the growth and development of *A. sinensis* have mainly focused on the mechanism of early flowering (Yu et al., 2019; Gao et al., 2021), or the effects of rhizosphere microorganisms on the quality of *A. sinensis* under different soil microenvironments (Zhu et al., 2021). Some of these isolated and identified autotoxic allelochemicals from the rhizosphere soil (Xin et al., 2019). The effects of enhanced UV-B on different *A. sinensis* cultivars and the responses of physiology, metabolites, and comparative transcriptome have not been sufficiently studied.

Abbreviations: ABA, abscisic acid; ACX, acyl-CoA oxidase; BR, brassinosteroid; CHS, chalcone synthase; CTK, cytokinin; CYP, cytochrome P450; DEG, differentially expressed gene; DFR, dihydroflavonol 4-reductase; EH, epoxide hydrolase; ET, ethylene; F3H, flavanone-3-hydroxylase; FAD, fatty acid desaturase; FAE, fatty acid epoxydase; FAH, fatty acid hydroxylase; FPKM, fragments per kilobase million; GA, gibberellin; GSH, glutathione; GST, glutathione s-transferase; HCT, shikimate O-hydroxycinnamoyl transferase; IAA, indole acetic acid; JA, jasmonic acid; KEGG, Kyoto Encyclopedia of Genes and Genomes; LOX, lipoxygenase; MDA, malondialdehyde; NR, non-redundant protein sequences; PAL, phenylalanine ammonia-lyase; PXG, peroxygenase; RAS, Radix Angelica Sinensis; ROS, reactive oxygen species; SA, salicylic acid; SD, standard deviation; TF, transcription factor; UV-B, Ultraviolet-B.

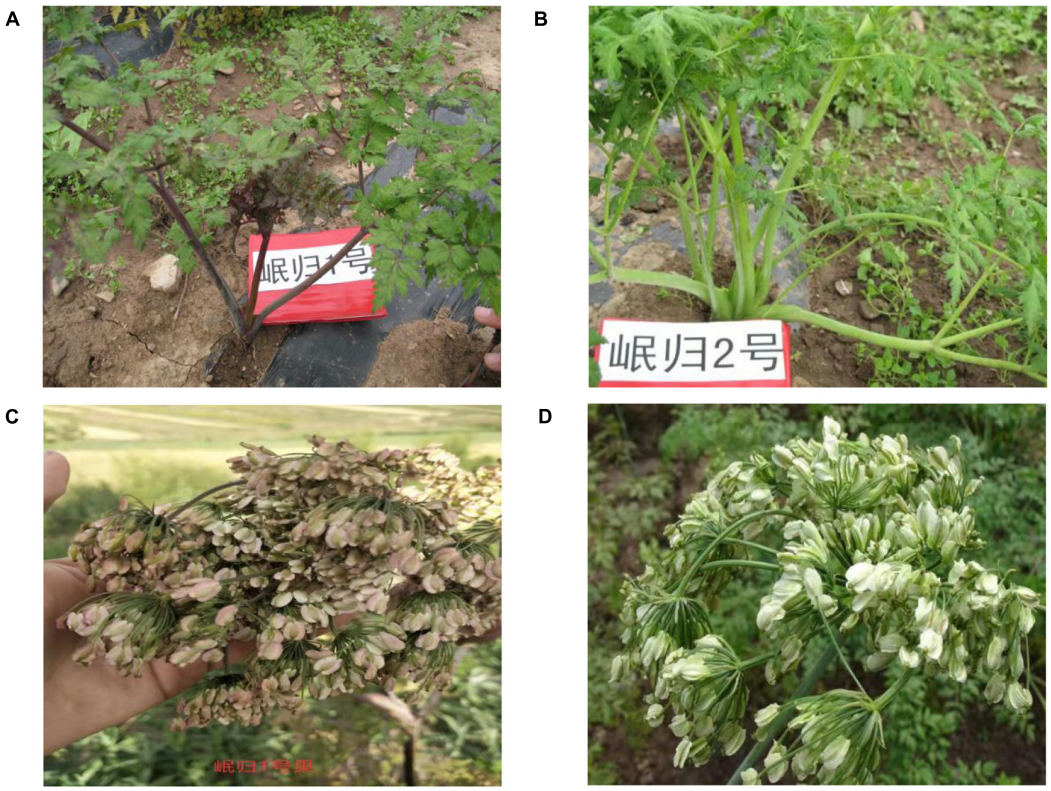

FIGURE 1 | Morphological performance of **(A)** Mingui 1 (C1) plants, **(B)** Mingui 2 (C2) plants, **(C)** C1 flowers and fruits, and **(D)** C2 flowers and fruits.

Therefore, in this study, we investigated the physiological and biochemical responses of two *A. sinensis* cultivars to exposure to enhanced UV-B radiation as well as the underlying molecular mechanisms.

MATERIALS AND METHODS

Plant Material and Enhanced Ultraviolet-B Radiation Treatment

Two *A. sinensis* cultivars [Mingui 1 (C1) and Mingui 2 (C2)] were used. Seedlings were obtained from the Dingxi Academy of Agricultural Sciences in Gansu, China. The experiment was run in Min County, Gansu Province (34°59′ N, 103°57′E, 2,340 m above sea level) from April 2019 to November 2019.

Enhanced UV-B radiation treatment was carried out using an adjustable UV-B lamp (wavelength range: 280∼400 nm) set 0.25∼0.5 m above the top of the plants (**Supplementary Figure 1**). The stress intensity of UV was set at two levels, natural light (U0) and the radiation dose equivalent at 2,600 m above sea level (or 14.11 $kJ{\cdot}m^{-2}{\cdot}D^{-1}$, Ut). Hence, the four treatment groups were: C1 plants exposed to U0 (U0C1), C2 plants exposed to U0 (U0C2), C1 plants exposed to Ut (UtC1), and C2 plants exposed to Ut (UtC2). Each treatment was repeated three times. Treatments started on July 5; for each treatment, the UV lamp was turned on at 8:30 a.m. and turned off at 5:30 p.m. After *A. sinensis* leaves were collected, they were rinsed with distilled water, immediately frozen in liquid nitrogen, and stored at –80°C for further analyses including physiological and biochemical index determination and high-throughput sequencing.

Photosynthesis Parameters

The gas exchange parameters, including photosynthetic rate (Pn), transpiration rate (Tr), and stomatal conductance (Gs), were recorded using an infrared gas analyzer (IRGA) (Li-Cor) between 09:00 and 11:00 a.m. We used an LI-6400–40 portable photosynthesis system (Li-Cor, Lincoln, NE). The CO_2 concentration was set at 350 $\mu mol{\cdot}mol^{-1}$, the light intensity was 1,000 $\mu mol{\cdot}m^{-2}{\cdot}s^{-1}$, and the temperature was 28°C. Each leaf was measured three times and the average value was calculated. Water use efficiency (WUE) was calculated as the ratio of Pn/Tr.

Photosynthetic and Photoprotective Pigments

Samples (0.25 g) were ground in liquid nitrogen and incubated in 2.5 mL 80% acetone at 4°C in darkness. The levels of chlorophyll (Chl a), Chl b, carotenoids (Car), and total chlorophyll (TChl) were determined using a UV-vis spectrophotometer (Cary-50), measuring the optical density (OD) of leaf extracts as previously described. Car was measured using a Car measurement kit (Qincheng Bio, Shanghai, China), according to the manual.

Antioxidant Activity

According to the manufacturer's instructions, the levels of Superoxide dismutase (SOD), peroxidase (POD), catalase (CAT), and malondialdehyde (MDA) were measured with commercially available SOD assay kits, POD assay kit, CAT assay kit, and MDA assay kit (Jiancheng Bioengineering Institute, Nanjing, China), respectively.

Extraction of Bioactive Compounds and HPLC Analysis

The RAS samples were dried in the shade, pulverized into powder, and sieved through a 0.25 mm filter. The powder (0.5 g) was placed in a 150 ml vial containing 20 ml of 70% MeOH, sealed, weighed, and then sonicated at 220 W, 80 Hz for 40 min. Next, they were shaken with 70% MeOH, extracted, and verbed on a 0.22 μm microporous membrane. The filtered solution was stored at 4°C and quantified by HPLC using Agilent 1260 (Agilent, United States) and Merk RP-C18 (250 mm × 4.6 mm, 5 μm) devices. A mobile phase consisting of 0.1% glacial acetic acid (A) and acetonitrile (B) was used for separation with the following gradient: 0∼20 min: 19% B; > 20∼60 min: 19∼95% B; > 60∼75 min: 95∼100% B. The mobile phase flow rate was 1 mL/min, and the column temperature was 30°C. The detection wavelength was 280 nm.

RNA Isolation, cDNA Library Construction, and Sequencing

Briefly, total RNA was digested using DNase. Then poly A-containing mRNA was enriched using oligo (dT)-attached magnetic beads, and then randomly fragmented into small segments. The first and second strands of cDNA were synthesized using the fragments as templates, and then end repair was done. The double-stranded cDNAs were purified with a QiaQuick PCR extraction kit (Qiagen) and eluted with EB buffer for end repair and poly (A) addition. Finally, sequencing adapters were ligated to the 5′ and 3′ ends of the fragments. The fragments were purified via agarose gel electrophoresis and amplified via PCR to create a cDNA library. The cDNA library was sequenced on an Illumina sequencing platform (Illumina HiSeq^{TM}2500) by Shanghai OE Biotech. Co., Ltd., Shanghai, China (Bolger et al., 2014).

Bioinformatic Analyses

Raw data in fastq format were first filtered by removing reads containing adapters and/or ploy-N and other low-quality reads. The remaining clean data were assembled using the Trinity program (Grabherr et al., 2011). The functions of unigenes were annotated by aligning them with the NCBI non-redundant (NR), SwissProt, and Clusters of Orthologous Groups for Eukaryotic Complete Genomes (KOG) databases using Blastx (Altschul et al., 1990) with a threshold *E*-value of 10^{-5}. Differential expression analyses were performed using the DESeq R package. A *P*-value < 0.01 with Foldchange ≥ 2.0-fold was set as the threshold for significant differential expression. KEGG enrichment analysis of differentially expressed genes (DEGs) was performed using R based on a hypergeometric distribution.

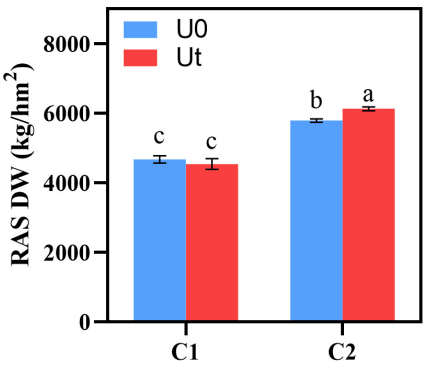

FIGURE 2 | Biomass of two *Angelica sinensis* cultivars in response to enhanced UV-B radiation. Different letters indicated the significant difference ($P < 0.05$). Error bars were represented standard deviation (SD).

qRT-PCR

Identical RNA samples as those used in the RNA-seq experiments were used for qRT-PCR. The relative expression patterns of six genes differentially expressed in transcriptome data were evaluated. Quantification was performed via a two-step reaction process: reverse transcription (RT) and PCR. Each RT reaction consisted of 0.5 μg RNA, 2 μL 5 × TransScript All-in-one SuperMix for qPCR and 0.5 μL gDNA Remover, in a total volume of 10 μL. Reactions were performed on a GeneAmp®PCR System 9700 (Applied Biosystems, United States) for 15 min at 42°C, 5 s at 85°C. Then the 10 μL RT reaction mix was diluted × 10 in nuclease-free water and held at −20°C. The expression levels of mRNAs were normalized to the reference gene and were calculated using the 2-ΔΔCt method.

Data Analysis

All data were analyzed using SPSS Statistics software (IBM, New York, United States). Differences in physiological response effects and bioactive compound levels between the two cultivars at different UV-B doses were analyzed via analysis of variance (ANOVA). The least significant difference (LSD) was calculated for significant data at $P < 0.05$. The reported values represent arithmetic averages of three replicates, and the data are expressed as mean ± standard deviation (SD).

RESULTS

Biomass

To evaluate the effect of enhanced UV-B radiation, the dry weight (DW) was measured in RAS after drying. DW of C2 was higher than that of C1 regardless of whether UV-B radiation enhancement was carried out, and DW of enhanced UV-B radiation was significantly higher than that of natural light ($P < 0.05$) (**Figure 2**).

Photosynthesis Response

As photosynthesis is one of the first processes affected by enhanced UV-B radiation, it is crucial to evaluate its

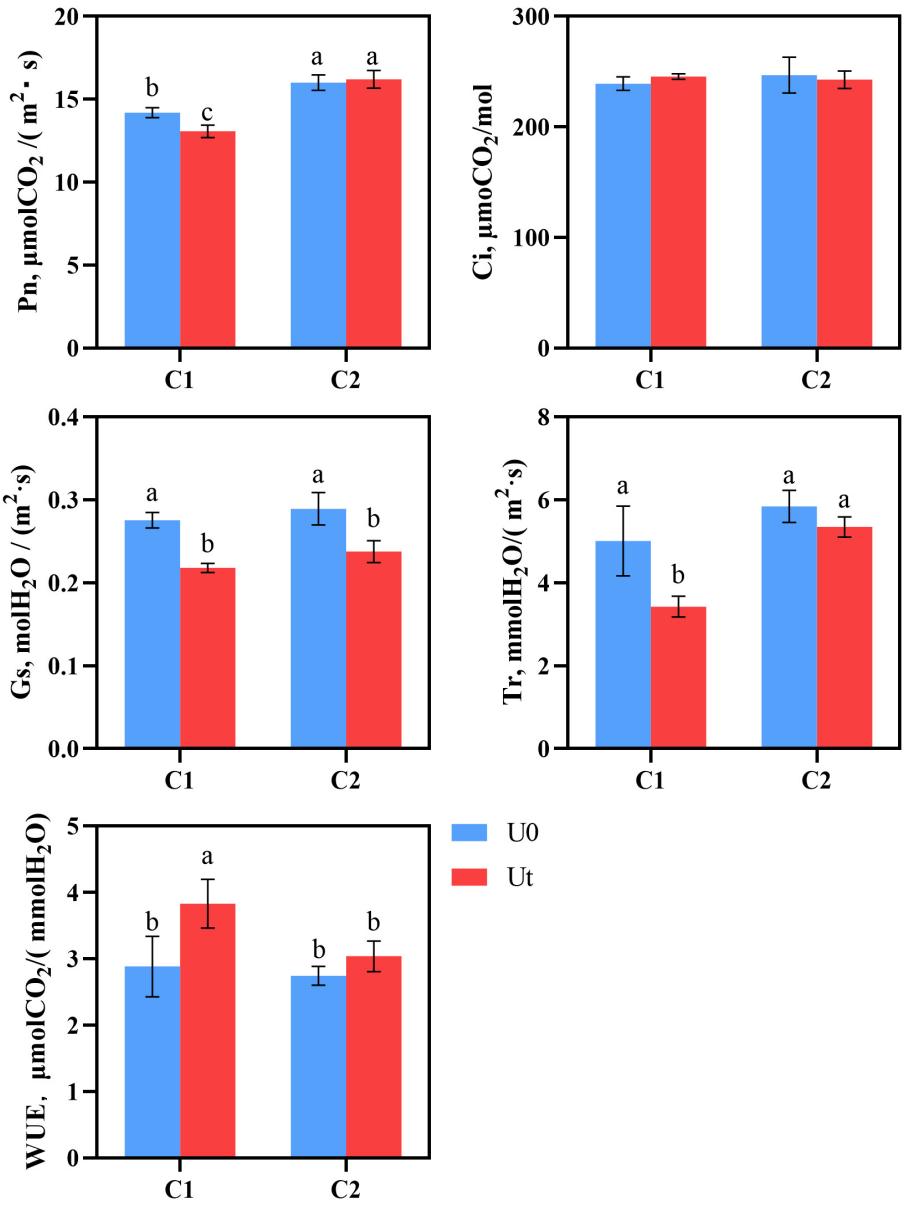

FIGURE 3 | Photosynthesis of two *Angelica sinensis* cultivars in response to enhanced UV-B radiation. Different letters indicated the significant difference ($P < 0.05$). Error bars were represented standard deviation (SD).

response. There were significant differences in the photosynthesis parameters, including Pn, Ci, Gs, Tr, and WUE between C1 and C2 under each treatment. In C1, enhanced UV-B radiation significantly decreased Pn, Gs, and Tr by 8.3, 26.3, 46.1, and 33.0%, respectively, compared to natural light. In C2, Gs was significantly decreased by 17.2%. Pn was 1.24 times higher in C2 than in C1 under radiation. It can be speculated that C2 maintains its photosynthesis by closing stomata and reducing the loss of water dispersion (**Figure 3**).

Photosynthetic Pigments

Chl content in plant leaves is an important physiological index to measure plant stress resistance (Ben-Asher et al., 2006). No differences were found in the photosynthetic pigments (Chl b, Chla + b, and Chl a/b) of C1, whereas Car was 1.11 times higher under radiation. In C2, radiation significantly affected all pigments except Chl b and Car, levels of Chl a, Chla + b, and Chla/b increased by 22.6, 7.1, and 20.5%, respectively, and Chlb decreased by 7.5%. It can be inferred that C1 can adapt to enhanced UV-B radiation by increasing levels of Car, a light absorption auxiliary pigment, clearing excess ROS in tissues, and protecting Chl. By contrast, the higher Chl a/b of C2 indicates that the thylakoid membrane structure of C2 was stable under enhanced UV-B radiation, it had better adaptability under radiation, and the accumulation of Chl content was somewhat promoted (**Figure 4**).

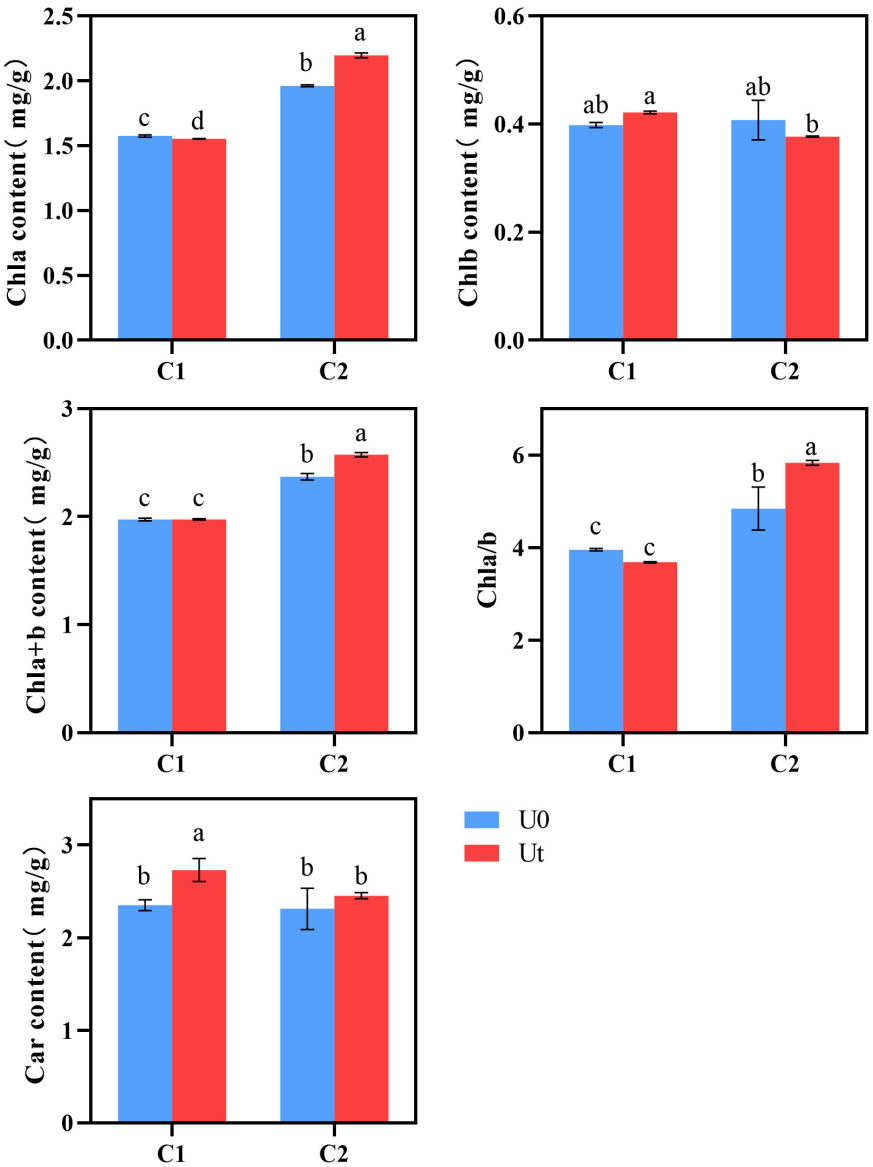

FIGURE 4 | Photosynthetic pigment of two *Angelica sinensis* cultivars in response to enhanced UV-B radiation. Different letters indicated the significant difference ($P < 0.05$). Error bars were represented standard deviation (SD).

Oxidative Damage and the Antioxidant Defense System

Compared to natural light, enhanced UV-B radiation increased the activities of antioxidant enzymes, such as SOD, POD, and CAT in leaves of *A. sinensis*. In detail, the increases were 9.7 and 28.8% for SOD, 20.1 and 53.9% for POD, and 16.9 and 59.6% for CAT in C1 and C2, respectively. To evaluate the effects of UV-B stress on membrane lipid peroxidation in leaves, MDA levels were measured. No significant differences were noted between the treatments. Plant tissues and cells protect against injuries derived from UV-B oxidative stress through the upregulation of multiple antioxidant enzymes. It shows that under enhanced UV-B radiation, increasing antioxidant enzyme activity (SOD, POD, and CAT) is the common adaptation method of C1 and C2, and the three protective enzymes can synergistically scavenge stress-induced ROS (**Figure 5**).

Bioactive Compounds

Radiation positively impacted the accumulation of senkyunolide A and 3-butylphthalide in both cultivars compared to natural light. It increased the content of Z-ligustilide by 19.27% and levistilide A by 9.7% in C1, and decreased the content of Z-ligustilide by 2.3% and levistilide A by 2.9% in C2. Senkyunolide I of C1 was significantly increased by 16.7%, but there were no significant differences in C2. Coniferyl ferulate can be regarded as the "reserve pool" of ferulic acid in RAS. Coniferyl ferulate can be easily decomposed into ferulic acid. Therefore, ferulic acid in RAS should be judged in combination

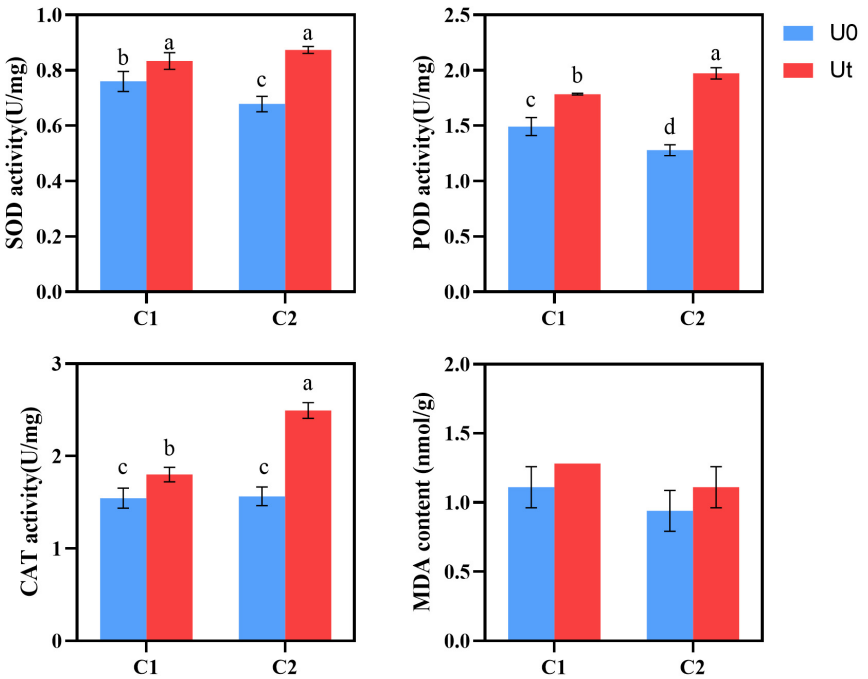

FIGURE 5 | SOD, POD, and CAT activities and MDA content of two *Angelica sinensis* cultivars in response to enhanced UV-B radiation. Different letters indicated the significant difference ($P < 0.05$). Error bars were represented standard deviation (SD).

with coniferyl ferulate. Generally speaking, C2 will not have a negative impact on the accumulation of ferulic acid content under enhanced UV-B radiation, on the contrary, C1 may be reduced. UV-B had a positive effect on the accumulation of C1 lactones (**Figure 6**).

Identification and Validation of Differentially Expressed Genes

A total of 6596 DEGs (2851 upregulated and 3745 downregulated) were identified in C1 between treatments (UtC1 vs. U0C1). Only 2583 DEGs (822 upregulated and 1761 downregulated) were found in C2 (UtC2 vs. U0C2). The number of DEGs caused by radiation was 3603 and 2600 in C1 and C2, respectively. The number of DEGs shared by the two cultivars was 1257 (**Figures 7A–C**).

To verify the sequencing data, we selected six unigenes for qRT-PCR verification. Of these, several unigenes encoding *psaH*, *SAUR*, *FAH*, *Lhca4*, *WIN1*, and *C2H2* were experimentally validated by quantitative RT-PCR, and there was good concordance ($R^2 = 0.976$) between RNA-seq data and qRT-PCR analysis (**Figure 7D**), indicating that the gene expression levels were reliable. The primers are shown in **Supplementary Table 1**.

Kyoto Encyclopedia of Genes and Genomes Pathway Analysis of Differentially Expressed Genes

KEGG analysis illustrated that the two cultivars responded differently to radiation. DEGs in C1 were significantly enriched in photosynthetic antenna protein (ko00196), indicating that radiation had a significant effect on light-harvesting ability (Jobe et al., 2019; **Figure 8A**). C2 was significantly enriched in the TCA cycle (ko00020), glutathione metabolism (ko00480), inositol phosphate metabolism (ko00562), cyanoamino acid metabolism (ko00460), flavonoid biosynthesis (ko00941), and brassinosteroid biosynthesis (ko00905) pathways (**Figure 8B**). This indicates that radiation widely affected the synthesis and accumulation of primary and secondary metabolites. Both C1 and C2 were enriched in the cutin, suberine, and wax biosynthesis pathways (ko00073), indicating that UV-B affects the production of wax and lignin on the leaf surface (**Figure 8C**).

Differentially Expressed Genes Related to the Photosynthetic System

KEGG enrichment analysis revealed that photosynthetic systems in C1 and C2 responded differently to enhanced UV-B radiation. A total of 48 DEGs between natural light and irradiation conditions were annotated to three pathways: 22 for photosynthesis (ko00195), 17 for photosynthesis-antenna proteins (ko00196), and 9 for carbon fixation (ko00710). These DEGs were concentrated in C1. In total, 22 genes (17 downregulated, 5 upregulated) participated in the photosynthetic reaction center including the PSI (*Psa A*, *Psa G*, *Psa H*, *Psa K*, *Psa N*, and *Psa O*) and PSII complexes (*Psb P*, *Psb Q*, *Psb R*, and *Psb 27*) and photosynthetic electron transport (*PetF*) in C1. One gene encoding *Psa H* and one encoding *Psa O* were downregulated in the photosynthetic reaction center in C2 (**Figure 9A**). In C1, *Lhca3* was significantly up-regulated, and one lhca1 coding gene and one *Lhcb2* coding gene were up-regulated. In C2, *Lhca4*, *Lhcb2*, and *Lhcb6* were significantly downregulated, although

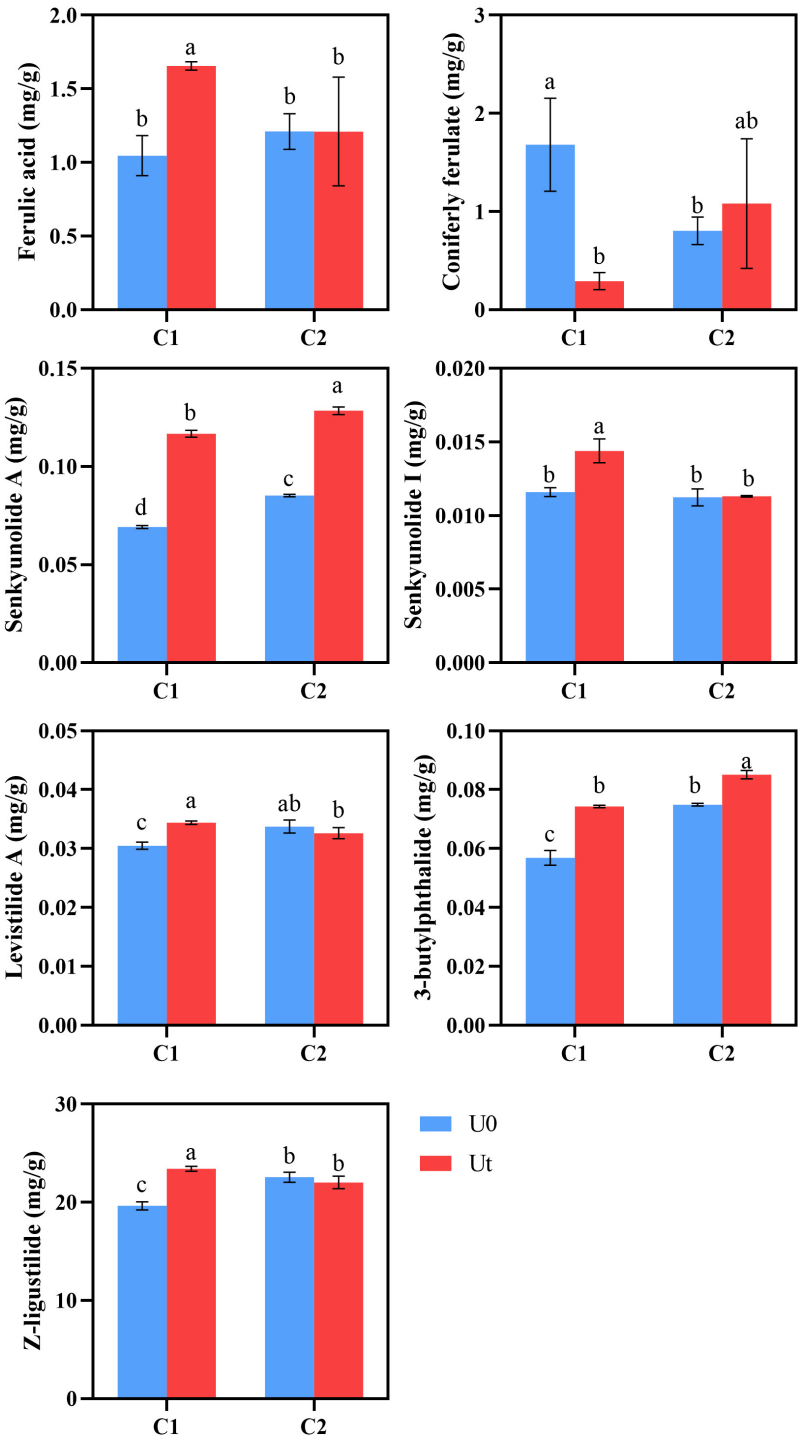

FIGURE 6 | Levels of bioactive compounds of two RAS cultivars in response to enhanced UV-B radiation. Different letters indicated the significant difference ($P < 0.05$). Error bars were represented standard deviation (SD).

overall the number of downregulated genes was much lower than in C1 (**Figure 9B**). Among the photosynthetic-related pathways in KEGG, only the photosynthetic antenna protein pathway was significantly downregulated in C1 (**Figure 9C**). However, there is no significant enrichment of photosynthetic system related pathways in C2. In C1, under UV-B enhanced radiation, most of the nine coding DEGs of the key enzymes *rbcL*, *rbcs*, *PGK*, *GAPDH*, and *GAPA* in the photosynthetic biological carbon fixation pathway were down-regulated. In C2, the expression of related genes in the photosynthetic system is stable (**Figure 9D**).

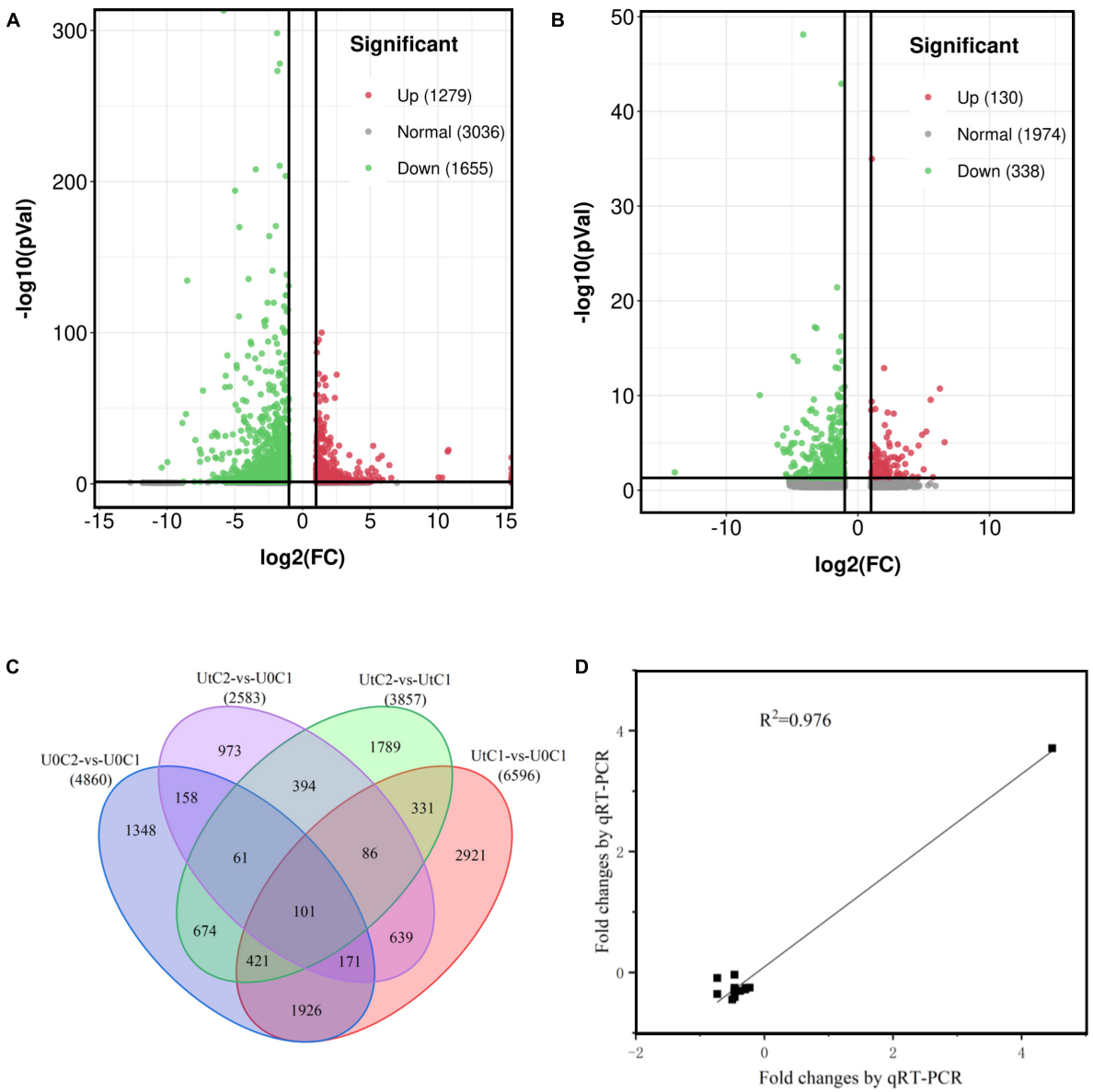

FIGURE 7 | Annotation and differentially expressed genes (DEGs) of the *Angelica sinensis* transcriptome. **(A,B)** Volcanic plots of the upregulated and downregulated genes of *Angelica sinensis* in two cultivars under enhanced UV-B radiation and natural light. **(C)** Unigene Venn diagrams for each group. **(D)** Correlation analysis between qRT-PCR and RNA-seq results of six genes.

However, the photosynthetic system of C1 is more sensitive to enhanced UV-B radiation, most DEGs are downregulated, and photosynthesis may be adversely affected.

The adaptability of plants to UV-B stress is inextricably related to chlorophyll metabolism (ko00860) and carotenoid biosynthesis (ko00960). One gene encoding *EARS* was significantly upregulated, and one gene encoding *hemE* and one encoding *chlH* were downregulated after radiation exposure in C1. Only one gene encoding *hemB* was upregulated in C2. In addition, one gene of *CrtL-e* was downregulated after radiation in C1. One gene of *Crt-b* and one gene of *CrtZ* were downregulated after radiation in C2 (**Figure 9E**). In conclusion, enhanced UV-B radiation was more beneficial for the accumulation of photosynthetic pigments in C2 than in C1.

Differentially Expressed Genes Involved in Defense Responses

Antioxidant System

UV-B stress causes the accumulation of ROS in plants (Hideg et al., 2013). ROS scavenging enzymes such as SOD, CAT, POD, and ascorbate peroxidase (APX), as well as non-enzymatic antioxidants (glutathione, carotenoids, etc.) After 30 days of exposure to enhanced UV-B radiation, there were 97 DEGs in C1 (30 upregulated, 60 downregulated). Among up-regulated

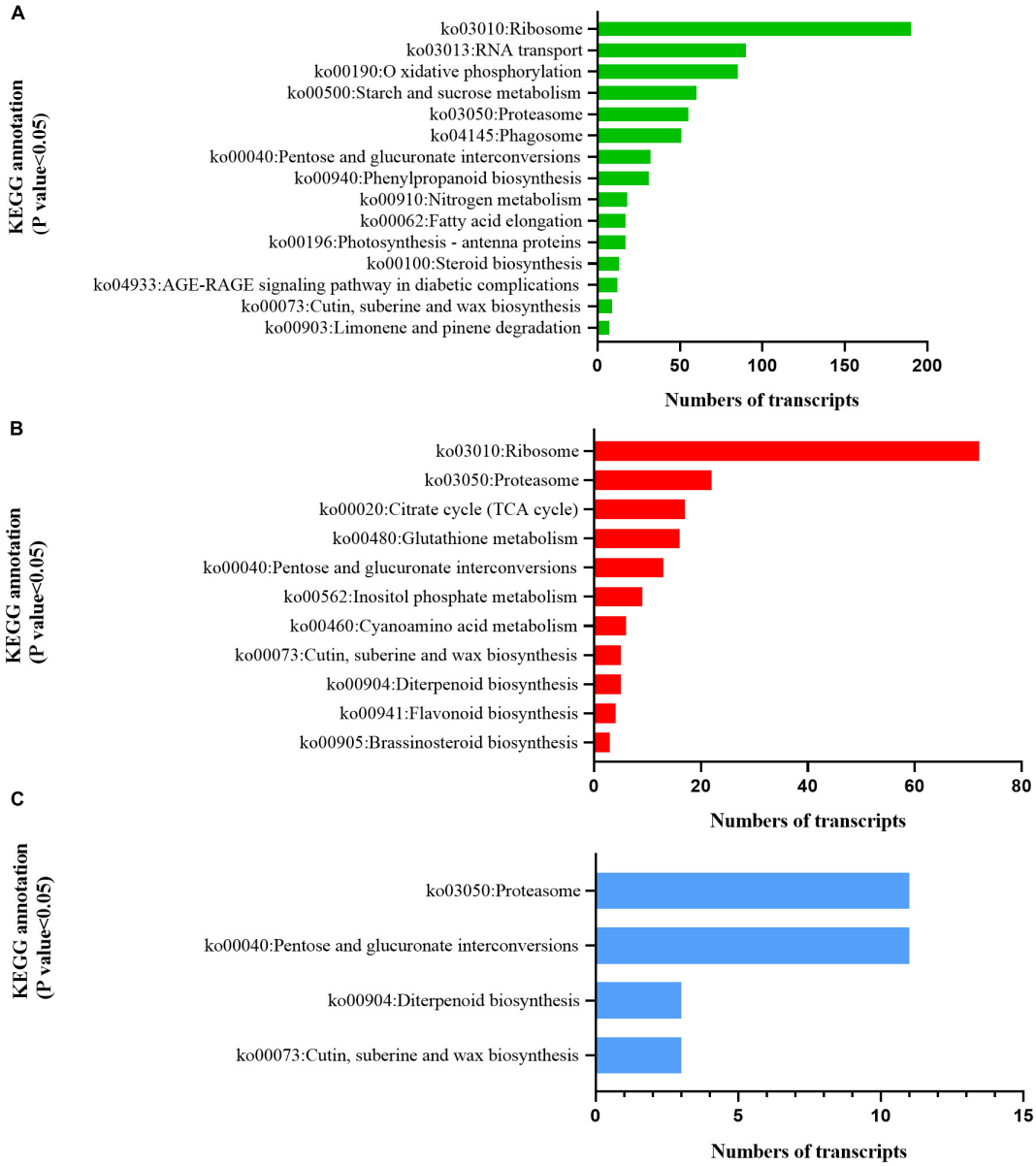

FIGURE 8 | Kyoto Encyclopedia of Genes and Genomes (KEGG) enrichment analysis of pathways involved in the response to enhanced UV-B radiation. **(A)** Mingui 1, **(B)** Mingui 2, **(C)** common pathways of two cultivars.

genes, 11 ASA-GSH cycle-related genes (6 GSTs, 1 GR, and 4 GLRS), 11 GPX-related pathway genes (4 PODS, 1 GPX, and 6 GLRS), 15 PrxR/Trx pathway-related coding genes (2 PrxR, 13 Trx), and 5 SOD encoding genes were identified (**Figure 10A**). There were only 5 upregulated and 32 downregulated DEGs in C2 (**Figure 10B**). The upregulated DEGs in both cultivars were focused on the AsA-GSH cycle and PrxR/Trx pathways.

Transcription Factors

A total of 177 and 50 TF-encoding genes were differentially expressed in irradiated C1 and C2 (and classified into 39 and 23 families), respectively, compared to natural light (**Figures 11A,B**). The largest number of such genes identified belonged to the TF families *C2H2* (27), *bHLH* (22), and *AP2/ERF-ERF* (21), making up more than 36.08% of the total number of TFs. Among *C2H2* and *AP2/ERF-ERF* TFs, about half were upregulated and half downregulated after radiation exposure in C1. However, these were mostly downregulated in C2. In C1, all *WRKY* (*WRK72*, *WRK50*, and *WRK22*) and one heat shock TF (*HSF*) were significantly upregulated after irradiation. In the *NAC* family, except for *NAC* domain-containing protein 41, the remaining 12 coding genes were also upregulated, but *bHLH* families were significantly downregulated after irradiation. MYB TFs are positive regulators of flavonoid biosynthesis, and

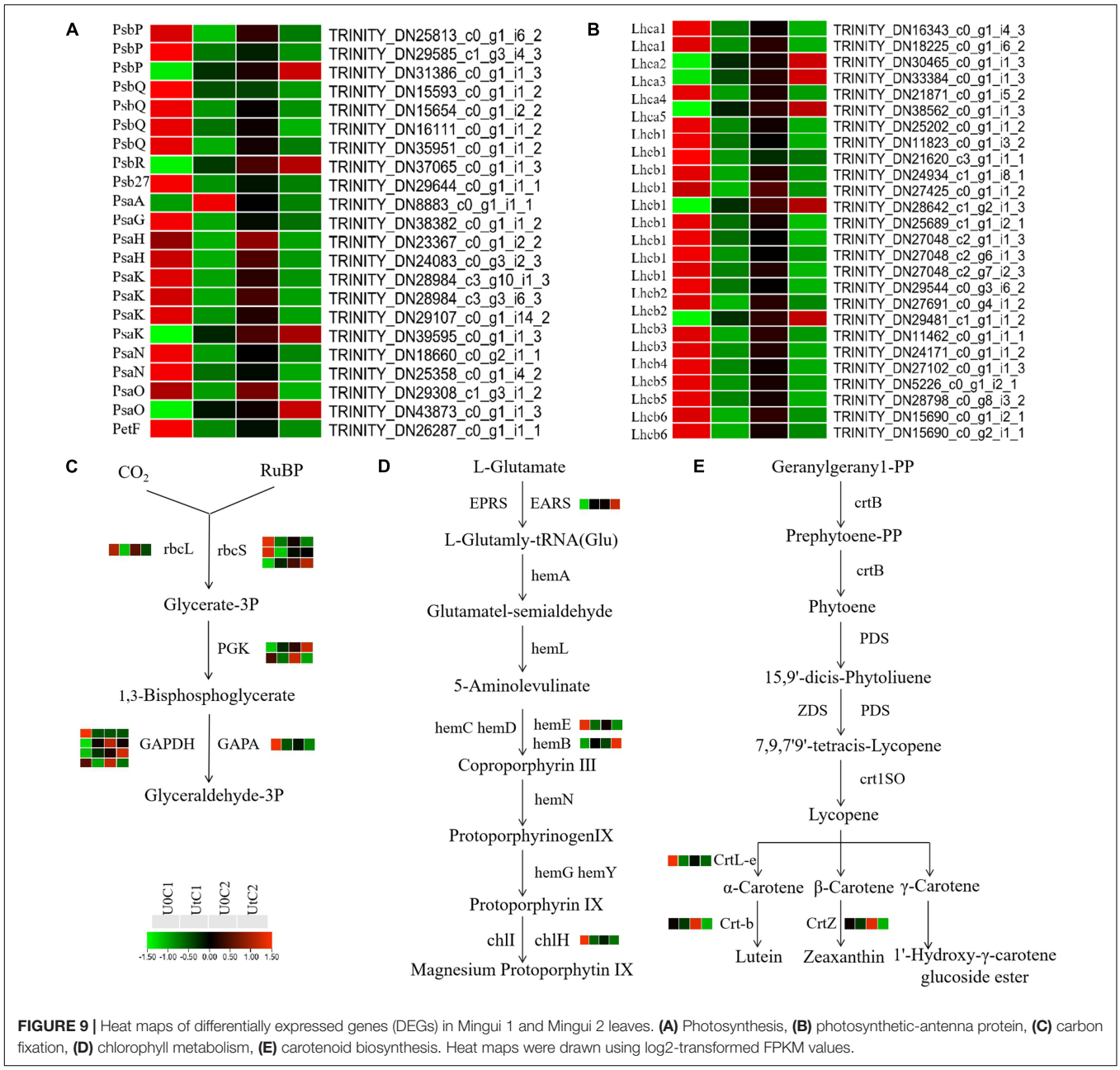

FIGURE 9 | Heat maps of differentially expressed genes (DEGs) in Mingui 1 and Mingui 2 leaves. **(A)** Photosynthesis, **(B)** photosynthetic-antenna protein, **(C)** carbon fixation, **(D)** chlorophyll metabolism, **(E)** carotenoid biosynthesis. Heat maps were drawn using log2-transformed FPKM values.

two genes encoding *MYB78* were upregulated; the remaining encoding genes were downregulated after radiation exposure in C1. In C2, one coding gene each was downregulated after radiation for *WRKY*, *MYB*, and *HSF*, namely, *WRK15*, *MYB73*, and *cytochrome P450 711A1*, respectively. In addition, one *NAC* family gene was upregulated (**Figure 11C**).

Phytohormone Signaling

Phytohormone signaling plays a key role in plant development, and hormones such as IAA, ethylene (ET), brassinosteroid (Br), ABA, jasmonic acid (JA), salicylic acid (SA), and cytokinins (CTK) are deeply involved in the regulation of plant morphology and metabolic responses (**Figure 12**). C1 had 44 DEGs (11 upregulated, 33 downregulated) in pathways related to phytohormones, and 30, 4, 5, 2, 1, and 2 DEGs in the IAA, CYT, ABA, ET, Br, and JA pathways, respectively. C2 had 7, 2, 2, and 1 DEG in the IAA, ABA, JA, and SA pathways, respectively, and most were downregulated after radiation treatment. In both cultivars, most DEGs were in the IAA signal transduction pathway. In this pathway, there were four times more downregulated IAA genes than upregulated ones. The *GH3*, *PP2C*, and *ABF* genes were significantly upregulated in C1, while one *PP2C* gene was upregulated and one was downregulated in C2. These results showed that in C1, *MPK6* and *ERF1/2* were significantly upregulated in ET signaling pathway, *A-ARR* and *B-ARR* were significantly downregulated in ZT signaling pathway,

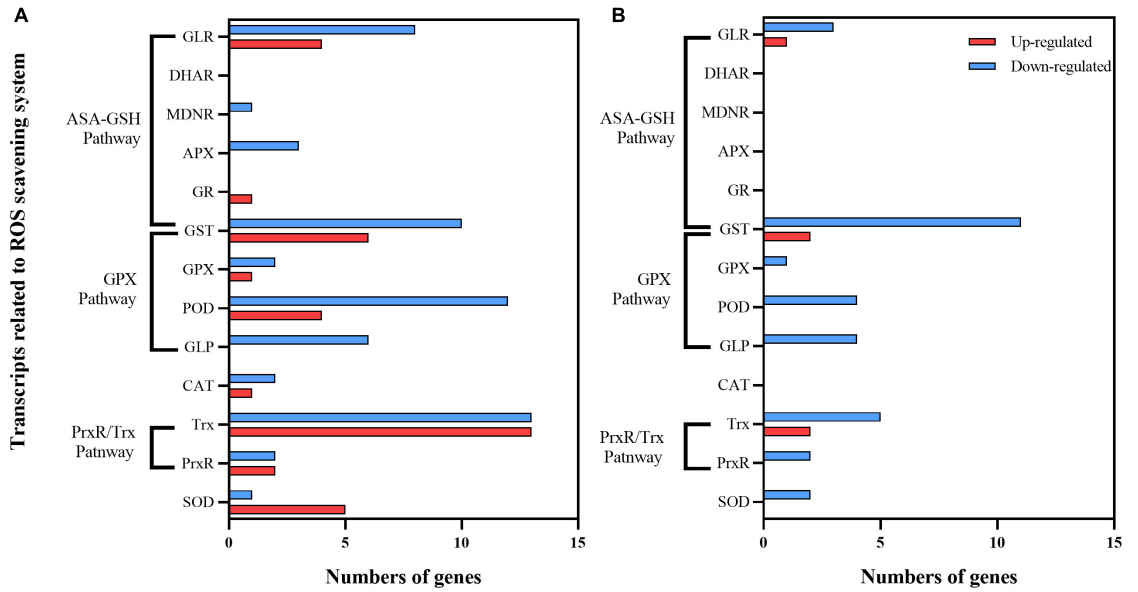

FIGURE 10 | ROS scavenging system of **(A)** Mingui 1 and **(B)** Mingui 2 under enhanced UV-B radiation.

and *BKI1* and *MYC2* were downregulated in BR and JA signaling pathway. In C2, in JA and SA pathways, the expression of *JAZ* and *TGA* were significantly downregulated.

Differentially Expressed Genes Related to Secondary Metabolism

Ferulic Acid Biosynthesis

Ferulic acid has antioxidant, antibacterial, and anti-inflammatory effects, among many other beneficial features, and is internationally recognized as an anti-cancer substance. It is easily absorbed by the human body and can be metabolized and excreted from urine. It has low toxicity and is relatively safe to use. Its medicinal value has attracted increasing attention (Sitarek et al., 2017). To further explore the metabolic mechanism of ferulic acid under enhanced UV-B radiation, its pathway and the expression level of related genes were visualized. KEGG data showed that the phenylpropanoid biosynthesis pathway was significantly enriched in C1, with a total of 31 DEGs (5 upregulated, 26 downregulated); there were only 9 DEGs in this pathway in C2. The key enzymes were *4CL*, *HCT*, *C3H*, *PAL*, *C4H*, *CCR*, *COMT*, and *CCOAMT*; the *4CL*, *CCR*, and *HCT* genes were all downregulated in C1. Only one gene encoding *COMT* was downregulated in C2 after radiation treatment in genes related to these key enzymes (**Figure 13**).

Lactone Biosynthesis

New evidence suggests that Z-ligustilide has a wide range of pharmacological properties, including anticancer, anti-inflammatory, antioxidant, and neuroprotective activities (Donkor et al., 2016; Xie et al., 2020). **Figure 14** shows the changes in key enzymes (*CYP*, *FAD*, *EH*, *ACX*, *PXG*) in lactone synthesis in C1 and C2 under irradiation, compared to natural light. The number of DEGs was much lower in C2 than in C1, and the number of upregulated DEGs was much higher in C1 than in C2. In this synthetic pathway, most DEGs encoded *CYP* in C1 (20 upregulated, 27 downregulated) and C2 (3 upregulated, 14 downregulated). Both *ACX* and *PXG* were significantly upregulated in C1, while only one coding gene was downregulated in *EH*; the rest were also significantly overexpressed. In C1, the upregulated number of DEGs encoding *FAD* and *FAH* was close to the downregulated number, while in C2, all DEGs encoding *FAD* were down-regulated. We conclude that the accumulation of lactones has a positive effect on C1 and may be neutral or has a slight adverse effect on C2.

Flavonoid Biosynthesis

Flavonoids have analgesic, hypotensive, anticoagulant, and cerebrovascular protective effects (Lovegrove et al., 2017). After irradiation, C2 was significantly enriched in flavonoid biosynthesis, with dihydroflavonol 4-reductase (*DFR*), chalcone synthase (*CHS*), and anthocyanin synthase (*ANS*) being significantly upregulated. In C1, three DEGs were significantly downregulated in this pathway, including *CHS*, chalcone isomerase (*CHI*), and shikimate o-hydroxycinnamoyl transferase (*HCT*). Therefore, after irradiation, more flavonoids were accumulated in the leaves of C2 (**Figure 15**).

DISCUSSION

Photosynthesis Response

Plants can adapt to different environmental stresses by changing gene expression. In our study, PSI and PSII of C1 were more susceptible to enhanced UV-B radiation. The peripheral subunits (*PsbP*, *PsbQ*, and *PsbR*) of the oxygen-evolving complex (OEC) responsible for the stabilization of PSII were differentially

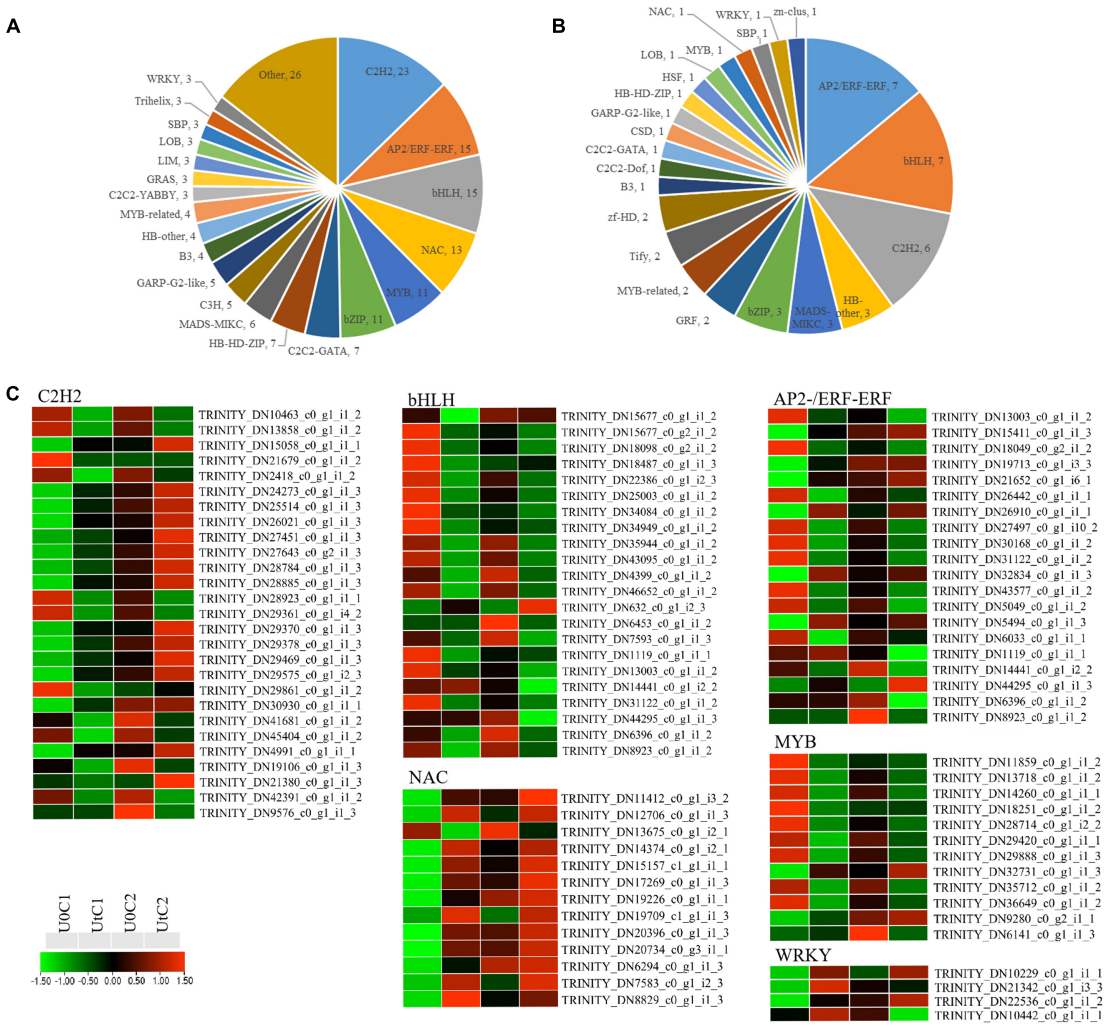

FIGURE 11 | Differentially expressed genes (DEGs) related to transcription factor (TF) families in *Angelica sinensis*. **(A)** Mingui 1, **(B)** Mingui 2, **(C)** Heatmap.

expressed after radiation treatment, whereas most DEGs were downregulated. *PsbR* plays an important role in polymerization stability, photosynthetic protection, and water oxidation. It may be that its coding gene was significantly upregulated and maintained the efficiency of PS II in C1 (De Las Rivas et al., 2007). *Psb27* protein is one of the most important assembly and repair factors. It plays an important role in maintaining efficient assembly and repair of PSII under stresses such as low temperature, high light, and a rapid change in light intensity (Roose and Pakrasi, 2008). One coding gene of *Psb27* was significantly downregulated in C1. *PsaA* is the most important protein in PS I, and membrane mosaic proteins such as *PsaG*, *PsaH*, *PsaK, PsaN*, and *PsaO* surround its core. In C1, the upregulation of *PsaA* plays an important role in maintaining PSI function (Jagannathan and Golbeck, 2009). In our study, the photosynthetic system of C2 was stable under enhanced UV-B radiation, and only one coding gene of *PsaH* and *PsaO* was downregulated in PS I. This indicates that enhanced UV-B radiation has a negative effect on the transfer of light energy from PS II to the center of PS I. The photosystem is composed of a photosynthetic reaction center and a peripheral antenna. Antenna proteins are the most important part of the light-harvesting complex (LHC) in photosynthesis. Under irradiation, the photosynthesis antenna protein pathway of C1 was significantly enriched, and the expression of several genes encoding *Lhcb* and *Lhca* were downregulated. This indicates that UV-B stress may affect the LHC of *A. sinensis*, consistent with previous experimental studies (Khudyakova et al., 2019). There was no significant enrichment in this pathway for C2.

Antioxidant System

To protect plants from ROS, plants have evolved a self-protection system that can eliminate ROS by combining antioxidant enzymes and small-molecule antioxidants (Fan et al., 2021). The ASA-GSH cycle and PrxP/TRX pathway play an important role in the resistance of the two varieties to UV-B stress. The number of DEGs was lower in C2 than in C1. These results indicate that

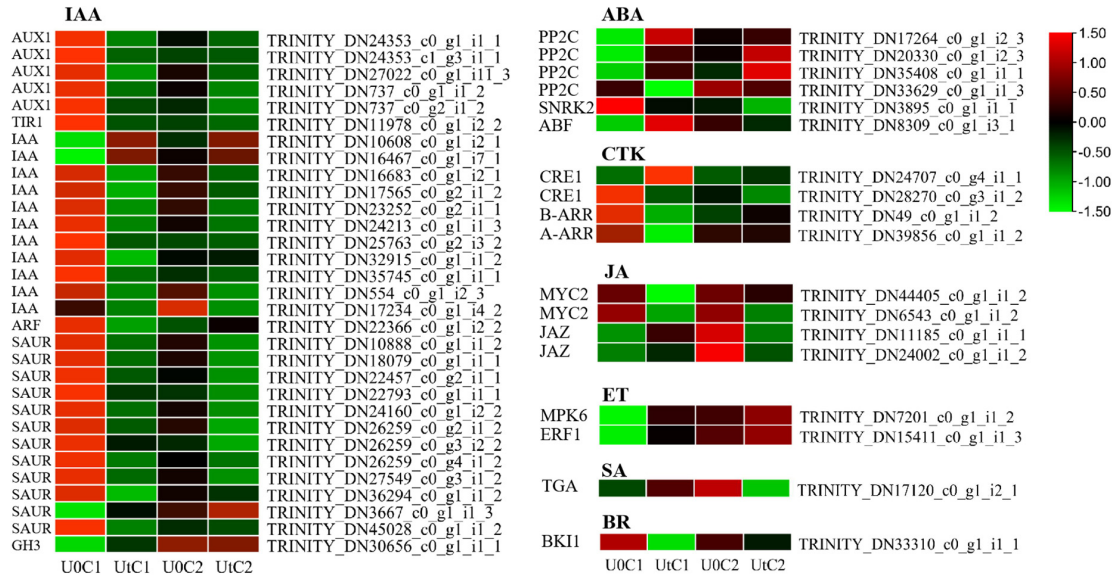

FIGURE 12 | Heatmap of differentially expressed genes (DEGs) related to plant hormone signal transduction of Mingui 1 and Mingui 2. Heat maps were drawn using log2-transformed FPKM values.

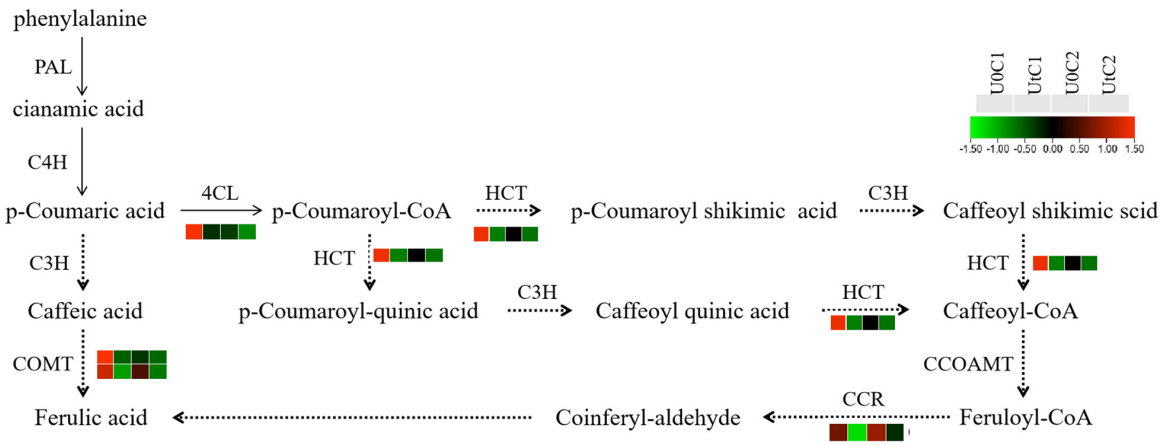

FIGURE 13 | Heatmap of differentially expressed genes (DEGs) related to ferulic acid synthesis in Mingui 1and Mingui 2. Heat maps were drawn using log2-transformed FPKM values.

the activities of antioxidant enzymes in leaves increased under enhanced UV-B radiation, which maintained the ability of plants to scavenge ROS and prevented damage to leaves, thus preserving photosynthetic efficiency. These results support the results of gene expression levels.

Transcription Factors

The expression of plant TFs is typically quickly altered in response to environmental stimuli, leading to the establishment of a pleiotropic phenotype to enhance stress tolerance (Joshi et al., 2016). Enhanced UV-B radiation affects phenolic metabolic pathways, as well as the levels of various phenols, by regulating the expression of various genes in the bHLH-MYB-WD40 complex (Zhou et al., 2015). In our study, almost all *bHLH* and *MYB* coding genes were downregulated, which shows that phenols had a poor response to enhanced UV-B radiation in C1. Among these TFs, *WRKY* is one of the most important in higher plants, as it participates in pathogen defense responses (Shi et al., 2020). *Arabidopsis AtWRKY22* and *AtWRKY29* proteins are essential components of MAPK-mediated plant defense responses against pathogens (Asai et al., 2002). Knockout of *WRKY22* enhances susceptibility to *Magnaporthe oryzae*, and overexpression of *WRKY22* enhances resistant phenotypes in rice (Abbruscato et al., 2012). *Arabidopsis AtWRKY50* might function as a positive regulator of the SA-mediated signaling pathway and a negative regulator of the JA acid-mediated signaling pathway, thereby enhancing resistance to gray mold disease (Gao et al., 2011). *WRKY72* and its *Arabidopsis* homolog *AtWRKY72*

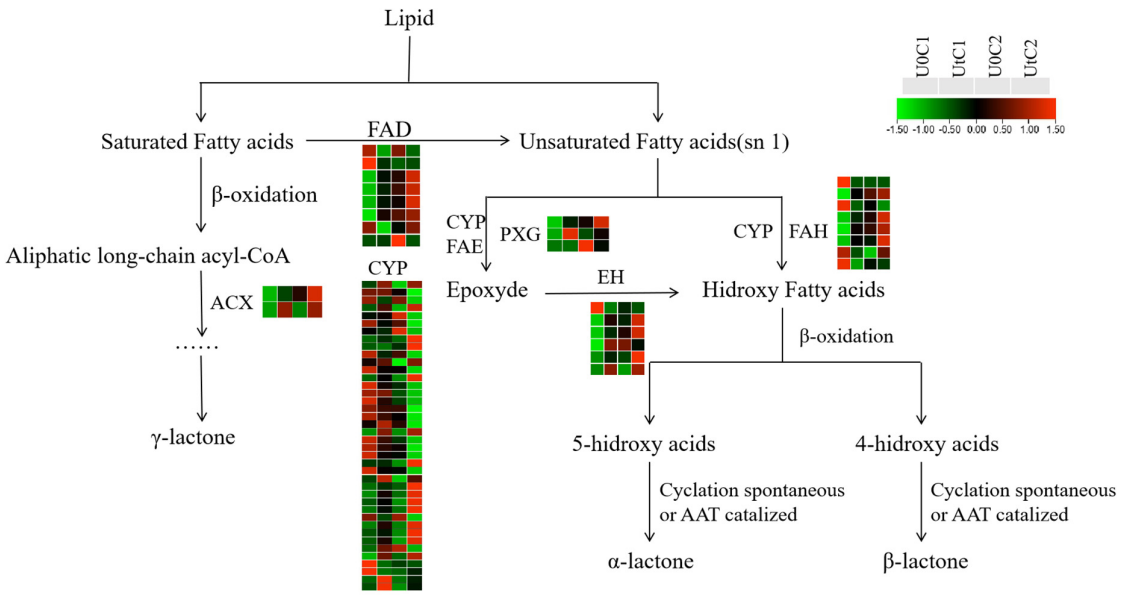

FIGURE 14 | Heatmap of differentially expressed genes (DEGs) related to lactone biosynthesis in Mingui 1 and Mingui 2. Heat maps were drawn using log2-transformed FPKM values.

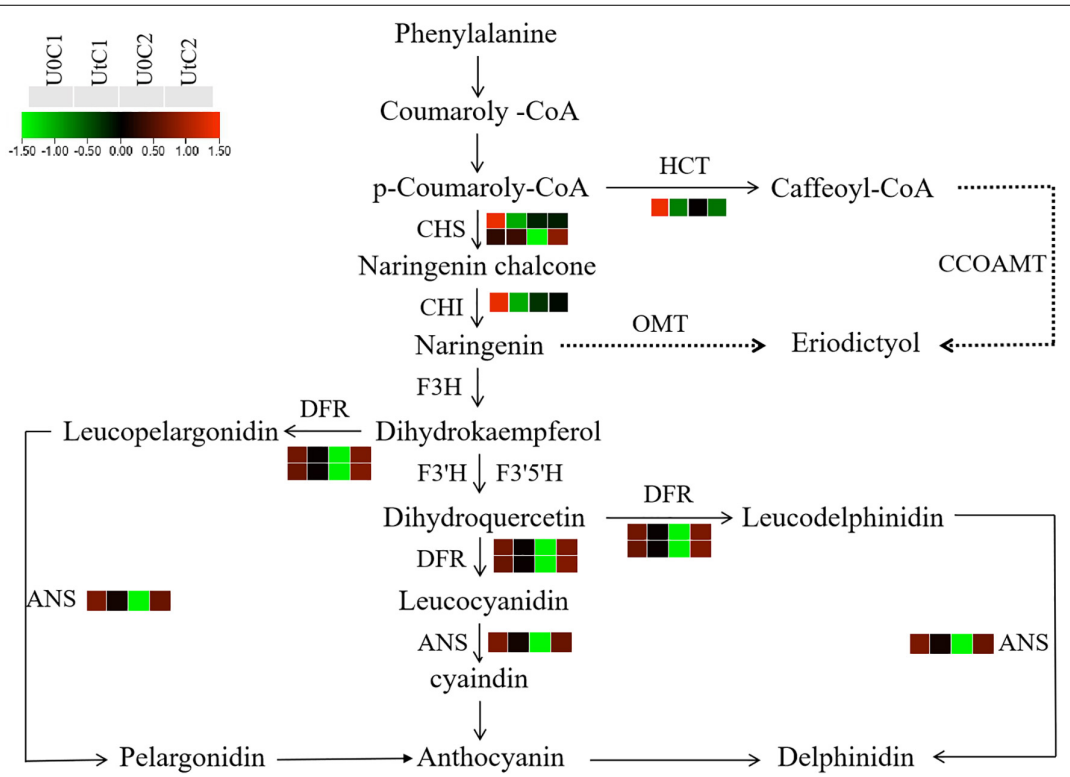

FIGURE 15 | Heatmap of differentially expressed genes (DEGs) related to flavonoid biosynthesis in Mingui 1 and Mingui 2. Heat maps were drawn using log2-transformed FPKM values.

are similarly involved in the pathogen defense process of *Meloidogyne* and Oomycota, and this process is most likely independent of the SA pathway (Bhattarai et al., 2010). In our study, *WRKY22*, *WRKY50*, and *WRKY72* were highly expressed in C1. *NAC* TFs are ubiquitous in plants, and their expression significantly changes under abiotic stresses (Yang et al., 2015). In

our dataset, the expression of the *NAC* TFs genes was upregulated under enhanced UV-B radiation, compared to natural light. The involvement of *NAC* TFs in UV-B tolerance has been demonstrated in various crops such as wheat. Some less common TFs such as C2H2-zinc finger proteins are also essential in plant stress responses, although their transcriptional regulatory mechanisms remain largely unclear. In addition, one *HSF* with high expression was detected in C1 under enhanced UV-B radiation, consistent with previous studies that *HSF* plays a crucial role in protecting against oxidative stress. This suggests that the regulation of development and metabolism by TFs is more prominent in C1. The details of the interactions among these genes and how they function require further research.

Phytohormone Signaling

Plant hormones play a key role in abiotic tolerance by mediating a wide range of responses. In this study, under enhanced UV-B radiation, the number of DEGs involved in the hormone signaling pathway was far less in C2 than in C1. Auxin and gibberellin are growth-promoting molecules. In response to auxin, many genes were downregulated, but the expression of DEGs encoding IAA was higher in C2 than C1. Biomass of C1 did not change significantly, it may be that the *GH3* gene was significantly upregulated and the *GH3* protein participated in the binding of free IAA and amino acids, thus controlling auxin homeostasis, while *GH3* gene was not found in C2, so the activity of IAA under enhanced UV-B radiation was higher than that of under natural light, resulting in a significant increase in its biomass (Feng et al., 2019). ABA, SA, and JA were mainly involved in the stress response and adaptation. *PP2C* and *ABF* were significantly upregulated in C1, and may thus constitute its adaptive response to UV-B stress. Under enhanced UV-B radiation, there were few genes involved in the response of each hormone in C2, indicating that this cultivar was stable under irradiation.

Bioactive Compounds

The absorbance of flavonoids is 280∼340 nm, which is equivalent to that of sunscreen (Tienaho et al., 2021). It can act as a UV filter in plants to prevent rays from penetrating tissues, to protect the photosynthetic system from damage (McLay et al., 2020). In our study, *DRF* and *CHS* were the key enzymes in flavonoid biosynthesis, which were significantly upregulated in C2. The upregulation of key enzymes in the flavonoid biosynthesis pathway has a positive effect on the accumulation of flavonoids. Given the function of flavonoids in scavenging and absorbing UV-B, it is speculated that C2 has strong resistance to enhanced UV-B radiation. The secondary metabolism gene of ferulic acid in RAS may promote blood circulation and prevent blood stasis (Yuan et al., 2019). In our study, there was no significant difference in the gene expression of enzymes related to ferulic acid synthesis in C2, while *4CL*, *CCR*, and *COMT* were downregulated in C1. This indicates that C1 is less favorable to the accumulation of ferulic acid under enhanced UV-B radiation. In this pathway, the *COMT* gene can also regulate the synthesis of lignin, and an increase in the content of lignin is conducive to the response to UV-B stress. Despite the importance of lactones for RAS quality, there is a lack of information on the enzymes and genes associated with their biosynthesis. Nevertheless, it seems clear that lactone biosynthesis starts from fatty acids with the introduction of an O atom to form hydroxy fatty acids. In our study, most DEGs were highly expressed in C1. *ACX* is widely involved in embryo development, seed germination, seedling establishment, and the biosynthesis of JA in response to stresses (Baker et al., 2006). Plant *cytochrome P450* is a monooxygenase, in the process of plant growth and development, P450 participates in secondary metabolic reactions such as the synthesis and degradation of alkaloids, terpenoids, fatty acids, plant hormones, signal molecules, and flavonoids (Cheng et al., 2020). In addition, it also plays an important role in the response mechanism to biological and abiotic stresses. *PXG* can protect plants from peroxyhydroxy fatty acids produced by lipoxygenase (*LOX*) enzymatic reactions and stress, and can also be transformed into derivatives to prevent fungal infection. The vast majority of genes encoding *PXG*, *CYP*, and *ACX* were upregulated in C1 in the present study. Under enhanced UV-B stress, the accumulation of lactones may have a positive effect in C1, leading to strong disease resistance. It may be neutral or have a slight adverse effect in C2.

CONCLUSION

Resistance to UV-B radiation is a complex phenomenon, often a fusion of multiple adaptive properties. The tolerance mechanisms include an increase in photosynthetic pigment levels, enhancement of antioxidant enzyme activity, accumulation of plant growth hormones, and an increase in phenolic and flavonoid levels.

In the present study, Pn, levels of photosynthetic pigments (Chl a, Chl b, and Car), antioxidant enzyme activities (SOD, POD, and CAT), and accumulation of bioactive substances (ferulic acid and flavonoid) were maintained or were enhanced in C2, and MDA accumulation was stable under enhanced UV-B radiation. It can be proved that enhanced UV-B radiation has a positive regulatory effect on C2 growth. C2 outperformed C1.

We identified the genes involved in the response to enhanced UV-B radiation. They are involved in photosynthesis and photosynthetic pigment biosynthesis, TFs and ROS scavenging systems, hormone biosynthesis and signal transduction, and biosynthetic pathways of ferulic acid, lactones and flavonoids. The results were consistent with the differences in physiological and biochemical indexes. C1 has poor resistance to enhanced UV-B stress, while C2 has a positive regulatory effect on it. Finally, a large number of *A. sinensis* transcriptome data generated here will be used as a source to find effective methods to alleviate UV-B enhancement, and also help to improve the lack of genetic information of non-model plant species.

DATA AVAILABILITY STATEMENT

The datasets presented in this study can be found in online repositories. The names of the repository/repositories and

accession number(s) can be found below: https://www.ncbi.nlm.nih.gov/bioproject/PRJNA767269.

AUTHOR CONTRIBUTIONS

YW designed the project and performed the literature research. TP acquired the main data, performed the statistical analysis, and edited the manuscript. TY, FW, JL, and YZ participated in the research and analyzed the data. All authors read and approved the final manuscript.

FUNDING

This work was supported by the National Key Research and Development Program of China (2017YFC1700705), the National Natural Science Foundation of China (81660625), the Double First-Class Major Scientific Research Project of Gansu Provincial Department of Education (GSSYLXM-05), the Special Program of Poverty Alleviation Science and Technology of Gansu University of Traditional Chinese medicine (2019FPZX-1), and the Advanced Technology Integration Demonstration (DX2020N10). The funders had no role in the design of the study; the collection, analysis, and/or interpretation of data; or the preparation of the manuscript.

ACKNOWLEDGMENTS

We are grateful to Caixia Yang (OE Biotechnology Co., Ltd., Shanghai, China) for assistance with RNA-Seq analysis.

SUPPLEMENTARY MATERIAL

The Supplementary Material for this article can be found online at: https://www.frontiersin.org/articles/10.3389/fpls.2021.805407/full#supplementary-material

REFERENCES

Abbruscato, P., Nepusz, T., Mizzi, L., Del Corvo, M., Morandini, P., Fumasoni, I., et al. (2012). OsWRKY22, a monocot WRKY gene, plays a role in the resistance response to blast. *Mol. Plant. Pathol.* 13, 828–841. doi: 10.1111/j.1364-3703.2012.00795

Altschul, S. F., Gish, W., Miller, W., Myers, E. W., and Lipman, D. J. (1990). Basic local alignment search tool. *J. Mo.l Biol.* 215, 403–410. doi: 10.1016/s0022-2836(05)80360-2

An, Z., Guo, F., Chen, Y., Bai, G., and Chen, Z. (2020). Rhizosphere bacterial and fungal communities during the growth of Angelica sinensis seedlings cultivated in an Alpine uncultivated meadow soil. *PeerJ.* 8:e8541. doi: 10.7717/peerj.8541

Asai, T., Tena, G., Plotnikova, J., Willmann, M. R., Chiu, W. L., Gomez-Gomez, L., et al. (2002). MAP kinase signalling cascade in *Arabidopsis* innate immunity. *Nature* 415, 977–983. doi: 10.1038/415977a

Baker, A., Graham, I. A., Holdsworth, M., Smith, S. M., and Theodoulou, F. L. (2006). Chewing the fat: beta-oxidation in signalling and development. *Trends. Plant. Sci.* 11, 124–132. doi: 10.1016/j.tplants.2006.01.005

Ben-Asher, J., Tsuyuki, I., Bravdo, B.-A., and Sagih, M. (2006). Irrigation of grapevines with saline water: I. Leaf area index, stomatal conductance, transpiration and photosynthesis. *Agric. Water Manag.* 83, 13–21.

Bhattarai, K. K., Atamian, H. S., Kaloshian, I., and Eulgem, T. (2010). WRKY72-type transcription factors contribute to basal immunity in tomato and *Arabidopsis* as well as gene-for-gene resistance mediated by the tomato R gene Mi-1. *Plant J.* 63, 229–240. doi: 10.1111/j.1365-313X.2010.04232

Bolger, A. M., Lohse, M., and Usadel, B. (2014). Trimmomatic: a flexible trimmer for Illumina sequence data. *Bioinformatics* 30, 2114–2120. doi: 10.1093/bioinformatics/btu170

Chao, W. W., and Lin, B. F. (2011). Bioactivities of major constituents isolated from Angelica sinensis (Danggui). *Chin. Med.* 6:29. doi: 10.1186/1749-8546-6-29

Chen, H., Feng, Y., Wang, L., Yonezawa, T., Crabbe, M. J., Zhang, X., et al. (2015). Transcriptome profiling of the UV-B stress response in the desert shrub *Lycium ruthenicum*. *Mol. Biol. Rep.* 42, 639–649. doi: 10.1007/s11033-014-3809-y

Cheng, Y., Liu, H., Tong, X., Liu, Z., Zhang, X., Li, D., et al. (2020). Identification and analysis of CYP450 and UGT supergene family members from the transcriptome of Aralia elata (Miq.) seem reveal candidate genes for triterpenoid saponin biosynthesis. *Res. Square* 20:214. doi: 10.21203/rs.2.20462/v5

De Las Rivas, J., Heredia, P., and Roman, A. (2007). Oxygen-evolving extrinsic proteins (PsbO,P,Q,R): bioinformatic and functional analysis. *Biochim. Biophys. Acta* 1767, 575–582. doi: 10.1016/j.bbabio.2007.01.018

Donkor, P. O., Chen, Y., Ding, L., and Qiu, F. (2016). Locally and traditionally used Ligusticum species - A review of their phytochemistry, pharmacology and pharmacokinetics. *J. Ethnopharmacol.* 194, 530–548. doi: 10.1016/j.jep.2016.10.012

Fan, Y., Lu, X., Chen, X., Wang, J., Wang, D., Wang, S., et al. (2021). Cotton transcriptome analysis reveals novel biological pathways that eliminate reactive oxygen species (ROS) under sodium bicarbonate ($NaHCO_3$) alkaline stress. *Genomics* 113, 1157–1169. doi: 10.1016/j.ygeno.2021.02.022

Feng, L., Li, G., He, Z., Han, W., and Chen, Y. (2019). The ARF, GH3, and Aux/IAA gene families in castor bean (*Ricinus communis* L.): genome-wide identification and expression profiles in high-stalk and dwarf strains. *Ind. Crops Prod.* 141:111804. doi: 10.1016/j.indcrop.2019.111804

Gao, Q. M., Venugopal, S., Navarre, D., and Kachroo, A. (2011). Low oleic acid-derived repression of jasmonic acid-inducible defense responses requires the WRKY50 and WRKY51 proteins. *Plant. Physiol.* 155, 464–476. doi: 10.1104/pp.110.166876

Gao, X., Guo, F., Chen, Y., Bai, G., Liu, Y., Jin, J., et al. (2021). Full-length transcriptome analysis provides new insights into the early bolting occurrence in medicinal Angelica sinensis. *Sci. Rep.* 11:13000. doi: 10.1038/s41598-021-92494-4

Gong, L., Gao, J., Xu, T., Qu, J., and You, J. (2020). Transcriptome analysis of field-grown Asian ginseng provides clues to environmental conditions and developmental mechanisms related to red skin root syndrome. *Ind. Crops Prod.* 153:112486. doi: 10.1016/j.indcrop.2020.112486

Grabherr, M. G., Haas, B. J., Yassour, M., Levin, J. Z., Thompson, D. A., Amit, I., et al. (2011). Full-length transcriptome assembly from RNA-Seq data without a reference genome. *Nat. Biotechnol.* 29, 644–652. doi: 10.1038/nbt.1883

Henry-Kirk, R. A., Plunkett, B., Hall, M., McGhie, T., Allan, A. C., Wargent, J. J., et al. (2018). Solar UV light regulates flavonoid metabolism in apple (Malus x domestica). *Plant. Cell. Environ.* 41, 675–688. doi: 10.1111/pce.13125

Hideg, E., Jansen, M. A., and Strid, A. (2013). UV-B exposure, ROS, and stress: inseparable companions or loosely linked associates? *Trends Plant. Sci.* 18, 107–115. doi: 10.1016/j.tplants.2012.09.003

Hook, I. L. (2014). Danggui to Angelica sinensis root: are potential benefits to European women lost in translation? A review. *J. Ethnopharmacol.* 152, 1–13. doi: 10.1016/j.jep.2013.12.018

Inostroza-Blancheteau, C., Acevedo, P., Loyola, R., Arce-Johnson, P., Alberdi, M., and Reyes-Díaz, M. (2016). Short-term UV-B radiation affects photosynthetic performance and antioxidant gene expression in highbush blueberry leaves. *Plant. Physiol. Biochem.* 107, 301–309. doi: 10.1016/j.plaphy.2016.06.019

Jagannathan, B., and Golbeck, J. H. (2009). Understanding of the binding interface between PsaC and the PsaA/PsaB heterodimer in photosystem I. *Biochemistry* 48, 5405–5416. doi: 10.1021/bi900243f

Jansen, M., Gaba, V., and Greenberg, B. M. (1998). Higher plants and UV-B radiation: balancing damage, repair and acclimation. *Trends Plant Sci.* 3, 131–135. doi: 10.1016/S1360-1385(98)01215-1

Jenkins, G. I. (2009). Signal transduction in responses to UV-B radiation. *Annu. Rev. Plant. Biol.* 60, 407–431. doi: 10.1146/annurev.arplant.59.032607.092953

Jobe, T. O., Zenzen, I., Rahimzadeh Karvansara, P., and Kopriva, S. (2019). Integration of sulfate assimilation with carbon and nitrogen metabolism in transition from C3 to C4 photosynthesis. *J. Exp. Bot.* 70, 4211–4221. doi: 10.1093/jxb/erz250

Joshi, R., Wani, S. H., Singh, B., Bohra, A., Dar, Z. A., Lone, A. A., et al. (2016). Transcription factors and plants response to drought stress: current understanding and future directions. *Front. Plant. Sci.* 7:1029. doi: 10.3389/fpls.2016.01029

Kataria, S., Jajoo, A., and Guruprasad, K. N. (2014). Impact of increasing Ultraviolet-B (UV-B) radiation on photosynthetic processes. *J. Photochem. Photobiol. B.* 137, 55–66. doi: 10.1016/j.jphotobiol.2014.02.004

Khudyakova, A. Y., Kreslavski, V. D., Shmarev, A. N., Lyubimov, V. Y., Shirshikova, G. N., Pashkovskiy, P. P., et al. (2019). Impact of UV-B radiation on the photosystem II activity, pro-/antioxidant balance and expression of light-activated genes in *Arabidopsis thaliana* hy4 mutants grown under light of different spectral composition. *J. Photochem. Photobiol. B.* 194, 14–20. doi: 10.1016/j.jphotobiol.2019.02.003

Lovegrove, J. A., Stainer, A., and Hobbs, D. A. (2017). Role of flavonoids and nitrates in cardiovascular health. *Proc. Nutr. Soc.* doi: 10.1017/s0029665116002871 [Epub Online ahead of Print].

McLay, E. R., Pontaroli, A. C., and Wargent, J. J. (2020). UV-B Induced flavonoids contribute to reduced biotrophic disease susceptibility in lettuce seedlings. *Front. Plant. Sci.* 11:594681. doi: 10.3389/fpls.2020.594681

Mosadegh, H., Trivellini, A., Lucchesini, M., Ferrante, A., Maggini, R., Vernieri, P., et al. (2019). UV-B Physiological changes under conditions of distress and eustress in sweet basil. *Plants (Basel)* 8:396. doi: 10.3390/plants8100396

Nawkar, G. M., Maibam, P., Park, J. H., Sahi, V. P., Lee, S. Y., and Kang, C. H. (2013). UV-Induced cell death in plants. *Int. J. Mol. Sci.* 14, 1608–1628. doi: 10.3390/ijms14011608

Neugart, S., Fiol, M., Schreiner, M., Rohn, S., Zrenner, R., Kroh, L. W., et al. (2014). Interaction of moderate UV-B exposure and temperature on the formation of structurally different flavonol glycosides and hydroxycinnamic acid derivatives in kale (Brassica oleracea var. sabellica). *J Agric. Food. Chem.* 62, 4054–4062. doi: 10.1021/jf4054066

Parihar, P., Singh, S., Singh, R., Singh, V. P., and Prasad, S. M. (2015). Changing scenario in plant UV-B research: UV-B from a generic stressor to a specific regulator. *J. Photochem. Photobiol. B* 153, 334–343. doi: 10.1016/j.jphotobiol.2015.10.004

Robson, T. M., Aphalo, P. J., Banaś, A. K., Barnes, P. W., Brelsford, C. C., Jenkins, G. I., et al. (2019). A perspective on ecologically relevant plant-UV research and its practical application. *Photochem. Photobiol. Sci.* 18, 970–988. doi: 10.1039/c8pp00526e

Roose, J. L., and Pakrasi, H. B. (2008). The Psb27 protein facilitates manganese cluster assembly in photosystem II. *J. Biol. Chem.* 283, 4044–4050. doi: 10.1074/jbc.M708960200

Shi, W., Zhao, S. L., Liu, K., Sun, Y. B., Ni, Z. B., Zhang, G. Y., et al. (2020). Comparison of leaf transcriptome in response to Rhizoctonia solani infection between resistant and susceptible rice cultivars. *BMC Genomics* 21:245. doi: 10.1186/s12864-020-6645-6

Sitarek, P., Rijo, P., Garcia, C., Skała, E., Kalemba, D., Białas, A. J., et al. (2017). Antibacterial, anti-inflammatory, antioxidant, and antiproliferative properties of essential oils from hairy and normal roots of *Leonurus sibiricus* L. and their chemical composition. *Oxid. Med. Cell Longev.* 2017:7384061. doi: 10.1155/2017/7384061

Tienaho, J., Silvan, N., Muilu-Mäkelä, R., Kilpeläinen, P., Poikulainen, E., and Sarjala, T. (2021). Ultraviolet absorbance of *Sphagnum magellanicum*, S. fallax and S. fuscum extracts with seasonal and species-specific variation. *Photochem. Photobiol. Sci.* 20, 379–389. doi: 10.1007/s43630-021-00026-w

Vandenbussche, F., Yu, N., Li, W., Vanhaelewyn, L., Hamshou, M., Van Der Straeten, D., et al. (2018). An ultraviolet B condition that affects growth and defense in *Arabidopsis*. *Plant Sci.* 268, 54–63. doi: 10.1016/j.plantsci.2017.12.005

Vanhaelewyn, L., Prinsen, E., Van Der Straeten, D., and Vandenbussche, F. (2016). Hormone-controlled UV-B responses in plants. *J. Exp. Bot.* 67, 4469–4482. doi: 10.1093/jxb/erw261

Wei, W. L., Zeng, R., Gu, C. M., Qu, Y., and Huang, L. F. (2016). Angelica sinensis in China-A review of botanical profile, ethnopharmacology, phytochemistry and chemical analysis. *J. Ethnopharmacol.* 190, 116–141. doi: 10.1016/j.jep.2016.05.023

Xiao, Z., Qiu, X., Xie, Y., Zhao, B., Wang, Y., Liang, Z., et al. (2019). Temporal-spatial variations characteristics of UV erythemal dose over China. *J. Earth Environ.* 10, 291–298.

Xie, Q., Zhang, L., Xie, L., Zheng, Y., Liu, K., Tang, H., et al. (2020). Z-ligustilide: a review of its pharmacokinetics and pharmacology. *Phytother. Res.* 34, 1966–1991. doi: 10.1002/ptr.6662

Xin, A., Li, X., Jin, H., Yang, X., Zhao, R., Liu, J., et al. (2019). The accumulation of reactive oxygen species in root tips caused by autotoxic allelochemicals – A significant factor for replant problem of Angelica sinensis (Oliv.) Diels. *Ind. Crops Prod.* 138, 111432–111432. doi: 10.1016/j.indcrop.2019.05.081

Yan, M. C., Jin, L., Zhu, T. T., Li, Y. D., and Zhu, J. Q. (2014). Identification of Angelica sinensis varieties by ISSR-PCR. *Trad. Chin. Med.* 37, 236–239. doi: 10.13863/j.issn1001-4454.2014.02.020

Yang, Y. W., Chen, H. C., Jen, W. F., Liu, L. Y., and Chang, M. C. (2015). Comparative transcriptome analysis of shoots and roots of TNG67 and TCN1 rice seedlings under cold stress and following subsequent recovery: insights into metabolic pathways, phytohormones, and transcription factors. *PLoS One* 10:e0131391. doi: 10.1371/journal.pone.0131391

Yin, R., and Ulm, R. (2017). How plants cope with UV-B: from perception to response. *Curr. Opin. Plant Biol.* 37, 42–48. doi: 10.1016/j.pbi.2017.03.013

Yu, G., Zhou, Y., Yu, J., Hu, X., Tang, Y., Yan, H., et al. (2019). Transcriptome and digital gene expression analysis unravels the novel mechanism of early flowering in Angelica sinensis. *Sci. Rep.* 9:10035. doi: 10.1038/s41598-019-46414-2

Yu, H., and Liu, R. (2013). Effect of UV-B radiation on the synthesis of UV-absorbing compounds in a terrestrial cyanobacterium, Nostoc flagelliforme. *J. Appl. Phycol.* 25, 1441–1446. doi: 10.1007/s10811-013-9978-6

Yuan, Z., Zhong, L., Hua, Y., Ji, P., Yao, W., Ma, Q., et al. (2019). Metabolomics study on promoting blood circulation and ameliorating blood stasis: investigating the mechanism of Angelica sinensis and its processed products. *Biomed. Chromatogr.* 33:e4457. doi: 10.1002/bmc.4457

Zhou, M., Wei, L., Sun, Z., Gao, L., Meng, Y., Tang, Y., et al. (2015). Production and transcriptional regulation of proanthocyanidin biosynthesis in forage legumes. *Appl. Microbiol. Biotechnol.* 99, 3797–3806. doi: 10.1007/s00253-015-6533-1

Zhu, L., Yan, H., Zhou, G. S., Jiang, C. H., Liu, P., Yu, G., et al. (2021). Insights into the mechanism of the effects of rhizosphere microorganisms on the quality of authentic Angelica sinensis under different soil microenvironments. *BMC Plant. Biol.* 21:285. doi: 10.1186/s12870-021-03047-w

Conflict of Interest: The authors declare that the research was conducted in the absence of any commercial or financial relationships that could be construed as a potential conflict of interest.

Publisher's Note: All claims expressed in this article are solely those of the authors and do not necessarily represent those of their affiliated organizations, or those of the publisher, the editors and the reviewers. Any product that may be evaluated in this article, or claim that may be made by its manufacturer, is not guaranteed or endorsed by the publisher.

Copyright © 2021 Peng, Wang, Yang, Wang, Luo and Zhang. This is an open-access article distributed under the terms of the Creative Commons Attribution License (CC BY). The use, distribution or reproduction in other forums is permitted, provided the original author(s) and the copyright owner(s) are credited and that the original publication in this journal is cited, in accordance with accepted academic practice. No use, distribution or reproduction is permitted which does not comply with these terms.

frontiers in Plant Science

ORIGINAL RESEARCH
published: 09 March 2022
doi: 10.3389/fpls.2022.852956

Nitric Oxide Crosstalk With Phytohormone Is Involved in Enhancing Photosynthesis of *Tetrastigma hemsleyanum* for Photovoltaic Adaptation

Zhuomi Xie[1,2], Chuyun Yang[1,2], Mingjie Li[1,2], Zhongyi Zhang[1,2], Yao Wu[3], Li Gu[1,2] and Xin Peng[3,4]**

[1] College of Agriculture, Fujian Agriculture and Forestry University, Fuzhou, China, [2] Key Laboratory of Ministry of Education for Genetics, Breeding and Multiple Utilization of Crops, Fujian Agriculture and Forestry University, Fuzhou, China, [3] College of Food Science, Ningbo Research Institute of Zhejiang University, Ningbo, China, [4] Medicinal Plant Resource Center, Ningbo Research Institute of Traditional Chinese Medicine, Ningbo, China

OPEN ACCESS

Edited by:
Zhihua Liao,
Southwest University, China

Reviewed by:
Qingsong Shao,
Zhejiang A&F University, China
Qianru Hui,
University of Manitoba, Canada
Yuyun Lu,
National University of Singapore, Singapore

***Correspondence:**
Li Gu
guli5101@163.com
Xin Peng
pengx@nit.zju.edu.cn

Specialty section:
This article was submitted to Plant Metabolism and Chemodiversity, a section of the journal Frontiers in Plant Science

Received: *11 January 2022*
Accepted: *28 January 2022*
Published: *09 March 2022*

Citation:
Xie Z, Yang C, Li M, Zhang Z, Wu Y, Gu L and Peng X (2022) Nitric Oxide Crosstalk With Phytohormone Is Involved in Enhancing Photosynthesis of Tetrastigma hemsleyanum for Photovoltaic Adaptation. Front. Plant Sci. 13:852956. doi: 10.3389/fpls.2022.852956

Photovoltaic agriculture is a newly emerging ecological planting pattern. In view of the adverse effect on production, a better understanding of photovoltaic adaptation responses is essential for the development of the innovative agriculture mode in sustainable crop production. Here, we investigated the impact of photovoltaic condition on endogenous hormone composition and transcriptome profile of *Tetrastigma hemsleyanum*. A total of 16 differentially accumulated phytohormones and 12,615 differentially expressed genes (DEGs) were identified. Photovoltaic adaptation significantly decreased the contents of phytohormones especially salicylic acid (SA) and jasmonic acid (JA). DEGs were the most relevant to photosynthesis and mitogen-activated protein kinase (MAPK) signaling pathway especially the key genes encoding proteins involved in photosystem I (PS I) and photosystem II (PS II) reaction center. Nitric oxide (NO), JA, and SA treatment alone significantly enhanced the photosynthetic efficiency which was decreased by exposure to photovoltaic condition, but the combined treatment of "NO + SA" could weaken the enhancement effect by regulating the expression level of *psaL, CHIL, petF1, psbQ,* and *psaE* genes. Exogenous phytohormones and NO treatment mitigated the accumulation of reactive oxygen species (ROS) and potentiated antioxidant capacity, which would be weakened by the combined treatment of "NO + SA." SA and JA significantly decreased endogenous NO burst triggered by photovoltaic adaptation. SA might be a potent scavenger of NO and counter the restoration effect of NO on growth and photosynthetic potential in *T. hemsleyanum*. The results could provide reference for the application of phytohormones/other signaling molecules in photovoltaic agriculture.

Keywords: photovoltaic adaptation, *Tetrastigma hemsleyanum*, nitric oxide, salicylic acid, crosstalk

INTRODUCTION

A sustainable and effective supply of crops to satisfy the demand in food supply is a global challenge especially under the background of climatic variation. In recent years, as the demand for clean energy continues to grow, the photovoltaic industry has developed rapidly. To rationally strengthen the intensified utilization of land resources, a new pattern of combining photovoltaic power generation and agricultural production, namely, photovoltaic agriculture, have largely emerged. Photovoltaic materials installed on the roof of greenhouses offer a protected opportunity for crop cultivation. As the principal energy source of photosynthesis, light plays a crucial role in crop growth and development. Light quality and quantity transmitted are significantly modified by cover materials, and then, generate a series of microclimate changes. So far, photovoltaic application system research is still in the initial stage. Recent research has been mainly focused on developing innovative cover materials to improve solar energy capture and light transmission. However, limited information was available about the ecological effect of the complex planting pattern on the physiological activity of crops. Some research showed that transmitted light changed by photovoltaic materials can have negative impacts on the plant production. For instance, 50% photovoltaic materials covering the roof of the greenhouse decreased tomato production significantly (Cossu et al., 2014). In contrast, a UV transmission film promotes cucumber yield (Allardyce et al., 2017), and the light cascade technology increases the fresh weight and yield of fruit (Lemarié et al., 2018). It was presumed that the photovoltaic agriculture was probably not suitable for those crops requiring high-light intensity, however, it could be developed for the cultivation of other industrial crops. Therefore, a deeper understanding of photovoltaic materials-mediated modulation/regulation of gene expression, protein, and metabolite composition in plants is essential for the development of the innovative complex ecological agriculture mode in sustainable crop production.

The metabolic processes of plants would become largely affected when subjected to abiotic stress. These adaptive responses are mediated through inducing a series of different cellular and physiological changes. Some reactive chemical species, such as reactive oxygen species (ROS), reactive nitrogen species (RNS), are generated at low concentrations and act as signaling molecules regulating secondary messengers (Zhou et al., 2021a), and interacts with other signaling components (Farnese et al., 2016; Singhal et al., 2021). There is quite a number of research indicating that ROS in plant cells are involved in various aspects of physiological responses (Campos et al., 2019; Jahan et al., 2019). Recent research found a metabolic interaction between ROS and RNS by detecting the peroxyinitrite content and glutathione concentrations in root of wheat (Zhao et al., 2022). Another research found that the plant decreased Cu toxicity through nitric oxide (NO)-mediated pathways to modulate reactive ROS accumulation and oxidative damage (Xu et al., 2022). However, all RNS family members derive from NO. RNS is emerging as a topic of great interest with the increase in the reports about various functions of RNS in plants.

For the initial years after its discovery, NO was extensively studied in animals for its potential neurological functions. NO's role in plants gradually turned from being a reactive species to its involvement in stress response/signaling, plant growth, and development (Zhou et al., 2021b). It is well-known that several phytohormones are essential components for the regulation of these processes, such as gibberellins (GA), brassinosteroids (BRs), abscisic acid (ABA), auxins, ethylene (ET), jasmonic acid (JA), and salicylic acid (SA). For instance, ABA and GA were reported previously for inducing seed germination. In recent years, NO and sodium nitroprusside (SNP) were reported to regulate the seed germination of apple embryos through phyto-hormonal crosstalk (Xiao-Ping and Xi-Gui, 2010; Krasuska et al., 2017). It is still not clear whether the mechanism of GA- and NO-promoting germination acts antagonistically or synergistically. Abiotic stresses adversely affect the plant growth and development by producing ROS, and regulating phytohormones, signaling, and metabolism in plants. Moreover, NO has been reported to improve the salt tolerance of plants by activating superoxide dismutase (Klein et al., 2018), waterlogging tolerance in wheat (Li et al., 2021), and decrease in toxic ion accumulation (Gadelha et al., 2017). Further research about the concerted participation between NO and phytohormones in signal pathways under environmental stress, would provide data for generating new eco-agricultural technologies based on the regulation of signal molecules for the plants.

Tetrastigma hemsleyanum Diels et Gilg is a perennial herbal plant distributed in subtropical areas of China. Wild *T. hemsleyanum* plants are close to deracinate due to over exploitation and environmental deterioration. Recently, it has become one of the most important varieties of artificial planting medicinal materials in Zhejiang province (Ji et al., 2021). At present, the technology of the greenhouses photovoltaic solar energy construction has been applied in planting *T. hemsleyanum* (**Figure 1**). Herein, we investigated the impact of photovoltaic condition on endogenous hormone composition and transcriptome profile of *T. hemsleyanum*. The role of NO effectors and/or phytohormones in mediating the photosynthetic adaptability was evaluated in terms of photosynthetic parameters, ROS accumulation, antioxidase activities, and gene expression level of CO_2 assimilation enzymes. The effect of phytohormones on endogenous NO burst triggered by photovoltaic adaptation was also explored. The results could provide reference for the application of phytohormones/other signaling molecules in photovoltaic agriculture.

MATERIALS AND METHODS

Plant Materials and Growth Conditions

Healthy cutting seedlings of *T. hemsleyanum* were grown under standard greenhouse conditions set as follows: 16 h day/8 h night cycle, 23 ± 2°C temperature, 50% relative humidity, and 250 $\mu mol\ m^{-2}s^{-1}$ light intensity. Then, 6 months seedlings showing similar growth potential were selected and uniformly divided

FIGURE 1 | The photovoltaic planting base of Zhejiang Guangsheng Group Co., Ltd. for planting *Tetrastigma hemsleyanum*.

into two groups, GZ (covered with transparent glass plate) and GF (covered with photovoltaic panel). The photovoltaic panel (ODA-60M) was provided by Ningbo Osda Solar Co., Ltd., China. Each treatment was repeated three times with ten plants. Phenotypic changes were observed and biochemical indexes were determined at 15, 30, and 45 days, respectively. The leaves were sampled on 30 days, frozen in liquid nitrogen immediately, and stored at −80℃ for phytohormones and gene expression analysis. The experiment was repeated three times, and each biological replicate consisted of a sample pool from 10 seedlings.

Exogenous Sodium Nitroprusside and Phytohormones Treatment

Based on our pre-experiment, plants of GF group were either sprayed (foliar application 2 times every 24 h, the application amount was 10 ml for every pot for each time) with ultrapure water or with 100 μM NO-donor SNP or with 300 μM NO scavenger 2-(4-carboxyphenyl)-4,4,5,5-tetramethylimidazoline-1-oxyl-3-oxide (cPTIO) or with phytohormones (50 μM SA, 50 μM MeJA, 50 μM ABA, or 50 mg/L GA, used independently). The treated plants were sampled for detection and analysis after 15 days of treatment. Each test included five seedlings, and three replicates were performed for each treatment.

Determination of Photosynthetic Efficiency

Five seedlings of the two groups were randomly selected and ten leaves at the same position of plant were sampled. The photosynthetic and fluorescence parameters of *T. hemsleyanum*, such as net photosynthetic rate (Pn), transpiration rate (Tr), stomatal conductance (Cond), mesophyll intercellular CO_2 (Ci), and the maximum light energy conversion efficiency (Fv/Fm), were determined using the LI-6400 portable photosynthesis meter (Li-COR company, United States) and PAM-2500 portable chlorophyll fluorescence meter (WALZ company, Germany), respectively. Five seedlings of each group were randomly selected, respectively, then values of the upper, middle, and lower leaves were determined uniformly, and the average value was used to reflect the value of this sample. Three replicates were performed for each treatment.

Determination of Antioxidative Capacity and Fluorescent Imaging of H_2O_2, O^{2-}, and Reactive Oxygen Species

Approximately 2 g of leaves were homogenized in 3 ml of 50 mM potassium phosphate buffer (pH 7.0). The supernatant was collected by centrifugation at 10,000 × g for 10 min at 4°C, and then be used for the activity determination of peroxidase (POD, EC 1.11.1.7), catalase (CAT, EC 1.11.1.6), superoxide dismutase (SOD, EC 1.15.1.1), and malondialdehyde (MDA) content. POD activity was determined as guaiacol oxidation by H_2O_2. SOD activity was analyzed based on the inhibiting rates of the reduction of nitro blue tetrazolium (NBT), CAT activity was determined as the H_2O_2 consumption, MDA content was extracted and determined by the thiobarbituric acid reaction method, according to our previous report (Peng et al., 2019).

Leaf and root samples were used to detect the presence of *in situ* accumulation of superoxide and H_2O_2 by staining with NBT and 3,3-diaminobenzidine (DAB), respectively. Then, 2.0–2.5 cm of the roots were immediately immersed in a 0.05% solution of NBT or an aqueous solution of 1 mg/ml DAB in 50 mM potassium phosphate buffer (pH 6.4), vacuum infiltrated, and incubated for 12 h in the dark, according to the previous report (Hu et al., 2018; Recalde et al., 2018). Stained segments were washed 3 times by water before photography. Furthermore, 10–15 individuals randomly sampled from each group were used for each experiment.

Quantification of Phytohormones

Approximately 30 g of each fresh sample was harvested and rapidly frozen in liquid nitrogen, and homogenized into powder. The extraction was conducted by methanol/water/formic acid (15:4:1, V/V/V), 10 μl internal standard mixed solution (100 ng/ml) was added as internal standards, followed by evaporation to dryness, dissolved in 100 μl 80% methanol (V/V), and filtrated through a 0.22 μm membrane filter before liquid chromatography-mass spectrometry (LC-MS/MS) analysis. The extracts were detected using an ultra-high performance liquid chromatography-mass spectrometry (UPLC-ESI-MS/MS) system (UPLC, ExionLC^{TM} AD; MS, Applied Biosystems 6500 Triple Quadrupole). A Waters ACQUITY UPLC HSS T3 C18 (2.1 mm × 100 mm × 1.8 μm) was used. Solvent system were

water (0.04 acetic acid): ACN (0.05% acetic acid). The gradient program was as follows: 95:5 V/V at 0–1 min, 5:95 V/V at 1–8 min, 5:95 V/V at 8–9 min, and 95:5 V/V at 9.1–12 min.

The effluent was alternatively connected to acquire linear ion trap (LIT) and triple quadrupole (QQQ) scans on an electrospray ionization (ESI)-triple quadrupole-LIT (Q TRAP)-MS, AB 6500 Q TRAP LC/MS/MS system, and controlled by Analyst 1.6 software (AB Sciex). The ESI source operation parameters were as follows: ion source, ESI ±; source temperature 550°C; ion spray voltage (IS) −4,500 V (negative), 5,500 V (positive); the collision gas (CAD) was medium; and curtain gas was 35.0 psi. A specific set of multiple reaction monitoring (MRM) transitions was monitored to analyze. Phytohormones contents were quantified by Multiquant 3.0.3 software (Sciex) based on the AB Sciex QTRAP 6500 LC-MS/MS platform. Three replications of each sample were performed.

Measurement of Nitric Oxide and Reactive Oxygen Species Production by Confocal Microscopy

To monitor NO and ROS production in *T. hemsleyanum*, root tips (1 cm) were incubated in darkness for 2 h in the presence of 10 μM fluorescent probe DAF-FM DA (4-amino-5-methy-lamino-2, 7-diamino-fluorescein diacetate, sigma) or 10 μM 2′,7′-Dichlorodihydrofluorescein diacetate (DCFH-DA) prepared in 50 mM Tris–HCl (pH 7.4). It was shaken every 3–5 min during the incubation, and then, washed three times for 10 min with fresh buffer. About 10–15 individuals randomly sampled from each group were used for each experiment. Fluorescence signals were observed using a Leica laser scanning confocal microscopy (LEICA TCS SP8, Germany), and monitored with an excitation line from 495 nm and an emission window from 515 nm. Fluorescence intensity was analyzed using ImageJ software. Fluorescence intensity was quantified by determining green pixels in a defined area. Fluorescence intensity was observed from five micrographs for each treatment.

RNA Extraction and Transcriptome Analysis

Total RNA was extracted with Plant RNA Reagent (Invitrogen, Carlsbad, CA, United States), and the RNA quality was checked using the kaiaoK5500®Spectrophotometer (Kaiao, Beijing, China) and the RNA Nano 6000 Assay Kit of the Bioanalyzer 2100 system (Agilent Technologies, CA, United States). The cDNA was synthesized using a cDNA Synthesis Kit (TaKaRa, Dalian, China). The sequencing of cDNA libraries was performed using the Illumina sequencing system (HiSeq^{TM} 2000, San Diego, CA, United States). Clean reads were obtained using the SOAPnuke (v1.4.0), and were mapped using Bowtie 2(v2.2.3). Fragments per kilo-base of exon per million fragments mapped (FPKMs) were calculated and differential expression analysis was carried out using the DEseq2 (Love et al., 2014). Transcripts with a p-adjusted < 0.05 and $|\log 2\text{-fold change}| \geq 1$ were identified as the differentially expressed genes (DEGs). Gene Ontology (GO) and Kyoto Encyclopedia of Genes and Genomes (KEGG) enrichment analyses were performed to reveal the biological functions and the signal transduction pathways of the DEGs, $q < 0.05$ was considered to be significantly enriched.

Quantitative Real-Time PCR Analysis

Total RNA was isolated from 100 mg (fresh-weight) of leaves using the plant RNA extraction kit (Nanjing Vazyme Biotech Co., Ltd.) and synthesis of cDNA was performed with Evo M-MLV Mix Kit with gDNA Clean for qPCR AG11728 (Accurate biotechnology (Hunan) Co., Ltd.). Each reaction contained 10 μl of 2xSYBR Green Pro Taq HS Premix AG11701 (Accurate biotechnology (Hunan) Co., Ltd.), 2 μl of template cDNA, 0.4 μl of forward and reverse primers each (10 μM). GAPDH gene was used as an internal reference (**Table 1**). The PCR reaction procedure was as follows, incubation at 95°C for 2 min followed by 40 cycles of 95°C for 5 s and 60°C for 30 s. Each gene was tested in three biological replicates, with three technical repeats. The expression level for each sample was expressed as $2^{-\Delta\Delta Ct}$. The data were exhibited as the mean ± SD of three independent experiments.

RESULTS

Photovoltaic Condition Decreased Phytohormones Levels, Especially Salicylic Acid and Jasmonic Acid

We comprehensively compared the accumulation of multiple phytohormones between GZ and GF groups to explore the contributions of phytohormones in response to the photovoltaic planting pattern.

We detected 37 phytohormones grouped into 8 categories (**Supplementary Table 1**), such as 2 ABA, 9 Auxin, 15 CK, 1 ETH, 1 GA, 6 JA, 2 SA, and 1Soligolactone (SL) (**Figure 2A**). The differentially accumulated phytohormones (DAP) between GZ and GF were screened using $|\log 2\text{-fold change}| \geq 1$ and $p < 0.05$. A total of 16 DAP were identified in GZ _vs._ GF, such as 4 auxin, 8 CK, 1 GA, 1 JA, and 2 SA. Overall, the levels of ABA, ETH, and SL have no significant differences between GZ and GF. The content of tryptamine increased in the GF, while the levels of other auxins, i.e., indole-3-acetyl-L-valine methyl ester (IAA-Val-Me), indole-3-acetyl-L-aspartic acid (IAA-Asp), and L-tryptophan (TRP) decreased in response to the photovoltaic treatment. The content of JA and SA (such as, SA and SA 2-O-β-glucoside) were significantly decreased by photovoltaic treatment. GF group had higher contents of cytokinins than GZ except for 6-benzyladenine (BAP) and 2-methylthio-N6- isopentenyladenine (2MeSiP). The levels of N6-isopentenyladenine (IP), cis-Zeatin riboside (cZR), trans-Zeatin (tZ), and ortho-Topolin riboside (oTR), which are naturally occurring cytokinin, decreased after photovoltaic treatment. Although the level of GA was significantly induced by photovoltaic treatment, it could hardly be detectable both in GZ and in GF. Overall, we noticed that GF decreased significantly the contents of phytohormones especially in SA and JA, while no significant differences were detected in the case of ABA, ETH, and SL (**Figure 2B**).

TABLE 1 | Primers sequences used for quantitative real-time PCR analysis (qRT-PCR) for detecting gene expression.

Gene annotation	Primer F (5′–3′)	Primer R (5′–3′)	Tm	Length (bp)
Photosystem I reaction center subunit XI (psaL)	CTTCACTTCACCATCAACC	GTCTCAAGGCTTCCGATA	60	183
Magnesium-chelatase subunit (ChlI)	CATCCTGCTCGGTTTATTC	CTCTCCTCCACAATCTTCA	60	143
Ferredoxin (petF)	GGAGAAGGAGTTTGAATGC	AAGTCAGAACCCATCCAG	60	194
Photosystem II oxygen-evolving enhancer protein (psbQ)	CCTTGATCTGCCATTGAAG	ACAGTGTTGAGGTCGTAG	60	189
Photosystem I subunit IV (psaE)	ACCTCCATGCTCATCTTC	TCCTTCCTCAGAATCTTCAC	60	194
Carbonic anhydrase (cynT)	GCCTTTCCCAGAACAATG	TCCACCCTTCAATGATAGAG	60	124
Nitrate reductase (NAD(P)H), (NR1)	CGGGAAGGTGTATGATGTA	GAGGAACGCTTGATGAATC	60	179
Nitrate reductase (NAD(P)H), (NR2)	TTCAAGACGGTGGTAGTG	CAAGGAGAGGAACGAAGA	60	144
Abscisic-aldehyde oxidase (AAO)	CAGTTCCAGACGAAGACA	CAGTAGCAACAGGCATTG	60	177
9-cis-epoxycarotenoid dioxygenase (NCED1)	CCACTTGTGAGGTGATAGA	CGTAACGGCTACAGAAGA	60	189
9-cis-epoxycarotenoid dioxygenase (NCED2)	GGAAGGAGACATTGAGACT	GAATCGGAAGTAGGTTAGGA	60	151
Phenylalanine–tRNA ligase beta subunit (pheT)	GATGTGGTTGAGGATGTTG	CAGTGGCTTCAATGATACAG	60	78
Phenylalanine ammonia-lyase (PAL)	GGATGAAGTGAAGCGTATG	GCTGTCTGTACCATTGTTC	60	199
Hydroxymethylbilane synthase (hemC)	TCACGAGGTTACCAGATTAG	GAAGCATATCCAGCAATAGG	60	93
Magnesium chelatase subunit H (CHLH)	CTATGTGGCTGTGATTATGG	CGAACGGCTTCTTAGTAAC	60	128
GAPDH	AGCAGCCTTGTCCTTGTCAGTG	GATTGGACGTTTGGTTGCGAG	60	150

Tm, melting temperature.

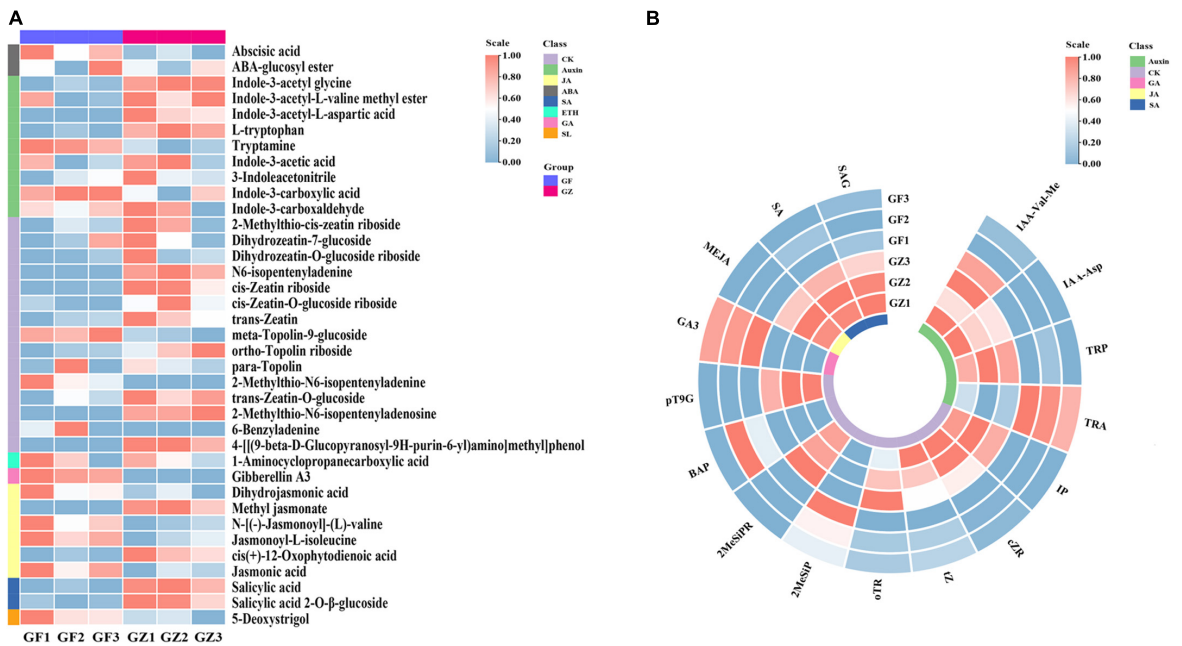

FIGURE 2 | (A) The overall heatmap of 8 categories of phytohormones in *T. hemsleyanum*. **(B)** The heatmap of significantly different phytohormones between GZ and GF in *T. hemsleyanum*. The color bar represents the normalized fold change values.

Transcriptome Analysis Revealed Key Factors Involved in Photovoltaic Adaptation

A total of 42.43–44.67 million clean reads were obtained, and the Q30 of the raw reads in the 6 RNA-seq libraries ranged from 91.7 to 95.241%. A total of 111,428 unigenes were generated, and the mean length was 1,313 bp with N50 length of 2,167 bp. Based on *de novo* assembly, we found that 7,024 upregulated and 5,591 downregulated genes in GZ _vs._ GF comparison (**Figure 3A**).

A total of 31 genes related to hormone synthesis were detected, most of them were downregulated in GF group compared with GZ group (**Figure 3B**). The results of GO functional and enrichment analyses demonstrated that the top-ten enriched GO terms were related to "proteasome-mediated ubiquitin-dependent protein catabolic process,""ribulose-1,5-bisphosphate carboxylase/oxygenase activator activity," "oxidoreductase activity," "chloroplast strom," "oxidoreductase activity, acting on paired donors, with incorporation or reduction of molecular oxygen, NAD(P)H as one donor," "heme

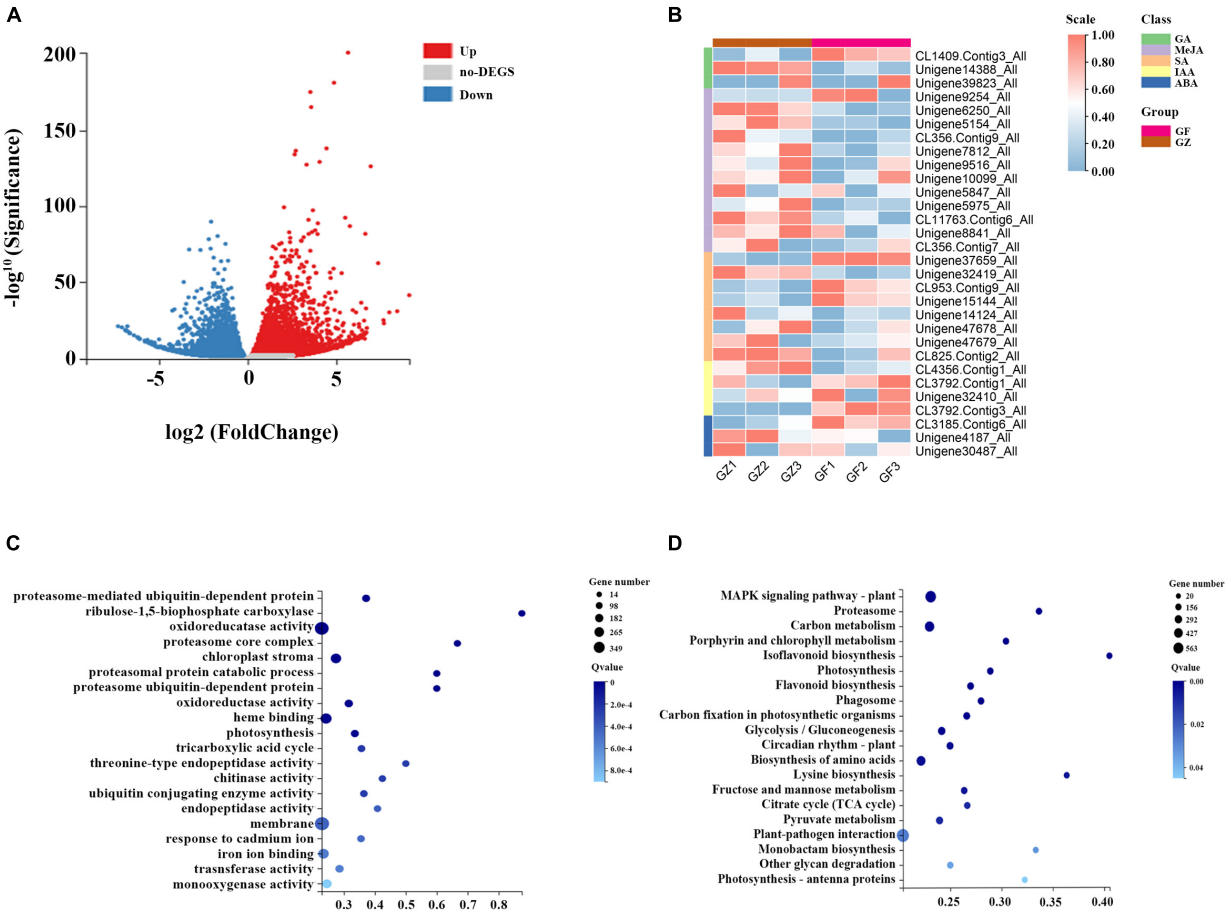

FIGURE 3 | (A) Volcano plot of differential gene expression analysis. **(B)** Heatmap of hormone-related genes expression level. **(C)** Gene Ontology (GO) level terms classification of differential genes. **(D)** Kyoto Encyclopedia of Genes and Genomes (KEGG) pathway analysis for differential gene expression analysis between GZ and GF in *T. hemsleyanum*.

binding," "photosynthesis," etc. (**Figure 3C**). Furthermore, the DEGs were significantly enriched using the KEGG database. The top enriched KEGG terms contributed by these DEGs included "mitogen-activated protein kinase (MAPK) signaling pathway-plant," "carbon metabolism," "porphyrin and chlorophyll metabolism," "photosynthesis," bioflavonoid biosynthesis," "carbon fixation in photosynthetic organisms," "circadian rhythm-plant," "photosynthesis- antenna proteins," etc. (**Figure 3D**).

The above analyses indicated that the identified DEGs were the most relevant to photosynthesis, MAPK signaling pathway, carbohydrate metabolism, and oxidation-reduction reaction. A total of 441 DEGs were annotated in MAPK signaling pathway, which was the top enriched KEGG term. MAPK cascade plays a prominent role in plant growth, stress response, and signal transduction of hormones. ROS are likely to directly or indirectly activate MAPKs. MAPK activation is an important step in the biosynthesis of various phytohormones. The largest number of DEGs was identified to link to the oxidoreductase activity in the GO enrichment analysis. A transcriptome analysis detected 277 genes encoding multiple enzymes in plant hormone signal transduction pathway. Of these genes, the Auxin signal transduction protein family was the most represented with 42 members, such as 31 Auxin-responsive proteins, 1 Auxin transporter-like protein, and 10 Auxin-induced proteins (**Supplementary Table 2**).

We selected 10 genes from photosynthesis and hormone signaling pathway to assess the relative expression levels by the quantitative real-time PCR (qRT-PCR) analysis. This independent evaluation revealed that the patterns of RNA-Seq expressions on these genes were highly consistent with the qRT-PCR data, and a correlation coefficient (R2) of 90.89% between the two techniques was obtained (**Figure 4**).

Exogenous Phytohormones and Nitric Oxide Enhance Photosynthetic Efficiency and Modulate-Related Gene Expression Under Photovoltaic Condition

Exposure to photovoltaic condition reduced the Pn, Tr, Cond, and Fv/Fm by 29.1, 18.0, 26.1, and 27.8%, respectively, compared with GZ group, whereas intercellular carbon dioxide

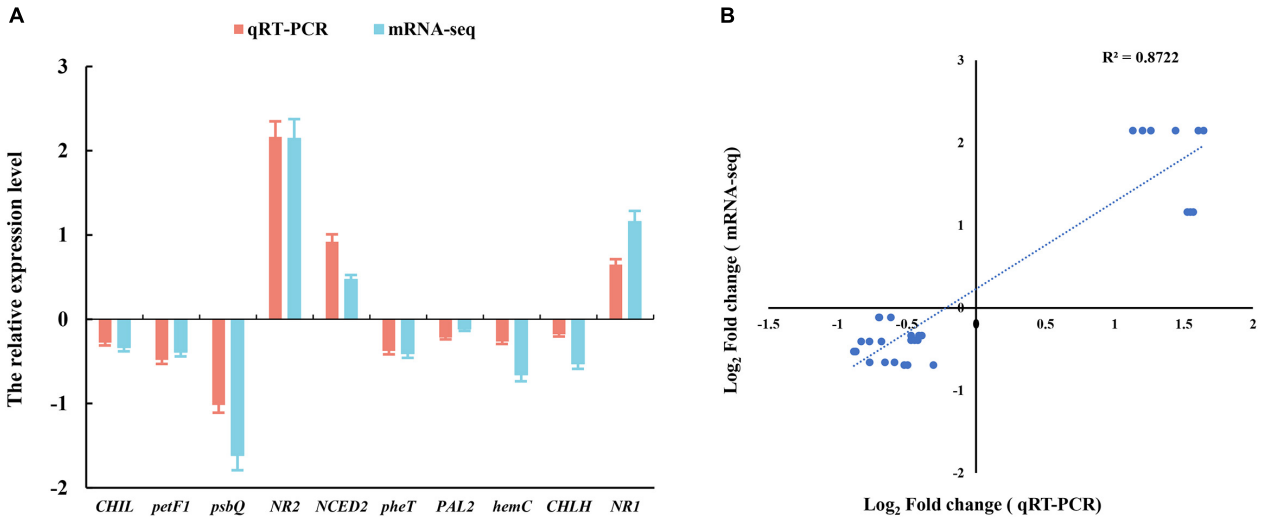

FIGURE 4 | (A) Verification of RNA-Seq data by the quantitative real-time PCR (qRT-PCR) assay. **(B)** Pearson's correlation coefficients of the log2 of gene expression ratios obtained from RNA-seq data and qRT-PCR. All the genes information is showed in **Table 1**. Three biological replicates and three technical replicates were collected for each sample.

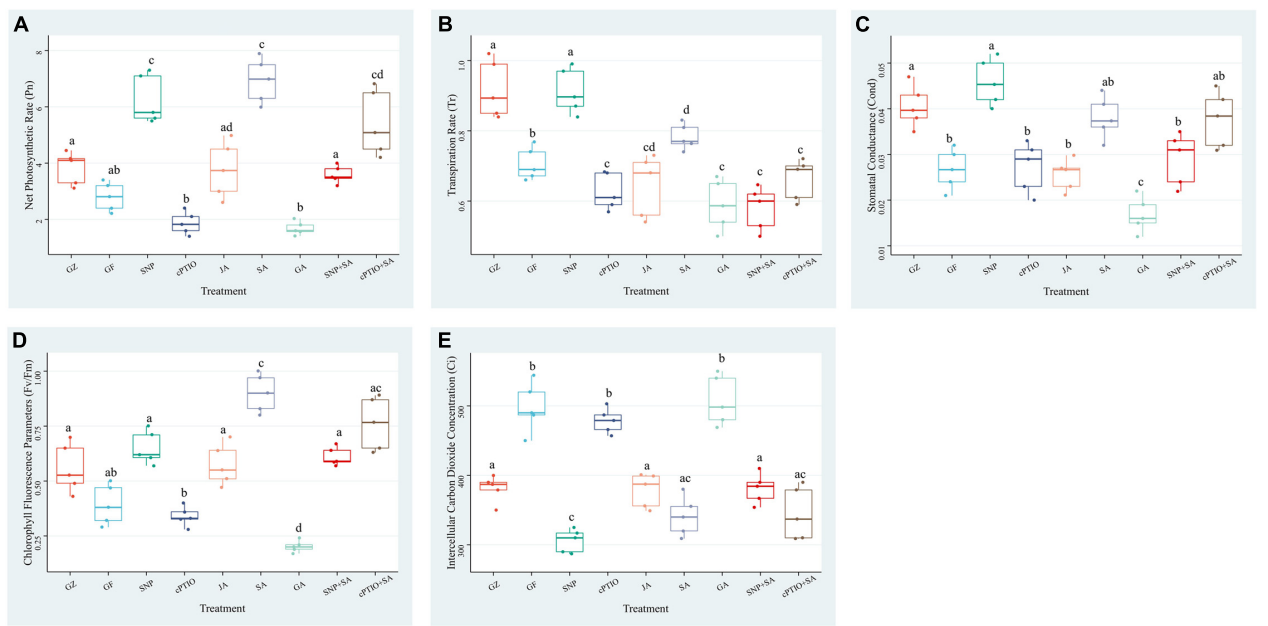

FIGURE 5 | Effect of nitric oxide (NO) effectors and/or phytohormones on **(A)** net photosynthetic rate (Pn), **(B)** transpiration rate (Tr), **(C)** stomatal conductance (Cond), **(D)** chlorophyll fluorescence parameters (Fv/Fm), and **(E)** intercellular carbon dioxide concentration (Ci) of *T. hemsleyanum* under photovoltaic condition (GF) and normal light condition (GZ). Data are means ± DE of the three technical replicates from five seedlings for each treatment. Means that do not share a same letter are significantly different at $p \leq 0.05$ level according to Tukey's test.

concentration (Ci) showed a significant increase of 26.6%. Although the Pn was significantly lower in GF group than in GZ group, JA supplementation narrowed that gap, SNP and SA treatment even greatly enhanced Pn to 1.52- and 1.76-fold of that of GZ group, respectively. Applying with cPTIO decreased Pn by 33.2% compared with GZ group. The enhancement effect of the combination of NO quencher cPTIO and SA treatment was decreased by 22.9% than that of SA treatment alone. However, when plants were treated with the combination of "SA + SNP," the enhancement effect of SA on Pn was markedly counteracted by 49.4%. On the contrary, GA showed no significant effect on the Pn level. Similar trends were noted for Tr, Cond, and Fv/Fm. On the other hand, Ci was increased under photovoltaic condition when compared with control. Exogenous SA, SNP,

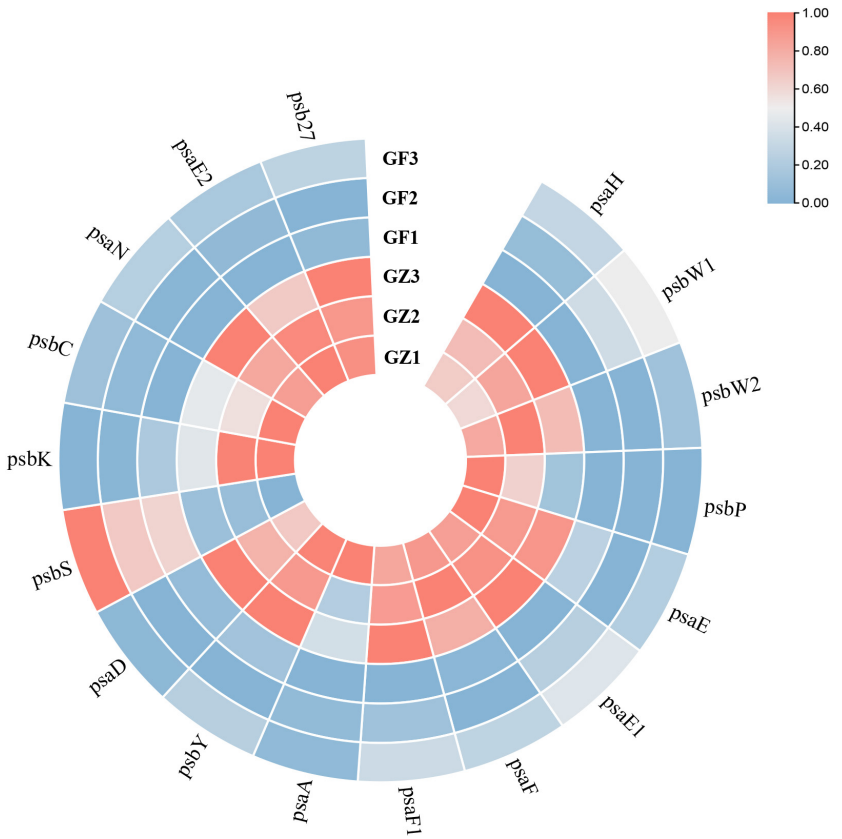

FIGURE 6 | The heatmap of significantly different genes encoding proteins involved in photosystem I (PS I) and photosystem II (PS II) reaction center between GZ and GF in *T. hemsleyanum*. The color bar represents the normalized fold change values.

and JA alleviated the increment, and the combined treatment of SA + SNP showed a higher Ci level than the combined treatment of SA + CPTIO (**Figure 5**). These data indicated that NO, JA, and SA treatment alone significantly enhanced the photosynthetic efficiency which was decreased by exposure to photovoltaic condition, but the combined treatment of NO + SA could weaken the enhancement effect.

Responses of Photosynthesis-Related Genes

Based on the transcriptome information, we investigated the whole genome expression level of the genes involved in photosynthesis. A total of 79 unigenes encoding multiple proteins or enzymes in the chlorophyll and photosystem biosynthesis and metabolism pathway (**Supplementary Table 3**). From **Figure 6**, we could see that a majority of genes involved in photosynthesis (69/79) were specifically downregulated in the GF group, compared with the GZ group. A total of 17 key genes encoding proteins involved in photosystem I (PS I) and photosystem II (PS II) reaction center (**Supplementary Table 4**), among them 16 genes were downregulated, such as PS I reaction center subunit IV B (Unigene48386), PS I reaction center subunit VI (CL5676.Contig2), and PS II oxygen-evolving enhancer protein (CL2591.Contig1) of GF were repressed to 31.3, 53.4, and 42.3% of GZ, respectively (**Figure 6**). In particular, 3 of 8 unigenes encoding psbP domain-containing protein were almost completely not expressed. The above results indicated that photosynthetic electron transport machinery was repressed to a certain degree in response to GF treatment.

To confirm the effect of photovoltaic condition and each treatment on photosynthetic efficiency, an RT-PCR was performed to determine the relative expression levels of 5 key genes in the photosystem biosynthesis and metabolism pathway: *psaL, CHIL, petF1, psbQ,* and *psaE* (**Figure 7**). Although 5 key genes showed different degrees of expression changes among each group, they generally have a similar variation trend. The expression levels of the GF group were below or close to the GZ group. SNP and SA treatment dramatically increased genes expression levels, while the GA and cPTIO treatment significantly lower their expression levels. The difference relative transcript level of *psaL* reached a maximum at 21.3 in "SNP vs. CK" and 13.5 in "SA vs. CK," respectively, while the difference multiple of "GA vs. CK" and "JA vs. CK" was 0.40 and 1.01, respectively. It suggested that *psaL* was inhibited by GA but were not significantly influenced by JA. Surprisingly, SA + SNP combined treatment only upregulated the gene expression level by 4.4-fold compared with CK, it was obviously lower than that in the SNP or in SA individual treatment group. On the other hand, cPTIO + SA combined treatment up-regulated the

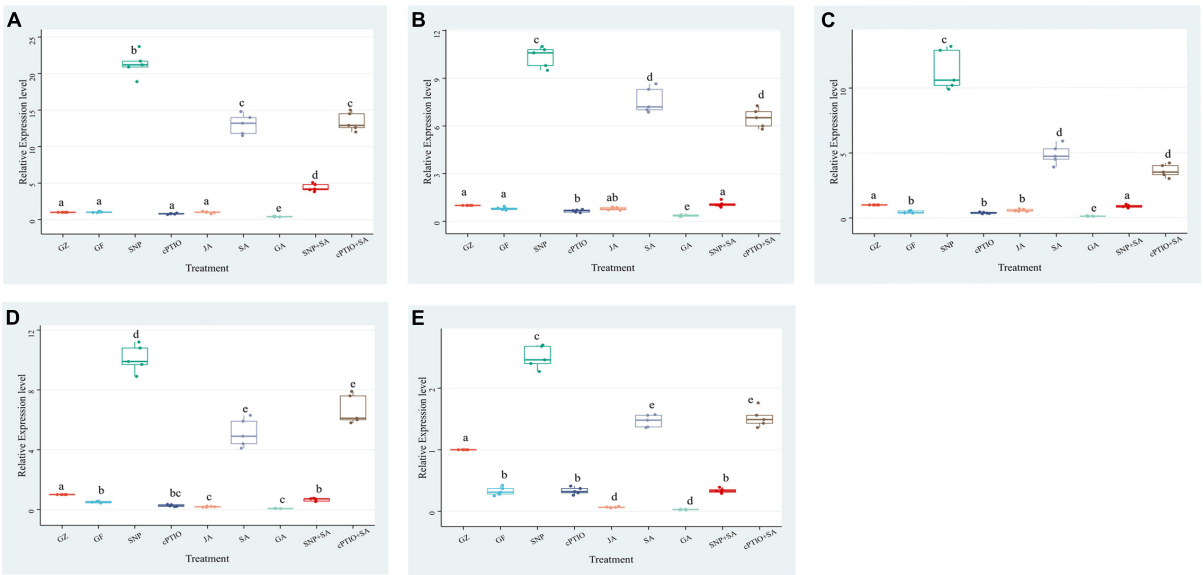

FIGURE 7 | Effect of NO effectors and/or phytohormones on expression levels of **(A)** *psaL*, **(B)** *CHlL*, **(C)** *petF1*, **(D)** *psbQ*, and **(E)** *psaE*, of *T. hemsleyanum* under photovoltaic condition (GF) and normal light condition (GZ). Data are means ± SE of the three technical replicates from five seedlings for each treatment. Means that do not share a same letter are significantly different at $p \leq 0.05$ level through Tukey's test.

gene expression level by 13.3-fold, close to the SA treatment group. It suggested that SA had no synergistic effect with NO in promoting the expression level of *psaL*, instead, an antagonistic link between them might even be possible. The expression of another gene, *psbQ*, also showed 9.9- and 5.1-fold upregulation under SNP and SA treatment, respectively. The difference multiple of "SNP + SA vs. CK" and "cPTIO + SA vs. CK" reached 0.65 and 6.6, respectively. It suggested that the inhibition of NO generation is beneficial for the activating effect of SA on *psbQ*.

Exogenous Phytohormones and Nitric Oxide Treatment Mitigated the Accumulation of Reactive Oxygen Species and Potentiated Antioxidant Capacity

The NBT- and DAB-staining were performed to show H_2O_2 and O^{2-} accumulation, respectively. Results of **Figure 8** revealed more intense brown or dark blue patches on the roots/leaves of the GF group than on those from the GZ group, and indicated overproduction of H_2O_2 and O^{2-} in response to the photovoltaic condition. A similar amount of H_2O_2 and O^{2-} was observed in GA-treatment seedlings, compared with the GF group. However, SA, SNP, or JA treatment alone considerably diminished the H_2O_2 and O^{2-} accumulation in the leaves/roots of the GF seedlings. This indicated that the SA-, JA-, and NO-mediated response was closely coupled with the H_2O_2 and O^{2-} level. On the other hand, applying cPTIO to quench endogenous NO would increase the accumulation of H_2O_2 and O^{2-} in seedlings. Similarly, accumulation of H_2O_2 and O^{2-} was promoted by cPTIO + SA combined treatment as compared with the SA treatment alone. But the leaves/roots of SNP + SA combined treatment group were stained more deeply by the two chemicals than those in SA or SNP treatment alone group, indicating more amount of H_2O_2 and O^{2-} was produced when SA coexisted with NO. These data indicated that NO, JA, and SA alleviated H_2O_2 and O^{2-} production, while GA and NO quencher led to the overproduction of H_2O_2 and O^{2-}, NO donor could weaken the scavenging effect of SA.

The DCFH-DA staining was performed to show ROS accumulation, respectively. Results of **Figure 9** revealed more intense green fluorescence on the roots of GF group than on those from the GZ group, and indicated overproduction of ROS in response to photovoltaic condition. However, SA, SNP, or JA treatment alone considerably diminished an ROS accumulation in the roots of the GF seedlings, especially SA and SNP. This indicated that the SA-, JA-, and NO-mediated response was closely coupled with the ROS level. Similarly, accumulation of ROS was promoted by cPTIO + SA combined treatment as compared with the SA treatment alone. However, the roots of SNP + SA combined treatment group were stained more deeply by the two chemicals than those in SA or SNP treatment alone group, indicating that more amount of ROS was produced when SA coexisted with NO. These data indicated that NO, JA, and SA alleviated ROS production, while GA and NO quencher led to the overproduction of ROS. NO donor could weaken the scavenging effect of SA.

The aforementioned results suggested that ROS accumulation varied among the photovoltaic condition and different treatments. Since enzymatic scavenging had an important influence in ROS accumulation, investigation of the antioxidant system was thus conducted by measuring the activities of SOD, CAT, and POD. The three enzymes exhibited almost the

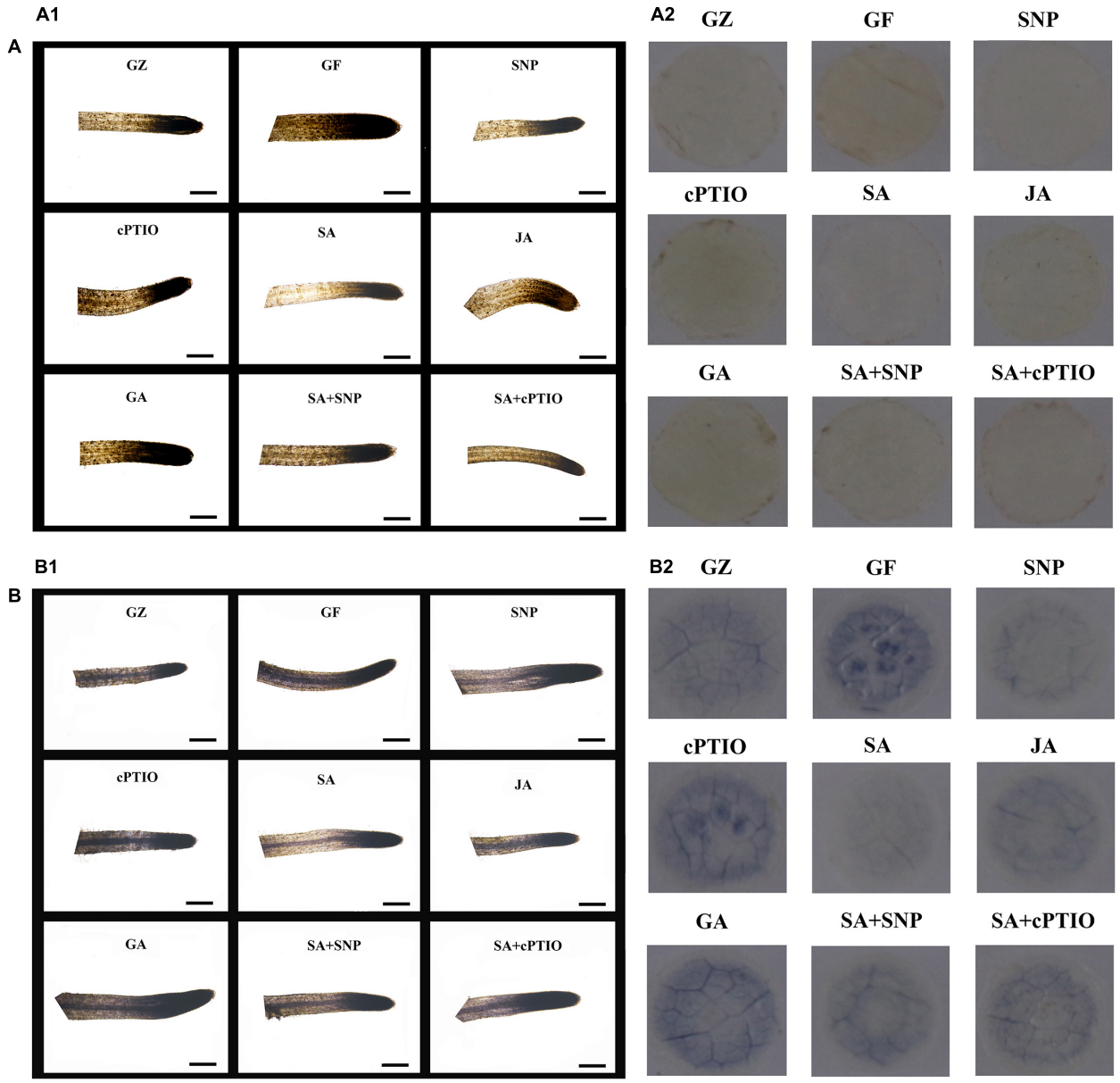

FIGURE 8 | *In situ* accumulation of H_2O_2 and O^{2-} by 3,3-diaminobenzidine (DAB) **(A)** and nitro blue tetrazolium (NBT) **(B)**. Staining of the roots **(A1,B1)** and leaves **(A2,B2)** after the respective treatment of NO effectors and/or phytohormones under the photovoltaic condition (GF) and the normal light condition (GZ). The figure is representative of ten segments stained in each experiment.

same trends among different treatment groups, although they differed in the order of magnitude. Under the photovoltaic condition, a considerable ($p \leq 0.05$) decrease by 60.8, 33.9, and 16.4% was observed in the activities of SOD, CAT, and POD enzymes, and a considerable ($p \leq 0.05$) increase by 47.0% was observed in the content of MDA yet, compared with normal illumination group (**Figure 10**). Exogenous application of SNP, SA, and JA significantly ($p \leq 0.05$) improved the POD activity by 67.8, 100.4, and 26.3%, respectively, they also improved the CAT activity by 80.8, 215.3, and 46.8%, respectively. While the SOD activity was improved by 56.0% only in response to SA. Application of cPTIO alone had no perceptible effect on the antioxidant system, but applying with cPTIO and SA combination counteracted the enhancement effect of SA on the activity of POD, SOD, and CAT by 5.9 ($p > 0.05$), 5.8% ($p > 0.05$), and 29.6% ($p \leq 0.05$), respectively. The SNP + SA combined treatment further counteracted the enhancement effect of SA on the activities of POD, SOD, and CAT by 20.8% ($p \leq 0.05$), 18.3% ($p > 0.05$), and 33.6% ($p \leq 0.05$), respectively. On the other hand, GA-treated samples had the lowest antioxidant enzyme activity and the highest MDA content among all the treatments. The above

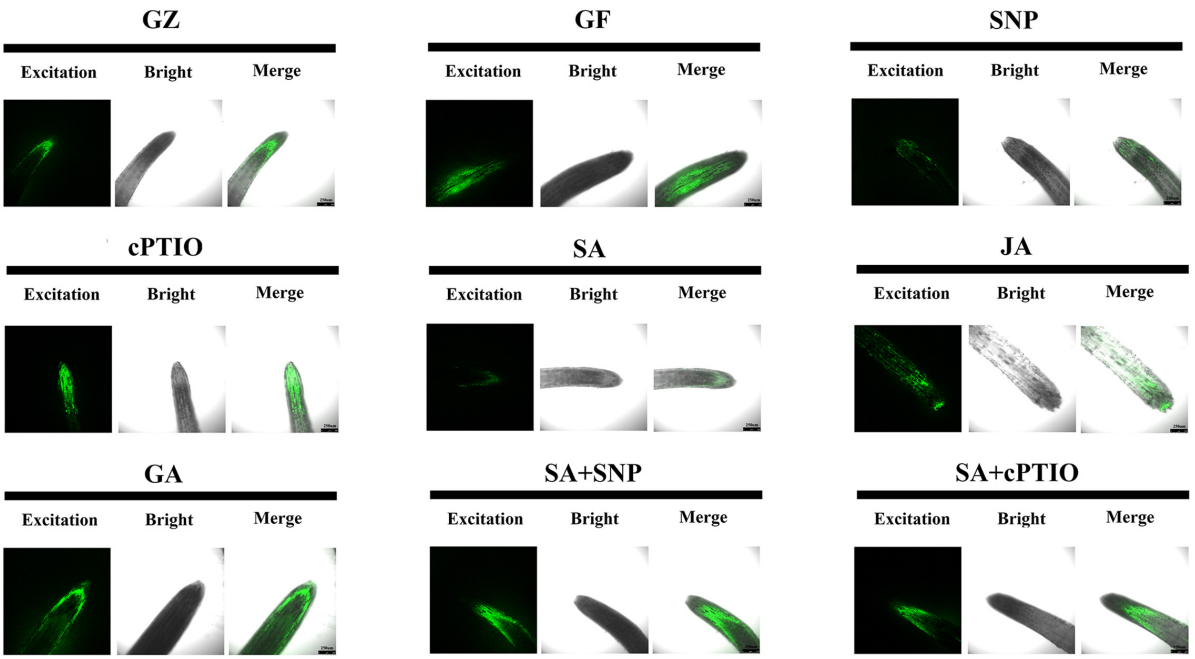

FIGURE 9 | Reactive oxygen species (ROS) accumulation of the roots after the respective treatment of NO effectors and/or phytohormones under the photovoltaic condition (GF) and the normal light condition (GZ), using 10 μM DCFH-DA as a fluorescent probe. The figure is representative of ten segments stained in each experiment.

results had a good agreement with the ROS accumulation dynamics (**Figure 9**).

The results of the antioxidant system demonstrated that the photovoltaic condition significantly increased ROS accumulation and decreased the antioxidant capacity. The antioxidant enzyme activities were consistent with the NO, SA, and JA levels, but negatively correlated with the ROS accumulation, thereby suggesting that NO, SA, and JA had protective roles, but the combined treatment of NO + SA could weaken the protective effect.

Phytohormones Reduced Endogenous Nitric Oxide Burst Triggered by Photovoltaic Adaptation

Semi-quantitative measurement of NO generation in root tips after different treatments was performed using the fluorescent probe 4,5-diaminofluorescein diacetate (DAF-2DA). As shown in **Figure 11**, the level of NO was 11.2% higher under the photovoltaic condition than under the normal light condition. This suggests that the production of endogenous NO was triggered by photovoltaic adaptation. Moreover, SNP strongly increased the level of NO, reaching an approximately 22.0 and 35.4% higher level in relation to the normal light and photovoltaic condition groups, respectively. In contrast, the photovoltaic condition-induced endogenous NO burst was weakened by treatment with the NO scavenger cPTIO, the level of NO decreased by 26.0%. The results suggested that NO was involved in photovoltaic condition-induced ROS accumulation and boosted photosynthesis in *T. hemsleyanum*.

To gain further insight into the possible interaction between NO generation and phytohormone signaling in response to the photovoltaic condition, the *in situ* NO level regulated by several kinds of phytohormones was analyzed. All phytohormones, except GA, significantly decreased the storage of NO message, especially under the SA treatment. The level of NO decreased by 22.3% under the SA treatment, similar to that of cPTIO treatment, while SNP increased the level of NO by 22.0%, however, SNP + SA combined treatment significantly strengthened the inhibitory effect on NO accumulation by 58.7% ($p \leq 0.05$), similar to that of JA treatment (**Figure 12**).

DISCUSSION

Greenhouse horticulture is essential in satisfying the increasing global food demand under climatic variation situation. As an increasingly important clean source of energy, solar photovoltaic energy system has attracted much attention. Due to the large land occupation of photovoltaic panel, it is economic to develop the photovoltaic planting pattern under photovoltaic panels. Research about energy-efficient cover materials on yield and photosynthesis have been examined in main vegetables, such as tomato (Ezzaeri et al., 2018) and cucumber (Alsadon et al., 2016). The result indicated that the covers had significant effects on photosynthate allocation, yield, and the nutrient composition in vegetables. However, the potential molecular and physiological mechanisms of photovoltaic response in horticultural crops are rarely studied.

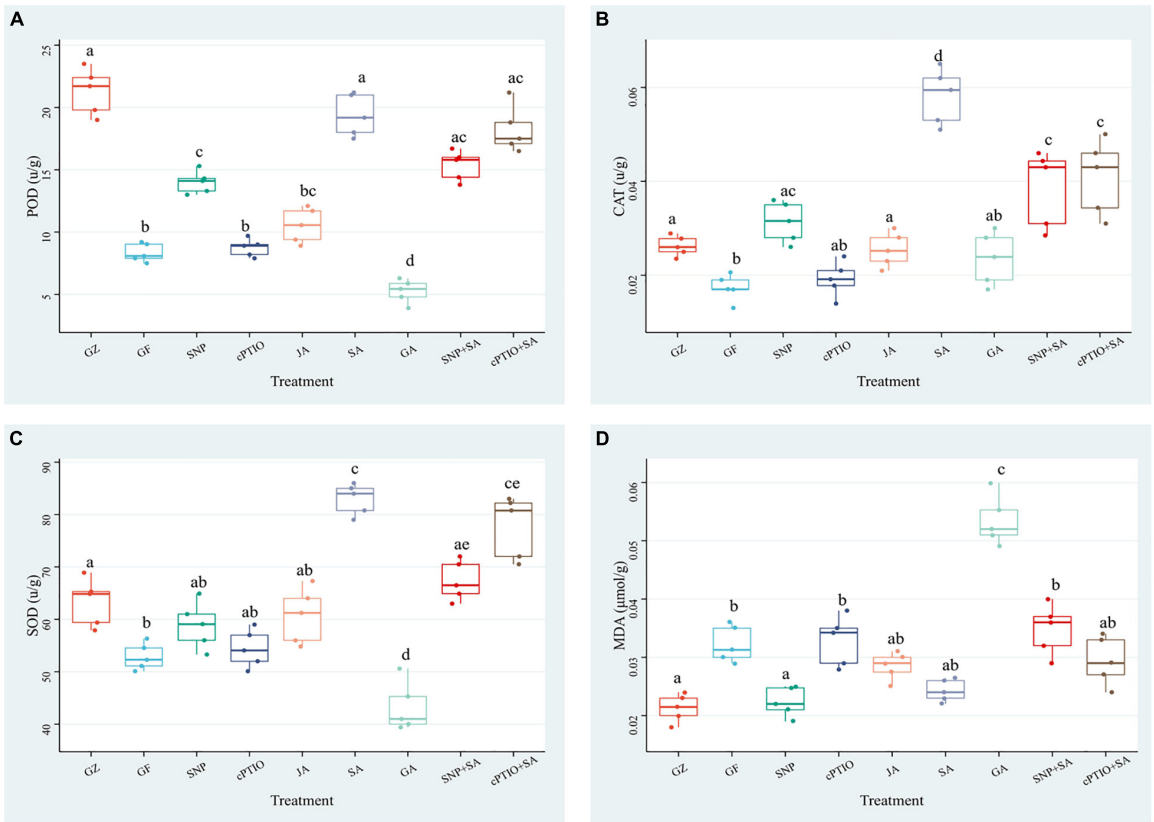

FIGURE 10 | Effect of NO effectors and/or phytohormones on the activities of determination of peroxidase (POD) **(A)**, catalase (CAT) **(B)**, superoxide dismutase (SOD) **(C)**, and the content of malondialdehyde (MDA) **(D)** in *T. hemsleyanum* under the photovoltaic condition (GF) and the normal light condition (GZ). Data are means ± SE of the three technical replicates from five seedlings for each treatment. Means that do not share a same letter are significantly different at $p \leq 0.05$ level through a Tukey's test.

In this study, exposure to the photovoltaic condition reduced the photosynthetic efficiency, decreased phytohormones levels, provoked endogenous NO burst, and disrupted the redox homeostasis of *T. hemsleyanum* and the transcriptome analysis verified that the largest number of DEGs were the most relevant to photosynthesis, plant hormone signal transduction pathway, MAPK signaling pathway, and oxidation-reduction reaction.

Mitogen-activated protein kinase cascade plays an important role in plant growth, stress response, and signal transduction of hormones. ROS are likely to directly or indirectly activate MAPKs. There are increasing experimental evidence that various gaseous signaling molecules are involved in MAPK cascades. NO could activate MAPK cascades during stress, and MAPK cascades could also mediate NO-dependent physiological processes (Wu et al., 2021).

It has been proved that various environmental stresses might cause many physiological disorders of plants, such as a decline in biomass production, chlorophyll content, and photosynthetic rate, directly or indirectly, through oxidative damage. A frequent occurrence is the generation of reactive chemical species, such as RNS and ROS. Numerous studies have been conducted to explore the roles of ROS as signaling molecules or as oxidative burst causing-agents. The RNS biology, however, is emerging as recent research hotspot. NO was thought to be an important precursor of RNS members. In this study, the photovoltaic condition provoked endogenous NO and ROS burst, similar to the responses to environmental stress. However, photovoltaic condition-induced ROS accumulation could be alleviated by exogenous NO to the upregulating activities of CAT, POD, and SOD, thus resulting in the alleviation of oxidative damage, while the NO inhibitor cPTIO reversed these responses. These responses are in agreement with several previous findings. Similar protective effects were obtained for *Pistia stratiotes* under arsenic stress (Farnese et al., 2017). NO donor SNP pretreatment conferred salt and drought tolerance by the activation of antioxidase (SOD, POD, and CAT) and lowering the oxidative stress, while the inhibitor L-NAME or cPTIO application made the seedlings more sensitive to both the two types of stresses (Fan and Liu, 2012; Kaya and Ashraf, 2021).

Sodium nitroprusside significantly increased the photochemical efficiency, alleviated the decrease of the Chl content, and decreased NPQ of PSII of ryegrass seedling leaves under alkaline stress (Procházková et al., 2013). NO has been reported to regulate the chlorophyll production (Romero-Puertas et al., 2004). SNP treatment decelerated chlorophyll loss and improved the photosynthetic efficiency under either

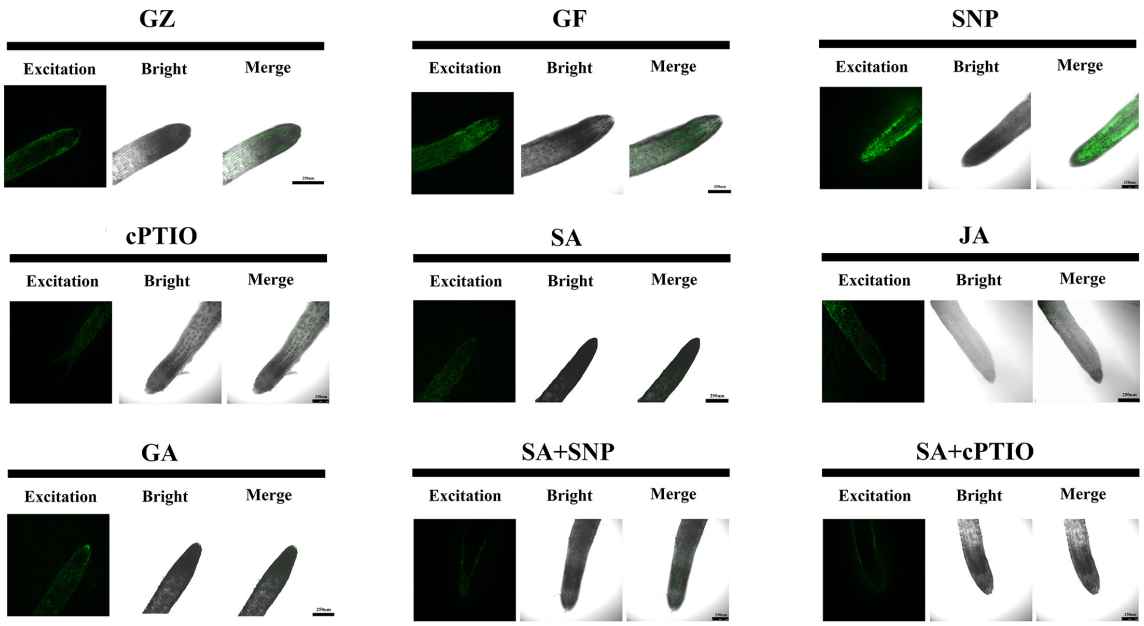

FIGURE 11 | Nitric oxide (NO) accumulation in roots of *T. hemsleyanum* after the respective treatment of NO effectors and/or phytohormones under the photovoltaic condition (GF) and the normal light condition (GZ), using 10 μM DAF-2DA as a fluorescent probe. The figure is representative of ten segments stained in each experiment.

dehydration or drought stress (Fan and Liu, 2012). NO plays an important role in CO_2 elevation-induced stomatal closure, and therefore enhance the photosynthesis of Arabidopsis, while NO inhibitor tungstate and L-NAME significantly inhibited stomatal closure by scavenging NO and reversed the enhancement of photosynthesis (Wang et al., 2015). In our study, the photovoltaic condition significantly decreased Fv/Fm, Pn, Tr, and Cond, and increased Ci. The presence of GA or cPTIO intensified the degree of change, while SNP, SA, and JA alleviated the decline of photosynthesis in different degrees, especially SNP and SA. Transcriptome analysis revealed that a majority of genes (69 of 79) involved in was specifically down-regulated in response of the photovoltaic condition, such as *psaL, CHIL, petF1, psbQ,* and *psaE*, and these key genes were proved to be upregulated by the SNP-treatment and downregulated by the cPTIO-treatment. The results suggested that both NO and SA play a significant role in recovering the suppression of photosynthesis induced by photovoltaic condition. It is surprising that the integration of NO and SA treatment provides no additional functionality, but it significantly weakened those restoration effects, much lower than NO or SNP treatment alone, than cPTIO and SA treatment. It indicates that there is some kind of antagonism between NO and SA. These conclusions are further confirmed by expression levels determination of the key genes for photosynthesis. The key gene expression levels of SNP + SA combined treatment were obviously lower than that in SNP or in SA individual treatment group. On the other hand, cPTIO + SA combined treatment upregulated the gene expression level, and close to the SA treatment group. It suggested that the inhibition of NO generation is beneficial for the activating effect of SA on photosynthesis.

Nowadays, the application of phytohormones/growth regulators has become an effective approach to regulate the plant metabolism and strengthen plant tolerance against various stresses. Not only synergistic but also antagonistic interactions between phytohormones and other signaling molecules have been reported to mediate the tolerance mechanisms of plants. Over the last decade, intricate crosstalk between NO and phytohormones during the regulation of several plant responses have been described by some studies. NO increased lettuce's resistance to salt stress by regulating its hormonal

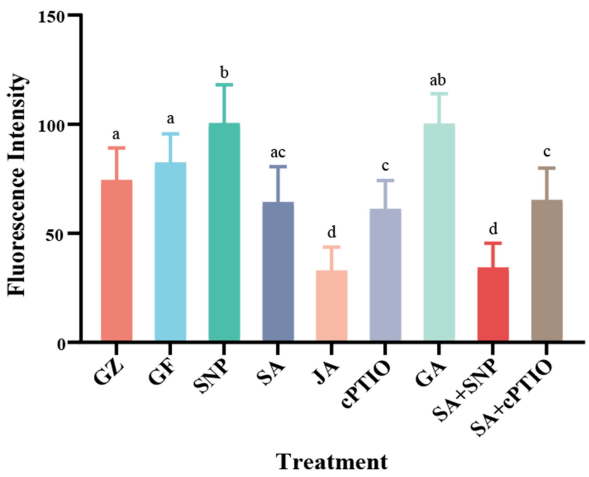

FIGURE 12 | The values of fluorescence intensity. Means in that do not share a same letter are significantly different at $p \leq 0.05$ level through Tukey's test.

balance. NO and CKs showed positive interaction in regulating photosynthesis and improving adaptability of *Zea mays* to drought stress (Mishina et al., 2007). *In vivo* NO detection showed that NO generation inside the guard cells is important for ABA-regulated stomatal closure (Neill et al., 2002). Both antagonistic and positive promotion effect between NO and GAs has been observed for several. NO could inhibit the GA synthesis by reducing the expression levels of GA20 oxidase3 (GA20ox3), which encodes a key enzyme in the synthesis pathway of active GAs. Moreover, NO promotes the expression of DELLA proteins, which are repressors of GA signaling (Lozano-Juste and León, 2011). On the contrary, under low- and high-phosphorus levels, NO showed antagonistic action against GA in regulating the primary root growth of Arabidopsis thaliana (Wu et al., 2014). Exogenous NO decreased the detrimental influence of overproduced ET under abiotic stresses by inhibiting 1-aminocyclopropane-1-carboxylic acid (ACC) synthase and ACC oxidase activities, which were responsible for the production of ET (Manjunatha et al., 2010). Under salt stress, the synergistic interaction between SA and NO was found in decreasing the damages in Soybean plants by more significantly activating CAT, ascorbate peroxidase (APX), and guaiacol peroxidase (GPX), and the protective action of SA + SNP combined treatment was more effective than that of SA and SNP alone (Simaei et al., 2011). On the contrary, our study demonstrated that the photovoltaic condition significantly increased ROS accumulation and decreased antioxidant capacity. NO, JA, and SA alleviated ROS production, while GA and NO quencher led to overproduction of ROS. The protective action of SA + SNP combined treatment against oxidative damage induced by photovoltaic condition was often less efficient than effects of SA and SNP alone. Similarly, SA was reported to antagonize the ability of NO to decline respiration, thereby causing oxidative stress (Fatima et al., 2021).

The above results indicated that although the crosstalk mode among NO and other signaling compounds was not always synergistic, sometimes antagonist responses under unfavorable situations. The NO crosstalk response under similar stress would vary plant by plant due to the complex signaling cascades of signaling compounds and their interacting signals. Therefore, future research considering the interaction between multiple phytohormones and NO under environmental stress is required to elucidate the biochemical mechanisms of how hormones interact with NO to fine tune the plant metabolism.

So far, little is known about the upstream and downstream relation between NO and phytohormones in the environmental response as indicated by a series of studies in this field with often conflicting results. NO and SA synergistically interact to ameliorate oxidative damage and alleviate salt/osmotic stress, and NO signaling action may occur downstream of SA (Liu et al., 2014; Naser et al., 2014). Increased Cd tolerance of Arabidopsis thaliana was mediated by auxin-induced NO accumulation (Xu et al., 2011).

The composition and content of hormones were altered in response to high saline conditions and they trigger NO production. Thus, after NO production, the balance of phytohormones will be rebuilt through feedback mechanisms (Nawaz et al., 2017). Under heat stress, exogenous melatonin increased the NO burst along with the expression of nitrate reductase- and NO synthase-related genes, which facilitated the scavenging of excess ROS and confronting oxidative damage induced by the heat stress in tomato seedlings. On the contrary, NO has been considered to be one of the first molecules in response to Cd stress, which in turn suppressed AUX carriers and AUX accumulation, resulting in inhibition of root elongation in Arabidopsis seedlings (Yuan and Huang, 2016). Some studies have shown that NO levels were unchanged or even low in mutant/transgenic plants with the higher level of CK. However, other reports have revealed CK treatment increased NO production (Freschi, 2013). CKs reduced NO generation in guard cells and stimulated stomatal opening. Moreover, CKs even abolished NO generation and thereby facilitated reopening of closed stomata under dark conditions. SA prevented NO accumulation in Arabidopsis under salt stress conditions indicating an antagonistic relationship between NO and SA (Khokon et al., 2011). In our study, all phytohormones, except GA, significantly decreased an endogenous NO burst triggered by photovoltaic adaptation, especially under an SA treatment. SA might also be a potent scavenger of NO and counter the restoration effect of NO on growth and photosynthetic potential in *T. hemsleyanum*.

To sum up, maintaining hormone homeostasis is a pressing challenge for plants under stress conditions, the NO crosstalk with various phytohormones in plant growth regulation in response to stress conditions is ever-present and very complicated, and our knowledge of crosstalk signaling pathways is fragmentary so far, most known signaling have not been connected to stress sensors. NO influences on the transcriptional regulation of gene encoding hormone-associated proteins are far from being clarified. Further, the large number of potential targets of NO action would be an important challenge for future research on the signaling networks of NO–phytohormone crosstalk in plant responses to environment, which would reveal new ideas to manipulate the responses of plant to adverse environmental conditions under the background of global climate change.

DATA AVAILABILITY STATEMENT

The datasets presented in this study can be found in online repositories. The names of the repository/repositories and accession number(s) can be found in the article/**Supplementary Material**.

AUTHOR CONTRIBUTIONS

XP and LG conceived the study. ML performed GO and KEGG pathways enrichment analysis and designed the experiments.

ZX performed physiological indicators determination and endogenous hormone determination. CY performed RNA extraction and quality determination. ZZ and YW carried out the analysis. All authors have read and approved the manuscript.

FUNDING

This work was supported by the National Natural Science Foundation of China (81903743), the China Postdoctoral Science Special Foundation (2019T120552), the Major Science and Technology Projects of Breeding New Varieties of Agriculture in Zhejiang Province (2021C02074), and the Ningbo City Science and Technology Innovation 2025 Major Research Project (2019B10008).

SUPPLEMENTARY MATERIAL

The Supplementary Material for this article can be found online at: https://www.frontiersin.org/articles/10.3389/fpls.2022.852956/full#supplementary-material

Supplementary Table 1 | All phytohormones identified in *Tetrastigma. hemsleyanum* in GZ and GF groups.

Supplementary Table 2 | All differentially accumulated genes encoding multiple enzymes in plant hormone signal transduction pathway between GZ vs. GF group.

Supplementary Table 3 | All differentially expressed genes (DEGs) encoding multiple well-known proteins or enzymes in the chlorophyll and photosystem biosynthesis and metabolism pathway between GZ vs. GF group.

Supplementary Table 4 | All DEGs encoding proteins involved in photosystem I (PS I) and photosystem II (PS II) reaction center between GZ vs. GF group.

REFERENCES

Allardyce, C. S., Fankhauser, C., Zakeeruddin, S. M., Grätzel, M., and Dyson, P. J. (2017). The influence of greenhouse-integrated photovoltaics on crop production. *Sol. Energy* 155, 517–522. doi: 10.1016/j.solener.2017.06.044

Alsadon, A., Al-Helal, I., Ibrahim, A., Abdel-Ghany, A., Al-Zaharani, S., Ashour, T., et al. (2016). The effects of plastic greenhouse covering on cucumber (*Cucumis sativus* L.) growth. *J. Ecol. Eng.* 87, 305–312. doi: 10.1016/j.ecoleng.2015.12.005

Campos, F. V., Oliveira, J. A., Pereira, M. G., and Farnese, F. S. (2019). Nitric oxide and phytohormone interactions in the response of *Lactuca sativa* to salinity stress. *Planta* 250, 1475–1489. doi: 10.1007/s00425-019-03236-w

Cossu, M., Murgia, L., Ledda, L., Deligios, P. A., Sirigu, A., Chessa, F., et al. (2014). Solar radiation distribution inside a greenhouse with south-oriented photovoltaic roofs and effects on crop productivity. *Appl. Energy* 133, 89–100. doi: 10.1016/j.apenergy.2014.07.070

Ezzaeri, K., Fatnassi, H., Bouharroud, R., Gourdo, L., and Bouirden, L. (2018). The effect of photovoltaic panels on the micro-climate and on the tomato production under photovoltaic Canarian greenhouses. *Sol. Energy* 173, 1126–1134. doi: 10.1016/j.solener.2018.08.043

Fan, Q. J., and Liu, J. H. (2012). Nitric oxide is involved in dehydration/drought tolerance in *Poncirus trifoliata* seedlings through regulation of antioxidant systems and stomatal response. *Plant Cell Rep.* 31, 145–154. doi: 10.1007/s00299-011-1148-1

Farnese, F. S., Menezes-Silva, P. E., Gusman, G. S., and Oliveira, J. A. (2016). When bad guys become good ones: the key role of reactive oxygen species and nitric oxide in the plant responses to abiotic stress. *Front. Plant Sci.* 7:471. doi: 10.3389/fpls.2016.00471

Farnese, F. S., Oliveira, J. A., Paiva, E. A. S., Menezes-Silva, P. E., Silva, A. A., Campos, F. V., et al. (2017). The involvement of nitric oxide in integration of plant physiological and ultrastructural adjustments in response to arsenic. *Front. Plant Sci.* 8:516. doi: 10.3389/fpls.2017.00516

Fatima, A., Husain, T., Suhel, M., Prasad, S. M., and Singh, V. P. (2021). Implication of nitric oxide under salinity stress: the possible interaction with other signaling molecules. *J. Plant Growth Regul.* 41, 163–177. doi: 10.1007/s00344-020-10255-5

Freschi, L. (2013). Nitric oxide and phytohormone interactions: current status and perspectives. *Front. Plant Sci.* 4:398. doi: 10.3389/fpls.2013.00398

Gadelha, C. G., Miranda, R. D. S., Alencar, N. L. M., Costa, J. H., Prisco, J. T., Gomes-Filho, E., et al. (2017). Exogenous nitric oxide improves salt tolerance during establishment of *Jatropha curcas* seedlings by ameliorating oxidative damage and toxic ion accumulation. *J. Plant Physiol.* 212, 69–79. doi: 10.1016/j.jplph.2017.02.005

Hu, L., Zhou, K., Li, Y., Chen, X., Liu, B., Li, C., et al. (2018). Exogenous *myo*-inositol alleviates salinity-induced stress in *Malus hupehensis* Rehd. *Plant Physiol. Biochem.* 133, 116–126. doi: 10.1016/j.plaphy.2018.10.037

Jahan, M. S., Sheng, S., Yu, W., Zheng, C., and Guo, S. (2019). Melatonin alleviates heat-induced damage of tomato seedlings by balancing redox homeostasis and modulating polyamine and nitric oxide biosynthesis. *BMC Plant Biol.* 19:414. doi: 10.1186/s12870-019-1992-7

Ji, T., Ji, W. W., Wang, J., Chen, H. J., Peng, X., Cheng, K. J., et al. (2021). A comprehensive review on traditional uses, chemical compositions, pharmacology properties and toxicology of *Tetrastigma hemsleyanum*. *J. Ethnopharmacol.* 264:113247. doi: 10.1016/j.jep.2020.113247

Kaya, C., and Ashraf, M. (2021). Nitric oxide is required for aminolevulinic acid-induced salt tolerance by lowering oxidative stress in maize (*Zea mays*). *J. Plant Growth Regul.* 40, 617–627. doi: 10.1007/s00344-020-10126-z

Khokon, M., Okuma, E. I., Hossain, M. A., Munemasa, S., Uraji, M., Nakamura, Y., et al. (2011). Involvement of extracellular oxidative burst in salicylic acid-induced stomatal closure in *Arabidopsis*. *Plant Cell Environ.* 34, 434–443. doi: 10.1111/j.1365-3040.2010.02253.x

Klein, A., Hüsselmann, L., Keyster, M., and Ludidi, N. (2018). Exogenous nitric oxide limits salt-induced oxidative damage in maize by altering superoxide dismutase activity. *S. Afr. J. Bot.* 115, 44–49. doi: 10.1016/j.sajb.2017.12.010

Krasuska, U., Ciacka, K., and Gniazdowska, A. (2017). Nitric oxide-poly-amines cross-talk during dormancy release and germination of apple embryos. *Nitric Oxide* 68, 8–50. doi: 10.1016/j.niox.2016.11.003

Lemarié, S., Guérin, V., Sakr, S., Jouault, A., and Peilleron, F. (2018). Impact of innovative optically active greenhouse films on melon, watermelon, raspberry and potato crops. *Acta Hortic.* 1252, 191–200. doi: 10.17660/ActaHortic.2019.1252.25

Li, W. Q., Challa, G. S., Gupta, A., Gu, L. P., Wu, Y. J., and Li, W. L. (2021). Physiological and transcriptomic characterization of sea-wheatgrass-derived waterlogging tolerance in wheat. *Plants* 11:108. doi: 10.3390/plants11010108

Liu, S., Dong, Y., Xu, L., and Kong, J. (2014). Effects of foliar applications of nitric oxide and salicylic acid on salt-induced changes in photosynthesis and antioxidative metabolism of cotton seedlings. *Plant Growth Regul.* 73, 67–78.

Love, M. I., Huber, W., and Anders, S. (2014). Moderated estimation of fold change and dispersion for RNA-seq data with DESeq2. *Genome Biol.* 15:550. doi: 10.1186/s13059-014-0550-8

Lozano-Juste, J., and León, J. (2011). Nitric oxide regulates DELLA content and PIF expression to promote photomorphogenesis in Arabidopsis. *Plant Physiol.* 156, 1410–1423. doi: 10.1104/pp.111.177741

Manjunatha, G., Lokesh, V., and Neelwarne, B. (2010). Nitric oxide in fruit ripening: trends and opportunities. *Biotechnol. Adv.* 28, 489–499. doi: 10.1016/j.biotechadv.2010.03.001

Mishina, T. E., Lamb, C., and Zeier, J. (2007). Expression of a nitric oxide degrading enzyme induces a senescence programme in *Arabidopsis*. *Plant Cell Environ.* 30, 39–52. doi: 10.1111/j.1365-3040.2006.01604.x

Naser, A. S. M., Arvin, M. J., and Manoochehri, K. K. (2014). Salicylic acid and nitric oxide alleviate osmotic stress in wheat (*Triticum aestivum* L.) seedlings. *J. Plant Interact.* 9, 683–688. doi: 10.1080/17429145.2014.900120

Nawaz, F., Shabbir, R. N., Shahbaz, M., Majeed, S., and Sohail, M. A. (2017). "Cross talk between nitric oxide and phytohormones regulate plant development during abiotic stresses," in *Phytohormones: Signaling Mechanisms and Crosstalk in Plant Development and Stress Responses*, ed. M. A. El-Esawi (Rijeka: InTech), 117–141. doi: 10.5772/intechopen.69812

Neill, S. J., Desikan, R., Clarke, A., and Hancock, J. T. (2002). Nitric oxide is a novel component of abscisic acid signaling in stomatal guard cells. *Plant Physiol.* 128, 13–16. doi: 10.1104/pp.128.1.13

Peng, X., Wu, H., Chen, H., Zhang, Y., Qiu, D., and Zhang, Z. (2019). Transcriptome profiling reveals candidate flavonol-related genes of *Tetrastigma hemsleyanum* under cold stress. *BMC Genomics* 20:687. doi: 10.1186/s12864-019-6045-y

Procházková, D., Haisel, D., Wilhelmová, N., Pavlíková, D., and Száková, J. (2013). Effects of exogenous nitric oxide on photosynthesis. *Photosynthetica* 51, 483–489. doi: 10.1007/s11099-013-0053-y

Recalde, L., Vázquez, A., Groppa, M. D., and Benavides, M. P. (2018). Reactive oxygen species and nitric oxide are involved in polyamine-induced growth inhibition in wheat plants. *Protoplasma* 255, 1295–1307. doi: 10.1007/s00709-018-1227-z

Romero-Puertas, M. C., Perazzolli, M., Zago, E. D., and Delledonne, M. (2004). Nitric oxide signalling functions in plant-pathogen interactions. *Cell. Microbiol.* 6, 795–803. doi: 10.1111/j.1462-5822.2004.00428.x

Simaei, M., Khavarinejad, R. A., Saadatmand, S., Bernard, F., and Fahimi, H. (2011). Interactive effects of salicylic acid and nitric oxide on soybean plants under NaCl salinity. *Russ. J. Plant Physiol.* 58, 783–790. doi: 10.1134/s1021443711050220

Singhal, R. K., Jatav, H. S., Aftab, T., Pandey, S., Mishra, U. N., Chauhan, J., et al. (2021). Roles of nitric oxide in conferring multiple abiotic stress tolerance in plants and crosstalk with other plant growth regulators. *J. Plant Growth Regul.* 40, 2303–2328. doi: 10.1007/s00344-021-10446-8

Wang, H., Xiao, W., Niu, Y., Chai, R., Jin, C., and Zhang, Y. (2015). Elevated carbon dioxide induces stomatal closure of *Arabidopsis thaliana* (L.) Heynh. Through an increased production of nitric oxide. *J. Plant Growth Regul.* 34, 372–380. doi: 10.1007/s00344-014-9473-6

Wu, A. P., Gong, L., Chen, X., and Wang, J. X. (2014). Interactions between nitric oxide, gibberellic acid, and phosphorus regulate primary root growth in *Arabidopsis*. *Biol. Plant.* 58, 335–340.

Wu, X., Liu, Z., and Liao, W. (2021). The involvement of gaseous signaling molecules in plant MAPK cascades: function and signal transduction. *Planta* 254:127. doi: 10.1007/s00425-021-03792-0

Xiao-Ping, S., and Xi-Gui, S. (2010). Cytokinin-and auxin-induced stomatal opening is related to the change of nitric oxide levels in guard cells in broad bean. *Physiol. Plant.* 128, 569–579. doi: 10.1111/j.1399-3054.2006.00782.x

Xu, J., Wang, W., Sun, J., Zhang, Y., Ge, Q., Du, L., et al. (2011). Involvement of auxin and nitric oxide in plant Cd-stress responses. *Plant Soil* 346, 107–119. doi: 10.1007/s11104-011-0800-4

Xu, L., Song, J. Q., Wang, Y. L., Liu, X. H., Li, X. L., Zhang, B., et al. (2022). Thymol improves salinity tolerance of tobacco by increasing the sodium ion efflux and enhancing the content of nitric oxide and glutathione. *BMC Plant Biol.* 22:31. doi: 10.1186/s12870-021-03395-7

Yuan, H. M., and Huang, X. (2016). Inhibition of root meristem growth by cadmium involves nitric oxide-mediated repression of auxin accumulation and signalling in Arabidopsis. *Plant Cell Environ.* 39, 120–135. doi: 10.1111/pce.12597

Zhao, H. C., Qian, R. Y., Liang, X., Ou, Y., Sun, C. L., and Lin, X. Y. (2022). Indium induces nitro-oxidative stress in roots of wheat (*Triticum aestivum*). *J. Hazard. Mater.* 428:128260. doi: 10.1016/j.jhazmat.2022.128260

Zhou, X., Joshi, S., Patil, S., Khare, T., and Kumar, V. (2021a). Reactive oxygen, nitrogen, carbonyl and sulfur species and their roles in plant abiotic stress responses and tolerance. *J. Plant Growth Regul.* 41, 1–24. doi: 10.1007/s00344-020-10294-y

Zhou, X., Joshi, S., Khare, T., Patil, S., and Kumar, V. (2021b). Nitric oxide, crosstalk with stress regulators and plant abiotic stress tolerance. *Plant Cell Rep.* 40, 1395–1414. doi: 10.1007/s00299-021-02705-5

Conflict of Interest: The authors declare that the research was conducted in the absence of any commercial or financial relationships that could be construed as a potential conflict of interest.

Publisher's Note: All claims expressed in this article are solely those of the authors and do not necessarily represent those of their affiliated organizations, or those of the publisher, the editors and the reviewers. Any product that may be evaluated in this article, or claim that may be made by its manufacturer, is not guaranteed or endorsed by the publisher.

Copyright © 2022 Xie, Yang, Li, Zhang, Wu, Gu and Peng. This is an open-access article distributed under the terms of the Creative Commons Attribution License (CC BY). The use, distribution or reproduction in other forums is permitted, provided the original author(s) and the copyright owner(s) are credited and that the original publication in this journal is cited, in accordance with accepted academic practice. No use, distribution or reproduction is permitted which does not comply with these terms.

frontiers | Frontiers in Plant Science

REVIEW
published: 08 April 2022
doi: 10.3389/fpls.2022.877304

Environmental and Genetic Factors Involved in Plant Protection-Associated Secondary Metabolite Biosynthesis Pathways

Xiaori Zhan[1,2], Zhehao Chen[1], Rong Chen[3] and Chenjia Shen[1,2]**

[1] College of Life and Environmental Sciences, Hangzhou Normal University, Hangzhou, China, [2] Zhejiang Provincial Key Laboratory for Genetic Improvement and Quality Control of Medicinal Plants, Hangzhou Normal University, Hangzhou, China, [3] School of Public Health, Hangzhou Normal University, Hangzhou, China

Plant specialized metabolites (PSMs) play essential roles in the adaptation to harsh environments and function in plant defense responses. PSMs act as key components of defense-related signaling pathways and trigger the extensive expression of defense-related genes. In addition, PSMs serve as antioxidants, participating in the scavenging of rapidly rising reactive oxygen species, and as chelators, participating in the chelation of toxins under stress conditions. PSMs include nitrogen-containing chemical compounds, terpenoids/isoprenoids, and phenolics. Each category of secondary metabolites has a specific biosynthetic pathway, including precursors, intermediates, and end products. The basic biosynthetic pathways of representative PSMs are summarized, providing potential target enzymes of stress-mediated regulation and responses. Multiple metabolic pathways share the same origin, and the common enzymes are frequently to be the targets of metabolic regulation. Most biosynthetic pathways are controlled by different environmental and genetic factors. Here, we summarized the effects of environmental factors, including abiotic and biotic stresses, on PSM biosynthesis in various plants. We also discuss the positive and negative transcription factors involved in various PSM biosynthetic pathways. The potential target genes of the stress-related transcription factors were also summarized. We further found that the downstream targets of these Transcription factors (TFs) are frequently enriched in the synthesis pathway of precursors, suggesting an effective role of precursors in enhancing of terminal products. The present review provides valuable insights regarding screening targets and regulators involved in PSM-mediated plant protection in non-model plants.

Keywords: abiotic stress, biotic stress, plant specialized metabolites, plant protection, transcription factor

OPEN ACCESS

Edited by:
Zhihua Liao,
Southwest University, China

Reviewed by:
Qian Shen,
Shanghai Jiao Tong University, China
Guoyin Kai,
Zhejiang Chinese Medical University, China

****Correspondence:***
Chenjia Shen
shencj@hznu.edu.cn
Rong Chen
rongchen1984@hznu.edu.cn

Specialty section:
This article was submitted to Plant Metabolism and Chemodiversity, a section of the journal Frontiers in Plant Science

Received: *16 February 2022*
Accepted: *14 March 2022*
Published: *08 April 2022*

Citation:
Zhan X, Chen Z, Chen R and Shen C (2022) Environmental and Genetic Factors Involved in Plant Protection-Associated Secondary Metabolite Biosynthesis Pathways. Front. Plant Sci. 13:877304. doi: 10.3389/fpls.2022.877304

INTRODUCTION

The ability of plants to synthesize an extremely wide arsenal of diverse metabolites makes them preeminent chemists (Fernie et al., 2004). Traditionally, plant metabolites are classified into two groups: primary and secondary (Patra et al., 2013). Primary metabolites are ubiquitous in all plants and play crucial housekeeping roles in plant growth and development (Fabregas and Fernie, 2021).

Secondary metabolites, also called plant specialized metabolites (PSMs), are involved in various physiological and biochemical processes, such as defense and adaptation to adverse environments (Chapman et al., 2019; Sic Zlabur et al., 2021). With the development of detection technology, more PSMs have been identified and characterized in plants.

On the basis of their core structures, PSMs form three major categories: nitrogen-containing chemical compounds, terpenoids/isoprenoids, and phenolics (Marone et al., 2022). Nitrogen-containing compounds, consisting of cyanogenic glycosides, alkaloids, and glucosinolates, have been widely identified in natural plant products and synthetic compounds (Aharoni and Galili, 2011). Terpenoids/isoprenoids can be divided into five subgroups: monoterpenes, sesquiterpenes, diterpenes, triterpenes, and tetraterpenes, on the basis of the number of isoprene structural units (Bohlmann et al., 1998). Phenolics, containing at least one aromatic ring and one hydroxyl group, can be divided into four functional classes: phenolic acids, flavonoids, tannins, and stilbenes (Aharoni and Galili, 2011; Rasouli et al., 2016). Most of PSMs are produced by individual metabolic pathways and unequally accumulate in different tissues and organs. The structural complexity and uneven distribution ensure different biological functions of PSMs under changing environmental conditions (Desmet et al., 2021).

The roles of PSMs in human health and their potential as pharmaceutical drugs have been studied extensively (Hamilton, 2004; Tungmunnithum et al., 2018). Medicinal plants produce valuable PSM-derived drugs, such as, taxol from *Taxus media,* quinine from *Cinchona officinalis,* withanolide from *Physalis angulate*, and artemisinin from *Artemisia annua*, are widely applied in the treatment of a variety of serious diseases (Ravishankara et al., 2001; Zhan et al., 2018; Shi et al., 2021; Wani et al., 2021; Yu et al., 2021). In plants, PSMs are essential for several physiological processes, such as plant protection, pollinator attraction, signal transduction, and seed germination, which are required for their survival in harsh environments (Chae et al., 2014; Liu et al., 2021d; Singh et al., 2021; Wari et al., 2021).

Plant specialized metabolites contribute to plant protection against different types of biotic and abiotic stresses, similar to the adaptive immune system in animals (Castro-Moretti et al., 2020; Desmet et al., 2021). To adapt to stress conditions, plants gear their metabolism toward the biosynthesis of PSMs, which, although energy-costly, is beneficial for their survival (Abdala-Roberts et al., 2016). PSMs serve in various parts of a complete plant defense system, acting as message molecules and/or antioxidants (Kumar and Pandey, 2013). Some PSMs act as key components of complex signaling pathways and trigger both the extensive expression of defense-related genes and the accumulation of other metabolites (Maag et al., 2015). Other PSMs serve as antioxidants, participating in the scavenging of rapidly rising reactive oxygen species (ROS) and in the chelation of heavy-metal ions under stress conditions (Pacifico et al., 2021). They not only act as powerful antioxidants, they may also be toxic to herbivores, microbial pathogens, and competing plant species (Glas et al., 2012). Overall, some of the credit for a plant's capability to tolerate or adapt to a changing environment goes to PSMs. The purpose of this review is to summarize the basic biosynthetic pathways of protection-related PSMs on a limited scale. Furthermore, the environmental and genetic factors involved in the biosynthesis of PSMs are also briefly summarized.

BASIC BIOSYNTHETIC PATHWAY OF PLANT SPECIALIZED METABOLITES

There are more than 400,000 vascular plants with up to one million metabolites on the Earth (Fang et al., 2019). Although there are many PSMs, their chemical structures are not random (Fernie et al., 2004). The vast majority of PSMs are variations on a core derived from several typical backbones having structural modifications, such as glycosylation, acylation, methylation, hydroxylation, and prenylation (Wang et al., 2019c). On the basis of the representative structures, PSMs can be grouped into major classes, such as nitrogen-containing compounds, terpenoids, and phenolics (D'Auria and Gershenzon, 2005). Here, we summarize the basic biosynthetic pathways of representative PSMs and attempt to better understand the potential targets of stress-mediated regulation.

Key Enzymes Involved in the Biosynthesis of Alkaloids

Alkaloids originally consisted of a large class of heterocyclic nitrogen-containing organic compounds (Zhang et al., 2021b). The nitrogen atom in the heterocyclic ring generally originates from an amino acid. On the basis of their amino acid precursors and chemical structures, alkaloids are classified into five subgroups: terpenoid indole alkaloids (TIAs), benzylisoquinoline alkaloids (BIAs), tropine alkaloids, purine alkaloids, and pyrrolizidine alkaloids (Bhambhani et al., 2021). From precursors to final products, a series of biochemical modification reactions occur during the different alkaloidal conversion steps, ensuring diverse arrays of chemical structures and biological activities (Lichman, 2021; Zhang et al., 2021c). The present review uses TIA and BIA as examples to investigate the complexity of alkaloid biosynthesis.

Terpenoid indole alkaloids are a class of PSMs found in various non-model medicinal plants, such as *Catharanthus roseus*, *Rauvolfia serpentina*, *Ophiorrhiza pumila,* and *Vinca minor* (Luijendijk et al., 1996; Schlager and Drager, 2016; Shi et al., 2020a; Zhan et al., 2020; Yang et al., 2021a; Vrabec et al., 2022). *Catharanthus roseus* is frequently used as the model plant to reveal a complete TIA biosynthetic pathway (O'Connor and Maresh, 2006). Strictosidine, a key skeleton unique to TIAs, is synthesized by strictosidine synthase with tryptamine, an indole ring donor derived from decarboxylated tryptophan, and secologanin, a terpenoid donor from the methylerythritol 4-phosphate (MEP) pathway (Moreno et al., 1993; Rai et al., 2013; Kumar et al., 2015). A series of key enzymes, including geraniol synthase, geraniol 10-hydroxylase, 10-hydroxygeraniol oxidoreductase, iridoid synthase, iridoid oxidase, 7-deoxyloganetic acid glucosyltransferase, 7-deoxyloganic acid, loganic acid-O-methyltransferase, and secologanin synthase, are involved in TIA skeleton biosynthesis

(Geu-Flores et al., 2012; Simkin et al., 2013; Shen et al., 2017; Sandholu et al., 2020; Jeena et al., 2021). Then, the intermediate strictosidine is modified by different enzymes to produce species-specific TIAs (Qu et al., 2018; Williams et al., 2019). As detection technology progresses, more novel TIAs and TIA-related enzymes are being identified in different plant species.

Benzylisoquinoline alkaloids are also members of a structurally diverse class of PSMs that mainly exist in the *Ranunculales* order (Ziegler and Facchini, 2008). The biosynthesis of BIAs starts with dopamine and 4-hydroxyphenylacetaldehyde, a tyrosine derivative, to produce a fundamental precursor trihydroxylated alkaloid (*S*)-norcoclaurine by norcoclaurine synthase (Sheng and Himo, 2019). *O*-methylation, *N*-methylation, and hydroxylation successively occur on 4-hydroxyphenylacetaldehyde to synthetize (*S*)-3′-hydroxy-*N*-methylcoclaurine (Liu et al., 2021c). The conversion of (*S*)-3′-hydroxy-*N*-methylcoclaurine to (*S*)-reticuline, a branch-point product, in the production of morphine, tetrahydropalmatine, sanguinarine, and noscapine, is conducted by 3′-hydroxy-*N*-methylcoclaurine 4′-hydroxylase (He et al., 2018). Finally, cytochrome P450 superfamily proteins are responsible for several modification reactions, such as hydroxylation, isomerization, and coupling, on the BIA backbone that produce species-specific BIAs (Hori et al., 2018; Menendez-Perdomo and Facchini, 2018).

Key Enzymes Involved in the Biosynthesis of Glucosinolates

As a class of wound-induced PSMs, glucosinolates highly accumulate in the Brassicaceae family of plants (Sanchez-Pujante et al., 2017). Most of glucosinolates can be grouped into three major subgroups, aliphatic, indole-, and aromatic glucosinolates, on the basis of their amino acid features (Ishida et al., 2014). The complete biosynthetic pathway of glucosinolates in *Brassica* genus consists of three steps: side-chain elongation, core structure formation, and side-chain secondary modifications (Sotelo et al., 2016).

During side-chain elongation, aliphatic and aromatic amino acids are utilized to produce 2-oxo acids by branched-chain amino acid aminotransferase family enzymes. Then, 2-oxo acid and acetyl-CoA are condensed by methylthioalkylmalate synthase (Kochevenko et al., 2012). Side-chain elongation ends with an isomerization process and an oxidative decarboxylation by isopropylmalate isomerase and isopropylmalate dehydrogenase, respectively (Sanchez-Pujante et al., 2017). To produce the core structure of glucosinolates, the conversion of side-chain-elongated amino acids to aldoximes is catalyzed by cytochrome P450 mono-oxygenases, such as CYP79 and CYP83, to produce *S*-alkyl-thiohydroximate and thiohydroximate (Robin et al., 2016). Then, thiohydroximate is catalyzed to form the glucosinolate core structure by two key enzymes, uridine diphosphate glycosyltransferase 74 and sulfotransferases (Sonderby et al., 2010; Robin et al., 2016). Finally, side-chain modifications, such as oxidation, hydroxylation, methoxylation, alkenylation, and benzoylation, are required for the formation of the terminal glucosinolate products (Halkier and Gershenzon, 2006; Nguyen et al., 2020).

Key Enzymes Involved in the Biosynthesis of Terpenoids

Terpenoids are a structurally diverse group of PSMs in which each member has a core isoprene unit. The central core of the terpenoids is synthesized by one-unit dimethylallyl diphosphate (DMAPP) and three-units isopentenyl diphosphates (IPP) (Yu et al., 2017). Both DMAPP and IPP originate from the MEP pathway, occurring in the plastids, and from the mevalonate pathway, occurring in the cytoplasm, endoplasmic reticulum, and peroxisomes (Mahmoud et al., 2021).

Here, we take model plant *Arabidopsis* as an example. Isopentenyl phosphate kinase, common to most plants, catalyzes the conversion of isopentenyl monophosphate and dimethylallyl monophosphate to IPP and DMAPP (Henry et al., 2015). In plants, there is a classic upstream pathway that forms prenyl diphosphates having varied chain lengths, such as geranyl diphosphate (GPP), having 10 isoprene units, farnesyl diphosphate (FPP), having 15 isoprene units, and geranylgeranyl diphosphate (GGPP), having 20 isoprene units (Tholl, 2015; Jia and Chen, 2016). Next, terpene synthases participate in the conversion of FPP, GGPP, and GPP into mono-/sesquiterpenes (Pichersky and Raguso, 2018; Zhou and Pichersky, 2020). Two units of FPP and one unit of GGPP can be condensed by squalene synthase to produce squalene and by phytoene synthase to produce phytoene, which are the precursors of sterols and carotenoids, respectively (Christianson, 2017). Thousands of different terpenoids having the same core skeleton are produced by various modifications, such as hydroxylation, dehydrogenation, reduction, glycosylation, methylation, and acylation (Liu et al., 2022a).

Key Enzymes Involved in the Biosynthesis of Phenolics

Phenolic Acids

Phenolic acids are important active ingredients in numerous medicinal plants (Chen et al., 2021b). Bioactivities, biosynthesis and biotechnological production of phenolic acids have been well revealed in *Salvia miltiorrhiza* (Shi et al., 2019). On the basis of the number aromatic ring structures, phenolic acids can be classified into different groups (Choi et al., 2021). Taking *S. miltiorrhiza* as an example, most phenolic acids are synthesized through the phenylpropanoid and tyrosine metabolic pathways (Wang et al., 2015). In the phenylpropanoid pathway, phenylalanine is treated as a substrate to produce cinnamic acid by phenylalanine ammonia-lyase (PAL) (Reyes Jara et al., 2022). Then, cinnamic acid is catalyzed to *p*-coumaroyl-CoA by two enzymes, cinnamic acid 4-hydroxylase (C4H), and 4-coumarate: CoA ligase (Huang et al., 2008). In the tyrosine pathway, tyrosine aminotransferase and hydroxyphenylpyruvate reductase are involved in the conversion of tyrosine to 3,4-dihydroxyphenyllactic acid (Rizi et al., 2021).

Subsequently, rosmarinic acid, an important precursor for downstream species-specific phenolic acids, is synthetized by

rosmarinic acid synthase and cytochrome P450-dependent monooxygenase CYP98A14 (Deng et al., 2020b; Chen et al., 2021b). Over-expression of rosmarinic acid synthase and CYP98A14 resulted in higher content of phenolic acids in *S. miltiorrhiza* hairy roots (Fu et al., 2020).

Flavonoids

Flavonoids are a class of water-soluble pigments stored in the cell vacuoles (Dong and Lin, 2021). In plants, more than 9,000 flavonoids have been identified and classified into different groups on the basis of the number of hydroxyl/methyl groups on their heterocyclic or benzene ring (Noda et al., 2017). As phenolics, flavonoids also originated from the phenylpropanoid pathway (Wang et al., 2018b). Specific flavonoid biosynthesis starts with the conversion of *p*-coumaroyl-CoA, together with malonyl-CoA and acetyl-CoA, to naringenin chalcone by chalcone synthase, which is the first rate-limiting enzyme in the flavonoid biosynthetic pathway (Zhang et al., 2017). Naringenin chalcone, a basic skeleton for the downstream pathway, is converted to naringenin by the catalysis of chalcone isomerase, or it is converted to naringenin chalcone 2'-glucoside by the catalysis of chalcone 2'-glucosyltransferase (Miyahara et al., 2018).

Chalcone is a central intermediate product in different branch pathways, such as the flavanone biosynthesis, flavone biosynthesis, isoflavone biosynthesis, and flavonol biosynthesis (Liu et al., 2021b). In the cytoplasm, chalcone isomerase participates in the cyclization of chalcones to produce flavanones, opening a route to the heterocyclic C-ring-containing flavonoids (Nabavi et al., 2020). In addition, naringenin is the precursor for eriodictyol biosynthesis by flavanone 3′-hydroxylase catalysis, and for pentahydroxyflavanone biosynthesis by flavanone 3′,5′-hydroxylase catalysis (Grotewold, 2006). Flavone biosynthesis is another branch of the flavonoid biosynthetic pathway. Flavone synthase catalyzes the conversion of flavanones to flavones, such as apigenin, dihydroxyflavone, luteolin, and tricetin (Zuk et al., 2019). Flavanones can also be converted to apigenin *C*-glycosides and luteolin *C*-glycosides by flavanone-2-hydroxylase (Lam et al., 2019).

Multiple metabolic pathways have the same origin, and the common enzymes are frequently to be the targets of metabolic regulation. The MEP pathway provides common precursors for the TIA biosynthesis and terpenoid biosynthesis pathways. The phenylalanine pathway provided common precursors for the phenolic acid biosynthesis and flavonoid biosynthesis pathways. Manipulation of these common enzymes affects multiple metabolic pathways to response to environmental stresses.

EFFECTS OF ENVIRONMENTAL FACTORS ON PLANT SPECIALIZED METABOLITES BIOSYNTHESIS

The synthesis and tissue-specific accumulation of PSMs are strictly controlled in spatio-temporal mode and affected by various biotic and abiotic factors (Yang et al., 2012). Environmental stresses influence the formation and accumulation of PSMs in plants (Gupta and Dutta, 2011).

Effects of Environmental Factors on Alkaloid Biosynthesis

Over a hundred TIAs, such as bisindole alkaloids, have been detected in the medicinal plant *C. roseus* (Shukla et al., 2006). *Catharanthus roseus* seedlings under drought- and salinity-stress conditions exhibit a greatly higher alkaloid content compared with under control conditions (Hassan et al., 2021; Yahyazadeh et al., 2021). Furthermore, the impact of drought and salt stresses on the biosynthesis and accumulation of alkaloids, such as dihydrocoptisine, has also been revealed in *Chelidonium majus* (Yahyazadeh et al., 2018). Cadmium chloride elicitation increases the yields of reserpine and ajmalicine, two important MIAs, in the endangered medicinal plant *Rauvolfia serpentina* (Zafar et al., 2020).

Under herbivore attack, the biosynthesis of physostigmine, an approved antiherbivore alkaloid, rapidly increases in the damaged area (Rivero et al., 2021). Various stresses elevate the content of a mixture of toxic pyrrolizidine alkaloids in *Echium plantagineum* plants, protecting them from insect and livestock herbivory (Skoneczny et al., 2019). Aphid predation induces the biosynthesis of quinolizidine alkaloids, a type of toxic secondary metabolites produced in lupin species (Frick et al., 2019). As a type of PSM, both of biotic and abiotic stresses up-regulate the content of alkaloids, suggesting their important roles of in resistance to environmental stress.

Effects of Environmental Factors on Glucosinolate Biosynthesis

Glucosinolates are important precursors to various active ingredients in the Brassicaceae family of plants (Moreno et al., 2006). In pak choi (*Brassica rapa*), strong light, high-temperature, and drought increase the accumulation of glucosinolates (Park et al., 2021; Rao et al., 2021). *Brassica oleracea* has a powerful tolerance to chilling and freezing, and the low temperature-induced content of glucosinolates is hypothesized to be involved in the protective mechanism that enables this tolerance (Ljubej et al., 2021). In addition to low temperature, other postharvest stresses, such as wounding, also induce the biosynthesis of glucosinolates in *B. oleracea* (Villarreal-Garcia et al., 2016). In *Broccoli* sprouts, both of UV-A and UV-B light doses affect the tailored glucosinolate and phenolic profiles, suggesting an important role for light stress in glucosinolate biosynthesis (Moreira-Rodriguez et al., 2017).

Biotic stresses also can influence the glucosinolate composition in plants. The aphid-induced expression of *CYP79B2*, *CYP79B3*, and *PAD33* leads to the accumulation of indolyl glucosinolates (Mewis et al., 2012). A gain-of-function *Arabidopsis* mutant, *cml42*, with a higher aliphatic glucosinolate content than the wild type, shows a strong resistance to herbivory (Vadassery et al., 2012).

Effects of Environmental Factors on Terpenoid Biosynthesis

Terpenoids play frequent roles in plant protection in the form of phytohormones, particularly as diterpene gibberellins, triterpene brassinosteroids (BRs), and sesquiterpene abscisic acid (ABA)

(Patra et al., 2013; Chen et al., 2021a; Liu et al., 2021a). In lettuce, long-term high temperature expose facilitates the accumulation of gibberellin to accelerate bolting (Liu et al., 2020). Under drought-stress conditions, significant accumulations of ABA occur in wheat guard cells (Wang et al., 2021). In maize sprouts, NaCl stress greatly increases the content of carotenoid, which is a typical tetraterpenoid with an intense antioxidant capacity, by up-regulating the expression of several carotenoid biosynthetic pathway genes (He et al., 2021). In winter wheat, cold treatments elevate the endogenous BR content, indicating a role of triterpene BR in improving the cold tolerance of winter cereals (Janeczko et al., 2019).

Biotic stresses can also influence the terpenoid contents of plants. In various Iranian cultivars of basil, water-deficit stress enhances the accumulations of linalool, germacrene D, and γ-cadinene, three important aromatic terpenes with verified cytotoxic activities (Khakdan et al., 2021). The ability to synthesize specialized antimicrobial avenacins, belonging to the triterpenoids, is likely to have allowed oats (*Avena* spp.) to combat various diseases (Qi et al., 2004). Terpenoids are rich in *Euphorbia peplus* latex and function as defensive chemical substances against insect herbivores and various agricultural phytopathogenic fungi (Hua et al., 2017).

A large number of works showed that terpenoids are involved in the resistance to environmental stress in the form of phytohormones. Phytohormones, as signal molecules, transmit environmental signals to plant cells.

Effects of Environmental Factors on Phenolic Acid Biosynthesis

The biosynthesis of phenolic compounds is significantly affected by various abiotic stress conditions (Sharma et al., 2019). In many inbred maize lines, long-term drought treatments cause significant reductions in various phenolic acids, such as protocatechuic, caffeic, and sinapic (Kravic et al., 2021). In Chinese cabbage, salt stress leads to great decreases in phenolic compounds, such as sinapic acid, salicylic acid, and ferulic acid (Linic et al., 2021). Under alkaline conditions, rice enhances phenolic acid secretions in the root epidermis and stele, which effectively increases ion uptake and alleviates the Fe-deficiency responses (Li et al., 2021b). In *Achillea pachycephala*, drought stress dramatically increases the contents of phenolic acids, such as chlorogenic and caffeic (Gharibi et al., 2019).

Rhizobacteria-mediated systemic resistance helps protect plants from pathogens and insects (Singh et al., 2002). Phenolic acid-induced systemic resistance provides bio-protection to plants under pathogenic stress conditions (Nicholson and Hammerschmidt, 2003). In rice, the correlation between phenolics and seedling protection from *Rhizobium solani* has been revealed. An High Performance Liquid Chromatography analysis showed that the biosynthesis of phenolic acids is more enhanced in Rhizobium-infected seedlings compared with uninfected controls (Mishra et al., 2006). In the orchid *D. officinale*, a *Dendrobium* viroid infection increases the total phenolic acid content, which may play an important role in the activation of pathogen defense responses (Li et al., 2022).

Phenolic acid has complex biological functions. Some stresses inhibit phenolic acid synthesis, and some other stresses promote phenolic acid contents, suggesting that phenolic acids may play both positive and negative roles in the process of resisting environmental stress.

Effects of Environmental Factors on Flavonoid Biosynthesis

Flavonoids, common polyphenols, are antioxidants required in plant stress resistance (Laoue et al., 2022). Plants with high flavonoid contents have potential cellular antioxidant capacities under environmental stress conditions (Hidayat and Wulandari, 2021). The over-accumulation of several flavonoids, such as kaempferol, quercetin, and cyanidin, has been well documented in model plants (Nakabayashi et al., 2014). In Chinese liquorice, the contents of some ortho-dehydroxylated B-ring flavonoids, effective scavengers of ROS, increase under UV-B exposure (Zhang et al., 2018). In rice, salt and heat stresses enhance flavonoid accumulation, which is crucial for stress tolerance (Jan et al., 2021). In some plant species, abiotic stresses play negative roles in flavonoid accumulation. For example, accumulated Na^{2+} in *Apocynum venetum* leaves reduces the flavonoid concentration and decreases salt tolerance under salt-stress conditions (Xu et al., 2021).

The protective roles of hesperidin and hesperetin, the major flavonoids in citrus fruit, against invading microbes and toxins have been well investigated (Iranshahi et al., 2015). Several flavonol glycosides, such as quercetin and kaempferol glycosides, increase under short-wavelength radiation, which enhances plant defenses against various herbivorous insects (Rechner et al., 2017).

Anthocyanins, another subgroup of flavonoids, are frequently induced in plants by biotic and abiotic stresses (Li et al., 2021a). Various environmental factors play distinct roles in anthocyanin biosynthesis and tissue-specific accumulation in plants (Li et al., 2012; An et al., 2020). In apple, drought, low temperature, UV-B, and light exposure significantly up-regulate the accumulation of anthocyanins in fruit, and high temperature and increased nitrogen fertilizer significantly down-regulate the accumulation of anthocyanins in fruit (Gao et al., 2021).

EFFECTS OF GENETIC FACTORS ON THE BIOSYNTHESIS OF PLANT SPECIALIZED METABOLITES

Accumulations of PSMs under stressful environment conditions is controlled by an intricate network containing a large number of Transcription factors (TFs). Many key enzyme-encoding genes involved in PSM biosynthesis are the downstream targets of different TFs (Patra et al., 2013).

Transcription Factors Involved in the Biosynthesis of Alkaloids

Previous studies have identified several TFs that control specific steps and branches of the TIA and BIA biosynthetic

pathways. In *C. roseus*, an ORCA3 TF regulates the expression of TIA biosynthetic pathway-related genes, such as *GEISSOSCHIZINE SYNTHASE*, *STRICTOSIDINE SYNTHASE*, and *DEACETYLVINDOLINE ACETYLTRANSFERASE* (Khataee et al., 2020). The interaction of MYC2 and GBFs governs TIA biosynthesis by modulating the TIA pathway genes in *C. roseus* (Sui et al., 2018). WRKY1 is a positive regulator of the TIA biosynthetic pathway (Suttipanta et al., 2011). A MAP kinase cascade modulates the TIA biosynthetic pathway by activating its downstream target *AP2/ERF* TF genes (Paul et al., 2017). In addition, the zinc-finger TF ZCT1 acts as a transcriptional repressor in the TIA biosynthetic pathway (Mortensen et al., 2019). In *Ophiorrhiza pumila*, OpWRKY2 and OpWRKY3 were identified as two positive regulators in the biosynthesis of camptothecin (Wang et al., 2019a; Hao et al., 2021).

In lotus (*Nelumbo nucifera*), WRKY40a and WRKY40b participate in the BIA biosynthetic pathway by regulating the *TYDC*, *NCS*, *CYP80G*, and *7OMT* genes (Meelaph et al., 2018; Li et al., 2019a). In narrow-leafed lupin, the TF RAP2-7 is involved in the regulation of the quinolizidine alkaloid biosynthetic pathway (Czepiel et al., 2021). Two jasmonate-responsive TFs, ERF189 and ERF199, are involved in the biosynthesis of nicotine, the predominant alkaloid in tobacco leaves (Kato et al., 2014; Kajikawa et al., 2017). Under high temperature-stress conditions, MYC2 enhances the nicotine content by regulating the expression of the *PMT1* gene, which encodes a putrescine *N*-methyl transferase involved in the key step of the pyridine alkaloid pathway (Yang et al., 2016). In *Coptis japonica*, isoquinoline alkaloid biosynthesis is controlled by CjbHLH1 homologs (Yamada et al., 2011).

Transcription Factors Involved in the Biosynthesis of Glucosinolates

Arabidopsis is a model plant used to reveal the transcriptional regulation of glucosinolate biosynthesis (Hirai et al., 2004). An analysis of the R2R3-MYB family in *Arabidopsis* showed that MYB34, MYB51, and MYB122 control the biosynthesis of indolic glucosinolates, whereas MYB28, MYB29, and MYB76 control the biosynthesis of aliphatic glucosinolates (Frerigmann and Gigolashvili, 2014; Baskar and Park, 2015). Another two *Arabidopsis* TFs, FRS7 and FRS12, are transcriptional repressors in the glucosinolate biosynthetic pathway (Fernandez-Calvo et al., 2020). In addition, a well-identified central circadian clock regulator, CCA1, participates in the host resistance of plants to the caterpillar *Trichoplusia ni* by enhancing basal indole glucosinolate biosynthesis (Lei et al., 2019). A bHLH TF, IAA-LEUCINE RESISTANT3, modulates the accumulation of glucosinolates under iron deficiency conditions and during pathogen infection (Samira et al., 2018). A proteomic analysis identified a jasmonate-responsive MYC2 TF that has opposite effects on the indolic and aliphatic glucosinolate pathways (Guo et al., 2012).

Short-term temperature treatments can enhance the accumulation of glucosinolates in *B. rapa*. A co-expression analysis identified a MYB family member, MYB51, that regulates the biosynthesis of glucosinolates after a short-term high temperature treatment (Rao et al., 2021). In addition, MYB28.3, MYB29.1, and MYB122.2, which are highly responsive to various abiotic and biotic stresses, are positive regulators of aliphatic glucosinolate biosynthesis in *B. rapa* (Baskar and Park, 2015; Seo et al., 2017).

Transcription Factors Involved in the Biosynthesis of Terpenoids

A number of TFs are involved in the terpenoid biosynthetic pathway (Patra et al., 2013). Artemisinin is an important sesquiterpene lactone in sweet wormwood, and several artemisinin biosynthesis-related TFs have been identified (Efferth, 2017). In sweet wormwood, two JA responsive TFs, ERF1 and ERF2, affect artemisinin biosynthesis by regulating the expression of *AMORPHA-4,11-DIENE SYNTHASE* and *CYP SEQUITERPENE OXIDASE* genes (Yu et al., 2012). AaWRKY1 controls the expression of *3-HYDROXY 3-METHYLGLUTARYL-COA REDUCTASE* and *ARTEMISINIC ALDEHYDE*Δ*11(13) REDUCTASE*, which are key genes in the artemisinin biosynthetic pathway (Jiang et al., 2016).

Several stress-related TFs are involved in the biosynthesis of terpenoids. In cotton (*Gossypium arboretum*), GaWRKY1 regulates the conversion of sesquiterpenes to gossypol, which plays a role in responses to fungal infection (Xu et al., 2004). Terpenoids are enriched in the latex products from the rubber tree (*Hevea brasiliensis*). HbWRKY1 and HbEREBP1 are positive and negative regulators, respectively, of latex biosynthesis induced by wounding (Chen et al., 2012; Wang et al., 2013). Clade Iva bHLH TFs in the JA-signaling pathway participate in the regulation of bioactive terpenoid biosynthesis (Mertens et al., 2016b). In *Medicago truncatula*, two bHLH TFs, TSAR1 and TSAR2, affect triterpene saponin biosynthesis by regulating the expression of *HMGR1*, which encodes the rate-limiting enzyme for triterpene biosynthesis, under stress conditions (Mertens et al., 2016a). In roses, the over-expression of the *PAP1* TF gene significantly activates the terpenoid biosynthetic pathway to enhance the production of terpenoid scent compounds (Zvi et al., 2012). The JA-responsive TF WRKY24 promotes the biosynthesis of saponin by increasing the expression of terpenoid biosynthetic pathway genes in *Conyza blini* (Sun et al., 2018). In *Taxus media*, a phloem-specific MYB3 affects the transcriptional regulation of paclitaxel biosynthesis, a classic diterpenoid compound, by activating the expression of *TBT*, *DBTNBT*, and *TS* genes (Yu et al., 2020).

Transcription Factors Involved in the Biosynthesis of Phenolic Acids

Several TFs act as regulators of the phenolic acid pathway in the Chinese medicinal plant *S. miltiorrhiza* (Sun et al., 2019a). A large number of TFs, including two ERF family members (SmERF115 and SmERF1L1), three MYB family members (SmMYB2a, SmMYB2b, and SmMYB52), four bHLH family members (SmbHLH3, SmbHLH37, SmbHLH51, and SmbHLH148), one ZIP family member (SmZIP1), and two GRAS family members (SmGRAS1 and SmGRAS2), are involved in the regulation of the phenolic acid biosynthetic pathway (Zhou et al., 2016;

Du et al., 2018; Li et al., 2019b; Deng et al., 2020a; Zhang et al., 2020). Furthermore, the corresponding downstream targets of the above TFs also have been identified in *S. miltiorrhiza*. SmMYC2a/b binds to the E-boxes in the promoter regions of *SmHCT6* and *SmCYP98A14*, which are key genes involved in the synthesis of 4-coumaroyl-3′,4′-dihydroxyphenyllactic acid and rosmarinic acid, respectively (Zhou et al., 2016). SmGRAS1, together with SmGRSA2, binds to the GARE box in the promoter region of *SmKSL1*, which catalyzes the biosynthesis of tanshinones from GGPP (Li et al., 2019b). SmbZIP1, an ABA-responsive TF, binds to the G-Box-like1 motif in the promoter region of *SmC4H1*, which is involved in the biosynthesis of phenolic acid precursors (Deng et al., 2020a). SmbHLH148 and SmMYB1 regulate phenolic acid biosynthesis by activating the expression of downstream genes, such as *PAL1*, *C4H1*, *TAT*, *HPPR*, *RAS*, and *CYP98A14* (Xing et al., 2018; Zhou et al., 2021b). SmMYB52 simultaneously affects the production of phenolic acids by binding to the MBE elements in promoter regions of *SmTAT1*, *Sm4CL9*, *SmC4H1*, and *SmHPPR1* (Yang et al., 2021b). Furthermore, SmbHLH3 acts a repressor in the biosynthesis of phenolic acids in *S. miltiorrhiza* hairy roots by reducing the expression of *DXS3*, *DXR*, *HMGR1*, *KSL1*, *CPS1* and *CYP76AH1* (Zhang et al., 2020). In *S. miltiorrhiza* hairy roots, tanshinone and salvianolic acid biosynthesis are controlled by SmMYB09 (Hao et al., 2020). Interestingly, over-expression of *Arabidopsis* MYC2 simultaneous promotes the biosynthesis of tanshinone and phenolic acid in *S. miltiorrhiza* hairy roots (Shi et al., 2020b). Additionally, SmJRB1 was identified as a positive regulator in regulation of phenolic acid biosynthesis (Zhou et al., 2021a).

Transcription Factors Involved in the Biosynthesis of Flavonoids

The complete flavonoid biosynthetic pathway, consisting of three major branches, has been well-studied in plants. Recently, TFs from different families, such as MYB, bHLH, and WRKY, have also been characterized (Lloyd et al., 2017; Yan et al., 2021).

In *M. truncatula*, MtMYB134 activates flavonol biosynthesis by binding the promoters of *MtFLS1*, *MtFLS2*, and *MtCHS2* (Naik et al., 2021). In apple, MdNAC52 regulates the biosynthesis of anthocyanin and proanthocyanidin by activating the promoters of *MdMYB9* and *MdMYB11* genes (Sun et al., 2019b). In buckwheat, MYBF1 regulates the flavonol biosynthetic pathway by up-regulating the *DFR* and *LDOX* genes (Matsui et al., 2018). In *Fagopyrum tataricum*, light-induced FtMYB116 promotes the accumulation of rutin by binding directly to the promoter region of *F3'H* (Zhang et al., 2019). In pear (*Pyrus pyrifolia*), PpMYB17 positively controls the flavonoid biosynthetic pathway by activating the promoters of *PpCHS*, *PpCHI*, *PpF3H*, *PpFLS*, and *PpUFGT* (Premathilake et al., 2020). Another pear (*Pyrus* × *bretschneideri*) TF, PbWRKY75 affects flavonoid biosynthesis by regulating the expression of *PbDFR*, *PbUFGT*, and *PbMYB10b* (Cong et al., 2021). In *Populus tomentosa*, PtMYB6 promotes anthocyanin and

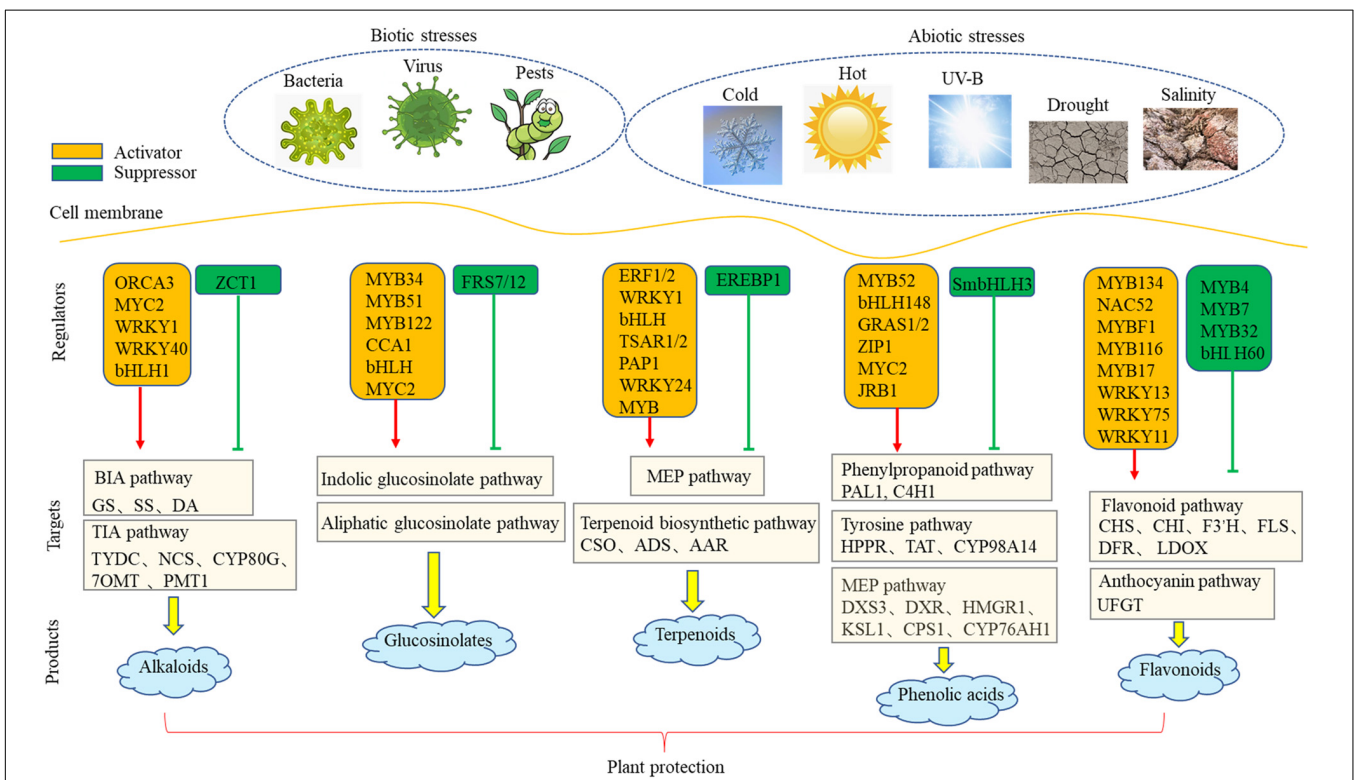

FIGURE 1 | The network of transcriptional regulation of plant under biotic and abiotic stresses. Red arrow indicated activation pathways and green arrow indicated inhibition pathways.

proanthocyanidin biosynthesis by interacting physically with KNAT7 (Wang et al., 2019b). In potato (*Solanum tuberosum*), StWRKY13 promotes anthocyanin biosynthesis in tubers by activating the promoters of *StCHS*, *StF3H*, *StDFR*, and *StANS* (Zhang et al., 2021a). The over-expression of MdWRKY11 in apple calli revealed its novel function in promoting the accumulation of flavonoids and anthocyanin by binding to the promoter of *MdHY5* (Wang et al., 2018a; Liu et al., 2019).

Furthermore, many negative regulators of the flavonoid biosynthetic pathway have been identified in different plant species. AtMYB4 and its close homologs AtMYB7 and AtMYB32 inhibit flavonoid accumulation by down-regulating the expression of *ADT6*, which catalyzes the key step that supplies phenylalanine (Wang et al., 2020). The over-expression of *MYB15L* in red-fleshed apple calli represses anthocyanin accumulation and cold tolerance (Xu et al., 2018). Homodimers of MdMYB16 inhibit anthocyanin synthesis through their C-terminal EARs, which are weakened by interactions with the TF MdbHLH33 (Xu et al., 2017). The over-expression of *Arabidopsis* MYB60 in lettuce plants significantly reduces the production and accumulation of anthocyanin pigments by inhibiting the expression of *DIHYDROFLAVONOL-4-REDUCTASE* gene (Park et al., 2008). The loss of *MYB2-1* expression causes the purple color in cabbage leaves, suggesting that it encodes a potential negative regulator of the flavonoid biosynthetic pathway (Song et al., 2018). In *Ginkgo biloba*, a negative regulator, GbMYBF2, affects flavonoid biosynthesis by down-regulating several key genes, such as *GbPAL*, *GbANS*, *GbFLS*, and *GbCHS2* (Xu et al., 2014). A *Brassica napus* WRKY TF, BnWRKY41-1, acts as a repressor of anthocyanin biosynthesis (Duan et al., 2018). In *S. miltiorrhiza*, SmbHLH60 was identified as a negative regulator in anthocyanin biosynthesis mainly *via SmDRF* gene (Liu et al., 2022b).

Environmental signals pass through cell membrane through a large number of TFs to activate downstream functional genes. To date, a number of TF involved in metabolic pathway have been identified in different plants. Our review summarizes a network that is involved in the transcriptional regulation of PSM biosynthesis under environmental stresses (**Figure 1**). To date, a large number of positive TFs have been identified, but the number of negative TFs is still limited. Negative regulatory TFs are also the key factors in the establishment of dynamic balance of plant secondary metabolism. In the future research, cloning and identification of negative regulatory TFs has become an urgent research hotspot.

CONCLUSION AND FUTURE PERSPECTIVES

Plants produce a large number of PSMs having diversified structures, and they play important physiological and ecological roles in stress tolerance. The biosynthesis of stress-related PSMs is controlled by environmental and genetic factors. Artificial regulation of PSM biosynthesis is helpful to enhance plant resistance to environmental stresses. We summarized potential genetic and environmental factors and their targets, particularly in MYB, bHLH, and WRKY families. For plant genetic improvement, overexpression of activating TFs or inhibition of expression of inhibitory TFs can increase the yield of PSM and enhance the resistance of plants to environmental stress. We further found that the downstream targets of these TFs are frequently enriched in the synthesis pathway of precursors, suggesting an effective role of precursors in enhancing of terminal products. Although most of PSM-related TFs have been identified in different plant species, including the model plant *Arabidopsis*, medicinal plant *C. roseus*, and woody plant poplar, these results also provide good guides for the regulation in other plants. This review summarizes the key enzymes and TFs involved in PSM biosynthetic pathways, providing valuable insights for screening targets and regulators in non-model plants.

AUTHOR CONTRIBUTIONS

RC was involved in the review writing. RC and ZC were involved in manuscript refinement. XZ and CS initiated the idea of the review and were involved in the manuscript writing. All authors contributed to the article and approved the submitted version.

FUNDING

This work was supported by the National Natural Science Foundation of China (32000255 and 82173919) and the Natural Science Foundation of Zhejiang Province (LY21C050004 and LY19C150005).

REFERENCES

Abdala-Roberts, L., Rasmann, S., Berny-Mier, Y. T. J. C., Covelo, F., Glauser, G., and Moreira, X. (2016). Biotic and abiotic factors associated with altitudinal variation in plant traits and herbivory in a dominant oak species. *Am. J. Bot.* 103, 2070–2078. doi: 10.3732/ajb.1600310

Aharoni, A., and Galili, G. (2011). Metabolic engineering of the plant primary-secondary metabolism interface. *Curr. Opin. Biotechnol.* 22, 239–244. doi: 10.1016/j.copbio.2010.11.004

An, J. P., Liu, Y. J., Zhang, X. W., Bi, S. Q., Wang, X. F., You, C. X., et al. (2020). Dynamic regulation of anthocyanin biosynthesis at different light intensities by the BT2-TCP46-MYB1 module in apple. *J. Exp. Bot.* 71, 3094–3109. doi: 10.1093/jxb/eraa056

Baskar, V., and Park, S. W. (2015). Molecular characterization of BRMYB28 and BRMYB29 paralogous transcription factors involved in the regulation of aliphatic glucosinolate profiles in *Brassica rapa* ssp. pekinensis. *C. R. Biol.* 338, 434–442. doi: 10.1016/j.crvi.2015.04.001

Bhambhani, S., Kondhare, K. R., and Giri, A. P. (2021). Diversity in chemical structures and biological properties of plant alkaloids. *Molecules* 26:3374. doi: 10.3390/molecules26113374

Bohlmann, J., Meyer-Gauen, G., and Croteau, R. (1998). Plant terpenoid synthases: molecular biology and phylogenetic analysis. *Proc. Natl. Acad. Sci. U.S.A.* 95, 4126–4133. doi: 10.1073/pnas.95.8.4126

Castro-Moretti, F. R., Gentzel, I. N., Mackey, D., and Alonso, A. P. (2020). Metabolomics as an emerging tool for the study of plant–pathogen interactions. *Metabolites* 10:52.

Chae, L., Kim, T., Nilo-Poyanco, R., and Rhee, S. Y. (2014). Genomic signatures of specialized metabolism in plants. *Science* 344, 510–513. doi: 10.1126/science.1252076

Chapman, J. M., Muhlemann, J. K., Gayomba, S. R., and Muday, G. K. (2019). RBOH-dependent ROS synthesis and ROS scavenging by plant specialized metabolites to modulate plant development and stress responses. *Chem. Res. Toxicol.* 32, 370–396. doi: 10.1021/acs.chemrestox.9b00028

Chen, R., Cao, Y., Wang, W., Li, Y., Wang, D., Wang, S., et al. (2021b). Transcription factor SmSPL7 promotes anthocyanin accumulation and negatively regulates phenolic acid biosynthesis in Salvia miltiorrhiza. *Plant Sci.* 310, 110993. doi: 10.1016/j.plantsci.2021.110993

Chen, L., Lu, B., Liu, L., Duan, W., Jiang, D., Li, J., et al. (2021a). Melatonin promotes seed germination under salt stress by regulating ABA and GA3 in cotton (*Gossypium hirsutum* L.). *Plant Physiol. Biochem.* 162, 506–516. doi: 10.1016/j.plaphy.2021.03.029

Chen, Y. Y., Wang, L. F., Dai, L. J., Yang, S. G., and Tian, W. M. (2012). Characterization of HBEREBP1, a wound-responsive transcription factor gene in laticifers of *Hevea brasiliensis* muell. *Arg. Mol. Biol. Rep.* 39, 3713–3719. doi: 10.1007/s11033-011-1146-y

Choi, M., Sathasivam, R., Nguyen, B. V., Park, N. I., Woo, S. H., and Park, S. U. (2021). Expression analysis of phenylpropanoid pathway genes and metabolomic analysis of phenylpropanoid compounds in adventitious, hairy, and seedling roots of tartary buckwheat. *Plants* 11:90. doi: 10.3390/plants11010090

Christianson, D. W. (2017). Structural and chemical biology of terpenoid cyclases. *Chem. Rev.* 117, 11570–11648. doi: 10.1021/acs.chemrev.7b00287

Cong, L., Qu, Y., Sha, G., Zhang, S., Ma, Y., Chen, M., et al. (2021). PBWRKY75 promotes anthocyanin synthesis by activating PBDFR, PbUFGT, and PbMYB10b in pear. *Physiol. Plant* 173, 1841–1849. doi: 10.1111/ppl.13525

Czepiel, K., Krajewski, P., Wilczura, P., Bielecka, P., Swiecicki, W., and Kroc, M. (2021). Expression profiles of alkaloid-related genes across the organs of narrow-leafed lupin (*Lupinus angustifolius* L.) and in response to anthracnose infection. *Int. J. Mol. Sci.* 22:2676. doi: 10.3390/ijms22052676

D'Auria, J. C., and Gershenzon, J. (2005). The secondary metabolism of *Arabidopsis thaliana*: growing like a weed. *Curr. Opin. Plant Biol.* 8, 308–316. doi: 10.1016/j.pbi.2005.03.012

Deng, C., Wang, Y., Huang, F., Lu, S., Zhao, L., Ma, X., et al. (2020b). SMMYB2 promotes salvianolic acid biosynthesis in the medicinal herb *Salvia miltiorrhiza*. *J. Integr. Plant Biol.* 62, 1688–1702. doi: 10.1111/jipb.12943

Deng, C., Shi, M., Fu, R., Zhang, Y., Wang, Q., Zhou, Y., et al. (2020a). ABA-responsive transcription factor bZIP1 is involved in modulating biosynthesis of phenolic acids and tanshinones in *Salvia miltiorrhiza*. *J. Exp. Bot.* 71, 5948–5962. doi: 10.1093/jxb/eraa295

Desmet, S., Morreel, K., and Dauwe, R. (2021). Origin and function of structural diversity in the plant specialized metabolome. *Plants* 10:2393. doi: 10.3390/plants10112393

Dong, N. Q., and Lin, H. X. (2021). Contribution of phenylpropanoid metabolism to plant development and plant-environment interactions. *J. Integr. Plant Biol.* 63, 180–209. doi: 10.1111/jipb.13054

Du, T., Niu, J., Su, J., Li, S., Guo, X., Li, L., et al. (2018). SmbHLH37 Functions Antagonistically With SMMYC2 in Regulating Jasmonate-mediated biosynthesis of phenolic acids in *Salvia miltiorrhiza*. *Front. Plant Sci.* 9:1720. doi: 10.3389/fpls.2018.01720

Duan, S., Wang, J., Gao, C., Jin, C., Li, D., Peng, D., et al. (2018). Functional characterization of a heterologously expressed *Brassica napus* WRKY41-1 transcription factor in regulating anthocyanin biosynthesis in *Arabidopsis thaliana*. *Plant Sci.* 268, 47–53. doi: 10.1016/j.plantsci.2017.12.010

Efferth, T. (2017). From ancient herb to modern drug: *Artemisia annua* and artemisinin for cancer therapy. *Semin. Cancer Biol.* 46, 65–83. doi: 10.1016/j.semcancer.2017.02.009

Fabregas, N., and Fernie, A. R. (2021). The interface of central metabolism with hormone signaling in plants. *Curr. Biol.* 31, R1535–R1548. doi: 10.1016/j.cub.2021.09.070

Fang, C., Fernie, A. R., and Luo, J. (2019). Exploring the diversity of plant metabolism. *Trends Plant Sci.* 24, 83–98. doi: 10.1016/j.tplants.2018.09.006

Fernandez-Calvo, P., Inigo, S., Glauser, G., Vanden Bossche, R., Tang, M., Li, B., et al. (2020). FRS7 and FRS12 recruit NINJA to regulate expression of glucosinolate biosynthesis genes. *New Phytol.* 227, 1124–1137. doi: 10.1111/nph.16586

Fernie, A. R., Trethewey, R. N., Krotzky, A. J., and Willmitzer, L. (2004). Metabolite profiling: from diagnostics to systems biology. *Nat. Rev. Mol. Cell. Biol.* 5, 763–769. doi: 10.1038/nrm1451

Frerigmann, H., and Gigolashvili, T. (2014). Update on the role of R2R3-MYBs in the regulation of glucosinolates upon sulfur deficiency. *Front. Plant Sci.* 5:626. doi: 10.3389/fpls.2014.00626

Frick, K. M., Foley, R. C., Siddique, K. H. M., Singh, K. B., and Kamphuis, L. G. (2019). The role of jasmonate signalling in quinolizidine alkaloid biosynthesis, wounding and aphid predation response in narrow-leafed lupin. *Funct. Plant Biol.* 46, 443–454. doi: 10.1071/FP18278

Fu, R., Shi, M., Deng, C., Zhang, Y., Zhang, X., Wang, Y., et al. (2020). Improved phenolic acid content and bioactivities of *Salvia miltiorrhiza* hairy roots by genetic manipulation of RAS and CYP98A14. *Food Chem.* 331:127365. doi: 10.1016/j.foodchem.2020.127365

Gao, H. N., Jiang, H., Cui, J. Y., You, C. X., and Li, Y. Y. (2021). Review: The effects of hormones and environmental factors on anthocyanin biosynthesis in apple. *Plant Sci.* 312:111024. doi: 10.1016/j.plantsci.2021.111024

Geu-Flores, F., Sherden, N. H., Courdavault, V., Burlat, V., Glenn, W. S., Wu, C., et al. (2012). An alternative route to cyclic terpenes by reductive cyclization in iridoid biosynthesis. *Nature* 492, 138–142. doi: 10.1038/nature11692

Gharibi, S., Sayed Tabatabaei, B. E., Saeidi, G., Talebi, M., and Matkowski, A. (2019). The effect of drought stress on polyphenolic compounds and expression of flavonoid biosynthesis related genes in *Achillea* pachycephala Rech.f. *Phytochemistry* 162, 90–98. doi: 10.1016/j.phytochem.2019.03.004

Glas, J. J., Schimmel, B. C., Alba, J. M., Escobar-Bravo, R., Schuurink, R. C., and Kant, M. R. (2012). Plant glandular trichomes as targets for breeding or engineering of resistance to herbivores. *Int. J. Mol. Sci.* 13, 17077–17103. doi: 10.3390/ijms131217077

Grotewold, E. (2006). The genetics and biochemistry of floral pigments. *Annu. Rev. Plant Biol.* 57, 761–780. doi: 10.1146/annurev.arplant.57.032905.105248

Guo, J., Pang, Q., Wang, L., Yu, P., Li, N., and Yan, X. (2012). Proteomic identification of MYC2-dependent jasmonate-regulated proteins in *Arabidopsis thaliana*. *Proteome Sci.* 10:57. doi: 10.1186/1477-5956-10-57

Gupta, M. L., and Dutta, A. (2011). Stress-mediated adaptive response leading to genetic diversity and instability in metabolite contents of high medicinal value: an overview on *Podophyllum hexandrum*. *OMICS* 15, 873–882. doi: 10.1089/omi.2011.0096

Halkier, B. A., and Gershenzon, J. (2006). Biology and biochemistry of glucosinolates. *Annu. Rev. Plant Biol.* 57, 303–333. doi: 10.1146/annurev.arplant.57.032905.105228

Hamilton, A. (2004). Medicinal plants, conservation and livelihhods. *Biodivers. Conserv.* 13, 1477–1517.

Hao, X., Pu, Z., Cao, G., You, D., Zhou, Y., Deng, C., et al. (2020). Tanshinone and salvianolic acid biosynthesis are regulated by SmMYB98 in *Salvia miltiorrhiza* hairy roots. *J. Adv. Res.* 23, 1–12. doi: 10.1016/j.jare.2020.01.012

Hao, X., Xie, C., Ruan, Q., Zhang, X., Wu, C., Han, B., et al. (2021). The transcription factor OpWRKY2 positively regulates the biosynthesis of the anticancer drug camptothecin in *Ophiorrhiza pumila*. *Hortic. Res.* 8:7. doi: 10.1038/s41438-020-00437-3

Hassan, F. A. S., Ali, E., Gaber, A., Fetouh, M. I., and Mazrou, R. (2021). Chitosan nanoparticles effectively combat salinity stress by enhancing antioxidant activity and alkaloid biosynthesis in *Catharanthus roseus* (L.) G. *Don. Plant Physiol. Biochem.* 162, 291–300. doi: 10.1016/j.plaphy.2021.03.004

He, S. M., Liang, Y. L., Cong, K., Chen, G., Zhao, X., Zhao, Q. M., et al. (2018). Identification and characterization of genes involved in benzylisoquinoline alkaloid biosynthesis in coptis species. *Front. Plant Sci.* 9:731. doi: 10.3389/fpls.2018.00731

He, W., Luo, H., Xu, H., Zhou, Z., Li, D., Bao, Y., et al. (2021). Effect of exogenous methyl jasmonate on physiological and carotenoid composition of yellow maize sprouts under NaCl stress. *Food Chem.* 361:130177. doi: 10.1016/j.foodchem.2021.130177

Henry, L. K., Gutensohn, M., Thomas, S. T., Noel, J. P., and Dudareva, N. (2015). Orthologs of the archaeal isopentenyl phosphate kinase regulate terpenoid production in plants. *Proc Natl Acad. Sci. U.S.A.* 112, 10050–10055. doi: 10.1073/pnas.1504798112

Hidayat, R., and Wulandari, P. (2021). Effects of *Andrographis paniculata* (Burm. F.). *Rep. Biochem. Mol. Biol.* 10, 445–454. doi: 10.52547/rbmb.10.3.445

Hirai, M. Y., Yano, M., Goodenowe, D. B., Kanaya, S., Kimura, T., Awazuhara, M., et al. (2004). Integration of transcriptomics and metabolomics for understanding of global responses to nutritional stresses in *Arabidopsis thaliana*. *Proc. Natl. Acad. Sci. U.S.A.* 101, 10205–10210. doi: 10.1073/pnas.0403218101

Hori, K., Yamada, Y., Purwanto, R., Minakuchi, Y., Toyoda, A., Hirakawa, H., et al. (2018). Mining of the uncharacterized cytochrome P450 genes involved in alkaloid biosynthesis in california poppy using a draft genome sequence. *Plant Cell Physiol.* 59, 222–233. doi: 10.1093/pcp/pcx210

Hua, J., Liu, Y., Xiao, C. J., Jing, S. X., Luo, S. H., and Li, S. H. (2017). Chemical profile and defensive function of the latex of *Euphorbia peplus*. *Phytochemistry* 136, 56–64. doi: 10.1016/j.phytochem.2016.12.021

Huang, B., Yi, B., Duan, Y., Sun, L., Yu, X., Guo, J., et al. (2008). Characterization and expression profiling of tyrosine aminotransferase gene from *Salvia miltiorrhiza* (Dan-shen) in rosmarinic acid biosynthesis pathway. *Mol. Biol. Rep.* 35, 601–612. doi: 10.1007/s11033-007-9130-2

Iranshahi, M., Rezaee, R., Parhiz, H., Roohbakhsh, A., and Soltani, F. (2015). Protective effects of flavonoids against microbes and toxins: the cases of hesperidin and hesperetin. *Life Sci.* 137, 125–132. doi: 10.1016/j.lfs.2015.07.014

Ishida, M., Hara, M., Fukino, N., Kakizaki, T., and Morimitsu, Y. (2014). Glucosinolate metabolism, functionality and breeding for the improvement of Brassicaceae vegetables. *Breed Sci.* 64, 48–59. doi: 10.1270/jsbbs.64.48

Jan, R., Kim, N., Lee, S. H., Khan, M. A., Asaf, S., Lubna, et al. (2021). Enhanced flavonoid accumulation reduces combined salt and heat stress through regulation of transcriptional and hormonal mechanisms. *Front. Plant Sci.* 12:796956. doi: 10.3389/fpls.2021.796956

Janeczko, A., Pociecha, E., Dziurka, M., Jurczyk, B., Libik-Konieczny, M., Oklestkova, J., et al. (2019). Changes in content of steroid regulators during cold hardening of winter wheat - Steroid physiological/biochemical activity and impact on frost tolerance. *Plant Physiol. Biochem.* 139, 215–228. doi: 10.1016/j.plaphy.2019.03.020

Jeena, G. S., Kumar, S., and Shukla, R. K. (2021). Characterization of MYB35 regulated methyl jasmonate and wound responsive geraniol 10-hydroxylase-1 gene from *Bacopa monnieric*. *Planta* 253:89. doi: 10.1007/s00425-021-03614-3

Jia, Q., and Chen, F. (2016). Catalytic functions of the isoprenyl diphosphate synthase superfamily in plants: a growing repertoire. *Mol. Plant* 9, 189–191. doi: 10.1016/j.molp.2015.12.020

Jiang, W., Fu, X., Pan, Q., Tang, Y., Shen, Q., Lv, Z., et al. (2016). Overexpression of AaWRKY1 leads to an enhanced content of artemisinin in *Artemisia annua*. *Biomed. Res. Int.* 2016:7314971. doi: 10.1155/2016/7314971

Kajikawa, M., Sierro, N., Kawaguchi, H., Bakaher, N., Ivanov, N. V., Hashimoto, T., et al. (2017). Genomic insights into the evolution of the nicotine biosynthesis pathway in tobacco. *Plant Physiol.* 174, 999–1011. doi: 10.1104/pp.17.00070

Kato, K., Shoji, T., and Hashimoto, T. (2014). Tobacco nicotine uptake permease regulates the expression of a key transcription factor gene in the nicotine biosynthesis pathway. *Plant Physiol.* 166, 2195–2204. doi: 10.1104/pp.114.251645

Khakdan, F., Govahi, M., Mohebi, Z., and Ranjbar, M. (2021). Water deficit stress responses of monoterpenes and sesquiterpenes in different Iranian cultivars of basil. *Physiol. Plant* 173, 896–910. doi: 10.1111/ppl.13485

Khataee, E., Karimi, F., and Razavi, K. (2020). Different carbon sources and their concentrations change alkaloid production and gene expression in *Catharanthus roseus* shoots in vitro. *Funct. Plant Biol.* 48, 40–53. doi: 10.1071/FP19254

Kochevenko, A., Klee, H. J., Fernie, A. R., and Araújo, W. L. (2012). Molecular identification of a further branched-chain aminotransferase 7 (BCAT7) in tomato plants. *J. Plant Physiol.* 169, 437–443. doi: 10.1016/j.jplph.2011.12.002

Kravic, N., Babic, V., Vukadinovic, J., Ristic, D., Dragicevic, V., Mladenovic Drinic, S., et al. (2021). Alteration of metabolites accumulation in maize inbreds leaf tissue under long-term water deficit. *Biology* 10:694. doi: 10.3390/biology10080694

Kumar, K., Kumar, S. R., Dwivedi, V., Rai, A., Shukla, A. K., Shanker, K., et al. (2015). Precursor feeding studies and molecular characterization of geraniol synthase establish the limiting role of geraniol in monoterpene indole alkaloid biosynthesis in *Catharanthus roseus* leaves. *Plant Sci.* 239, 56–66. doi: 10.1016/j.plantsci.2015.07.007

Kumar, S., and Pandey, A. K. (2013). Chemistry and biological activities of flavonoids: an overview. *ScientificWorldJournal* 2013:162750. doi: 10.1155/2013/162750

Lam, P. Y., Lui, A. C. W., Yamamura, M., Wang, L., Takeda, Y., Suzuki, S., et al. (2019). Recruitment of specific flavonoid B-ring hydroxylases for two independent biosynthesis pathways of flavone-derived metabolites in grasses. *New Phytol* 223, 204–219. doi: 10.1111/nph.15795

Laoue, J., Fernandez, C., and Ormeno, E. (2022). Plant flavonoids in mediterranean species: a focus on flavonols as protective metabolites under climate stress. *Plants* 11:172. doi: 10.3390/plants11020172

Lei, J., Jayaprakasha, G. K., Singh, J., Uckoo, R., Borrego, E. J., Finlayson, S., et al. (2019). CIRCADIAN CLOCK-ASSOCIATED1 controls resistance to aphids by altering indole glucosinolate production. *Plant Physiol.* 181, 1344–1359. doi: 10.1104/pp.19.00676

Li, C., Shi, L., Li, X., Wang, Y., Bi, Y., Li, W., et al. (2021a). ECAP is a key negative regulator mediating different pathways to modulate salt stress-induced anthocyanin biosynthesis in *Arabidopsis*. *New Phytol.* 233, 2216–2231. doi: 10.1111/nph.17937

Li, H., Chen, H., Deng, S., Cai, H., Shi, L., Xu, F., et al. (2021b). Inhibition of nitric oxide production under alkaline conditions regulates iron homeostasis in rice. *Physiol. Plant* 172, 1465–1476. doi: 10.1111/ppl.13333

Li, S., Wu, Z. G., Zhou, Y., Dong, Z. F., Fei, X., Zhou, C. Y., et al. (2022). Changes in metabolism modulate induced by viroid infection in the orchid *Dendrobium officinale*. *Virus Res.* 308:198626. doi: 10.1016/j.virusres.2021.198626

Li, W., Bai, Z., Pei, T., Yang, D., Mao, R., Zhang, B., et al. (2019b). SmGRAS1 and SmGRAS2 regulate the biosynthesis of tanshinones and phenolic acids in *Salvia miltiorrhiza*. *Front. Plant Sci.* 10:1367. doi: 10.3389/fpls.2019.01367

Li, J., Xiong, Y., Li, Y., Ye, S., Yin, Q., Gao, S., et al. (2019a). Comprehensive Analysis and Functional Studies of WRKY Transcription Factors in Nelumbo nucifera. *Int J Mol Sci* 20, 5006. doi: 10.3390/ijms20205006

Li, Y. Y., Mao, K., Zhao, C., Zhao, X. Y., Zhang, H. L., Shu, H. R., et al. (2012). MdCOP1 ubiquitin E3 ligases interact with MdMYB1 to regulate light-induced anthocyanin biosynthesis and red fruit coloration in apple. *Plant Physiol.* 160, 1011–1022. doi: 10.1104/pp.112.199703

Lichman, B. R. (2021). The scaffold-forming steps of plant alkaloid biosynthesis. *Nat. Prod. Rep.* 38, 103–129. doi: 10.1039/d0np00031k

Linic, I., Mlinaric, S., Brkljacic, L., Pavlovic, I., Smolko, A., and Salopek-Sondi, B. (2021). Ferulic acid and salicylic acid foliar treatments reduce short-term salt stress in chinese cabbage by increasing phenolic compounds accumulation and photosynthetic performance. *Plants* 10:2346. doi: 10.3390/plants10112346

Liu, Y., Watanabe, M., Yasukawa, S., Kawamura, Y., Aneklaphakij, C., Fernie, A. R., et al. (2021d). Cross-species metabolic profiling of floral specialized metabolism facilitates understanding of evolutional aspects of metabolism among Brassicaceae species. *Front. Plant Sci.* 12:640141. doi: 10.3389/fpls.2021.640141

Liu, X., Bu, J., Ma, Y., Chen, Y., Li, Q., Jiao, X., et al. (2021c). Functional characterization of (S)-N-methylcoclaurine 3′-hydroxylase (NMCH) involved in the biosynthesis of benzylisoquinoline alkaloids in *Corydalis yanhusuo*. *Plant Physiol. Biochem.* 168, 507–515. doi: 10.1016/j.plaphy.2021.09.042

Liu, W., Feng, Y., Yu, S., Fan, Z., Li, X., Li, J., et al. (2021b). The flavonoid biosynthesis network in plants. *Int. J. Mol. Sci.* 22:12824. doi: 10.3390/ijms222312824

Liu, C., Wang, H., Zhang, X., Ma, F., Guo, T., and Li, C. (2021a). Activation of the ABA signal pathway mediated by GABA improves the drought resistance of apple seedlings. *Int. J. Mol. Sci.* 22:12676. doi: 10.3390/ijms222312676

Liu, C. L., Xue, K., Yang, Y., Liu, X., Li, Y., Lee, T. S., et al. (2022a). Metabolic engineering strategies for sesquiterpene production in microorganism. *Crit. Rev. Biotechnol.* 42, 73–92. doi: 10.1080/07388551.2021.1924112

Liu, R., Su, Z., Zhou, H., Huang, Q., Fan, S., Liu, C., et al. (2020). LsHSP70 is induced by high temperature to interact with calmodulin, leading to higher bolting resistance in lettuce. *Sci. Rep.* 10:15155. doi: 10.1038/s41598-020-72443-3

Liu, S., Wang, Y., Shi, M., Maoz, I., Gao, X., Sun, M., et al. (2022b). SmbHLH60 and SmMYC2 antagonistically regulate phenolic acids and anthocyanins biosynthesis in Salvia miltiorrhiza. *J. Adv. Res.* doi: 10.1016/j.jare.2022.02.005

Liu, W., Wang, Y., Yu, L., Jiang, H., Guo, Z., Xu, H., et al. (2019). MdWRKY11 participates in anthocyanin accumulation in red-fleshed apples by affecting

MYB transcription factors and the photoresponse factor MdHY5. *J. Agric. Food Chem.* 67, 8783–8793. doi: 10.1021/acs.jafc.9b02920

Ljubej, V., Radojcic Redovnikovic, I., Salopek-Sondi, B., Smolko, A., Roje, S., and Samec, D. (2021). Chilling and freezing temperature stress differently influence glucosinolates content in *Brassica oleracea* var. acephala. *Plants* 10:1305. doi: 10.3390/plants10071305

Lloyd, A., Brockman, A., Aguirre, L., Campbell, A., Bean, A., Cantero, A., et al. (2017). Advances in the MYB-bHLH-WD Repeat (MBW) pigment regulatory model: addition of a WRKY factor and co-option of an anthocyanin MYB for betalain regulation. *Plant Cell Physiol.* 58, 1431–1441. doi: 10.1093/pcp/pcx075

Luijendijk, T. J., van der Meijden, E., and Verpoorte, R. (1996). Involvement of strictosidine as a defensive chemical in *Catharanthus roseus*. *J. Chem. Ecol.* 22, 1355–1366. doi: 10.1007/BF02027718

Maag, D., Erb, M., Kollner, T. G., and Gershenzon, J. (2015). Defensive weapons and defense signals in plants: some metabolites serve both roles. *Bioessays* 37, 167–174. doi: 10.1002/bies.201400124

Mahmoud, S. S., Maddock, S., and Adal, A. M. (2021). Isoprenoid metabolism and engineering in glandular trichomes of Lamiaceae. *Front. Plant Sci.* 12:699157. doi: 10.3389/fpls.2021.699157

Marone, D., Mastrangelo, A. M., Borrelli, G. M., Mores, A., Laido, G., Russo, M. A., et al. (2022). Specialized metabolites: physiological and biochemical role in stress resistance, strategies to improve their accumulation, and new applications in crop breeding and management. *Plant Physiol. Biochem.* 172, 48–55. doi: 10.1016/j.plaphy.2021.12.037

Matsui, K., Oshima, Y., Mitsuda, N., Sakamoto, S., Nishiba, Y., Walker, A. R., et al. (2018). Buckwheat R2R3 MYB transcription factor FeMYBF1 regulates flavonol biosynthesis. *Plant Sci.* 274, 466–475. doi: 10.1016/j.plantsci.2018.06.025

Meelaph, T., Kobtrakul, K., Chansilpa, N. N., Han, Y., Rani, D., De-Eknamkul, W., et al. (2018). Coregulation of biosynthetic genes and transcription factors for aporphine-type alkaloid production in wounded lotus provides insight into the biosynthetic pathway of nuciferine. *ACS Omega* 3, 8794–8802. doi: 10.1021/acsomega.8b00827

Menendez-Perdomo, I. M., and Facchini, P. J. (2018). Benzylisoquinoline alkaloids biosynthesis in sacred lotus. *Molecules* 23:2899. doi: 10.3390/molecules23112899

Mertens, J., Van Moerkercke, A., Vanden Bossche, R., Pollier, J., and Goossens, A. (2016b). Clade IVa basic helix-loop-helix transcription factors form part of a conserved jasmonate signaling circuit for the regulation of bioactive plant terpenoid biosynthesis. *Plant Cell Physiol.* 57, 2564–2575. doi: 10.1093/pcp/pcw168

Mertens, J., Pollier, J., Vanden Bossche, R., Lopez-Vidriero, I., Franco-Zorrilla, J. M., and Goossens, A. (2016a). The bHLH transcription factors TSAR1 and TSAR2 regulate Triterpene saponin biosynthesis in *Medicago truncatula*. *Plant Physiol.* 170, 194–210. doi: 10.1104/pp.15.01645

Mewis, I., Khan, M. A., Glawischnig, E., Schreiner, M., and Ulrichs, C. (2012). Water stress and aphid feeding differentially influence metabolite composition in *Arabidopsis thaliana* (L.). *PLoS One* 7:e48661. doi: 10.1371/journal.pone.0048661

Mishra, R. P., Singh, R. K., Jaiswal, H. K., Kumar, V., and Maurya, S. (2006). Rhizobium-mediated induction of phenolics and plant growth promotion in rice (*Oryza sativa L.*). *Curr. Microbiol.* 52, 383–389. doi: 10.1007/s00284-005-0296-3

Miyahara, T., Sugishita, N., Ishida-Dei, M., Okamoto, E., Kouno, T., Cano, E. A., et al. (2018). Carnation I locus contains two chalcone isomerase genes involved in orange flower coloration. *Breed Sci.* 68, 481–487. doi: 10.1270/jsbbs.18029

Moreira-Rodriguez, M., Nair, V., Benavides, J., Cisneros-Zevallos, L., and Jacobo-Velazquez, D. A. (2017). UVA, UVB light doses and harvesting time differentially tailor glucosinolate and phenolic profiles in broccoli sprouts. *Molecules* 22:1065. doi: 10.3390/molecules22071065

Moreno, D. A., Carvajal, M., Lopez-Berenguer, C., and Garcia-Viguera, C. (2006). Chemical and biological characterisation of nutraceutical compounds of broccoli. *J. Pharm. Biomed. Anal.* 41, 1508–1522. doi: 10.1016/j.jpba.2006.04.003

Moreno, P. R., Schlatmann, J. E., Van der Heijden, R., van Gulik, W. M., Ten Hoopen, H. J., Verpoorte, R., et al. (1993). Induction of ajmalicine formation and related enzyme activities in *Catharanthus roseus* cells: effect of inoculum density. *Appl. Microbiol. Biotechnol.* 39, 42–47. doi: 10.1007/BF00166846

Mortensen, S., Weaver, J. D., Sathitloetsakun, S., Cole, L. F., Rizvi, N. F., Cram, E. J., et al. (2019). The regulation of ZCT1, a transcriptional repressor of monoterpenoid indole alkaloid biosynthetic genes in *Catharanthus roseus*. *Plant Direct* 3:e00193. doi: 10.1002/pld3.193

Nabavi, S. M., Samec, D., Tomczyk, M., Milella, L., Russo, D., Habtemariam, S., et al. (2020). Flavonoid biosynthetic pathways in plants: versatile targets for metabolic engineering. *Biotechnol. Adv.* 38:107316. doi: 10.1016/j.biotechadv.2018.11.005

Naik, J., Rajput, R., Pucker, B., Stracke, R., and Pandey, A. (2021). The R2R3-MYB transcription factor MtMYB134 orchestrates flavonol biosynthesis in *Medicago truncatula*. *Plant Mol. Biol.* 106, 157–172. doi: 10.1007/s11103-021-01135-x

Nakabayashi, R., Mori, T., and Saito, K. (2014). Alternation of flavonoid accumulation under drought stress in *Arabidopsis thaliana*. *Plant Signal Behav.* 9:e29518. doi: 10.4161/psb.29518

Nguyen, V. P. T., Stewart, J., Lopez, M., Ioannou, I., and Allais, F. (2020). Glucosinolates: natural occurrence, biosynthesis, accessibility, isolation, structures, and biological activities. *Molecules* 25:4537. doi: 10.3390/molecules25194537

Nicholson, R. L., and Hammerschmidt, R. E. (2003). Phenolic compounds and their role in disease resistance. *Ann. Rev. Phytopathol.* 30, 369–389.

Noda, N., Yoshioka, S., Kishimoto, S., Nakayama, M., Douzono, M., Tanaka, Y., et al. (2017). Generation of blue chrysanthemums by anthocyanin B-ring hydroxylation and glucosylation and its coloration mechanism. *Sci. Adv.* 3:e1602785. doi: 10.1126/sciadv.1602785

O'Connor, S. E., and Maresh, J. J. (2006). Chemistry and biology of monoterpene indole alkaloid biosynthesis. *Nat. Prod. Rep.* 23, 532–547. doi: 10.1039/b512615k

Pacifico, D., Lanzanova, C., Pagnotta, E., Bassolino, L., Mastrangelo, A. M., Marone, D., et al. (2021). sustainable use of bioactive compounds from solanum tuberosum and *Brassica*ceae wastes and by-products for crop protection-a review. *Molecules* 26:2174. doi: 10.3390/molecules26082174

Park, J. E., Kim, J., Purevdorj, E., Son, Y. J., Nho, C. W., and Yoo, G. (2021). Effects of long light exposure and drought stress on plant growth and glucosinolate production in pak choi (*Brassica rapa* subsp. Chinensis). *Food Chem.* 340:128167. doi: 10.1016/j.foodchem.2020.128167

Park, J. S., Kim, J. B., Cho, K. J., Cheon, C. I., Sung, M. K., Choung, M. G., et al. (2008). Arabidopsis R2R3-MYB transcription factor AtMYB60 functions as a transcriptional repressor of anthocyanin biosynthesis in lettuce (*Lactuca sativa*). *Plant Cell Rep.* 27, 985–994. doi: 10.1007/s00299-008-0521-1

Patra, B., Schluttenhofer, C., Wu, Y., Pattanaik, S., and Yuan, L. (2013). Transcriptional regulation of secondary metabolite biosynthesis in plants. *Biochim. Biophys. Acta* 1829, 1236–1247. doi: 10.1016/j.bbagrm.2013.09.006

Paul, P., Singh, S. K., Patra, B., Sui, X., Pattanaik, S., and Yuan, L. (2017). A differentially regulated AP2/ERF transcription factor gene cluster acts downstream of a MAP kinase cascade to modulate terpenoid indole alkaloid biosynthesis in *Catharanthus roseus*. *New Phytol.* 213, 1107–1123. doi: 10.1111/nph.14252

Pichersky, E., and Raguso, R. A. (2018). Why do plants produce so many terpenoid compounds? *New Phytol.* 220, 692–702. doi: 10.1111/nph.14178

Premathilake, A. T., Ni, J., Bai, S., Tao, R., Ahmad, M., and Teng, Y. (2020). R2R3-MYB transcription factor PpMYB17 positively regulates flavonoid biosynthesis in pear fruit. *Planta* 252:59. doi: 10.1007/s00425-020-03473-4

Qi, X., Bakht, S., Leggett, M., Maxwell, C., Melton, R., and Osbourn, A. (2004). A gene cluster for secondary metabolism in oat: implications for the evolution of metabolic diversity in plants. *Proc. Natl. Acad. Sci. U.S.A.* 101, 8233–8238. doi: 10.1073/pnas.0401301101

Qu, Y., Thamm, A. M. K., Czerwinski, M., Masada, S., Kim, K. H., Jones, G., et al. (2018). Geissoschizine synthase controls flux in the formation of monoterpenoid indole alkaloids in a *Catharanthus roseus* mutant. *Planta* 247, 625–634. doi: 10.1007/s00425-017-2812-7

Rai, A., Smita, S. S., Singh, A. K., Shanker, K., and Nagegowda, D. A. (2013). Heteromeric and homomeric geranyl diphosphate synthases from *Catharanthus roseus* and their role in monoterpene indole alkaloid biosynthesis. *Mol. Plant* 6, 1531–1549. doi: 10.1093/mp/sst058

Rao, S. Q., Chen, X. Q., Wang, K. H., Zhu, Z. J., Yang, J., and Zhu, B. (2021). Effect of short-term high temperature on the accumulation of glucosinolates in *Brassica rapa*. *Plant Physiol. Biochem.* 161, 222–233. doi: 10.1016/j.plaphy.2021.02.013

Rasouli, H., Farzaei, M. H., Mansouri, K., Mohammadzadeh, S., and Khodarahmi, R. (2016). Plant cell cancer: may natural phenolic compounds prevent onset and development of plant cell malignancy? A literature review. *Molecules* 21:1104. doi: 10.3390/molecules21091104

Ravishankara, M. N., Shrivastava, N., Padh, H., and Rajani, M. (2001). HPTLC method for the estimation of alkaloids of *Cinchona officinalis* stem bark and its marketed formulations. *Planta Med.* 67, 294–296. doi: 10.1055/s-2001-11995

Rechner, O., Neugart, S., Schreiner, M., Wu, S., and Poehling, H. M. (2017). Can narrow-bandwidth light from UV-A to green alter secondary plant metabolism and increase *Brassica* plant defenses against aphids? *PLoS One* 12:e0188522. doi: 10.1371/journal.pone.0188522

Reyes Jara, A. M., Gomez Lobato, M. E., Civello, P. M., and Martinez, G. A. (2022). Phenylalanine ammonia lyase is more relevant than Chalcone synthase and *Chalcone isomerase* in the biosynthesis of flavonoids during postharvest senescence of broccoli. *J. Food Biochem.* 46:e14054. doi: 10.1111/jfbc.14054

Rivero, J., Lidoy, J., Llopis-Gimenez, A., Herrero, S., Flors, V., and Pozo, M. J. (2021). Mycorrhizal symbiosis primes the accumulation of antiherbivore compounds and enhances herbivore mortality in tomato. *J. Exp. Bot.* 72, 5038–5050. doi: 10.1093/jxb/erab171

Rizi, M. R., Azizi, A., Sayyari, M., Mirzaie-Asl, A., and Conti, L. (2021). Increased phenylpropanoids production in UV-B irradiated *Salvia verticillata* as a consequence of altered genes expression in young leaves. *Plant Physiol. Biochem.* 167, 174–184. doi: 10.1016/j.plaphy.2021.07.037

Robin, A. H., Yi, G. E., Laila, R., Yang, K., Park, J. I., Kim, H. R., et al. (2016). Expression Profiling of glucosinolate biosynthetic genes in *Brassica oleracea* L. var. Capitata inbred lines reveals their association with glucosinolate content. *Molecules* 21:787. doi: 10.3390/molecules21060787

Samira, R., Li, B., Kliebenstein, D., Li, C., Davis, E., Gillikin, J. W., et al. (2018). The bHLH transcription factor ILR3 modulates multiple stress responses in *Arabidopsis*. *Plant Mol Biol* 97, 297–309. doi: 10.1007/s11103-018-0735-8

Sanchez-Pujante, P. J., Borja-Martinez, M., Pedreno, M. A., and Almagro, L. (2017). Biosynthesis and bioactivity of glucosinolates and their production in plant in vitro cultures. *Planta* 246, 19–32. doi: 10.1007/s00425-017-2705-9

Sandholu, A. S., Mujawar, S. P., Ramakrishnan, K., Thulasiram, H. V., and Kulkarni, K. (2020). Structural studies on 10-hydroxygeraniol dehydrogenase: a novel linear substrate-specific dehydrogenase from *Catharanthus roseus*. *Proteins* 88, 1197–1206. doi: 10.1002/prot.25891

Schlager, S., and Drager, B. (2016). Exploiting plant alkaloids. *Curr. Opin Biotechnol.* 37, 155–164. doi: 10.1016/j.copbio.2015.12.003

Seo, M. S., Jin, M., Sohn, S. H., and Kim, J. S. (2017). Expression profiles of BrMYB transcription factors related to glucosinolate biosynthesis and stress response in eight subspecies of *Brassica rapa*. *FEBS Open Biol.* 7, 1646–1659. doi: 10.1002/2211-5463.12231

Sharma, A., Shahzad, B., Rehman, A., Bhardwaj, R., Landi, M., and Zheng, B. (2019). Response of phenylpropanoid pathway and the role of polyphenols in plants under abiotic stress. *Molecules* 24:2452. doi: 10.3390/molecules24132452

Shen, C., Guo, H., Chen, H., Shi, Y., Meng, Y., Lu, J., et al. (2017). Identification and analysis of genes associated with the synthesis of bioactive constituents in *Dendrobium officinale* using RNA-Seq. *Sci. Rep.* 7:187. doi: 10.1038/s41598-017-00292-8

Sheng, X., and Himo, F. (2019). Enzymatic pictet-spengler reaction: computational study of the mechanism and enantioselectivity of norcoclaurine synthase. *J. Am. Chem. Soc.* 141, 11230–11238. doi: 10.1021/jacs.9b04591

Shi, M., Gong, H., Cui, L., Wang, Q., Wang, C., Wang, Y., et al. (2020a). Targeted metabolic engineering of committed steps improves anti-cancer drug camptothecin production in *Ophiorrhiza pumila* hairy roots. *Ind. Crops Prod.* 148:112277. doi: 10.1016/j.indcrop.2020.112277

Shi, M., Huang, F., Deng, C., Wang, Y., and Kai, G. (2019). Bioactivities, biosynthesis and biotechnological production of phenolic acids in *Salvia miltiorrhiza*. *Crit. Rev. Food Sci. Nutr.* 59, 953–964. doi: 10.1080/10408398.2018.1474170

Shi, M., Liao, P., Nile, S. H., Georgiev, M. I., and Kai, G. (2021). Biotechnological exploration of transformed root culture for value-added products. *Trends Biotechnol.* 39, 137–149. doi: 10.1016/j.tibtech.2020.06.012

Shi, M., Wang, Y., Wang, X., Deng, C., Cao, W., Hua, Q., et al. (2020b). Simultaneous promotion of tanshinone and phenolic acid biosynthesis in *Salvia miltiorrhiza* hairy roots by overexpressing *Arabidopsis* MYC2. *Ind. Crops Prod.* 155:112826. doi: 10.1016/j.indcrop.2020.112826

Shukla, A. K., Shasany, A. K., Gupta, M. M., and Khanuja, S. P. (2006). Transcriptome analysis in *Catharanthus roseus* leaves and roots for comparative terpenoid indole alkaloid profiles. *J. Exp. Bot.* 57, 3921–3932. doi: 10.1093/jxb/erl146

Sic Zlabur, J., Radman, S., Fabek Uher, S., Opacic, N., Benko, B., Galic, A., et al. (2021). Plant response to mechanically-induced stress: a case study on specialized metabolites of leafy vegetables. *Plants* 10:2650. doi: 10.3390/plants10122650

Simkin, A. J., Miettinen, K., Claudel, P., Burlat, V., Guirimand, G., Courdavault, V., et al. (2013). Characterization of the plastidial geraniol synthase from Madagascar periwinkle which initiates the monoterpenoid branch of the alkaloid pathway in internal phloem associated parenchyma. *Phytochemistry* 85, 36–43. doi: 10.1016/j.phytochem.2012.09.014

Singh, P., Arif, Y., Bajguz, A., and Hayat, S. (2021). The role of quercetin in plants. *Plant Physiol. Biochem.* 166, 10–19. doi: 10.1016/j.plaphy.2021.05.023

Singh, U. P., Sarma, B. K., Singh, D. P., and Bahadur, A. (2002). Plant growth-promoting rhizobacteria-mediated induction of phenolics in pea (*Pisum sativum*) after infection with *Erysiphe pisi*. *Curr. Microbiol.* 44, 396–400. doi: 10.1007/s00284-001-0007-7

Skoneczny, D., Zhu, X., Weston, P. A., Gurr, G. M., Callaway, R. M., and Weston, L. A. (2019). Production of pyrrolizidine alkaloids and shikonins in *Echium plantagineum* L. in response to various plant stressors. *Pest Manag. Sci.* 75, 2530–2541. doi: 10.1002/ps.5540

Sonderby, I. E., Geu-Flores, F., and Halkier, B. A. (2010). Biosynthesis of glucosinolates–gene discovery and beyond. *Trends Plant Sci.* 15, 283–290. doi: 10.1016/j.tplants.2010.02.005

Song, H., Yi, H., Lee, M., Han, C. T., Lee, J., Kim, H., et al. (2018). Purple *Brassica oleracea* var. capitata F. rubra is due to the loss of BoMYBL2-1 expression. *BMC Plant Biol.* 18:82. doi: 10.1186/s12870-018-1290-9

Sotelo, T., Velasco, P., Soengas, P., Rodriguez, V. M., and Cartea, M. E. (2016). Modification of leaf glucosinolate contents in *brassica oleracea* by divergent selection and effect on expression of genes controlling glucosinolate pathway. *Front. Plant Sci.* 7:1012. doi: 10.3389/fpls.2016.01012

Sui, X., Singh, S. K., Patra, B., Schluttenhofer, C., Guo, W., Pattanaik, S., et al. (2018). Cross-family transcription factor interaction between MYC2 and GBFs modulates terpenoid indole alkaloid biosynthesis. *J. Exp. Bot.* 69, 4267–4281. doi: 10.1093/jxb/ery229

Sun, M., Shi, M., Wang, Y., Huang, Q., Yuan, T., Wang, Q., et al. (2019a). The biosynthesis of phenolic acids is positively regulated by the JA-responsive transcription factor ERF115 in *Salvia miltiorrhiza*. *J. Exp. Bot.* 70, 243–254. doi: 10.1093/jxb/ery349

Sun, Q., Jiang, S., Zhang, T., Xu, H., Fang, H., Zhang, J., et al. (2019b). Apple NAC transcription factor MdNAC52 regulates biosynthesis of anthocyanin and proanthocyanidin through MdMYB9 and MdMYB11. *Plant Sci.* 289:110286. doi: 10.1016/j.plantsci.2019.110286

Sun, W. J., Zhan, J. Y., Zheng, T. R., Sun, R., Wang, T., Tang, Z. Z., et al. (2018). The jasmonate-responsive transcription factor CbWRKY24 regulates terpenoid biosynthetic genes to promote saponin biosynthesis in *Conyza blinii* H. *Lev. J. Genet* 97, 1379–1388.

Suttipanta, N., Pattanaik, S., Kulshrestha, M., Patra, B., Singh, S. K., and Yuan, L. (2011). The transcription factor CrWRKY1 positively regulates the terpenoid indole alkaloid biosynthesis in *Catharanthus roseus*. *Plant Physiol.* 157, 2081–2093. doi: 10.1104/pp.111.181834

Tholl, D. (2015). Biosynthesis and biological functions of terpenoids in plants. *Adv. Biochem. Eng. Biotechnol.* 148, 63–106. doi: 10.1007/10_2014_295

Tungmunnithum, D., Thongboonyou, A., Pholboon, A., and Yangsabai, A. (2018). Flavonoids and other phenolic compounds from medicinal plants for pharmaceutical and medical aspects: an overview. *Medicines* 5:93. doi: 10.3390/medicines5030093

Vadassery, J., Reichelt, M., Hause, B., Gershenzon, J., Boland, W., and Mithofer, A. (2012). CML42-mediated calcium signaling coordinates responses to *Spodoptera herbivory* and abiotic stresses in *Arabidopsis*. *Plant Physiol* 159, 1159–1175. doi: 10.1104/pp.112.198150

Villarreal-Garcia, D., Nair, V., Cisneros-Zevallos, L., and Jacobo-Velazquez, D. A. (2016). Plants as biofactories: postharvest stress-induced accumulation of phenolic compounds and glucosinolates in broccoli subjected to wounding stress and exogenous phytohormones. *Front. Plant Sci.* 7:45. doi: 10.3389/fpls.2016.00045

Vrabec, R., Marikova, J., Locarek, M., Korabecny, J., Hulcova, D., Hostalkova, A., et al. (2022). Monoterpene indole alkaloids from *Vinca minor* L. (Apocynaceae): Identification of new structural scaffold for treatment of Alzheimer's disease. *Phytochemistry* 194:113017. doi: 10.1016/j.phytochem.2021.113017

Wang, B., Sun, W., Li, Q., Li, Y., Luo, H., Song, J., et al. (2015). Genome-wide identification of phenolic acid biosynthetic genes in *Salvia miltiorrhiza*. *Planta* 241, 711–725. doi: 10.1007/s00425-014-2212-1

Wang, S., Alseekh, S., Fernie, A. R., and Luo, J. (2019c). The structure and function of major plant metabolite modifications. *Mol. Plant* 12, 899–919. doi: 10.1016/j.molp.2019.06.001

Wang, L., Lu, W., Ran, L., Dou, L., Yao, S., Hu, J., et al. (2019b). R2R3-MYB transcription factor MYB6 promotes anthocyanin and proanthocyanidin biosynthesis but inhibits secondary cell wall formation in *Populus tomentosa*. *Plant J.* 99, 733–751. doi: 10.1111/tpj.14364

Wang, C., Wu, C., Wang, Y., Xie, C., Shi, M., Nile, S., et al. (2019a). Transcription factor OpWRKY3 is involved in the development and biosynthesis of camptothecin and its precursors in *Ophiorrhiza pumila* hairy roots. *Int. J. Mol. Sci.* 20:3996. doi: 10.3390/ijms20163996

Wang, J., Li, Y., Wu, T., Miao, C., Xie, M., Ding, B., et al. (2021). Single-cell-type transcriptomic analysis reveals distinct gene expression profiles in wheat guard cells in response to abscisic acid. *Funct. Plant Biol.* 48, 1087–1099. doi: 10.1071/FP20368

Wang, Z. L., Wang, S., Kuang, Y., Hu, Z. M., Qiao, X., and Ye, M. (2018b). A comprehensive review on phytochemistry, pharmacology, and flavonoid biosynthesis of *Scutellaria baicalensis*. *Pharm Biol.* 56, 465–484. doi: 10.1080/13880209.2018.1492620

Wang, N., Liu, W., Zhang, T., Jiang, S., Xu, H., Wang, Y., et al. (2018a). Transcriptomic analysis of red-fleshed apples reveals the novel role of MdWRKY11 in flavonoid and anthocyanin biosynthesis. *J. Agric. Food Chem.* 66, 7076–7086. doi: 10.1021/acs.jafc.8b01273

Wang, X. C., Wu, J., Guan, M. L., Zhao, C. H., Geng, P., and Zhao, Q. (2020). *Arabidopsis* MYB4 plays dual roles in flavonoid biosynthesis. *Plant J* 101, 637–652. doi: 10.1111/tpj.14570

Wang, Y., Guo, D., Li, H. L., and Peng, S. Q. (2013). Characterization of HbWRKY1, a WRKY transcription factor from *Hevea brasiliensis* that negatively regulates HbSRPP. *Plant Physiol. Biochem.* 71, 283–289. doi: 10.1016/j.plaphy.2013.07.020

Wani, K. I., Choudhary, S., Zehra, A., Naeem, M., Weathers, P., and Aftab, T. (2021). Enhancing artemisinin content in and delivery from *Artemisia annua*: a review of alternative, classical, and transgenic approaches. *Planta* 254:29. doi: 10.1007/s00425-021-03676-3

Wari, D., Aboshi, T., Shinya, T., and Galis, I. (2021). Integrated view of plant metabolic defense with particular focus on chewing herbivores. *J. Integr. Plant Biol.* 64, 449–475. doi: 10.1111/jipb.13204

Williams, D., Qu, Y., Simionescu, R., and De Luca, V. (2019). The assembly of (+)-vincadifformine- and (-)-tabersonine-derived monoterpenoid indole alkaloids in *Catharanthus roseus* involves separate branch pathways. *Plant J.* 99, 626–636. doi: 10.1111/tpj.14346

Xing, B., Liang, L., Liu, L., Hou, Z., Yang, D., Yan, K., et al. (2018). Overexpression of SmbHLH148 induced biosynthesis of tanshinones as well as phenolic acids in *Salvia miltiorrhiza* hairy roots. *Plant Cell Rep.* 37, 1681–1692. doi: 10.1007/s00299-018-2339-9

Xu, F., Ning, Y., Zhang, W., Liao, Y., Li, L., Cheng, H., et al. (2014). An R2R3-MYB transcription factor as a negative regulator of the flavonoid biosynthesis pathway in *Ginkgo biloba*. *Funct. Integr. Genomics* 14, 177–189. doi: 10.1007/s10142-013-0352-1

Xu, H., Wang, N., Liu, J., Qu, C., Wang, Y., Jiang, S., et al. (2017). The molecular mechanism underlying anthocyanin metabolism in apple using the MdMYB16 and MdbHLH33 genes. *Plant Mol. Biol.* 94, 149–165. doi: 10.1007/s11103-017-0601-0

Xu, H., Yang, G., Zhang, J., Wang, Y., Zhang, T., Wang, N., et al. (2018). Overexpression of a repressor MdMYB15L negatively regulates anthocyanin and cold tolerance in red-fleshed callus. *Biochem. Biophys. Res. Commun.* 500, 405–410. doi: 10.1016/j.bbrc.2018.04.088

Xu, Y. H., Wang, J. W., Wang, S., Wang, J. Y., and Chen, X. Y. (2004). Characterization of GaWRKY1, a cotton transcription factor that regulates the sesquiterpene synthase gene $^{(+)}$-delta-cadinene synthase-A. *Plant Physiol.* 135, 507–515. doi: 10.1104/pp.104.038612

Xu, Z., Wang, M., Ren, T., Li, K., Li, Y., Marowa, P., et al. (2021). Comparative transcriptome analysis reveals the molecular mechanism of salt tolerance in *Apocynum venetum*. *Plant Physiol. Biochem.* 167, 816–830. doi: 10.1016/j.plaphy.2021.08.043

Yahyazadeh, M., Jerz, G., Winterhalter, P., and Selmar, D. (2021). The complexity of sound quantification of specialized metabolite biosynthesis: the stress related impact on the alkaloid content of *Catharanthus roseus*. *Phytochemistry* 187:112774. doi: 10.1016/j.phytochem.2021.112774

Yahyazadeh, M., Meinen, R., Hansch, R., Abouzeid, S., and Selmar, D. (2018). Impact of drought and salt stress on the biosynthesis of alkaloids in *Chelidonium majus* L. *Phytochemistry* 152, 204–212. doi: 10.1016/j.phytochem.2018.05.007

Yamada, Y., Kokabu, Y., Chaki, K., Yoshimoto, T., Ohgaki, M., Yoshida, S., et al. (2011). Isoquinoline alkaloid biosynthesis is regulated by a unique bHLH-type transcription factor in *Coptis japonica*. *Plant Cell Physiol.* 52, 1131–1141. doi: 10.1093/pcp/pcr062

Yan, H., Pei, X., Zhang, H., Li, X., Zhang, X., Zhao, M., et al. (2021). MYB-mediated regulation of anthocyanin biosynthesis. *Int. J. Mol. Sci.* 22:3103. doi: 10.3390/ijms22063103

Yang, C. Q., Fang, X., Wu, X. M., Mao, Y. B., Wang, L. J., and Chen, X. Y. (2012). Transcriptional regulation of plant secondary metabolism. *J. Integr. Plant Biol.* 54, 703–712. doi: 10.1111/j.1744-7909.2012.01161.x

Yang, L., Li, J., Ji, J., Li, P., Yu, L., Abd Allah, E. F., et al. (2016). High temperature induces expression of tobacco transcription factor NtMYC2a to regulate nicotine and JA biosynthesis. *Front. Physiol.* 7:465. doi: 10.3389/fphys.2016.00465

Yang, M., Wang, Q., Liu, Y., Hao, X., Wang, C., Liang, Y., et al. (2021a). Divergent camptothecin biosynthetic pathway in *Ophiorrhiza pumila*. *BMC Biol.* 19:122. doi: 10.1186/s12915-021-01051-y

Yang, R., Wang, S., Zou, H., Li, L., Li, Y., Wang, D., et al. (2021b). R2R3-MYB transcription factor SmMYB52 positively regulates biosynthesis of salvianolic acid B and inhibits root growth in *Salvia miltiorrhiza*. *Int. J. Mol. Sci.* 22:9538. doi: 10.3390/ijms22179538

Yu, C., Guo, H., Zhang, Y., Song, Y., Pi, E., Yu, C., et al. (2017). Identification of potential genes that contributed to the variation in the taxoid contents between two *Taxus* species (*Taxus media* and *Taxus mairei*). *Tree Physiol.* 37, 1659–1671. doi: 10.1093/treephys/tpx091

Yu, C., Luo, X., Zhang, C., Xu, X., Huang, J., Chen, Y., et al. (2020). Tissue-specific study across the stem of *Taxus media* identifies a phloem-specific TmMYB3 involved in the transcriptional regulation of paclitaxel biosynthesis. *Plant J.* 103, 95–110. doi: 10.1111/tpj.14710

Yu, C., Zhan, X., Zhang, C., Xu, X., Huang, J., Feng, S., et al. (2021). Comparative metabolomic analyses revealed the differential accumulation of taxoids, flavonoids and hormones among six Taxaceae trees. *Sci. Hortic.* 285:110196. doi: 10.1016/j.scienta.2021.110196

Yu, Z. X., Li, J. X., Yang, C. Q., Hu, W. L., Wang, L. J., and Chen, X. Y. (2012). The jasmonate-responsive AP2/ERF transcription factors AaERF1 and AaERF2 positively regulate artemisinin biosynthesis in *Artemisia annua* L. *Mol. Plant* 5, 353–365. doi: 10.1093/mp/ssr087

Zafar, N., Mujib, A., Ali, M., Tonk, D., Gulzar, B., Malik, M. Q., et al. (2020). Cadmium chloride (CdCl2) elicitation improves reserpine and ajmalicine yield in *Rauvolfia serpentina* as revealed by high-performance thin-layer chromatography (HPTLC). *3 Biotech* 10:344. doi: 10.1007/s13205-020-02339-6

Zhan, G., Miao, R., Zhang, F., Chang, G., Zhang, L., Zhang, X., et al. (2020). Monoterpene indole alkaloids with acetylcholinesterase inhibitory activity from the leaves of *Rauvolfia vomitoria*. *Bioorg. Chem.* 102:104136. doi: 10.1016/j.bioorg.2020.104136

Zhan, X., Liao, X., Luo, X., Zhu, Y., Feng, S., Yu, C., et al. (2018). Comparative metabolomic and proteomic analyses reveal the regulation mechanism underlying MeJA-induced bioactive compound accumulation in cutleaf groundcherry (*Physalis angulata L.*) hairy roots. *J. Agric. Food Chem.* 66, 6336–6347. doi: 10.1021/acs.jafc.8b02502

Zhang, C., Xing, B., Yang, D., Ren, M., Guo, H., Yang, S., et al. (2020). SmbHLH3 acts as a transcription repressor for both phenolic acids and tanshinone biosynthesis in *Salvia miltiorrhiza* hairy roots. *Phytochemistry* 169:112183. doi: 10.1016/j.phytochem.2019.112183

Zhang, D., Jiang, C., Huang, C., Wen, D., Lu, J., Chen, S., et al. (2019). The light-induced transcription factor FtMYB116 promotes accumulation of rutin

in *Fagopyrum tataricum*. *Plant Cell Environ.* 42, 1340–1351. doi: 10.1111/pce.13470

Zhang, J., Morris-Natschke, S. L., Ma, D., Shang, X. F., Yang, C. J., Liu, Y. Q., et al. (2021b). Biologically active indolizidine alkaloids. *Med. Res. Rev.* 41, 928–960. doi: 10.1002/med.21747

Zhang, S., Zhang, L., Zou, H., Qiu, L., Zheng, Y., Yang, D., et al. (2021c). Effects of light on secondary metabolite biosynthesis in medicinal plants. *Front. Plant Sci.* 12:781236. doi: 10.3389/fpls.2021.781236

Zhang, H., Zhang, Z., Zhao, Y., Guo, D., Zhao, X., Gao, W., et al. (2021a). StWRKY13 promotes anthocyanin biosynthesis in potato (*Solanum tuberosum*) tubers. *Funct. Plant Biol.* 49, 102–114. doi: 10.1071/FP21109

Zhang, X., Abrahan, C., Colquhoun, T. A., and Liu, C. J. (2017). A proteolytic regulator controlling chalcone synthase stability and flavonoid biosynthesis in *Arabidopsis*. *Plant Cell* 29, 1157–1174. doi: 10.1105/tpc.16.00855

Zhang, X., Ding, X., Ji, Y., Wang, S., Chen, Y., Luo, J., et al. (2018). Measurement of metabolite variations and analysis of related gene expression in Chinese liquorice (*Glycyrrhiza uralensis*) plants under UV-B irradiation. *Sci. Rep.* 8:6144. doi: 10.1038/s41598-018-24284-4

Zhou, F., and Pichersky, E. (2020). More is better: the diversity of terpene metabolism in plants. *Curr. Opin. Plant Biol.* 55, 1–10. doi: 10.1016/j.pbi.2020.01.005

Zhou, W., Shi, M., Deng, C., Lu, S., Huang, F., Wang, Y., et al. (2021b). The methyl jasmonate-responsive transcription factor SmMYB1 promotes phenolic acid biosynthesis in *Salvia miltiorrhiza*. *Hortic. Res.* 8:10. doi: 10.1038/s41438-020-00443-5

Zhou, W., Li, S., Maoz, I., Wang, Q., Xu, M., Feng, Y., et al. (2021a). SmJRB1 positively regulates the accumulation of phenolic acid in *Salvia miltiorrhiza*. *Ind. Crops Prod.* 164:113417. doi: 10.1016/j.indcrop.2021.113417

Zhou, Y., Sun, W., Chen, J., Tan, H., Xiao, Y., Li, Q., et al. (2016). SmMYC2a and SmMYC2b played similar but irreplaceable roles in regulating the biosynthesis of tanshinones and phenolic acids in Salvia miltiorrhiza. *Sci Rep* 6, 22852. doi: 10.1038/srep22852

Ziegler, J., and Facchini, P. J. (2008). Alkaloid biosynthesis: metabolism and trafficking. *Annu. Rev. Plant Biol.* 59, 735–769. doi: 10.1146/annurev.arplant.59.032607.092730

Zuk, M., Szperlik, J., Hnitecka, A., and Szopa, J. (2019). Temporal biosynthesis of flavone constituents in flax growth stages. *Plant Physiol. Biochem.* 142, 234–245. doi: 10.1016/j.plaphy.2019.07.009

Zvi, M. M. B., Shklarman, E., Masci, T., Kalev, H., Debener, T., Shafir, S., et al. (2012). PAP1 transcription factor enhances production of phenylpropanoid and terpenoid scent compounds in rose flowers. *New Phytol.* 195, 335–345. doi: 10.1111/j.1469-8137.2012.04161.x

Conflict of Interest: The authors declare that the research was conducted in the absence of any commercial or financial relationships that could be construed as a potential conflict of interest.

Publisher's Note: All claims expressed in this article are solely those of the authors and do not necessarily represent those of their affiliated organizations, or those of the publisher, the editors and the reviewers. Any product that may be evaluated in this article, or claim that may be made by its manufacturer, is not guaranteed or endorsed by the publisher.

Copyright © 2022 Zhan, Chen, Chen and Shen. This is an open-access article distributed under the terms of the Creative Commons Attribution License (CC BY). The use, distribution or reproduction in other forums is permitted, provided the original author(s) and the copyright owner(s) are credited and that the original publication in this journal is cited, in accordance with accepted academic practice. No use, distribution or reproduction is permitted which does not comply with these terms.

frontiers | Frontiers in Plant Science

ORIGINAL RESEARCH
published: 06 May 2022
doi: 10.3389/fpls.2022.904105

The Superoxide Dismutase Gene Family in *Nicotiana tabacum*: Genome-Wide Identification, Characterization, Expression Profiling and Functional Analysis in Response to Heavy Metal Stress

*Chunsong Huo[1], Linshen He[1], Ting Yu[1], Xue Ji[1], Rui Li[1], Shunqin Zhu[2], Fangyuan Zhang[2], He Xie[3] and Wanhong Liu[1]**

[1] Chongqing Key Laboratory of Industrial Fermentation Microorganism, School of Chemistry and Chemical Engineering, Chongqing University of Science and Technology, Chongqing, China, [2] School of Life Sciences, Southwest University, Chongqing, China, [3] Tobacco Breeding and Biotechnology Research Center, Yunnan Academy of Tobacco Agricultural Sciences, Kunming, China

OPEN ACCESS

Edited by:
Lei Zhang, Second Military Medical University, China

Reviewed by:
Zhichao Xu, Northeast Forestry University, China
Guoyin Kai, Zhejiang Chinese Medical University, China
Pengda Ma, Northwest A&F University, China

***Correspondence:**
Wanhong Liu
liuwanh@163.com

Specialty section:
This article was submitted to Plant Metabolism and Chemodiversity, a section of the journal Frontiers in Plant Science

Received: *25 March 2022*
Accepted: *11 April 2022*
Published: *06 May 2022*

Citation:
Huo C, He L, Yu T, Ji X, Li R, Zhu S, Zhang F, Xie H and Liu W (2022) The Superoxide Dismutase Gene Family in Nicotiana tabacum: Genome-Wide Identification, Characterization, Expression Profiling and Functional Analysis in Response to Heavy Metal Stress. Front. Plant Sci. 13:904105. doi: 10.3389/fpls.2022.904105

Superoxide dismutases (SODs) play an important role in protecting plants against ROS toxicity induced by biotic and abiotic stress. Recent studies have shown that the SOD gene family is involved in plant growth and development; however, knowledge of the SOD gene family in tobacco is still limited. In the present study, the SOD gene family was systematically characterized in the tobacco genome. Based on the conserved motif and phylogenetic tree, 15 *NtSOD* genes were identified and classified into three subgroups, including 5 *NtCSDs*, 7 *NtFSDs* and 3 *NtMSDs*. The predicted results of the transport peptide or signal peptide were consistent with their subcellular localization. Most *NtSOD* genes showed relatively well-maintained exon-intron and motif structures in the same subgroup. An analysis of *cis*-acting elements in *SOD* gene promoters showed that *NtSOD* expression was regulated by plant hormones, defense and stress responses, and light. In addition, multiple transcription factors and miRNAs are predicted to be involved in the regulation of *NtSOD* gene expression. The qPCR results indicated specific spatial and temporal expression patterns of the NtSOD gene family in different tissues and developmental stages, and this gene family played an important role in protecting against heavy metal stress. The results of functional complementation tests in the yeast mutant suggested that *NtCSD1a*, *NtFSD1e* and *NtMSD1b* scavenge ROS produced by heavy metal stress. This study represents the first genome-wide analysis of the NtSOD gene family, which lays a foundation for a better understanding of the function of the NtSOD gene family and improving the tolerance of plants to heavy metal toxicity.

Keywords: tobacco, superoxide dismutase (SOD), heavy metal, expression profiles, functional analysis

INTRODUCTION

Increasingly severe heavy metal pollution has exerted serious effects on crop growth, yield and quality. However, heavy metals such as Cu, Zn, Fe and Mn are essential for plant growth and development as micronutrient elements but become toxic when present in excess concentrations. Moreover, trace amounts of non-essential elements such as Cd and Hg are highly toxic to plants. For example, exposure of plants to Cd triggers severe symptoms, including chlorosis, root tip browning, stunted growth, and even plant death (Nagajyoti et al., 2010). Generally, heavy metals cause harmful physiological processes in plant cells, including the induction of reactive oxygen species (ROS) generation by changing the intracellular antioxidant defense system, binding the sulfhydryl, histidine and carboxyl groups of proteins and inactivating proteins. The substitution of essential ions at specific sites of proteins causes a loss of function (Hossain et al., 2012). Oxidative stress induced by heavy metals causes oxidative damage to cell membranes, proteins and nucleic acids and even increases cell death (Mittler, 2002). Therefore, scavenging excessive ROS in plant cells is an important strategy for plants to resist the toxicity induced by heavy metals.

Maintaining an optimal intracellular ROS level is essential for plant growth and development (Mittler, 2017). Generally, the ROS generated in chloroplasts, mitochondria and other organelles are maintained in a stable balance by the antioxidant defense system (ADS) in plant cells. The ADS in plants usually contains two categories of molecules: non-enzymatic antioxidant active substances, including ascorbic acid, glutathione, phenolic acid, and flavonoids; and antioxidants, such as superoxide dismutase and catalase. The excessive accumulation of intracellular ROS is scavenged by the complex ADS in plant cells. Among antioxidant systems, superoxide dismutase (SOD, EC 1.15.1.1) plays a pioneer role in scavenging ROS by activating a series of biochemical processes. Its main biofunction is to convert superoxide radicals into oxygen and hydrogen peroxide and protect plant cells from oxidative damage (Su et al., 2021). SODs are metalloproteinases, which are usually encoded by a gene family. According to the different metal cofactors, the SOD family genes in higher plants are classified into three subfamilies: copper zinc SOD (CSD), ferrum SOD (FSD) and manganese SOD (MSD) (Fink and Scandalios, 2002; Abreu and Cabelli, 2010). CSD is most widely distributed in the cytoplasm, chloroplast, peroxisomes, glyoxalic acid cycle and extracellular space. FSD is mainly located in chloroplasts, while MSD is usually located in the mitochondrial matrix and peroxisome (Pilon et al., 2011). In addition to scavenging ROS, SODs also play important roles in electron transport, photosynthesis and signal transmission. For example, CSD loss-of-function in *Arabidopsis* results in significant inhibition of plant growth and development and decreased chloroplast size, chlorophyll content and photosynthetic activity compared with the wild-type plant (Rizhsky et al., 2003). The *Arabidopsis thaliana fsd1* mutant extends fewer lateral roots than the WT strain, but root growth was resumed by expressing FSD (Dvořák et al., 2020). Based on these results, SOD plays an important role in plant growth and responses to environmental changes by maintaining ROS homeostasis.

Superoxide dismutase plays a key role in plant resistance to drought, cold, salinity, and heavy metal toxicity, and regulates plant senescence (Sahu et al., 2017; Pan et al., 2019; Zang et al., 2020; Liu et al., 2021). In recent years, a positive correlation was observed between plant metal toxicity tolerance and antioxidant enzyme activity in heavy metal stress studies (Hasanuzzaman et al., 2020). For example, Ni stress significantly activated the antioxidant enzymes such as SOD and glutathione peroxidase (GPX) in rice leaves (Hasanuzzaman et al., 2019). Cd stimulates the activity of the antioxidant enzymes SOD, CAT and POD in *Pseudochlorella pringsheimii* to scavenge heavy metal-induced ROS and exhibits a dose-dependent effect (Ismaiel and Said, 2018). Over-expression of the *SaCSD* gene from *Sedum alfredii* in *Arabidopsis* increases Cd tolerance in transgenic plants by scavenging ROS (Li et al., 2017). However, the response of different SOD isozymes to heavy metal stress differed. Significantly higher activity of CSD was observed in the leaves and roots of *Tagetes patula* under Cd stress, while MSD activity was lower (Liu et al., 2011). In *Pisum sativum* plants, the activity of CSD localized in the cytoplasm was significantly inhibited by Cd, and FSD was more resistant than CSD, while MSD, the most resistant isoform to Cd, maintained 50% activity under 40 μM Cd stress (Sandalio et al., 2001). Therefore, an in-depth understanding of the fine-tuned mechanisms of ROS homeostasis depends on systematic studies of the functions of plant SOD gene family members.

Genome-wide identification of the SOD gene family has been performed in several plants, including monocots such as rice (Yadav et al., 2019), wheat (Jiang et al., 2019), and sorghum (Filiz and Tombuloğlu, 2015), and dicots such as cotton (Wang et al., 2016), alfalfa (Song et al., 2018), and rapeseed (Su et al., 2021). Tobacco is the most widely cultivated non-food cash crop worldwide. To date, studies on the genome-wide identification of the SOD gene family in tobacco have not been reported. In the present study, the SOD gene family of tobacco cultivar TN90 was identified at the whole genome level, and its sequence characteristics and gene structure were systematically analyzed. The promoter sequences and *cis*-acting elements of SOD gene family members were predicted and analyzed. Transcription factors and miRNAs that may be involved in the regulation of *SOD* gene expression were analyzed. The tissue expression pattern and induced expression pattern of the *NtSOD* genes in plants under different metal stresses were analyzed using qPCR to further explore the function of the *NtSOD* genes. This study laid a foundation for further study of *SOD* gene function in tobacco exposed to heavy metal stress.

MATERIALS AND METHODS

Identification and Sequence Analysis of the NtSOD Gene Family

The annotation information of genomic coding and protein sequences of *N. tabacum* cultivar TN90 were downloaded

from the NCBI Genome database[1]. The HMM profiles of CSD (PF00080), FSD (PF02777) and MSD (PF00081) were downloaded from the Pfam database[2], which was used as the query for searching the deduced protein sequences using the HMMER search program[3]. The candidate protein sequences were submitted to the SMART database[4] and NCBI-CCD website[5] to verify the conserved domains of SOD proteins. The molecular weight and theoretical iso-electric point of NtSOD proteins were calculated using the ProtParam tool in ExPASy web[6]. The subcellular localization of NtSOD proteins was predicted using the BUSCA web server[7] (Savojardo et al., 2018).

Phylogenetic Analysis

Twenty-three SOD proteins were selected to construct an unrooted phylogenetic tree using MEGA 7 with the neighbor-joining (NJ) algorithm and 1,000 bootstrap replicates to investigate the phylogenetic relationships of the *SOD* genes between tobacco and *A. thaliana*; other parameters all used the default setting. Finally, the iTOL online tool[8] was used to visualize the phylogenetic trees.

Multiple Sequence Alignment, Motif Composition and Gene Structure

Multiple sequence alignment was performed with the MAFFT software (Katoh and Standley, 2013) using the FFT-NS-2 algorithm and subsequently visualized using Jalview software packages to construct consensus sequences of NtSOD family members (Waterhouse et al., 2009). An internal consistency analysis was conducted on each of the three groups of *NtSOD* genes using BioEdit software. Multiple EM for Motif Elicitation (MEME) suite (http://meme-suite) was used with the default parameters to determine the distribution of conserved motifs within the NtSOD proteins (Bailey et al., 2015). The diagrams of the exon-intron structure of *NtSOD* genes were generated using the online tool GSDS[9] according to the available coding sequence and their respective genomic sequence (Hu et al., 2015). The composite picture of the phylogenetic tree, motif distribution and gene structure of *NtSOD* genes was generated using the Gene Structure View program of TBtools software (Chen et al., 2020).

Prediction of *Cis*-Acting Elements

Two thousand-bp sequences upstream of the translation start site were extracted as promoter regions using the Gtf/Gff3 Sequences Extract program of TBtools software to further understand the potential functions of the *cis*-regulatory elements in *NtSOD* genes. The *cis*-regulatory elements in the promoter sequences were analyzed with the PlantCare online tool[10], and then the results were visualized with the Simple BioSequence Viewer of TBtools software (Chen et al., 2020).

Prediction of Transcription Factors and miRNAs Involved in Regulating NtSOD Expression

As a method to better understand the transcription factors and miRNAs involved in regulating *NtSOD* expression, the promoter and mRNA sequences were used to predict possible transcription factor binding sites and target miRNAs, respectively. In detail, 2000-bp promoter sequences of *NtSOD* genes were submitted to the PlantRegMap website[11] to predict the transcription factors involved in regulating *NtSOD* expression with the Regulation Prediction tool at a p value $\leq 1e^{-6}$ (Tian et al., 2020). For the miRNA target gene analysis, NtSOD mRNA sequences were submitted to the psRNATarget online server[12], and then the network map was generated using Cytoscape software (Dai et al., 2018).

Plant Materials and Heavy Metal Treatments

Seeds of tobacco cultivar TN90 were sown in uncontaminated nutrient soil and generated plantlets in a greenhouse at $25 \pm 2°C$ under a 16/8 h (light/dark) photoperiod. Two-week-old tobacco seedlings were transplanted to hydroponic tanks and cultured with half-strength Hoagland's solution for 7 days. Heavy metal stress was induced by replacing the solution in hydroponic tanks with fresh Hoagland's solution containing 200 μM $CuSO_4$, 200 μM $ZnSO_4$, 200 μM $MnSO_4$, 200 μM Fe-EDTA, or 50 μM $CdCl_2$. For ion-deficiency treatments, the solutions were replaced with fresh Hoagland's solution lacking Cu, Zn, Mn and Fe (Yu et al., 2021). The tobacco seedlings were cultured with the abovementioned treatments for 7 days. Subsequently, the leaves and roots of the seedlings were separately harvested. For the analysis of the tissue expression profile, five tissue samples, including roots, stems, old leaves, young leaves and flowers, were collected from four-month-old tobacco plants grown in the natural environment. All samples were frozen immediately in liquid nitrogen and stored at −80°C until total RNA was isolated. Each experimental group consisted of three biological replicates and technical duplicates.

Determination of the Heavy Metal Content in Tobacco Plants

The metal ion concentrations in the roots and shoots of tobacco plants treated with various heavy metals were measured in this study. The roots of tobacco plants were soaked in a 20 mM EDTA solution for half an hour and then washed three times with distilled water to remove heavy metal ions and precipitates adsorbed on the root surface with sterile absorbent paper for laboratory. The plant materials, including roots and shoots, were

[1] https://www.ncbi.nlm.nih.gov/genome/425?genome_assembly_id=274804
[2] https://pfam.xfam.org/
[3] http://hmmer.org
[4] http://smart.embl.de/
[5] https://www.ncbi.nlm.nih.gov/Structure/bwrpsb/bwrpsb.cgi
[6] http://www.expasy.org/
[7] http://busca.biocomp.unibo.it/
[8] https://itol.embl.de/
[9] http://gsds.gao-lab.org/
[10] http://bioinformatics.psb.ugent.be/webtools/plantcare/html/
[11] http://plantregmap.gao-lab.org/regulation_prediction.php
[12] http://plantgrn.noble.org/psRNATarget/

dried in an oven at 80°C for 3 days until a constant weight was obtained. Subsequently, the dried roots and shoots were separately ground into powders, and 20 mg of powdered sample was digested with 7 mL of concentrated HNO_3 for 2 h at 115°C. The contents of Cd, Cu, Zn, Fe and Mn were determined using flame atomic absorption spectrometry (TAS-986, China) at wavelengths of 228.8 nm, 324.8 nm, 213.9 nm, 248.3 nm and 279.5 nm, respectively.

Analysis of the Pattern of NtSOD Gene Expression

Total RNA was extracted from the abovementioned plant materials using an RNAsimple Total RNA kit (DP419, Tiangen Biotech, Beijing, China) according to the manual, and then the quality and concentration of RNA were determined using a BioPhotometer Plus instrument (Eppendorf, Germany). Subsequently, 5 μg of total RNA were used to synthesize first-strand cDNAs *via* reverse transcription using the GoScriptTM Reverse Transcriptase Kit (Promega, Madison, WI, United States) according to the manufacturer's protocol. All cDNA samples were diluted 25 times with RNase-free water and stored at −20°C until qPCR was performed.

In the present study, *NtSOD* gene expression was analyzed based on transcriptome data and qPCR results. The raw transcriptome data (PRJNA208209) of tobacco cultivar TN90 were downloaded from NCBI-BioProject, including SRA data from roots, stems, young leaves, mature leaves, senescent leaves, young flowers, mature flowers, and senescent flowers. The relative abundance of each gene transcript was calculated as transcripts per kilobase million (TPM) values using the Salmon program and visualized in a heatmap using the Heatmap tool of TBtools. qPCR was performed with a CFX96TM real-time fluorescence quantification platform (Bio-Rad, United States) using SYBR Green enzyme (Novoprotein, China) with the following procedure to further verify the results of transcriptome data analysis: 95°C for 1 min, followed by 45 cycles of 95°C for 15 s and 60°C for 30 s. The qPCR primers were designed using Primer Premier 6.0 and are listed in **Supplementary Table 1**. The relative mRNA expression levels of *NtSOD* genes were normalized to *NtEF1α* (accession number: AF120093) (Liu et al., 2022), and relative fold changes were calculated using the $2^{-\Delta\Delta CT}$ method (Livak and Schmittgen, 2001).

Heterologous Expression and Functional Verification of NtSOD Family Genes in Yeast

The CDSs of three NtSOD family members, *NtCSD1a*, *NtFSD1e* and *NtMSD1b*, were cloned by PCR with the primers listed in **Supplementary Table 1** to verify the potential function of NtSOD proteins in scavenging ROS produced in response to heavy metal stress. The PCR fragment and pYES2 vector were digested using the restriction enzymes *Bam*HI *and Eco*RI (TaKaRa, Dalian, China) for 3 h at 37°C. Subsequently, the CDS of the three genes were inserted into the expression vector pYES2 using the DNA Ligation Kit Ver. 2.1 (TaKaRa, Dalian, China) and transformed into *E. coli* strain DH5α. The inserted sequences in the resulting recombinant plasmids, named pYES2:NtCSD1a, pYES2:NtFSD1e and pYES2:NtMSD1b, were verified by DNA sequencing (BGI, Shenzhen, China). The recombinant plasmids were amplified in DH5α cells and extracted according to the operation manual of a high purity plasmid extraction kit (Biomed, Beijing, China). The oxidation-sensitive yeast mutant strain Δ*yap1* (*MATα ura3lys2 ade2 trp1 leu2 yap1:leu2*) was transformed with the three recombinant plasmids using the lithium acetate transformation protocol, and the empty plasmid pYES2 was used as the control (Kawai et al., 2010; Rodrigues-Pousada et al., 2019). Yeast cells were cultured in SD/-URA liquid medium until reaching the logarithmic phase (OD_{600} = 0.6) to assess the sensitivity of the cells to heavy metal-induced oxidative stress. The cultures were successively diluted 10 times from 1 to 10^{-3} and spotted onto SD plates containing 50 μM $CdCl_2$, 2.5 mM $CuSO_4$, 5 mM $ZnSO_4$, 2.5 mM $FeSO_4$, or 2.5 mM $MnSO_4$ and grown for 3 days before being photographed.

Statistical Analysis

Data are presented as the means ± SD derived from at least three biological replicates, unless indicated otherwise. All data were analyzed using one-way ANOVA, and significant differences were analyzed using Dunnett's multiple range test ($P < 0.05$) with GraphPad Prism 8.0 (GraphPad Software, San Diego, CA, United States).

RESULTS

Identification and Phylogenetic Analysis of NtSOD Genes

According to the results of the HMM search and BlastP, 17 candidate genes were originally obtained from the Pfam SOD family in tobacco. Based on the domain analysis, 5 proteins were shown to have a Cu/Zn-SOD domain (PF00080), 7 proteins contained an Fe/Mn-SOD alpha-hairpin domain (PF00081), and 3 proteins contained an Fe/Mn-SOD C-terminal domain (PF02777). Additionally, 2 proteins contained both a Cu/Zn-SOD domain and an N-terminal heavy metal-associated domain (HMA; PF000403) (**Figure 1B**), which were considered copper chaperones for Cu/Zn superoxide dismutase in tobacco (NtCCS) due to their clustering with AtCCS in the phylogenetic tree (**Figure 1A**). CCS is essential for transporting Cu to SOD but has no dismutase activity (Cohu et al., 2009). After excluding 2 NtCCS members from 17 candidate proteins, we identified 15 NtSOD proteins in *N. tabacum* cultivar TN90.

A neighbor-joining phylogenetic rootless tree was constructed using SOD protein sequences from *A. thaliana* and tobacco to further clarify the evolutionary relationship of *SOD* genes in tobacco. All *NtSOD* genes were assigned specific names according to their phylogenetic relationships with *AtSOD* genes. The results of phylogenetic analysis showed that SOD family members in tobacco were classified into three subfamilies with high bootstrap values, including the Cu/Zn-SOD subfamily (NtCSD1a/1b, NtCSD2a/2b, and NtCSD3), Fe-SOD subfamily (NtFSD1a/1b/1c/1d/1e and NtFSD3a/3b) and Mn-SOD subfamily (NtMSD1a/1b/1c). The NtFSD

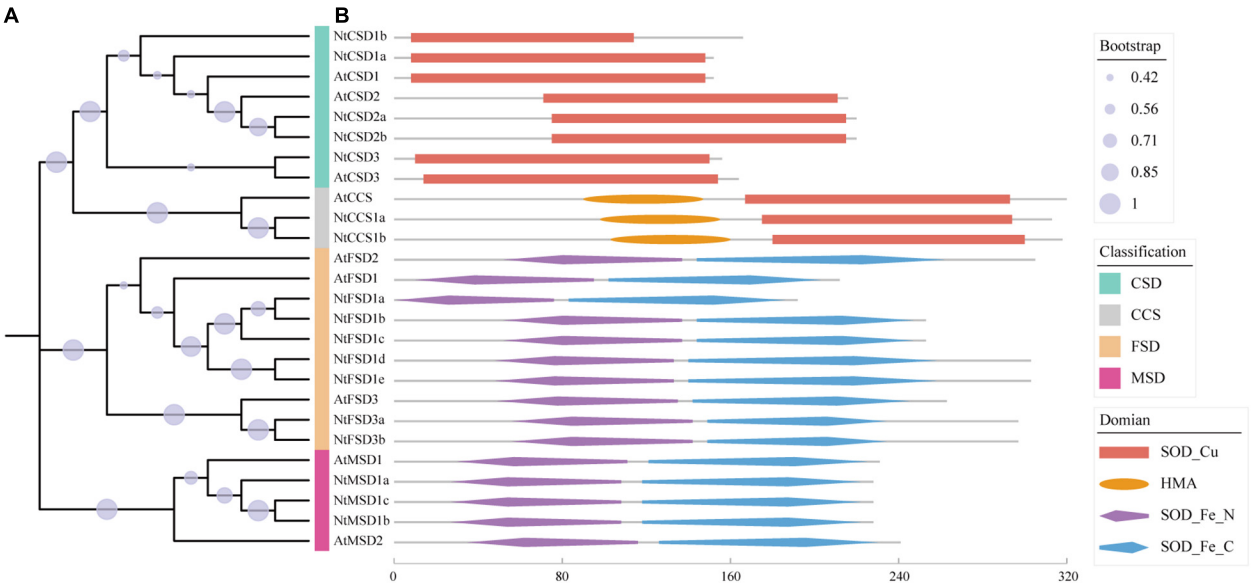

FIGURE 1 | Phylogenetic analysis and distribution of conserved structural domains of SOD gene family members in *N. tabacum* and *Arabidopsis*. **(A)** Phylogenetic tree of AtSODs and NtSODs. **(B)** Distribution of conserved structural domains of AtSODs and NtSODs. Red squares indicate the SOD_Cu structural domain (PF00080), orange oval blocks indicate the HMA structural domain (PF00403), and purple and blue diamond blocks represent the SOD_Fe_N structural domain (PF00081) and SOD_Fe_C structural domain (PF02777), respectively.

subfamily exhibited a closer phylogenetic relationship with NtMSD than with NtFSD, potentially because NtFSD and NtMSD have the same conserved domains SOD_Fe_N and SOD_Fe_C (**Figure 1B**).

The protein sequences and physicochemical properties of NtSOD family members were characterized in the present study. The *NtSOD* gene CDSs ranged from 459 bp to 912 bp and encoded NtSOD proteins with lengths ranging from 153–304 amino acids. The molecular weight of the NtSOD proteins ranged from 15.2 kDa to 34.7 kDa, and the theoretical isoelectric points (pIs) ranged from 5.08 (NtCSD1b) to 8.82 (NtMSD1c). Additionally, the results for the predicted subcellular localization showed that SOD proteins in the same subfamily may be located in different organelles. Except for NtFSD1a that is located in the cytoplasm, other members in the NtFSD subfamily are located in chloroplasts. NtCSD2a/2b is located in chloroplasts, while NtCSD1a/1b/3 is located in the extracellular space. NtMSD1c is the only tobacco SOD protein located in mitochondria (**Table 1**).

Multiple Sequence Alignment of NtSOD Proteins

Multiple sequence alignment was conducted to analyze the differences among the fifteen NtSOD proteins, and the results are shown in **Figure 2**. Among the five members of the NtCSD subfamily, NtCSD2a and NtCSD2b had the highest sequence consistency of 95%. NtCSD1b showed low consistency with the other four subfamily members, ranging from 29.2% to 64.8%. The N-terminal and C-terminal regions of NtCSD2a/2b contained chloroplast transporter peptide sequences and transmembrane alpha-helical structures, respectively, suggesting that NtCSD2a/2b was localized in the chloroplast membrane. These results were consistent with the predicted subcellular localization of NtCSD2a/2b. Eight metal binding sites were identified in the protein sequence of the NtCSD gene subfamily, of which three sites bind Cu, four sites bind Zn, and H63 binds both Cu and Zn (**Figure 2A**). In the NtFSD subfamily, the sequence consistency between NtFSD1b and NtFSD1c, NtFSD1d and NtFSD1e, and NtFSD3a and NtFSD3b was greater than 97%, suggesting that they may be the products of gene doubling events. All NtFSD proteins (except NtFSD1a) have a chloroplast transit peptide and transmembrane alpha-helix, suggesting that these enzymes function on the chloroplast membrane. Although NtFSD1a has a transmembrane structure, the absence of its chloroplast transporter peptide leads to its localization in the cytoplasm, consistent with the predicted subcellular localization. In addition, the four Fe ion binding sites were highly conserved in all members of the NtFSD gene subfamily (**Figure 2B**). The three members of the NtMSD subfamily exhibit high sequence consistency, among which NtMSD1b and NtMSD1c have only 5 amino acid differences, and the similarity is 97.8%. The mitochondrial transit peptide and transmembrane alpha-helix are closely linked at the N-terminus of NtMSD, consistent with the prediction that NtMSD is located in mitochondria by the subcellular localization analysis. The four Mn binding sites are extremely conserved in NtMSD subfamily members (**Figure 2C**).

Conserved Motifs and Gene Structure Analysis of NtSOD Genes

We further analyzed the conserved motifs of the NtSOD family genes in tobacco, and 7 motifs were identified using MEME

TABLE 1 | The data of 15 *NtSOD* genes identified in tobacco genome.

Gene Name	Gene ID	Length of protein (aa)	MW (kDa)	pI	Subcellular prediction
NtCSD1a	LOC107790449	153	15.20	5.47	Extracellular space
NtCSD1b	LOC107774639	167	17.75	5.08	Extracellular space
NtCSD2a	LOC107806960	221	22.54	5.95	Chloroplast thylakoid membrane
NtCSD2b	LOC107767528	221	22.57	6.23	Chloroplast thylakoid membrane
NtCSD3	LOC107826236	157	15.71	6.78	Extracellular space
NtFSD1a	LOC107767307	193	21.84	5.51	Cytoplasm
NtFSD1b	LOC107805394	254	28.34	8.60	Chloroplast thylakoid membrane
NtFSD1c	LOC107800004	254	28.38	7.90	Chloroplast thylakoid membrane
NtFSD1d	LOC107819573	304	34.78	6.03	Chloroplast outer membrane
NtFSD1e	LOC107832827	304	34.69	5.91	Chloroplast outer membrane
NtFSD3a	LOC107797648	298	33.81	7.68	Chloroplast outer membrane
NtFSD3b	LOC107820063	298	33.87	7.71	Chloroplast outer membrane
NtMSD1a	LOC107803567	229	25.59	8.40	Organelle membrane
NtMSD1b	LOC107829594	229	25.55	7.86	Organelle membrane
NtMSD1c	LOC107830263	229	25.49	8.82	Mitochondrion membrane

software with the default parameters (**Figure 3B**). As expected, most of the closely related members in the same subfamily had common motif compositions; however, no common motifs were shared in all fifteen *NtSOD* genes. Among them, motifs 4 and 6 were associated with the Cu/Zn-SOD domain (PF00080) and were only identified in Cu/Zn-SOD subfamily members. Motif 1, motif 7 and motif 5 were specific to NtFSD and NtMSD proteins, respectively. Motif 2 and motif 3 correspond to the Fe/Mn-SOD alpha-hairpin domain (PF00081) and Fe/Mn-SOD C-terminal domain (PF02777), respectively. Except for NtFSD1a, motif 3 was the common conserved motif in the NtFSD subfamily. Motif2 was shared by the NtFSD subfamily and NtMSD subfamily.

The number of introns and gene structure are usually related to the evolution of gene family members (Zhang et al., 2021). In the present study, cDNA and corresponding DNA sequences of NtSOD family genes were compared to analyze the gene structure (**Figure 3C**). *NtFSD1b* was the smallest gene at 1,124 bp, while *NtFSD3b* was the longest gene at 9,355 bp. All *NtSOD* genes contain introns, and the number of introns ranges from 2 to 8. Among them, *NtFSD1a* has the least number of introns at 2, while *NtFSD1c/1d/1e* has the most at 8 introns. Notably, the three *NtFSD1c/1d/1e* genes showed highly similar genetic structures, and their cDNA and DNA sequences were highly consistent, suggesting that they may be the result of gene replication. The same replication event occurs in *NtCSD1a/1b* and *NtCSD2a/2b*.

Cis-Acting Elements in the Promoter Regions of NtSOD Genes

Based on accumulating evidence, *SOD* genes play important roles in the plant response to abiotic stress. The *cis*-acting elements in the promoter regions of the NtSOD family genes, except *NtFSD1e* due to incomplete assembly of the tobacco genome sequence, were scanned using plantCARE to better understand the potential regulatory mechanism of *NtSOD* genes in abiotic stress or hormonal responses of tobacco. Nineteen elements involved in defense and stress responsiveness, phytohormone responsiveness and light responsiveness were detected in the *NtSOD* promoters and divided into three categories, as shown in **Figure 4**. These elements were irregularly dispersed in the promoter regions of NtSOD family genes (**Supplementary Figure 3**). No similar distribution pattern was observed between two genes, even those that are evolutionarily close. Many of the hormone-related *cis*-acting elements, including ABRE (abscisic acid), AuxRR core/TGA element (auxin), GARE motif/P Box/TATC Box (gibberellin), CGTCA motif/TGACG motif (MeJA), and TCA element (salicylic acid), were identified in the promoter region of *NtSOD* genes. ABRE and CGTCA/TGACG motifs were widely distributed in *NtFSD* and *NtCSD* promoter sequences, suggesting that ABA and MeJA are involved in the regulation of *NtFSD* and *NtCSD*. *NtMSD* was predicted to be regulated by auxin and salicylic acid based on the presence of TGA elements and TCA elements in their promoter regions, respectively. Elements associated with auxin and gibberellin responses are scattered in the promoters of NtSOD family genes (**Figure 4**). These results suggested that plant hormones might exert a modulatory effect on the regulation of *NtSOD* gene expression. MYC, one of the key motifs responding to thrilling, was identified in all NtSOD family gene promoter regions. The anaerobic induction regulation-related element ARE was mainly present in the promoters of NtFSD subfamily and NtMSD subfamily genes, especially in the promoter region of *NtMSD1b*, which contained 16 ARE elements. In addition, a large number of light-responsive elements were present in almost all promoter regions of *NtSOD* genes, among which Box4 and G-box were significantly enriched.

Analysis of Potential Regulatory Interactions Between Transcription Factors and NtSODs

The online software PlantRegMap was employed to predict the potential regulatory interactions between transcription factors (TFs) and NtSOD family genes. Sixteen TFs that may be involved in regulating NtSOD family gene expression were identified. The number of potential binding motifs for TFs

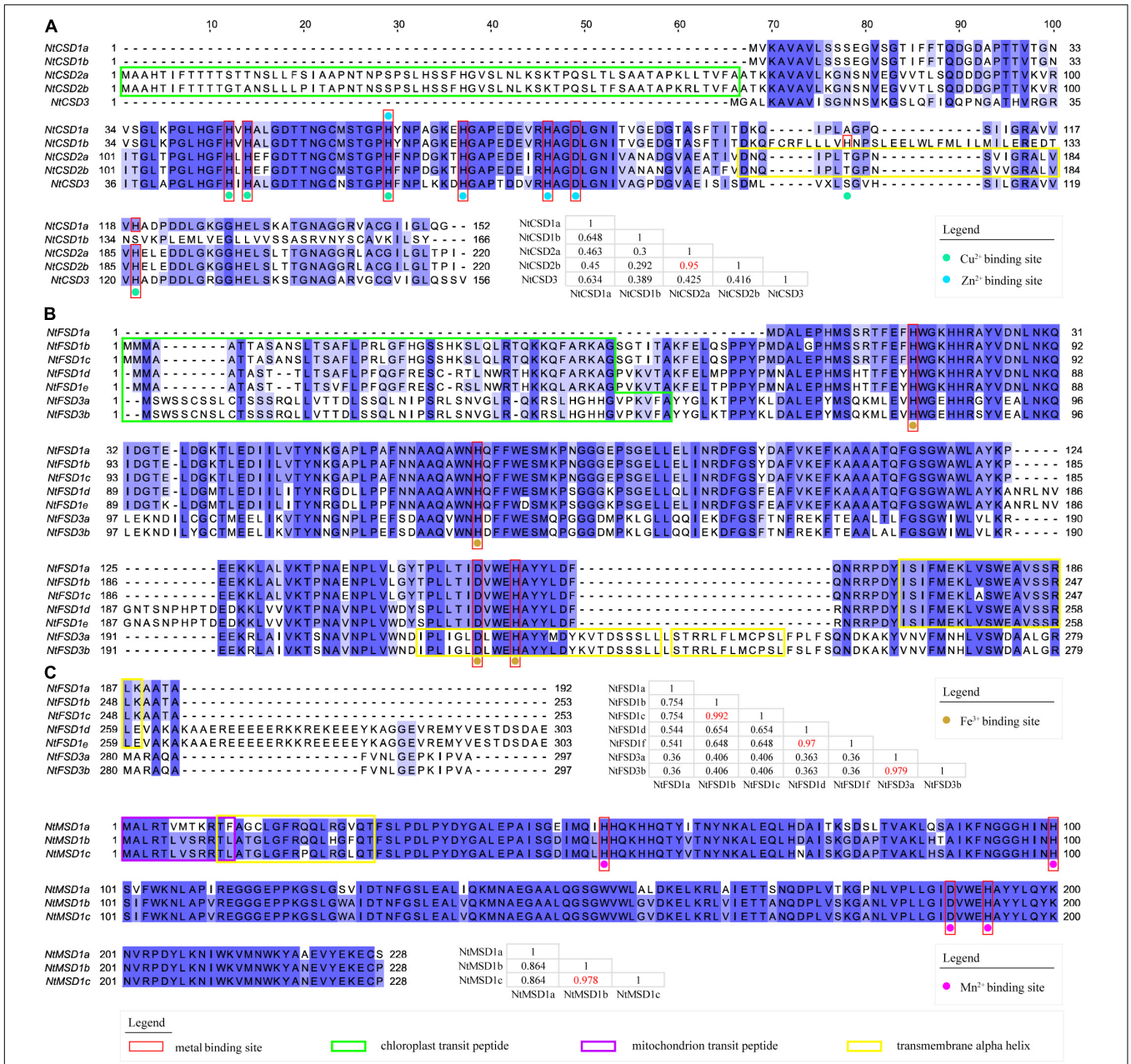

FIGURE 2 | Multiple sequence alignment of deduced amino acid sequences of NtSOD proteins. **(A)** Multiple sequence alignment of NtCSD proteins. The metal-binding sites for Cu^{2+} and Zn^{2+} are marked with green and blue dots, respectively. **(B)** Multiple sequence alignment of NtFSD proteins. Metal-binding sites of Fe^{3+} are marked with brown dots. **(C)** Multiple sequence alignment of NtMSD proteins. Metal-binding sites of Mn^{2+} are marked with purple dots. The similarity between amino acid sequences was recorded in the table, and the chloroplast transit peptide, mitochondrial transit peptide, and membrane transit peptide are marked using green, purple and yellow boxes, respectively, and red boxes mark the metal-binding sites of these SOD proteins.

in NtSOD family gene promoters was counted to conduct a clustering analysis and construct a heatmap (**Figure 5A**). The regulatory patterns of *NtMSD1a*, *NtCSD1a*, *NtCSD1b* and *NtFSD3a* were similar, all of which were regulated by Dof, AP2 and MIKC_MADS. Additionally, three *NtSOD* genes, *NtFSD1c*, *NtFSD1e* and *NtMSD1c*, constitute another group with similar regulatory patterns, which were all regulated by MYB, ERF and LBD. Notably, the *NtCSD3* promoter only contains one C2H2 transcription factor binding site, suggesting that *NtCSD3* may not be regulated by transcription factors other than C2H2.

Analysis of miRNAs Targeting NtSOD Genes

MicroRNAs (miRNAs) are a class of single-stranded small (20–24 nucleotides) non-coding RNAs that regulate gene expression

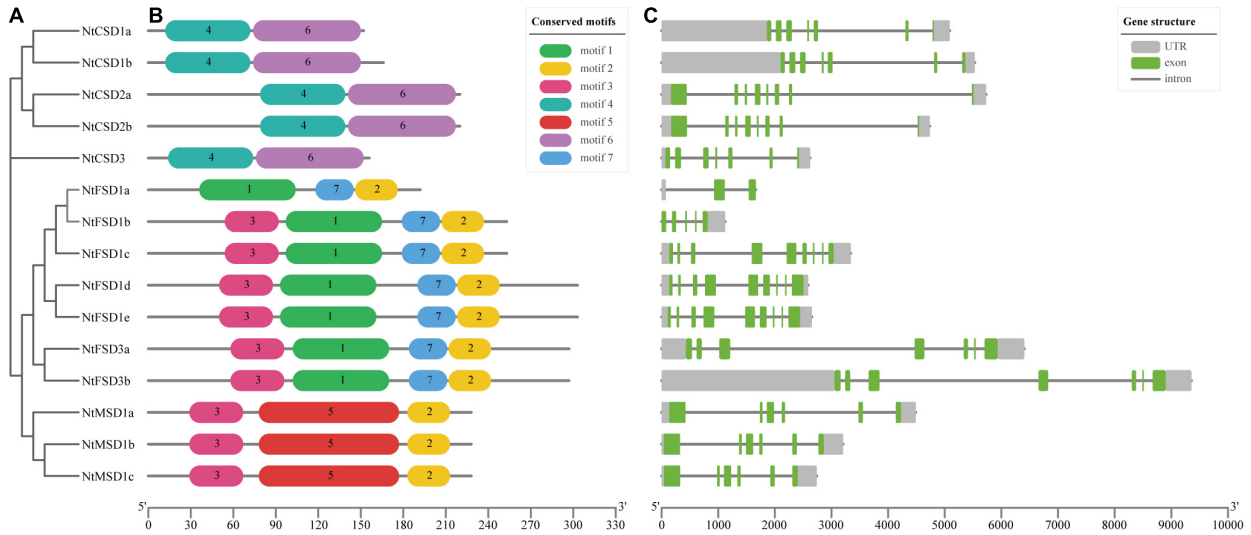

FIGURE 3 | Phylogenetic tree, conserved motifs of NtSOD proteins, and exon-intron structures of *NtSOD* genes. **(A)** A neighbor-joining tree of NtSOD proteins. **(B)** Seven motifs in NtSOD proteins identified using the MEME tool are marked by different colors. **(C)** Exon-intron structures of *NtSOD* genes. Introns, UTRs, and CDSs are displayed with gray lines, gray boxes, and green boxes, respectively.

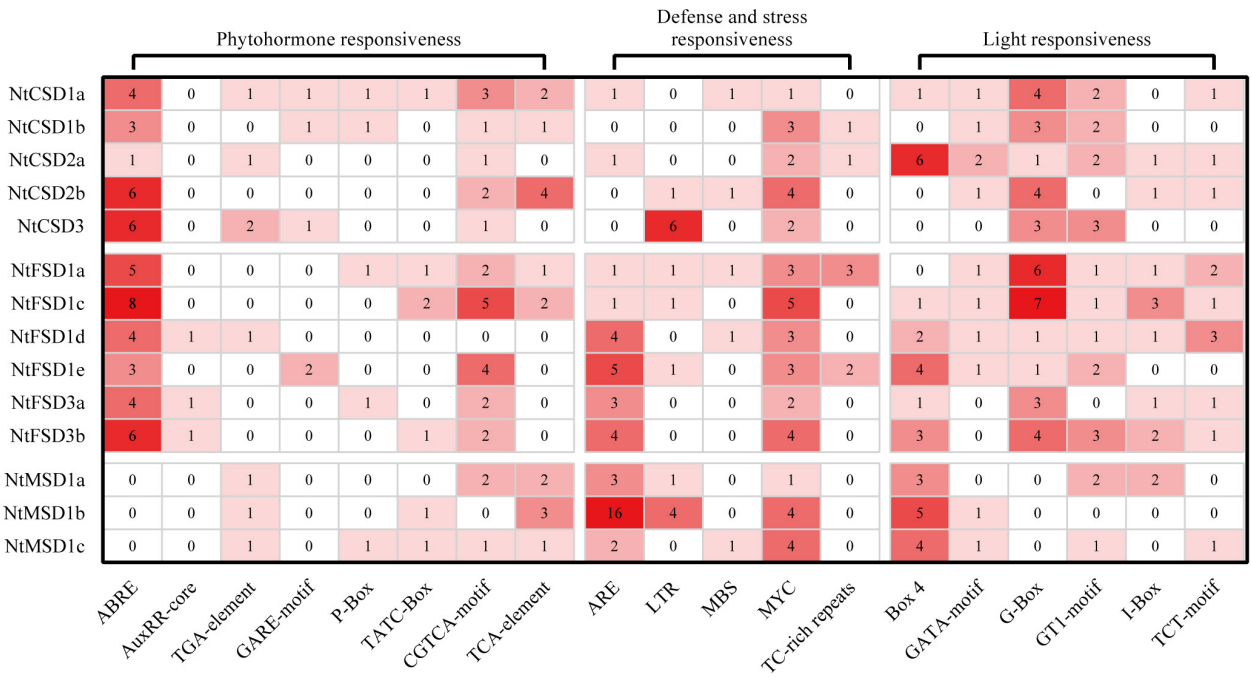

FIGURE 4 | *Cis*-acting elements in the promoters of *NtSOD* genes. The frequencies of *cis*-acting elements are represented by numbers and different colors of shading.

by binding to target gene transcripts to inhibit their translation or promote mRNA degradation. psRNATarget online software was used to analyze miRNA binding sites in 15 *NtSOD* genes and to provide insights into the miRNA-mediated regulation of the *NtSOD* genes. Nine *NtSOD* genes were predicted to be targeted by 13 known miRNA families, of which 5 target genes were cleaved by 5 conserved miRNA families, including miR156, miR398, miR482, miR172 and miR164, and 7 target genes were cleaved by unique miRNAs in *Solanaceae* plants, including miR6025, miR6020, miR6144, miR6150, miR6024, miR6155 and miR6021 (**Figure 5B**). As expected, miR398 was predicted to target *NtCSD1a/1b*. The miR164 family and miR6021 may be involved in regulating the expression of *NtMSD1b*, which was the only gene regulated by miRNAs in the NtMSD subfamily of genes.

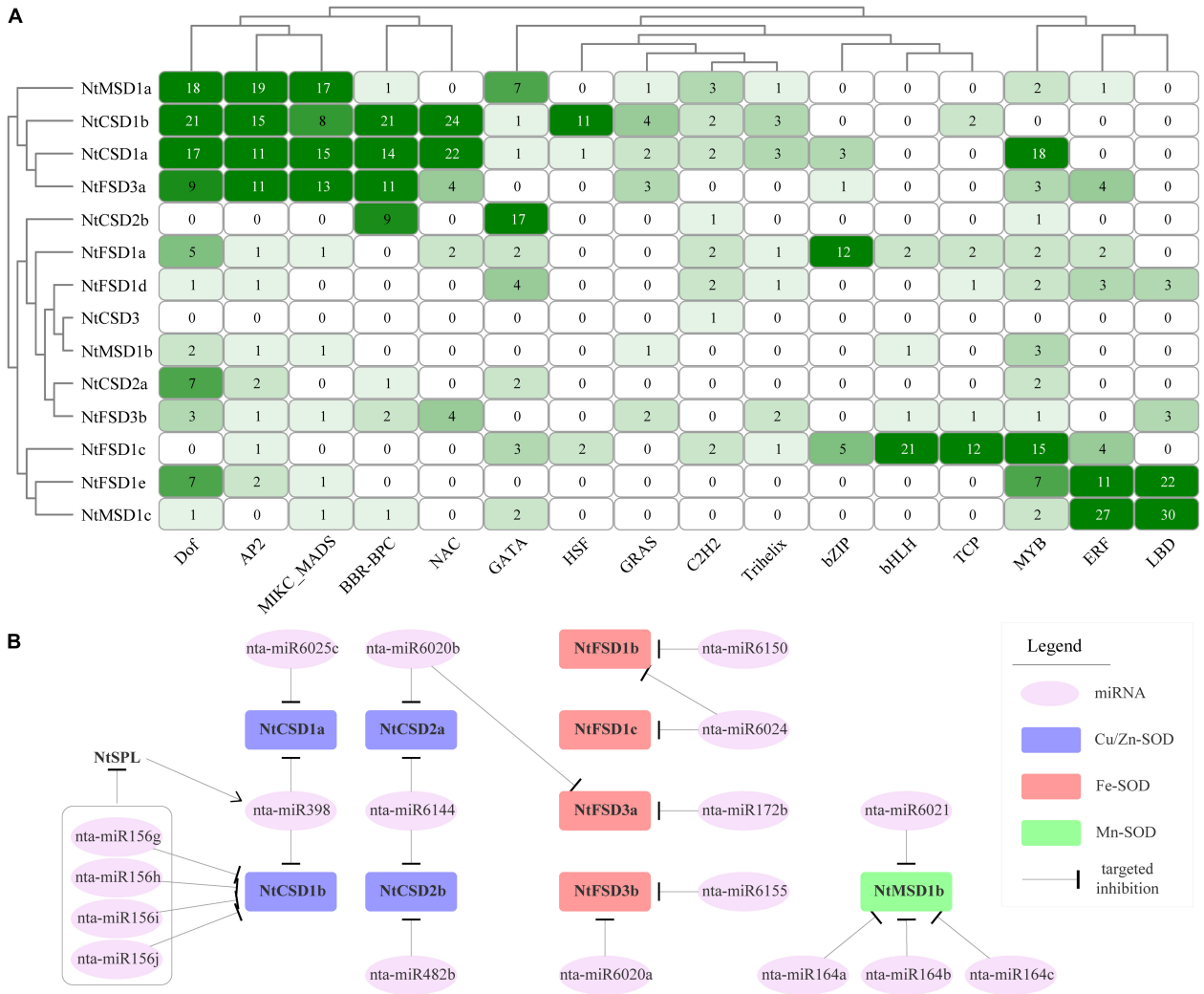

FIGURE 5 | Predicted factors regulating the expression of *NtSOD* genes. **(A)** Transcription factor binding sites in the promoters of *NtSOD* genes. The frequencies of *cis*-acting elements are represented by numbers and different colors of shading. **(B)** The predicted miRNAs regulating the expression of *NtSOD* genes.

Based on accumulating evidence, miR156-SPL and miR164-NAC modules regulate plant abiotic stress tolerance by maintaining ROS homeostasis (Fang et al., 2014; Yin et al., 2019). Interestingly, miR156 and miR164 were associated with the expression of *NtCSD1b* and *NtMSD1b* in tobacco, respectively. Therefore, the regulation of NtSOD family genes in tobacco involves a complex regulatory network of transcription factors and miRNAs.

Tissue-Specific Expression Profiles of NtSOD Family Genes

qPCR was used to analyze the relative tissue-specific expression levels of NtSOD family genes in different organs (stem, taproot, lateral root, terminal bud, 1st leaf, 2nd leaf, 3rd leaf and 4th leaf) at the vegetative stage of tobacco grown under normal growth conditions. Taken together, the expression levels of NtSOD family genes in taproots and lateral roots were lower than those in shoots of tobacco plants. Similar expression patterns were observed among *NtSOD* genes in the same subfamily, which were hierarchically clustered in the heatmap (**Figure 6**). Additionally, the qPCR results were generally consistent with the results from the transcriptome data (**Supplementary Figure 2**). NtCSD subfamily genes, except *NtCSD3*, were expressed at relatively high levels in terminal buds and the 1st leaves but expressed at low levels in mature leaves. NtFSD subfamily genes shared a similar expression pattern and exhibited higher expression levels in leaves than in roots, while *NtFSD1d/1e* was expressed at high levels in stems. A lower expression level of NtMSD subfamily genes was detected in lateral roots, and no significant difference was observed in the other tissues.

Heavy Metal Stress-Induced Expression Profiles of NtSOD Family Genes

Two-week-old tobacco seedlings were divided into two treatment groups, including a heavy metal toxicity group (hydroponic

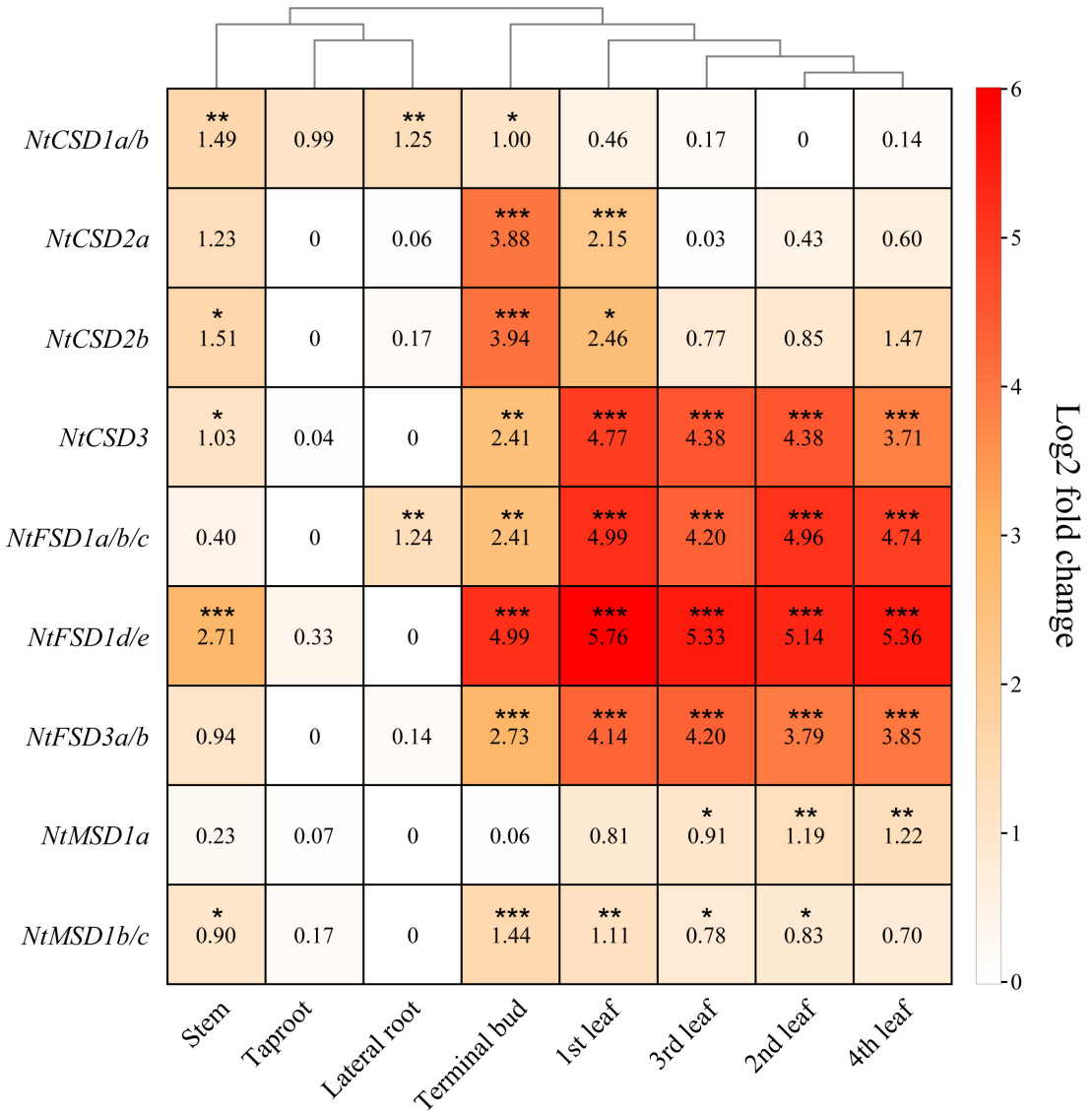

FIGURE 6 | The relative expression levels of *NtSOD* genes in different tobacco tissues. The expression data were obtained from the real-time RT-PCR (RT-qPCR) analysis data and are shown as log2 values calculated as averages. High expression levels are shown in red, and lower expression levels are shown in white. Statistically significant differences are indicated using asterisks (Dunnett's test, $^{*}p < 0.05$, $^{**}p < 0.01$, and $^{***}p < 0.001$). Data are presented as the means ± SD of three replicates.

solution containing Cd or excess Cu, Zn, Fe or Mn) and an ion-deficiency treatment group (Hoagland's solution without Cu, Zn, Fe or Mn), to understand the effect of heavy metal stress on the expression pattern of NtSOD family genes. After 7 days of treatment, chlorosis and growth inhibition were observed as significant toxicity symptoms for tobacco seedlings treated with Cd and Cu. Additionally, the growth of roots of tobacco seedlings under Cu stress was substantially inhibited (**Figure 7A**). In the present study, the ion concentrations in all the treated tobacco seedlings were determined using flame atomic absorption spectrometry. The results were consistent with the expectation. In the ion-deficient stress groups, the ion contents in the roots and shoots of tobacco seedlings were significantly lower than those in the control group. In contrast, the ion content was higher in the heavy metal toxicity group than that in the control group (**Figure 7C**). Notably, the copper ions mainly accumulated in the roots of tobacco after treatment with 200 μM Cu, while the concentration of copper ions in the shoots of Cu-treated tobacco was lower than that in the control group. This phenomenon may be due to Cu stress inhibiting the growth and development of roots in tobacco, which blocked ion transport from roots to shoots. Thus, heavy metal stress disrupted ion homeostasis in tobacco plants in the present study.

Antioxidant enzymes, especially SOD, play important roles in scavenging ROS generated in response to heavy metal stress in plants. qPCR was used to analyze the relative expression levels

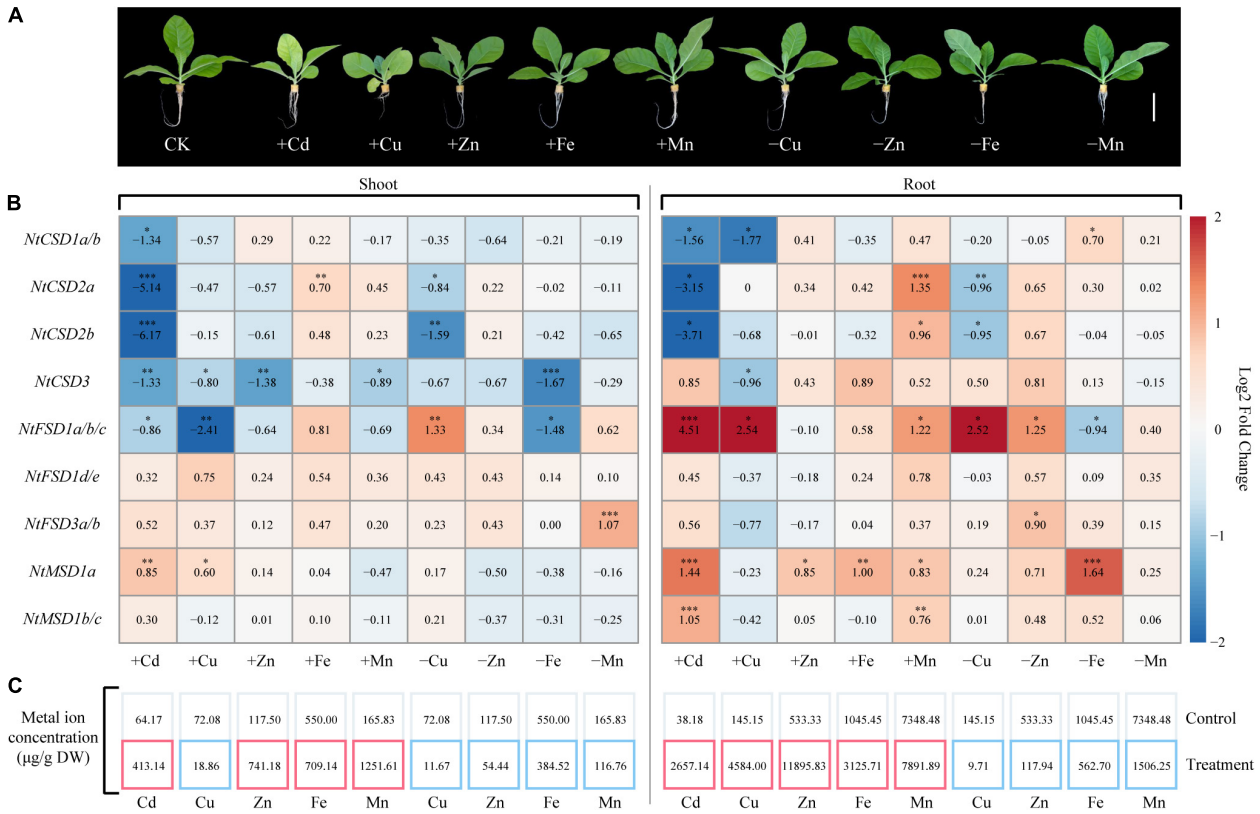

FIGURE 7 | Expression of *NtSOD* genes in tobacco shoots and roots treated with Cd, Cu, Zn, Fe, or Mn stress and without Cu, Zn, Fe, or Mn. **(A)** The phenotypes of tobacco seedlings subjected to different heavy metal treatments. **(B)** qRT-PCR analysis of *NtSOD* gene expression in response to various heavy metal stresses. The numbers in the box represent the average ratio of gene expression levels in the treatment and control groups. The asterisks on the number indicate significant differences (Dunnett's test, $^{*}p < 0.05$, $^{**}p < 0.01$, and $^{***}p < 0.001$). The population size was $n = 3$. **(C)** Content of metals contained in tobacco tissues subjected to different heavy metal treatments. The red box indicates that the corresponding metal content is higher than that of the control, while the blue box indicates that the corresponding metal content is lower than that of the control.

of NtSOD family genes in tobacco seedlings with heavy metal toxicity and ion deficiency to clarify the expression patterns of NtSOD family genes in tobacco in response to oxidative stress induced by different heavy metals. Cd exposure significantly inhibited the expression of NtCSD subfamily genes and induced the upregulation of NtMSD subfamily genes (**Figure 7B**). The expression levels of *NtFSD1a/1b/1c* were significantly altered in the tobacco seedlings under Cu-related stress compared with the control group. However, the expression levels of *NtFSD1d/1e* were not affected by Cu toxicity or Cu deficiency. *NtCSD3* expression was downregulated in shoots but not in roots exposed to zinc toxicity. Except for *NtCSD2a* and *NtMSD1a*, iron toxicity had no effect on the expression of other NtSOD family genes. On the other hand, iron-deficient stress resulted in the downregulation of *NtCSD3* and *NtFSD1a/1b/1c* expression in shoots and significantly upregulated *NtMSD1a* expression in roots. Excessive accumulation of Mn in roots upregulated the expression of NtSOD family genes, including *NtCSD2a*, *NtMSD1b/1c*, *NtFSD1a/1b/1c*, *NtCSD2b* and *NtMSD1a*. However, Mn-deficient stress only induced the upregulation of *NtFSD3a/3b* expression in shoots. In summary, NtSOD family genes displayed a wide variety of expression patterns in tobacco seedlings in response to heavy metal toxicity and ion-deficient stresses.

Heterologous Expression of *NtSOD* Genes in Yeast Mutant Δ*yap1*

The oxidative stress-hypersensitive yeast mutant Δ*yap1* was transformed with *NtCSD1a*, *NtFSD1e* and *NtMSD1b* and compared with the control to investigate the ability of NtSOD family genes to resist oxidative stress induced by heavy metals. Four serial dilutions (10 ×) of yeast cells were dropped on solid SD/-URA medium containing different heavy metals, including Cd, Zn and Mn, and cultured for 3 days at 30°C. The dilution dot assay showed no significant differences in cell growth under normal culture conditions following the heterologous expression of three *NtSOD* genes in yeast and the control group. The Cd and Zn tolerance in *NtMSD1b*-overexpressing yeast was stronger than that in the control group. All yeast cells expressing *NtSOD* genes exhibited better growth than the control under Cu stress and Fe stress. Additionally, the heterologous expression of *NtMSD1b* or *NtFSD1e*, but not *NtCSD1a*, conferred tolerance to high concentrations of Mn (**Figure 8**). Based on these results,

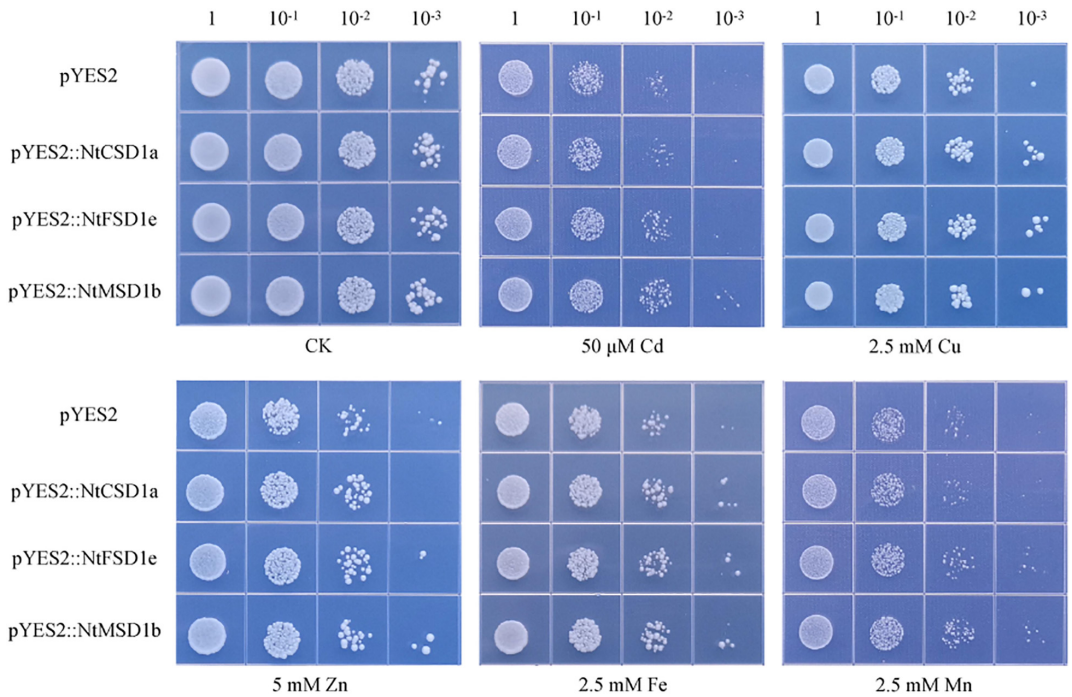

FIGURE 8 | Effect of *NtSOD* gene expression in oxidation-sensitive yeast Δ*yap1* on yeast cell growth in response to different heavy metal stresses (50 μM Cd, 2.5 mM Cu, 5 mM Zn, 2.5 mM Fe, and 2.5 mM Mn). The numbers above the data represent the dilution times of the bacterial solution.

the overexpression of *NtSOD* genes in the mutant Δ*yap1* yeast effectively enhanced the resistance of yeast to heavy metal stress.

DISCUSSION

Tobacco is the most widely cultivated non-food cash crop in the world. ROS accumulation caused by stresses such as drought, high temperature and heavy metals exerts adverse effects on tobacco growth and development (Rizhsky et al., 2002). SOD is the first line of defense against oxidative stress and removes ROS that accumulate in plant cells under stress (Alscher et al., 2002). Previous studies have shown that SOD overexpression confers abiotic stress resistance to tobacco (Pitcher et al., 1991; Zhang et al., 2017; Pan et al., 2019). To date, studies on SOD family genes in tobacco have been limited. A complete characterization of the characteristics and functions of the SOD gene family in tobacco is helpful to enrich our understanding of the SOD gene family in plants. The systematic identification of the *NtSOD* genes as the best candidate genes for screening and enhancing tobacco heavy metal toxicity tolerance is very important to cope with the increasingly serious soil heavy metal pollution.

In this study, 15 *NtSOD* genes were identified from the tobacco genome and classified into three subfamilies according to their domains and motifs, including 5 *NtCSDs*, 7 *NtFSDs* and 3 *NtMSDs* (**Table 1**). Although NtCCS has a conserved SOD_Cu domain (**Figure 1**), its HMA domain and evolutionary relationship closely with *A. thaliana* suggested that NtCCS may be a copper chaperone for NtCSD. The N-terminus of the NtCCS protein contains a conserved metal-binding motif MxCxxC, consistent with AtCCS and MaCCS sequences (Chu et al., 2005; Leitch et al., 2009). In previous studies, the CCS gene has been classified as a member of the SOD family (Feng et al., 2016). Since NtCCS lacks the common motif of the NtCSD subfamily, NtCCS does not belong to the NtSOD gene family, and the NtCCS subfamily was not included in the subsequent gene family analysis. Additionally, the NtFSD2 subfamily is lacking in tobacco (**Figure 1**). Just like the NtMT family genes (Yu et al., 2021), The NtFSD2 subfamily gene loss events possibly occurred during the formation of tobacco tetraploid genome.

The phylogenetic analysis showed that NtFSDs and NtMSDs were clustered into one group with a high bootstrap value (**Figure 3A**). In addition, an analysis of conserved domains showed that NtFSD and NtMSD shared Motif 3 and Motif 7, while the conserved domains in the NtCSD subfamily were Motif 4 and Motif 6 (**Figure 3B**). These results suggest different origins of NtCSD and NtFSD/NtMSD. The emergence of SOD family enzymes is an important event of biological evolution on earth. Before the Great Oxidation Event, Fe and Mn were relatively abundant and highly available in the early reductive ocean, while Zn and Cu were bound to unavailable sulfur-bearing minerals in the crust (Saito et al., 2003). Thus, FSD and MSD were generally considered more ancient than CSD and evolved from a common ancestor (Wang et al., 2017). CSD, however, evolved separately in bryophytes. These two groups evolved independently. In addition, according to the distribution characteristics of motifs, we speculated that NtFSD1a might be an intermediate transition type between NtFSDs and NtMSDs (**Figure 3B**).

The NtCSDs were mainly localized in the cytoplasm (NtCSD1a/1b) and chloroplasts (NtCSD2a/2b) (**Table 1**), and exhibit low amino acid sequence identity (**Figure 2**). The gene structure analysis revealed significant differences in the number and location of introns between NtCSD1a/1b and NtCSD2a/2b (**Figure 3**), which is a feature that distinguishes cytoplasmic and chloroplast CSDs. The cytoplasmic CSD in *Marchantia paleacea* shares high homology with the chloroplast CSD, and MaCSD is speculated to be the closest relative to the original ancestral plant CSD (Fink and Scandalios, 2002). Unlike other NtFSD subfamily members, NtFSD1a is predicted to be expressed in the cytoplasm. Actually, FSDs were also expressed in the cytoplasm of cowpea and *L. japonicus* (Moran et al., 2003; Rubio et al., 2007). Plant MSDs are generally located in the mitochondria of plants, where NtMSD1c is predicted to be localized in the mitochondria. In addition, MSDs are expressed in peroxisomes (del Río et al., 2003), which explains the prediction that NtMSD1a/1b is expressed in organelle membranes (**Table 1**).

The analysis of *cis*-acting elements in promoters provides important information for studying the regulation of SOD expression. Due to the lack of NtFSD1b promoter information in the tobacco genome database, we extracted 14 *NtSOD* gene promoter sequences and performed a *cis*-acting element analysis. A large number of *cis*-acting elements related to plant hormone response existed in the promoter region of NtSOD family genes (**Figure 4**), which was consistent with the fact that SOD was regulated by ABA and MeJA in plants (Agarwal et al., 2005; Cao et al., 2009; Lu et al., 2009; Jiang et al., 2015). Plant SODs play an important role in defense and stress responses. Drought, low temperature, heavy metal toxicity, and biotic stresses usually lead to an imbalance in ROS homeostasis, which induces the expression of plant *SOD* genes. We identified multiple *cis*-acting elements associated with defense and stress resistance in the *NtSOD* gene promoter region (**Figure 4**). MYC and LRT, two *cis*-acting elements associated with freezing injury and low-temperature stress, were distributed in each *NtSOD* gene promoter region, a prediction that suggests an important role for the tobacco NtSOD family in responding to low-temperature stress. Overexpression of the *NtMSD* gene in alfalfa significantly enhanced the cold tolerance and next-year yield of transgenic plants (McKersie et al., 1993). ARE, a key *cis*-acting element involved in anaerobic induction, is widely distributed in the promoter region of the *NtSOD* gene, which might explain why SOD activity is increased in plants under hypoxic conditions (Chen and Qualls, 2003). *NtSOD* gene transcripts were significantly increased under light conditions, and conversely, *NtSOD* gene expression was significantly downregulated in the absence of light (Tsang et al., 1991). This phenomenon is consistent with our finding of a large number of *cis*-acting elements associated with light response in the tobacco *SOD* gene promoter. The analysis of *cis*-acting elements in the promoter indicated that *NtSOD* genes play an important role in the tobacco response to stress resistance.

The expression of *SOD* genes in response to stress is regulated by transcription factors and miRNAs in plants. *SOD* gene expression levels were significantly upregulated in transgenic peanut overexpressing *MuWRKY3*, which subsequently effectively enhanced drought stress tolerance in transgenic plants (Kiranmai et al., 2018). The transcription factor SPL7 is the main transcription factor that regulates *CSD* genes and negatively regulates the expression of *CSD* genes to adapt to Cu deficiency stress (Mermod et al., 2019). Activation of rat *SOD* gene expression by ginsenoside Rb2 from a ginseng extract is regulated by the AP2 transcription factor (Kim et al., 1996). Expression of the transcription factor NAC derived from maize (*Glycine max*) in tobacco resulted in transgenic plants that were more sensitive to drought, and the molecular mechanism was that NAC functioned as a negative regulator, reducing the expression of plant *SOD* genes and leading to ROS accumulation (Jin et al., 2013). Multiple transcription factor binding sites were predicted in the promoter region of the *NtSOD* genes, including Dof, AP2, NAC, MADS, and MYB (**Figure 5**). This result implies that *NtSOD* genes have different regulatory modalities to cope with the complex external environment. In recent years, an increasing number of studies have shown that miRNAs play a key role in the posttranscriptional regulation of plant *SOD* genes. miRNA398 is the first miRNA identified to negatively regulate *CSD* expression and plays an important role in plant resistance to stress. In *A. thaliana*, oxidative stress does not directly regulate the expression of *CSD* genes but represses miRNA398 expression, thereby protecting CSD mRNAs from cleavage (Zhou et al., 2019).

Plant *SOD* genes show different expression patterns at different growth stages or in different tissues. Some *SOD* genes exhibit constitutive expression in all tissues (Lin and Lai, 2013), while other *SOD* genes show tissue-specific expression patterns (Feng et al., 2015). In the present study, we detected the expression patterns of *NtSOD* genes in different tissues and at different stages using qPCR and nine-pair primers. The results of the qPCR analysis (**Figure 6**) were consistent with the results obtained from transcriptomic data (**Supplementary Figure 2**). Furthermore, *NtSOD* gene expression profiles showed that genes in the same subfamily have similar expression patterns, consistent with the tissue expression profile of cotton SOD family genes (Wang et al., 2017). Differences in the expression levels of NtSOD family members were observed in different tissues and leaves at different developmental stages. For example, the higher expression level of *NtFSD1a/b/c* in the lateral root, compared to other *NtSOD* genes, implies that it is associated with the development of the lateral root. The *fsd1* knockout mutant in *Arabidopsis* significantly suppressed the development of the lateral roots (Dvořák et al., 2021). *NtSOD* was expressed at a relatively high level in the terminal bud of tobacco, consistent with the continuous increase in SOD activity observed in buds of *Ficus carica* during the dormancy to germination period (Sedaghat et al., 2022). Briefly, the expression of tobacco NtSOD family genes show spatiotemporal specificity and play an important role in different tissues and organs and developmental stages.

The regulation of plant *SOD* gene expression by heavy metals is mainly reflected in two aspects. First, the toxic effects of heavy metal stress on cells induce the accumulation of ROS and a subsequent imbalance of cellular redox homeostasis;

ROS removal usually depends on the expression of SOD. Second, metals such as Fe, Cu, Mn and Zn are essential to ensure SOD activity, and their deficiency also induces SOD expression. SOD expression levels in plants are usually upregulated by Cd, which is a non-essential and poisonous heavy metal (Pan et al., 2019). In contrast to our expectations, we found that Cd stress caused a significant decrease in the expression levels of NtCSD subfamily genes, consistent with the observation that Cd treatment exerted a significant inhibitory effect on the CSD mRNA and protein levels and activity in pea (Romero-Puertas et al., 2007). However, Cd stress significantly increased the expression levels of *NtFSD1a/b/c* and *NtMSD1a/b/c* (**Figure 7**), indicating that NtSOD family genes employ a differential division of labor in resisting Cd stress. Compared to toxicity induced by other essential metals, Mn toxicity significantly altered the expression level of *NtSOD* genes, especially in tobacco roots (**Figure 7**). A significant increase in SOD activity was detected in soybean roots treated with excess Mn (Santos et al., 2017). The SPL7-miR398 module is an important regulator of Cu homeostasis in *Arabidopsis*. Cu deficiency induces miR398 expression and results in degradation of the CSD mRNA (Yamasaki et al., 2009). The expression level of the NtCSD subfamily in tobacco was significantly downregulated under Cu-deficient conditions, suggesting that SPL7-mir398 is involved in a conserved regulatory module in plants to address disrupted Cu homeostasis. In addition, Cu deficiency induced the expression of *NtFSD1a/b/c* to complement the functional deficiency of *NtCSD*. Fe deficiency downregulated *NtFSD* expression but induced the expression of the *NtMSD* genes, consistent with the upregulation of MSD expression in *Chlamydomonas reinhardtii* under Fe deficiency (Allen et al., 2007). Consequently, *NtSOD* expression is regulated by a complex regulatory network to counteract the imbalance of heavy metal homeostasis in tobacco.

A yeast (*Saccharomyces cerevisiae*) mutant strain was used in this study to analyze the biological functions of NtSOD in resisting oxidative stress induced by heavy metal exposure. Yeast is generally acknowledged as a well-understood eukaryote in the field of stress response. The yeast activator protein (YAP) protein family is the largest bZIP subfamily in *S. cerevisiae* and consists of 8 members (Yap1 to Yap8) (Rodrigues-Pousada et al., 2019). In yeast cells, functional deficiency of Yap1 caused cellular sensitivity to ROS generated by the disruption of metal homeostasis (Schnell et al., 1992). Therefore, utilization of the yeast mutant strain delta yap represents a convenient method to test the ability of heterologously expressed SOD to remove ROS in response to heavy metal stress. In the present study, three tobacco *SOD* genes, *NtCSD1a*, *NtFSD1e* and *NtMSD1b*, were introduced into the yeast mutant strain Δ*yap1*. The results of the dilution dot assay showed that all three tobacco *SOD* genes alleviated oxidative stress induced by heavy metals (**Figure 8**). Compared to *NtMSD1b* and *NtFSD1e*, *NtCSD1a* may have a slightly weaker ability to remove ROS induced by heavy metals. Thus, *NtSOD* genes show differences in their abilities to remove ROS generated in response to heavy metals.

CONCLUSION

In the present study, 15 *SOD* genes were identified in tobacco variety TN90. The NtSOD gene family is divided into three subfamilies: NtCSD, NtFSD and NtMSD. The specific characteristics of the *SOD* genes were investigated, including the subcellular localization, conserved domain and gene structure. *Cis*-regulatory elements of the *NtSOD* gene promoter region in response to plant hormones, abiotic stress and light were also identified. Meanwhile, the transcription factors and miRNAs that may be involved in regulating *NtSOD* gene expression were predicted. The analysis of the tissue expression profile showed that the NtSOD gene family played an important role in tobacco during the growth and development stages. The expression pattern of the NtSOD gene family in response to heavy metals indicated that the *NtSOD* genes were the key proteins mediating tobacco resistance to heavy metal toxicity, but their functions were different. In addition, the biological function of the NtSOD gene family in protecting against oxidative stress induced by heavy metals was verified in the yeast mutant strain. These results provide a good understanding of the biological characteristics and functions of the NtSOD gene family in tobacco and provide important information for the analysis of tobacco resistance to heavy metal-induced oxidative stress.

DATA AVAILABILITY STATEMENT

The original contributions presented in the study are included in the article/**Supplementary Material**, further inquiries can be directed to the corresponding author/s.

AUTHOR CONTRIBUTIONS

CH: data curation, methodology, and writing-original draft. CH and LH: investigation. LH: software. TY and SZ: methodology. RL and XJ: validation. WL, RL, and HX: funding acquisition. WL and FZ: writing-review. HX: resources. WL: conceptualization, editing, supervision, and project administration. All authors contributed to the article and approved the submitted version.

FUNDING

This work was supported by the Science and Technology Research Program of Chongqing Municipal Education Commission (Grant No. KJZD-K202001504), CNTC (Grant No. 110202001025-JY08), YNTC (Grant No. 2021530000241014), and the Postgraduate Science and Technology Innovation Program of Chongqing University of Science and Technology (Grant Nos. YKJCX2020503 and YKJCX2020537).

ACKNOWLEDGMENTS

We would like to thank Prof. Xiaoling Liao and Dr. Shuang Yang for technical support.

SUPPLEMENTARY MATERIAL

The Supplementary Material for this article can be found online at: https://www.frontiersin.org/articles/10.3389/fpls.2022.904105/full#supplementary-material

Supplementary Figure 1 | Conserved motifs of NtSODs. The number on the X-axis indicates the position of the amino acid, and the number on the Y-axis indicates the conservation of the amino acid in the protein. The height of a letter indicates its relative frequency at the given position (X-axis) in the motif.

Supplementary Figure 2 | Expression patterns of the tobacco *NtSOD* genes in various tissues. Heatmap generated with TPM values. The depth of the red color in the figure reflects the levels of gene expression.

Supplementary Figure 3 | Distribution of *cis*-acting element positions in *NtSOD* promoters.

REFERENCES

Abreu, I. A., and Cabelli, D. E. (2010). Superoxide dismutases—a review of the metal-associated mechanistic variations. *Biochim. Biophys. Acta* 1804, 263–274. doi: 10.1016/j.bbapap.2009.11.005

Agarwal, S., Sairam, R. K., Srivastava, G. C., Tyagi, A., and Meena, R. C. (2005). Role of ABA, salicylic acid, calcium and hydrogen peroxide on antioxidant enzymes induction in wheat seedlings. *Plant Sci.* 169, 559–570. doi: 10.1016/j.plantsci.2005.05.004

Allen, M. D., Kropat, J., Tottey, S., Del Campo, J. A., and Merchant, S. S. (2007). Manganese deficiency in Chlamydomonas results in loss of photosystem II and MnSOD function, sensitivity to peroxides, and secondary phosphorus and iron deficiency. *Plant Physiol.* 143, 263–277. doi: 10.1104/pp.106.088609

Alscher, R. G., Erturk, N., and Heath, L. S. (2002). Role of superoxide dismutases (SODs) in controlling oxidative stress in plants. *J. Exp. Bot.* 53, 1331–1341. doi: 10.1093/jexbot/53.372.1331

Bailey, T. L., Johnson, J., Grant, C. E., and Noble, W. S. (2015). The MEME suite. *Nucleic Acids Res.* 43, W39–W49. doi: 10.1093/nar/gkv416

Cao, S., Zheng, Y., Wang, K., Jin, P., and Rui, H. (2009). Methyl jasmonate reduces chilling injury and enhances antioxidant enzyme activity in postharvest loquat fruit. *Food Chem.* 115, 1458–1463. doi: 10.1016/j.foodchem.2009.01.082

Chen, C., Chen, H., Zhang, Y., Thomas, H. R., Frank, M. H., He, Y., et al. (2020). TBtools: an integrative toolkit developed for interactive analyses of big biological data. *Mol. Plant* 13, 1194–1202. doi: 10.1016/j.molp.2020.06.009

Chen, H., and Qualls, R. G. (2003). Anaerobic metabolism in the roots of seedlings of the invasive exotic *Lepidium latifolium*. *Environ. Exp. Bot.* 50, 29–40. doi: 10.1016/S0098-8472(02)00112-0

Chu, C. C., Lee, W. C., Guo, W. Y., Pan, S. M., Chen, L. J., Li, H., et al. (2005). A copper chaperone for superoxide dismutase that confers three types of copper/zinc superoxide dismutase activity in Arabidopsis. *Plant Physiol.* 139, 425–436. doi: 10.1104/pp.105.065284

Cohu, C. M., Abdel-Ghany, S. E., Gogolin Reynolds, K. A., Onofrio, A. M., Bodecker, J. R., Kimbrel, J. A., et al. (2009). Copper delivery by the copper chaperone for chloroplast and cytosolic copper/zinc-superoxide dismutases: regulation and unexpected phenotypes in an *Arabidopsis* mutant. *Mol. Plant* 2, 1336–1350. doi: 10.1093/mp/ssp084

Dai, X., Zhuang, Z., and Zhao, P. X. (2018). psRNATarget: a plant small RNA target analysis server (2017 release). *Nucleic Acids Res.* 46, W49–W54. doi: 10.1093/nar/gky316

del Río, L. A., Sandalio, L. M., Altomare, D. A., and Zilinskas, B. A. (2003). Mitochondrial and peroxisomal manganese superoxide dismutase: differential expression during leaf senescence. *J. Exp. Bot.* 54, 923–933. doi: 10.1093/jxb/erg091

Dvořák, P., Krasylenko, Y., Ovečka, M., Basheer, J., Zapletalová, V., Šamaj, J., et al. (2020). FSD1: developmentally-regulated plastidial, nuclear and cytoplasmic enzyme with anti-oxidative and osmoprotective role. *Plant Cell Environ.* doi: 10.1111/pce.13773 [Epub ahead of print].

Dvořák, P., Krasylenko, Y., Ovečka, M., Basheer, J., Zapletalová, V., Šamaj, J., et al. (2021). *In vivo* light-sheet microscopy resolves localisation patterns of FSD1, a superoxide dismutase with function in root development and osmoprotection. *Plant Cell Environ.* 44, 68–87. doi: 10.1111/pce.13894

Fang, Y., Xie, K., and Xiong, L. (2014). Conserved miR164-targeted NAC genes negatively regulate drought resistance in rice. *J. Exp. Bot.* 65, 2119–2135. doi: 10.1093/jxb/eru072

Feng, K., Yu, J., Cheng, Y., Ruan, M., Wang, R., Ye, Q., et al. (2016). The *SOD* gene family in tomato: identification, phylogenetic relationships, and expression patterns. *Front. Plant Sci.* 7:1279. doi: 10.3389/fpls.2016.01279

Feng, X., Lai, Z., Lin, Y., Lai, G., and Lian, C. (2015). Genome-wide identification and characterization of the superoxide dismutase gene family in *Musa acuminata* cv. Tianbaojiao (AAA group). *BMC Genomics* 16:823. doi: 10.1186/s12864-015-2046-7

Filiz, E., and Tombuloğlu, H. (2015). Genome-wide distribution of superoxide dismutase (SOD) gene families in *Sorghum bicolor*. *Turk. J. Biol.* 39, 49–59. doi: 10.3906/biy-1403-9

Fink, R. C., and Scandalios, J. G. (2002). Molecular evolution and structure–function relationships of the superoxide dismutase gene families in angiosperms and their relationship to other eukaryotic and prokaryotic superoxide dismutases. *Arch. Biochem. Biophys.* 399, 19–36. doi: 10.1006/abbi.2001.2739

Hasanuzzaman, M., Alam, M. M., Nahar, K., Mohsin, S. M., Bhuyan, M. H. M. B., Parvin, K., et al. (2019). Silicon-induced antioxidant defense and methylglyoxal detoxification works coordinately in alleviating nickel toxicity in *Oryza sativa* L. *Ecotoxicology* 28, 261–276. doi: 10.1007/s10646-019-02019-z

Hasanuzzaman, M., Bhuyan, M. H. M. B., Zulfiqar, F., Raza, A., Mohsin, S. M., Mahmud, J. A., et al. (2020). Reactive oxygen species and antioxidant defense in plants under abiotic stress: revisiting the crucial role of a universal defense regulator. *Antioxidants* 9:681. doi: 10.3390/antiox9080681

Hossain, M. A., Piyatida, P., da Silva, J. A. T., and Fujita, M. (2012). Molecular mechanism of heavy metal toxicity and tolerance in plants: central role of glutathione in detoxification of reactive oxygen species and methylglyoxal and in heavy metal chelation. *J. Bot.* 2012, 1–37. doi: 10.1155/2012/872875

Hu, B., Jin, J., Guo, A. Y., Zhang, H., Luo, J., and Gao, G. (2015). GSDS 2.0: an upgraded gene feature visualization server. *Bioinformatics* 31, 1296–1297. doi: 10.1093/bioinformatics/btu817

Ismaiel, M. M. S., and Said, A. A. (2018). Tolerance of *Pseudochlorella pringsheimii* to Cd and Pb stress: role of antioxidants and biochemical contents in metal detoxification. *Ecotoxicol. Environ. Saf.* 164, 704–712. doi: 10.1016/j.ecoenv.2018.08.088

Jiang, L., Jin, P., Wang, L., Yu, X., Wang, H., and Zheng, Y. (2015). Methyl jasmonate primes defense responses against *Botrytis cinerea* and reduces disease development in harvested table grapes. *Sci. Hortic.* 192, 218–223. doi: 10.1016/j.scienta.2015.06.015

Jiang, W., Yang, L., He, Y., Zhang, H., Li, W., Chen, H., et al. (2019). Genome-wide identification and transcriptional expression analysis of superoxide dismutase (SOD) family in wheat (*Triticum aestivum*). *PeerJ* 7:e8062. doi: 10.7717/peerj.8062

Jin, H., Huang, F., Cheng, H., Song, H., and Yu, D. (2013). Overexpression of the *GmNAC2* gene, an NAC transcription factor, reduces abiotic stress tolerance in tobacco. *Plant Mol. Biol. Rep.* 31, 435–442. doi: 10.1007/s11105-012-0514-7

Katoh, K., and Standley, D. M. (2013). MAFFT multiple sequence alignment software version 7: improvements in performance and usability. *Mol. Biol. Evol.* 30, 772–780. doi: 10.1093/molbev/mst010

Kawai, S., Hashimoto, W., and Murata, K. (2010). Transformation of *Saccharomyces cerevisiae* and other fungi: methods and possible underlying mechanism. *Bioeng. Bugs* 1, 395–403. doi: 10.4161/bbug.1.6.13257

Kim, Y. H., Park, K. H., and Rhoxy, H. M. (1996). Transcriptional activation of the Cu, Zn-superoxide dismutase gene through the AP2 site by ginsenoside Rb_2 extracted from a medicinal plant, *Panax ginseng*. *J. Biol. Chem.* 271, 24539–24543. doi: 10.1074/jbc.271.40.24539

Kiranmai, K., Lokanadha Rao, G., Pandurangaiah, M., Nareshkumar, A., Amaranatha Reddy, V., Lokesh, U., et al. (2018). A novel WRKY transcription factor, *MuWRKY3* (*Macrotyloma uniflorum* Lam. Verdc.) enhances drought stress tolerance in transgenic groundnut (*Arachis hypogaea* L.) plants. *Front. Plant Sci.* 9:346. doi: 10.3389/fpls.2018.00346

Leitch, J. M., Jensen, L. T., Bouldin, S. D., Outten, C. E., Hart, P. J., and Culotta, V. C. (2009). Activation of Cu, Zn-superoxide dismutase in the absence of oxygen and the copper chaperone CCS. *J. Biol. Chem.* 284, 21863–21871. doi: 10.1074/jbc.M109.000489

Li, Z., Han, X., Song, X., Zhang, Y., Jiang, J., Han, Q., et al. (2017). Overexpressing the *Sedum alfredii* Cu/Zn superoxide dismutase increased resistance to oxidative stress in transgenic *Arabidopsis*. *Front. Plant Sci.* 8:1010. doi: 10.3389/fpls.2017.01010

Lin, Y. L., and Lai, Z. X. (2013). Superoxide dismutase multigene family in longan somatic embryos: a comparison of CuZn-SOD, Fe-SOD, and Mn-SOD gene structure, splicing, phylogeny, and expression. *Mol. Breed.* 32, 595–615. doi: 10.1007/s11032-013-9892-2

Liu, J., Xu, L., Shang, J., Hu, X., Yu, H., Wu, H., et al. (2021). Genome-wide analysis of the maize superoxide dismutase (SOD) gene family reveals important roles in drought and salt responses. *Genet. Mol. Biol.* 44:e20210035. doi: 10.1590/1678-4685-gmb-2021-0035

Liu, W., Huo, C., He, L., Ji, X., Yu, T., Yuan, J., et al. (2022). The NtNRAMP1 transporter is involved in cadmium and iron transport in tobacco (*Nicotiana tabacum*). *Plant Physiol. Biochem.* 173, 59–67. doi: 10.1016/j.plaphy.2022.01.024

Liu, Y. T., Chen, Z. S., and Hong, C. Y. (2011). Cadmium-induced physiological response and antioxidant enzyme changes in the novel cadmium accumulator, *Tagetes patula*. *J. Hazard Mater.* 189, 724–731. doi: 10.1016/j.jhazmat.2011.03.032

Livak, K. J., and Schmittgen, T. D. (2001). Analysis of relative gene expression data using real-time quantitative PCR and the $2^{-\Delta\Delta CT}$ method. *Methods* 25, 402–408. doi: 10.1006/meth.2001.1262

Lu, S., Su, W., Li, H., and Guo, Z. (2009). Abscisic acid improves drought tolerance of triploid bermudagrass and involves H_2O_2- and NO-induced antioxidant enzyme activities. *Plant Physiol. Biochem.* 47, 132–138. doi: 10.1016/j.plaphy.2008.10.006

McKersie, B. D., Chen, Y., de Beus, M., Bowley, S. R., Bowler, C., Inzé, D., et al. (1993). Superoxide dismutase enhances tolerance of freezing stress in transgenic alfalfa (*Medicago sativa* L.). *Plant Physiol.* 103, 1155–1163. doi: 10.1104/pp.103.4.1155

Mermod, M., Takusagawa, M., Kurata, T., Kamiya, T., Fujiwara, T., and Shikanai, T. (2019). SQUAMOSA promoter-binding protein-like 7 mediates copper deficiency response in the presence of high nitrogen in *Arabidopsis thaliana*. *Plant Cell Rep.* 38, 835–846. doi: 10.1007/s00299-019-02422-0

Mittler, R. (2002). Oxidative stress, antioxidants and stress tolerance. *Trends Plant Sci.* 7, 405–410. doi: 10.1016/S1360-1385(02)02312-9

Mittler, R. (2017). ROS Are Good. *Trends Plant Sci.* 22, 11–19. doi: 10.1016/j.tplants.2016.08.002

Moran, J. F., James, E. K., Rubio, M. C., Sarath, G., Klucas, R. V., and Becana, M. (2003). Functional characterization and expression of a cytosolic iron-superoxide dismutase from cowpea root nodules. *Plant Physiol.* 133, 773–782. doi: 10.1104/pp.103.023010

Nagajyoti, P. C., Lee, K. D., and Sreekanth, T. V. M. (2010). Heavy metals, occurrence and toxicity for plants: a review. *Environ. Chem. Lett.* 8, 199–216. doi: 10.1007/s10311-010-0297-8

Pan, C., Lu, H., Yu, J., Liu, J., Liu, Y., and Yan, C. (2019). Identification of Cadmium-responsive *Kandelia obovata* SOD family genes and response to Cd toxicity. *Environ. Exp. Bot.* 162, 230–238. doi: 10.1016/j.envexpbot.2019.02.018

Pilon, M., Ravet, K., and Tapken, W. (2011). The biogenesis and physiological function of chloroplast superoxide dismutases. *BBA* 1807, 989–998. doi: 10.1016/j.bbabio.2010.11.002

Pitcher, L. H., Brennan, E., Hurley, A., Dunsmuir, P., Tepperman, J. M., and Zilinskas, B. A. (1991). Overproduction of petunia chloroplastic copper/zinc superoxide dismutase does not confer ozone tolerance in transgenic tobacco. *Plant Physiol.* 97, 452–455. doi: 10.1104/pp.97.1.452

Rizhsky, L., Liang, H., and Mittler, R. (2002). The combined effect of drought stress and heat shock on gene expression in tobacco. *Plant Physiol.* 130, 1143–1151. doi: 10.1104/pp.006858

Rizhsky, L., Liang, H., and Mittler, R. (2003). The water-water cycle is essential for chloroplast protection in the absence of stress. *J. Biol. Chem.* 278, 38921–38925. doi: 10.1074/jbc.M304987200

Rodrigues-Pousada, C., Devaux, F., Caetano, S. M., Pimentel, C., da Silva, S., Cordeiro, A. C., et al. (2019). Yeast AP-1 like transcription factors (Yap) and stress response: a current overview. *Microb. Cell* 6, 267–285. doi: 10.15698/mic2019.06.679

Romero-Puertas, M. C., Corpas, F. J., Rodríguez-Serrano, M., Gómez, M., Del Río, L. A., and Sandalio, L. M. (2007). Differential expression and regulation of antioxidative enzymes by cadmium in pea plants. *J. Plant Physiol.* 164, 1346–1357. doi: 10.1016/j.jplph.2006.06.018

Rubio, M. C., Becana, M., Sato, S., James, E. K., Tabata, S., and Spaink, H. P. (2007). Characterization of genomic clones and expression analysis of the three types of superoxide dismutases during nodule development in *Lotus japonicus*. *Mol. Plant Microbe Interact.* 20, 262–275. doi: 10.1094/MPMI-20-3-0262

Sahu, A. K., Sahu, B., Soni, A., and Naithani, S. C. (2017). Active oxygen species metabolism in neem (*Azadirachta indica*) seeds exposed to natural ageing and controlled deterioration. *Acta Physiol. Plant* 39, 1–12. doi: 10.1007/s11738-017-2494-6

Saito, M. A., Sigman, D. M., and Morel, F. M. M. (2003). The bioinorganic chemistry of the ancient ocean: the co-evolution of cyanobacterial metal requirements and biogeochemical cycles at the Archean–Proterozoic boundary? *Inorg. Chim. Acta* 356, 308–318. doi: 10.1016/S0020-1693(03)00442-0

Sandalio, L. M., Dalurzo, H. C., Gomez, M., Romero-Puertas, M. C., and del Río, L. A. (2001). Cadmium-induced changes in the growth and oxidative metabolism of pea plants. *J. Exp. Bot.* 52, 2115–2126. doi: 10.1093/jexbot/52.364.2115

Santos, E. F., Santini, J. M. K., Paixão, A. P., Júnior, E. F., Lavres, J., Campos, M., et al. (2017). Physiological highlights of manganese toxicity symptoms in soybean plants: Mn toxicity responses. *Plant Physiol. Biochem.* 113, 6–19. doi: 10.1016/j.plaphy.2017.01.022

Savojardo, C., Martelli, P. L., Fariselli, P., Profiti, G., and Casadio, R. (2018). BUSCA: an integrative web server to predict subcellular localization of proteins. *Nucleic Acids Res.* 46, W459–W466. doi: 10.1093/nar/gky320

Schnell, N., Krems, B., and Entian, K. D. (1992). The *PAR1* (*YAP1/SNQ3*) gene of *Saccharomyces cerevisiae*, ac-*jun* homologue, is involved in oxygen metabolism. *Curr. Genet.* 21, 269–273. doi: 10.1007/BF00351681

Sedaghat, S., Gaaliche, B., Rahemi, M., Zare, H., and Jafari, M. (2022). Enzymatic activity and physico-chemical changes of terminal bud in rain-fed fig (*Ficus carica* L. 'Sabz') during dormant season. *Hortic. Plant J.* 8, 195–204. doi: 10.1016/j.hpj.2021.03.010

Song, J., Zeng, L., Chen, R., Wang, Y., and Zhou, Y. (2018). In silico identification and expression analysis of superoxide dismutase (SOD) gene family in *Medicago truncatula*. *3 Biotech* 8:348. doi: 10.1007/s13205-018-1373-1

Su, W., Raza, A., Gao, A., Jia, Z., Zhang, Y., Hussain, M. A., et al. (2021). Genome-wide analysis and expression profile of superoxide dismutase (SOD) gene family in rapeseed (*Brassica napus* L.) under different hormones and abiotic stress conditions. *Antioxidants* 10:1182. doi: 10.3390/antiox10081182

Tian, F., Yang, D. C., Meng, Y. Q., Jin, J., and Gao, G. (2020). PlantRegMap: charting functional regulatory maps in plants. *Nucleic Acids Res.* 48, D1104–D1113. doi: 10.1093/nar/gkz1020

Tsang, E. W. T., Bowler, C., Hérouart, D., Van Camp, W., Villarroel, R., Genetello, C., et al. (1991). Differential regulation of superoxide dismutases in plants exposed to environmental stress. *Plant Cell* 3, 783–792. doi: 10.1105/tpc.3.8.783

Wang, W., Xia, M., Chen, J., Deng, F., Yuan, R., Zhang, X., et al. (2016). Genome-wide analysis of superoxide dismutase gene family in *Gossypium raimondii* and *G. arboreum*. *Plant Gene* 6, 18–29. doi: 10.1016/j.plgene.2016.02.002

Wang, W., Zhang, X., Deng, F., Yuan, R., and Shen, F. (2017). Genome-wide characterization and expression analyses of superoxide dismutase (*SOD*) genes in *Gossypium hirsutum*. *BMC Genomics* 18:376. doi: 10.1186/s12864-017-3768-5

Waterhouse, A. M., Procter, J. B., Martin, D. M. A., Clamp, M., and Barton, G. J. (2009). Jalview Version 2—a multiple sequence alignment editor and analysis workbench. *Bioinformatics* 25, 1189–1191. doi: 10.1093/bioinformatics/btp033

Yadav, S., Gill, S. S., Passricha, N., Gill, R., Badhwar, P., Anjum, N. A., et al. (2019). Genome-wide analysis and transcriptional expression pattern-assessment of superoxide dismutase (SOD) in rice and *Arabidopsis* under abiotic stresses. *Plant Gene* 17:100165. doi: 10.1016/j.plgene.2018.10.001

Yamasaki, H., Hayashi, M., Fukazawa, M., Kobayashi, Y., and Shikanai, T. (2009). SQUAMOSA promoter binding protein–like7 is a central regulator for copper homeostasis in *Arabidopsis*. *Plant Cell* 21, 347–361. doi: 10.1105/tpc.108.060137

Yin, H., Hong, G., Li, L., Zhang, X., Kong, Y., Sun, Z., et al. (2019). miR156/SPL9 regulates reactive oxygen species accumulation and immune response in

Arabidopsis thaliana. *Phytopathology* 109, 632–642. doi: 10.1094/phyto-08-18-0306-r

Yu, Q., He, L., Huo, C., Jiang, X., Chen, H., Wang, R., et al. (2021). Genome-wide identification and expression analysis of heavy metal stress–responsive metallothionein family genes in *Nicotiana tabacum*. *Plant Mol. Biol. Rep.* 39, 443–454. doi: 10.1007/s11105-020-01262-7

Zang, Y., Chen, J., Li, R., Shang, S., and Tang, X. (2020). Genome-wide analysis of the superoxide dismutase (SOD) gene family in *Zostera marina* and expression profile analysis under temperature stress. *PeerJ* 8:e9063. doi: 10.7717/peerj.9063

Zhang, L., Sun, L., Zhang, L., Qiu, H., Liu, C., Wang, A., et al. (2017). A Cu/Zn superoxide dismutase gene from *Saussurea involucrata* Kar. & Kir., *SiCSD*, enhances drought, cold, and oxidative stress in transgenic tobacco. *Can. J. Plant Sci.* 97, 816–826. doi: 10.1139/cjps-2016-0180

Zhang, X., Zhang, L., Chen, Y., Wang, S., Fang, Y., Zhang, X., et al. (2021). Genome-wide identification of the SOD gene family and expression analysis under drought and salt stress in barley. *Plant Growth Regul.* 94, 49–60. doi: 10.1007/s10725-021-00695-8

Zhou, C., Zhu, C., Fu, H., Li, X., Chen, L., Lin, Y., et al. (2019). Genome-wide investigation of *superoxide dismutase* (*SOD*) gene family and their regulatory miRNAs reveal the involvement in abiotic stress and hormone response in tea plant (*Camellia sinensis*). *PLoS One* 14:e0223609. doi: 10.1371/journal.pone.0223609

Conflict of Interest: The authors declare that the research was conducted in the absence of any commercial or financial relationships that could be construed as a potential conflict of interest.

Publisher's Note: All claims expressed in this article are solely those of the authors and do not necessarily represent those of their affiliated organizations, or those of the publisher, the editors and the reviewers. Any product that may be evaluated in this article, or claim that may be made by its manufacturer, is not guaranteed or endorsed by the publisher.

Copyright © 2022 Huo, He, Yu, Ji, Li, Zhu, Zhang, Xie and Liu. This is an open-access article distributed under the terms of the Creative Commons Attribution License (CC BY). The use, distribution or reproduction in other forums is permitted, provided the original author(s) and the copyright owner(s) are credited and that the original publication in this journal is cited, in accordance with accepted academic practice. No use, distribution or reproduction is permitted which does not comply with these terms.

frontiers | Frontiers in Plant Science

REVIEW
published: 06 May 2022
doi: 10.3389/fpls.2022.850949

Natural Composition and Biosynthetic Pathways of Alkaloids in Medicinal *Dendrobium* Species

Cheng Song[1,2†], Jingbo Ma[1†], Guohui Li[1], Haoyu Pan[1], Yanfang Zhu[3], Qing Jin[4], Yongping Cai[4*] and Bangxing Han[1,2*]*

[1]College of Biological and Pharmaceutical Engineering, West Anhui University, Lu'an, China, [2]Anhui Engineering Laboratory for Conservation and Sustainable Utilization of Traditional Chinese Medicine Resources, West Anhui University, Lu'an, China, [3]College of Life Science, Huaibei Normal University, Huaibei, China, [4]College of Life Sciences, Anhui Agricultural University, Hefei, China

Dendrobium is the second biggest genus in the Orchidaceae family, some of which have both ornamental and therapeutic values. Alkaloids are a group of active chemicals found in *Dendrobium* plants. Dendrobine has emerged specific pharmacological and therapeutic properties. Although *Dendrobium* alkaloids have been isolated and identified since the 1930s, the composition of alkaloids and their biosynthesis pathways, including metabolic intermediates, alkaloid transporters, concrete genes involved in downstream pathways, and associated gene clusters, have remained unresolved scientific issues. This paper comprehensively reviews currently identified and tentative alkaloids from the aspect of biogenic pathways or metabolic genes uncovered based on the genome annotations. The biosynthesis pathways of each class of alkaloids are highlighted. Moreover, advances of the high-throughput sequencing technologies in the discovery of *Dendrobium* alkaloid pathways have been addressed. Applications of synthetic biology in large-scale production of alkaloids are also described. This would serve as the basis for further investigation into *Dendrobium* alkaloids.

Keywords: alkaloid, *Dendrobium*, secondary metabolism, chemicals, pathway

OPEN ACCESS

Edited by:
Zhihua Liao,
Southwest University, China

Reviewed by:
Jungui Dai,
Chinese Academy of Medical Sciences and Peking Union Medical College, China
Guoyin Kai,
Zhejiang Chinese Medical University, China
Xiaozhong Lan,
Tibet Agricultural and Animal Husbandry College, China

***Correspondence:**
Qing Jin
qingjin@ahau.edu.cn
Yongping Cai
ypcaiah@163.com
Bangxing Han
hanbx1978@sina.com

†These authors have contributed equally to this work

Specialty section:
This article was submitted to Plant Metabolism and Chemodiversity, a section of the journal Frontiers in Plant Science

Received: *08 January 2022*
Accepted: *30 March 2022*
Published: *06 May 2022*

Citation:
Song C, Ma J, Li G, Pan H, Zhu Y, Jin Q, Cai Y and Han B (2022) Natural Composition and Biosynthetic Pathways of Alkaloids in Medicinal Dendrobium Species. Front. Plant Sci. 13:850949. doi: 10.3389/fpls.2022.850949

INTRODUCTION

Dendrobium is the second biggest genus in the Orchidaceae family, and many of them have high medicinal and ornamental benefits (Lam et al., 2015). For almost 2,000 years, *Dendrobium* has been used as a prized traditional Chinese medicine. This can be traced back to the monograph "Shen Nong Ben Cao Jing." The medicinal *Dendrobium* materials included in the Chinese Pharmacopoeia (11th Edition) are divided into two categories: one is the cultivated varieties from *D. nobile*, *D. huoshanense*, *D. chrysotoxum*, or *D. fimbriatum* Hook., and the fresh or dried stems of similar species in the same genus. The other is the dry stem of *D. officinale*. According to the records of the national general survey of key medicinal resources, the Ta-pieh Mountains in Anhui Province, as a natural wild progeny reserve, is home to numerous of wild *Dendrobium* species, including *D. moniliforme*, *D. officinale*, and *D. huoshanense*.

The chemical composition and categorization of different medicinal *Dendrobium* species vary massively due to the wide variety of medicinal *Dendrobium* species (Teixeira da Silva and Ng, 2017). At present, the chemical components isolated from *Dendrobium* spp. mainly included polysaccharides, alkaloids, amino acids, bibenzyls, phenanthrenes, sesquiterpenes, fluorenones, flavonoids, phenolic acids, phenylpropanoids, lignans, amides, alkaloids, steroids, etc. (Ng et al., 2012; Xu et al., 2013). Alkaloids were the first chemicals studied and structurally confirmed in *Dendrobium*. The total alkaloid content of *D. nobile* typically approached 0.5% (Wang et al., 2016). More than 40 sesquiterpene alkaloids and terpenes have been isolated and identified from *D. nobile* (Mou et al., 2021). *D. officinale* is one of the most frequently cultivated *Dendrobium* species in China. The chemical constituents have been thoroughly isolated and characterized (Wang et al., 2021). Polysaccharides, bibenzyl, phenanthrene, lignans, flavonoids, alkaloids, and other chemicals have been found in *D. officinale*. However, there have been few studies on the isolation and identification of alkaloids monomers from *D. officinale*. *D. huoshanense* is a second-class wild endangered plant in China, having extremely high medicinal and health benefits (Jin et al., 2016; Cakova et al., 2017; Yuan et al., 2018, 2019). The extraction, separation, and structural characterization of polysaccharides are the main focus of research on the active ingredients of *D. huoshanense* (Zha et al., 2017). There have also been some studies on the separation of other small molecule chemicals, such as flavonoids, terpenoids, and alkaloids (Chang et al., 2010; Song et al., 2020; Li et al., 2021). However, the biosynthesis pathway of alkaloids from *D. huoshanense* remain unclear.

Previous researches have indicated that *D. officinale* and *D. huoshanense* contain a substantial amount of nitrogen-containing compounds, including alkaloids, the composition of which varies greatly between the two *Dendrobium* species (Song et al., 2020). Aside from the complicated structure of alkaloids, the scarcity of high-quality genomes makes pinpointing key genes in the alkaloid biosynthesis pathway more challenging. Currently, the mining of alkaloid functional genes and the research of biosynthesis pathway in some model medicinal plants, such as *Artemisia annua*, *Papaver somniferum*, *Catharanthus roseus*, *Camptotheca acuminata*, and other species, has been carried out by using third-generation sequencing technologies like Pacbio and Oxford nanopore (Kellner et al., 2015a; Shen et al., 2018; Guo et al., 2018b; Kang et al., 2021). These findings have further spurred and enhanced research into the process of alkaloids production. Here, we highlighted recent progresses in the chemical identification and biosynthesis processes of *Dendrobium* alkaloids, and also discussed the alkaloid biosynthesis pathways across diverse biogenic pathways. Meanwhile, we deeply discussed the significance of high-throughput sequencing technology in uncovering the critical genes of *Dendrobium* alkaloid biosynthesis pathways. Biosynthetic gene clusters were exploited to construct the heterologous pathways for *Dendrobium* alkaloids biosynthesis based on the synthetic biology approaches, which could fulfill large-scale production and market demand.

COMPOSITION OF *DENDROBIUM* ALKALOIDS

Alkaloids are a class of nitrogen-containing alkaline organic compounds that exist in organisms (mostly plants; Facchini, 2001; Zhan et al., 2020). Most alkaloids have a complex ring structure, and nitrogen atom is mostly contained in ring. Alkaloids have a high level of biological activity and are one of the most important active substances in herbal medicines (Facchini and St-Pierre, 2005; Kiss et al., 2017). Chinese herbal medicines abundant in alkaloids have been discovered in more than 100 families with the most dicotyledonous plants, followed by monocots, gymnosperms, and ferns. Among them, *Papaveraceae*, *Leguminosae*, *Fangchiaceae*, *Ranunculaceae*, *Apocynaceae*, *Solanaceae*, and *Amaryllidaceae* are all rich in alkaloids (Kishimoto et al., 2016). Most alkaloids are derived from L-amino acids (such as tyrosine, phenylalanine, tryptophan, lysine, and arginine), or combined with steroids, secoiridoids, and other ligands (Kumar et al., 2018). Under the catalysis of a set of specific enzymes, natural amino acids can be converted into highly specialized alkaloid precursors *via* the TCA cycle (Lichman, 2021). Alkaloids are the first compounds to be isolated and validated in the structure, among which sesquiterpene alkaloids are even more studied (Kreis and Carreira, 2012). The isolation and identification of dendrobine first occurred in *D. nobile* as a significant therapeutic substance (Wang et al., 2016). Afterward, dozens of alkaloid monomers were identified from *D. parishii* Rchb.f, *D. chrysanthum* Wall, *D. crepidatum* Lind, *D. findlayanum* par.et Rchb.f, *D. friedricksianum* Lindl., *D. hilderbrandii*, and *D. loddigesii* Rolfe (Liu et al., 2007, 2020a; Zhang et al., 2017; Yang et al., 2018, 2020; Wang et al., 2019, 2020). Based on the chemical structure of the separated alkaloids, they were divided into sesquiterpene alkaloids, imidazole alkaloids, pyrrolidine alkaloids, phthalide alkaloids, indolizidine alkaloids, and other types (Mou et al., 2021; Wang et al., 2022). At least 60 alkaloids were characterized by structure, including 35 sesquiterpene alkaloids, 14 indolizidine alkaloids, five pyrrolidine alkaloids, four phthalide alkaloids, two organic amine alkaloids, one imidazole type, and one indole alkaloid (**Figure 1**). Among these alkaloids, the activities of total alkaloid extracts and several monomers have been verified *in vivo* or *in vitro* at various levels (Nie et al., 2018; Huang et al., 2019; Song et al., 2019; Hu et al., 2020). Some alkaloids have shown significant anti-inflammatory, anti-cancer, anti-viral, and neuroprotective properties (**Table 1**). Different types of alkaloids exhibit significantly different pharmacological and pharmacodynamic effects. The total alkaloids and monomers from *D. nobile*, such as dendrobine, have obvious therapeutic effects in repairing nerve and liver injuries, improving memory, suppressing LPS-induced apoptosis, and anti-virus activity (Li et al., 2011, 2017c; Nie et al., 2016; Zhou et al., 2020). In *D. crepidatum*, homocrepidines and dendrocrepidine F exhibit anti-inflammatory properties (Hu et al., 2016). Shihunine and related extracts from *D. loddigesii* have significant anti-inflammatory and diabetic symptom alleviation effects (Chen et al., 2018; Li et al., 2019). Dendrofindline A from *D. findlayanum* exhibits notable cytotoxic effects on human tumor cells while

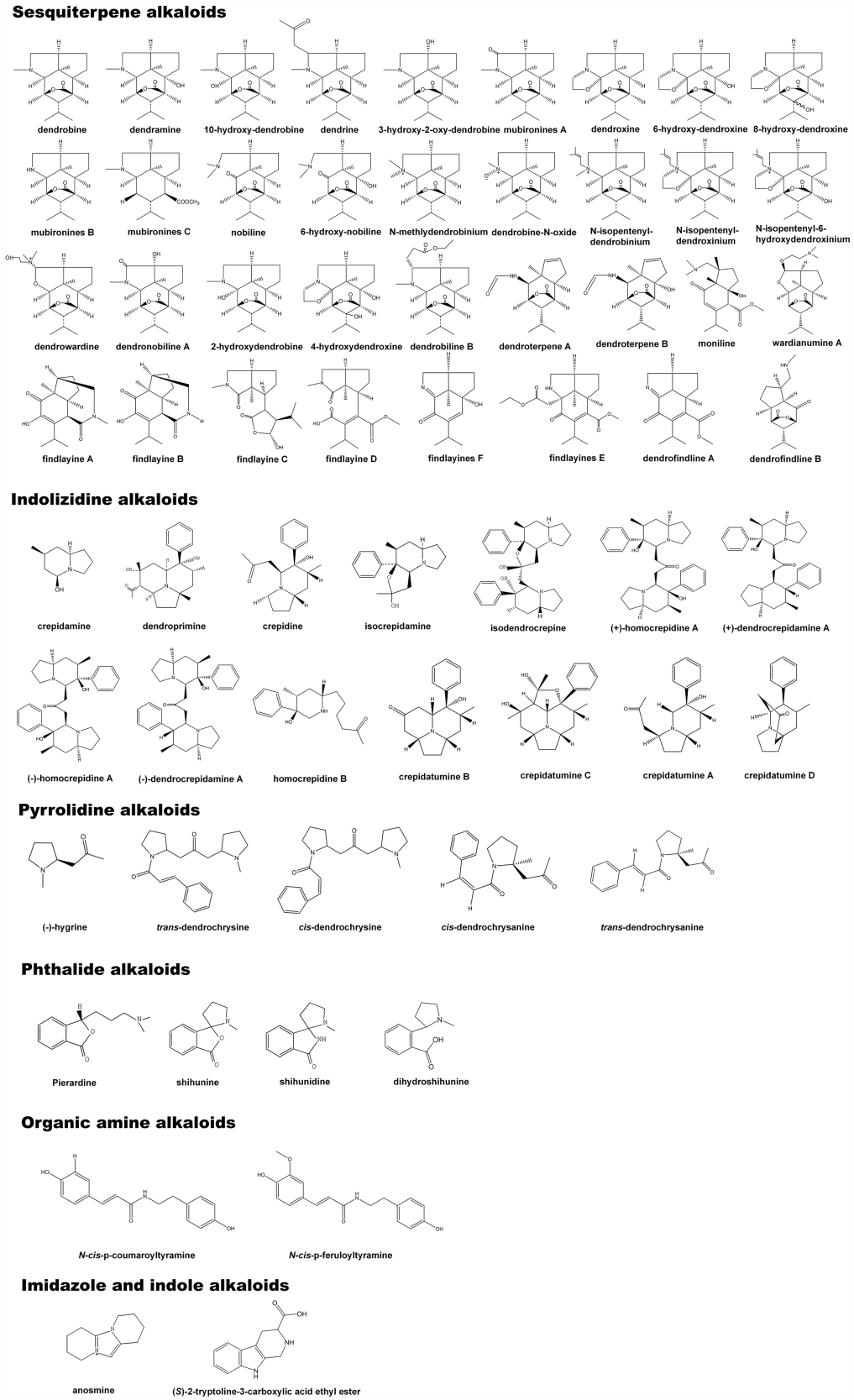

FIGURE 1 | The composition and chemical structure of *Dendrobium* alkaloids.

TABLE 1 | *Dendrobium* spp. and alkaloid constituents with biological properties.

***Dendrobium* species (organ)**	**Active molecule/type of extract**	**Experimental subjects**	**Activity**	**Ref.**
D. nobile (stem)	Total alkaloids (90.7% dendrobine)	Rat's cortical neurons (*in vitro*)	Attenuation of neuronal damage on cortical neurons injured by oxygen–glucose deprivation/reperfusion	Wang et al., 2010
	Total alkaloids (90.7% dendrobine)	Rat's hippocampus	Inhibition of LPS-induced memory impairment	Li et al., 2011
	Total alkaloids (30.5% dendrobine)	Tau protein in rat's hippocampus	Inhibition of hyperphosphorylation and LPS-induced apoptosis	Yang et al., 2014
	Total alkaloids (92.6% dendrobine)	Aβ25-35-induced memory impairment in mice	Prevention of Aβ25-35-induced neuronal and synaptic loss	Nie et al., 2016
	Total alkaloids (92.6% dendrobine)	8-week-old male Kunming mice with given doses of DNLA	Glucose-lowering and antihyperlipidemia effects in diabetic rats on the expression of the Nrf2-antioxidant pathway genes	Xu et al., 2017
	Total alkaloids (92.6% dendrobine)	Male APPswe/PS11E9 transgenic (APP/PS1) mice and wild-type (WT) littermates	Improvement of learning and memory function in APP/PS1 mice by increasing v-ATPase A1 and autolysosomal proteolysis	Nie et al., 2018
	Total alkaloids (79.8% dendrobine)	HFD-induced Male C57BL/6 mice	Balance hepatic lipid homeostasis in HFD-fed mice by increasing the taurine-conjugated bile acids and decreasing the CA/CDCA ratio	Huang et al., 2019
D. nobile	Dendrobine standard	Influenza A (H1N1,H3N2)	Anti-viral activity against influenza A viruses by restraining viral NP and its oligomerization	Li et al., 2017c
	Dendrobine standard	Human lung cancer cell line A549	Induced cytotoxicity and apoptosis of A549 NSCLC cells through JNK/Bim signaling pathway	Song et al., 2019
	Total alkaloids	8- to 10-week-old male wild-type and Nrf2 knockout mice	Protection of CCl4-induced mitochondrial dysfunction and mice liver injury by Nrf2 signaling pathway	Zhou et al., 2020
D. nobile (whole plant)	Anosmine	LPS-activated RAW264.7 cells	Inhibitory activity against NO production and a weak α-glucosidase inhibitory activity	Chen et al., 2018
D. crepidatum (stem)	Homocrepidine B	LPS-activated RAW264.7 cells	Moderate inhibition on LPS-induced NO production	Hu et al., 2016
	(–)-Dendrocrepidine F	LPS-activated peritoneal macrophages in mice	Higher anti-inflammatory effects by inhibiting NO production	Hu et al., 2018
	(+)-Homocrepidine A	LPS-activated RAW264.7 cells	Inhibitory effects on NO production and protective effect against LPS-induced acute lung injury in mice	Hu et al., 2016, 2020
D. loddigesii (stem)	Isocrepidamine	HepG2 cells	Potent hypoglycemic effect *in vitro* without cytotoxicity	Xu et al., 2019
	Dendrocrepine	HepG2 cells	Potential hypoglycemic effect on high glucose model *in vitro*	Xu et al., 2020
	Shihunine	LPS-activated RAW264.7 cells	Inhibitory activity against NO production and a weak α-glucosidase inhibitory activity	Chen et al., 2018
	Shihunine-rich extract	3T3-L1 preadipocytes induced with insulin and 3-isobutyl-1-methylxanthine, db/db, and C57BL/6 mice	Anti-diabetic effect on db/db mice by reducing the oil droplets and TG and promoting 2-NBDG uptake in 3T3-L1 cell	Li et al., 2019
D. findlayanum (whole plant)	Dendrofindline A Dendrofindline B Findlayine A	Cytotoxic effects on human tumor cell lines (A172, SHSY5Y, Hela) and zebrafish gastrointestinal motility	Inactive cytotoxicity against tumor cell lines but promoting gastrointestinal motility activities	Liu et al., 2020a
D. Snowflake "Red Star"	Flakinins A Flakinins B Mubironine C	Murine leukemia L1210 cells	Moderate cytotoxicity against murine leukemia	Morita et al., 2000
D. officinale (leaf, stem, root)	Total alkaloids	Not stated	Not stated	Shen et al., 2017
D. officinale (Protocorm-like bodies)	Carapanaubine, sempervirine, glycoperine, xanthoplanine, senkirkine, pelletierine	Not stated	Not stated	Jiao et al., 2018
D. officinale (leaf, stem)	Hordenine, piperidine, quinine, betaine Isohemiphloin, Theobromine, Trigonelline	Not stated	Not stated	Cao et al., 2019
D. officinale (leaf)	Total alkaloids	Not stated	Not stated	Chen et al., 2019
D. officinale (stem)	Caffeoylcholine 6-glucoside, cocamidopropyl βine, dopamine hydrochloride, putrescine-based derivatives	Not stated	Not stated	Zuo et al., 2020
D. officinale (Protocorm-like bodies)	Total alkaloids	Not stated	Not stated	Wang et al., 2021

also promoting gastrointestinal motility (Liu et al., 2020a). Although several alkaloids have been identified in *D. officinale*, no relevant pharmacological effects have been reported for these substances.

SESQUITERPENE ALKALOIDS AND RELATED BIOSYNTHESIS PATHWAY

Sesquiterpene alkaloids are the most abundant alkaloids found in *Dendrobium* plants. Dendrobine is one of the most rigorously studied alkaloids, with significant pharmacological effects in anti-tumor, cardiovascular and gastrointestinal inhibitory effects, and neuroprotection (Ohc and Claisen, 2012; Song et al., 2019; Zhou et al., 2020). Picrotoxane-type sesquiterpene lactone is the fundamental skeleton of this type of alkaloid. Most alkaloids have a nitrogen atom that is bonded to the C2 and C11 positions of a sesquiterpene to create a five-membered heterocyclic ring. The nitrogen atom is commonly linked to functional groups, such as methyl and isopentenyl (Morita et al., 2000; Guo et al., 2018a; Yang et al., 2019). This conformation is considered to be directly correlated with the biogenic origins of picrotoxin and tutin (Ma et al., 2019a). The isotope tracer test demonstrated that mevalonic acid is involved in the formation of the carbon skeleton of dendrobine by using substances containing radioactive isotopes ^{14}C, ^{2}H, and ^{3}H to cultivate and feed *D. nobile* (Meng et al., 2017). The canonical precursor of all sesquiterpene alkaloids (2-*trans*-6-*trans*-farnesol) is initially determined by 2-*trans*-6-*trans*-farnesyl diphosphate under the catalysis of farnesyl pyrophosphate synthesase (FPS). After farnesol undergo a cycloaddition event to form germacradiene, the electrons of germacrene follow the H_R transition from C11 to C1 to form a germacrene cation immediately. The reaction center is also shifted from C11 to C1. This stereoisomerization yields the diastereomers of the germacrene cation. Since the reaction center meets the cyclization conditions at the C1 position, the intermediate muurolane is achieved. The C2-C3 double bond is then broken, and the C3 and C7 bonds occur simultaneously, resulting in the tricyclic intermediate copaborneol. It is a common precursor in the biosynthesis of picrotoxin, tutin, and dendrobine (Wang et al., 2019). Following that, the C2-C3 bond of copaborneol is broken to form intermediate 1 (5-isopropyl-7a-methyl-1-methyleneoctahydro-1H-inden-4-yl) methanol, which is further oxidized to form intermediate 2 (5-isopropyl-7a-methyl-1-methyleneoctahydro-^{1}H-indene-4-carboxylic acid), to which a H_2O is incorporated to form intermediate 3. Dioxygenase catalyzes the hydroxylation of intermediate 3 at the C8 and C9 positions, resulting in the formation of picrotoxane (Li et al., 2017b). Picrotoxane esterifies to produce picrotoxane-lactone. Picrotoxin and tutin are synthesized by a series of oxidation reactions catalyzed by CYP450 enzymes (**Figure 2**). Furthermore, under the action of monooxygenase, aminotransferase, and methyltransferase, picrotoxane-lactone could ultimately be converted to dendrobine (Li et al., 2017b; Mou et al., 2021).

INDOLIZIDINE ALKALOIDS AND RELATED BIOSYNTHESIS PATHWAY

Indolizidine alkaloids are a type of heterocyclic compounds with specific biological and pharmacological activities that are discovered mostly in the *Apocynaceae*, *Convolvulaceae*, *Orchidaceae*, *Pandanaceae*, and *Leguminosae* (Hu et al., 2018). Currently, a large number of indolizidine alkaloids have been found in marine and terrestrial animals and plants. The fundamental structure of indolizidine alkaloids is a 5-membered ring joined with a 6-membered ring sharing a nitrogen atom (Hu et al., 2020; Zhang et al., 2021a). The biogenic pathway of indolizidine alkaloids originates from L-lysine in terms of molecular structure. L-lysine undergoes a deamination in the lysine degradation pathway, which is catalyzed by saccharopine dehydrogenase (SD) to form saccharopine. Saccharopine is catalyzed by SD to form 2-aminoadipate 6-semialdehyde, which then cyclized to form 1-piperideine-6-L-carboxylate. Under the catalysis of L-pipecolate oxidase, 1-piperideine-6-L-carboxylate degrades into pipecolate (PO). Pipecolate and acetic acid are catalyzed by cyclase to yield 1-indolizidinone. 1-Indolizidinone undergoes a multi-step reaction involving CYP450 monooxygenase, reductase, and methyltransferase to form intermediate 3 (**Figure 3**). It is believed that the C2 and C3 in 1-indolizidinone came from acetate *via* malonate; however, the enzyme that catalyzes this step has not been found. Intermediate 3 is catalyzed by phenyltransferase (PT) and malonyl-CoA-ACP transacylase (MCAT) to generate crepidatumine A, crepidatumine D, and crepidine, based on the location of the malonyl group binding (Xu et al., 2019, 2020). Depending on CYP450 enzyme, crepidatumine A and crepidine polymerize to form two type of enantiomeric octahydroindolizine alkaloids—homocrepidine A and dendrocrepidamine A (Hu et al., 2016). Crepidatumine A was converted to dendroprimine *via* CYP450 and cyclase (Kobayashi et al., 2012). Crepidine underwent the cyclization to yield isocrepidamine, which then combined with intermediate 3 to form isodendrocrepine (Xu et al., 2019).

PYRROLIDINE ALKALOIDS AND RELATED BIOSYNTHESIS PATHWAY

Pyrrolidine alkaloids are a family of structurally related substances found in *Asteraceae*, *Leguminosae*, and *Boraginaceae*. Some of them have pharmacological effects on liver toxicity to humans and livestock (Khosravi et al., 2019; Lichman, 2021). Pyrrolidine alkaloids are abundant in several edible plants, including *Senecio*, *Crotalaria*, and *Heliotropium* (Seigler, 1998). Some plants featuring pyrrolidine alkaloids are also utilized to make herbal remedies and medicinal teas. Japanese daisy tea, for example, is rich in pyrrolidine alkaloids. Currently, almost 700 pyrrolidine alkaloids have been identified from diverse plants. L-ornithine is the source of pyrrolidine alkaloids. L-ornithine is initially catalyzed by ornithine decarboxylase (ODC) to produce putrescine, which then catalyzed by putrescine N-methyltransferase (PMT) to obtain methylputrescine. Under the catalysis of primary amine: oxygen oxidoreductase (AOC), methylputrescine is deaminated and

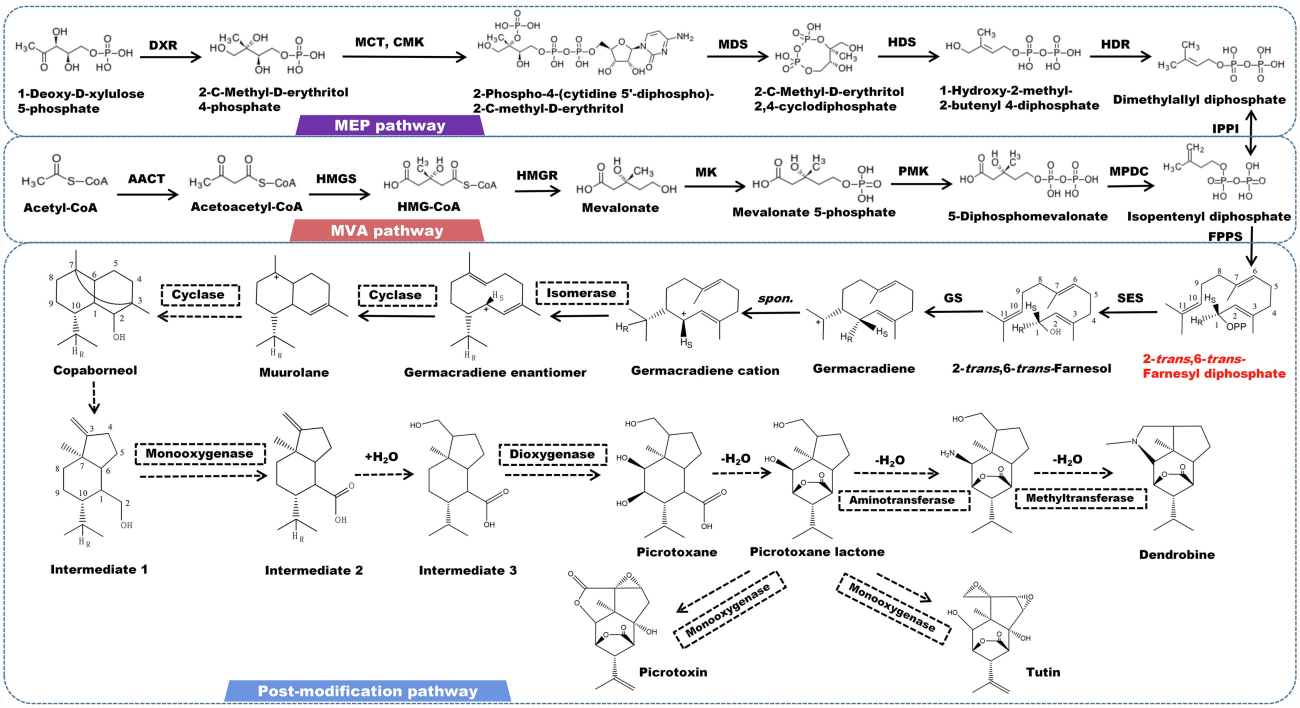

FIGURE 2 | A plausible biosynthesis pathway of sesquiterpene alkaloids. The dashed box represents the putative enzymes. The dashed arrow represents the speculated pathway. Acetyl-CoA acetyltransferase (AACT), HMG-CoA synthase (HMGS), HMG-CoA reductase (HMGR), mevalonate kinase (MK), phosphomevalonate kinase (PMK), mevalonate diphosphate decarboxylase (MPDC), 1-deoxy-D-xylulose 5-phosphate reductoisomerase (DXR), 2-C-methyl-D-erythritol 4-phosphate cytidylyltransferase (MCT), 4-diphosphocytidyl-2-C-methyl-D-erythritol kinase (CMK), 2-C-methyl-D-erythritol 2,4-cyclodiphosphate synthase (MDS), 4-hydroxy-3-methylbut-2-enyl diphosphate synthase (HDS), 4-hydroxy-3-methylbut-2-enyl diphosphate reductase (HDR), isopentenyl pyrophosphate: dimethylallyl pyrophosphate isomerase (IPPI), farnesyl diphosphate synthase (FPPS), sesquiterpene synthase (SES), germacradiene synthase (GS). SES catalyzes the formation of the precursor 2-*trans*-6-*trans*-farnesol by 2-*trans*-6-*trans*-farnesyl diphosphate.

oxidized to form 1-methylpyrrolinium—the precursor of all pyrrolidine alkaloids (**Figure 4**). Depending on acetyl-CoA acetyltransferase (AACT), one molecule 1-methylpyrrolinium and two molecules of acetyl-CoA link to form two enantiomers (−)-hygrine and (+)-hygrine (Nguyen et al., 2015). In addition, (R)-2-acetoacetyl-CoA-1-methylpyrrolidine can also be combined with 1-methylpyrrolinium to form cuscohygrine. Cuscohygrine coupled with *p*-cinnamoyl-CoA form *trans*- and *cis*-dendrochrysine. In addition, (−)-hygrine and *p*-cinnamoyl-CoA condense to produce *cis*- and *trans*-dendrochrysanine (Yang et al., 2006).

BIOSYNTHESIS PATHWAYS OF IMIDAZOLE AND INDOLE ALKALOIDS

A rare imidazolium-type alkaloid called anosmine was isolated from *D. nobile* (Chen et al., 2018). L-lysine is the starting point for the production of this kind of alkaloids (Hemscheidt and Spenser, 1993). Lysine decarboxylase catalyzes the conversion of L-lysine to cadaverine. Simultaneously, saccharopine dehydrogenase (SD) and L-pipecolate oxidase (PO) catalyze the formation of L-pipecolate. Cadaverine is oxidized by amine oxidase to form 1-piperideinium. L-Pipecolate and 1-piperideinium combine to form [1,2′-bipiperidine]-2-carboxylic acid, which is dehydrated to form intermediates 1 and 2. The latter is subjected to a series of oxidation to produce anosmine (**Figure 5A**). Other alkaloids, such as terpenoid indole alkaloids (TIAs), are also found in some *Dendrobium* spp. However, there have been few studies on the isolation and identification of indole alkaloids, with only the β-carbolin-type indole alkaloid (S)-2-tryptoline-3-carboxylic acid ethyl ester being isolated and characterized. Based on the chemical structure, the biosynthetic pathway of (S)-2-tryptoline-3-carboxylic acid ethyl ester is assumed to have originated from tryptophan metabolism (**Figure 5B**). L-tryptophan is converted to tryptamine *via* the tryptophan degradation pathway, which is catalyzed by L-tryptophan decarboxylase (TDC). Based on Pictet–Spengler reaction, tryptamine is catalyzed by strictosidine synthase (STR) to form strictosidine, which is then cracked to become tetrahydroharman (Pressnitz et al., 2018; Sharma et al., 2018; Yang et al., 2021; You et al., 2021). Through a multi-step enzymatic reaction, tetrahydroharman finally creates (S)-2-tryptoline-3-carboxylic acid ethyl ester.

PHTHALIDE ALKALOIDS AND RELATED BIOSYNTHESIS PATHWAY

Phthalide alkaloids mainly distributed in *D. loddigesii* (Li et al., 2019). The carbon skeleton structure is o-succinylbenzoate, and

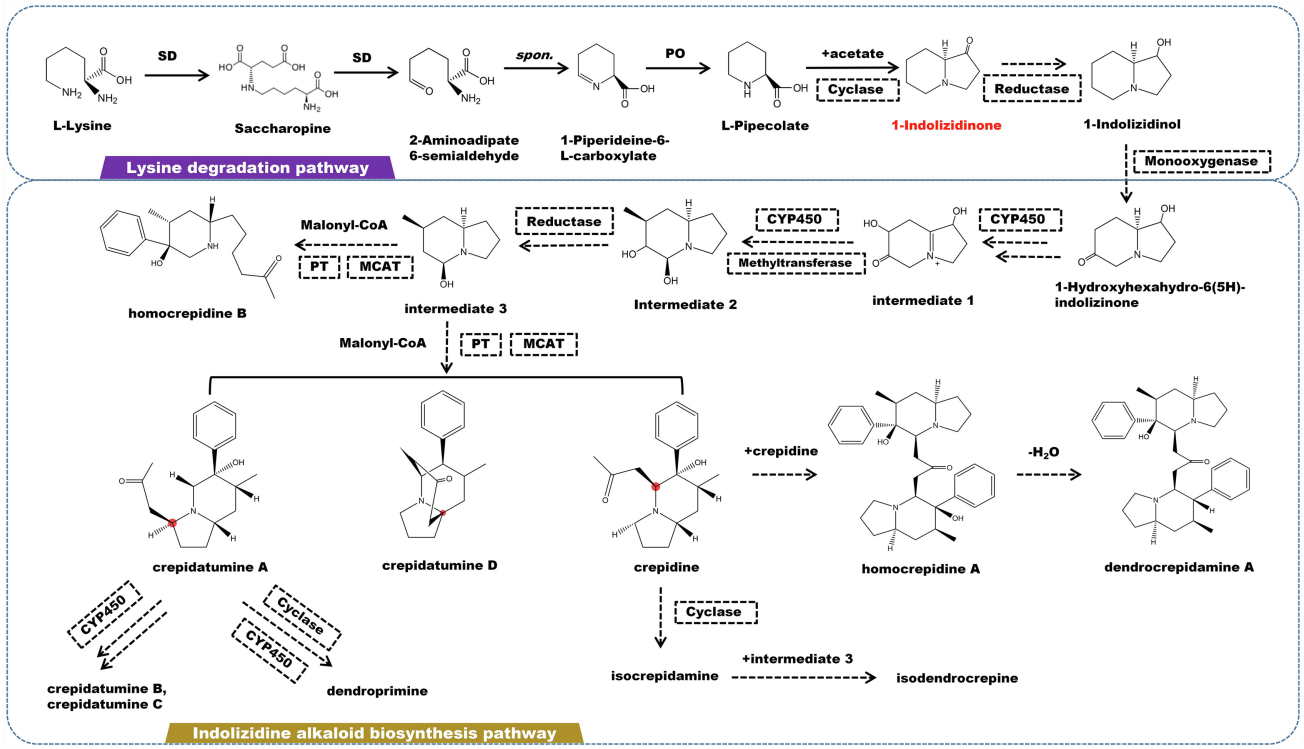

FIGURE 3 | A plausible biosynthesis pathway of indolizidine alkaloids. The dashed box represents the putative enzymes. The dashed arrow represents the speculated pathway. The multiple arrows represent multi-step reactions. Saccharopine dehydrogenase (SD), L-pipecolate oxidase (PO), phenyltransferase (PT), malonyl-CoA-ACP transacylase (MCAT). Cyclase catalyzes the connection of pipecolate and acetic acid to produce the precursor 1-indolizidinone.

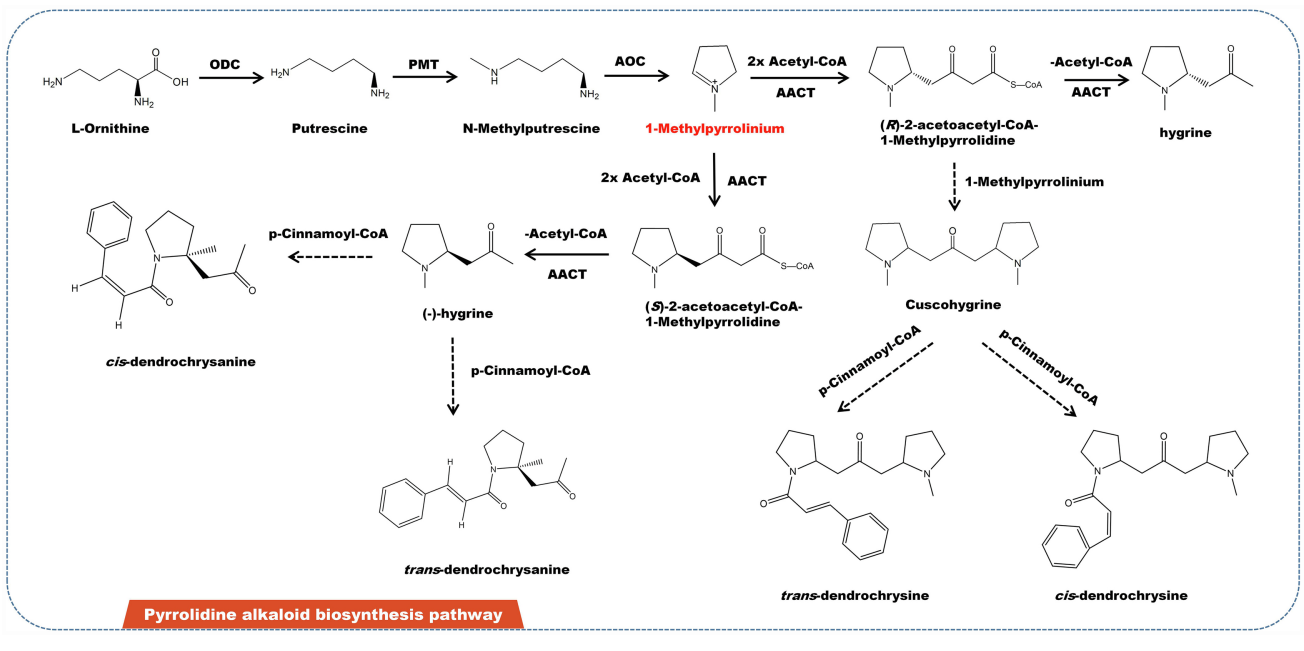

FIGURE 4 | A plausible biosynthesis pathway of pyrrolidine alkaloids. The dashed box represents the putative enzymes. The dashed arrow represents the speculated pathway. Ornithine decarboxylase (ODC), putrescine N-methyltransferase (PMT), primary amine: oxygen oxidoreductase (AOC), acetyl-CoA acetyltransferase (AACT). Under the catalysis of AOC, methylputrescine is deaminated and oxidized to produce the precursor 1-methylpyrrolinium.

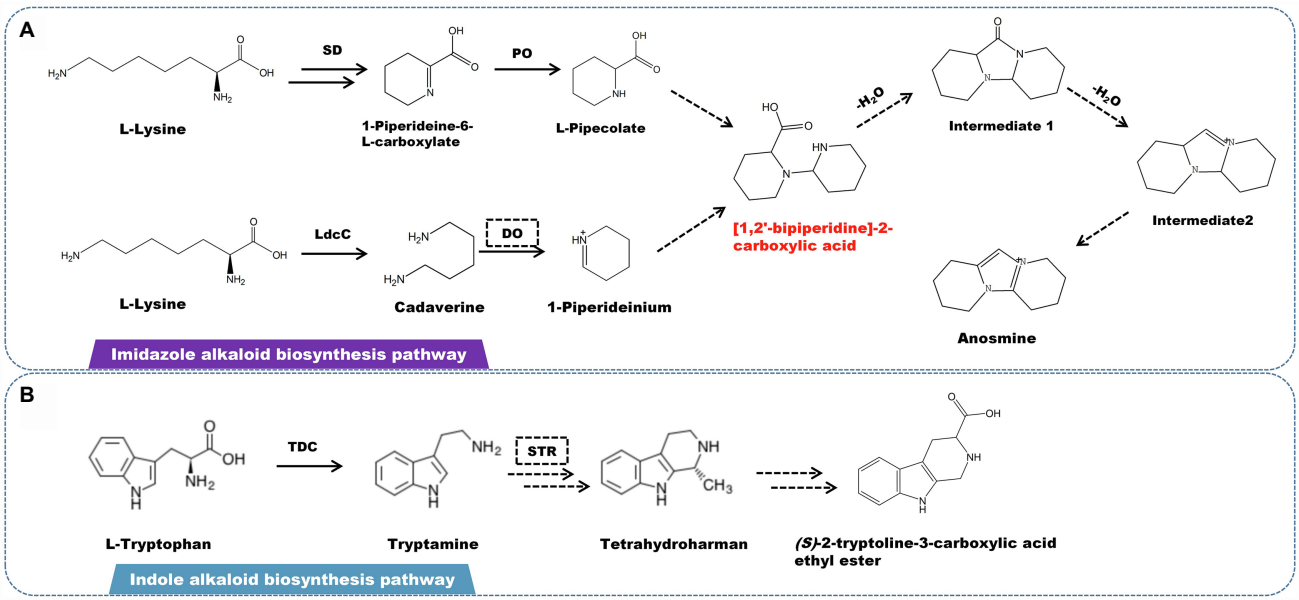

FIGURE 5 | A plausible biosynthesis pathway of imidazole and indole alkaloids. **(A)** The imidazole alkaloid biosynthetic pathway. **(B)** The indole alkaloid biosynthetic pathway. The dashed box represents the putative enzymes. The dashed arrow represents the speculated pathway. The multiple arrows represent multi-step reactions. Saccharopine dehydrogenase (SD), L-pipecolate oxidase (PO), diamine oxidase (DO), lysine decarboxylase (LdcC), L-tryptophan decarboxylase (TDC), strictosidine synthase (STR). The precursor [1,2′-bipiperidine]-2-carboxylic acid is synthesized by linking L-pipecolate with 1-piperideinium derived from lysine.

the shikimic acid/o-succinyl benzoate pathway is thought to be involved in the synthesis of this kind of alkaloid (**Figure 6**). O-succinylbenzoate (OSB) is also the precursor of menaquinones. A number of OSB-CoA synthetase family genes have been characterized in some bacteria (Lu et al., 2012). The isochorismic acid (derived from the shikimate pathway), α-ketoglutarate (originated from TCA cycle), and thiamine diphosphate (TPP) eventually form OSB under the successive reaction of 2-succinyl-5-enolpyruvyl-6-hydroxy-3-cyclohexene-1- carboxylic acid synthase (SEPHCHC synthase), 2-succinyl-6-hydroxy-2,4-cyclohexadiene-1-carboxylate synthase (SHCHC synthase) and o-succinylbenzoate synthetase (OSBS). This process lead to the release of one molecule of CO_2 and one molecule of phosphoenolpyruvate (PEP), respectively (Thoden et al., 2004). Following that, OSB is reduced to aldehydes and ketones, which are subsequently catalyzed by aminotransferase to generate 2-(4-aminobutanoyl) benzoic acid. The carbonyl group undergoes a reduction and combines with the oxygen on the ortho carboxyl group to produce a lactone, which is accompanied by methylation on the nitrogen atom. Pierardine is the final outcome of the chemical reaction. Simultaneously, 2-(4-Aminobutanoyl)benzoic acid can be cyclized to form 2-(3,4-dihydro-2H-pyrrol-5-yl) benzoic acid. As a precursor, 2-(3,4-dihydro-2H-pyrrol-5-yl) benzoic acid is transformed into lactone by an addition reaction, followed by methylation on the nitrogen atom to yield shihunine (Chen et al., 2018). Shihunidine is structurally related to shihunine. It is hypothesized that the hydroxyl group on 2-(3,4-dihydro-2H-pyrrol-5-yl)benzoic acid is substituted by a phenyl group, which first becomes an aniline form and then cyclizes and methylates to produce shihunidine.

USE OF HIGH-THROUGHPUT SEQUENCING TECHNOLOGY TO IDENTIFY THE METABOLIC PATHWAYS OF *DENDROBIUM* ALKALOIDS

High-throughput sequencing has been widely employed in the discovery of novel genes and the investigation of gene structural variation in recent years (Balilashaki et al., 2019). By integrating two or more "omics," the transcription regulators and hub genes that impact plant growth and secondary metabolism have been uncovered in many non-model plants (Kellner et al., 2015b; Saiman et al., 2018). *D. officinale*, *D. huoshanense*, *D. chrysotoxum*, and other varieties with significant medicinal benefit have undertaken *de novo* genome sequencing (Han et al., 2020; Niu et al., 2021; Zhang et al., 2021d). Combining with RNA-seq results, some researchers have systematically studied the regulatory mechanism of genes transcription and spatiotemporal characteristics under different conditions (Zheng et al., 2018; Yuan et al., 2020). The biosynthetic genes and metabolic pathways involved in *Dendrobium* alkaloids have been increasingly elucidated by the approaches described above (Zhang et al., 2021b). The genome of *D. officinale* has been upgraded in three versions, and the sequencing accuracy and assembly quality have massively improved (Yan et al., 2015; Zhang et al., 2016b; Niu et al., 2021). The *polyneuridine-aldehyde esterase* (*PNAE*) was tentatively identified based on the genomic annotation of *D. officinale* grown in Yunnan. Since *PNAE* is a crucial gene in the downstream pathway of monoterpene indole alkaloids, it is suggested that the alkaloid production of *D. officinale* may extend to the branch of

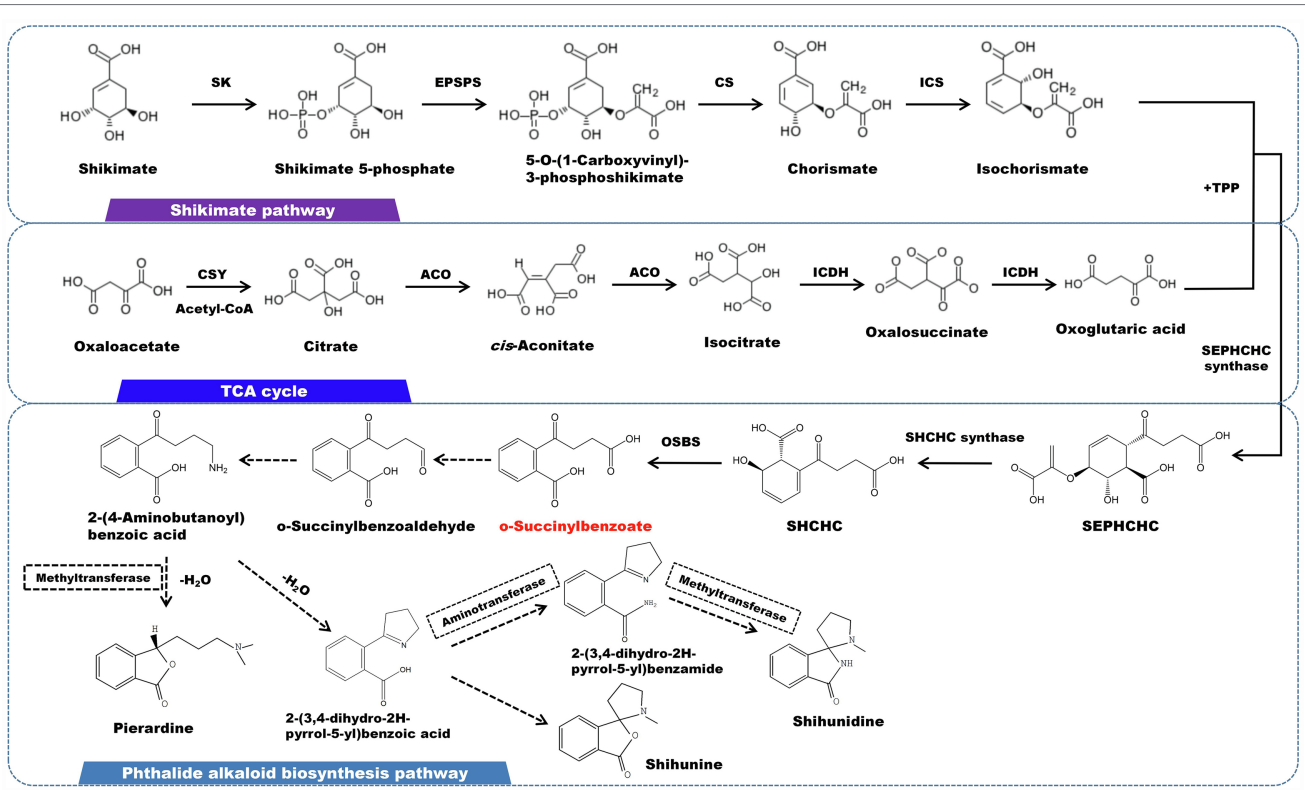

FIGURE 6 | A plausible biosynthesis pathway of phthalide alkaloids. The dashed box represents the putative enzymes. The dashed arrow represents the speculated pathway. Shikimate kinase (SK), 5-enolpyruvylshikimate 3-phosphate synthase (EPSPS), chorismate synthase (CS), isochorismate synthase (ICS), citrate synthase (CSY), aconitate hydratase (ACO), isocitrate dehydrogenase (ICDH), 2-succinyl-5-enolpyruvyl-6-hydroxy-3-cyclohexene-1-carboxylic acid synthase (SEPHCHC synthase), 2-succinyl-6-hydroxy-2,4-cyclohexadiene-1-carboxylate synthase (SHCHC synthase), o-succinylbenzoate synthase (OSBS). O-succinylbenzoate served as the core structure for the biosynthesis of the phthalide alkaloid, which is produced *via* the catalysis of OSBS.

16-epivellosimine (Yan et al., 2015). Through KEGG functional enrichment on the transcriptome of *D. officinale*, 25 genes were identified as being involved in the formation of the alkaloid skeleton (Guo et al., 2013). The expression of five key enzyme genes, *geraniol 10-hydroxylase* (*G10H*), *β-subunit of tryptophan synthase* (*TSB*), *tryptophan decarboxylase* (*TDC*), *secretoganin synthase* (*SCS*), and *strictosidine synthase* (*STR*) suggested that monoterpene indole alkaloids are mainly produced in the leaves of *D. officinale*. Many studies have indicated that MeJA treatment could stimulate the expression of most genes in the MEP and MVA pathways, as well as the accumulation of total alkaloids (Jiao et al., 2018; Chen et al., 2019). A comparative transcriptome analysis of *D. officinale* tissues and protocorm-like bodies showed 42 genes involved in the alkaloid biosynthesis pathway, and dozens of alkaloid-coding genes were identified. The expressions of some aminotransferases and CYP450 genes were significantly higher in protocorm-like bodies than in leaves, and the total alkaloid content in protocorm-like bodies likewise exhibited a similar accumulation (Wang et al., 2021). The qRT-PCR method was used to examine the expression levels of monoterpene indole alkaloid downstream pathway genes *STR*, *strictosidine-D-glucosidase* (*SG*), *PNAE*, and *vinorine synthase* (*VS*), which also revealed that the expressions of these genes are higher in protocorm-like bodies than in leaves. Transcriptome sequencing on *D. officinale* yielded a total of 2,115 unigenes related to secondary metabolism, including 4 sequences related to the indole alkaloids biosynthetic pathway, 34 sequences related to isoquinoline alkaloids biosynthetic pathway, and 38 sequences related to tropine, pyridine, and pyridine alkaloids biosynthesis (Zhang et al., 2016b). Previous studies had indicated that *DoSTR* was localized in vacuoles and that its expression was regulated by hormones, such as MeJA and ABA (Zhu et al., 2020). Recent studies generated a high-quality *D. officinale* genome at the chromosomal level, demonstrating that the sequencing data contained a contig N50 of 1.44 Mb and a Hi-C anchored rate of 93.5% (Niu et al., 2021). A total of 98 alkaloid-related genes were identified, including 56 genes encoding 25 enzymes associated with the biosynthesis of sesquiterpene alkaloids, terpenoid indole alkaloids, and their upstream pathways, including the shikimate, MVA, and MEP pathways. These genes comprise *primary amine oxidase* (*AOC*), *aspartate aminotransferase* (*AAT*), *tyrosine aminotransferase* (*TAT*), *tyrosine decarboxylase* (*TDC*), *1-benzyl-1,2,3,4-tetrahydroisoquinoline N-methyltransferase* (*CNMT*), *norbelladine O-methyltransferase* (*N4OMT*), *tropinone reductase I* (*TR1*), *PNAE*, etc. Transcriptome sequencing of *D. nobile* co-cultured with the endophytic fungus MF23 showed that a total of 16 genes were involved in the synthesis of terpenoid backbone or sesquiterpene alkaloids (Li et al., 2017b). The expression levels of *PMK* and *MVD* increased

in the ninth week of co-cultivation, which was consistent with the accumulation pattern of dendrobine. The expression of *TPS21* is negatively correlated with the biosynthesis of dendrobine, and the expression of *AACT* is positively correlated with the biosynthesis of dendrobine. Further analysis of 9 post-modification enzymes found that the expression levels of *CYP1D10*, *METTL23*, *ATX4*, and *BCAT2* were higher than other culture stages after 9 weeks inoculation. The expression of *ATX4* was at a low level at 6 weeks and was activated at 9 weeks. It demonstrates that *ATX4* is essential in the modulation of the biosynthesis of *Dendrobium* alkaloids that is altered by MF23. Besides the crucial genes, some transcription factors have important regulatory roles in stress responses and secondary metabolite production in *Dendrobium* plants (Zhang et al., 2021d). DcTCP4 and DcTCP9 are involved in JA-dependent leaf developmental processes (Zhang et al., 2021b). In *D. catenatum*, the bHLH-MYB-WD40 module is deeply engaged in anthocyanin biosynthesis. DcTT8, a IIIf bHLH transcription factor, strongly regulates the expression of the anthocyanin-related genes *F3'H* and *UFGT* (Jia et al., 2021). By binding to the promoters of *CHS*, *CHI*, and *F3H*, a light-induced WD40-repeat TF DoTTG1 regulates their expression and promotes anthocyanin formation (Jia et al., 2021). MYB2 could interact with bHLH1 to enhance the expressions of *DFR* and *ANS* (Li et al., 2017a). WRKY TFs are well-studied transcriptional regulators that are mainly involved in the stress of *D. officinale* and the production of active components. Some WRKY genes commonly activated by cold stress and MeJA treatment, while others may be involved in polysaccharide biosynthesis and hydrolysis (He et al., 2017; Wang et al., 2018). DoMYB25 participated in the positive regulation of water-soluble polysaccharides (He et al., 2019). DcWRKY22, DcWRKY36, and DcWRKY45 are involved in plant drought, cold, and salt stress (Zhang et al., 2022). DobHLHs are induced by ABA and MeJA treatments. DobHLH4 positively regulates the expression of *TPS10*, therefore boosting linalool production (Wang and Liu, 2020; Yu et al., 2021). So far, there are limited reports on transcription factors that regulate dendrobium alkaloids biosynthesis. We previously isolated a MYC2 transcription factor from *D. officinale*. Overexpression of *DoMYC2* in *A. thaliana* reduces the expression of *HMGR2*, *FPS1*, and *FPS2*, implying that DoMYC2 functions as a negative regulator to regulate the expression of JA-responsive genes. DoMYC2 typically binds to the E-box in the promoters to influence transcription (Zhu et al., 2017). We highlight the classification of alkaloids and main enzyme coding genes of different *Dendrobium* species found by high-throughput sequencing in recent years (**Table 2**).

APPLICATION OF SYNTHETIC BIOLOGY IN THE LARGE-SCALE PRODUCTION OF *DENDROBIUM* ALKALOIDS

Next generation sequencing technology provided a strong foundation for the acquisition of high-quality genome datasets of the medicinal plants, which facilitated the investigation of crucial genes in the secondary metabolism (Goossens and Rischer, 2007; Liu et al., 2020b). However, the industry still faces constraints, such as lack of raw materials and a long cultivated period. Meanwhile, alkaloid contents in most *Dendrobium* spp. are generally limited, which makes it tricky to obtain a large quantity of alkaloids rapidly. The utilization of microbial fermentation plants and synthetic biology can provide technological support for the secondary development and sustainable utilization of *Dendrobium* resources (Ehrenworth and Peralta-Yahya, 2017; Li et al., 2018a). Based on existing studies, there are two main technological methods for using synthetic biology in natural products: one is the heterologous expression of synthetic gene clusters of natural products in suitable chassis cells (Ro et al., 2006; Dangel et al., 2010; Gwak et al., 2017); the other is to introduce positive regulatory regulatory elements or delete negative regulatory elements in the original host to achieve regulation or overexpression of related genes (Zhuang et al., 2017; Ma et al., 2018). Since the synthetic route of natural products is generally extended, the problem of heavy metabolic load and low yield of single bacteria are often stressful to overcome. The exploration of multicellular systems provides flexibility and personalization for the production of such complex substances (Li et al., 2018b). By rationally designing and constructing an artificial multi-cell culture system, the metabolic pathways could be dispersed and assembled into multiple independent cells, which can lower the metabolic burden of a single bacteria. The optimal module combination could be achieved by engineering and maximizing the metabolic capacity of a single chassis cell (Zhang and Wang, 2016). The goal of synthetic biology has gradually evolved from the synthesis of biological components and devices (the first stage of synthetic biology) to the construction of multicellular life systems (the second stage of synthetic biology; Paddon et al., 2013; Ma et al., 2019b). With the gradual development of gene editing and *de novo* synthesis technologies, the chassis of synthetic biology is becoming more abundant, mainly including microbial chassis (*Saccharomyces cerevisiae* and *Escherichia coli*, etc.) and plant chassis (tobacco, suspension cells, hairy roots, etc.). The heterologous synthesis of iridoids, isoflavin, and vinblastine in yeast and the heterologous synthesis of triterpenoids, such as artemisinin and its precursors, β-amyrin and oleanolic acid in tobacco, provide scientific reference for *in vitro* synthesis of dendrobium alkaloids (Farhi et al., 2011; Miettinen et al., 2014; Brown et al., 2015; Fuentes et al., 2016; Malhotra et al., 2016; Kumar et al., 2018; Saiman et al., 2018).

Recent research found that specialized metabolic enzymes usually clustered in a few chromosomes, forming metabolic gene clusters. These gene clusters are widely present in the biosynthesis pathways of secondary metabolites in dicotyledonous and monocotyledonous plants (Nützmann et al., 2016). Generally, genes in some gene clusters are arranged continuously and tightly on chromosomes (Polturak and Osbourn, 2021). The thaliano-synthetic gene cluster in over 80% of *Arabidopsis* ecotypes, the acylated tyramine gene cluster in rice, and the diterpene casbene gene cluster present a continuous arrangement (Zhan et al., 2020; Shen et al., 2021). Some gene clusters are scattered in distant areas, such as the genes that synthesize the sterol alkaloid α-solanine in tomato clusters on chromosome 7 (Itkin et al., 2013). This

TABLE 2 | Identification of alkaloid-related compounds and key genes in *Dendrobium* spp.

Species	Sequencing platform or technique	Classification	Annotated genes	Ref.
D. nobile	Molecular Cloning	Pyrrolidine alkaloid	*TR1*	Chen et al., 2013
D. nobile	Molecular Cloning	Pyrrolidine alkaloid	*TR2*	Cheng et al., 2013
D. officinale	Roche 454 GS FLX Titanium	terpenoid indole alkaloids	*AACT,HMGS,HMGR,MVK,PMK, MVD,IPI,DXS,DXR,CMS,CMK, MCS,HDS,FPS,TSB,TDC,G10H, SCS,STR,10-HGO*	Guo et al., 2013
D. officinale	Illumina Hiseq 2000 and PacBio Sequel	Monoterpene indole alkaloids	*AACT,HMGS,HMGR, MVK, PMK, MVD,IPI, DXS,DXR,CMS,CMK, MCS,HDS,FPS, PNAE*	Yan et al., 2015
D. officinale	Molecular Cloning	Precursor of terpenoid	*DXS,DXR*	Fan et al., 2016
D. catenatum	Illumina HiSeq 2000	Precursor of terpenoid	*TPS-a, TPS-b, TPS-e/f, TPS-c, TPS-g*	Zhang et al., 2016a
D. officinale	Illumina Hiseq 2000	Indole alkaloids, isoquinoline alkaloid, tropane, piperidine, and pyridine alkaloid	*Not stated*	Zhang et al., 2016b
D. nobile	Agilent Bioanalyzer 2,100	Sesquiterpene alkaloids	*AACT,HMGS,HMGR,MK,PMK, MVD,GPPS,FPS,TPS21,CYP71D55,CYP735A,CYP71D10,CYP94C1, METTL23,ATX4,AAT2,DAT, BCAT2*	Li et al., 2017b
D. officinale	Agilent Bioanalyzer 2,100	terpenoid indole alkaloids	*AACT,HMGS,HMGR,MVK,PMK, MVD,IPI,DXS,DXR,CMS,CMK, MCS,HDS,FPS,TSB,TDC,STR*	Shen et al., 2017
D. officinale	Molecular Cloning	Precursor of terpenoid	*MYC2*	Zhu et al., 2017
D. huoshanense	Illumina Hiseq 2,500	terpenoid indole alkaloids	*FPS,AACT,HMGS,HMGR,MVK, PMK,MVD,IPI,DXS,DXR,CMS, CMK,MCS,TDS,TSB,HDR*	Yuan et al., 2018
D. officinale	Illumina Hiseq 4,000	Sesquiterpene alkaloids	*AACT,HMGS,HMGR,MVK,PMK, MVD,DXS,DXR,MCT,CMK,MDS, HDS,HDR,FPS,IPI*	Chen et al., 2019
D. officinale	Molecular Cloning	Monoterpene indole alkaloids	*STR*	Zhu et al., 2020
D. officinale	Genome-wide identification	Precursor of indole alkaloids	*GAD,HDC,TYDC,TDC*	Zhang et al., 2020
D. officinale	Genome-wide identification	Precursor of terpenoid	*TPS-a, TPS-b, TPS-c, TPS-e/f*	Yu et al., 2020
D. chrysotoxum	MGISEQ-2000 and PacBio Sequel	Precursor of terpenoid	*TPS-a, TPS-b, TPS-c, TPS-e/f, TPS-g*	Zhang et al., 2021c
D. officinale	Illumina Hiseq 4,000 and PacBio Sequel II	Sesquiterpene alkaloids, isoquinoline alkaloid, pyrrolidine alkaloid, terpenoid indole alkaloids	*AOC, AAT, TAT, TDC, CNMT, N4OMT,TR1 ,PNAE,HMGS,HMGR,MVK,PMK,MVD,DXS,DXR, CMS,CMK,MCS,PNAE,SDR,AAE, TPS21,FDFT1,SQLE,FLDH, CYP71D55*	Niu et al., 2021
D. officinale	BGIseq 500	Monoterpene indole alkaloids	*TS,TDC,STR,HDR,GPPS,GES, G10H,UGT8,7-DLH,LAMT,SG, GS,PNAE,VS,AACT,HMGS, HMGR, MVK,PMK,MVD,IPI, DXD,DXR,CMS,CMK,MCS,HDS, SCS*	Wang et al., 2021
D. officinale	Illumina HiSeq 4,000	Precursor of terpenoid	*TPS-a, TPS-b, TPS-c, TPS-e/f*	Li et al., 2021

encompasses two upstream pathway genes, *GAME11* and *GAME6*, as well as four glycosyltransferase genes, *GAME1*, *GAME17*, *GAME18*, and *GAME2*. The other two structural genes, *GAME12* and *GAME4*, which encode aminotransferases, are adjacent to each other on chromosome 12. Based on genome and transcriptome co-expression analysis, it is feasible to carry out initial mining of gene clusters of specific metabolic pathways (Jeon et al., 2020; Liu et al., 2020c). Some software and algorithms are capable of rapidly identifying potential gene clusters in non-model plants. Plant Cluster Finder is a more developed tool that has studied 18 plants and identified approximately 12,000 possible biosynthetic gene clusters (Schläpfer et al., 2017). PlantiSMASH and PhytoClust employ a more accurate hidden Markov model to identify distinct biosynthetic enzymes and integrate the gene locations to predict candidate gene clusters (Kautsar et al., 2017; Töpfer et al., 2017). It should be noted that *Dendrobium* alkaloids are mostly composed of TIAs and sesquiterpene alkaloids (**Table 1**). By altering particular critical enzymes in the MEP and MVA pathways, heterologous expression strategies can supply richer terpene precursors for the production of these two kinds of alkaloids (Zhu et al., 2014).

CONCLUSION AND FUTURE CHALLENGES

With the rapid development of sequencing technology and various "omics" technologies, plant-specific metabolic biosynthesis has rapidly progressed from small-scale sequencing and functional identification of individual genes to the large-scale sequencing and comparative genomics studies. Transcriptomics and

metabolomics-associated analysis, including co-expression and co-response analysis, have been successfully employed in the functional identification of unknown genes in many non-model plants. The completion of high-quality genome sequencing and re-sequencing of natural populations has also provided considerable prospects for the exploration of crop metabolic pathways and valuable Chinese herbal medicines. The metabolome genome-wide association study (mGWAS) is a new approach to decipher in-depth analyses of complicated metabolic pathways and their regulatory mechanisms, as well as other basic theoretical studies. However, this technology is rarely applied in the research of active specific metabolites of medicinal plants. The main reason for this is that medicinal plants, unlike commercial crops, do not typically have systematic classification and whole germplasm lines. Synthetic biology is the design or modification of living systems at the molecular level to meet certain purposes. Plants can transform light energy and CO_2 from the environment into their own energy and carbon sources. The use of synthetic biology to rebuild metabolic networks in plant cells and reroute carbon flow to more useful plant-specific metabolites has enormous potential. The convergence of cutting-edge technologies, such as improved genome editing, sophisticated gene module assembly, tobacco transient expression technology, rapid and efficient genetic modification with magnetic nanoparticles as carriers, and computer-aided design, will propel synthetic biology into the next era in the future.

AUTHOR CONTRIBUTIONS

CS, QJ, and YC discussed the writing plan. CS and JM drafted the manuscript. CS, JM, GL, HP, and YZ edited the manuscript. BH and QJ acquired the funding. All authors have read, reviewed, and approved the submitted version.

FUNDING

This work was supported by China Agricultural Research System of MOF and MARA. The authors are also grateful for the financial support of National Industry Technology System of Traditional Chinese Medicine (CARS-21), Anhui University Collaborative Innovation Project (GXXT-2019-043 and GXXT-2019-049), High-level Talents Research Initiation Funding Project of West Anhui University (WGKQ2022025), and Natural Science Foundation of Anhui (2108085MC80).

REFERENCES

Balilashaki, K., Zakizadeh, H., Olfati, J. A., Vahedi, M., Kumar, A., and Indracanti, M. (2019). Recent advances in phalaenopsis orchid improvement using omics approaches. *Plant Tissue Cult. Biotechnol.* 29, 133–149. doi: 10.3329/ptcb.v29i1.41986

Brown, S., Clastre, M., Courdavault, V., and O'Connor, S. E. (2015). De novo production of the plant-derived alkaloid strictosidine in yeast. *Proc. Natl. Acad. Sci. U. S. A.* 112, 3205–3210. doi: 10.1073/pnas.1423555112

Cakova, V., Bonte, F., and Lobstein, A. (2017). Dendrobium: sources of active ingredients to treat age-related pathologies. *Aging Dis.* 8, 827–849. doi: 10.14336/AD.2017.0214

Cao, H., Ji, Y., Li, S., Lu, L., Tian, M., Yang, W., et al. (2019). Extensive metabolic profiles of leaves and stems from the medicinal plant *Dendrobium officinale* kimura et migo. *Meta* 9, 13–18. doi: 10.3390/metabo9100215

Chang, C. C., Ku, A. F., Tseng, Y. Y., Yang, W. B., Fang, J. M., and Wong, C. H. (2010). 6,8-Di-C-glycosyl flavonoids from dendrobium huoshanense. *J. Nat. Prod.* 73, 229–232. doi: 10.1021/np900252f

Chen, W., Cheng, X., Zhou, Z., Liu, J., and Wang, H. (2013). Molecular cloning and characterization of a tropinone reductase from *Dendrobium nobile* Lindl. *Mol. Biol. Rep.* 40, 1145–1154. doi: 10.1007/s11033-012-2156-0

Chen, H., Li, X., Xu, Y., Lo, K., Zheng, H., Hu, H., et al. (2018). Study on the polar extracts of *Dendrobium nobile, D. officinale, D. loddigesii*, and *flickingeria fimbriata*: metabolite identification, content evaluation, and bioactivity assay. *Molecules* 23:1185. doi: 10.3390/molecules23051185

Chen, Y., Wang, Y., Lyu, P., Chen, L., Shen, C., and Sun, C. (2019). Comparative transcriptomic analysis reveal the regulation mechanism underlying MeJA-induced accumulation of alkaloids in *Dendrobium officinale*. *J. Plant Res.* 132, 419–429. doi: 10.1007/s10265-019-01099-6

Cheng, X., Chen, W., Zhou, Z., Liu, J., and Wang, H. (2013). Functional characterization of a novel tropinone reductase-like gene in *Dendrobium nobile* Lindl. *J. Plant Physiol.* 170, 958–964. doi: 10.1016/j.jplph.2013.02.007

Dangel, V., Westrich, L., Smith, M. C. M., Heide, L., and Gust, B. (2010). Use of an inducible promoter for antibiotic production in a heterologous host. *Appl. Microbiol. Biotechnol.* 87, 261–269. doi: 10.1007/s00253-009-2435-4

Ehrenworth, A. M., and Peralta-Yahya, P. (2017). Accelerating the semisynthesis of alkaloid-based drugs through metabolic engineering. *Nat. Chem. Biol.* 13, 249–258. doi: 10.1038/nchembio.2308

Facchini, P. J. (2001). Alkaloid biosynthesis in plants: biochemistry, cell biology, molecular regulation, and metabolic engineering applications. *Annu. Rev. Plant Biol.* 52, 29–66. doi: 10.1146/annurev.arplant.52.1.29

Facchini, P. J., and St-Pierre, B. (2005). Synthesis and trafficking of alkaloid biosynthetic enzymes. *Curr. Opin. Plant Biol.* 8, 657–666. doi: 10.1016/j.pbi.2005.09.008

Fan, H., Wu, Q., Wang, X., Wu, L., Cai, Y., and Lin, Y. (2016). Molecular cloning and expression of 1-deoxy-d-xylulose-5-phosphate synthase and 1-deoxy-d-xylulose-5-phosphate reductoisomerase in *Dendrobium officinale*. *Plant Cell Tissue Organ Cult.* 125, 381–385. doi: 10.1007/s11240-016-0945-1

Farhi, M., Marhevka, E., Ben-Ari, J., Algamas-Dimantov, A., Liang, Z., Zeevi, V., et al. (2011). Generation of the potent anti-malarial drug artemisinin in tobacco. *Nat. Biotechnol.* 29, 1072–1074. doi: 10.1038/nbt.2054

Fuentes, P., Zhou, F., Erban, A., Karcher, D., Kopka, J., and Bock, R. (2016). A new synthetic biology approach allows transfer of an entire metabolic pathway from a medicinal plant to a biomass crop. *elife* 5, 1–26. doi: 10.7554/eLife.13664

Goossens, A., and Rischer, H. (2007). Implementation of functional genomics for gene discovery in alkaloid producing plants. *Phytochem. Rev.* 6, 35–49. doi: 10.1007/s11101-006-9018-0

Guo, L., Frey, W., and Plietker, B. (2018a). Catalytic enantioselective total synthesis of the Picrotoxane alkaloids (-)-Dendrobine, (-)-Mubironine B, and (-)-Dendroxine. *Org. Lett.* 20, 4328–4331. doi: 10.1021/acs.orglett.8b01782

Guo, X., Li, Y., Li, C., Luo, H., Wang, L., Qian, J., et al. (2013). Analysis of the *Dendrobium officinale* transcriptome reveals putative alkaloid biosynthetic genes and genetic markers. *Gene* 527, 131–138. doi: 10.1016/j.gene.2013.05.073

Guo, L., Winzer, T., Yang, X., Li, Y., Ning, Z., He, Z., et al. (2018b). The opium poppy genome and morphinan production. *Science* 347, 343–347. doi: 10.1126/science.aat4096

Gwak, Y. S., Han, J. Y., Adhikari, P. B., Ahn, C. H., and Choi, Y. E. (2017). Heterologous production of a ginsenoside saponin (compound K) and its precursors in transgenic tobacco impairs the vegetative and reproductive growth. *Planta* 245, 1105–1119. doi: 10.1007/s00425-017-2668-x

Han, B., Jing, Y., Dai, J., Zheng, T., Gu, F., Zhao, Q., et al. (2020). A chromosome-level genome assembly of *Dendrobium Huoshanense* using long reads and Hi-C data. *Genome Biol. Evol.* 12, 2486–2490. doi: 10.1093/gbe/evaa215

He, C., Teixeira da Silva, J. A., Tan, J., Zhang, J., Pan, X., Li, M., et al. (2017). A genome-wide identification of the WRKY family genes and a survey of

potential WRKY target genes in *Dendrobium officinale*. *Sci. Rep.* 7, 1–14. doi: 10.1038/s41598-017-07872-8

He, C., Teixeira da Silva, J. A., Wang, H., Si, C., Zhang, M., Zhang, X., et al. (2019). Mining MYB transcription factors from the genomes of orchids (*Phalaenopsis* and *Dendrobium*) and characterization of an orchid R2R3-MYB gene involved in water-soluble polysaccharide biosynthesis. *Sci. Rep.* 9, 13818–13819. doi: 10.1038/s41598-019-49812-8

Hemscheidt, T., and Spenser, I. D. (1993). Biosynthesis of anosmine: incorporation of the intact six-carbon chain of lysine and of pipecolic acid. *J. Nat. Prod.* 56, 1281–1287. doi: 10.1021/np50098a012

Huang, S., Wu, Q., Liu, H., Ling, H., He, Y., Wang, C., et al. (2019). Alkaloids of dendrobium nobile lindl. altered hepatic lipid homeostasis via regulation of bile acids. *J. Ethnopharmacol.* 241:111976. doi: 10.1016/j.jep.2019.111976

Hu, Y., Ren, J., Wang, L., Zhao, X., Zhang, M., Shimizu, K., et al. (2018). Protective effects of total alkaloids from *Dendrobium crepidatum* against LPS-induced acute lung injury in mice and its chemical components. *Phytochemistry* 149, 12–23. doi: 10.1016/j.phytochem.2018.02.006

Hu, Y., Yang, H., Ding, X., Liu, J., Wang, X., Hu, L., et al. (2020). Anti-inflammatory octahydroindolizine alkaloid enantiomers from *Dendrobium crepidatum*. *Bioorg. Chem.* 100:103809. doi: 10.1016/j.bioorg.2020.103809

Hu, Y., Zhang, C., Zhao, X., Wang, Y., Feng, D., Zhang, M., et al. (2016). (±)-Homocrepidine A, a pair of anti-inflammatory enantiomeric octahydroindolizine alkaloid dimers from *Dendrobium crepidatum*. *J. Nat. Prod.* 79, 252–256. doi: 10.1021/acs.jnatprod.5b00801

Itkin, M., Heinig, U., Tzfadia, O., Bhide, A. J., Shinde, B., Cardenas, P. D., et al. (2013). Biosynthesis of antinutritional alkaloids in solanaceous crops is mediated by clustered genes. *Science* 341, 175–179. doi: 10.1126/science.1240230

Jeon, J. E., Kim, J. G., Fischer, C. R., Mehta, N., Dufour-Schroif, C., Wemmer, K., et al. (2020). A pathogen-responsive gene cluster for highly modified fatty acids in tomato. *Cell* 180, 176–187.e19. doi: 10.1016/j.cell.2019.11.037

Jia, N., Wang, J. J., Liu, J., Jiang, J., Sun, J., Yan, P., et al. (2021). DcTT8, a bHLH transcription factor, regulates anthocyanin biosynthesis in *Dendrobium candidum*. *Plant Physiol. Biochem.* 162, 603–612. doi: 10.1016/j.plaphy.2021.03.006

Jia, N., Wang, J., Wang, Y., Ye, W., Liu, J., Jiang, J., et al. (2021). The light-induced WD40-repeat transcription factor DcTTG1 regulates anthocyanin biosynthesis in *Dendrobium candidum*. *Front. Plant Sci.* 12:633333. doi: 10.3389/fpls.2021.633333

Jiao, C., Song, C., Zheng, S., Zhu, Y., Jin, Q., Cai, Y., et al. (2018). Metabolic profiling of *Dendrobium officinale* in response to precursors and methyl jasmonate. *Int. J. Mol. Sci.* 19:728. doi: 10.3390/ijms19030728

Jin, Q., Jiao, C., Sun, S., Song, C., Cai, Y., Lin, Y., et al. (2016). Metabolic analysis of medicinal Dendrobium officinale and Dendrobium huoshanense during different growth years. *PLoS One* 11. doi: 10.1371/journal.pone.0146607

Kang, M., Fu, R., Zhang, P., Lou, S., Yang, X., Chen, Y., et al. (2021). A chromosome-level *Camptotheca acuminata* genome assembly provides insights into the evolutionary origin of camptothecin biosynthesis. *Nat. Commun.* 12, 3531–3512. doi: 10.1038/s41467-021-23872-9

Kautsar, S. A., Suarez Duran, H. G., Blin, K., Osbourn, A., and Medema, M. H. (2017). PlantiSMASH: automated identification, annotation and expression analysis of plant biosynthetic gene clusters. *Nucleic Acids Res.* 45, W55–W63. doi: 10.1093/nar/gkx305

Kellner, F., Geu-Flores, F., Sherden, N. H., Brown, S., Foureau, E., Courdavault, V., et al. (2015a). Discovery of a P450-catalyzed step in vindoline biosynthesis: a link between the aspidosperma and eburnamine alkaloids. *Chem. Commun.* 51, 7626–7628. doi: 10.1039/c5cc01309g

Kellner, F., Kim, J., Clavijo, B. J., Hamilton, J. P., Childs, K. L., Vaillancourt, B., et al. (2015b). Genome-guided investigation of plant natural product biosynthesis. *Plant J.* 82, 680–692. doi: 10.1111/tpj.12827

Khosravi, E., Mousavi, A., Farhadpour, M., Ghashghaie, J., Ghanati, F., and Haghbeen, K. (2019). Pyrrolizidine alkaloids-free extract from the cell culture of *Lithospermum officinale* with high antioxidant capacity. *Appl. Biochem. Biotechnol.* 187, 744–752. doi: 10.1007/s12010-018-2830-3

Kishimoto, S., Sato, M., Tsunematsu, Y., and Watanabe, K. (2016). Evaluation of biosynthetic pathway and engineered biosynthesis of alkaloids. *Molecules* 21:1078. doi: 10.3390/molecules21081078

Kiss, T., Borcsa, B., Orvos, P., Tálosi, L., Hohmann, J., and Csupor, D. (2017). Diterpene lipo-alkaloids with selective activities on cardiac K + channels. *Planta Med.* 83, 1321–1328. doi: 10.1055/s-0043-109556

Kobayashi, T., Hasegawa, F., Hirose, Y., Tanaka, K., Mori, H., and Katsumura, S. (2012). Stereocontrolled synthesis of substituted chiral piperidines via one-pot asymmetric 6π-azaelectrocyclization: asymmetric syntheses of (−)-dendroprimine, (+)-7-epidendroprimine, (+)-5-epidendroprimine, and (+)-5,7-epidendroprimine. *J. Org. Chem.* 77, 1812–1832. doi: 10.1021/jo202350z

Kreis, L. M., and Carreira, E. M. (2012). Total synthesis of (−)-Dendrobine. *Angew. Chemie* 124, 3492–3495. doi: 10.1002/ange.201108564

Kumar, S. R., Shilpashree, H. B., and Nagegowda, D. A. (2018). Terpene moiety enhancement by overexpression of geranyl(Geranyl) diphosphate synthase and geraniol synthase elevates monomeric and dimeric monoterpene indole alkaloids in transgenic *Catharanthus roseus*. *Front. Plant Sci.* 9:942. doi: 10.3389/fpls.2018.00942

Lam, Y., Ng, T. B., Yao, R. M., Shi, J., Xu, K., Sze, S. C. W., et al. (2015). Evaluation of chemical constituents and important mechanism of pharmacological biology in *Dendrobium* plants. *Evidence-based Complement. Altern. Med.* 2015, 1–25. doi: 10.1155/2015/841752

Li, Q., Ding, G., Li, B., and Guo, S. X. (2017b). Transcriptome analysis of genes involved in dendrobine biosynthesis in *Dendrobium nobile* Lindl. infected with mycorrhizal fungus MF23 (Mycena sp.). *Sci. Rep.* 7, 1–16. doi: 10.1038/s41598-017-00445-9

Li, N., Dong, Y., Lv, M., Qian, L., Sun, X., Liu, L., et al. (2021). Combined analysis of volatile terpenoid metabolism and transcriptome reveals transcription factors related to terpene synthase in two cultivars of *Dendrobium officinale* flowers. *Front. Genet.* 12:661296. doi: 10.3389/fgene.2021.661296

Li, X. W., Huang, M., Lo, K., Chen, W. L., He, Y. Y., Xu, Y., et al. (2019). Anti-diabetic effect of a shihunine-rich extract of *Dendrobium loddigesii* on 3t3-l1 cells and db/db mice by up-regulating AMPK–GLUT4–PPARα. *Molecules* 24, 1–20. doi: 10.3390/molecules24142673

Li, S., Li, Y., and Smolke, C. D. (2018a). Strategies for microbial synthesis of high-value phytochemicals. *Nat. Chem.* 10, 395–404. doi: 10.1038/s41557-018-0013-z

Li, Y., Li, F., Gong, Q., Wu, Q., and Shi, J. (2011). Inhibitory effects of dendrobium alkaloids on memory impairment induced by lipopolysaccharide in rats. *Planta Med.* 77, 117–121. doi: 10.1055/s-0030-1250235

Li, Y., Li, S., Thodey, K., Trenchard, I., Cravens, A., and Smolke, C. D. (2018b). Complete biosynthesis of noscapine and halogenated alkaloids in yeast. *Proc. Natl. Acad. Sci. U. S. A.* 115, E3922–E3931. doi: 10.1073/pnas.1721469115

Li, R., Liu, T., Liu, M., Chen, F., Liu, S., and Yang, J. (2017c). Anti-influenza A virus activity of dendrobine and its mechanism of action. *J. Agric. Food Chem.* 65, 3665–3674. doi: 10.1021/acs.jafc.7b00276

Li, C., Qiu, J., Ding, L., Huang, M., Huang, S., Yang, G., et al. (2017a). Anthocyanin biosynthesis regulation of DhMYB2 and DhbHLH1 in *Dendrobium* hybrids petals. *Plant Physiol. Biochem.* 112, 335–345. doi: 10.1016/j.plaphy.2017.01.019

Lichman, B. R. (2021). The scaffold-forming steps of plant alkaloid biosynthesis. *Nat. Prod. Rep.* 38, 103–129. doi: 10.1039/d0np00031k

Liu, Z., Cheema, J., Vigouroux, M., Hill, L., Reed, J., Paajanen, P., et al. (2020c). Formation and diversification of a paradigm biosynthetic gene cluster in plants. *Nat. Commun.* 11, 1–11. doi: 10.1038/s41467-020-19153-6

Liu, Y., Cui, Y., Lu, L., Gong, Y., Han, W., and Piao, G. (2020b). Natural indole-containing alkaloids and their antibacterial activities. *Arch. Pharm.* 353, e2000120–e2000110. doi: 10.1002/ardp.202000120

Liu, W. H., Hua, Y. F., and Zhan, Z. J. (2007). Moniline, a new alkaloid from *Dendrobium moniliforme*. *J. Chem. Res.* 38, 317–318. doi: 10.3184/030823407X218048

Liu, G. Y., Tan, L., Cheng, L., Ding, L. S., Zhou, Y., Deng, Y., et al. (2020a). Dendrobine-type alkaloids and bibenzyl derivatives from *Dendrobium findlayanum*. *Fitoterapia* 142:104497. doi: 10.1016/j.fitote.2020.104497

Lu, X., Zhou, R., Sharma, I., Li, X., Kumar, G., Swaminathan, S., et al. (2012). Stable analogues of OSB-AMP: potent inhibitors of MenE, the o-Succinylbenzoate-CoA Synthetase from bacterial Menaquinone biosynthesis. *Chembiochem* 13, 129–136. doi: 10.1002/cbic.201100585

Ma, C., Meng, C. W., Zhou, Q. M., Peng, C., Liu, F., Zhang, J. W., et al. (2019a). New sesquiterpenoids from the stems of *Dendrobium nobile* and their neuroprotective activities. *Fitoterapia* 138:104351. doi: 10.1016/j.fitote.2019.104351

Ma, D., Reichelt, M., Yoshida, K., Gershenzon, J., and Constabel, C. P. (2018). Two R2R3-MYB proteins are broad repressors of flavonoid and phenylpropanoid metabolism in poplar. *Plant J.* 96, 949–965. doi: 10.1111/tpj.14081

Ma, T., Shi, B., Ye, Z., Li, X., Liu, M., Chen, Y., et al. (2019b). Lipid engineering combined with systematic metabolic engineering of *Saccharomyces cerevisiae* for high-yield production of lycopene. *Metab. Eng.* 52, 134–142. doi: 10.1016/j.ymben.2018.11.009

Malhotra, K., Subramaniyan, M., Rawat, K., Kalamuddin, M., Qureshi, M. I., Malhotra, P., et al. (2016). Compartmentalized metabolic engineering for artemisinin biosynthesis and effective malaria treatment by oral delivery of plant cells. *Mol. Plant* 9, 1464–1477. doi: 10.1016/j.molp.2016.09.013

Meng, C. W., He, Y. L., Peng, C., Ding, X. J., Guo, L., and Xiong, L. (2017). Picrotoxane sesquiterpenoids from the stems of *Dendrobium nobile* and their absolute configurations and angiogenesis effect. *Fitoterapia* 121, 206–211. doi: 10.1016/j.fitote.2017.07.017

Miettinen, K., Dong, L., Navrot, N., Schneider, T., Burlat, V., Pollier, J., et al. (2014). The seco-iridoid pathway from *Catharanthus roseus*. *Nat. Commun.* 5:3606. doi: 10.1038/ncomms4606

Morita, H., Fujiwara, M., Yoshida, N., and Kobayashi, J. (2000). New Picrotoxinin-type and Dendrobine-type Sesquiterpenoids from *Dendrobium Snowflake* 'Red Star'. *Tetrahedron* 56, 5801–5805. doi: 10.1016/S0040-4020(00)00530-5

Mou, Z., Zhao, Y., Ye, F., Shi, Y., Kennelly, E. J., Chen, S., et al. (2021). Identification, biological activities and biosynthetic pathway of *Dendrobium* alkaloids. *Front. Pharmacol.* 12:605994. doi: 10.3389/fphar.2021.605994

Ng, T. B., Liu, J., Wong, J. H., Ye, X., Wing Sze, S. C., Tong, Y., et al. (2012). Review of research on *Dendrobium*, a prized folk medicine. *Appl. Microbiol. Biotechnol.* 93, 1795–1803. doi: 10.1007/s00253-011-3829-7

Nguyen, T. K. O., Jamali, A., Lanoue, A., Gontier, E., and Dauwe, R. (2015). Unravelling the architecture and dynamics of tropane alkaloid biosynthesis pathways using metabolite correlation networks. *Phytochemistry* 116, 94–103. doi: 10.1016/j.phytochem.2015.03.005

Nie, J., Jiang, L. S., Zhang, Y., Tian, Y., Li, L. S., Lu, Y. L., et al. (2018). *Dendrobium nobile* Lindl. Alkaloids decreases the level of intracellular β-amyloid by improving impaired Autolysosomal proteolysis in APP/PS1 mice. *Front. Pharmacol.* 9:1479. doi: 10.3389/fphar.2018.01479

Nie, J., Tian, Y., Zhang, Y., Lu, Y. L., Li, L. S., and Shi, J. S. (2016). *Dendrobium* alkaloids prevent aß25-35-induced neuronal and synaptic loss via promoting neurotrophic factors expression in mice. *PeerJ* 4, 1–16. doi: 10.7717/peerj.2739

Niu, Z., Zhu, F., Fan, Y., Li, C., Zhang, B., Zhu, S., et al. (2021). The chromosome-level reference genome assembly for *Dendrobium officinale* and its utility of functional genomics research and molecular breeding study. *Acta Pharm. Sin. B* 11, 2080–2092. doi: 10.1016/j.apsb.2021.01.019

Nützmann, H. W., Huang, A., and Osbourn, A. (2016). Plant metabolic clusters – from genetics to genomics. *New Phytol.* 211, 771–789. doi: 10.1111/nph.13981

Ohc, C., and Claisen, I. (2012). Synthesis of (−)-Dendrobine. *Synfacts* 8:592. doi: 10.1055/s-0031-1291052

Paddon, C. J., Westfall, P. J., Pitera, D. J., Benjamin, K., Fisher, K., McPhee, D., et al. (2013). High-level semi-synthetic production of the potent antimalarial artemisinin. *Nature* 496, 528–532. doi: 10.1038/nature12051

Polturak, G., and Osbourn, A. (2021). The emerging role of biosynthetic gene clusters in plant defense and plant interactions. *PLoS Pathog.* 17, e1009698–e1009611. doi: 10.1371/journal.ppat.1009698

Pressnitz, D., Fischereder, E. M., Pletz, J., Kofler, C., Hammerer, L., Hiebler, K., et al. (2018). Asymmetric synthesis of (R)-1-alkyl-substituted Tetrahydro-ß-carbolines catalyzed by Strictosidine synthases. *Angew. Chem. Int. Ed.* 57, 10683–10687. doi: 10.1002/anie.201803372

Ro, D. K., Paradise, E. M., Quellet, M., Fisher, K. J., Newman, K. L., Ndungu, J. M., et al. (2006). Production of the antimalarial drug precursor artemisinic acid in engineered yeast. *Nature* 440, 940–943. doi: 10.1038/nature04640

Saiman, M. Z., Miettinen, K., Mustafa, N. R., Choi, Y. H., Verpoorte, R., and Schulte, A. E. (2018). Metabolic alteration of *Catharanthus roseus* cell suspension cultures overexpressing geraniol synthase in the plastids or cytosol. *Plant Cell Tissue Organ Cult.* 134, 41–53. doi: 10.1007/s11240-018-1398-5

Schläpfer, P., Zhang, P., Wang, C., Kim, T., Banf, M., Chae, L., et al. (2017). Genome-wide prediction of metabolic enzymes, pathways, and gene clusters in plants. *Plant Physiol.* 173, 2041–2059. doi: 10.1104/pp.16.01942

Seigler, D. S. (1998). "Pyrrolizidine, quinolizidine, and indolizidine alkaloids," *Plant Secondary Metabolism*. Boston, MA: Springer.

Sharma, A., Verma, P., Mathur, A., and Mathur, A. K. (2018). Overexpression of tryptophan decarboxylase and strictosidine synthase enhanced terpenoid indole alkaloid pathway activity and antineoplastic vinblastine biosynthesis in *Catharanthus roseus*. *Protoplasma* 255, 1281–1294. doi: 10.1007/s00709-018-1233-1

Shen, C., Guo, H., Chen, H., Shi, Y., Meng, Y., Lu, J., et al. (2017). Identification and analysis of genes associated with the synthesis of bioactive constituents in *Dendrobium officinale* using RNA-Seq. *Sci. Rep.* 7, 187–111. doi: 10.1038/s41598-017-00292-8

Shen, S., Peng, M., Fang, H., Wang, Z., Zhou, S., Jing, X., et al. (2021). An Oryza-specific hydroxycinnamoyl tyramine gene cluster contributes to enhanced disease resistance. *Sci. Bull.* 66, 2369–2380. doi: 10.1016/j.scib.2021.03.015

Shen, Q., Zhang, L., Liao, Z., Wang, S., Yan, T., Shi, P., et al. (2018). The genome of *Artemisia annua* provides insight into the evolution of Asteraceae Family and Artemisinin biosynthesis. *Mol. Plant* 11, 776–788. doi: 10.1016/j.molp.2018.03.015

Song, T. H., Chen, X. X., Lee, C. K. F., Sze, S. C. W., Feng, Y. B., Yang, Z. J., et al. (2019). Dendrobine targeting JNK stress signaling to sensitize chemotoxicity of cisplatin against non-small cell lung cancer cells in vitro and in vivo. *Phytomedicine* 53, 18–27. doi: 10.1016/j.phymed.2018.06.018

Song, C., Jiao, C., Jin, Q., Chen, C., Cai, Y., and Lin, Y. (2020). Metabolomics analysis of nitrogen-containing metabolites between two *Dendrobium* plants. *Physiol. Mol. Biol. Plants.* 26, 1425–1435. doi: 10.1007/s12298-020-00822-1

Teixeira da Silva, J. A., and Ng, T. B. (2017). The medicinal and pharmaceutical importance of *Dendrobium* species. *Appl. Microbiol. Biotechnol.* 101, 2227–2239. doi: 10.1007/s00253-017-8169-9

Thoden, J. B., Taylor Ringia, E. A., Garrett, J. B., Gerlt, J. A., Holden, H. M., and Rayment, I. (2004). Evolution of enzymatic activity in the Enolase superfamily: structural studies of the promiscuous o-Succinylbenzoate synthase from *Amycolatopsis*. *Biochemistry* 43, 5716–5727. doi: 10.1021/bi0497897

Töpfer, N., Fuchs, L. M., and Aharoni, A. (2017). The PhytoClust tool for metabolic gene clusters discovery in plant genomes. *Nucleic Acids Res.* 45, 7049–7063. doi: 10.1093/nar/gkx404

Wang, Y., Avula, B., Abe, N., Wei, F., Wang, M., Ma, S., et al. (2016). Tandem mass spectrometry for structural characterization of dendrobine-type sesquiterpene alkaloids from the stems of *Dendrobium nobile* using LC-MS/MS. *Planta Med.* 82, 662–670. doi: 10.1055/s-0042-103031

Wang, P., Chen, X., Cai, C. H., Kong, F. D., Huang, S. Z., Yuan, J. Z., et al. (2020). A new picrotoxane-type sesquiterpene from *Dendrobium nobile* Lindl. *Nat. Prod. Res.* 36, 2112–2117. doi: 10.1080/14786419.2020.1851224

Wang, P., Chen, X., Wang, H., Huang, S., Cai, C., Yuan, J., et al. (2019). Four new picrotoxane-type sesquiterpenes from *Dendrobium nobile* Lindl. *Front. Chem.* 7:812. doi: 10.3389/fchem.2019.00812

Wang, Q., Gong, Q., Wu, Q., and Shi, J. (2010). Neuroprotective effects of Dendrobium alkaloids on rat cortical neurons injured by oxygen-glucose deprivation and reperfusion. *Phytomedicine* 17, 108–115. doi: 10.1016/j.phymed.2009.05.010

Wang, Z., Jiang, W., Liu, Y., Meng, X., Su, X., Cao, M., et al. (2021). Putative genes in alkaloid biosynthesis identified in *Dendrobium officinale* by correlating the contents of major bioactive metabolites with genes expression between Protocorm-like bodies and leaves. *BMC Genomics* 22, 579–518. doi: 10.1186/s12864-021-07887-6

Wang, Y., and Liu, A. (2020). Genomic characterization and expression analysis of basic helix-loop-helix (BHLH) family genes in traditional chinese herb *Dendrobium officinale*. *Plan. Theory* 9, 1–23. doi: 10.3390/plants9081044

Wang, T., Song, Z., Wei, L., and Li, L. (2018). Molecular characterization and expression analysis of WRKY family genes in *Dendrobium officinale*. *Genes Genomics* 40, 265–279. doi: 10.1007/s13258-017-0602-z

Wang, Y., Tong, Y., Adejobi, O. I., Wang, Y., and Liu, A. (2022). Research advances in multi-Omics on the traditional Chinese herb *Dendrobium officinale*. *Front. Plant Sci.* 12:808228. doi: 10.3389/fpls.2021.808228

Xu, X., Chen, X., Yang, R., Li, Z., Zhou, H., Bai, Y., et al. (2020). Crepidtumines A and B, two novel Indolizidine alkaloids from *Dendrobium crepidatum*. *Sci. Rep.* 10, 9564–9568. doi: 10.1038/s41598-020-66552-2

Xu, J., Han, Q. B., Li, S. L., Chen, X. J., Wang, X. N., Zhao, Z. Z., et al. (2013). Chemistry, bioactivity and quality control of *Dendrobium*, a commonly used tonic herb in traditional Chinese medicine. *Phytochem. Rev.* 12, 341–367. doi: 10.1007/s11101-013-9310-8

Xu, X., Li, Z., Yang, R., Zhou, H., Bai, Y., Yu, M., et al. (2019). Crepidatumines C and D, two new indolizidine alkaloids from *Dendrobium crepidatum* lindl. ex Paxt. *Molecules* 24, 2–10. doi: 10.3390/molecules24173071

Xu, Y. Y., Xu, Y. S., Wang, Y., Wu, Q., Lu, Y. F., Liu, J., et al. (2017). *Dendrobium nobile* Lindl. alkaloids regulate metabolism gene expression in livers of mice. *J. Pharm. Pharmacol.* 69, 1409–1417. doi: 10.1111/jphp.12778

Yan, L., Wang, X., Liu, H., Tian, Y., Lian, J., Yang, R., et al. (2015). The genome of *Dendrobium officinale* illuminates the biology of the important traditional Chinese orchid herb. *Mol. Plant* 8, 922–934. doi: 10.1016/j.molp.2014.12.011

Yang, D., Cheng, Z. Q., Hou, B., Yang, L., Zi, C. T., Dong, F. W., et al. (2020). Two unusual dendrobine-type alkaloids from *Dendrobium findlayanum*. *Fitoterapia* 144:104607. doi: 10.1016/j.fitote.2020.104607

Yang, D., Cheng, Z. Q., Yang, L., Hou, B., Yang, J., Li, X. N., et al. (2018). Seco-Dendrobine-type alkaloids and bioactive Phenolics from *Dendrobium findlayanum*. *J. Nat. Prod.* 81, 227–235. doi: 10.1021/acs.jnatprod.7b00150

Yang, D., Cheng, Z. Q., Zi, C. T., Yang, L., Dong, F. W., Hu, J. M., et al. (2019). Four new sesquiterpene derivatives from *Dendrobium findlayanum*. *Chin. J. Nat. Med.* 17, 900–905. doi: 10.1016/S1875-5364(19)30110-4

Yang, S., Gong, Q., Wu, Q., Li, F., Lu, Y., and Shi, J. (2014). Alkaloids enriched extract from *Dendrobium nobile* Lindl. attenuates tau protein hyperphosphorylation and apoptosis induced by lipopolysaccharide in rat brain. *Phytomedicine* 21, 712–716. doi: 10.1016/j.phymed.2013.10.026

Yang, L., Qin, L. H., Bligh, S. W. A., Bashall, A., Zhang, C. F., Zhang, M., et al. (2006). A new phenanthrene with a spirolactone from *Dendrobium chrysanthum* and its anti-inflammatory activities. *Bioorgan. Med. Chem.* 14, 3496–3501. doi: 10.1016/j.bmc.2006.01.004

Yang, M., Wang, Q., Liu, Y., Hao, X., Wang, C., Liang, Y., et al. (2021). Divergent camptothecin biosynthetic pathway in *Ophiorrhiza pumila*. *BMC Biol.* 19, 122–116. doi: 10.1186/s12915-021-01051-y

You, D., Feng, Y., Wang, C., Sun, C., Wang, Y., Zhao, D., et al. (2021). Cloning, characterization, and enzymatic identification of a new tryptophan decarboxylase from *Ophiorrhiza pumila*. *Biotechnol. Appl. Biochem.* 68, 381–389. doi: 10.1002/bab.1935

Yu, Z., Zhang, G., Teixeira da Silva, J. A., Zhao, C., and Duan, J. (2021). The methyl jasmonate-responsive transcription factor DobHLH4 promotes DoTPS10, which is involved in linalool biosynthesis in *Dendrobium officinale* during floral development. *Plant Sci.* 309:110952. doi: 10.1016/j.plantsci.2021.110952

Yu, Z., Zhao, C., Zhang, G., Teixeira da Silva, J. A., and Duan, J. (2020). Genome-wide identification and expression profile of tps gene family in *Dendrobium officinale* and the role of dotps10 in linalool biosynthesis. *Int. J. Mol. Sci.* 21, 1–22. doi: 10.3390/ijms21155419

Yuan, Y., Liu, X., Wang, J., and Zhang, J. (2019). Morphological and microscopic identification of three major medicinal *Dendrobium* species in Ta-Pieh Mountains area. *Microsc. Res. Tech.* 82, 483–493. doi: 10.1002/jemt.23191

Yuan, Y., Yu, M., Jia, Z., Song, X., Liang, Y., and Zhang, J. (2018). Analysis of *Dendrobium huoshanense* transcriptome unveils putative genes associated with active ingredients synthesis. *BMC Genomics* 19, 978–916. doi: 10.1186/s12864-018-5305-6

Yuan, Y., Zhang, B., Tang, X., Zhang, J., and Lin, J. (2020). Comparative transcriptome analysis of different dendrobium species reveals active ingredients-related genes and pathways. *Int. J. Mol. Sci.* 21:861. doi: 10.3390/ijms21030861

Zhan, C., Lei, L., Liu, Z., Zhou, S., Yang, C., Zhu, X., et al. (2020). Selection of a subspecies-specific diterpene gene cluster implicated in rice disease resistance. *Nat. Plants* 6, 1447–1454. doi: 10.1038/s41477-020-00816-7

Zhang, J., He, C., Wu, K., Teixeira da Silva, J. A., Zeng, S., Zhang, X., et al. (2016b). Transcriptome analysis of *Dendrobium officinale* and its application to the identification of genes associated with polysaccharide synthesis. *Front. Plant Sci.* 7:5. doi: 10.3389/fpls.2016.00005

Zhang, L., Jiao, C., Cao, Y., Cheng, X., Wang, J., Jin, Q., et al. (2020). Comparative analysis and expression patterns of the PLP_dec genes in *Dendrobium officinale*. *Int. J. Mol. Sci.* 21:54. doi: 10.3390/ijms21010054

Zhang, L., Li, C., Yang, D., Wang, Y., Yang, Y., and Sun, X. (2021b). Genome-wide analysis of the tcp transcription factor genes in *Dendrobium catenatum* lindl. *Int. J. Mol. Sci.* 22:10269. doi: 10.3390/ijms221910269

Zhang, C., Liu, S. J., Yang, L., Yuan, M. Y., Li, J. Y., Hou, B., et al. (2017). Sesquiterpene amino ether and cytotoxic phenols from *Dendrobium wardianum* Warner. *Fitoterapia* 122, 76–79. doi: 10.1016/j.fitote.2017.08.015

Zhang, J., Morris-Natschke, S. L., Ma, D., Shang, X. F., Yang, C. J., Liu, Y. Q., et al. (2021a). Biologically active indolizidine alkaloids. *Med. Res. Rev.* 41, 928–960. doi: 10.1002/med.21747

Zhang, G. Q., Xu, Q., Bian, C., Tsai, W. C., Yeh, C. M., Liu, K. W., et al. (2016a). The *Dendrobium catenatum* Lindl. genome sequence provides insights into polysaccharide synthase, floral development and adaptive evolution. *Sci. Rep.* 6, 1–10. doi: 10.1038/srep19029

Zhang, H., and Wang, X. (2016). Modular co-culture engineering, a new approach for metabolic engineering. *Metab. Eng.* 37, 114–121. doi: 10.1016/j.ymben.2016.05.007

Zhang, T., Xu, Y., Ding, Y., Yu, W., Wang, J., Lai, H., et al. (2022). Identification and expression analysis of WRKY gene family in response to abiotic stress in *Dendrobium catenatum*. *Front. Genet.* 13:800019. doi: 10.3389/fgene.2022.800019

Zhang, M., Yu, Z., Zeng, D., Si, C., Zhao, C., Wang, H., et al. (2021c). Transcriptome and metabolome reveal salt-stress responses of leaf tissues from *Dendrobium officinale*. *Biomol. Ther.* 11, 1–16. doi: 10.3390/biom11050736

Zhang, Y., Zhang, G. Q., Zhang, D., Liu, X. D., Xu, X. Y., Sun, W. H., et al. (2021d). Chromosome-scale assembly of the *Dendrobium chrysotoxum* genome enhances the understanding of orchid evolution. *Hortic. Res.* 8:183. doi: 10.1038/s41438-021-00621-z

Zha, X. Q., Deng, Y. Y., Li, X. L., Wang, J. F., Pan, L. H., and Luo, J. P. (2017). The core structure of a Dendrobium huoshanense polysaccharide required for the inhibition of human lens epithelial cell apoptosis. *Carbohydr. Polym.* 155, 252–260. doi: 10.1016/j.carbpol.2016.08.087

Zheng, S.-g., Hu, Y.-d., Zhao, R.-x., Yan, S., Zhang, X.-q., Zhao, T.-m., et al. (2018). Genome-wide researches and applications on *Dendrobium*. *Planta* 248, 769–784. doi: 10.1007/s00425-018-2960-4

Zhou, J., Zhang, Y., Li, S., Zhou, Q., Lu, Y., Shi, J., et al. (2020). *Dendrobium nobile* Lindl. alkaloids-mediated protection against CCl4-induced liver mitochondrial oxidative damage is dependent on the activation of Nrf2 signaling pathway. *Biomed. Pharmacother.* 129:110351. doi: 10.1016/j.biopha.2020.110351

Zhu, Y. F., Fan, H. H., Li, D. H., Jin, Q., Zhang, C. M., Zhu, L. Q., et al. (2020). Molecular cloning, bioinformation analysis and expression of the strictosidine synthase in *Dendrobium officinale*. *Acta Sci. Pol. Hortorum Cultus* 19, 111–124. doi: 10.24326/asphc.2020.3.10

Zhu, Y., Meng, C., Zhu, L., Li, D., Jin, Q., Song, C., et al. (2017). Cloning and characterization of DoMYC2 from Dendrobium officinale. *Plant Cell. Tissue Organ Cult.* 129, 533–541. doi: 10.1007/s11240-017-1198-3

Zhu, X., Zeng, X., Sun, C., and Chen, S. (2014). Biosynthetic pathway of terpenoid indole alkaloids in *Catharanthus roseus*. *Front. Med. China* 8, 285–293. doi: 10.1007/s11684-014-0350-2

Zhuang, Y., Yang, G. Y., Chen, X., Liu, Q., Zhang, X., Deng, Z., et al. (2017). Biosynthesis of plant-derived ginsenoside Rh2 in yeast via repurposing a key promiscuous microbial enzyme. *Metab. Eng.* 42, 25–32. doi: 10.1016/j.ymben.2017.04.009

Zuo, S. M., Yu, H. D., Zhang, W., Zhong, Q., Chen, W., Chen, W., et al. (2020). Comparative metabolomic analysis of *Dendrobium officinale* under different cultivation substrates. *Meta* 10, 1–14. doi: 10.3390/metabo10080325

Conflict of Interest: The authors declare that the research was conducted in the absence of any commercial or financial relationships that could be construed as a potential conflict of interest.

Publisher's Note: All claims expressed in this article are solely those of the authors and do not necessarily represent those of their affiliated organizations, or those of the publisher, the editors and the reviewers. Any product that may be evaluated in this article, or claim that may be made by its manufacturer, is not guaranteed or endorsed by the publisher.

Copyright © 2022 Song, Ma, Li, Pan, Zhu, Jin, Cai and Han. This is an open-access article distributed under the terms of the Creative Commons Attribution License (CC BY). The use, distribution or reproduction in other forums is permitted, provided the original author(s) and the copyright owner(s) are credited and that the original publication in this journal is cited, in accordance with accepted academic practice. No use, distribution or reproduction is permitted which does not comply with these terms.

frontiers | Frontiers in Plant Science

ORIGINAL RESEARCH
published: 20 May 2022
doi: 10.3389/fpls.2022.878796

Increasing Expression of *PnGAP* and *PnEXPA4* Provides Insights Into the Enlargement of *Panax notoginseng* Root Size From *Qing* Dynasty to Cultivation Era

Mu-Yao Yu[1†], Zhong-Yi Hua[1†], Pei-Ran Liao[2], Han Zheng[1], Yan Jin[1], Hua-Sheng Peng[1], Xiu-Ming Cui[3], Lu-Qi Huang[1*] and Yuan Yuan[1*]*

[1] State Key Laboratory Breeding Base of Dao-di Herbs, National Resource Center for Chinese Materia Medica, China Academy of Chinese Medical Sciences, Beijing, China, [2] School of Traditional Chinese Medicine, Guangdong Pharmaceutical University, Guangzhou, China, [3] Faculty of Life Science and Technology, Kunming University of Science and Technology, Kunming, China

OPEN ACCESS

Edited by:
Lei Zhang,
Second Military Medical University, China

Reviewed by:
Fangyuan Zhang,
Southwest University, China
Qingsong Shao,
Zhejiang Agriculture and Forestry University, China

***Correspondence:**
Yuan Yuan
y_yuan0732@163.com
Lu-Qi Huang
huangluqi01@126.com
Xiu-Ming Cui
sanqi37@vip.sina.com

[†] These authors have contributed equally to this work

Specialty section:
This article was submitted to Plant Metabolism and Chemodiversity, a section of the journal Frontiers in Plant Science

Received: 18 February 2022
Accepted: 07 April 2022
Published: 20 May 2022

Citation:
Yu M-Y, Hua Z-Y, Liao P-R, Zheng H, Jin Y, Peng H-S, Cui X-M, Huang L-Q and Yuan Y (2022) Increasing Expression of PnGAP and PnEXPA4 Provides Insights Into the Enlargement of Panax notoginseng Root Size From Qing Dynasty to Cultivation Era. Front. Plant Sci. 13:878796. doi: 10.3389/fpls.2022.878796

Root size is a key trait in plant cultivation and can be influenced by the cultivation environment. However, physical evidence of root size change in a secular context is scarce due to the difficulty in preserving ancient root samples, and how they were modified during the domestication and cultivation stays unclear. About 100 ancient root samples of *Panax notoginseng,* preserved as tribute in the Palace Museum (A.D. 1636 to 1912, *Qing* dynasty), provided an opportunity to investigate the root size changes during the last 100 years of cultivation. The dry weight of ancient root samples (~120 *tou* samples, *tou* represents number of roots per 500 g dry weight) is 0.22-fold of the modern samples with the biggest size (20 *tou* samples). Transcriptome analysis revealed that *PnGAP* and *PnEXPA4* were highly expressed in 20 *tou* samples, compared with the 120 *tou* samples, which might contribute to the thicker cell wall and a higher content of lignin, cellulose, and callose in 20 *tou* samples. A relatively lower content of dencichine and higher content of ginsenoside Rb_1 in 20 *tou* samples are also consistent with higher expression of ginsenoside biosynthesis-related genes. PnPHL8 was filtrated through transcriptome analysis, which could specifically bind the promoters of *PnGAP*, *PnCYP716A47,* and *PnGGPPS3*, respectively. The results in this study represent the first physical evidence of root size changes in *P. notoginseng* in the last 100 years of cultivation and contribute to a comprehensive understanding of how the cultivation environment affected root size, chemical composition, and clinical application.

Keywords: root size, cultivation, GPI-anchored, expansin, *Panax notoginseng*, cell wall

INTRODUCTION

Plant root size is a key trait for improving water and nitrogen uptake efficiency. In cultivation, temperature (Teskey and Hinckley, 2010; Chathurika et al., 2018), precipitation (Ba Rraclough et al., 2010; Ghaffari et al., 2021), light transmittance (Cheon et al., 2004; Kuang et al., 2015), fertilization (Ba Rraclough et al., 2010; Goodsman et al., 2010), and agrotype

(Hiroyoshi et al., 2004; Chen, 2017) can lead to deformation of plant root phenotype. Except for the environmental factors, the genotype is the main factor determining the root size, and a number of quantitative trait loci (QTL) or genes associated with root size have been identified (Jeong et al., 2013; Tamirisa et al., 2014; Yao et al., 2014; Cheng et al., 2016; Ding et al., 2016). It was reported that glycosylphosphatidylinositol (GPI)-anchored protein (*GAP*) has diverse function on root architecture, by affecting cell wall architecture (Macmillan et al., 2010), cell elongation (Niu et al., 2018), cytoderm thickness, and content of lignin, cellulose, and callose (Liu, 2009; Bundy et al., 2016; Zhao et al., 2020). High temperature decreased the expression of *OsGAP18,* leading to a thinner cell wall (Zhao et al., 2020), while several *GAP*s were prominently upregulated during cold acclimation (Daisuke et al., 2016) and nitrogen supply (Engelsberger and Schulze, 2012). Expansin (EXP) also plays significant role in root architecture, and the expression of EXPAs could be induced under cold acclimation, water stress, and higher application of fertilizer (Bian, 2006; Kozbial et al., 2010; Li et al., 2013, 2019b; Sun, 2013; Han et al., 2014; Ren et al., 2019).

Panax notoginseng is a popular functional food and traditional medicine, whose benefits are considered to be represented by the root size and ginsenoside content. The main root of *P. notoginseng* cultivated at higher altitude is significantly larger (Zheng et al., 2014). Root diameter is directly proportional to light transmittance within limit (Kuang et al., 2014; Wang et al., 2018a), and the application of phosphorus and potassium can increase root weight and promote root thickening (Wang et al., 2008; Zhang et al., 2008). A suitable soil texture possesses great fertilizer preserving capability and abundant mineral elements, promoting the growth of root system (Cui et al., 2005; Li et al., 2016).

Cultivation also affects the content of ginsenosides and amino acids, as well as the transcriptional level of corresponding biosynthetic genes in *P. notoginseng*. High precipitation inhibits the accumulation of total ginsenosides, while low temperature induced upregulation of *HMGR*, *SS,* and *SE* and increased the ginsenoside content (Liu et al., 2016b; Ma et al., 2021). Increasing the concentration of potassium, nitrogen, magnesium, and calcium brings a remarkable boost to the ginsenoside content, in a certain range (Konsler et al., 1990; Yu et al., 2001). As a key enzyme in dencichine biosynthesis, activity of serine acetyltransferase (*SAT*) can be decreased by drought stress (Ahmad et al., 2016; Yang et al., 2021).

The cultivation of *P. notoginseng* can be tracked back to *Jiaqing* year in *Qing* dynasty, which is around A.D. 1800 (Wu, 1963). The Palace Museum (Beijing, China) has abundant and well-preserved *P. notoginseng* samples from *Qing* dynasty, and those ancient root samples were tributes from Guangxi or Yunnan provinces to the emperor, which represented the best quality of *P. notoginseng* at that time. The cultivation environments of *P. notoginseng* showed a great improvement toward planting temperature and humidity (Hua, 1967; He and Deng, 1981; China Association of Chiniese Medicine., 2019), light transmittance (Chen, 1958; Huang et al., 2007; China Association of Chiniese Medicine., 2019), soil type (He and Deng, 1981; China Association of Chiniese Medicine., 2019), and fertilizer application (Chen, 1958; He and Deng, 1981; China Association of Chiniese Medicine., 2019) during past 100 years, with root size also showing an enlargement since 1950s (Jin et al., 1996; Xu, 2016). Tributes from *Qing* dynasty ought to be an excellent material to investigate how long cultivation influenced root development.

In this study, we compared the root length, diameter, and weight of *P. notoginseng* from the Palace Museum (Beijing, China) and modern market and performed detailed RNA-seq, UPLC-QQQ-MS, and desorption electrospray ionization analyses of two types of root size (SRW samples, 120 *tou* with small root weight, representing substitutes for *Qing* dynasty tribute; and LRW samples, 20 *tou* with large root weight, representing for highest benefits in modern market). We used these datasets to explore how domestication and cultivation lead to deformation of *P. notoginseng* root size and to investigate the gene-level regulatory mechanisms that control a better-architected cell wall obtained in LRW samples, providing guidance on artificial cultivation of *P. notoginseng*.

MATERIALS AND METHODS

Plant Materials

About 100 root samples of *P. notoginseng* in *Qing* dynasty were obtained from The Palace Museum, Beijing. Six types of dry root samples with different sizes (20 *tou*, 40 *tou*, 60 *tou*, 80 *tou*, 120 *tou,* and >120 *tou*, *tou* represents the number of roots per 500 g dry weight) were purchased from Anhui Tienho Herbal Source Company. Fresh root samples were collected in Wenshan, Yunnan Province, and stored at −80°C (Zheng et al., 2017). According to the drying rate (Xu, 2016), 21 fresh roots of *P. notoginseng* were divided into two groups: (1) Seven LRW samples that have fresh weight of 14.27 ± 2.54 g and are equivalent to 20 *tou* samples, and (2) 14 SRW samples that have fresh weight of 5.17 ± 0.62 g and are equivalent to 120 *tou* samples (**Supplementary Table 1**).

Analysis of RNA Sequencing Profiles

Raw data from transcript database of *P. notoginseng* (Zheng et al., 2017) were used for further analysis. Clean data were obtained by removing reads with low quality from raw data. Filtered reads were aligned to the *P. notoginseng* genome (Jiang et al., 2020) using STAR (Valencia, 2014) and counted using RSEM (Dewey and Li, 2011). Differentially expressed genes (DEGs) were obtained by comparing the gene expression in LRW and SRW *P. notoginseng* using DESeq2 (Love et al., 2014). Genes with padj below 0.05 and log2 (fold change) >1 were considered as DEGs.

Microscope Observation

Root material was cut into 3-mm tissue samples and dehydrated with a gradient of 70, 80, 95, and 100% of ethanol. The tissue was treated with xylene twice for cell permeabilization and then was soaked and embedded with paraffin. After that, the tissue was cut into 5-μm slice, which was heated and dewaxed in water. Microsection was observed using an Olympus BX51 microscope. The diameter of vessel and the thickness of cell wall were measured using DP2-BSW software. The diameters of vessels in

one field of view were measured and averaged, and six fields of view of each five biological replicates were obtained for *t*-test. Measurement of cell wall thickness in each tissue was same as that of the vessel diameter, and the thickness of 10 cells in one field of view was measured and averaged.

Cell Wall Component Measurement

Sulfuric acid hydrolysis method was used to determine the lignin content (Xiong et al., 2005; Chen et al., 2010). LRW and SRW samples were freeze-dried and ground into powder. About 100 mg of powder was weighed and extracted with 1% acetic acid solution twice. The precipitate was soaked in a mixture of ethanol and diethyl ether (1:1) for three times and evaporated to residue. About 3 mL of 72% (w/v) sulfuric acid was mixed up with the precipitate and stood for 16 h at room temperature. Then, 10 mL of distilled water was added and placed in boiling water bath for 5 min. After cooling, 5 mL of distilled water and 0.5 mL of 10% (w/v) barium chloride solution were added, and the residue was washed with distilled water subsequently. About 10 mL of 10% (w/v) sulfuric acid solution and 10 mL of 0.1 mol·L^{-1} potassium dichromate solution were added to the residue and heated in boiling water for 15 min. The supernatant after cooling was transferred to flask and then mixed up with 5 mL of 20% (w/v) KI solution and 1 mL of 0.5% (w/v) starch solution for titration. The titrant was 0.2 mol·L^{-1} of sodium thiosulfate.

Determination of cellulose was performed using enzyme-linked immunosorbent assay (ELISA), according to the manufacturer's instructions (Jiangsu Jingmei Biological Technology Co. Ltd., China. Item number, JM-110113P1). Homogenized LRW and SRW samples were extracted in 900-μL PBS buffer (pH 7.4), and then, supernatant was obtained by centrifugation at 2,000 rpm for 20 min. Microtitration plates were coated with purified cellulose antibody. After 5 times dilution, the sample solution was added to coated micropore, which subsequently bound with HRP-labeled cellulose antibody at 37°C for 30 min. Tetramethylbenzidine (TMB) was added as substrate and then incubated in the dark at 37°C for 10 min. The reaction was terminated using 1 mol·L^{-1} of sulfuric acid, and the absorbance value was determined at 450 nm. Calibration curve was obtained using cellulose standard solution of 400, 200, 100, 50, and 25 ng·L^{-1}.

Callose determination was performed according to the published method (Khle et al., 1985) with some modification. Briefly, 100 mg of fresh plant materials was washed with ethanol for three times to eliminate autofluorescence, ground in liquid nitrogen, and extracted with 1 mL of 1 mol·L^{-1} NaOH at 80°C for 15 min. After centrifugation (10,000× g, 15 min), the supernatant was mixed with 0.1% (w/v) aniline blue to produce a violet-red color. Then, 1 mol·L^{-1} of glycine/NaOH buffer (pH 9.5) was added and incubated at 50°C for 20 min, and then at room temperature for 20 min. Fluorescence was recorded using a HITACHI F-7000 spectrofluorometer (Tokyo, Japan) with the following parameters: excitation wavelength of 400 nm, emission wavelength of 510 nm, and slit width of 10 nm. Calibration curve was obtained using β-1,3-glucan in 1 mol·L^{-1} of NaOH.

qRT-PCR Analysis

Total RNA was extracted from root of *P. notoginseng*, using the Plant RNA Purification Reagent (Invitrogen, USA), according to the manufacturer's instructions. qRT-PCR was performed on a LightCycler 480 Real-Time PCR System (Roche Diagnostics, Basel, Switzerland), with primers listed in **Supplementary Table 2**.

Determination of Ginsenosides Using UPLC-QTRAP-MS/MS

The ginsenoside content was measured as described previously (Liu et al., 2020), with some modifications. *P. notoginseng* samples were first ground into powder, and 0.1 g powder was weighed accurately into 5-mL centrifuge tubes and extracted with 2 mL of 70% ethanol solution. The tubes were then sonicated for 30 min at room temperature. The supernatant was collected after being centrifuged for 10 min at 13,000 g. The test solution was obtained by filtrating the supernatant through 0.22-μm Millipore filter.

UPLC was performed on a Waters ACQUITY UPLC I-Class system. Chromatographic separations were performed on a ACQUITY BEH C18 column (2.1 × 100 mm, 1.7 μm) with a flow rate of 0.5 mL·min^{-1} at 40°C. The mobile phase was composed of 0.1% of formic acid–acetonitrile (A) and 0.05% of formic acid–water (B). Gradient elution program was as follows: 0–0.5 min, 20% A; 0.5–3 min, 20–80% A; 3–3.1 min, 80–98% A; 3.1–5 min, 98% A; 5–5.1 min, 98–20% A; 5.1–8 min 20% A. The injection volume was 1 μL for each sample.

Mass analysis was performed on a ABSCIEX 6500 QTRAP mass spectrometer. Mass spectrometer was performed in a positive ion mode using multiple reaction monitoring (MRM) mode. Optimized MS/MS parameters of saponins are shown in **Supplementary Table 3**. Ion spray voltage was set at 5500 eV, and turbo spray temperature was 550°C. Both gas 1 and gas 2 were set at 50 psi.

Quantitation of Dencichine Using UPLC-UV-MS

Determination of dencichine was performed as reported with some modification (Ju et al., 2015). About 0.1 g of root power was added with 5 mL of 70% methanol solution, and the mixture was sonicated for 2 h subsequently. The supernatant was obtained through centrifugation at 12,000 × g for 15 min and then diluted with 70% of methanol for 10 times before quantification. Dencichine was detected on a Waters ACQUITY UPLC I-Class system, equipped with a PDA detector under a UV wavelength of 213 nm. An ACQUITY BEH C18 column (2.1 × 100 mm, 1.7 μm) was used for separation, with a flow rate of 0.3 mL·min^{-1}. Mobile phase A consisted of 0.05% phosphoric acid in water, while mobile phase B was methanol, and an isocratic elution of 53% A was used. Injection of samples was 1 μL.

Yeast One-Hybrid Assay

Y1H assay was performed as described previously (Zheng et al., 2021). The sequences of *proPnEXPA4*, *proPnGGPPS3*, *proPnFPS*, *proPnCYP716A47*, *proPnCYP716A53v2,* and *proPnGAP* were nested PCR-amplified according to genomic sequences

(Jiang et al., 2020). The probable binding domains of promoters were inserted into pAbAi vector as baits and were integrated into Y1HGold, and then, the minimal inhibitory concentration of aureobasidin (AbA) was tested on SD/-Uracil (Ura) plates. A pGADT7-*PnPHL8* recombinant plasmid was synthesized by RuiBiotech Co. Ltd., as prey. The pGADT7-*PnPHL8* construct and a blank pGADT7 were introduced into bait reporter strains, while blank pGADT7 was used as control. Positive transformants were selected on SD/-Leucine (Leu)/-Ura plates with an appropriate concentration of AbA. Primers used for promotor nested PCR amplification and bait construction are listed in **Supplementary Table 2**.

Electrophoretic Mobility Shift Assay

EMSA was performed as described previously (Zheng et al., 2021). The full-length cDNA of *PnPHL8* was first cloned into a pMAL-c2x vector and then transformed into a Rosetta (DE3) competent cell. Prokaryotic expression was performed at 20°C for 12 h, and then, recombinant protein was purified using Amylose Resin High Flow (NEB, Ipswich, MA, USA). EMSA was performed according to the manufacturer's instructions, using chemiluminescent EMSA kit (Beyotime, Item number, GS009). Primers and probes are listed in **Supplementary Table 2**.

RESULTS

Transition of Root Size of *P. notoginseng* From *Qing* Dynasty to Modern Times

To investigate the morphological difference between *Qing* dynasty tributes and modern commodities, root length, diameter, and root weight of ancient samples (**Figure 1A**) from the Palace Museum and six types of root samples (20 *tou*, 40 *tou*, 60 *tou*, 80 *tou*, 120 *tou,* and >120 *tou*) bought from modern market (**Figure 1B**) were measured. The root of *P. notoginseng* in *Qing* dynasty had a similar diameter and dry weight with 120 *tou* samples, while the length of ancient samples was relatively shorter than the 120 *tou* samples (**Figure 1C**).

After 1950s, artificial cultivation techniques, for example, the application of chemical fertilizers, reduced light transmittance and temperature has been applied to the cultivation of *P. notoginseng* (**Supplementary Table 4**), and the biggest root weight increased from 6.25 to 12.5 g in 1950s (Jin et al., 1996) to 25 g at present (Liu et al., 2016a; Xu, 2016). The dry weight of *Qing* root samples is around 5.17 g, which is 0.22-fold of the biggest of modern samples (20 *tou* samples), suggesting that a transition in root size of *P. notoginseng* has occurred following the change in cultivation practices and environment among *Qing* dynasty, 1950's, and modern time.

Higher Expression of GPI-Anchored Protein and Thicker Cell Wall in Root With Larger Weight

To further investigate the probable molecular mechanism behind the transition of root size, transcriptome sequencing was performed on 21 *P. notoginseng* root samples with two types of root size (LRW and SRW). A total of nine DEGs were identified between LRW and SRW samples, and the transcriptional levels of eight genes, namely a MYB-CC transcriptional factor, AUX/IAA, DNA ligase, ceramide glucosyltransferase, L-type lectin-domain containing receptor kinase, berberine bridge enzyme-like (*BBE*), β-1,3-galactosyltransferase (*GALT*), and E3 ubiquitin-protein ligase (*RIE*), were decreased in LRW samples (**Table 1**). Among the nine DEGs, only *BBE* was enriched into phenylpropanoid biosynthesis pathway in KEGG analysis, while no DEGs were enriched in GO analysis.

The expression of an uncharacterized GPI-anchored protein (GAP) was upregulated in LRW, with a 3.14-fold increase, compared with that in SRW. *GAP*s were reported to be associated with cell wall architecture (Macmillan et al., 2010; Niu et al., 2018), so we speculated that higher expression of *PnGAP* in LRW samples may lead to the thicker cell wall. We then measured the structure and component of cell wall in *P. notoginseng* root. Compared with SRW samples, cell wall in phloem and xylem of LRW samples was significantly thicker. An extremely significantly thicker cytoderm of vessel was detected in LRW, which was 1.41-fold of that in SRW. There was no remarkable difference of the cell wall thickness in cork and cortex between LRW and SRW samples (**Figure 2A**). In addition, LRW samples possessed a prominently larger vessel width than SRW samples (**Figure 2B**). As major components of cell walls, the content of lignin, cellulose, and callose was significantly higher in LRW samples (**Figure 2C**).

Expansin (*EXP*) and extension (*EXT*), which possess a membrane-binding mode of GPI-anchored, could be associated with thickening of *P. notoginseng* root through cell wall expansion pathway (Li et al., 2019b; Zhou, 2019). *PnEXPA5* (PN022438) showed a prominently higher transcriptional level in SRW samples, while *PnEXPA4* (PN017088) expressed significantly higher transcriptional level in LRW samples, which was 1.44-fold higher than that in SRW samples (**Figure 3**). Phylogenetic tree using 39 *AtEXP*s and multiple sequence alignments indicated that *PnEXPA4* (PN017088) shows most similarity with *AtEXPA4*, and *PnEXPA5* (PN022438) is homologous with *AtEXPA5*, both possessing a DPBB domain and a pollen allergen domain. In addition, a WCNP domain in front of a HFD motif was found in PN017088, which is particularly owned in alpha-expansin (**Supplementary Figures 1A,B**). Since *AtEXPA4* had positively correlated with the cell wall thickness and root size (Ren et al., 2019), we speculated that *PnEXPA4* (PN017088) is associated with root enlargement of *P. notoginseng* as an essential factor.

Higher Root Weight Was Accompanied by Higher Content of Ginsenoside Rb_1 and Lower Content of Dencichine

To investigate whether the chemical composition is related to root size of *P. notoginseng*, we analyzed the expression of the genes related to ginsenosides biosynthesis, and the accumulation of ginsenosides and dencichine in LRW and SRW samples. In LRW, the expression level of *GGPPS1* (PN000021), *GGPPS3* (PN029682), *GGPPS4* (PN016696), *FPS* (PN009896), *CYP716A47* (PN011429), and *CYP716A53v2* (PN006374) was

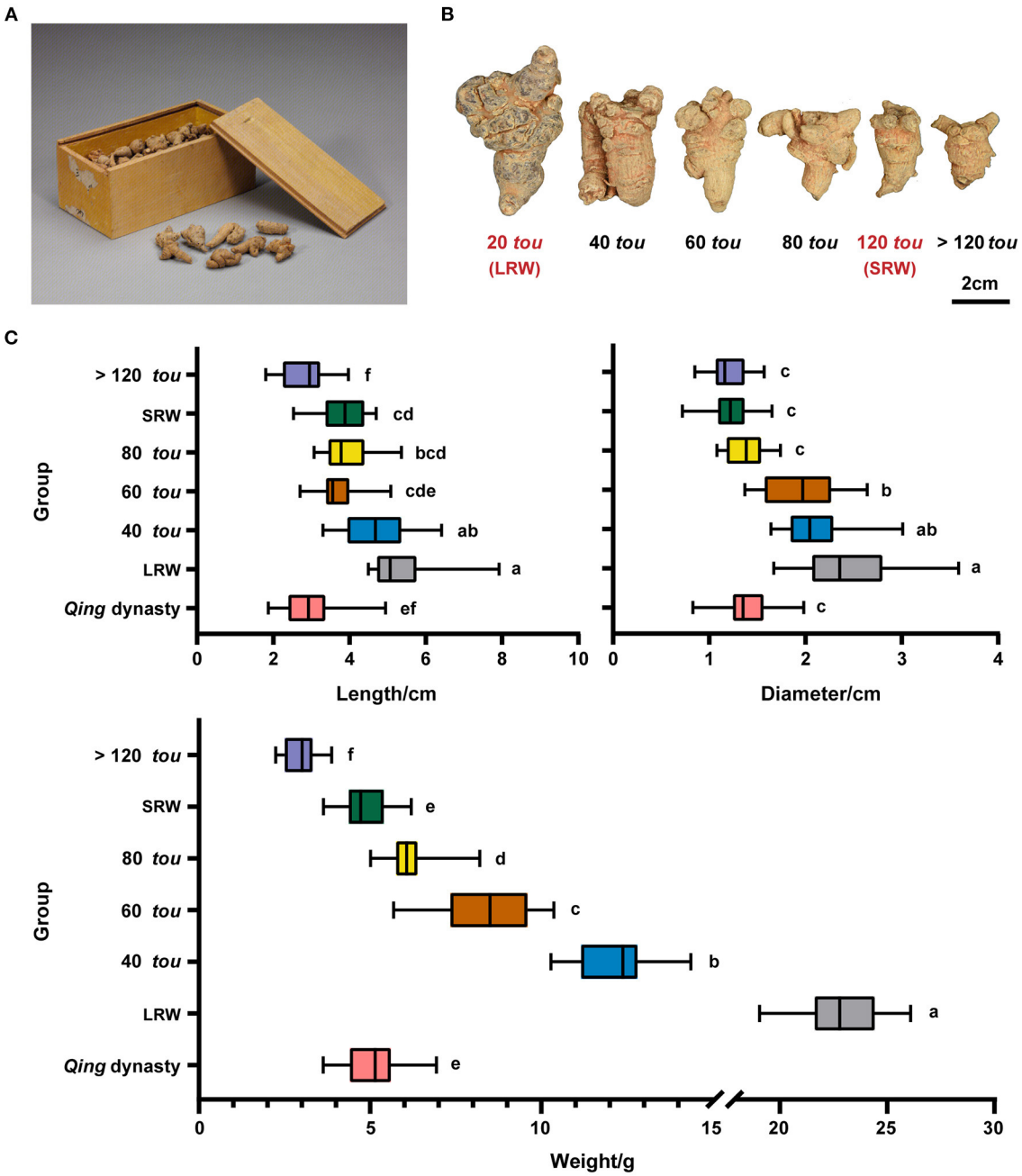

FIGURE 1 | Morphological features of *P. notoginseng* in *Qing* dynasty and modern times. **(A)** *P. notoginseng* in *Qing* dynasty, relic number, Gu00172482-8/9. **(B)** *P. notoginseng* of different root sizes (20 *tou*, 40 *tou*, 60 *tou*, 80 *tou*, 120 *tou,* and >120 *tou*; *tou* is the number of roots per 500 g). **(C)** Length, diameter, and weight of *P. notoginseng* in *Qing* dynasty ($n = 30$) and in modern times ($n = 20$). Data are shown in box plot, and the different letters indicate values that vary significantly at $P < 0.05$ (one-way ANOVA).

3.25-, 4.54-, 3.42-, 1.84-, 1.46-, and 1.68-fold higher than that in SRW, respectively (**Figure 4A**). The content of ginsenoside Rb_1 was significantly lower in SRW samples than that in LRW samples, while the content of dencichine in SRW samples was 1.28-fold higher than that in LRW samples (**Figure 4B**). It was reported that the content of protopanaxadiol and ginsenoside Rb_1 was considerably increased under overexpression of *FPS* and *CYP716A47*, respectively (Han et al., 2012; Yang et al., 2017; Li et al., 2019a), indicating that higher expression level of *FPS* and *CYP716A47* led to remarkably higher content of ginsenoside Rb_1 in LRW. In addition, WGCNA showed a significantly positive correlation between transcriptional level

TABLE 1 | Identification of nine DEGs in *P. notoginseng* of different sizes.

ID	Description	FPKM	
		LRW	SRW
PN010249	DNA ligase	5.08	46.60
PN012351	Berberine bridge enzyme-like 8 (*BBE*)	3.52	41.78
PN018218	L-type lectin-domain containing receptor kinase S4	0.05	1.03
PN023854	Uncharacterized GPI-anchored protein	5.99	1.91
PN024060	Auxin-responsive protein (*IAA7*)	20.94	79.16
PN024675	β-1,3-galactosyltransferase (*GALT1*)	0.11	1.95
PN024679	MYB family transcription factor (*PHL8*)	1.32	5.16
PN025758	Ceramide glucosyltransferase 3	1.82	4.96
PN035878	E3 ubiquitin protein ligase (*RIE1*)	1.21	5.32

of *PnEXPA4* and *PnGGPPS*3, which were positively associated with root weight (**Supplementary Figures 2A,B**), suggesting that LRW samples with the thicker cell wall may be related to a higher content of ginsenosides.

PnPHL8 Had Potential to Bind With *PnGAP*, *PnCYP716A47,* and *PnGGPPS3 in Vitro*

PHR transcription factor, belonging to MYB-CC family, participates in plant transcriptional responses to phosphate starvation (Wang et al., 2018b; Sega and Pacak, 2019). A PHR-like transcriptional factor PN024679 was filtrated through transcriptome analysis, which had a higher transcriptional level in SRW samples. PN024679 contains a 1074bp open reading frame (ORF) encoding 357 amino acids. A constructed phylogenetic tree using 14 AtPHLs indicated that PN024679 (named as PnPHL8) is homologous with AtPHL8 (**Supplementary Figure 3A**). Multiple sequence alignment showed PN024679 possessing a MYB DNA-binding domain and coiled-coil domain (**Supplementary Figure 3B**).

We investigated whether PnPHL8 regulates genes related to root size and ginsenosides biosynthesis *in vitro* by Y1H method. Promoter sequences of *PnGAP*, *PnEXPA4*, *PnGGPPS3*, *PnFPS*, *PnCYP716A47,* and *PnCYP716A53v2* were PCR-amplified, all of which except *proPnFPS* and *proPnCYP716A53v2* contained either a P1BS binding site (GNATATNC) or a P1BS-like element (Sun, 2015). MBS domain was also existed in *proPnGAP*, *proPnFPS*, *proPnCYP716A53v2,* and *proPnGGPPS3* (Ding et al., 2017; Mabuchi et al., 2018). Specific P1BS domain and MBS domain of *proPnGAP*, *proPnEXPA4*, *proPnGGPPS3*, *PnFPS*, *PnCYP716A47,* and *PnCYP716A53v2* were integrated into yeast, individually. After cotransformation with pGADT7-PnPHL8, we found that yeast strains carrying proPnGAP-MBS, proPnCYP716A47-P1BS, and proPnGGPPS3-P1BS could grow on SD minus leucine and uracil with aureobasidin (**Figures 5A,B**).

To avoid false-positive results caused by Y1H assay, we further performed EMSA to verify the interaction of PnPHL8 with the promoters of *PnGAP*, *PnCYP716A47,* and *PnGGPPS3 in vitro*. Fragments of *proPnGAP*, *PnCYP716A47,* and *proPnGGPPS3*, containing MBS or P1BS motif, were synthesized as specific probes for EMSA, while mutated probes were synthesized by replacing MBS/P1BS motif with poly-A/T. We found that MBP-PnPHL8 was able to bind to the promoter fragments of *PnGAP*, *PnCYP716A47,* and *PnGGPPS3*, but failed to bind to the mutated probes. Moreover, the cold competing probes, which contain high concentration of unlabeled promotor fragments, impaired the interaction between PnPHL8 and specific probes (**Figure 5C**). These results indicate that PnPHL8 specifically binds the promoters of *PnGAP*, *PnCYP716A47,* and *PnGGPPS3 in vitro*, suggesting that PnPHL8 may synergistically regulate biosynthesis of diterpenoid and triterpenoid, as well as cell wall architecture.

DISCUSSION

Cell Wall Architecture Involved in Transition of Root Size of *P. notoginseng*

In this study, we revealed that the root of *P. notoginseng* exhibited a faster growth rate and better-developed root system during the past 100 years. Plant possessing larger diameter of vessels usually has a faster growth rate and water carrying capacity of vessel (Ian et al., 2008). Lignin also serves as a major component of vessel, which agreed with the significantly larger vessels and a higher content of lignin in LRW samples. In LRW samples, width of root, thickness of vessels and xylem cell wall, and the content of cellulose and callose were significantly higher than that in SRW samples, which might be due to the higher expression of *PnGAP* and *PnEXPA4* in LRW. It was reported that GAPs related to cell wall architecture were mainly expressed in xylem vessels and adjacent parenchyma cells and then functioned in secondary wall deposition (Loopstra and No, 2000; Dahiya et al., 2006; Dai, 2015). In addition, the expression of *EXPA4* and *GAP*s was positively related to the cell wall thickness, with *GAP*s also showing a positive correlation with the content of cellulose (Sun, 2013; Ben-Tov et al., 2015; Mcnair, 2015; Ren et al., 2019).

P. notoginseng is now usually cultivated at higher altitude, lower light transmittance, lower temperature, and lower precipitation condition, compared with earlier times. Lower temperature increased the gene expression level of *PnGAP* (Daisuke et al., 2016; Zhao et al., 2020), while cold acclimation, water stress, and phosphorus application led to higher expression of *EXPA* and *EXT* (Bian, 2006; Kozbial et al., 2010; Li et al., 2013; Han et al., 2014). The expression of *EXPA*s was upregulated under green shade within limits, but was strongly inhibited under dark treatment (Ping et al., 1994; Sasidharan et al., 2009; Liu et al., 2011). The vessel diameter and vessel wall thickness showed a significant increase under drought (Xu and Chen, 2012; Aref et al., 2013). Following the transition of cultivation measures, lower temperature and drought could increase the vessel diameter and vessel wall thickness, and a faster growth

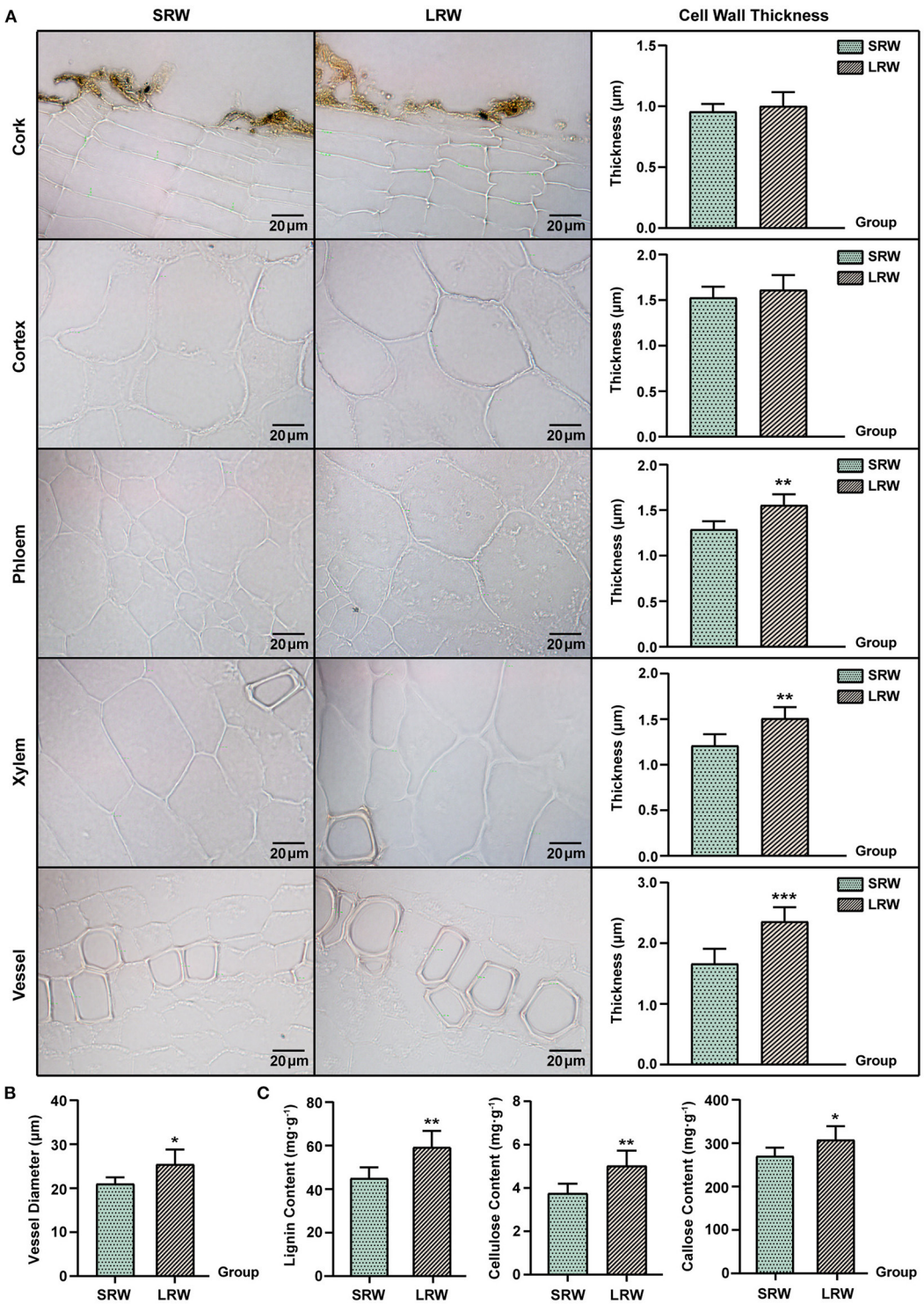

FIGURE 2 | Different tissues and cell morphology in *P. notoginseng*. SRW was an abbreviation of small root weight, while LRW represented large root weight. **(A)** Microscope morphology of different tissues including cork, cortex, phloem, xylem, and vessel, and comparison of the cell wall thickness. **(B)** Comparison of the vessel diameter of *P. notoginseng* with different root weights. **(C)** Determination of lignin and callose in *P. notoginseng* with different root weights. The thickness of 10 cell walls in one field of view were measured and averaged, and then in accordance with this, a total of six fields of view from five biological replicates were obtained for *t*-test. Measurement of the vessel diameters was same as that of the cell wall thickness, while the diameter of seven vessels was measured and averaged. Asterisks denote Student's t-test significance: $^{*}P < 0.05$ and $^{**}P < 0.01$.

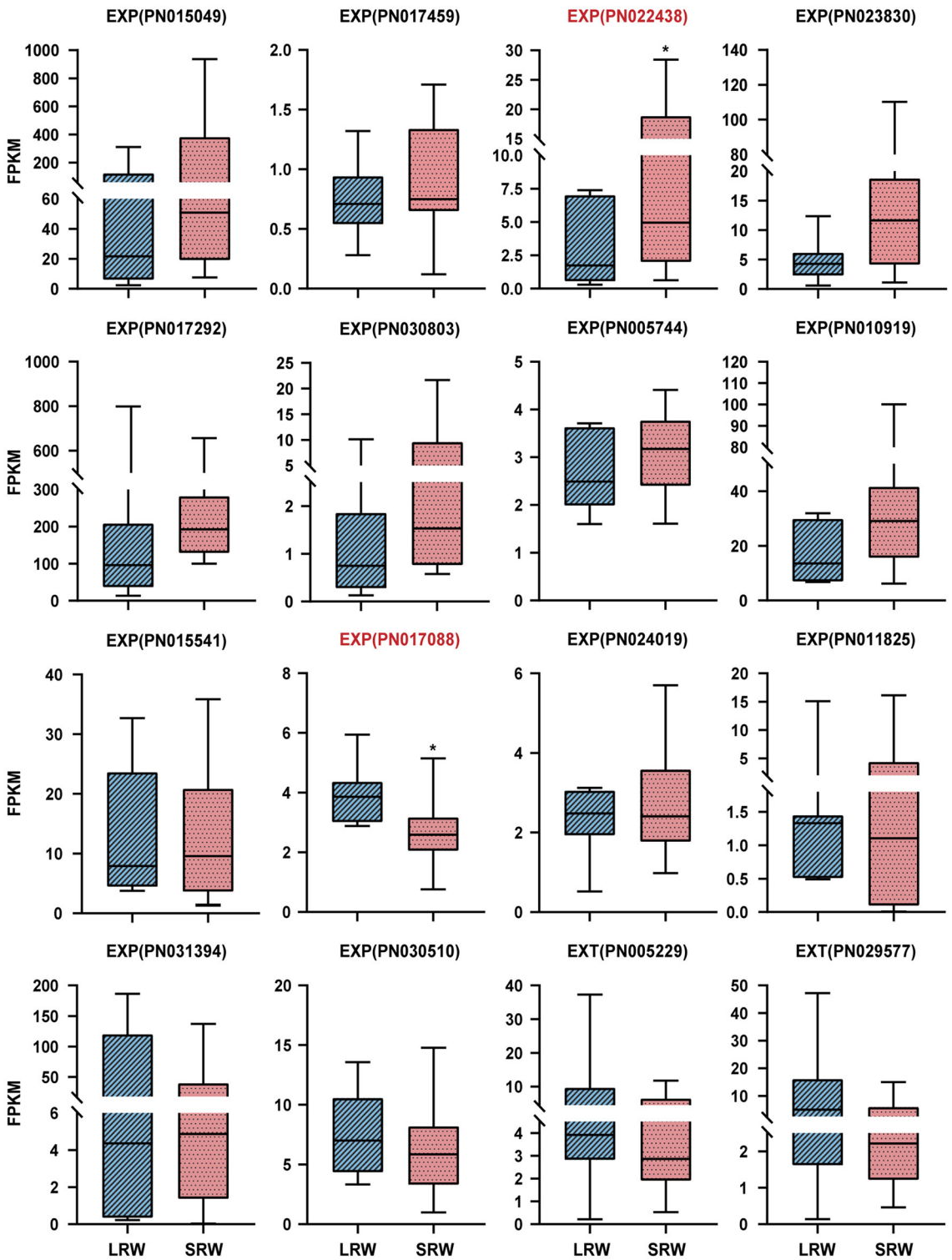

FIGURE 3 | Expression pattern of *EXP*s and *EXT*s in LRW and SRW samples. EXPA, alpha-expansin; EXPB, beta-expansin; EXT, extension. Asterisks denote student's *t*-test significance: $^*P < 0.05$.

rate and then a bigger root size of *P. notoginseng* were formed. Higher expression of *PnGAP* in vessels and xylem parenchyma contributed to a higher content of cellulose and callose, while higher expression of *PnEXPA4* led to better-architected cell wall. In addition, cell wall-mediated resistance is an important part of plant immune response system, to which the cell wall

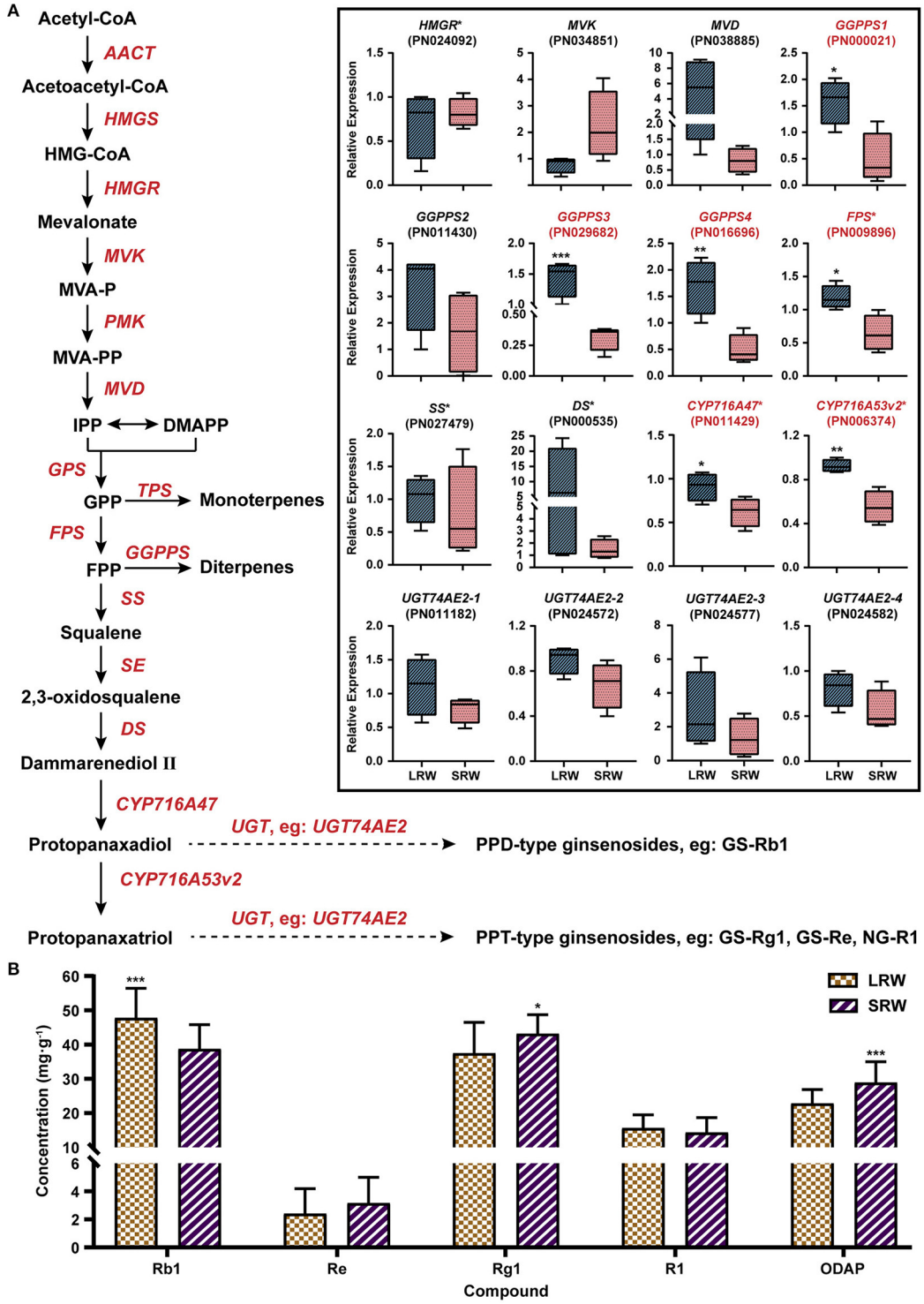

FIGURE 4 | Expression pattern of genes related to biosynthesis of ginsenosides and content of active components. **(A)** Expression pattern of genes related to biosynthesis of ginsenosides in LRW and SRW groups. **(B)** Content of active components in LRW and SRW groups. AACT, acetyl-CoA C-acetyltransferase; HMGS, hydroxymethylglutaryl-CoA synthase; HMG-CoA, 3-hydroxy-3-methylglutaryl CoA; HMGR, hydroxymethylglutaryl-CoA reductase; MVK, mevalonate kinase; MVAP, mevalonate-5-phosphate; PMK, phosphomevalonate kinase; MVAPP, mevalonate-5-pyrophosphate; MVD, diphosphomevalonate decarboxylase; IPP, isopentenyl diphosphate; DMAPP, dimethylallyl diphosphate; GPS, geranyl pyrophosphate synthase; GPP, geranyl pyrophosphate; FPS, farnesyl diphosphate synthase; FPP, farnesyl diphosphate; GGPPS, geranylgeranyl pyrophosphate synthase; SS, squalene synthase; SE, squalene epoxidase; DS, dammarenediol-II synthase; CYP, cytochrome P450 proteins; UGT, UDP-glycosyltransferase; GS, ginsenoside; NG, notoginsenoside. Genes obtained * on upper right were reported to be functional. Genes in red tag had statistical significance. Asterisks denote Student's *t*-test significance: $^{*}P < 0.05$, $^{**}P < 0.01$, and $^{***}P < 0.001$.

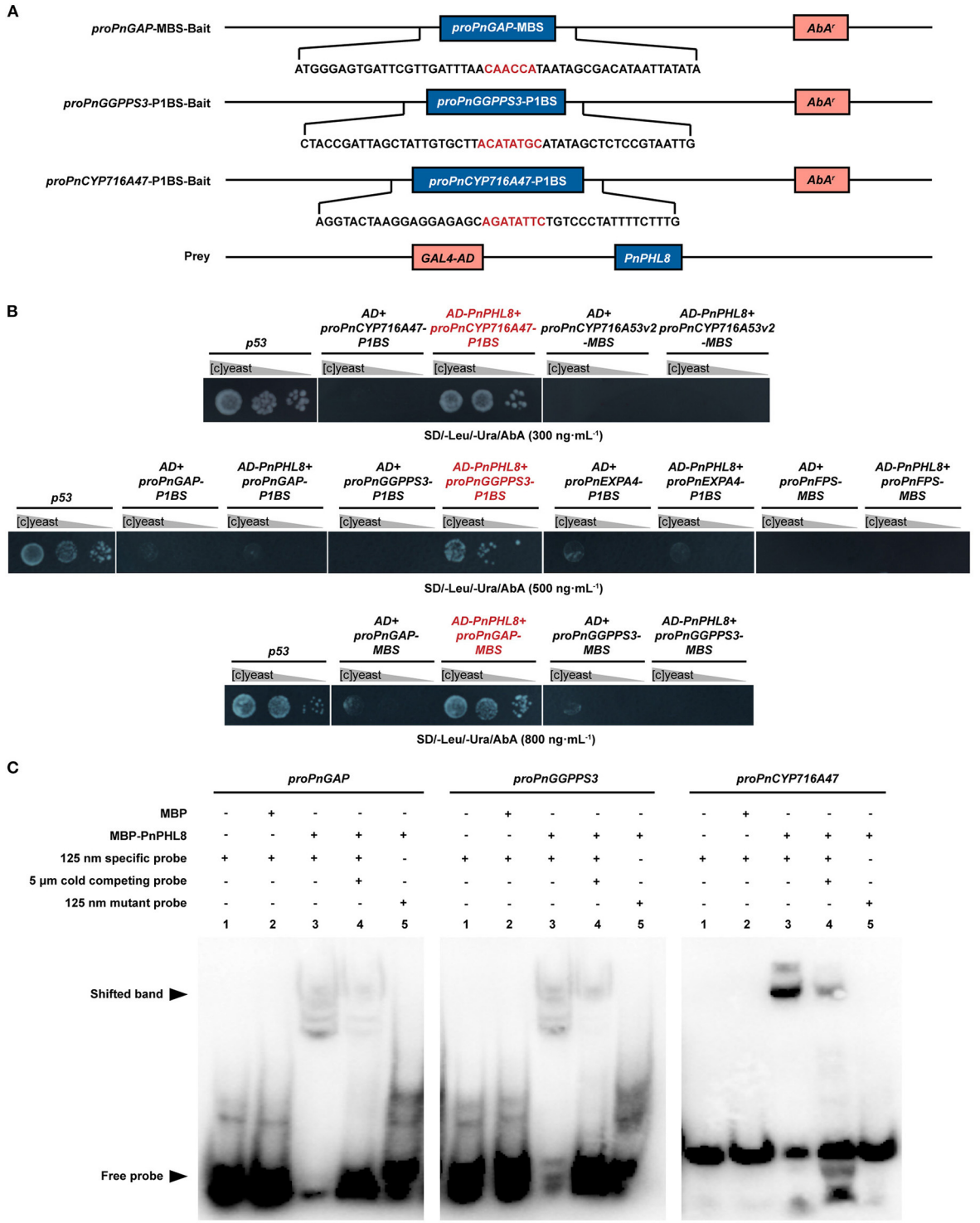

FIGURE 5 | PnPHL8 binds with the promoter sequence of *PnGAP*, *PnCYP716A47,* and *PnGGPPS3*. **(A)** Structural schematics of baits and prey in yeast one-hybrid (Y1H) assay. **(B)** Y1H assay between PnPHL8 and PIBS domains as well as MBS domains of *proPnGAP* (promoter of *PnGAP*), *proPnEXPA4* (promoter of *PnEXPA4*), *proPnGGPPS3* (promoter of *PnGGPPS3*), *proPnCYP716A47* (promoter of *PnCYP716A47*), *proPnCYP716A53v2* (promotor of *PnCYP716A53v2*), and *proPnFPS* (promotor of *PnFPS*). Gray triangles represent dilution factor of the yeast concentration, while *p53* served as a positive control. **(C)** EMSA among PnPHL8, *proPnGAP*, *proPnCYP716A47*, and *proPnGGPPS3*. GAP, glycosylphosphatidylinositol-anchored protein; PHL, phosphate starvation response transcription factor like; AbA, aureobasidin.

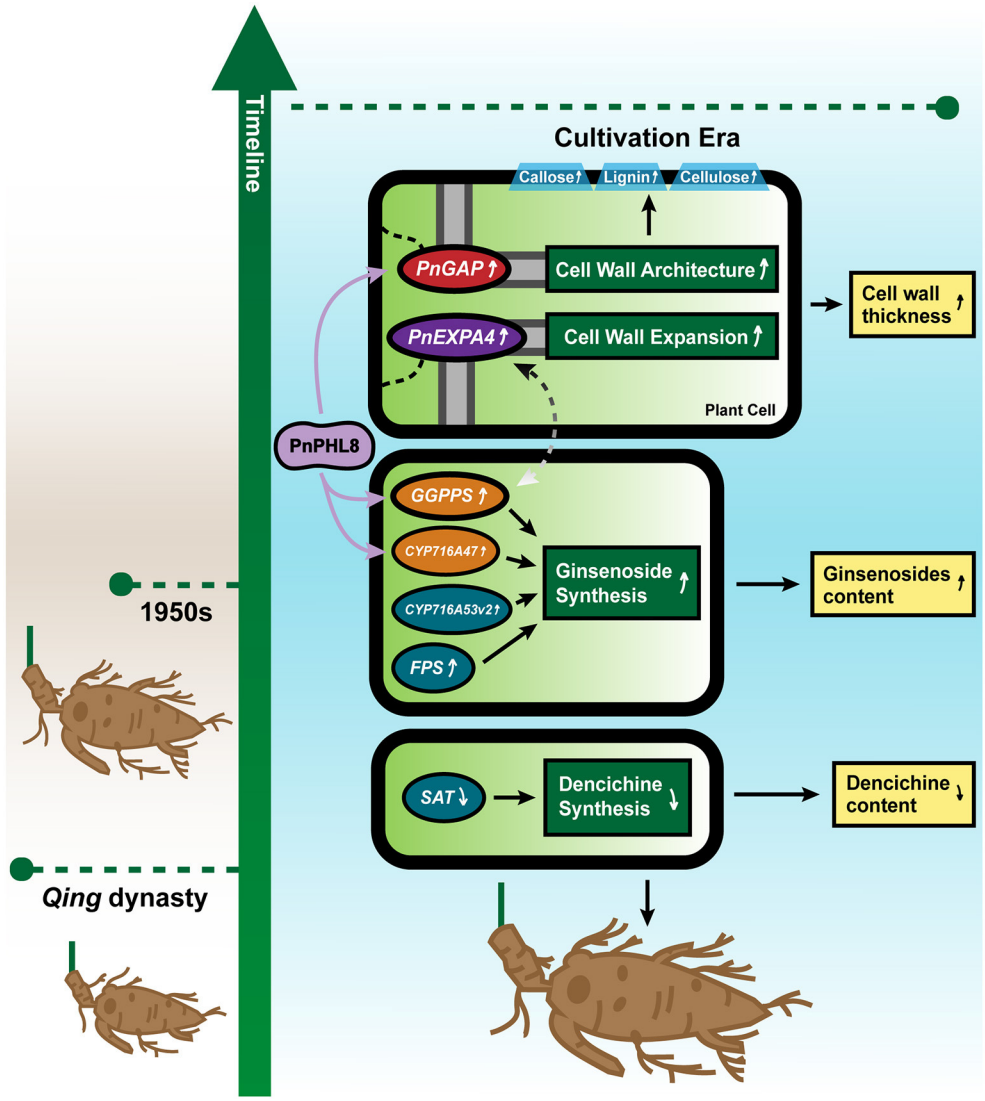

FIGURE 6 | Probable molecular mechanism model for cultivation influencing root architecture and chemical component of *P. notoginseng*. Changes in root size and active component accumulation of *P. notoginseng* are influenced by related genes and affected by changes in the cultivation environment. Increased expression of *PnGAP* and *PnEXPA4* results in the thicker cell wall and a higher content of lignin, cellulose, and callose in *P. notoginseng* of cultivation era. Higher expression of *GGPPS*, *FPS*, *CYP716A47,* and *CYP716A53v2* contributes to a higher content of ginsenosides, while lower expression of *SAT* might result in a lower content of dencichine. A PnPHL8 transcriptional factor participates in transcriptional regulation of *PnGAP*, *PnCYP716A47,* and *PnGGPPS3*, while dotted line between *PnEXPA4* and *PnGGPPS3* indicates that a probable positive correlation may exist.

thickness was positively related (Aquije et al., 2010; Rachid et al., 2016), and a large root size was reportedly associated with resistance (Chloupek, 2010). The PHR transcription factor family participates in plant transcriptional responses to phosphate starvation (Wang et al., 2018b; Sega and Pacak, 2019). Lower application of phosphate in *Qing* dynasty might result in higher transcriptional level of *PnPHL8*, which subsequently influenced the expression of *PnGAP* and affected cell wall architecture and expansion of *P. notoginseng*. Based on this, we speculate that cell wall architecture played an important role in transition of root size from *Qing* dynasty to the present.

The Variation of Chemical Components Content and Root Size of *P. notoginseng* Might Lead to Transition in Clinical Usage

Ginsenoside Rb_1 and dencichine, the major compounds in root of *P. notoginseng*, show diverse pharmacological activities. Ginsenoside Rb_1 has great effects on vascular endothelial function improvement (Ohashi et al., 2006), cerebral ischemia protection (Yuan et al., 2007), myocardial preservation (Zhao et al., 2010), and neuroprotection (Jin et al., 2005; Liang et al., 2010), while dencichine was used for the treatment of injury induced trauma, and its hemostatic function was proven by

clinical practice (Zhang and Yu, 2010). Modern cultivation condition, for example, lower temperature and drought, is beneficial to the accumulation of saponins in *P. notoginseng* (Konsler et al., 1990; Yu et al., 2001; Liu et al., 2016b; Ma et al., 2021). Here, we also found high content of ginsenosides Rb_1 in LRW samples. In addition, the PHL transcription factor negatively regulates secondary metabolism such as carotenoid (Lu et al., 2021), indicating that the higher expression of *PnPHL8* in SRW samples may lead to a lower content of secondary metabolism such as ginsenoside Rb_1. In contrast, the content of dencichine was lower in LRW samples, which may be resulted from the decreased activity of SAT induced by drought (Ahmad et al., 2016; Yang et al., 2021). As recorded in herbal records, *P. notoginseng* in *Qing* dynasty was mostly applied externally or prepared into powder for hemostasis (Chen, 2009). However, prescription containing *P. notoginseng* with a higher content of ginsenoside Rb_1 in recent years was mainly used to treat heart diseases and injuries (Chen et al., 2017). The change in root size, ginsenoside Rb_1 and dencichine content of *P. notoginseng* from *Qing* dynasty to modern cultivation era, may also influence the clinical usage.

Triterpenoid is reported as a regulator of cell wall biosynthesis (Jozwiak et al., 2020), and ginsenoside Rb_1 was localized to degrading primary cell wall of xylem in root of *Panax ginseng* (Yokota et al., 2011). In addition, a significantly positive correlation between the expression of *PnEXPA4* and *PnGGPPS*3 was also observed by WGCNA, suggesting that cell wall architecture pathway and ginsenosides biosynthesis pathway may jointly participate in root enlargement of *P. notoginseng* during past 100 years.

CONCLUSION

From *Qing* dynasty to modern times, cultivation increased the root size and changed the content of ginsenoside and dencichine of *P. notoginseng*. In this study, we revealed that large root size of modern *P. notoginseng* should be due to the high expression of *PnGAP* and *PnEXPA4*, by promoting better-architected cell walls and larger vessels. *GGPPS*, *FPS*, *CYP716A47,* and *CYP716A53v2* involved in ginsenosides biosynthesis pathway are also induced to contribute to a relatively higher content of ginsenosides, while depressed expression of *SAT* in LRW sample affected dencichine biosynthesis, leading to transition toward clinical efficacy from *Qing* dynasty to cultivation era. PnPHL8 participates in transcriptional regulation of *PnGAP*, *PnCYP716A47*, and *PnGGPPS3*, modulating cell wall architecture and ginsenosides biosynthesis pathway (**Figure 6**). Our results toward *P. notoginseng* of 2 eras separated by 100 years provided enlightenment on how long cultivation affected root size, chemical composition, and clinical usage.

DATA AVAILABILITY STATEMENT

The 10 *P. notoginseng* RNA-seq profiles (r9, r14, r20, r28, r29, r35, r36, r45, r48 and r55) are available in National Genomics Data Center under the GSA accession number CRA006118. The remaining 11 *P. notoginseng* RNA-seq profiles (r1, r13, r15, r18, r19, r23, r26, r32, r33, r53 and r59) have been deposited at DDBJ/EMBL/GenBank under the accession GFRX00000000 (Zheng et al., 2017).

AUTHOR CONTRIBUTIONS

X-MC, L-QH, and YY designed the study. M-YY, Z-YH, P-RL, HZ, and YJ performed the experiments. M-YY, Z-YH, and H-SP analyzed data. M-YY, Z-YH, and YY wrote the manuscript. All authors discussed the results and commented on the manuscript.

FUNDING

This research was financially supported by the National Natural Science Foundation of China (NSFC) (81891013/81891010), the Scientific and Technological Innovation project of China Academy of Chinese Medical Science (C12021A041), and the Key project at the central government level for the ability to the establishment of sustainable use for valuable Chinese Medicine Resources (2060302).

SUPPLEMENTARY MATERIAL

The Supplementary Material for this article can be found online at: https://www.frontiersin.org/articles/10.3389/fpls.2022.878796/full#supplementary-material

REFERENCES

Ahmad, N., Malagoli, M., Wirtz, M., and Hell, R. (2016). Drought stress in maize causes differential acclimation responses of glutathione and sulfur metabolism in leaves and roots. *BMC Plant Biol.* 16, 247–261. doi: 10.1186/s12870-016-0940-z

Aquije, G., Zorzal, P. B., Buss, D. S., Ventura, J. A., Fernandes, P., and Fernandes, A. (2010). Cell wall alterations in the leaves of fusariosis-resistant and susceptible pineapple cultivars. *Plant Cell Rep.* 29, 1109–1117. doi: 10.1007/s00299-010-0894-9

Aref, I. M., Ahmed, A. I., Khan, P. R., and El-Atta, H. (2013). Drought-induced adaptive changes in the seedling anatomy of Acacia ehrenbergiana and Acacia tortilis subsp. raddiana. *Trees* 27, 959–971. doi: 10.1007/s00468-013-0848-2

Ba Rraclough, P. B., Kuhlmann, H., and Weir, A. H. (2010). The effects of prolonged drought and nitrogen fertilizer on root and shoot growth and water uptake by winter wheat. *J. Agronomy Crop Sci.* 163, 352–360. doi: 10.1111/j.1439-037X.1989.tb00778.x

Ben-Tov, D., Abraham, Y., Stav, S., Thompson, K., Loraine, A., Elbaum, R., et al. (2015). COBRA-LIKE2, a member of the glycosylphosphatidylinositol-anchored COBRA-LIKE family, plays a role in cellulose deposition in arabidopsis seed coat mucilage secretory cells. *Plant Physiol.* 167, 711–724. doi: 10.1104/pp.114.240671

Bian, H. Y. (2006). *Effect of the Key Enzymes and Exogenous Materials on Fiber Strength Formation in Low Temperature Condition*. Nanjing: Nanjing Agricultural University.

Bundy, M. G., Kosentka, P. Z., Willet, A. H., Zhang, L., Miller, E., and Shpak, E. D. (2016). A mutation in the catalytic subunit of the glycosylphosphatidylinositol

transamidase disrupts growth, fertility, and stomata formation. *Plant Physiol.* 171, 974–985. doi: 10.1104/pp.16.00339

Chathurika, W., Raja, R. K., Shankle, M. W., Stephen, M., and Gao, W. (2018). Low and high-temperature effects on sweetpotato storage root initiation and early transplant establishment. *entia Horticulturae* 240, 38–48. doi: 10.1016/j.scienta.2018.05.052

Chen, G., Liu, C., He, H. Q., Gao, J. L., Li, J., Xing, Y. W., et al. (2017). Prescription rules of Chinese patent medicines containing Notoginseng Radix et Rhizoma. *Chin. J. Experi. Traditional Med. Formulae* 23, 191−197. doi: 10.13422/j.cnki.syfjx.2017070191

Chen, K. J. (2009). *Integration of Medical Records in Qing Dynasty*. Beijing: Science Press.

Chen, M. Y. (2017). *Effect of Different Irrigation Methods on Yield and Quality of Rice Under Different Soil Types*. Yangzhou University.

Chen, N. L., Hu, M., Qiao, C. P., Nai, X. Y., and Wang, R. (2010). Effects of BTH, SA and SiO_2 treatment on disease resistance and leaf HRGP and lignin contents of melon seedlings. *Sci. Agri. Sinica* 43, 535–541. doi: 10.4028/www.scientific.net/AMM.37-38.1549

Chen, Z. Z. (1958). Review of Panax notoginseng. *Bull. Chin. Materia Med.* 4, 224–230.

Cheng, H., Chen, X., Zhu, J., and Huang, H. (2016). Overexpression of a hevea brasiliensis *ErbB-3* binding protein 1 gene increases drought tolerance and organ size in *Arabidopsis*. *Front. Plant Sci.* 7, 1703–1713. doi: 10.3389/fpls.2016.01703

Cheon, S. K., Lee, T. S., Yoon, J. H., Lee, S. S., and Mok, S. K. (2004). Effect of light transmittance control on the root yield and quality during the growing season of panax ginseng. *J. Ginseng Res.* 4, 196–200. doi: 10.5142/JGR.2004.28.4.196

China Association of Chiniese Medicine. (2019). *"Daodi herbs (in Chinese)", in: Part 118: Sanqi*. Beijing: China Standard Press.

Chloupek, O. (2010). The size of the root system of lucerne varieties grown for forage and seed, and its relation to yield. *Plant Breeding* 101, 169–172. doi: 10.1111/j.1439-0523.1988.tb00284.x

Cui, X. M., Xu, L. S., Wang, Q., and Chen, Z. J. (2005). Analysis on the geologic background and physicochemical properties of soil for the cultivation of *Panax notoginseng* in Yunnan province. *China J. Chin. Materia Med.* 30:332. doi: 10.3321/j.issn:1001-5302.2005.05.003

Dahiya, P., Findlay, K., Roberts, K., and Mccann, M. C. (2006). A fasciclin-domain containing gene, ZeFLA11, is expressed exclusively in xylem elements that have reticulate wall thickenings in the stem vascular system of Zinnia elegans cv Envy. *Planta* 223, 1281–1291. doi: 10.1007/s00425-005-0177-9

Dai, Y. J. (2015). *Effects of Elevated Temperature During Flowering and Boll Formation Stage on Physiological Mechanisms of Cotton Leaves and Fiber*. Nanjing Agricultural University.

Daisuke, T., Yukio, K., and Matsuo, U. (2016). Cold acclimation is accompanied by complex responses of glycosylphosphatidylinositol (GPI)-anchored proteins in *Arabidopsis*. *J. Experi. Botany* 17, 5203–5215. doi: 10.1093/jxb/erw279

Dewey, C. N., and Li, B. (2011). RSEM: accurate transcript quantification from RNA-Seq data with or without a reference genome. *BMC Bioinformatics* 12, 323–323. doi: 10.1186/1471-2105-12-323

Ding, K., Pei, T., Bai, Z., Jia, Y., Ma, P., and Liang, Z. (2017). SmMYB36, a novel R2R3-MYB transcription factor, enhances tanshinone accumulation and decreases phenolic acid content in salvia miltiorrhiza hairy roots. *Sci. Rep.* 7:5104. doi: 10.1038/s41598-017-04909-w

Ding, W., Wang, Y., Fang, W., Gao, S., Li, X., and Xiao, K. (2016). *TaZAT8*, a C2H2-ZFP type transcription factor gene in wheat, plays critical roles in mediating tolerance to Pi deprivation through regulating P acquisition, ROS homeostasis and root system establishment. *Physiol. Plant.* 158, 297–311. doi: 10.1111/ppl.12467

Engelsberger, W. R., and Schulze, W. X. (2012). Nitrate and ammonium lead to distinct global dynamic phosphorylation patterns when resupplied to nitrogen-starved Arabidopsis seedlings. *Plant J.* 69, 978–995. doi: 10.1111/j.1365-313X.2011.04848.x

Ghaffari, H., Tadayon, M. R., Bahador, M., and Razmjoo, J. (2021). Investigation of the proline role in controlling traits related to sugar and root yield of sugar beet under water deficit conditions. *Agri. Water Manage.* 243:e106448. doi: 10.1016/j.agwat.2020.106448

Goodsman, D. W., Lieffers, V. J., Landh?Usser, S. M., and Erbilgin, N. (2010). Fertilization of lodgepole pine trees increased diameter growth but reduced root carbohydrate concentrations. *For. Ecol. Manage.* 260, 1914–1920. doi: 10.1016/j.foreco.2010.08.041

Han, J. Y., Hwang, H. S., Choi, S. W., Kim, H. J., and Choi, Y. E. (2012). Cytochrome P450 *CYP716A53v2* Catalyzes the Formation of Protopanaxatriol from Protopanaxadiol During Ginsenoside Biosynthesis in *Panax Ginseng*. *Plant Cell Physiol.* 53, 1535–1545. doi: 10.1093/pcp/pcs106

Han, Y. Y., Zhou, S., Chen, Y. H., Kong, X. Z., Xu, Y., and Wang, W. (2014). The involvement of expansins in responses to phosphorus availability in wheat, and its potentials in improving phosphorus efficiency of plants. *Plant Physiol. Biochem.* 78, 53–62. doi: 10.1016/j.plaphy.2014.02.016

He, Z. X., and Deng, X. Q. (1981). Investigation on cultivation of *Panax notoginseng* in Guangxi and Yunnan (in Chinese). *Chin Tradit Herbal Drugs* 12, 28–31.

Hiroyoshi, I., Satoshi, N., Seiji, M., Yasushi, T., and Yasuo, U. (2004). Interaction between genetic effects and soil type in diallel analysis of root shape and size of japanese radish (*Raphanus sativus* L.). *Breed. Sci.* 54, 313–318. doi: 10.1270/jsbbs.54.313

Hua, B. S. (1967). *County Annals of Baise*. Taibei: Chengwen Publishing House.

Huang, R. S., Yang, H. J., He, Z. J., Chen, C. J., Li, Z. W., and Zhang, C. L. (2007). Textual research on the origin in areas of *Panax notoginseng*. *Lishizhen Med. Materia Med. Res.* 18, 1610–1611. doi: 10.3969/j.issn.1008-0805.2007.07.035

Ian, C., Dodd, B. J., Ferguson, C., and Beveridge A. (2008). Apical wilting and petiole xylem vessel diameter of the rms2 branching mutant of pea are shoot controlled and independent of a long-distance signal regulating branching. *Plant Cell Physiol.* 49, 791–800. doi: 10.1093/pcp/pcn052

Jeong, J. S., Kim, Y. S., Redillas, M., Jang, G., Jung, H., Bang, S. W., et al. (2013). *OsNAC5* overexpression enlarges root diameter in rice plants leading to enhanced drought tolerance and increased grain yield in the field. *Plant Biotechnol. J.* 11, 101–114. doi: 10.1111/pbi.12011

Jiang, Z. Q., Tu, L. C., Yang, W. F., Zhang, Y. F., Hu, T. Y., Ma, B. W., et al. (2020). The chromosome-level reference genome assembly for *Panax notoginseng* and insights into ginsenoside biosynthesis. *Plant Commun.* 2:100113. doi: 10.1016/j.xplc.2020.100113

Jin, K. P., Namgung, U., Chang, J. L., Park, J. O., Jin, S. H., Kwon, O. B., et al. (2005). Calcium-independent CaMKII activity is involved in ginsenoside Rb1-mediated neuronal recovery after hypoxic damage. *Life Sci.* 76, 1013–1025. doi: 10.1016/j.lfs.2004.10.011

Jin, X. D., Qiao, R. Q., and Li, S. D. (1996). *County Annal of Guangxi*. Nanning: Guangxi People's Publishing House.

Jozwiak, A., Sonawane, P. D., Panda, S., Garagounis, C., and Aharoni, A. (2020). Plant terpenoid metabolism co-opts a component of the cell wall biosynthesis machinery. *Nat. Chem. Biol.* 740–748. doi: 10.1038/s41589-020-0541-x

Ju, Z. C., He, C. Y., Liu, Q., Yang, L., and Wang, Z. T. (2015). Determination of dencichine in Sanqi tablet by HILIC. *China J. Chin. Materia Madica* 40:4. doi: 10.4268/cjcmm20151320

Khle, H., Jeblick, W., Poten, F., Blaschek, W., and Kauss, H. (1985). Chitosan-elicited callose synthesis in soybean cells as a Ca-dependent process. *Plant Physiol.* 77, 544–551. doi: 10.1104/pp.77.3.544

Konsler, T. R., Zito, S. W., Shelton, J. E., and Staba, E. J. (1990). Lime and phosphorus effects on American ginseng: II. Root and leaf ginsenoside content and their relationship. *J. Am. Soc. Horticultural Sci.* 115, 575–580. doi: 10.21273/JASHS.115.4.575

Kozbial, P. Z., Jerzmanowski, A., Shirsat, A. H., and Kacperska, A. (2010). Transient freezing regulates expression of extensin-type genes in winter oilseed rape. *Physiol. Plant.* 103, 264–270. doi: 10.1034/j.1399-3054.1998.1030214.x

Kuang, S., Xu, X., Meng, Z., Zhang, G., and Chen, J. (2015). Effects of light transmittance on plant growth and root ginsenoside content of *Panax notoginseng*. *Chin. J. Appl. Environ. Biol.* 21, 279–286. doi: 10.3724/SP.J.1145.2014.08002

Kuang, S. B., Zhang, G. H., J., C. Z., Wei, F. G., Yang, S. C., et al. (2014). Changes in morphological and growth indexes of *Panax notoginseng* seedling under different light conditions. *J. Plant Resources Environ.* 2014, 54–59. doi: 10.3969/j.issn.1674-7895.2014.02.08

Li, F., Han, Y. Y., Feng, Y. N., Xing, S. C., Zhao, M. R., Chen, Y. H., et al. (2013). Expression of wheat expansin driven by the RD29 promoter in tobacco confers water-stress tolerance without impacting growth and development. *J. Biotechnol.* 163, 281–291. doi: 10.1016/j.jbiotec.2012.11.008

Li, J., Ma, L., Zhang, S. T., Zuo, C. L., Song, N., Zhu, S. S., et al. (2019a). Transcriptome analysis of 1- and 3-year-old *Panax notoginseng* roots and functional characterization of saponin biosynthetic genes *DS* and *CYP716A47*-like. *Planta* 249, 1229–1237. doi: 10.1007/s00425-018-03083-1

Li, X. J., Yang, J. L., Hao, B., Lu, Y. C., and Yang, S. C. (2019b). Comparative transcriptome and metabolome analyses provide new insights into the molecular mechanisms underlying taproot thickening in *Panax notoginseng*. *BMC Plant Biol.* 19, 451–468. doi: 10.1186/s12870-019-2067-5

Li, Y. X., Chen, X. F., Li, Y., Liang, Q., Shi, F., Dou, M. M., et al. (2016). Correlation of agronomic character of *Panax notoginseng* in Guangxi with soil physical and chemical properties. *J. Chin. Med. Mater.* 39, 1982–1988. doi: 10.13863/j.issn1001-4454.2016.09.013

Liang, W., Ge, S., Yang, L., Yang, M., Ye, Z., Yan, M., et al. (2010). Ginsenosides Rb_1 and Rg_1 promote proliferation and expression of neurotrophic factors in primary Schwann cell cultures. *Brain Res.* 1357, 19–25. doi: 10.1016/j.brainres.2010.07.091

Liu, B. (2009). *Biological Function Research of a GPI Anchored Protein Gene, OsGAP1 in Oryza sativa*. Sun Yat-sen University.

Liu, D. H., Xu, N., Guo, L. P., Jin, Y., Cui, X. M., Yang, Y., et al. (2016a). Qualitative characteristics and classification study on commodity specification and grade standard of *Panax notoginseng*. *China J. Chin. Mat. Med.* 41, 776–785. doi: 10.4268/cjcmm20160504

Liu, J., Chen, T., Zhang, J., Li, C., Xu, Y., Zheng, H., et al. (2020). Ginsenosides regulate adventitious root formation in *Panax ginseng* via a PgCLE45-PgWOX11 regulatory module. *J. Exp. Bot.* 71, 6396–6407. doi: 10.1093/jxb/eraa375

Liu, J., Quan, X. L., Jiang, M. L., Li, X. G., Quan, L. H., and Wu, S. Q. (2016b). Effect of cold stress on expression characteristic of gene families of ginsenoside biosynthesis pathway. *Chin. Traditional Herbal Drugs* 47, 1956–1961. doi: 10.7501/j.issn.0253-2670.2016.11.024

Liu, W. G., Tao, J., Zhou, X. R., and Yang, W. Y. (2011). Characteristics of expansins in soybean (Glycine max) internodes and responses to shade stress. *Asian J. Crop Sci.* 3:34. doi: 10.3923/ajcs.2011.26.34

Loopstra, C. A., and No, P. (2000). Purification and cloning of an arabinogalactan-protein from xylem of loblolly pine. *Planta* 210, 686–689. doi: 10.1007/s004250050061

Love, M. I., Huber, W., and Anders, S. (2014). Moderated estimation of fold change and dispersion for RNA-seq data with DESeq2. *Genome Biol.* 15:550. doi: 10.1186/s13059-014-0550-8

Lu, S., Ye, J., Zhu, K., Zhang, Y., and Deng, X. (2021). A citrus phosphate starvation response factor CsPHL3 negatively regulates carotenoid metabolism. *Plant Cell Physiol.* 62, 482–493. doi: 10.1093/pcp/pcab007

Ma, W.Q., Wang, H.Y., Zhang, W.J., Wang, S., and Guo, L.P. (2021). Effects of ecological factors on shape and ginsenoside of Panax ginseng. *China J. Chin. Materia Med.* 46, 1920–1926. doi: 10.19540/j.cnki.cjcmm.20210123.102

Mabuchi, K., Maki, H., Itaya, T., Suzuki, T., Nomoto, M., Sakaoka, S., et al. (2018). MYB30 links ROS signaling, root cell elongation, and plant immune responses. *Proc. Natl. Acad. Sci. U.S.A.* 115:E4710. doi: 10.1073/pnas.1804233115

Macmillan, C. P., Mansfield, S. D., Stachurski, Z. H., Evans, R., and Southerton, S. G. (2010). Fasciclin-like arabinogalactan proteins: specialization for stem biomechanics and cell wall architecture in *Arabidopsis* and *Eucalyptus*. *Plant J.* 62, 689–703. doi: 10.1111/j.1365-313X.2010.04181.x

Mcnair, G. (2015). *COBRA-like4: a GPI-Anchored Protein Functioning as a Mediator of Cellulose Ultrastructure in Herbaceous and Woody Plants*.

Niu, E., Fang, S., Shang, X., and Guo, W. (2018). Ectopic expression of *GhCOBL9A*, a cotton glycosyl-phosphatidyl inositol-anchored protein encoding gene, promotes cell elongation, thickening and increased plant biomass in transgenic *Arabidopsis*. *Mol. Genet. Genomics* 293, 1191–1204. doi: 10.1007/s00438-018-1452-3

Ohashi, R., Yan, S., Hong, M., Hong, C., Yao, Q., Lin, P. H., et al. (2006). Effects of homocysteine and ginsenoside Rb_1 on endothelial proliferation and superoxide anion production. *J. Surg. Res.* 133, 89–94. doi: 10.1016/j.jss.2005.09.016

Ping, W., Flores, H. E., and Humphrey, A. E. (1994). Production of expansin from light/dark growing Trichosanthes kirilowii var. Japonicum root cultures. *Biotechnol. Lett.* 16, 955–958. doi: 10.1007/BF00128632

Rachid, L., Saroj, K., Wang, L., Li, F., Nicole, S., Malgorzata, K., et al. (2016). Cell wall biomolecular composition plays a potential role in the host type II resistance to fusarium head blight in wheat. *Front. Microbiol.* 7, 910–921. doi: 10.3389/fmicb.2016.00910

Ren, H., Wen, L. Z., Guo, Y. H., Yu, Y. Y., Sun, C. H., Fan, H. M., et al. (2019). Expressional and functional verification of the involvement of CmEXPA4 in chrysanthemum root development. *J. Plant Growth Regul.* 38, 1375–1386. doi: 10.1007/s00344-019-09940-x

Sasidharan, R., Chinnappa, C. C., Voesenek, L., and Pierik, R. (2009). A molecular basis for the physiological variation in shade avoidance responses: A tale of two ecotypes. *Plant Signal. Behav.* 4, 528–529. doi: 10.4161/psb.4.6.8586

Sega, P., and Pacak, A. (2019). Plant PHR transcription factors: put on a map. *Genes.* 10, 1–14. doi: 10.3390/genes10121018

Sun, L. (2013). *The Soybean Expansion GmEXPA4 Gene Transformed Arabidopsis Thaliana and Functional Verification*.

Sun, L. (2015). *Arabidopsis Transcription Factors PHL2 and PHR1 Regulate the Transcriptional Responses to Phosphate Starvation*. Tsinghua University.

Tamirisa, S., Reddy, V. D., and Rao, K. V. (2014). Ectopic expression of pigeonpea cold and drought regulatory protein (CcCDR) in yeast and tobacco affords multiple abiotic stress tolerance. *Plant Cell Tissue Organ Culture* 119, 489–499. doi: 10.1007/s11240-014-0549-6

Teskey, R. O., and Hinckley, T. M. (2010). Influence of temperature and water potential on root growth of white oak. *Physiol. Plant.* 52, 363–369. doi: 10.1111/j.1399-3054.1981.tb06055.x

Valencia, A. (2014). *STAR: ultrafast universal RNA-seq aligner*. Bioinformatics.

Wang, J., Kuang, S. B., Zhou, P., Fan, W., Long, G. Q., Zhang, G. H., et al. (2018a). Agronomic and quality traits of two-year old *Panax notoginseng* response to environmental light intensity. *J. Trop Subtropical Botany*. 26, 57–64.

Wang, Z., Zheng, Z., Song, L., and Liu, D. (2018b). Functional characterization of arabidopsis PHL4 in plant response to phosphate starvation. *Other* 9:e01432. doi: 10.3389/fpls.2018.01432

Wang, Z. L., Wei, M. L., Sun, Y. Q., Hunag, T. W., Wang, B. Y., and Chen, Z. J. (2008). Study on the effect of applying phosphate fertilizer to *Panax notoginseng*. *Ginseng Res.* 2, 29–30. doi: 10.3969/j.issn.1671-1521.2008.02.007

Wu, Q. J. (1963). *Chi wu ming shi t'u k'ao.* Beijing: Zhonghua Book Company.

Xiong, S. M., Zuo, X. F., and Zhu, Y. Y. (2005). Determination of cellulose, hemi-cellulose and lignin in rice hull. *Cereal Feed Industry* 8:2. doi: 10.3969/j.issn.1003-6202.2005.08.018

Xu, N. (2016). *Research of the Factors Influencing Commodity Quality of Notoginseng Radix et Rhizoma*. Kunming University of Science and Technology.

Xu, Q., and Chen, Y. N. (2012). Response of anatomy hydraulic characteristics of xylem stem of *Populus euphratica* Oliv. to drought stress. *Chin. J. Eco-Agricult.* 8, 1059–1065. doi: 10.3724/SP.J.1011.2012.01059

Yang, Y., Ge, F., Sun, Y., Liu, D. Q., and Chen, C. Y. (2017). Strengthening triterpene saponins biosynthesis by over-expression of farnesyl pyrophosphate synthase gene and RNA interference of cycloartenol synthase gene in *Panax notoginseng* cells. *Molecules* 22, 581–592. doi: 10.3390/molecules22040581

Yang, Z. Y., Liu, G. Z., Zhang, G. H., Yan, J., Dong, Y., Lu, Y. C., et al. (2021). The chromosome: cale high quality genome assembly of *Panax notoginseng* provides insight into dencichine biosynthesis. *Plant Biotechnol. J.* 19, 869–871. doi: 10.1111/pbi.13558

Yao, Z. F., Liang, C. Y., Zhang, Q., Chen, Z. J., Xiao, B. X., Tian, J., et al. (2014). *SPX1* is an important component in the phosphorus signalling network of common bean regulating root growth and phosphorus homeostasis. *J. Experi. Botany* 12, 3299–3310. doi: 10.1093/jxb/eru183

Yokota, S., Onohara, Y., Uto, T., Tanaka, H., and Shoyama, Y. (2011). Localization of ginsenoside-Rb1 in Panax ginseng revealed by immunofluorescence and immunoelectron microscopic techniques. *J. Med. Plant Res.* 5, 3176–3187. doi: 10.1002/cbic.201100002

Yu, K. W., Gao, W. Y., Hahn, E. J., and Paek, K. Y. (2001). Effects of macro elements and nitrogen source on adventitious root growth and ginsenoside production in ginseng (*Panax ginseng C. A. Meyer). J. Plant Biol.* 44, 179–184. doi: 10.1007/BF03030349

Yuan, Q. L., Yang, C. X., Xu, P., Gao, X. Q., Deng, L., Chen, P., et al. (2007). Neuroprotective effects of ginsenoside Rb_1 on transient cerebral ischemia in rats. *Brain Res.* 1167, 1–12. doi: 10.1016/j.brainres.2007.06.024

Zhang, L. B., Sun, Y. Q., Wei, M. L., Wang, Z. L., and Chen, Z. J. (2008). Effect of potassium suppliment level on the growth and yield

of *Panax notoginseng*. *Special Wild Econ. Animal Plant Res.* 4, 46–48. doi: 10.3969/j.issn.1001-4721.2008.04.014

Zhang, Y.P., and Yu, Q. (2010). Experimental study on hemostatic activity and neurotoxic effect of Panax notoginseng. *Shandong J. Tradit. Chin. Med.* 43–45.

Zhao, B., Tang, Y., Zhang, B., Wu, P., Li, M., Xu, X., et al. (2020). The temperature-dependent retention of introns in *GPI8* transcripts contributes to a drooping and fragile shoot phenotype in rice. *Int. J. Mol. Sci.* 21, 299–315. doi: 10.3390/ijms21010299

Zhao, H., Lv, D., Zhang, W., Dong, W., Feng, J., Xiang, Z., et al. (2010). Ginsenoside-Rb_1 attenuates dilated cardiomyopathy in $cTnT^{R141W}$ transgenic mouse. *J. Pharmacol. Sci.* 112, 214–222. doi: 10.1254/jphs.09314FP

Zheng, D. M., Wang, L., Ou, X. H., Guo, L. P., Hao, Q. X., Liu, D. H., et al. (2014). Comparison of agronomic traits of *Panax notoginseng* between traditional cultivated fields and new cultivated fields. *China J. Chin. Materia Med.* 39, 558–565. doi: 10.4268/cjcmm20140402

Zheng, H., Jing, L., Jiang, X., Pu, C., Zhao, S., Yang, J., et al. (2021). The ERF-VII transcription factor SmERF73 coordinately regulates tanshinone biosynthesis in response to stress elicitors in Salvia miltiorrhiza. *New Phytol.* 231, 1940–1955. doi: 10.1111/nph.17463

Zheng, Y., Chen, K., Xu, Z., Liao, P., Zhang, X., Liu, L., et al. (2017). Small RNA profiles from *Panax notoginseng* roots differing in sizes reveal correlation between miR156 abundances and root biomass levels. *Rep* 7:9418. doi: 10.1038/s41598-017-09670-8

Zhou, K. (2019). Glycosylphosphatidylinositol-anchored proteins in *Arabidopsis* and one of their common roles in signaling transduction. *Front. Plant Sci.* 10, 1022–1041. doi: 10.3389/fpls.2019.01022

Conflict of Interest: The authors declare that the research was conducted in the absence of any commercial or financial relationships that could be construed as a potential conflict of interest.

Publisher's Note: All claims expressed in this article are solely those of the authors and do not necessarily represent those of their affiliated organizations, or those of the publisher, the editors and the reviewers. Any product that may be evaluated in this article, or claim that may be made by its manufacturer, is not guaranteed or endorsed by the publisher.

Copyright © 2022 Yu, Hua, Liao, Zheng, Jin, Peng, Cui, Huang and Yuan. This is an open-access article distributed under the terms of the Creative Commons Attribution License (CC BY). The use, distribution or reproduction in other forums is permitted, provided the original author(s) and the copyright owner(s) are credited and that the original publication in this journal is cited, in accordance with accepted academic practice. No use, distribution or reproduction is permitted which does not comply with these terms.

frontiers | Frontiers in Plant Science

ORIGINAL RESEARCH
published: 06 June 2022
doi: 10.3389/fpls.2022.885622

Basic Helix-Loop-Helix Transcription Factors AabHLH2 and AabHLH3 Function Antagonistically With AaMYC2 and Are Negative Regulators in Artemisinin Biosynthesis

Qian Shen[1], Huayi Huang[1], Lihui Xie[1], Xiaolong Hao[1,2], Sadaf-Ilyas Kayani[1], Hang Liu[1], Wei Qin[1], Tiantian Chen[1], Qifang Pan[1], Pin Liu[1] and Kexuan Tang[1]**

[1] Plant Biotechnology Research Center, SJTU–Fudan–Nottingham Plant Biotechnology R&D Center, School of Agriculture and Biology, Shanghai Jiao Tong University, Shanghai, China, [2] Laboratory of Medicinal Plant Biotechnology, College of Pharmacy, Zhejiang Chinese Medical University, Hangzhou, China

OPEN ACCESS

Edited by:
Zhihua Liao,
Southwest University, China

Reviewed by:
Wei Sun,
China Academy of Chinese Medical Sciences, China
Zhichao Xu,
Northeast Forestry University, China

***Correspondence:**
Qian Shen
qshen18@sjtu.edu.cn
Kexuan Tang
kxtang@sjtu.edu.cn

Specialty section:
This article was submitted to Plant Metabolism and Chemodiversity, a section of the journal Frontiers in Plant Science

Received: *28 February 2022*
Accepted: *09 May 2022*
Published: *06 June 2022*

Citation:
Shen Q, Huang H, Xie L, Hao X, Kayani S-I, Liu H, Qin W, Chen T, Pan Q, Liu P and Tang K (2022) Basic Helix-Loop-Helix Transcription Factors AabHLH2 and AabHLH3 Function Antagonistically With AaMYC2 and Are Negative Regulators in Artemisinin Biosynthesis. Front. Plant Sci. 13:885622. doi: 10.3389/fpls.2022.885622

Plants have evolved sophisticated systems for regulating the biosynthesis of specialized phytochemicals. Artemisinin, which is a sesquiterpene lactone widely used in anti-malaria treatment, is produced by the *Artemisia annua* L. plant. However, the artemisinin content in *A. annua* is low and difficult to meet market demands. Studies have shown that artemisinin biosynthesis in *A. annua* has complex temporal and spatial specificity and is under tightly transcriptional regulation. However, the mechanism of transcriptional regulation of artemisinin biosynthesis remains unclear. In this study, we identified two MYC-type bHLH transcription factors (AabHLH2 and AabHLH3) as novel regulators of artemisinin biosynthesis. These bHLH TFs act as transcription repressors and function redundantly to negatively regulate artemisinin biosynthesis. Furthermore, AabHLH2 and AabHLH3 are nuclear proteins that bind to DNA elements with similar specificity to that of AaMYC2, but lack the conserved activation domain, suggesting that repression is achieved by competition for the same *cis*-regulatory elements. Together, our findings reveal a novel artemisinin biosynthesis regulatory network, provide new insight into how specialized metabolites are modulated in plants, and propose a model in which different bHLH TFs coordinated in regulating artemisinin production in the plant. Finally, this study provides some useful target genes for metabolic engineering of artemisinin production via CRISPR/Cas9 gene editing.

Keywords: bHLH, MYC2, transcription regulation, *Artemisia annua*, artemisinin

INTRODUCTION

Artemisinin, a sesquiterpene lactone, extracted from the Chinese traditional medicinal plant *Artemisia annua* L, is the main component of artemisinin-based combinatory therapies (ACT) to treat malaria. Besides the antimalarial activities, artemisinin is also a multi-functional compound that has demonstrated cytotoxicity against cancer (Tin et al., 2012), schistosomiasis (Utzinger et al., 2007), virus (Obeid et al., 2013), and tuberculosis (Zheng et al., 2017). Due to the important

medicinal properties of artemisinin, understanding how the artemisinin biosynthetic pathway is regulated is of extreme importance. Despite the great achievement in producing artemisinin in microbes via semisynthetic synthesis (Ro et al., 2006; Paddon et al., 2013), the *A. annua* plant is still the most important resource for artemisinin (Peplow, 2016). However, the transcriptional regulation of this important pathway in *A. annua* is not yet well established.

The family of bHLH TFs is very widespread among eukaryotes and exists in plants, animals, and fungi (Feller et al., 2011). The bHLH family consists of an N-terminal stretch of basic amino acid residues responsible for DNA (Goossens et al., 2017), which recognizes the E-box sequences (CANNTG) in the promoter of their target genes (Ezer et al., 2017). It has been found that bHLH TFs play critical regulatory roles in the specialized metabolism of medicinal and crop species. In Arabidopsis, AtMYC2, AtMYC3, and AtMYC4 were reported to regulate some flavonoid compounds biosynthesis (Dombrecht et al., 2007; Schweizer et al., 2013). The bHLH members of CrMYC2, CrBIS1, and CrBIS2 were involved in monoterpene indole alkaloids biosynthesis in the *Catharanthus roseus* plant (Zhang et al., 2011; Van Moerkercke et al., 2015, 2016). The NbbHLH1 and NbbHLH2 were found to regulate the pyridine alkaloids biosynthesis in *Nicotiana benthamiana* (Todd et al., 2010). In the medical plant *Salvia miltiorrhiza*, the SmMYC2a and SmMYC2b participated in the transcriptional regulation of tanshinones and phenolic acids biosynthesis (Zhou et al., 2016; Yang et al., 2017).

With nearly 200 predicted members in *A. annua*, the bHLH TFs comprise one of the largest TF families in the *A. annua* plant (Shen et al., 2018). To date, several bHLH TFs were reported that positively regulate the accumulation of artemisinin in *A. annua* under different conditions (Ji et al., 2014; Shen et al., 2016; Li et al., 2019; Xiang et al., 2019). Of these, the best characterized and most multifunctional are the MYC-type (MYC2 and AabHLH1) transcription factors, which are the members of the bHLH subgroup IIIe according to the classification by Heim et al. (2003). The MYC2 type of bHLH TFs are usually acting as the positive regulators in secondary metabolism in many plant species (Dombrecht et al., 2007; Todd et al., 2010; Zhang et al., 2011; Ji et al., 2014; Shen et al., 2016; Li et al., 2019; Xiang et al., 2019). On the contrary, JA-ASSOCIATED MYC2-LIKE1 (AtJAM1), AtJAM2, and AtJAM3 (AtbHLH17, −13, and −3, respectively) belong to the bHLH IIId subgroup in *A. thaliana*, function as transcription repressors to antagonize the transcription activator MYC2, and display negative regulation functions (Sasaki-Sekimoto et al., 2013; Song et al., 2013; Fonseca et al., 2014; Qi et al., 2015). Considering the important roles and complex network regulation mechanisms of MYC-type TFs in regulating plant secondary metabolism, it is interesting to ask whether there are other MYC-type bHLH TFs that regulate the biosynthesis of artemisinin.

To identify novel regulators of the artemisinin biosynthesis in the *A. annua* plant, gene co-expression analysis and phylogenetic analysis were performed. In the present study, we identified AabHLH2 and AabHLH3 as two new artemisinin biosynthesis regulators that show high similarity to AaMYC2, and their expression pattern is correlated with the artemisinin synthetic pathway genes. We then conducted overexpression and RNAi experiments to explore the functions of AabHLH2 and AabHLH3 in the *A. annua* plant. The overexpressed transgenic plants showed significantly lower accumulations of artemisinin, while the RNAi transgenic plants displayed higher artemisinin content when compared with the wild-type plants. Thus, we propose that AabHLH2 and AabHLH3 are novel factors that function mostly antagonistically to AaMYC2 in regulating the artemisinin metabolic pathway in *A. annua*. Our research indicates that the coordinated regulation of artemisinin by the transcription activators and repressors provides clues about the previously unknown complex mechanism for directing the production of secondary metabolites.

RESULTS

Combining Phylogenetic Analysis and Global Gene Expression of bHLH Transcription Factors in *Artemisia annua*

The bHLH transcription factor family is one of the largest transcription factor families in the plant. However, up to now, there were only a few bHLH transcription factors, AabHLH1, AaMYC2, and AabHLH112, reported positively in regulating artemisinin biosynthesis in *A. annua* plant (Ji et al., 2014; Shen et al., 2016; Li et al., 2019; Xiang et al., 2019). Sequence analysis of those two genes showed that they both belong to the MYC-type bHLH transcription factor. MYC-type bHLH transcription factors extensively participate in the plant's secondary metabolism process (Ramsay et al., 2003; Dombrecht et al., 2007; Hong et al., 2012; Schmiesing et al., 2016; Zhou et al., 2016). Therefore, further investigations on the regulatory functions of this sub-family member in *A. annua* are noteworthy. Benefited by the completion of the *A. annua* genome sequence, genome-wide analysis of MYC-type bHLH TFs in *A. annua* is feasible. The genes which encode putative MYC-type proteins were identified using the conserved MYC-type domain (Pfam: PF14215) through the HMM (Hidden Markov Model) search program. The output contains 45 genes that harbor the MYC-type domain. After manually checking the turnout results, sequences with low confidence (E value $> 1 \times 10^{-10}$) and redundancy are removed; therefore, a total of 35 unique genes encoding proteins containing the MYC-type domain were gained. In this study, we focused on the MYC-type bHLH transcription factors, therefore, by comparing with the bHLH transcription factor family in *A. annua*, it showed that 20 of the 35 candidate MYC-type genes belonged to the bHLH family.

To identify novel bHLH transcription factor regulators of the artemisinin biosynthesis, we performed a combined analysis of genome-wide phylogenetic analysis and gene expression profiles of different tissues via RNA-seq data. The transcriptomic sequencing data of seven different tissues of *A. annua* were generated by our lab before (Shen et al., 2018). To investigate

whether, in addition to AabHLH1 and AaMYC2, other MYC-type bHLHs might contribute to the artemisinin biosynthesis of *A. annua*, phylogenetic analysis with characterized MYC-type in other plants was performed based on the clustering of their translated protein sequences in a Maximum Likelihood method. All the MYC-type genes were grouped into two distinct groups, the MYC-type bHLH group (Clade I) and the MYC-type non-bHLH group (Clade II) (**Figure 1A**). In Clade I, in which both AabHLH1 and AaMYC2 were grouped, there was a branch (highlighted in a red box) that was close to most of the MYC2-type transcription factors from different plants and with a specialty. There were nine MYC-type bHLH genes gathered on this branch, and to further understand the function of those genes, we launched the gene expression profiles analysis.

The result was shown as a hierarchical cluster analysis in a heatmap (**Figure 1B**) and showed that there were 12 MYC-type genes grouped with the specific artemisinin biosynthetic pathway genes (*ADS*, *CYP71AV1*, *DBR2,* and *ALDH1*) and demonstrated potential correlative with artemisinin biosynthesis. Together, combining the phylogenetic analysis and gene expression profile results indicated that there were two MYC-type bHLH genes, *AabHLH2* (AA095110) and *AabHLH3* (AA589050), which were located in the specific phylogenetic tree branch mentioned earlier, meanwhile showed co-expression pattern with pathway genes and demonstrated that they may have the potential roles in the regulation of artemisinin biosynthesis.

Characterization of AabHLH2 and AabHLH3, and They Act as Transcriptional Repressors

The full-length coding regions of *AabHLH2* and *AabHLH3* correspond to open reading frames of 1,461 bp and 1,254 bp, respectively, and were isolated from cDNA prepared from leaves of the *A. annua* Huhao 1# cultivar. AabHLH2 shows a 63% sequence similarity to the *Helianthus annuus* (sunflower) MYC2-like transcription factor (Badouin et al., 2017) and AabHLH3 shows a 65% sequence similarity to the *Cynara cardunculus* MYC4-like transcription factor (Scaglione et al., 2016).

To determine where the AabHLH2 and AabHLH3 proteins functions within the cell, we determined the subcellular localization of AabHLH2 and AabHLH3 via fused with YFP protein. In contrast to YFP, which was distributed throughout all the cells, both AabHLH2-YFP and AabHLH3-YFP fusion proteins were observed exclusively in the nuclei (**Supplementary Figure 1**) of *N. benthamiana* leaf epidermal cells, suggesting that AabHLH2 and AabHLH3 are nuclear-localized proteins and this consistent with their potential function as transcriptional regulators.

To further assess if AabHLH2 and AabHLH3 are regulators of artemisinin biosynthesis, we performed promoters (*ADS*, *CYP71AV1*, *DBR2,* and *ALDH1*) transactivation assays with AabHLH2 and AabHLH3 in *N. benthamiana* by Dual-LUC analysis (**Figure 2A**). To our surprise, when AabHLH2 and AabHLH3 were co-infiltrated in *N. benthamiana* leaf cells with proADS:LUC, proCYP71AV1:LUC, proDBR2:LUC, and proALDH1:LUC reporters, respectively, all the promoter activities were significantly decreased while comparing with the control set (**Figures 2B,C**). However, the AaMYC2 effector could upregulate the four aforementioned promoters' activities, which is consistent with the previous report (Shen et al., 2016; **Figure 2D**). Together, these results indicated that AabHLH2 and AabHLH3 have transcriptional repression activities and may play as the negative regulators of artemisinin biosynthesis.

Overexpression of *AabHLH2* or *AabHLH3* Decreases Artemisinin Content and Attenuated Expression of *AabHLH2* or *AabHLH3* Promotes Artemisinin Production in *Artemisia annua*

To further explore the physiological functions of AabHLH2 and AabHLH3 in *A. annua*, we generated transgenic *A. annua* plants, which include *AabHLH2* and *AabHLH3* overexpressing transgenic lines and *AabHLH2* and *AabHLH3* RNAi transgenic lines.

The transgenic plants were confirmed by genomic PCR, and subsequently, qRT-PCR was used to analyze the transcript levels of *AabHLH2* and *AabHLH3* in the transgenic plants. The transcript levels of *AabHLH2* and *AabHLH3* were significantly higher in the overexpressed transgenic lines than in the WT and vector control transgenic plants (**Figures 3A,B**). As expected, the results were consistent with the previous Dual-LUC results that AabHLH2 and AabHLH3 inhibit the promoter activities of those pathway genes, and the expression levels of *ADS*, *CYP71AV1*, *DBR2*, and *ALDH1* were all dramatically decreased in *AabHLH2* and *AabHLH3* overexpression plants, respectively, compared with the WT or vector control plants (**Figure 3D**). This suggests that AabHLH2 and AabHLH3 have the potential role of negatively regulating artemisinin biosynthesis in *A. annua*. We performed high-performance liquid chromatography (HPLC) to analyze the relevant metabolites in the transgenic and WT plants. In line with the downregulation of genes involved in artemisinin biosynthesis, the HPLC results showed that the artemisinin (AN) and dihydroartemisinic acid (DHAA) contents in *AabHLH2* overexpression lines significantly reduced by 27 to 66% and 73 to 88%, respectively, compared with WT (**Figure 3E**), whereas the artemisinic acid (AA) content was not altered too much (**Figure 3E**) and the AN and DHAA contents in *AabHLH3* overexpression lines significantly reduced by 20 to 61% and 72 to 84%, respectively, compared with WT (**Figure 3F**), and also the AA content was not influenced too much (**Figure 3F**) ($P < 0.05$, Student's *t*-test). No obvious phenotype differences were observed in the transgenic *A. annua* plants compared with the control vector (VC1) and WT plants. All these results indicate that AabHLH2 and AabHLH3 regulate artemisinin biosynthesis in the negative model.

To further verify the biological roles of AabHLH2 and AabHLH3 in controlling artemisinin biosynthesis, we silenced these genes' expression by RNA interference. The transcript levels of *AabHLH2* and *AabHLH3* were significantly reduced in the RNAi transgenic lines while compared with the WT and vector control plants (**Figures 4A,B**). As expected, the expression levels

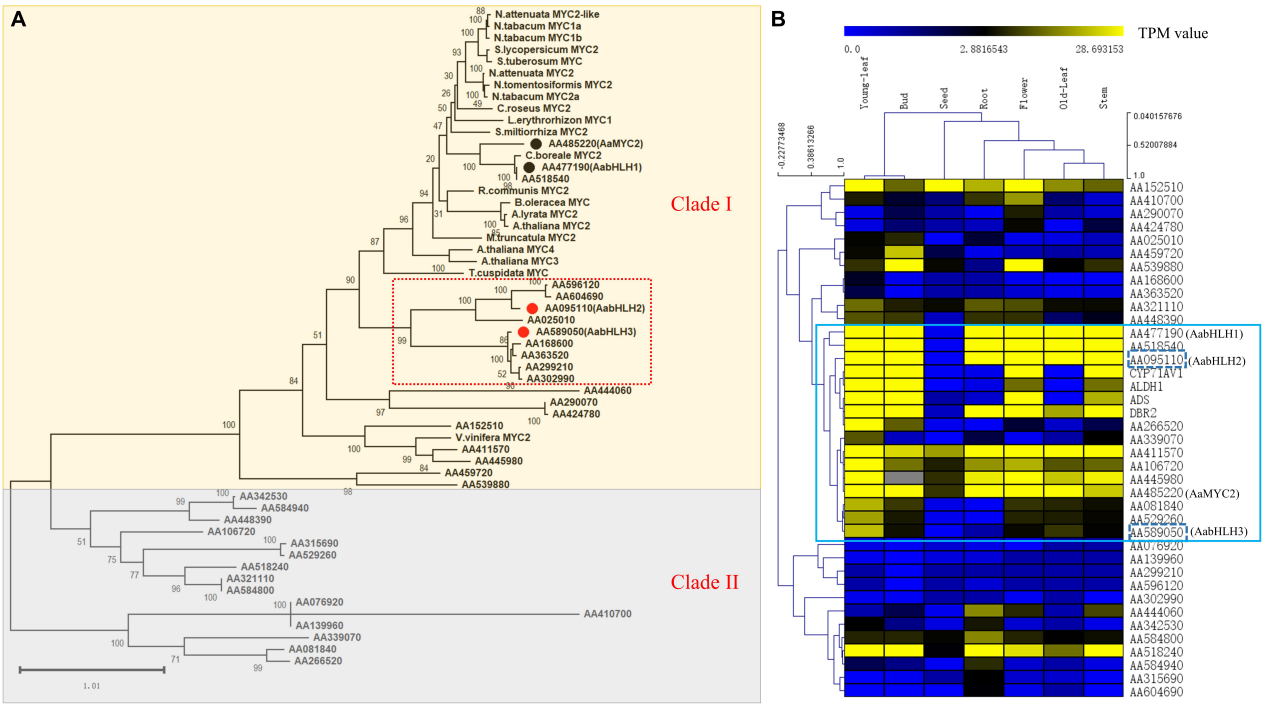

FIGURE 1 | Phylogenetic analysis and global gene expression of MYC-type transcription factors in *A. annua*. **(A)** Phylogenetic tree analysis of MYCs transcription factors in *A. annua* with other plants MYCs. **(B)** Gene co-expression analysis of the MYC transcription factor subfamily with artemisinin biosynthetic pathway genes in *A. annua*.

of *ADS*, *CYP71AV1*, *DBR2*, and *ALDH1* were all upregulated in *AabHLH2* and *AabHLH3* overexpression plants, respectively, compared with the WT or vector control plants (**Figures 4C,D**). Consistent with this, the contents of AN, DHAA, and AA in *AabHLH2* RNAi plants were increased by 42 to 87%, 10 to 90%, and 93 to 175%, respectively, compared with the WT plants (**Figure 4E**). Similarly, the contents of AN, DHAA, and AA in *AabHLH3* RNAi plants were increased by 35 to 60%, 29 to 79%, and 65 to 156%, respectively, compared with the WT plants (**Figure 4F**; $P < 0.05$, Student's *t*-test). No obvious differences were observed in *A. annua* plants that transformed with the control vector (VC2). Together, all the results indicate that AabHLH2 and AabHLH3 are the negative regulators of artemisinin biosynthesis and may be good targets in efforts to increase artemisinin production through CRISPR/Cas9 gene-editing knockout in *A. annua* plant. We also speculate that overexpressing *AaMYC2* and silencing/knockout *AabHLH2/3* simultaneously is a promising genetic engineering strategy to dramatically enhance concentrations of artemisinin.

AabHLH2 and AabHLH3 Inhibit Artemisinin Biosynthesis *via* Antagonizing AaMYC2 for Target Genes

Sequence alignment revealed that the basic HLH domain is highly conserved between AabHLH2, AabHLH3, and AaMYC2, as well as other MYC-type bHLH proteins (**Supplementary Figure 2**). The basic HLH domain is mainly involved in DNA binding activities (Carretero-Paulet et al., 2010; Fernandez-Calvo et al., 2011; Goossens et al., 2017), and we hypothesized that AabHLH2 and AabHLH3 may bind to the same promoter regions as AaMYC2. Previous studies suggested that usually the bHLH family proteins directly bind to the E-box (CANNTG) element in the promoter sequence of target genes and MYC-type bHLH subfamily members prefer the G-box (CACGTG) element which is one type of the E-box elements (Atchley and Fitch, 1997; Atchley et al., 2000; Boter et al., 2004; Dombrecht et al., 2007). Promoter analysis revealed that there were two G-box-like motifs in the promoter of *ADS*, three G-box-like motifs in the promoter of *CYP71AV1*, two G-box-like motifs in the promoter of *DBR2*, and two G-box-like motifs in the promoter of *ALDH1* (**Figure 5A**). Yeast one-hybrid assay revealed that the pB42AD-AabHLH2 fusion protein binding to the three tandem repeats of the ADS-Box1 motif, while the pB42AD-AabHLH3 fusion protein binding to the three tandem repeats of the ADS-Box1 and CYP-Box2 motif, respectively (**Figure 5B**). Meanwhile, we also performed the Y1H assay of AaMYC2 and showed that AaMYC2 binding to the ADS-Box 1, CYP-Box2, and DBR2-Box1, respectively (**Figure 5B**). Together, the above results demonstrate that AabHLH2 and AabHLH3 have similar but not the same DNA binding preferences as AaMYC2.

One of the possible mechanisms of AabHLH2 and AabHLH3 repressions of gene expression is that AabHLH2 and AabHLH3 may repress gene transcription competitively with MYC2 for target sequences. To test whether AabHLH2 and AabHLH3

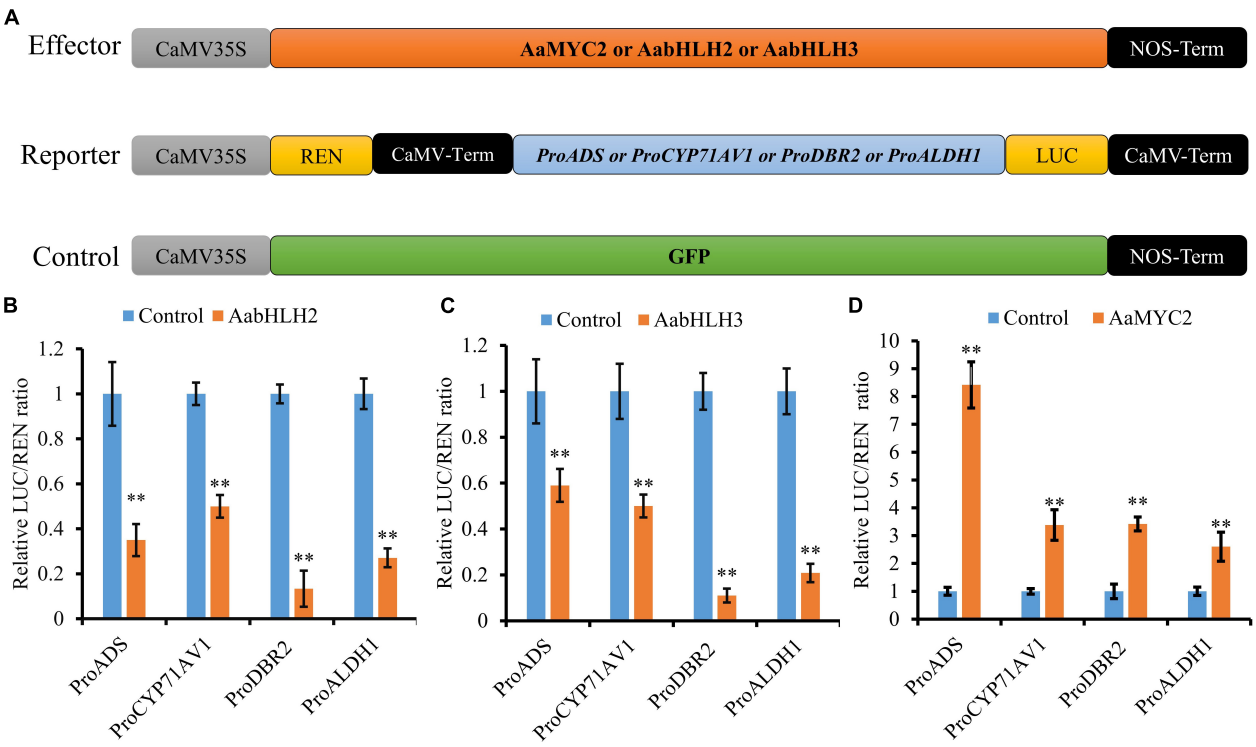

FIGURE 2 | AabHLH2 and AabHLH3 regulate artemisinin biosynthetic genes expression as transcriptional repressors. **(A)** Schematic representation of effector and reporter constructs used in the Dual-LUC assays; **(B,C)** Transient Dual-LUC analysis of AabHLH2 and AabHLH3 with four artemisinin biosynthesis specific pathway gene promoters. **(D)** Transient Dual-LUC analysis of AaMYC2 (positive control) with four artemisinin biosynthesis specific pathway gene promoters; The values were reached by calculating the relative ratio of LUC activities to REN activities (LUC/REN) and the GFP control was set to one. Data are means ± SD (n = 4). Student's t-test: *, $P < 0.05$; **, $P < 0.01$.

proteins antagonize the binding of AaMYC2 to its target promoters, we performed the competition assays by transient expression of *AabHLH2*, *AabHLH3*, and *AaMYC2* with the *ADS* and *CYP71AV1* promoter reporters, respectively. The Dual-LUC analysis showed that AaMYC2 was able to induce the activity of *ADS* and *CYP71AV1* promoters dramatically (**Figure 2D**). However, the transcriptional activation of the proADS-regulated LUC by AaMYC2 was attenuated in a dose-dependent manner by co-expression of AabHLH2 or AabHLH3 (**Figures 6A,B**). The proCYP71AV1-regulated LUC activation showed a similar pattern (**Figures 6C,D**). The transient expression analysis using the LUC reporter revealed the competition effect of AabHLH2 or AabHLH3 with AaMYC2 in regulating target genes. Taken together, these data demonstrate that AabHLH2 and AabHLH3 proteins antagonize AaMYC2 by binding to its target gene (*ADS* and *CYP71AV1*) promoters and act as transcriptional repressors.

DISCUSSION

Malaria is still a global health problem, according to the WHO world malaria report 2021 (World Health Organization [WHO], 2021). Artemisinin, a sesquiterpene lactone, extracted from the Chinese traditional medicinal plant *A. annua*, is the main component of artemisinin-based combinatory therapies (ACT) to treat malaria. Although tremendous amount of energy has been invested in increasing the artemisinin content such as semi-synthetic via engineering yeast (Ro et al., 2006; Paddon et al., 2013), heterogenous production in other plants (van Herpen et al., 2010; Fuentes et al., 2016; Ikram and Simonsen, 2017), the *A. annua*-derived artemisinin is still the main source. Therefore, current artemisinin production by plants is still not sufficient to meet global needs for malaria treatment. Several TF regulators have reported that they are involved in artemisinin biosynthesis in the plant, but a more in-depth understanding of the underlying mechanism of transcriptional regulation is still unclear.

Commonly, plant secondary metabolites are precisely synthesized within the specific tissues at a certain time to coordinate the plant development and response to environmental issues, which are usually tightly controlled at the transcriptional level. This means that in one particular metabolic pathway, the enzyme-encoding genes, the transcription factors, the transporter encoding genes, and other regulator genes usually exhibit a concerted expression pattern (Goossens, 2014). A striking feature of the *A. annua* genome is the existence of a large gene number that may be caused by the expansion of the gene family. Therefore, for effective gene discovery in plant secondary metabolism, co-expression analysis has been proved to be a powerful tool (Goossens, 2014). For instance, the

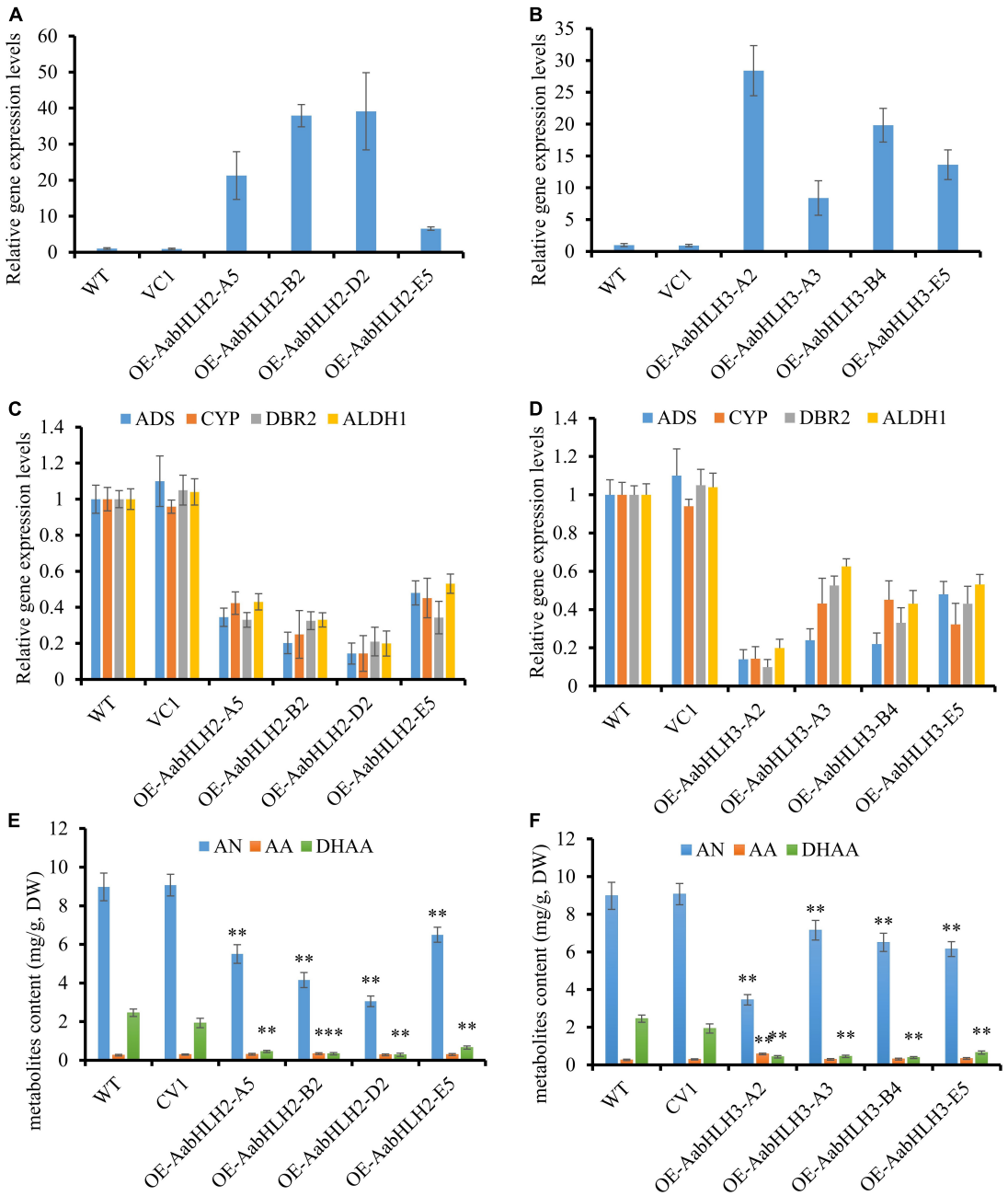

FIGURE 3 | Overexpressing of *AabHLH2* and *AabHLH3* affects artemisinin biosynthetic pathway gene expression levels and artemisinin-related metabolites contents. **(A)** Gene expression analysis of *AabHLH2* in the *AabHLH2* overexpressing transgenic plants. **(B)** Gene expression analysis of *AabHLH3* in the *AabHLH3* overexpressing transgenic plants. **(C)** Relative gene expression of *ADS*, *CYP71AV1*, *DBR2,* and *ALDH1* in the *AabHLH2* overexpressing transgenic plants. **(D)** Relative gene expression of *ADS*, *CYP71AV1*, *DBR2,* and *ALDH1* in the *AabHLH3* overexpressing transgenic plants. **(E)** The contents of artemisinin (AN), dihydroartemisinic acid (DHAA), and artemisinic acid (AA) in the *AabHLH2* overexpressed plants and wild-type plants, determined by HPLC analysis. **(F)** The contents of artemisinin (AN), dihydroartemisinic acid (DHAA), and artemisinic acid (AA) in the *AabHLH3* overexpressed plants and wild-type plants, determined by HPLC analysis. The metabolites contents in the transgenic plant leaves were compared to the wild-type plants. Asterisks indicate the difference between overexpressing transgenic plants and wild-type plants. Statistical significance was determined by Student's *t*-test: **, $P < 0.01$; *, $P < 0.05$.

terpenoid indole alkaloids biosynthesis regulators CrORCA3, CrBIS1, CrBIS2, and CrERF5 in *C. roseus* (Zhang et al., 2011; Van Moerkercke et al., 2015, 2016) and the artemisinin biosynthesis regulators AabZIP9, AaGSW1 in *A. annua* were all discovered via gene co-expression analysis (Chen et al., 2017; Shen et al., 2019). On the other hand, in many cases, the transcription factors involving plant specialized metabolites regulation are conserved among different species. These TFs control the expression level

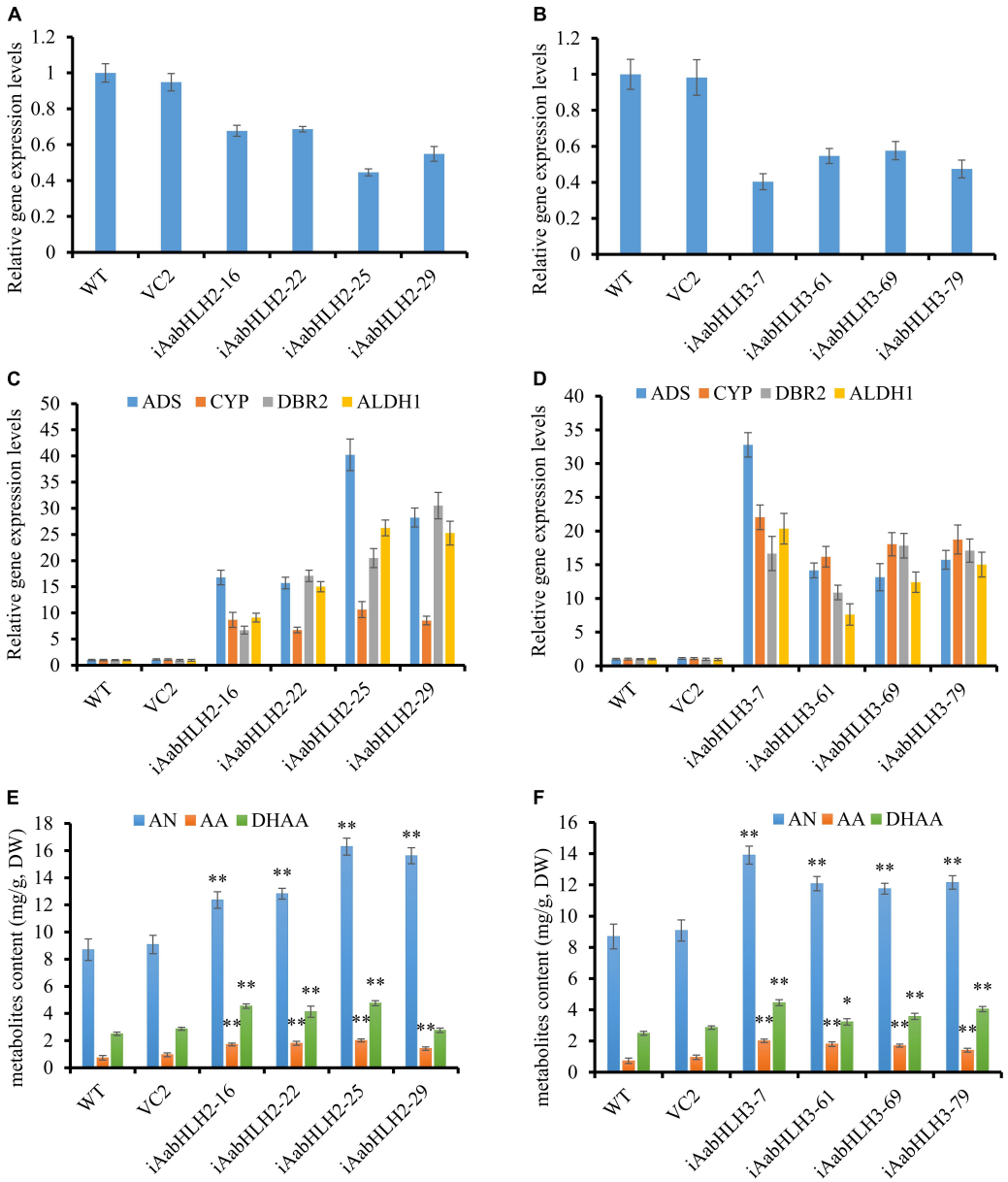

FIGURE 4 | RNA interference reducing *AabHLH2* and *AabHLH3* gene expression affects artemisinin biosynthetic pathway gene expression levels and artemisinin-related metabolites contents. **(A)** Gene expression analysis of *AabHLH2* in the *AabHLH2* RNAi transgenic plants. **(B)** Gene expression analysis of *AabHLH3* in the *AabHLH3* RNAi transgenic plants. **(C)** Relative gene expression of *ADS*, *CYP71AV1*, *DBR2,* and *ALDH1* in the *AabHLH2* RNAi transgenic plants. **(D)** Relative gene expression of *ADS*, *CYP71AV1*, *DBR2,* and *ALDH1* in the *AabHLH3* RNAi transgenic plants. **(E)** The contents of artemisinin (AN), dihydroartemisinic acid (DHAA), and artemisinic acid (AA) in the *AabHLH2* RNAi plants and wild-type plants were determined by HPLC analysis. **(F)** The contents of artemisinin (AN), dihydroartemisinic acid (DHAA), and artemisinic acid (AA) in the *AabHLH3* RNAi plants and wild-type plants were determined by HPLC analysis. The metabolites contents in the transgenic plant leaves were compared to the wild-type plants. Asterisks indicate the difference between RNAi transgenic plants and wild-type plants. Statistical significance was determined by Student's *t*-test: **, $P < 0.01$; *, $P < 0.05$.

of multiple biosynthetic enzyme genes of one specific pathway in a coordinated manner, resulting in the regulation of flux through the pathway (Van Moerkercke et al., 2015, 2016; Li et al., 2016; Goossens et al., 2017). Given their conserved role, these TFs can be considered potential candidates for metabolic engineering of plants and may be used in different plant species (Mertens et al., 2016; Shi et al., 2020). Consequently, fundamental research in model plants may transfers to other non-model plant species that produce specialized metabolites of interest for plants or humans.

The bHLH transcription factor family is one of the largest families in the plant. By combining the gene co-expression and phylogenetic analysis strategies, we demonstrated

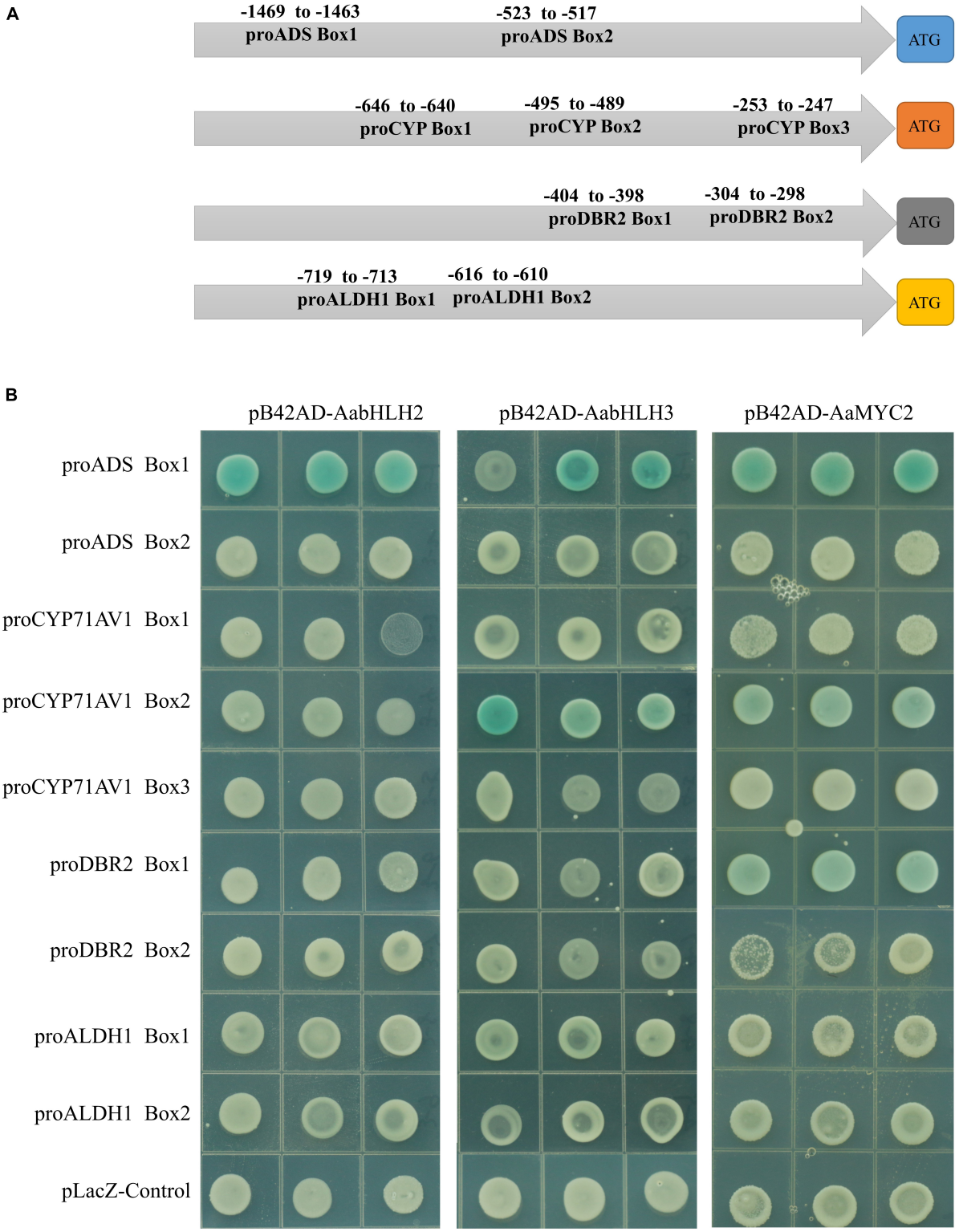

FIGURE 5 | Binding assay of AabHLH2 and AabHLH3 to G-box-like *cis*-elements in the promoters via yeast one-hybrid. **(A)** Schematic representation of all G-box-like *cis*-elements boxes position in the four pathway gene promoters. **(B)** The result of yeast one-hybrid assay for the interaction between AabHLH2 and AabHLH3 with DNA motifs.

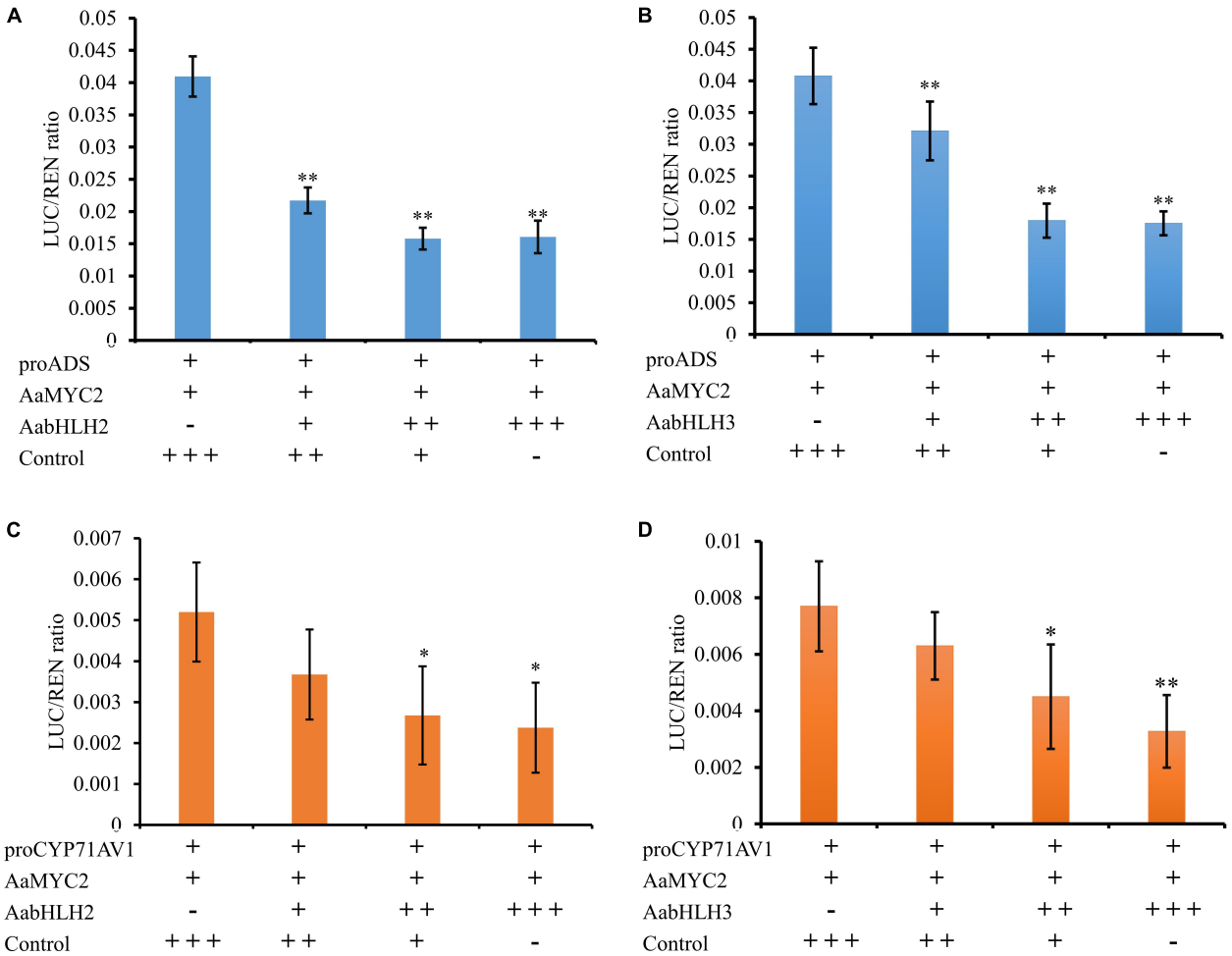

FIGURE 6 | AabHLH2 and AabHLH3 were competing with AaMYC2 to the target gene promoters. **(A,B)** The competition effect of AabHLH2/AabHLH3 with AaMYC2 in regulating *ADS* promoter, the activation of the *ADS* promoter was attenuated in a dose-dependent manner when co-expressing of *AabHLH2*/AabHLH3 and *AaMYC2*, respectively. **(C,D)** The competition effect of AabHLH2/AabHLH3 with AaMYC2 in regulating the *CYP71AV1* promoter, the activation of the *CYP71AV1* promoter was attenuated in a dose-dependent manner when co-expressing of *AabHLH2*/AabHLH3 and *AaMYC2*, respectively. The values were reached by calculating the relative ratio of LUC activities to REN activities (LUC/REN), and the GFP was added as a control. Data are means ± SD ($n = 4$). Student's *t*-test: *, $P < 0.05$; **, $P < 0.01$.

that two MYC-type bHLH TFs candidates (AabHLH2 and AabHLH3) displayed similar gene expression patterns with the artemisinin biosynthetic pathway genes closely clustered with all the other plant MYC2-type transcription factors (**Figure 1B**). Transactivation assays of AabHLH2 and AabHLH3 in *N. benthamiana* by Dual-LUC analysis revealed that AabHLH2 and AabHLH3 were both negatively regulating the transcriptional activity of the pathway genes promoters (**Figures 2B,C**). Our results demonstrated that gene co-expression analysis is not only useful for positive regulators discovery but also suitable for finding negative regulators.

AabHLH2 and AabHLH3 have higher homology to jasmonate-associated MYC2-like proteins (AtJAMs) 1 to 3, rather than AtMYC2 or AaMYC2 (**Supplementary Figure 2**). AaMYC2 and AtMYC2 are categorized as IIIe group of bHLH TFs, while AabHLH2, AabHLH3, and AtJAMs are categorized as IIId group of bHLH TFs (Goossens et al., 2017). It was reported in Arabidopsis that the bHLH subgroup IIId TFs, including AtJAM1/2/3, function as transcription repressors to antagonize the transcription activator MYC2 (Sasaki-Sekimoto et al., 2013; Song et al., 2013; Qi et al., 2015). Unlike the MYC2-types TFs, the IIId group TFs lacks a transcriptional activation domain (TAD) and fail to recruit the RNA polymerase II complex such as MED25 to activate transcription (An et al., 2017; Liu et al., 2019; Wang et al., 2019). In this study, we also found that AabHLH2 and AabHLH3 have a similar binding ability to AaMYC2, which likely provides the mechanism for negative regulation of artemisinin biosynthesis (**Figure 7**). The antagonistic functions between the bHLH subgroup IIId members (e.g., JAM1,2,3) and IIIe members (e.g., MYC2,3,4) appear to be a more general mechanism of the balanced output of plant secondary metabolites biosynthesis.

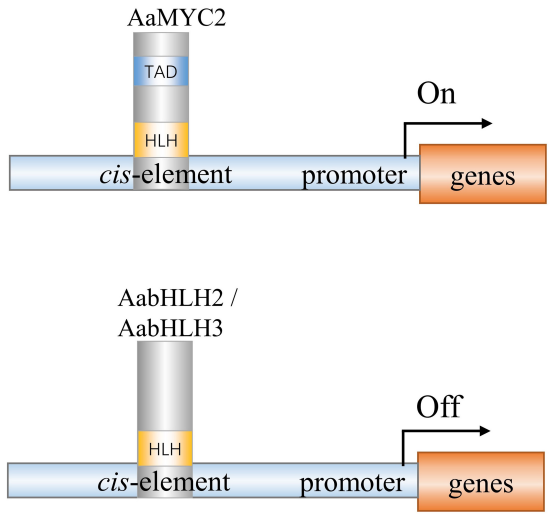

FIGURE 7 | A simplified model of action of AabHLH2, AabHLH3, and AaMYC2 in regulating artemisinin biosynthesis in *Artemisia annua*. AabHLH2, AabHLH3, and AaMYC2 were all able to bind the G-box-like motifs in the pathway gene promoters. AaMYC2 contains the conserved TAD domain and activates the transcription of the downstream gene. AabHLH2 and AabHLH3 were lacking the conserved TAD domain and repressing the transcription of the downstream genes.

Notably, there were several MYC-type non-bHLH genes clustered in the clade II branch that also showed similar gene expression patterns with the artemisinin biosynthetic pathway genes, such as AA081840, AA266520, and AA529260 (**Figure 1**). It will be interesting and worthwhile to investigate their functions whether they are positive regulators or negative regulators of artemisinin biosynthesis or maybe they are not involved in artemisinin biosynthesis regulation and have other functions.

Moreover, up to date, more and more artemisinin positive regulators were reported and only a few artemisinin negative regulators were investigated. With the development of gene-editing technology, the negative regulators are becoming more and more important. Our results indicate that AabHLH2 and AabHLH3 are the negative regulators of artemisinin biosynthesis and may be good targets in efforts to increase artemisinin production through CRISPR/Cas9 gene editing in *A. annua*. Screening for negative regulators suitable for gene editing to enhance artemisinin content may be a new strategy to improve the concentration of artemisinin in the plant.

MATERIALS AND METHODS

Plant Material

The seeds of *A. annua* (cultivar "Huhao 1") were bred by our lab for several years in Shanghai, China (Shen et al., 2016, 2018). Aseptic seedlings for genetic transformation were acquired according to the method reported previously. Seeds were surface-sterilized with 75% ethanol for 1 min and then treated using 20% (v/v) NaOCl for 10 min, followed by washing with sterilized water four times (Shen et al., 2016). The *Nicotiana benthamiana* (a close relative of tobacco) seeds were sown in pots and grown in a growth chamber under standard conditions of light, temperature, and humidity (16/8 light/dark period, 25 ± 2°C, 50%–70% relative humidity).

Gene Discovery and Bioinformatics Analysis

To search for the MYC-type subfamily in *A. annua*, the conserved MYC-type domain (Pfam: PF14215) was downloaded from the Pfam database.[1] The MYC-type homologs were identified through the HMM (Hidden Markov Model) search against the *A. annua* protein sequence database. Sequences with low confidence (*E* value $>1\times 10^{-10}$) and redundancy of the turnout results were then manually removed. The protein sequences of MYC2 type in other plants (retrieved from NCBI) and protein sequences of all the MYC-type in *A. annua* were aligned with ClustalW (Larkin et al., 2007). The non-rooted phylogenetic tree was generated with the MEGA6.1 software (Tamura et al., 2013), according to the Maximum Likelihood method with JTT matrix-based model and bootstrapping with 500 replicates to evaluate the accuracy of phylogenetic construction. The expression levels of each MYC-type TFs in seven different tissues (young leaf, old leaf, flower, bud, root, stem, and seed) were obtained by transcripts per million (TPM) normalization method as reported previously (Shen et al., 2018). Gene co-expression analysis was performed using the MultiExperiment Viewer (MeV4.9.0) software (Saeed et al., 2003) based on the TPM value of each gene. Sample clustering was carried out using the hierarchical clustering method, and the evolutionary distances were computed with Poisson correction (Eisen et al., 1998).

Cloning of the Candidate MYC-Type bHLH Genes

For gene isolation, the gene-specific primers, AabHLH2 F/R and AabHLH3 F/R, were designated according to assembled RNA-seq data generated by our lab before (Shen et al., 2018). PCR was performed according to the manufacturer's instructions for KOD DNA polymerase (Toyobo, Japan), using *A. annua* young leaf cDNA as the template. The PCR products were subcloned into the pLB vector (Tiangen, China) and confirmed by sequencing. All the primers used in the present study are listed in **Supplementary Table 1**.

Dual-Luciferase Assay

To obtain plant overexpression vectors and perform the dual-luciferase assay (Dual-LUC), AabHLH2 and AabHLH3 ORF were amplified with primers P1 F/R and P2 F/R, and then cloned into pHB vector, respectively. The four reporter constructs were previously generated by our lab (Hao et al., 2017), which were produced by inserting the promoters of *ADS*, *CYP71AV1*, *DBR2*, and *ALDH1* into the

[1]https://pfam.xfam.org/

pGreenII 0800-LUC plasmid (Hellens et al., 2005), respectively. The effector and reporter plasmids were transferred into the *A. tumefaciens* strain GV3101, respectively. The effector strain and reporter strain were mixed at the ratio 1:1, then the bacteria mixtures were transiently infiltrated into the *N. benthamiana* leaves as described previously (Shen et al., 2019). The effector strain that harbored pHB-GFP plasmid was used as the control. The firefly LUC and REN activities were analyzed using commercial Dual-LUC reaction reagents (Promega, United States) according to the manufacturer's instructions. Four biological replicates were measured for each sample.

Subcellular Localization Analysis

For subcellular localization analysis, AabHLH2 and AabHLH3 ORF were amplified with primers P3 F/R and P4 F/R and cloned into pENTR-SD/TOPO gateway vector (Invitrogen, United States) and subsequently recombined into pEarleyGate104 (Earley et al., 2006) by LR reaction (Invitrogen, United States) to generate YFP fusion vectors, pEarleyGate104-YFP-AabHLH2 and pEarleyGate104-YFP-AabHLH3, respectively. Subsequently, the above-mentioned plasmids were transferred into the *A. tumefaciens* strain GV3101 and transiently infiltrated into the *N. benthamiana* leaves as described previously (Shen et al., 2019). The YFP signals were observed after 3 days of cultivation using confocal microscopy (Leica, Germany), with argon laser excitation at 488 nm and a 505- to 550-nm emission filter set. Subcellular localization was done in three biological replicates.

Yeast One-Hybrid

For yeast one-hybrid experiments, the full-length coding sequences of AabHLH2 and AabHLH3 were amplified with primers P7 F/R and P8 F/R and then cloned into the pB42AD (*Eco*RI/*Xho*I) by using ClonExpress II (Vazyme, China) to generate the effector vectors. The artificial synthesized triplicate *cis*-element segments contain possible bHLH binding elements from the promoters of *ADS*, *CYP71AV1*, *DBR2*, and *ALDH1,* which were inserted into the pLacZ (*Eco*RI/*Xho*I) to create the reporter vectors. The sequences of artificially synthesized triplicate *cis*-elements were listed in **Supplementary Table 1**. The combinations of pB42AD-AabHLH2 and pB42AD-AabHLH3 with different *cis*-element motifs were co-transformed into the yeast strain EGY48 by using the LiAc method. The transformant yeasts were cultivated on synthetic-defined SD/-Trp/-Ura dropout (Clontech, Dalian) selected plates at 30°C and positive clones were transferred to and grown on SD/-Trp/-Ura plates with X-gal to test the interaction.

RNA Isolation and qPCR Analysis

Young leaves from 3-month-old transgenic and wild-type plants were harvested for gene expression analysis. Leaf samples were picked and immediately frozen in liquid nitrogen and stored at −80°C. The total RNA was extracted by RNAprep Pure Plant Kit (Tiangen, China) following the manufacturer's instructions. 1 μg of total RNA was used for first-strand cDNA synthesis by using PrimeScript RT Master Mix Kit (TaKaRa, Dalian). qRT-PCR experiments were performed by using SuperReal PreMix SYBR Green Kit (Tiangen, China) on the LightCycle96 machine (Roche, Switzerland) as reported previously (Shen et al., 2016). The relative expression levels of genes were normalized to the expression of the *A. annua* β-ACTIN gene and calculated by the $2^{-\Delta\Delta Ct}$. All the primers used for qPCR are listed in **Supplementary Table 1**.

Plant Transformation of *Artemisia nnua* and Genomic DNA PCR Analysis

To construct RNAi vector, approximately 400 bp length specific sequence of AabHLH2 and AabHLH3 is amplified with primers P5 F/R and P6 F/R and cloned into pENTR-SD/TOPO gateway vector (Invitrogen, United States) and is subsequently recombined into pHellsagate (Helliwell and Waterhouse, 2003) by LR reaction (Invitrogen, United States) to generate pHellsagate-iAabHLH2 and pHellsagate-iAabHLH3 vectors. The plant overexpression, RNAi, and control constructs (pHB-AabHLH2, pHB-AabHLH3, pHellsagate-iAabHLH2, pHellsagate-iAabHLH3, pHB-GUS, and pHellsagate) were introduced into *Agrobacterium tumefaciens* strain EHA105, respectively, and the resulting strains were used in the transformation of *A. annua*. The transgenic plants of *A. annua* were generated as described previously (Shen et al., 2012). To detect the positive transgenic plants, the genomic DNA was extracted from the *A. annua* plants by the CTAB method. The T_0 transgenic plants of overexpression *A. annua* were confirmed by genomic DNA-based PCR on both inserted gene and Hyg (Hygromycin) resistant gene. For RNAi transgenic plant confirmation, both the inserted fragment and NPT II (kanamycin) resistance gene were analyzed by PCR. All the primers used are listed in **Supplementary Table 1**

Quantification of Metabolites Using High-Performance Liquid Chromatography

Three-month-old plant leaves were harvested for HPLC analysis, and leaf samples of the transgenic plants and control plants were prepared as described previously (Lu et al., 2013). The leaves were dried in a drying oven at 45°C for 2 days and then ground into powder. A 0.1 g dried leaf powder of each sample was extracted with 2 ml methanol in an ultrasonic processor under the conditions of 25°C and 50W for 30 min. The samples were centrifuged for 10 min at 10,000 g and then the supernatants were passed through a 0.25-μm membrane filter. The filtrated solutions were then used for metabolites analysis via HPLC. The conditions for HPLC were set as described previously (Lu et al., 2013). Standard of artemisinin was purchased from Sigma and standard of dihydroartemisinic acid and artemisinic acid were bought from Guangzhou Honsea Sunshine BioScience and Technology

Co. Ltd. (Honsea Sunshine Bio, China). Three biological replicates were measured for each sample.

DATA AVAILABILITY STATEMENT

The original contributions presented in the study are included in the article/**Supplementary Material**, further inquiries can be directed to the corresponding author.

AUTHOR CONTRIBUTIONS

QS and KT designed the project. QS and HH performed most of the experiments and wrote the manuscript. LX, XH, and S-IK performed some of the experiments. HL, WQ, TC, and QP analyzed the data and discussed the article. PL performed the HPLC analysis. All authors have read and approved the manuscript.

FUNDING

This work was supported by the National Natural Science Foundation of China (31600231) and the Bill and Melinda Gates Foundation (OPP1199872).

SUPPLEMENTARY MATERIAL

The Supplementary Material for this article can be found online at: https://www.frontiersin.org/articles/10.3389/fpls.2022.885622/full#supplementary-material

REFERENCES

An, C., Li, L., Zhai, Q., You, Y., Deng, L., Wu, F., et al. (2017). Mediator subunit MED25 links the jasmonate receptor to transcriptionally active chromatin. *Proc. Natl. Acad. Sci. U.S.A.* 114, E8930–E8939. doi: 10.1073/pnas.1710885114

Atchley, W. R., and Fitch, W. M. (1997). A natural classification of the basic helix–loop–helix class of transcription factors. *Proc. Natl. Acad. Sci. U.S.A.* 94, 5172–5176. doi: 10.1073/pnas.94.10.5172

Atchley, W. R., Wollenberg, K. R., Fitch, W. M., Terhalle, W., and Dress, A. W. (2000). Correlations among amino acid sites in bHLH protein domains: an information theoretic analysis. *Mol. Biol. Evol.* 17, 164–178. doi: 10.1093/oxfordjournals.molbev.a026229

Badouin, H., Gouzy, J., Grassa, C. J., Murat, F., Staton, S. E., Cottret, L., et al. (2017). The sunflower genome provides insights into oil metabolism, flowering and Asterid evolution. *Nature* 546, 148–152. doi: 10.1038/nature22380

Boter, M., Ruiz-Rivero, O., Abdeen, A., and Prat, S. (2004). Conserved MYC transcription factors play a key role in jasmonate signaling both in tomato and *Arabidopsis*. *Genes Dev.* 18, 1577–1591. doi: 10.1101/Gad.297704

Carretero-Paulet, L., Galstyan, A., Roig-Villanova, I., Martinez-Garcia, J. F., Bilbao-Castro, J. R., and Robertson, D. L. (2010). Genome-wide classification and evolutionary analysis of the bHLH family of transcription factors in *Arabidopsis*, poplar, rice, moss, and algae. *Plant Physiol.* 153, 1398–1412. doi: 10.1104/pp.110.153593

Chen, M., Yan, T., Shen, Q., Lu, X., Pan, Q., Huang, Y., et al. (2017). GLANDULAR TRICHOME-SPECIFIC WRKY 1 promotes artemisinin biosynthesis in *Artemisia annua*. *New Phytol.* 214, 304–316. doi: 10.1111/nph.14373

Dombrecht, B., Xue, G. P., Sprague, S. J., Kirkegaard, J. A., Ross, J. J., Reid, J. B., et al. (2007). MYC2 differentially modulates diverse jasmonate-dependent functions in *Arabidopsis*. *Plant Cell* 19, 2225–2245. doi: 10.1105/tpc.106.048017

Earley, K. W., Haag, J. R., Pontes, O., Opper, K., Juehne, T., Song, K., et al. (2006). Gateway-compatible vectors for plant functional genomics and proteomics. *Plant J.* 45, 616–629. doi: 10.1111/j.1365-313X.2005.02617.x

Eisen, M. B., Spellman, P. T., Brown, P. O., and Botstein, D. (1998). Cluster analysis and display of genome-wide expression patterns. *Proc. Natl. Acad. Sci. U.S.A.* 95, 14863–14868. doi: 10.1073/pnas.95.25.14863

Ezer, D., Shepherd, S. J., Brestovitsky, A., Dickinson, P., Cortijo, S., Charoensawan, V., et al. (2017). The G-box transcriptional regulatory code in *Arabidopsis*. *Plant Physiol.* 175, 628–640. doi: 10.1104/pp.17.01086

Feller, A., Machemer, K., Braun, E. L., and Grotewold, E. (2011). Evolutionary and comparative analysis of MYB and bHLH plant transcription factors. *Plant J.* 66, 94–116. doi: 10.1111/j.1365-313X.2010.04459.x

Fernandez-Calvo, P., Chini, A., Fernandez-Barbero, G., Chico, J. M., Gimenez-Ibanez, S., Geerinck, J., et al. (2011). The Arabidopsis bHLH transcription factors MYC3 and MYC4 are targets of JAZ repressors and act additively with MYC2 in the activation of jasmonate responses. *Plant Cell* 23, 701–715. doi: 10.1105/tpc.110.080788

Fonseca, S., Fernández-Calvo, P., Fernández, G. M., Díez-Díaz, M., Gimenez-Ibanez, S., López-Vidriero, I., et al. (2014). bHLH003, bHLH013 and bHLH017 are new targets of JAZ repressors negatively regulating JA responses. *PLoS One* 9:e86182. doi: 10.1371/journal.pone.0086182

Fuentes, P., Zhou, F., Erban, A., Karcher, D., Kopka, J., and Bock, R. (2016). A new synthetic biology approach allows transfer of an entire metabolic pathway from a medicinal plant to a biomass crop. *elife* 5:e13664. doi: 10.7554/eLife.13664

Goossens, A. (2014). It is easy to get huge candidate gene lists for plant metabolism now, but how to get beyond? *Mol. Plant* 8, 2–5. doi: 10.1093/mp/ssu099

Goossens, J., Mertens, J., and Goossens, A. (2017). Role and functioning of bHLH transcription factors in jasmonate signalling. *J. Exp. Bot.* 68, 1333–1347. doi: 10.1093/jxb/erw440

Hao, X., Zhong, Y., Fu, X., Lv, Z., Shen, Q., Yan, T., et al. (2017). Transcriptome analysis of genes associated with the artemisinin biosynthesis by jasmonic acid treatment under the light in *Artemisia annua*. *Front. Plant Sci.* 8:971. doi: 10.3389/fpls.2017.00971

Heim, M. A., Jakoby, M., Werber, M., Martin, C., Weisshaar, B., and Bailey, P. C. (2003). The basic helix-loop-helix transcription factor family in plants: a genome-wide study of protein structure and functional diversity. *Mol. Biol. Evol.* 20:735. doi: 10.1093/molbev/msg088

Hellens, R. P., Allan, A. C., Friel, E. N., Bolitho, K., Grafton, K., Templeton, M. D., et al. (2005). Transient expression vectors for functional genomics, quantification of promoter activity and RNA silencing in plants. *Plant Methods* 1:13. doi: 10.1186/1746-4811-1-13

Helliwell, C., and Waterhouse, P. (2003). Constructs and methods for high-throughput gene silencing in plants. *Methods* 30, 289–295. doi: 10.1016/s1046-2023(03)00036-7

Hong, G. J., Xue, X. Y., Mao, Y. B., Wang, L. J., and Chen, X. Y. (2012). *Arabidopsis* MYC2 interacts with DELLA proteins in regulating sesquiterpene synthase gene expression. *Plant Cell* 24, 2635–2648. doi: 10.1105/tpc.112.098749

Ikram, N. K. B. K., and Simonsen, H. T. (2017). A review of biotechnological artemisinin production in plants. *Front. Plant Sci.* 8:1966. doi: 10.3389/fpls.2017.01966

Ji, Y., Xiao, J., Shen, Y., Ma, D., Li, Z., Pu, G., et al. (2014). Cloning and characterization of AabHLH1, a bHLH transcription factor that positively

regulates artemisinin biosynthesis in *Artemisia annua*. *Plant Cell Physiol.* 55, 1592–1604. doi: 10.1093/pcp/pcu090

Larkin, M. A., Blackshields, G., Brown, N., Chenna, R., McGettigan, P. A., McWilliam, H., et al. (2007). Clustal W and Clustal X version 2.0. *Bioinformatics* 23, 2947–2948. doi: 10.1093/bioinformatics/btm404

Li, L., Hao, X., Liu, H., Wang, W., Fu, X., Ma, Y., et al. (2019). Jasmonic acid-responsive AabHLH1 positively regulates artemisinin biosynthesis in *Artemisia annua*. *Biotechnol. Appl. Biochem.* 66, 369–375. doi: 10.1002/bab.1733

Li, P., Chen, B., Zhang, G., Chen, L., Dong, Q., Wen, J., et al. (2016). Regulation of anthocyanin and proanthocyanidin biosynthesis by *Medicago truncatula* bHLH transcription factor MtTT8. *New Phytol.* 210, 905–921. doi: 10.1111/nph.13816

Liu, Y., Du, M., Deng, L., Shen, J., Fang, M., Chen, Q., et al. (2019). MYC2 regulates the termination of jasmonate signaling via an autoregulatory negative feedback loop. *Plant Cell* 31, 106–127. doi: 10.1105/tpc.18.00405

Lu, X., Zhang, L., Zhang, F., Jiang, W., Shen, Q., Zhang, L., et al. (2013). AaORA, a trichome-specific AP2/ERF transcription factor of *Artemisia annua*, is a positive regulator in the artemisinin biosynthetic pathway and in disease resistance to *Botrytis cinerea*. *New Phytol.* 198, 1191–1202. doi: 10.1111/nph.12207

Mertens, J., Van Moerkercke, A., Bossche, R. V., Pollier, J., and Goossens, A. (2016). Clade IVa basic helix-loop-helix transcription factors form part of a conserved jasmonate signalling circuit for the regulation of bioactive plant terpenoid biosynthesis. *Plant Cell Physiol.* 57, 2564–2575. doi: 10.1093/pcp/pcw168

Obeid, S., Alen, J., Pham, V. C., Meuleman, P., Pannecouque, C., Le, T. N., et al. (2013). Artemisinin analogues as potent inhibitors of in vitro hepatitis C virus replication. *PLoS One* 8:e81783. doi: 10.1371/journal.pone.0081783

Paddon, C. J., Westfall, P. J., Pitera, D. J., Benjamin, K., Fisher, K., McPhee, D., et al. (2013). High-level semi-synthetic production of the potent antimalarial artemisinin. *Nature* 496, 528–532. doi: 10.1038/nature12051

Peplow, M. (2016). Synthetic biology's first malaria drug meets market resistance. *Nature* 530, 389–390. doi: 10.1038/530390a

Qi, T. C., Wang, J. J., Huang, H., Liu, B., Gao, H., Liu, Y. L., et al. (2015). Regulation of jasmonate-induced leaf senescence by antagonism between bHLH subgroup IIIe and IIId factors in *Arabidopsis*. *Plant Cell* 27, 1634–1649. doi: 10.1105/tpc.15.00110

Ramsay, N. A., Walker, A. R., Mooney, M., and Gray, J. C. (2003). Two basic-helix-loop-helix genes (MYC-146 and GL3) from *Arabidopsis* can activate anthocyanin biosynthesis in a white-flowered *Matthiola incana* mutant. *Plant Mol. Biol.* 52, 679–688. doi: 10.1023/A:1024852021124

Ro, D.-K., Paradise, E. M., Ouellet, M., Fisher, K. J., Newman, K. L., Ndungu, J. M., et al. (2006). Production of the antimalarial drug precursor artemisinic acid in engineered yeast. *Nature* 440, 940–943. doi: 10.1038/nature04640

Saeed, A., Sharov, V., White, J., Li, J., Liang, W., Bhagabati, N., et al. (2003). TM4: a free, open-source system for microarray data management and analysis. *Biotechniques* 34, 374–378. doi: 10.2144/03342mt01

Sasaki-Sekimoto, Y., Jikumaru, Y., Obayashi, T., Saito, H., Masuda, S., Kamiya, Y., et al. (2013). Basic Helix-Loop-Helix transcription factors JASMONATE-ASSOCIATED MYC2-LIKE1 (JAM1), JAM2, and JAM3 are negative regulators of jasmonate responses in *Arabidopsis*. *Plant Physiol.* 163, 291–304. doi: 10.1104/pp.113.220129

Scaglione, D., Reyes-Chin-Wo, S., Acquadro, A., Froenicke, L., Portis, E., Beitel, C., et al. (2016). The genome sequence of the outbreeding globe artichoke constructed de novo incorporating a phase-aware low-pass sequencing strategy of F1 progeny. *Sci. Rep.* 6:19427. doi: 10.1038/srep19427

Schmiesing, A., Emonet, A., Gouhier-Darimont, C., and Reymond, P. (2016). *Arabidopsis* MYC transcription factors are the target of hormonal salicylic acid/jasmonic acid cross talk in response to *Pieris brassicae* egg extract. *Plant Physiol.* 170, 2432–2443. doi: 10.1104/pp.16.00031

Schweizer, F., Fernández-Calvo, P., Zander, M., Diez-Diaz, M., Fonseca, S., Glauser, G., et al. (2013). *Arabidopsis* basic helix-loop-helix transcription factors MYC2, MYC3, and MYC4 regulate glucosinolate biosynthesis, insect performance, and feeding behavior. *Plant Cell* 25, 3117–3132. doi: 10.1105/tpc.113.115139

Shen, Q., Chen, Y., Wang, T., Wu, S., Lu, X., Zhang, L., et al. (2012). Overexpression of the cytochrome P450 monooxygenase (cyp71av1) and cytochrome P450 reductase (cpr) genes increased artemisinin content in *Artemisia annua* (Asteraceae). *Genet. Mol. Res.* 11, 3298–3309. doi: 10.4238/2012.September.12.13

Shen, Q., Huang, H., Zhao, Y., Xie, L., He, Q., Zhong, Y., et al. (2019). The transcription factor Aabzip9 positively regulates the biosynthesis of artemisinin in *Artemisia annua*. *Front. Plant Sci.* 10:1294. doi: 10.3389/fpls.2019.01294

Shen, Q., Lu, X., Yan, T., Fu, X., Lv, Z., Zhang, F., et al. (2016). The jasmonate-responsive AaMYC2 transcription factor positively regulates artemisinin biosynthesis in *Artemisia annua*. *New Phytol* 210, 1269–1281. doi: 10.1111/nph.13874

Shen, Q., Zhang, L., Liao, Z., Wang, S., Yan, T., Shi, P., et al. (2018). The genome of *Artemisia annua* provides insight into the evolution of Asteraceae family and artemisinin biosynthesis. *Mol. Plant* 11, 776–788. doi: 10.1016/j.molp.2018.03.015

Shi, M., Wang, Y., Wang, X., Deng, C., Cao, W., Hua, Q., et al. (2020). Simultaneous promotion of tanshinone and phenolic acid biosynthesis in *Salvia miltiorrhiza* hairy roots by overexpressing *Arabidopsis* MYC2. *Ind. Crops Prod.* 155:112826. doi: 10.1016/j.indcrop.2020.112826

Song, S., Qi, T., Fan, M., Zhang, X., Gao, H., Huang, H., et al. (2013). The bHLH subgroup IIId factors negatively regulate jasmonate-mediated plant defense and development. *PLoS Genet.* 9:e1003653. doi: 10.1371/journal.pgen.1003653

Tamura, K., Stecher, G., Peterson, D., Filipski, A., and Kumar, S. (2013). MEGA6: molecular evolutionary genetics analysis version 6.0. *Mol. Biol. Evol.* 30, 2725–2729. doi: 10.1093/molbev/mst197

Tin, A. S., Sundar, S. N., Tran, K. Q., Park, A. H., Poindexter, K. M., and Firestone, G. L. (2012). Antiproliferative effects of artemisinin on human breast cancer cells requires the downregulated expression of the E2F1 transcription factor and loss of E2F1-target cell cycle genes. *Anti Cancer Drug* 23, 370–379. doi: 10.1097/CAD.0b013e32834f6ea8

Todd, A. T., Liu, E., Polvi, S. L., Pammett, R. T., and Page, J. E. (2010). A functional genomics screen identifies diverse transcription factors that regulate alkaloid biosynthesis in *Nicotiana benthamiana*. *Plant J.* 62, 589–600. doi: 10.1111/j.1365-313X.2010.04186.x

Utzinger, J., Xiao, S.-H., Tanner, M., and Keiser, J. (2007). Artemisinins for schistosomiasis and beyond. *Curr. Opin. Investig. Drugs* 8, 105–116.

van Herpen, T. W., Cankar, K., Nogueira, M., Bosch, D., Bouwmeester, H. J., and Beekwilder, J. (2010). *Nicotiana benthamiana* as a production platform for artemisinin precursors. *PLoS One* 5:e14222. doi: 10.1371/journal.pone.0014222

Van Moerkercke, A., Steensma, P., Gariboldi, I., Espoz, J., Purnama, P. C., Schweizer, F., et al. (2016). The basic helix-loop-helix transcription factor BIS2 is essential for monoterpenoid indole alkaloid production in the medicinal plant *Catharanthus roseus*. *Plant J.* 88, 3–12. doi: 10.1111/tpj.13230

Van Moerkercke, A., Steensma, P., Schweizer, F., Pollier, J., Gariboldi, I., Payne, R., et al. (2015). The bHLH transcription factor BIS1 controls the iridoid branch of the monoterpenoid indole alkaloid pathway in *Catharanthus roseus*. *Proc. Natl. Acad. Sci. U.S.A.* 112, 8130–8135. doi: 10.1073/pnas.1504951112

Wang, H., Li, S., Li, Y. A., Xu, Y., Wang, Y., Zhang, R., et al. (2019). MED25 connects enhancer-promoter looping and MYC2-dependent activation of jasmonate signalling. *Nat. Plants* 5, 616–625. doi: 10.1038/s41477-019-0441-9

World Health Organization [WHO] (2021). *World Malaria Report 2021*. Available online at: https://www.who.int/teams/global-malaria-programme/reports/world-malaria-report-2021 (accessed December 6, 2021).

Xiang, L., Jian, D., Zhang, F., Yang, C., Bai, G., Lan, X., et al. (2019). The cold-induced transcription factor bHLH112 promotes artemisinin biosynthesis indirectly via ERF1 in *Artemisia annua*. *J. Exp. Bot.* 70, 4835–4848. doi: 10.1093/jxb/erz220

Yang, N., Zhou, W., Su, J., Wang, X., Li, L., Wang, L., et al. (2017). Overexpression of SmMYC2 increases the production of phenolic acids in *Salvia miltiorrhiza*. *Front. Plant Sci.* 8:1804. doi: 10.3389/fpls.2017.01804

Zhang, H., Hedhili, S., Montiel, G., Zhang, Y., Chatel, G., Pré, M., et al. (2011). The basic helix-loop-helix transcription factor CrMYC2 controls the jasmonate-responsive expression of the ORCA genes that regulate alkaloid biosynthesis in *Catharanthus roseus*. *Plant J.* 67, 61–71. doi: 10.1111/j.1365-313X.2011.04575.x

Zheng, H., Colvin, C. J., Johnson, B. K., Kirchhoff, P. D., Wilson, M., Jorgensen-Muga, K., et al. (2017). Inhibitors of *Mycobacterium tuberculosis* DosRST signaling and persistence. *Nat. Chem. Biol.* 13, 218–225. doi: 10.1038/nchembio.2259

Zhou, Y., Sun, W., Chen, J., Tan, H., Xiao, Y., Li, Q., et al. (2016). SmMYC2a and SmMYC2b played similar but irreplaceable roles in regulating the biosynthesis of tanshinones and phenolic acids in *Salvia miltiorrhiza*. *Sci. Rep.* 6:22852. doi: 10.1038/srep22852

Conflict of Interest: The authors declare that the research was conducted in the absence of any commercial or financial relationships that could be construed as a potential conflict of interest.

Publisher's Note: All claims expressed in this article are solely those of the authors and do not necessarily represent those of their affiliated organizations, or those of the publisher, the editors and the reviewers. Any product that may be evaluated in this article, or claim that may be made by its manufacturer, is not guaranteed or endorsed by the publisher.

Copyright © 2022 Shen, Huang, Xie, Hao, Kayani, Liu, Qin, Chen, Pan, Liu and Tang. This is an open-access article distributed under the terms of the Creative Commons Attribution License (CC BY). The use, distribution or reproduction in other forums is permitted, provided the original author(s) and the copyright owner(s) are credited and that the original publication in this journal is cited, in accordance with accepted academic practice. No use, distribution or reproduction is permitted which does not comply with these terms.

Advantages of publishing in Frontiers

OPEN ACCESS
Articles are free to read for greatest visibility and readership

FAST PUBLICATION
Around 90 days from submission to decision

HIGH QUALITY PEER-REVIEW
Rigorous, collaborative, and constructive peer-review

TRANSPARENT PEER-REVIEW
Editors and reviewers acknowledged by name on published articles

Frontiers
Avenue du Tribunal-Fédéral 34
1005 Lausanne | Switzerland

Visit us: www.frontiersin.org
Contact us: frontiersin.org/about/contact

REPRODUCIBILITY OF RESEARCH
Support open data and methods to enhance research reproducibility

DIGITAL PUBLISHING
Articles designed for optimal readership across devices

FOLLOW US
@frontiersin

IMPACT METRICS
Advanced article metrics track visibility across digital media

EXTENSIVE PROMOTION
Marketing and promotion of impactful research

LOOP RESEARCH NETWORK
Our network increases your article's readership